Synthesis of highly functionalised calix[4]resorcinarenes and their application as drug solubilising agents

Keele University

By

May Fahmi A Abdulrahman

A thesis submitted in partial fulfilment of the requirements of Keele University for the degree of Doctor of Philosophy in the School of Pharmacy and Bioengineering

July 2020

Abstract

The rate-limiting step for oral absorption of hydrophobic drugs and solubility is the drug dissolution rate in the GI fluids. Several novel and traditional methods have been used to improve the solubility rates of poorly water-soluble drugs. The proficient encapsulation of hydrophobic drugs in specially designed, functionalized carriers and controlling the drug dissolution and release is considered a major challenge. Approaches to prepare water soluble receptors based on calix[n]arene scaffolds capable of selectively binding guests, including hydrophobic drugs in aqueous media, have been reported but there is no universal solution.

The goal of this project was to study the self-assembly and potential applications of functionalised calix[4]resorcinarenes and calix[4]pyrogallolarenes as drug solubilising agents. These goals were addressed by synthesizing several series of calix[4]resorcinarene and calix[4]pyrogallolarene hosts bearing different lower rim alkyl chain lengths (C_4 and C_7). Further modifications were performed by functionalisation of the upper rim of the calix[4]resorcinarene and calix[4]pyrogallolarenes, by exploiting 2-substituted resorcinols and by attaching ester moieties to the phenolic hydroxyl groups. The synthesis of deep-cavity cavitands was explored also. These amphiphilic carriers were fully characterised using spectroscopy and physico-chemical measurements.

Six water-soluble hosts were formed into nanoparticles using the appropriate method. Their ability to self-assemble in aqueous environments and the resultant particle size and zeta potential of the aggregates were compared. These hosts were tested for their ability to improve the solubility, dissolution rate and release behaviour of different hydrophobic drugs. Interestingly, all of these novel formulations

significantly improved the aqueous solubility and dissolution of three of the hydrophobic drugs tested, indicating that these amphiphilic carriers can be used as drug solubilising agents for formulation. *In vitro* release profiles showed that all the novel formulations derived from calix[4]resorcinarenes and calix[4]pyrogallolarenes bearing long alkyl chains on the lower rim achieved sustained release.

Acknowledgments

I am very grateful to my two amazing supervisors Dr Anthony D.M. Curtis and Dr Clare Hoskins, whose expertise, support, patience, and guidance have been essential for completing this work. I could not have imagined having better supervisors for my PhD study.

I also owe a huge thanks to my country Iraq and particularly to the Iraqi Ministry of Higher Education and Scientific Research for giving me the opportunity to do a PhD and for funding and the continued support.

Most of all, I thank my family, especially my parents who have sacrificed so much for me, my lovely sisters and my brother for supporting me spiritually throughout writing this thesis and my life in general. In particular, very great thanks go to my husband Mohammed for his never-ending love, support, patience, and faith in me and our children Saif and Samara for brightening every day.

I would like to thank my colleagues in the Keele Nanopharmaceutics Research Group. Particular thanks go to Dr Ali Alsurafi for helping.

To all my friends in Jack Ashley Building and further away, thank you for your support and good times throughout the last four years, which I could not have done without. In particular, very warm thanks go to Laboratory technicians Mark Arrowsmith, Dr Neil Grazier and Melissa Kirkby for the assistance with the HPLC.

MAY

Table of Contents

Chapter One 1

Introduction 1

1.1 Supramolecular chemistry 2

1.2 Hydrophobic Drugs 3

1.3 Solubility Enhancement 7

1.3.1 Polymeric Micelles 9

1.3.2 Inclusion Complexes 13

1.4 Calix[n]arenes 14

1.4.1 Evolution of Calix[n]arene Chemistry 14

1.4.2 Structural Characteristics of Calix[n]arenes 16

1.4.3 Applications of Calix[n]arenes 17

1.5 Calix[4]resorcinarenes and Calix[4]pyrogallolarenes 33

1.5.1 History and Chemistry of Calix[4]resorcinarenes and Calix[4]pyrogallolarenes 33

1.5.2 Structural Characteristics of Calix[4]resorcinarenes and Calix[4]pyrogallolarenes 36

1.5.3 Functionalization of Calix[4]resorcinarenes and Calix[4]pyrogallolarenes 39

1.5.4 Bridged Calix[4]resorcinarenes 44

1.5.5 Self–organization of Amphiphilic Calix[4]resorcinarenes and Calix[4]pyrogallolarenes in Water 51

1.5.6 Application of Calix[4]resorcinarenes and Calix[4]pyrogallolarenes in Drug Delivery 59

1.6 Aims and Objectives 68

Chapter Two 72

Synthesis and Characterisation of Calix[4]resorcinarene and Calix[4]pyrogallolarene Nanocarriers and their Aggregation in an Aqueous Environment 72

2.1 Introduction 73

2.2 Nuclear magnetic resonance (NMR) spectroscopy 74

2.3 Infrared (IR) spectroscopy 75

2.4 Mass Spectrometry 76

2.5 Particle Size Analysis of Aggregation 76

2.6 Zeta Potential 77

2.7 Photon Correlation Spectroscopy in Nanoparticle Size and Zeta Potential Determination 77

2.8 Critical Aggregate Concentration Determination 78

2.8.1 Surface Tension 79

2.8.2 Conductivity Methods 80

2.8.3 UV Hydrophobic Probes 80

2.9 Synthesis and Characterisation of water-soluble Calix[4]resorcinarenes and Calix[4]pyrogallolarenes 80

2.9.1 Synthetic Strategy 80

2.10 Results 84

2.10.1 Synthesis of c-Alkyl Calix[4]resorcinarene octa-sodium Salts and c-Alkyl Calix[4]pyrogallolarenes dodeca-sodium Salts 84

2.10.2 Solubility 95

2.10.3 Photon Correlation Spectroscopy 95

2.10.4 Critical Aggregation Concentration CAC 120

2.11 Discussion 128

2.12 Conclusion 134

Chapter Three 136

Drug Loading and Release Studies of Calix[4]resorcinarene and Calix[4]pyrogallolarene Nanocarrier Formulations 136

3.1 Introduction 137

3.2 Model Hydrophobic Drugs used in this Study 138

3.3 UV-Visible Spectroscopy 139

3.4 High Performances Liquid Chromatography 140

3.5 Loading of Hydrophobic Drugs into Nanocarriers 140

3.5.1 Determination of Drug Loading Capacity 141

3.5.2 Particle Size, Zeta Potential and Conductivity Measurements of Aggregate Formed 158

3.6 Results 159

3.6.1 Drug Loading Evaluation 159

3.6.2 UV-Vis Spectroscopy 164

3.6.3 FTIR Analysis of Freeze Dried Formulations 167

3.6.4 NMR Analysis of Formulations 169

3.6.5 Photon Correlation Spectroscopy 177

3.6.6 *In Vitro* Drug Release from Nano-aggregates 191

3.7 Discussion 196

3.8 Conclusion 214

Chapter Four 216

Drug Loading and Release Studies of Calix[4]resorcinarene and Calix[4]pyrogallolarene Nanocarrier Formulations of 2,4-dimethoxy-*N*-(4-phenylbutyl)benzamide 216

4.1 Introduction 217

4.1.1 The Uses of Benzamide Derivatives in Medicinal Chemistry and their Pharmacological Potential 220

4.2 Preparation of LO9 **57** and Formulations and Characterisation Methods used 222

4.2.1 Drug Incorporation Studies 222

4.2.2 Determination of Drug Loading Capacity 223

4.2.3 Spectroscopic Analysis of the Formulation 229

4.2.4 Particle Size and Zeta Potential Measurement using Photon Correlation Spectroscopy 230

4.2.5 *In Vitro* Drug Release Studies 230

4.3 Results 231

4.3.1 Characterization of LO9 57 231

4.3.2 Determination of Drug Loading Capacity for LO9 57..... 233

4.3.3 *In Vitro* Drug Release from Nanoaggregates 247

4.4 Discussion 249

4.5 Conclusion..... 260

Chapter Five 262

Synthesis and Characterization of C-alkyl Substituted Calix[4]resorcinarenes and their Derivatives 262

5.1 Introduction..... 263

5.2 Results..... 266

5.2.1 Synthesis of Aminocalix[4]resorcinarenes 58a-b and 59a-b..... 267

5.2.2 Synthesis of Aminocalix[4]resorcinarenes 58c-d and 59c-d..... 268

5.2.3 Synthesis of Bridge Calix[4]resorcinarenes..... 270

5.2.4 Synthesis of Cavitands 60a-b..... 271

5.3 Discussion 278

5.4 Conclussion 283

Chapter Six..... 286

General Conclusion & Future Work 286

6.1 General conclusion..... 287

6.2 Future Work..... 292

Chapter Seven..... 295

Experimental Details..... 295

7.1 Materials, Analytical Techniques and Methods 296

7.1.1 Materials 296

7.1.2 Analytical Techniques 297

7.1.3 Methods 299

7.1.4 Modification of Calix[4]resorcinarenes **44**. 304

7.1.5 Synthesis of Calix[4]resorcinarenes Octa-Sodium Salt **46a-d** and Calix[4]pyrogallolarenes Dodeca-Sodium Salt **46e-f**. 309

7.1.6 Synthesis of Model Drug Analogue LO9 **57** 312

7.1.7 Modification of Calix[4]resorcinarenes **44a-b** to Prepare Aminocalix[4]resorcinarenes **58a-d**. 313

7.1.8 Synthesis of Calix[4]resorcinarene Cavitands 319

7.1.9 Bromination of Calix[4]resorcinarene Cavitands **60** 321

7.1.10 Modification of Calix[4]resorcinarene Cavitands **61** 322

7.1.11 Modification of Calix[4]resorcinarene Cavitands **62** 323

References 324

List of Figures

Figure 1: The envisaged ideal host–guest complex formed by a calixarene. 3

Figure 2: The molecular structures of model hydrophobic drugs..... 7

Figure 3: Different types of nanocarriers for oral drug delivery..... 8

Figure 4: Diagram showing various strategies that are used to increase solubility and bioavailability of drugs. 9

Figure 5: An illustration of polymer micelle formation as a core/shell structure in aqueous environments. 11

Figure 6: Representation of micelles formed by the self-assembly of block copolymers. 12

Figure 7: An illustration of the process of drug encapsulation into the hydrophobic core of a polymeric micelle. 13

Figure 8: The chemical structure and representation of the shape of some example macrocyclic molecules. 14

Figure 9: The general structure of a calix[4]arene. 15

Figure 10: General structure of calix[n]arenes where [n] = 4, 6, and 8. 16

Figure 11: The possible conformations of calix[4]arene. 17

Figure 12: Chiral calix[4]arenes bearing four L-alanine units at the upper rim..... 20

Figure 13: Chiral calix[4]arenes **6** and **7** functionalized with amino acid residues at the lower rim..... 20

Figure 14: Model of co-assembly of an amphiphilic drug with calix[4]arenes. 23

Figure 15: Model of pH-triggered drug release..... 24

Figure 16: Inclusion complexes of carbamazepine (CBMZ) with *para*-sulfonatocalix[6]arene 1:1(a) and carbamazepine (CBMZ) with *para*-sulfonatocalix[4]arene 1:2 (b). 25

Figure 17: Inclusion complexes of carvedilol (CDL) with *para*-sulfonatocalix[n]aren ..... …26

Figure 18: Inclusion complexes of tetracaine with *para*-sulfonatocalix[6]arene..... 27

Figure 19: The molecular structure of topotecan (TPT). 28

Figure 20: The molecular structures of furosemide and nifedipine..... 29

Figure 21: The complex between a calix[4]arene and carboplatin 30

Figure 22: The molecular structure of Paclitaxel (PTX)..... 31

Figure 23: The molecular structure of amphiphilic calix[4]arenes 32

Figure 24: 1:1 Inclusion complex between *para*-*t*-butyl calix[8]arene and curcumin. 33

Figure 25: The general structure of a calix[4]resorcinarene and calix[4]pyrogallolarene. 34

Figure 26: The possible conformations of calix[4]resorcinarenes and calix[4]pyrogallolarenes..... 37

Figure 27: Relative configurations at methylene bridges of calix[4]resorcinarenes and calix[4]pyrogallolarenes..... 38

Figure 29: The general structure of bromomethylated calix[4]resorcinarene-based cavitands..... 48

Figure 30**:** Structure of an amphiphilic deep cavitand 54

Figure 31: Representation of a vesicle derived from deep cavitand **33**; the small coloured balls represent three different types of guest molecules 55

Figure 32**:** An illustration of the structural behaviour of calix[4]resorcinarenes with glycine, D,L-alanine and D,L-valine in aqueous alkaline sodium and sodium dodecyl sulfate (SDS) solutions..... 56

Figure 33: Molecular structure of water soluble calix[4]resorcinarene **35** 57

Figure 34: The structure of the tris(hydroxymethyl)amide calix[4]resorcinarenes **36**. 58

Figure 35: The structure of the carbazoylmethyl derivative **37** of calix[4]pyrogallol. 59

Figure 36: Molecular structure of chiral calix[4]resorcinarene **38**. 60

Figure 37: The 2:1 inclusion complex between calix[4]resorcinarene **39** and MMF 61

Figure 38: 1:1 Inclusion complex of lamotrigine with compound **39** 62

Figure 39: Proposed 1:1 complex of calix[4]resorcinarene **39** with curcumin 63

Figure 40: Structural formulae of amphiphilic calix[4]resorcinarenes decorated with sulfonate moieties at the upper rim and different alkyl groups at the lower rim 64

Figure 41: The structure of the calix[4]resorcinarene cavitand **41** 65

Figure 42 : Structure of glycine *C*-methylcalix[4]resorcinarene **42** 66

Figure 43: The molecular structure of gabapentin. 67

Figure 44: Structure of tetraundecylcalix[4]resorcinarene–mPEG conjugate **43** 68

Figure 45: the electromagnetic spectrum showing regions of IR. 75

Figure 46: ^{1}H NMR spectrum of calix[4]resorcinarene **44c** in DMSO-d_6 carried out at 300 MHz at 25 °C. 86

Figure 47: ^{1}H NMR spectrum of calix[4]resorcinarene octa-sodium salt **46a** in D_2O at 300 MHz at 25 °C. 88

Figure 48: ^{1}H NMR spectrum of calix[4]resorcinarene octa-sodium salt **46b** in D_2O at 300 MHz at 25 °C. 89

Figure 49: ^{1}H NMR spectrum of calix[4]resorcinarene octa-sodium salt **46c** in D_2O at 300 MHz at 25 °C. 90

Figure 50: ^{1}H NMR spectrum of calix[4]resorcinarene octa-sodium salt **46d** in D_2O at 300 MHz at 25 °C. 91
Figure 51: ^{1}H NMR spectrum of calix[4]pyrogallolarene dodeca-sodium salt **46e** in D_2O at 300 MHz at 25 °C. 92
Figure 52: ^{13}C NMR spectrum of calix[4]pyrogallolarene dodeca-sodium salt **46e** in D_2O at 75 MHz at 25 °C. 93
Figure 53: ^{1}H NMR spectrum of calix[4]pyrogallolarene dodeca-sodium salt **46f** in D_2O at 300 MHz at 25 °C. 94
Figure 54:^{13}C NMR spectrum of calix[4]pyrogallolarene dodeca-sodium salt **46f** in D_2O at 75 MHz at 25 °C. 95
Figure 55: Photon correlation spectroscopy size correlation charts for unfiltered solutions of carrier **46a** with concentrations 0.1 mg/mL (A),1 mg/mL (B) and 5 mg/mL (C) in deionised water (n=3). 98
Figure 56: Photon correlation spectroscopy size correlation charts for filtered solutions of carrier **46a** with concentrations 0.1 mg/mL (A),1 mg/mL (B) and 5 mg/mL (C) in deionised water (n=3). 100
Figure 57: Photon correlation spectroscopy size correlation charts for unfiltered solutions of carrier **46b** with concentrations 0.1 mg/mL (A),1 mg/mL (B) and 5 mg/mL (C) in deionised water (n=3). 102
Figure 58: Photon correlation spectroscopy size correlation charts for filtered solutions of carrier **46b** with concentrations 0.1 mg/mL (A),1 mg/mL (B) and 5 mg/mL (C) in deionised water (n=3). 104
Figure 59: Photon correlation spectroscopy size correlation charts for unfiltered solutions of carrier **46c** with concentrations 0.1 mg/mL (A),1 mg/mL (B) and 5 mg/mL (C) in deionised water (n=3). 106

Figure 60: Photon correlation spectroscopy size correlation charts for filtered solutions of carrier **46c** with concentrations 0.1 mg/mL (A),1 mg/mL (B) and 5 mg/mL (C) in deionised water (n=3). 108

Figure 61: Photon correlation spectroscopy size correlation charts for unfiltered solutions of carrier **46d** with concentrations 0.1 mg/mL (A),1 mg/mL (B) and 5 mg/mL (C) in deionised water (n=3). 110

Figure 62: Photon correlation spectroscopy size correlation charts for filtered solutions of carrier **46d** with concentrations 0.1 mg/mL (A),1 mg/mL (B) and 5 mg/mL (C) in deionised water (n=3). 112

Figure 63: Photon correlation spectroscopy size correlation charts for unfiltered solutions of carrier **46e** with concentrations 0.1 mg/mL (A),1 mg/mL (B) and 5 mg/mL (C) in deionised water (n=3). 114

Figure 64: Photon correlation spectroscopy size correlation charts for filtered solutions of carrier **46e** with concentrations 0.1 mg/mL (A),1 mg/mL (B) and 5 mg/mL (C) in deionised water (n=3). 116

Figure 65: Photon correlation spectroscopy size correlation charts for unfiltered solutions of carrier **46f** with concentrations 0.1 mg/mL (A),1 mg/mL (B) and 5 mg/mL (C) in deionised water (n=3). 118

Figure 66: Photon correlation spectroscopy size correlation charts for filtered solutions of carrier **46f** with concentrations 0.1 mg/mL (A),1 mg/mL (B) and 5 mg/mL (C) in deionised water (n=3). 120

Figure 67: Methyl orange CMC/CAC measurement for the amphiphilic carriers **46a-f**. (Error bars have been omitted for clarity). 121

Figure 68: Surface tension of solutions of calix[4]resorcinarenes **46a-b** measured at 20 °C using a torsion balance (n = 3 ± SD). 123

Figure 69: Surface tension of solutions of calix[4]resorcinarenes **46c-d** measured at 20 °C using a torsion balance (n = 3 ± SD). 124
Figure 70: Surface tension of solutions of calix[4]pyrogallolarenes **46e-f** measured at 20 °C using a torsion balance (n = 3 ± SD). 124
Figure 71: Dependence of the conductivity of solutions of carrier **46a** with varying concentration. 125
Figure 72: Dependence of the conductivity of solutions of carrier **46b** with varying concentration. 126
Figure 73: Dependence of the conductivity of solutions of carrier **46c** with varying concentration. 126
Figure 74: Dependence of the conductivity of solutions of carrier **46d** with varying concentration. 127
Figure 75: Dependence of the conductivity of solutions of carrier **46e** with varying concentration. 127
Figure 76: Dependence of the conductivity of solutions of carrier **46f** with varying concentration. 128
Figure 77: Molecular structure of calix[4]resorcinarenes **46a-d** and calix[4]pyrogallolarenes **46e-f**. 129
Figure 78: Photon correlation spectroscopy size correlation charts for solutions of carrier **46a** with concentrations 0.1 mg/mL (A),1 mg/mL (B) and 5 mg/mL (C) in deionised water (n=3). 131
Figure 79: The molecular structures of hydrophobic drugs propofol, tetracaine and prednisolone. 139
Figure 80: The HPLC chromatogram of (A) standard pure drug propofol (B) carrier **46a** and (C) carrier: drug formulation. 142

Figure 81: The HPLC chromatogram of (A) standard pure drug propofol (B) carrier **46b** and (C) carrier: drug formulation. 143
Figure 82: The HPLC chromatogram of (A) standard pure drug propofol (B) carrier **46c** and (C) carrier: drug formulation. 144
Figure 83: The HPLC chromatogram of (A) standard pure drug propofol (B) carrier **46d** and (C) carrier: drug formulation. 145
Figure 84: The HPLC chromatogram of (A) standard pure drug propofol (B) carrier **46e** and (C) carrier: drug formulation. 146
Figure 85: The HPLC chromatogram of (A) standard pure drug propofol (B) carrier **46f** and (C) carrier: drug formulation. 147
Figure 86: The HPLC chromatogram of (A) standard pure drug prednisolone PLS (B) carrier **46a** and (C) carrier: drug formulation. 149
Figure 87: The HPLC chromatogram of (A) standard pure drug prednisolone PLS (B) carrier **46b** and (C) carrier: drug formulation. 150
Figure 88: The HPLC chromatogram of (A) standard pure drug prednisolone PLS (B) carrier **46c** and (C) carrier: drug formulation. 151
Figure 89: The HPLC chromatogram of (A) standard pure drug prednisolone PLS (B) carrier **46d** and (C) carrier: drug formulation. 152
Figure 90: The HPLC chromatogram of (A) standard pure drug prednisolone PLS (B) carrier **46e** and (C) carrier: drug formulation. 153
Figure 91: The HPLC chromatogram of (A) standard pure drug prednisolone PLS (B) carrier **46f** and (C) carrier: drug formulation. 154
Figure 92: The HPLC chromatogram of (A) standard pure drug TTC (B) carrier **46a** and (C) carrier: drug formulation. 156

Figure 93: The HPLC chromatogram of (A) standard pure drug TTC (B) carrier **46b** and (C) carrier: drug formulation. 157

Figure 94: Propofol- loading concentration at three different feed ratios (1:1, 5:1 and 10:1) of drug: carriers (calix[4]resorcinarenes **46a-d** and calix[4]pyrogallolarenes **46e-f**..... 161

Figure 95: Prednisolone- loading concentration at three different feed ratios (1:1, 5:1 and 10:1) drug: carriers concentrations (calix[4]resorcinarenes **46a-d** and calix[4]pyrogallolarenes **46e-f**). 163

Figure 96: Tetracaine- loading concentration at three different feed ratios (1:1, 5:1 and 10:1) for drug: carriers ratios for calix[4]resorcinarene **46a** (A) and calix[4]pyrogallolarene **46b** (B) 164

Figure 97: UV-Vis spectra of propofol; inclusion complex and carriers **46a-f**..... 165

Figure 98: UV-Vis spectra of prednisolone (PLS); inclusion complex and carriers **46a-f**..... .166

Figure 99: UV-Vis spectra of tetracaine (TTC); inclusion complex and carrier **46a** and carrier **46b.**..... 167

Figure 100: FT-IR spectral analysis of (pink) Propofol (red) inclusion complex (blue) carrier **46b.**..... 168

Figure 101: FT-IR spectral analysis of (pink) Prednisolone (blue) inclusion complex (red) carrier **46b**. 168

Figure 102: FT-IR spectral analysis of (blue) Tetracaine (red) inclusion complex (purple) carrier **46b** 169

Figure 103: ^{1}H NMR spectrum of a solution of propofol and carrier **46b** corresponding to an initial carrier concentration of 3 mg/mL and drug: carrier ratio of 1:1 in D_2O…….....170

Figure 104: ^{1}H NOESY NMR spectrum of a solution of propofol and carrier **46b** corresponding to an initial carrier concentration of 3 mg/mL and drug: carrier ratio of 1:1 in D_2O.....171

Figure 105: ^{1}H NMR spectrum of a solution of prednisolone and carrier **46b** corresponding to an initial carrier concentration of 3 mg/mL and drug: carrier ratio of 1:1 in D_2O.....173

Figure 106: ^{1}H NOESY NMR spectrum of a solution of prednisolone and carrier **46b** corresponding to an initial carrier concentration of 3 mg/mL and drug: carrier ratio of 1:1 in D_2O.....174

Figure 107: ^{1}H NMR spectrum of a solution of tetracaine and carrier **46b** corresponding to an initial carrier concentration of 3 mg/mL and drug: carrier ratio of 1:1 in D_2O.....175

Figure 108: ^{1}H ROESY NMR spectrum of a solution of tetracaine and carrier **46b** corresponding to an initial carrier concentration of 3 mg/mL and drug: carrier ratio of 1:1 in D_2O.....176

Figure 109: Photon correlation spectroscopy size correlation chart for propofol: carrier **46a** (10:1) at 3 mg/mL and 6 mg/mL in deionised water (n=3, ave).....178

Figure 110: Photon correlation spectroscopy size correlation chart for propofol: carrier **46b** (10:1) at 3 mg/mL and 6 mg/mL in deionised water (n=3, ave).....179

Figure 111: Photon correlation spectroscopy size correlation chart for propofol: carrier **46c** (10:1) at 3 mg/mL and 6 mg/mL in deionised water (n=3, ave).....180

Figure 112: Photon correlation spectroscopy size correlation chart for propofol: carrier **46d** (10:1) at 3 mg/mL and 6 mg/mL in deionised water (n=3, ave)..... 181
Figure 113: Photon correlation spectroscopy size correlation chart for propofol: carrier **46e** (10:1) at 3 mg/mL and 6 mg/mL in deionised water (n=3, ave)..... 183
Figure 114: Photon correlation spectroscopy size correlation chart for propofol: carrier **46f** (10:1) at 3 mg/mL and 6 mg/mL in deionised water (n=3, ave)..... 184
Figure 115: Photon correlation spectroscopy size correlation chart for prednisolone: carrier **46a** (1:1) at 1 mg/mL and 3 mg/mL in deionised water (n=3, ave)..... 185
Figure 116: Photon correlation spectroscopy size correlation chart for prednisolone: carrier **46b** (1:1) at 1 mg/mL and 3 mg/mL in deionised water (n=3, ave)..... 186
Figure 117: Photon correlation spectroscopy size correlation chart for prednisolone: carrier **46c** (1:1) at 1 mg/mL and 3 mg/mL in deionised water (n=3, ave)..... 187
Figure 118: Photon correlation spectroscopy size correlation chart for prednisolone: carrier **46d** (1:1) at 1 mg/mL and 3 mg/mL in deionised water (n=3, ave)..... 188
Figure 119: Photon correlation spectroscopy size correlation chart for prednisolone: carrier **46e** (5:1) at 1 mg/mL and 3 mg/mL in deionised water (n=3, ave)..... 189
Figure 120: Photon correlation spectroscopy size correlation chart for prednisolone: carrier **46f** (1:1) at 1 mg/mL and 3 mg/mL in deionised water (n=3, ave)..... 191
Figure 121: The drug propofol release from the optimal formulations derived from carrier **46a-f** at 20 ºC..... 192
Figure 122: The *in vitro* release profiles of prednisolone. 195
Figure 123: Maximum propofol concentration solubilised by calix[4]resorcinarenes **46a-d** and calix[4]pyrogallolarenes **46e-f**..... 198

Figure 124: Maximum prednisolone concentration solubilised by calix[4]resorcinarenes octa-sodium salt **46a-d** and calix[4]pyrogallolarenes dodeca-sodium salt **46e-f**.....200
Figure 125: Photon correlation spectroscopy size correlation chart for carrier with short chains and drug: carrier formulation in deionised water (n=3, ave). 201
Figure 126: Photon correlation spectroscopy size correlation chart for carrier with long chains and drug: carrier formulation in deionised water (n=3, ave). 202
Figure 127: Photon correlation spectroscopy size correlation chart for carrier with short chains and drug: carrier formulation in deionised water (n=3, ave). 203
Figure 128: Photon correlation spectroscopy size correlation chart for carrier with long chains and drug: carrier formulation in doubly distilled water (n=3, ave)…. 204
Figure 129: Comparison of the release profiles rate of propofol and prednisolone over (48 h) at 20 ºC. 207
Figure 130: Comparison of the drugs release profile rate between the long and short chain carriers over (72 h) at 20 ºC. 209
Figure 131: Potential mode of aggregation of propofol with carriers **46a** and **46c**. 211
Figure 132: Potential mode of aggregation of propofol with carriers **46b**, **46d** and **46f**.....212
Figure 133: Potential mode of aggregation of prednisolone with carriers **46a-f**.....213
Figure 134: Amide bonds in drug molecules (**47**-**49**) and natural products (**50**).....217
Figure 135: The structure of a benzamide derivative with different substituents. 221

Figure 136: The HPLC chromatogram of (A) standard pure drug LO9 **57** (B) carrier 46a and (C) carrier: drug formulation. 224
Figure 137: The HPLC chromatogram of (A) standard pure drug LO9 **57** (B) carrier 46b and (C) carrier: drug formulation. 225
Figure 138: The HPLC chromatogram of (A) standard pure drug LO9 **57** (B) carrier 46c and (C) carrier: drug formulation. 226
Figure 139: The HPLC chromatogram of (A) standard pure drug LO9 **57** (B) carrier 46d and (C) carrier: drug formulation. 227
Figure 140: The HPLC chromatogram of (A) standard pure drug LO9 **57** (B) carrier 46e and (C) carrier: drug formulation. 228
Figure 141: The HPLC chromatogram of (A) standard pure drug LO9 **57** (B) carrier 46f and (C) carrier: drug formulation. 229
Figure 142: FTIR spectrum of LO9 **57** 231
Figure 143: ^{1}H NMR spectrum of LO9 **57** in $CDCl_3$ solution at 25 °C..... 232
Figure 144: ^{13}C NMR spectrum of LO9 **57** in $CDCl_3$ solution at 25 °C. 233
Figure 145: LO9 **57** loading concentration at three different initial drug: carrier feed ratios (1:1, 5:1 and 10:1) for calix[4]resorcinarenes **46a-d** and calix[4]pyrogallolarenes **46e-f**. 235
Figure 146: UV-Vis spectra of LO9 **57**, carrier and the corresponding inclusion complex..... 236
Figure 147: UV-Vis spectra of LO9 **57**, carrier and the corresponding inclusion complex..... 236
Figure 148: UV-Vis spectra of LO9 **57**, carrier and the corresponding inclusion complex..... 237

Figure 149: FTIR spectral analysis of (green) LO9 **57** (red) inclusion complex (pink) carrier **46a**. 238

Figure 150: FTIR spectral analysis of (red) LO9 **57** (blue) inclusion complex (purple) carrier **46b**. 238

Figure 151: Expansion of the ^{1}H NMR of the host-guest formulation of carrier **46b:** LO9 **57** (1: 1) in D_2O carried out at 300 MHz at 25 °C. 239

Figure 152: ^{1}H NOESY NMR spectrum of a solution of LO9 **57** and carrier **46a** corresponding to an initial carrier concentration of 6 mg/mL and drug: carrier ratio of 1:1 in D_2O. 240

Figure 153: ^{1}H NOESY NMR spectrum of a solution of LO9 **57** and carrier **46b** corresponding to an initial carrier concentration of 6 mg/mL and drug: carrier ratio of 1:1 in D_2O. 241

Figure 154: Photon correlation spectroscopy size correlation chart for LO9 **57**: carrier **46a** and **46b** formulations in deionised water (n=3, ave). 244

Figure 155: Photon correlation spectroscopy size correlation chart for LO9 **57**: carrier **46c** and **46d** formulations in deionised water 245

Figure 156: Photon correlation spectroscopy size correlation chart for LO9 **57**: carrier **46e** and **46f** formulations in deionised water. 247

Figure 157: *In vitro* drug release from all formulations at two different temperatures (n=3, ± SD), (Error bars have been omitted for clarity). 248

Figure 158: Molecular structure of LO9 **57**, calix[4]resorcinarenes **46a-d** and calix[4]pyrogallolarenes **46e-f**. 250

Figure 159: Maximum LO9 **57** concentration solubilised by calix[4]resorcinarenes **46a-d** and calix[4]pyrogallolarenes **46e-f.** 252

Figure 160: Photon correlation spectroscopy size correlation charts for the carrier and drug: carrier formulation in doubly distilled water (n=3, ave). 255

Figure 161: The drug drug-like molecule LO9 **57** release from the carriers' formulations at 37 ºC and at 20 ºC (Error bars have been omitted for clarity)…….. 257

Figure 162: Potential mode of aggregation of LO9 **57** with carriers **46a**, **46c** and **46e**. 259

Figure 163: Potential mode of aggregation of LO9 **57** with carriers **46b** and **46f**..... ….260

Figure 164: ^{1}H NMR spectrum of aminocalix[4]resorcinarene **58a** in $CDCl_3$ carried out at 300 MHz at 25 °C..... 268

Figure 165: ^{1}H NMR spectrum of aminocalix[4]resorcinarene **59c** in $CDCl_3$ carried out at 300 MHz at 25 °C..... 269

Figure 166: ^{1}H NMR spectrum of aminocalix[4]resorcinarene **59d** in $CDCl_3$ carried out at 300 MHz at 25 °C..... 270

Figure 167: ^{1}H NMR spectrum of calix[4]resorcinarene **60a** in $CDCl_3$ carried out at 400 MHz at 25 °C..... 272

Figure 168: ^{1}H NMR spectrum of calix[4]resorcinarene **60b** in $CDCl_3$ carried out at 400 MHz at 25 °C..... 273

Figure 169: ^{1}H NMR spectrum of calix[4]resorcinarene **61a** in $CDCl_3$ carried out at 400 MHz at 25 °C..... 274

Figure 170: ^{1}H NMR spectrum of aminocalix[4]resorcinarene **61b** in $CDCl_3$ carried out at 400 MHz at 25 °C..... 275

Figure 171: ^{1}H NMR spectrum of calix[4]resorcinarene **62a** in $CDCl_3$ carried out at 300 MHz at 25 °C..... 276

Figure 172: ^{1}H NMR spectrum of calix[4]resorcinarene **62b** in $CDCl_3$ carried out at 300 MHz at 25 °C. 277

Figure 173: ^{1}H NMR spectrum of calix[4]resorcinarene **58a** in $CDCl_3$ carried out at 300 MHz at 25 °C. 279

Figure 174: ^{1}H NMR spectrum of calix[4]resorcinarene **58c** in $CDCl_3$ carried out at 300 MHz at 25 °C. 280

Figure 175: ^{1}H NMR spectrum of calix[4]resorcinarene **60a** in $CDCl_3$ carried out at 400 MHz at 25 °C. 281

Figure 176: ^{13}C NMR spectrum of calix[4]resorcinarene **62a** in $CDCl_3$ carried out at 100 MHz at 25 °C. 282

Figure 177: ^{13}C NMR spectrum of calix[4]resorcinarene **62b** in $CDCl_3$ carried out at 100 MHz at 25 °C. 283

Figure 178: Possible drug- loaded carriers and aggregation mechanisms of carriers calix[4]resorcinarenes and calix[4]pyrogallolalarenes with LO9 **57** ..... …….. 292

List of Tables

Table 1: Biopharmaceutics Classification System for approximate drug solubility. ..... …..4

Table 2**:** Hydrodynamic radius and polydispersity index analysis for solutions (0.1 mg/mL, 1 mg/mL, and 5 mg/mL) of compound **46a** before filtration. Samples were recorded in triplicate at 25°C..... 97

Table 3: Hydrodynamic radius and polydispersity index analysis for solutions (0.1 mg/mL, 1 mg/mL, and 5 mg/mL) of compound **46a** following filtration. Samples were recorded in triplicate at 25°C..... 99

Table 4: Hydrodynamic radius and polydispersity index analysis for solutions (0.1 mg/mL, 1 mg/mL, and 5 mg/mL) of compound **46b** before filtration. Samples were recorded in triplicate at 25°C..... 101

Table 5: Hydrodynamic radius and polydispersity index analysis for solutions (0.1 mg/mL, 1 mg/mL, and 5 mg/mL) of compound **46b** following filtration. Samples were recorded in triplicate at 25°C..... 103

Table 6: Hydrodynamic radius and polydispersity index analysis for solutions (0.1 mg/mL, 1 mg/mL, and 5 mg/mL) of compound **46c** before filtration. Samples were recorded in triplicate at 25°C..... 105

Table 7: Hydrodynamic radius and polydispersity index analysis for solutions (0.1 mg/mL, 1 mg/mL, and 5 mg/mL) of compound **46c** following filtration. Samples were recorded in triplicate at 25°C..... 107

Table 8: Hydrodynamic radius and polydispersity index analysis for solutions (0.1 mg/mL, 1 mg/mL, and 5 mg/mL) of compound **46d** before filtration. Samples were recorded in triplicate at 25°C..... 109

Table 9: Hydrodynamic radius and polydispersity index analysis for solutions (0.1 mg/mL, 1 mg/mL, and 5 mg/mL) of compound **46d** following filtration. Samples were recorded in triplicate at 25°C. 111

Table 10: Hydrodynamic radius and polydispersity index analysis for solutions (0.1 mg/mL, 1 mg/mL, and 5 mg/mL) of compound **46e** before filtration. Samples were recorded in triplicate at 25°C. 113

Table 11: Hydrodynamic radius and polydispersity index analysis for solutions (0.1 mg/mL, 1 mg/mL, and 5 mg/mL) of compound **46e** following filtration. Samples were recorded in triplicate at 25°C. 115

Table 12: Hydrodynamic radius and polydispersity index analysis for solutions (0.1 mg/mL, 1 mg/mL, and 5 mg/mL) of compound **46f** before filtration. Samples were recorded in triplicate at 25°C. 117

Table 13: Hydrodynamic radius and polydispersity index analysis for solutions (0.1 mg/mL, 1 mg/mL, and 5 mg/mL) of compound **46f** following filtration. Samples were recorded in triplicate at 25°C. 119

Table 14: Critical Association Concentrations (CAC, mg/mL) measured at 25 °C using a torsion balance and conductivity (n = 3 ± SD). 133

Table 15: Photon correlation spectrometry size analysis of optimal carrier **46a** formulations at different initial concentrations and initial drug: carrier mass ratio (n=3, ave). 177

Table 16: Photon correlation spectrometry size analysis of optimal carrier **46b** formulations at different initial concentrations and initial drug: carrier mass ratio (n=3, ave). 179

Table 17: Photon correlation spectrometry size analysis of optimal carrier **46c** formulations at different initial concentrations and initial drug: carrier mass ratio (n=3, ave)..... 180
Table 18: Photon correlation spectrometry size analysis of optimal carrier **46d** formulations at different initial concentrations and initial drug: carrier mass ratio (n=3, ave)..... 181
Table 19: Photon correlation spectrometry size analysis of optimal carrier **46e** formulations at different initial concentrations and initial drug: carrier mass ratio (n=3, ave)..... 182
Table 20: Photon correlation spectrometry size analysis of optimal carrier **46f** formulations at different initial concentrations and initial drug: carrier mass ratio (n=3, ave)..... 183
Table 21: Photon correlation spectrometry size analysis of optimal carrier **46a** formulations at different initial concentrations and initial drug: carrier mass ratio (n=3, ave)..... 185
Table 22: Photon correlation spectrometry size analysis of optimal carrier **46b** formulations at different initial concentrations and initial drug: carrier mass ratio (n=3, ave)..... 186
Table 23: Photon correlation spectrometry size analysis of optimal carrier **46c** formulations at different concentrations with different initial carrier: drug mass ratio (n=3, ave)..... 187
Table 24: Photon correlation spectrometry size analysis of optimal carrier **46d** formulations at different concentrations with different initial carrier: drug mass ratio (n=3, ave)..... 188

Table 25: Photon correlation spectrometry size analysis of optimal carrier **46e** formulations at different concentrations with different initial carrier: drug mass ratio (n=3, ave). 189

Table 26: Photon correlation spectrometry size analysis of optimal carrier **46f** formulations at different concentrations with different initial carrier: drug mass ratio (n=3, ave). 190

Table 27: Hydrodynamic radius and polydispersity index analysis for aqueous formulations of LO9 **57** and carriers **46a** and **46b**. Samples recorded in triplicate at 25 °C. 243

Table 28: Hydrodynamic radius and polydispersity index analysis for aqueous formulations of LO9 **57** and carriers **46c** and **46d**. Samples recorded in triplicate at 25 °C. 245

Table 29: Hydrodynamic radius and polydispersity index analysis for aqueous formulations of LO9 **57** and carriers **46e** and **46f**. Samples recorded in triplicate at 25 °C. 246

Abbreviations

Å	Ångstrom, 1×10^{-10} m
Ar	Aromatic
ß–CD	*Beta*-cyclodextrin
br	Broad
^{o}C	Degrees Celsius
CAC	Critical aggregates concentration
CBMZ	Carbamazepine
$CDCl_3$	Chloroform
CDL	Carvedilol
cm	Centimetre
CPZ	Chlorpromazine hydrochloride
CPF	Ciprofloxacin
d	Doublet
DCC	*N,N'*-Dicyclohexylcarbodiimide
DCM	Dichloromethane
DLOV theory	Derjaguin, Landau, Vervey, and Overbeek theory
DMAP	*N,N*-dimethylaminopyridine
DMF	Dimethyformamide
DMSO	Dimethyl sulfoxide
D_2O	Deuterium oxide
ESI-MS	Electrospray ionisation mass spectrometry
EtOH	Ethanol
Et_3N	Tryethylamine

FTIR	Fourier transform infrared
g	Gram
h	Hours
HCl (conc)	Concentrated Hydrochloric acid
Hz	Hertz
HPLC	High Performance Liquid Chromatography
J	coupling constant
LO9	2,4-Dimethoxy-*N*-(4-phenylbutyl)benzamide
Log P	Partition coefficient
MeCN	Acetonitrile
m	Multiplet
μM	Micromolar
MeOH	Methanol
MHz	MegaHertz
mg	Milligram
min	Minute
mL	Millilitres
mmol	Millimoles
mol	Moles
m.p.	Melting point
MW	Molecular weight
NBS	*N*-Bromosuccinimide
NMR	Nuclear magnetic resonance
PCS	Photon correlation spectroscopy
PDI	Polydispersity index

PLS	Prednisolone
Pt/C (5 %)	Palladium (5 %) on carbon
PTX	Pactitaxel
q	Quartet
s	Singlet
SC_4A	*p*-Sulfonatocalix[4]arene
RT	Room temperature
t	Triplet
TFA	Trifluoroacetic acid
THF	Tetrahydrofuran
TLC	Thin layer chromatography
TMS	Tetramethylsilane
TPT	Topotecan
TTC	Tetracaine
UV	Ultraviolet

Chapter One

Introduction

1.1 Supramolecular chemistry

Supramolecular chemistry has been defined as ‘‘chemistry beyond the molecule’’ by Jean-Marie Lehn, who won the Nobel Prize in Chemistry in 1987 along with Donald J. Cram and Charles J. Pedersen (Lehn, 1988; Steed & Atwood, 2009). Supramolecular chemistry can also be defined as “the chemistry of the non–covalent bond” and “non–molecular chemistry” (Lehn, 1987). It refers to the association of two or more chemical species arranged together by non-covalent intermolecular forces such as hydrogen bonds, π–π–stacking interactions, electrostatic and van der Waals forces in order to prepare structures with various sizes and forms (Lehn, 1988; Ventola, 2006; Pastor & Martínez-Viviente, 2008). It describes the weaker and reversible non–covalent interactions between molecules, whereas “traditional” chemistry concentrates on the covalent bond (Reinhoudt, 1992). Host-guest supramolecular chemistry focuses on one molecule (a host) associating non-covalently with another molecule (a guest) to produce a host–guest complex or super–molecule (Figure 1). Typically, a host is a molecule with convergent binding sites and which may also possess a sizeable central hole or cavity. On the other hand, the guest may be a molecule or ion that has divergent binding sites *(*Ventola *et al.*, 2005). The development of synthetic receptors capable of forming complexes with particular guests is an important principle in the advancement of supramolecular host–guest chemistry. The complementarity of the binding sites of host and guest must match correctly, in order to achieve optimal preorganization of host and guest (Cram *et al*., 1988). Research into supramolecular chemistry has been applied to drug delivery because of the limited toxicity of many supramolecular systems and potential enhancements in the bioavailability of guest drug molecules. Organic host molecules such as crown ethers, cyclophanes (including cavitands and calixarenes)

(Nimse & Kim, 2013), cucurbiturils (Kim *et al*., 2007), pillararenes (Yao *et al*., 2012) and cyclodextrins (Mellet *et al*., 2011) are the most common host molecules employed in such research (Hu *et al.,* 2014). Cavitands are essentially rigid scaffolds and the restricted conformation of their functionality has enabled the development of a variety of receptors for both charged particles and neutral species. Cavitands have also been applied extensively in of the preparation of capsule-like hosts, including capsules derived from self-assembly (Cram *et al.*, 1988; Cram & Cram, 1994).

Diverse host molecules with different supramolecular functions may be derived from calixarenes as the core unit. Calixarenes can be further classified into two main categories, the phenol–derived calix[n]arene macrocycles and resorcinol–derived macrocycles such as calix[4]resorcinarene (Bohmer, 1995; Gutsche, 1998; Valand & Menon, 2015).

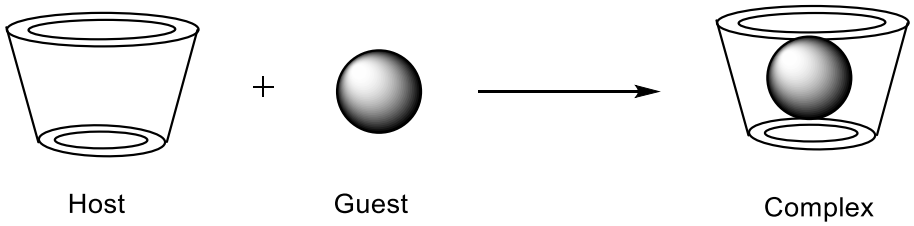

Figure 1: The envisaged ideal host–guest complex formed by a calixarene.

1.2 Hydrophobic Drugs

The majority of clinically effective drug molecules formulated for oral administration are poorly soluble in water (hydrophobic). Orally administered drugs show good bioavailability only when they have a degree of solubility on aqueous media and completely absorb in the gastrointestinal (GI) environment. It is frequently difficult to formulate a drug so that it can show a satisfactory bioavailability profile *in vivo* as a result of this hydrophobicity. Poor bioavailability can give rise to problems such as

ineffective therapy, the need for higher dosing regimes and/or undesirable side effects (Lacy *et al*., 1997).

Drug solubility can be defined as the maximum equilibrium amount of drug solute that can dissolve per amount of solvent under specific conditions (Jain *et al.*, 2010; Savjani *et al.*, 2012; Kadam *et al.*, 2013). The solubility of a drug can be expressed in several ways such as percentage, molarity, molality, volume fraction, and mole fraction (Vemula *et al.*, 2010). According to the Biopharmaceutical Classification System (BCS), drugs can be classified into four categories on the basis of solubility and intestinal permeability (Nagabandi *et al.*, 2011; Murtaza *et al.*, 2014; Shah & Amidon, 2014). These descriptive classes are listed in Table 1: Compounds which feature poor solubility and high permeability belong to Class II according to the Biopharmaceutical Classification System (BCS), while compounds which feature poor solubility and poor permeability belong to Class IV (Nagabandi *et al.*, 2011).

Table 1: Biopharmaceutics Classification System for approximate drug solubility.

Descriptive term	Amount of solvent required for one part of solute
Very soluble	Less than 1
Freely soluble	From 1 to 10
Soluble	From 10 to 30
Sparingly soluble	From 30 to 100
Slightly soluble	From 100 to 1000
Very slightly soluble	From 1000 to 10,000
Practically insoluble	10,000 and over

It is commonly recognized that in combinatorial libraries more than 40 % of newly discovered therapeutic compounds are classified as hydrophobic, or practically insoluble (solubility less than 100 µg/mL), which makes them unsuitable for further drug development because of difficulties associated with their delivery using traditional formulation techniques (Merisko *et al.*, 2008; Wang *et al.*, 2010). A number of potential vehicles are being studied currently for delivering hydrophobic drugs as these drugs require a more complex delivery system compared to their hydrophilic counterparts (Garbo & Morgan, 1988; Chutimaworapan *et al.*, 2000).

Local anaesthetics cause an absence of pain sensation in the area where they are administered. Local anaesthetics block nerve conduction by preventing the increase in membrane permeability to sodium ions that normally leads to nerve impulses. Local anaesthetics can be classified into two principal classes; aminoamide and aminoester local anaesthetics (Butterworth & Strichartz, 1990). Tetracaine (Figure 2) is in the aminoester class of local anaesthetics (Fernandes *et al*., 2007). It has been shown that the molecular mechanisms of both the cationic and the uncharged species of local anaesthesia that coexist at physiological pH is related to inactivation of the sodium ion channels in the nerve membranes, thus blocking the initiation and propagation of nervous impulses (Patton *et al*., 1992; West *et al.*, 1992). Owing to the short duration of action of the local anaesthetics, they may have adverse side effects such as cardiac and central nervous system (CNS) toxicity, accompanied sometimes by allergic reactions (Butterworth & Strichartz, 1990). A key characteristic of the local anaesthetics are that they are hydrophobic when they are in the uncharged state which is desirable for transfer across the skin, but they are typically formulated as the salt in order to overcome the hydrophobicity. Thus, new formulations are required to improve the bioavailability of these drugs.

Propofol, (2,6-diisopropylphenol) (Figure 2), is a hydrophobic anaesthetic as well as a sedative–hypnotic agent. It is widely used for both induction and maintenance of anaesthesia due to its rapid onset, short duration of action, minimal side effects, decreased cerebral oxygen consumption, and reduction of intracranial pressure (Angelini *et al.*, 2001). It is most commonly used in intensive care units and in outpatient procedures (Baker & Naguib, 2005; Imam, 2013). Compared to conventional sedation, propofol has a good level of safety for paediatric endoscopy and is suitable for patient-controlled administration (Kaddu *et al*., 2002; Kulling *et al*., 2001; Sultan, 2014). However, propofol is extremely hydrophobic and is formulated as an oil-in-water emulsion. Large volumes of the formulation are required to induce sedation which may also induce shock unless administered carefully.

There is an increased use of oral and inhaled corticosteroids to control and prevent the symptoms of asthma. They are desirable due to their ability to inhibit production and secretion of cytokines, prevent migration of eosinophils and other inflammatory cells to the airways, as well as reducing the leakage of small-vessel in the lung (Ahmed *et al.*, 2001). Oral corticosteroids are usually as effective as those given intravenously and are preferred because of the ease of using especially in children (Haskell *et al.*, 1984). Corticosteroids such as prednisolone are preferred and available for oral use because of their minimal mineralocorticoid effect, their relatively short half-life, as well as their limited effects on striated muscle (Becker, 2013). Prednisolone is most frequently used clinically for the treatment of inflammatory conditions such as arthritis and asthma. However, like the majority of steroids, prednisolone is significantly hydrophobic and requires a specific formulation in order to administer the correct dose to the patient.

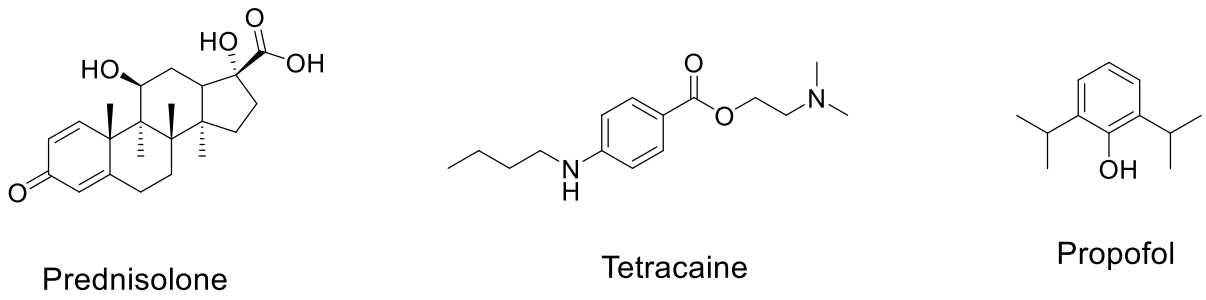

Figure 2: The molecular structures of model hydrophobic drugs.

1.3 Solubility Enhancement

There are two main reasons for insolubility of small organic molecule drugs in aqueous media, a limited ability to hydrogen bond with water or difficulty in disaggregating the molecules in the solid state. Water is a unique solvent due to the water molecules being tightly interlinked through hydrogen bonding. The solute molecule must successfully compete with these powerful intermolecular interactions in order for it to be soluble. Thus, solubility requires a modified formulation or delivery technology that is able to disrupt hydrogen bonding between water molecules (Kipp, 2004).

Approximately, one-third of drugs in development are insoluble in water and one-half fail in trials due to adverse pharmacokinetics. These poorly water soluble drugs are associated with slow drug absorption resulting in inadequate and variable bioavailability (Ahuja *et al.*, 2007; Khadka *et al.*, 2014). As solubility and permeability are the decisive factor for *in vivo* drug absorption, these can be changed or modified by formulation techniques which enhance solubility in aqueous media (Saharan *et al*., 2009).

Thus, improving drug solubility and hence its oral bioavailability is one of most challenging aspects of the drug development process especially for oral drug delivery

(Savjani *et al.*, 2012). Many formulation techniques are available to improve the solubility of hydrophobic drugs (Kumar *et al.*, 2011). The use of nanoparticles as drug carriers has become an important emerging area of nanotechnology (Figure 3) (Farokhzad & Langer, 2009; Chen *et al.*, 2010). Since most anticancer drugs are hydrophobic molecules, the development of nanomaterials to deliver these drugs has gained considerable attention (Liu *et al.*, 2008; Athar & Das, 2014).

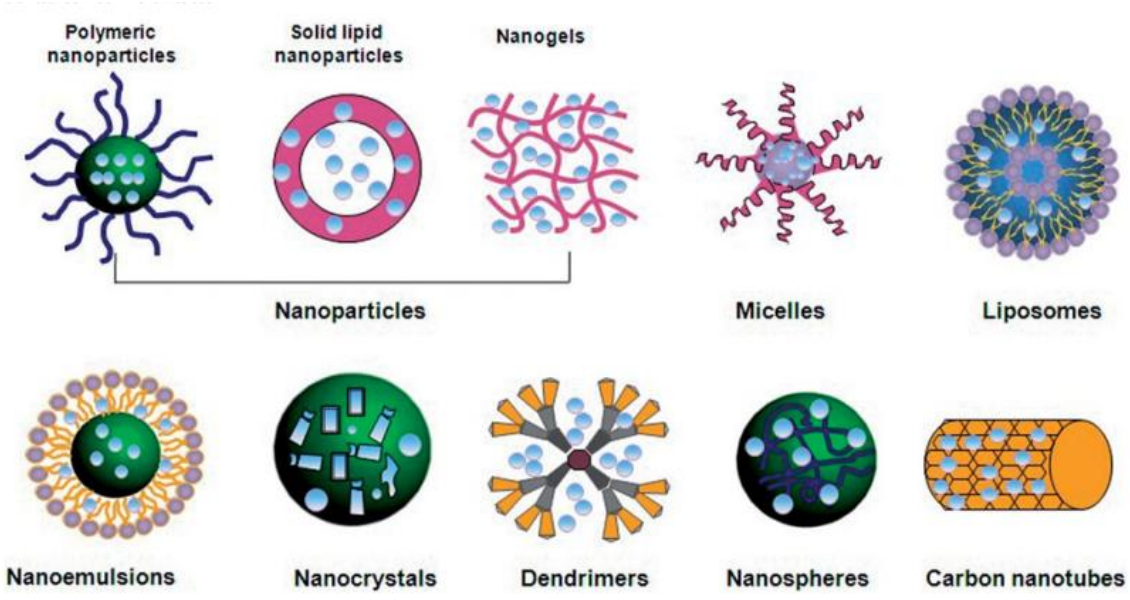

Figure 3: Different types of nanocarriers for oral drug delivery (Zhang *et al*., 2013).

In order to increase the dissolution rates and bioavailability of numerous poorly water soluble drugs, a variety of nanonization strategies (Figure 4) have been employed, included increasing the surface area to volume ratios of drug powders, changing the crystalline forms and designing novel nanomaterials that can serve as carriers for controlled release (Chen *et al.*, 2010).

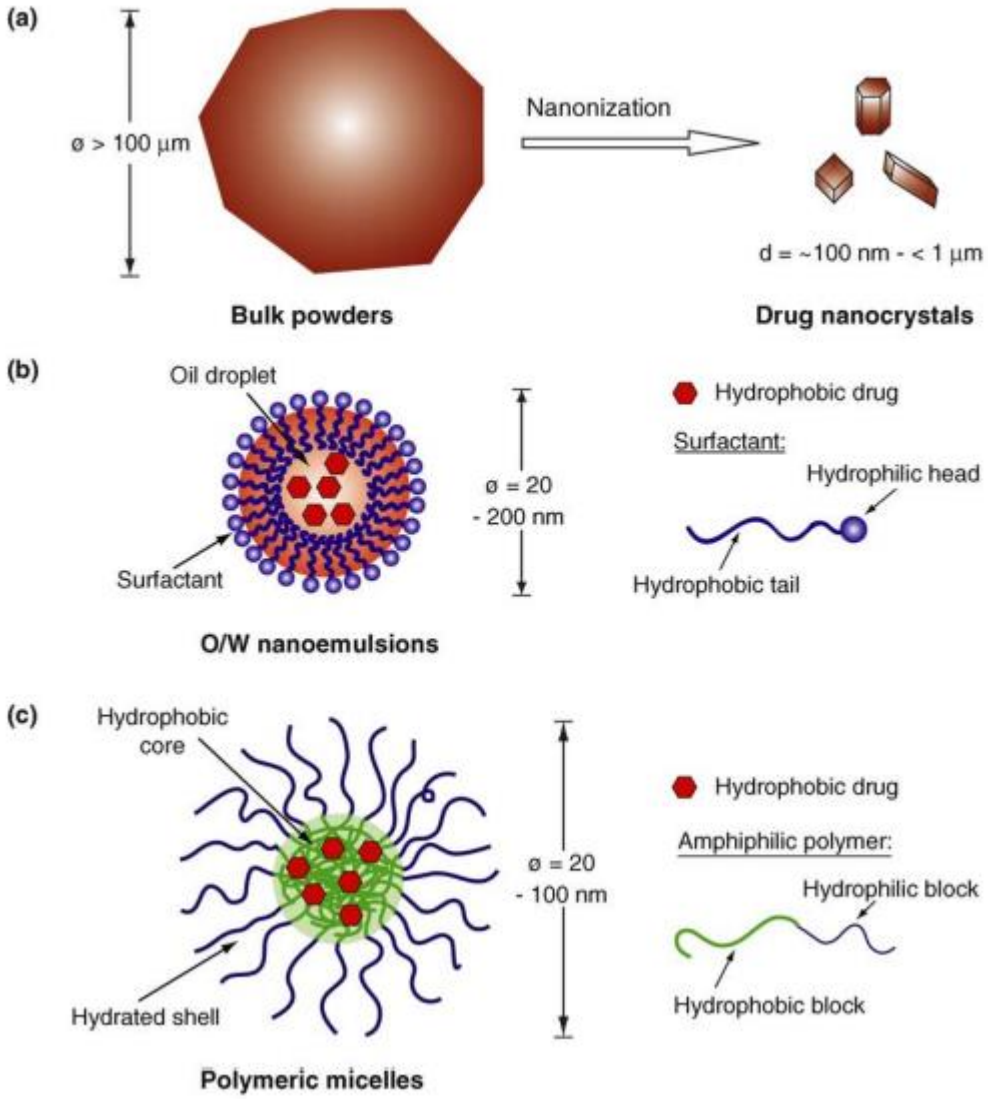

Figure 4: Diagram showing various strategies that are used to increase solubility and bioavailability of drugs (Chen *et al.*, 2010).

1.3.1 Polymeric Micelles

Polymers have been employed for many years as drug delivery vehicles, especially implants due to their beneficial mechanical properties (Kiick, 2007; Singh & Jr, 2009). Polymer-based materials, such as polymer particles, polymer-based micelles, polymer drug conjugates, polymer capsules, and polymersomes have important benefits as drug carriers due to their ability to increase the solubility of poorly water

soluble compounds (hydrophobic drugs), extend the circulation of drugs in the blood and increase the elimination by kidney secretion (Duncan *et al.*, 2003; Duncan, 2006).

Micelle formation from block copolymers has been reported, but the majority of such micelles were not synthesized from biocompatible materials (Bader *et al.*, 1984; Pratten *et al.*, 1985; Kabanov *et al.*, 1989; Masayuki *et al.*, 1990; Yokoyama *et al.*, 1992; Kwon *et al.*, 1993). Currently, biocompatible polymeric micelles are attracting a great deal of attention as novel colloidal delivery systems for poorly soluble drugs, which can meet the requirements of an ideal and versatile carrier for anticancer drugs, for example (Allen *et al.*, 1999; Gong *et al.*, 2012; Chen *et al.*, 2013). The micelles are formed by the self-assembly of amphiphilic polymers above the critical micellar concentration (CMC) in colloidal dispersions of molecular aggregates, with the micelles typically having a diameter of 20-100 nm (Kataoka *et al*., 1993). Polymeric micelles are characterized by a spherical, core/shell structure in which the hydrophobic core is formed by the aggregation of the hydrophobic blocks of various polymer chains and acts as a micro-reservoir suitable for the encapsulation of hydrophobic drugs, while the hydrophilic blocks create an outer shell that acts as stabilizing interface between the hydrophobic core and the biological environment (Figure 5) (Savic *et al.*, 2006; Simoes *et al.*, 2014). Pharmaceutical research on polymeric micelles has been mainly focused on copolymers which have an A-B di-block structure with A, the hydrophilic (shell) and B, the hydrophobic (core) polymers, respectively (Figure 6) (Jones *et al.*, 2004; Khadka *et al.*, 2014; Lukyanov & Torchilin, 2004; Wei *et al*., 2013). Due to the peculiar corona-core structure and unique properties of polymeric micelles they have the ability to enhance the aqueous solubility of hydrophobic substances (Nagarajan, 1997). An important property of

micelles is their ability to enhance the solubility of water-insoluble solute molecules because the micellar core provides a suitable microenvironment for the solubilisation (Nagarajan & Ganesh, 1989).

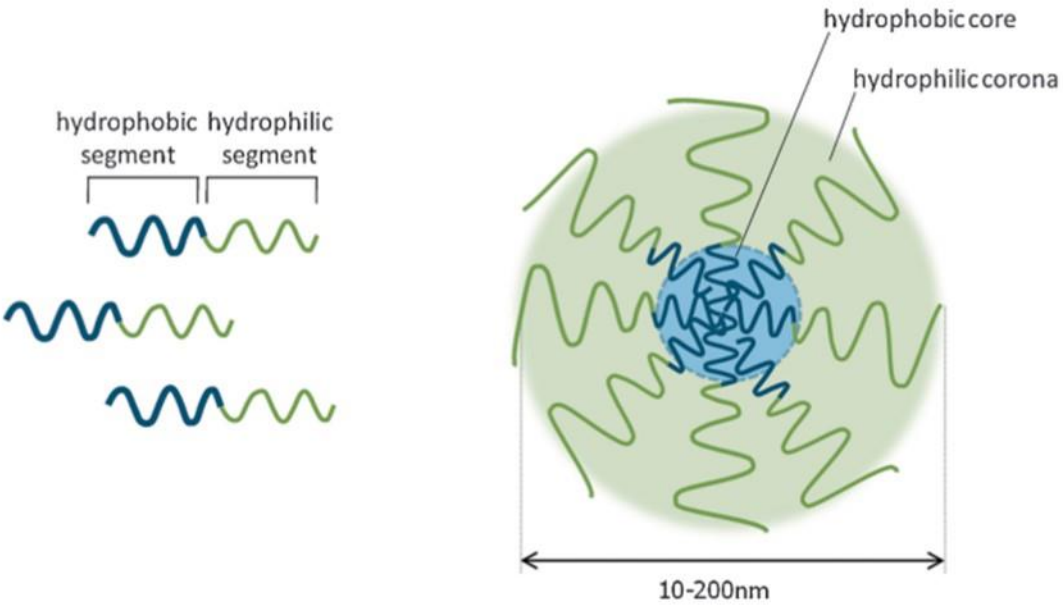

Figure 5: An illustration of polymer micelle formation as a core/shell structure in aqueous environments (Owen *et al.*, 2012).

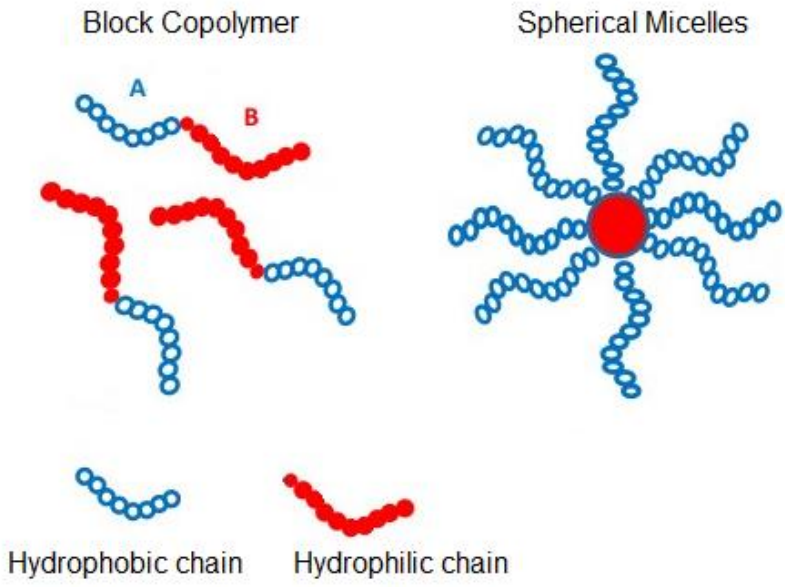

Figure 6: Representation of micelles formed by the self-assembly of block copolymers (Jones & Leroux, 1999).

1.3.1.1 Drug Loading and Release

Hydrophobic drug can be efficiently incorporated into the hydrophobic core of a polymeric micelle via physical entrapment (Figure 7). Thus, some advantages can be obtained such as: diminished side effects of the drug; protection of drug molecules from potential degradation under particular conditions (pH, temperature); increasing the water solubility of hydrophobic drugs; controlling the drug release rate (Torchilin, 2004). Three critical parameters have been improved in drug performance by the design and use of polymeric micellar delivery systems: solubility, release and biological distribution (Aliabadi & Lavasanifar, 2006). The aggregation number of the polymeric micelles affects the drug loading efficiency. The solubility of the given drugs in the inner core increases with a concomitant increase in the aggregation number of micelles (Hagan *et al.*, 1996). The drugs can be released from the micellar core through two routes, the separation of the drug from monomers by micelle

dissociation and the escape of the drug from the delivery system by diffusion due to weakened drug-polymer interactions within the micelle (Lavasanifar *et al.*, 2002).

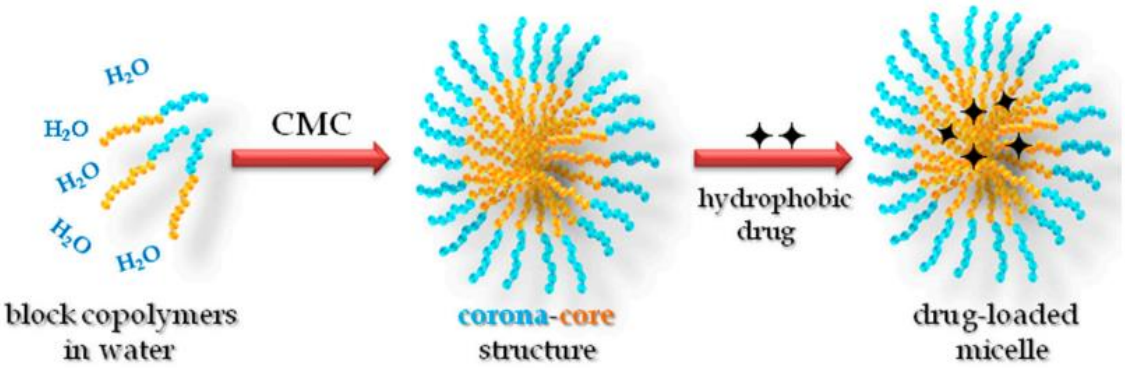

Figure 7: An illustration of the process of drug encapsulation into the hydrophobic core of a polymeric micelle (Hussein & Youssry, 2018).

1.3.2 Inclusion Complexes

It has been well demonstrated that solubility, dissolution and gastrointestinal permeability of drugs are a prime determinant in the rate and extent of absorption of poorly water-soluble drugs and their oral bioavailability (Horter & Dressman, 1997). The solubility rate of poorly water-soluble drugs have been shown to be improved through the formation of an inclusion complex which can potentially enhance the bioavailability of the drug (Shinde *et al.*, 2008; Savjani *et al.*, 2012). Macrocycle-based host-guest inclusion complexes are formed by introducing a guest molecule, the nonpolar molecule, inside the cavity of a host which can be a single molecule or an assembled group of molecules. A series of macrocyclic molecules and their derivatives have been developed to be used as hosts including calixarenes, cyclodextrins, cyclophanes, cucurbit[n]urils, and pillar[n]arenes (Figure 8).

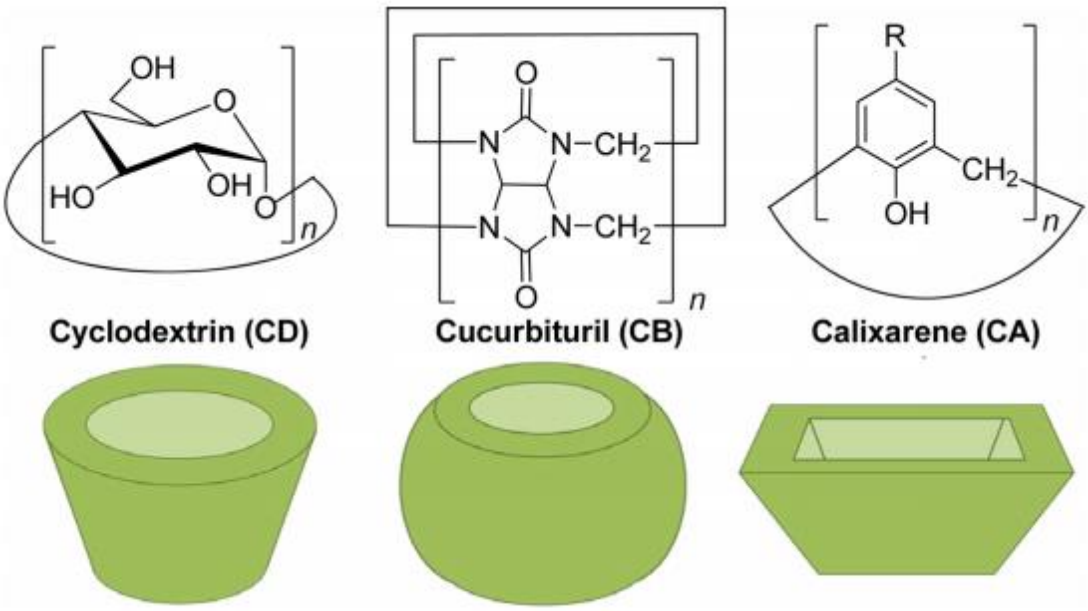

Figure 8: The chemical structure and representation of the shape of some example macrocyclic molecules (Ma & Zhao, 2015).

In a typical host−guest inclusion complex, the hosts possess a hydrophobic cavity to encapsulate the hydrophobic guest molecule through noncovalent interactions in aqueous solution (Ma & Zhao, 2015).

1.4 Calix[n]arenes

1.4.1 Evolution of Calix[n]arene Chemistry

Calix[n]arenes are the generation of supramolecular host compound which appeared after cyclodextrins and crown ethers (Arimura *et al.*, 1991; Arora *et al*., 2007). Calix[n]arenes were first discovered by Adolf von Baeyer in 1872. However, they were not reinvestigated until 1952, when Alois Zinke offered conclusive evidence of their structure (Figure 9). Because Baeyer could not isolate his products with purity he did not propose a structure (Gutsche, 2008). By 1970, Gutsche demonstrated that calix[n]arenes could be synthesized rapidly and in high yield. In the name

calix[n]arenes, “calix” describes how the molecules look like a cup or vase while “arene” refers to the aryl elements and the ordinal [n] denotes the number of aromatic (phenolic) units in the molecule (Gutsche, 1998; Li, 1996).

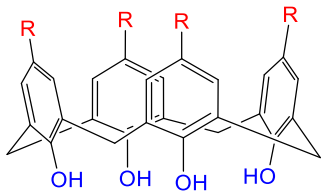

Figure 9: The general structure of a calix[4]arene.

Calix[n]arenes are cyclic oligomers and are easily produced from the base-induced condensation between substituted phenols (1) and formaldehyde (2) in a one–pot reaction (Scheme 1) (Sardjono & Rachmawati, 2017). They can exist as a “vase” shape with a distinct hydrophobic upper or “wide” rim and a hydrophilic lower or “narrow” rim, as well as a central annulus cavity with dimensions that can vary depending on the number of the phenolic units [n] that are contained within the oligomer (Gutsche, 1983; Chawla & Srinivas, 1996). Calix[n]arenes where [n] = 4, 6, or 8 are the most widely studied since they are readily prepared and purified (Figure 10) (Otsuka & Shinkai, 1996; Ukhatskaya *et al.*, 2013). By contrast, their preparation with an odd number of phenol units is more difficult and has attracted less attention. Therefore, relatively few studies can be found that focus only on calix[n]arenes where [n]= 5, 7, and 9 (Gallagher *et al.*, 1994; Gaeta *et al*., 2006). Calix[n]arenes, especially calix[4]arenes can be modified by introducing functional groups into two main places: the phenolic hydroxyl groups and the *para*-positions. In addition, the methylene bridge may be replaced or modified (Agrawal *et al.*, 2009). Calix[4]arenes can act as host molecules due to their rigid conformation which forms a hydrophobic cavity.

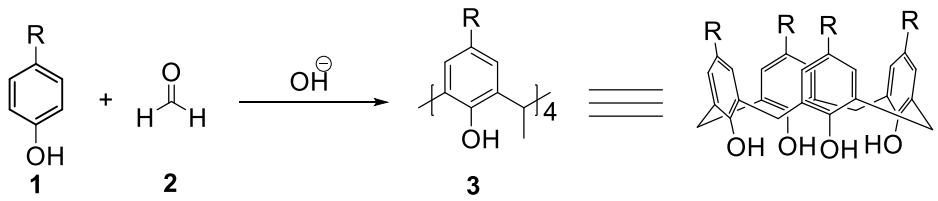

Scheme 1: Direct condensation in the synthesis of a calix[4]arene.

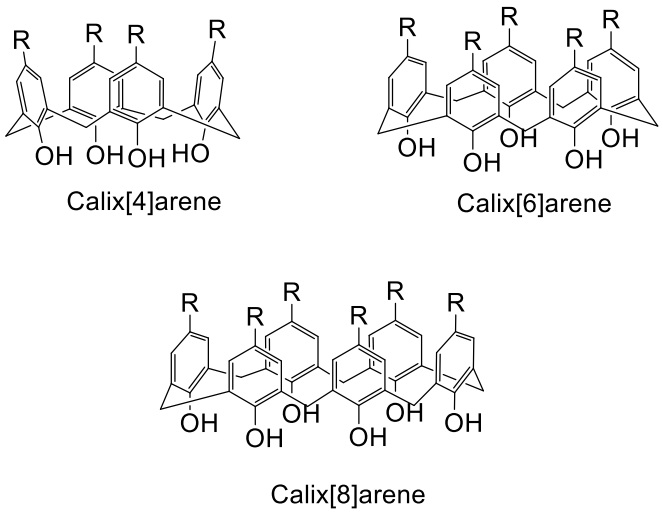

Figure 10: General structure of calix[n]arenes where [n] = 4, 6, and 8.

1.4.2 Structural Characteristics of Calix[n]arenes

Calix[n]arenes can exist in different conformations depending on the number of aromatic residues in the molecule. A calix[4]arene has four aromatic units in the molecule and it can exist in the cone, partial cone, 1,2 alternate and 1,3 alternate conformations (Figure 11). A calix[6]arene has six units in the molecule and can exist in eight main conformations. Calix[8]arenes have eight aromatic units in the molecule and can exist in sixteen principal conformations (Gutsche & Bauer, 1985). Changing the value of [n] controls the shape and size of the hydrophobic cavity (Hassen *et al.*, 2007).

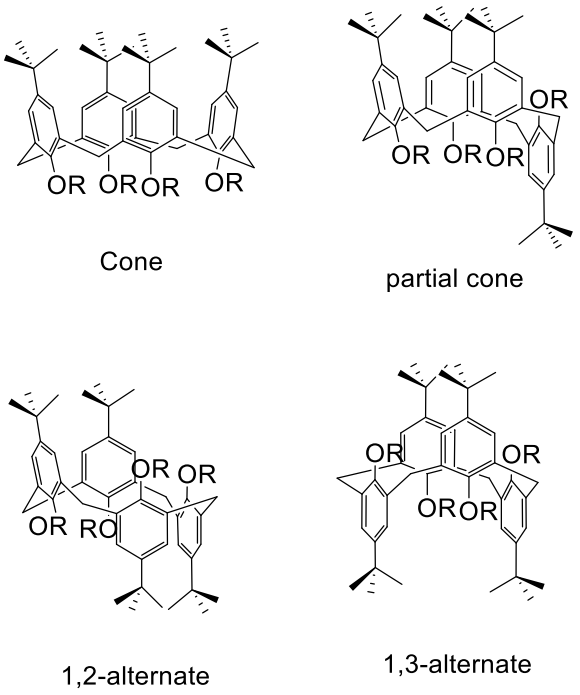

Figure 11: The possible conformations of calix[4]arene.

The upper rim is identified as the wider end of the cavity and the lower rim as the narrower hydroxylated end. Various derivatives of calix[n]arenes can be prepared by modifying the upper and/or the lower rims with different functionalities. Much research has been undertaken into the derivatives of calix[4]arenes, calix[6]arenes, and calix[8]arenes (Shinkai & Ikeda, 1997).

1.4.3 Applications of Calix[n]arenes

In recent years, research has shown that synthetic macromolecules have some biomedical applications, can act as drug molecules, and occupy a pivotal position in drug delivery systems. Among such synthetic macromolecules, calix[n]arenes and their derivatives have been extensively investigated for their potential advantages in pharmaceutical science (Yousaf *et al.*, 2015; Espanol & Villamil, 2019). In addition, calix[n]arenes have raised considerable interest as hosts that can encapsulate many

types of guests (Bohmer, 1995). Low inherent toxicity combined with low cost offers them an advantage (Karthauser, 2013; Shahgaldian *et al*., 2003). Various strategies have been used for the subsequent functionalization of calix[n]arenes at the *para*-positions. Also, hydroxyl groups at the lower rim provide clear locations to attach various functional groups (Jose & Menon, 2007). Modifications such as adding carboxylate, amide, nitrile, halide and phosphate functional groups have led to derivatives that are soluble in aqueous media (Akkus *et al*., 2008). Such water-soluble calix[n]arenes play a key role in the discovery of devices that imitate natural biological operations. For example, they have been investigated as enzyme inhibitors and anti–bacterial agents (Danylyuk & Suwinska, 2009). Calix[n]arenes with appropriate biocompatible functionalities make them suitable for gene delivery vectors, for example (Zhou *et al*., 2015).

1.4.3.1 Calix[n]arenes in Chiral Drug Recognition

One of the most important considerations in the design and manufacture of pharmaceuticals is chirality. Typically, one stereoisomer of a chiral drug is more biologically active than other possible stereoisomers. Subsequently, when designing drug molecules that will interact with biomolecules, it is important to consider the stereochemistry of the targeted entity. It is very important to develop synthesis techniques that result in pure optical isomer, but equally important is the design of hosts that are able to accommodate stereoisomers, maybe selectively (Shahgaldian & Pieles, 2006). Bearing this in mind, it was investigated whether a chiral calix[n]arene macrocycle could be used as a model to produce materials that, in principle, meet the above criteria (Arnott, 2017). The locus of chirality on the calix[n]arene platform may be due to modification with chiral moieties attached at the upper or lower rim, the modification in the *para*-positions of the phenyl rings resulting

in inherently chiral calix[n]arenes, or chiral substituents linked on the methylene bridges of the calix[n]arene (Li *et al.*, 2011; Fernandes & Mulay, 2014).

The first chiral water–soluble host molecules were derived from calix[6]arene, synthesised by Shinkai and co–workers (Shinkai *et al.*, 1984). Since then, many chiral calix[n]arenes have been synthesized by modification with various chiral groups at either upper or lower rims (Sirit & Yilmaz, 2009; Arimura *et al.*, 1991). The McKervey group, jointly with the Diamond group studied (*S*)-dinapthylprolinolcalix[4]arene, which has been used effectively in the chiral separation of enantiomers of phenylglycinol, phenylethylamine and norephedrine (Grady *et al.*, 1996; McMahon *et al.,* 2003). Different types of substituted calix[4]arene derivatives, which contain multiple chiral functional groups at the upper rim have been reported by Zadmard and co–workers. These receptors are able to associate with amino acids such as arginine and lysine selectively in polar solvents (Zadmard *et al*., 2011). Chiral calix[4]arene **4** and **5** in the cone conformation and modified with suitable peptide units at the upper rim was synthesized by Ungaro and co–workers. Calix[4]arene **4** and **5** showed antimicrobial activity against Gram positive bacteria *in vitro* as a result of their ability to bind D-alanyl-D-alanine residues (Casnati *et al.*, 1996; Sansone *et al.*, 1998) (Figure 12). In addition, the synthesis of chiral lower rim peptidocalix[4]arene derivatives **6** and **7** were described by Lamartine and co–workers in which two amino acids and their derivatives are attached at the lower rim of the parent calixarene (Sdira *et al.*, 2005) (Figure 13). Over a number of years, anionic calix[4]arenes have been investigated for their ability to complex biomolecules, including a wide range of proteins (Perret & Coleman, 2011; Tauran *et al.*, 2013).

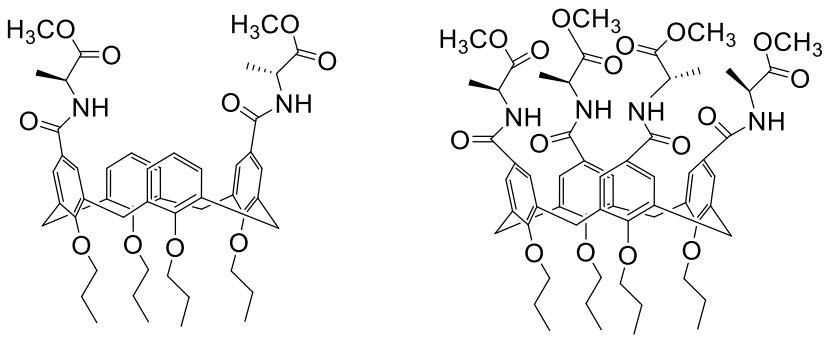

4 **5**

Figure 12: Chiral calix[4]arenes bearing four L-alanine units at the upper rim *(Sansone et al.*, 1998).

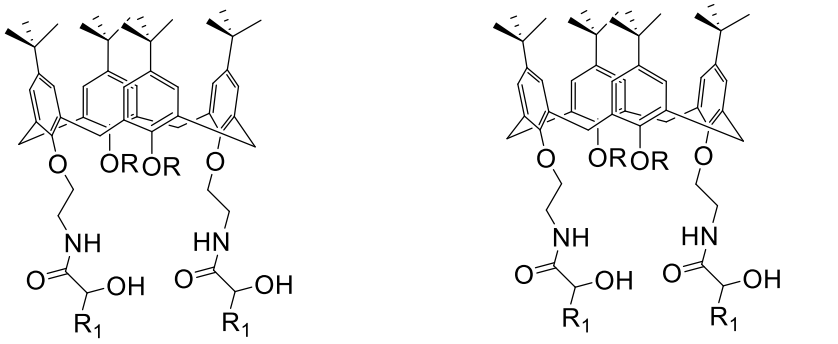

6a R= H, R_1= 2-thiophen
6b R= H, R_1= Ph

7a R= C_3H_7, R_1= 2-thiophen
7b R= C_3H_7, R_1= Ph

Figure 13: Chiral calix[4]arenes **6** and **7** functionalized with amino acid residues at the lower rim (Sansone *et al.*, 1998).

In comparison with the anionic calix[n]arenes, cationic calix[n]arenes are expected to have higher haemotoxicity due to their capability to react with a negatively charged membrane. This has resulted in fewer reports of cationic calix[n]arenes in the literature (Tauran, 2014).

1.4.3.2 Biomedical and Drug Delivery Applications

The main goal of a drug delivery system is to release therapeutics at the targeted site and maintain the concentration of the drug within the therapeutic range for the required period of time. Appropriate carriers, such as particles formed from supramolecular assemblies, are used to overcome undesirable physicochemical properties of drug molecules in an advanced pharmaceutical formulation. Thus, different types of high–performance biocompatible materials are continuously being developed to satisfy the research need for such advanced drug delivery systems (Uekama *et al.*, 1998). When used in drug delivery, host–guest complexes should ideally have the ability to target specific sites, for example specific tumour types, resulting in more effective treatment (Wang *et al*., 2015). They should also be soluble in polar, aqueous media while still allowing non–covalent interactions (such as hydrogen bonding, hydrophobic effects, ion–dipole interactions) to stabilize them (Kimizuka *et al.*, 1998; Zhang *et al*., 2007; Y. Wang *et al.*, 2013). Exploring different types of supramolecular host-guest interactions in pharmaceutical formulations has led to significant progress in improving the solubility of the drug molecules (Li & Loh, 2008). Calix[n]arenes are being investigated intensively for use in novel formulation strategies (Ghosh & Nau, 2012). In recent years, investigations into the use of calix[n]arenes has demonstrated some advantages in the pharmaceutical arena, mostly with calix[n]arenes that have been modified with functional groups at the upper and lower rims of the calix[n]arene platform, something which is easily achieved (Gutsche, 1998). Calix[n]arenes have been investigated as both drugs and drug delivery agents, particularly attractive due to their low inherent toxicity and cost (Yang & de Villiers, 2004; Coleman *et al.*, 2008; Espanol & Villamil, 2019). The modification of calix[n]arenes with appropriate biocompatible functional groups has

enabled them to be used for gene delivery (Zhou *et al.*, 2015). Many calix[n]arene-based amphiphiles have already been cited in the literature. However, most of them have focused on their self–assembling behaviour rather than on co–assembling with other amphiphiles (Wang *et al*., 2015). The most important calix[n]arene derivatives with high water solubility in addition to a strong ability to bind guests in their cavities in aqueous media are *para*-sulfonatocalix[n]arenes, where [n]= 4−8, first reported by Shinkai *et al*. in 1984 (Shinkai *et al.*, 1984; Guo *et al*., 2008; Guo & Liu, 2014). They have many useful features: Firstly, they can be synthesized easily in high yield through the direct sulfonation of the upper rim of calix[n]arenes. Secondly, the guest can be accommodated in their cavity through hydrophobic and π–stacking interactions, which are more effective in aqueous media than in organic media. Thirdly, they exhibit strong and highly selective binding ability to various organic cations as a result of the sulfonate groups present which provide anchoring points to make the inclusion complex more stable (Shinkai *et al.*, 1990; Liu *et al.*, 2006; Cui *et al.*, 2010; Zhao *et al*., 2013). Finally, they are biocompatible, which makes them useful for hosting guest molecules in aqueous solutions, including biological or pharmaceutical agents, offering many useful advantages in drug delivery (Koh *et al*., 1996; Paclet *et al.*, 2006; Wang *et al.*, 2009; Jiang *et al.*, 2014).

Chlorpromazine hydrochloride (CPZ) is a phenothiazine derivative which is commonly used in clinical medicine as an antipsychotic and a tranquilizing drug. It can form micelle–like aggregates through self–assembly at a critical concentration. Thus, CPZ can be used as an ideal model drug molecule for co-assembly. The co-assembly of an amphiphilic drug (CPZ) with a calix[n]arene–based amphiphilic molecule such as *para*-sulfonatocalix[4]arene (SC_4A) was reported by Qin and co-workers. They studied calix[n]arene–based supra-amphiphilic molecules and their

applications in drug delivery systems, where drug molecules are encapsulated by host–guest binary vesicles and then released. These systems can be easily adapted by disrupting the vesicles during formation using an appropriate method. The aim is to improve the efficiency of drug loading by reducing the use of inactive substances. Two different mechanisms were followed simultaneously: the 1:n complexation of *para*-sulfonatocalix[4]arene (SC_4A) with CPZ and also the amphiphilic co-assembly between anionic *para*-sulfonatocalix[4]arene tetraheptyl ether (SC_4AH) and cationic CPZ (Qin *et al*., 2014) (Figure 14).

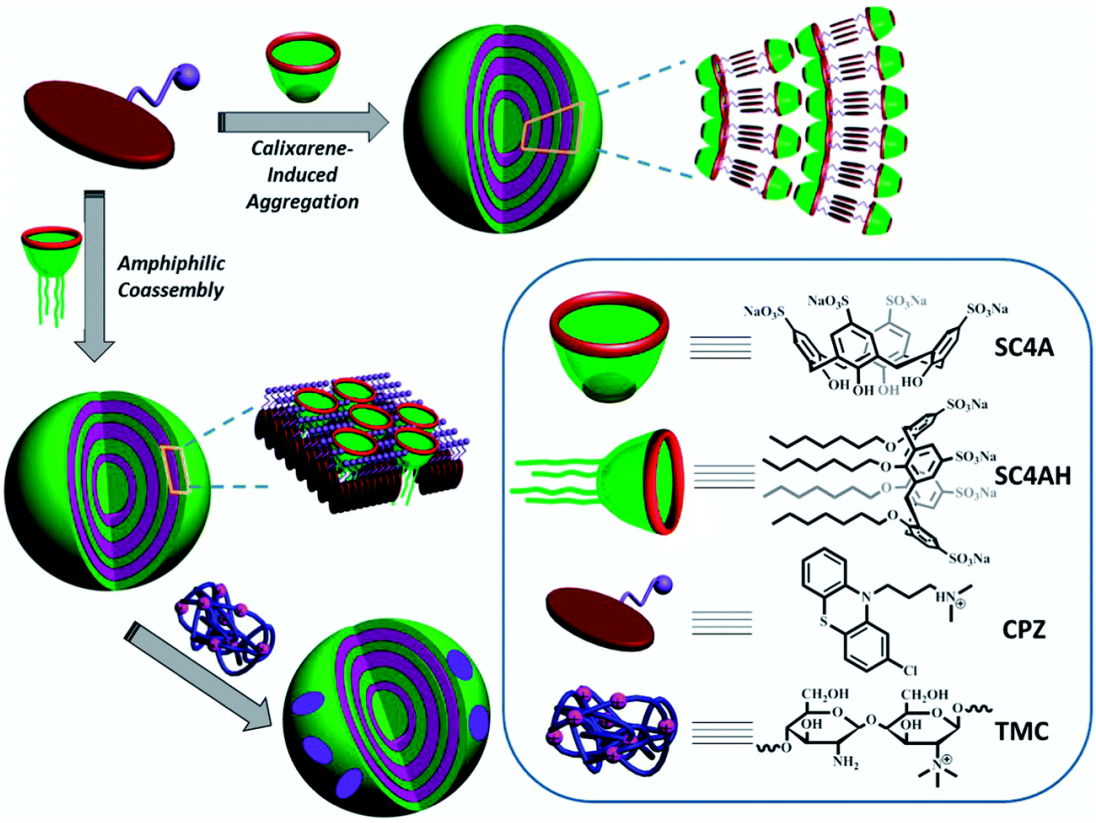

Figure 14: Model of co-assembly of an amphiphilic drug with calix[4]arenes (Qin *et al.*, 2014).

New ‘programmable’ drug delivery systems that are based on stimuli–sensitive drug carriers have emerged, in which the drug can be released by disrupting the carriers

with an appropriate stimulus such as temperature, pH, ionic strength, or enzymes (Meng *et al.*, 2009). A derivative of water–soluble *para*-sulfonatocalix[8]arene which is negatively charged at the upper rim and positively charged at the lower rim was reported by Xiao as a stimuli-responsive carrier model to investigate the pH–triggered release of the hydrophobic antimicrobial drug ciprofloxacin (CPF) as a model system. The modified calix[8]arene showed a good hydrophobic drug loading capacity as well as a pH–triggered drug releasing behaviour. Ciprofloxacin was retained in the hydrophobic cavity at neutral pH, with the electrostatic interactions between the upper and lower rims forming supramolecular structures. It was released when the capsule disassembled at higher or lower pH values (Xue *et al*., 2013) (Figure 15).

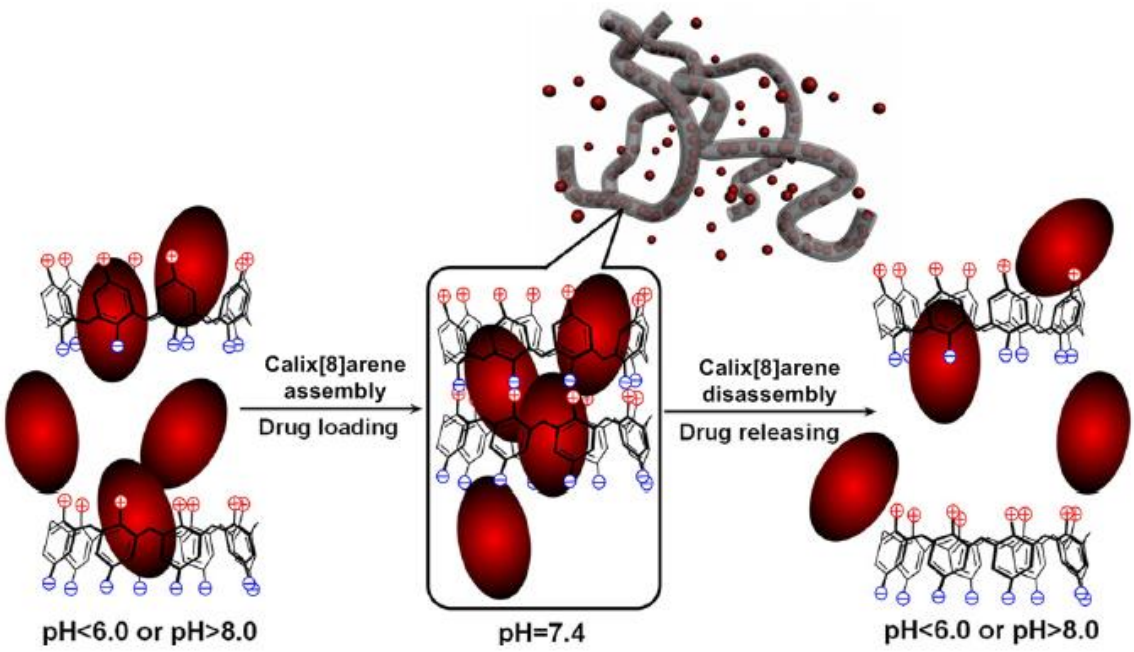

Figure 15: Model of pH-triggered drug release (Gangemi *et al.*, 2015).

Carbamazepine (CBMZ), an anticonvulsant drug, is poorly soluble in aqueous media. The formation of inclusion complexes with *para*-sulfonated calix[n]arene was investigated by Menon and co–workers to increase the solubilisation of CBMZ in

aqueous media and thus modify its bioavailability. They studied the 1:1 complex formation of CBMZ with *para*-sulfonatocalix[6]arene (Figure 16a) and the 1:2 complex formation of CBMZ with *para*-sulfonatocalix[4]arene (Figure 16b) (Panchal *et al.*, 2010). Such calix[n]arenes were also exploited to form inclusion complexes with another poorly water-soluble drug, carvedilol (CDL) (Figure 17). It is a nonselective adrenal β receptor antagonist, an α_1 receptor antagonist and a vasodilator used to treat mild to moderate hypertension. The complexation observed was similar to that observed with CBMZ, both *in vitro* and *in vivo*. The results showed that solubility was improved and toxicity was decreased by the formulations prepared as compared to the pure drugs (Menon *et al*., 2012).

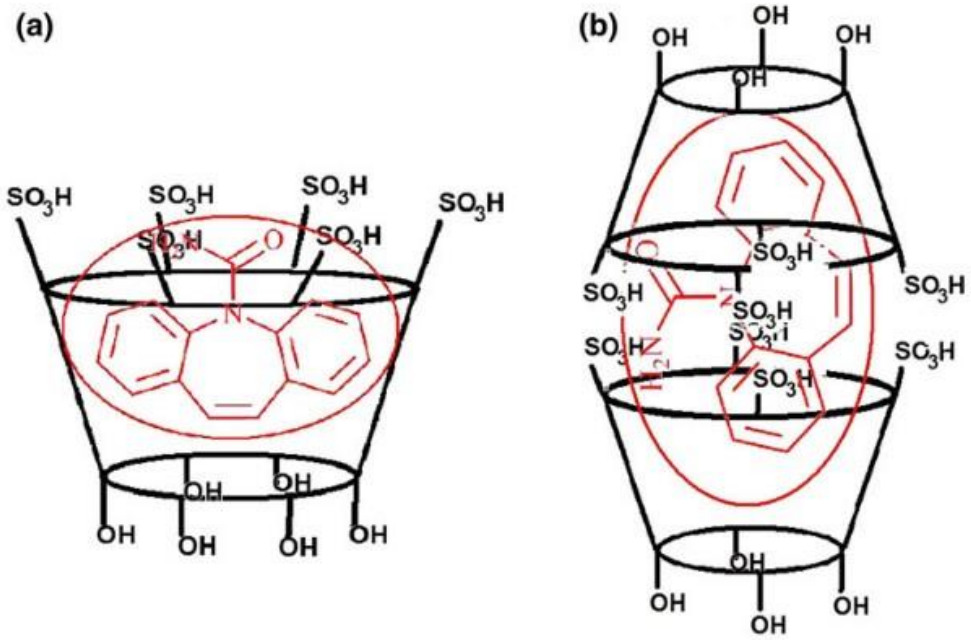

Figure 16: Inclusion complexes of carbamazepine (CBMZ) with *para*-sulfonatocalix[6]arene 1:1(a) and carbamazepine (CBMZ) with *para*-sulfonatocalix[4]arene 1:2 (b) (Panchal *et al.*, 2010).

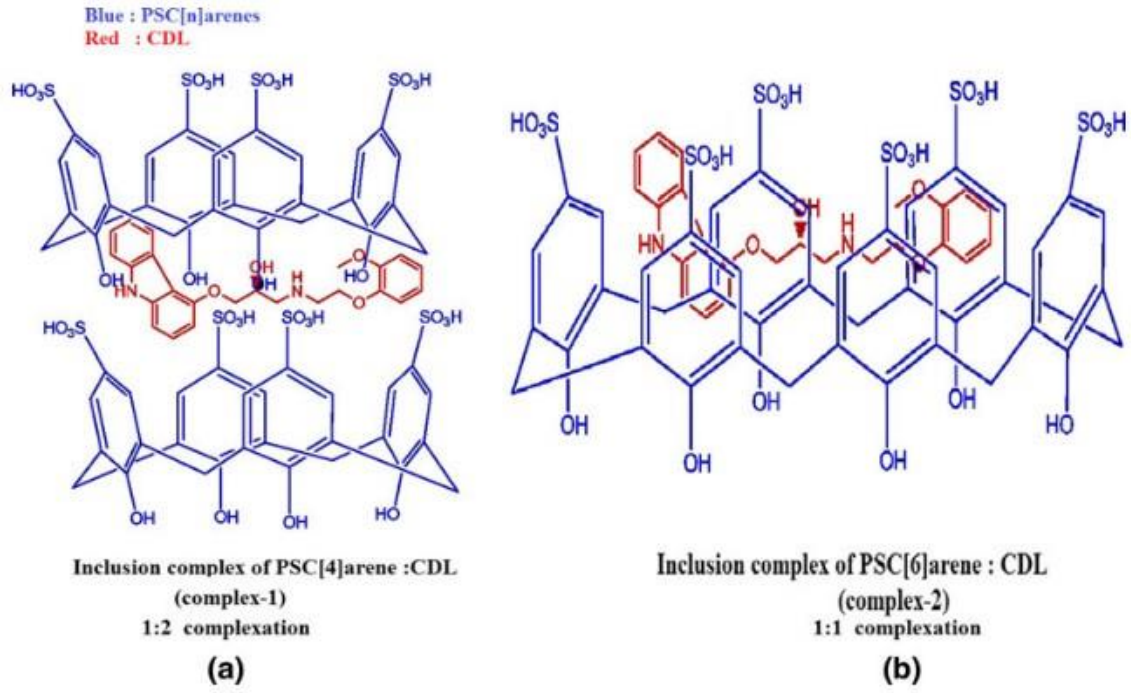

Figure 17: Inclusion complexes of carvedilol (CDL) with *para*-sulfonatocalix[n]arene (Menon *et al*., 2012).

Tetracaine (TTC), one of an important class of nociceptive agents, is a local anaesthetic drug belonging to the amino-ester family (Chalam *et al*., 2009; de Paula *et al*., 2010; Kuroda *et al*., 1996). It acts by preventing the transmission of impulses in neurons. However, poor chemical stability is still a limitation in the formulation of local anaesthetics, especially for esters such as tetracaine due to hydrolysis of the ester bond by plasma esterases. Also, systemic toxicity inhibits the clinical applications of TTC (Lee *et al*., 2009; Werdehausen *et al*., 2009). Thus, several approaches have been used to improve the pharmaceutical properties of TTC, including the use of novel drug-delivery systems. Formulations of TTC with β-cyclodextrin (β–CD) and with *para*-sulfonatocalix[6]arene were designed to improve the bioavailability and decrease the systemic toxicity of the drug. The results indicated that the complexation between the drug and *para*-sulfonatocalix[6]arene gives a more stable species due to the negative charge present on the sulfonate groups of the

calix[6]arene (Figure 18). The association of TTC with *para*-sulfonatocalix[6]arene was evaluated by nuclear magnetic resonance experiments which examined complexation-induced proton chemical shifts. Complexation between TTC and *para*-sulfonatocalix[6]arene induced large shielding effects in all the hydrogens of TTC, indicating interactions between the ammonium group of TTC with the SO^{3-} group of *para*-sulfonatocalix[6]arene (Fernandes *et al.*, 2007). Also β–CD or hydroxypropyl–β–cyclodextrin (HP–β–CD) have been employed to develop two new TTC formulations (TTC: β–CD and TTC: HP–β–CD) (de Lima *et al*., 2012).

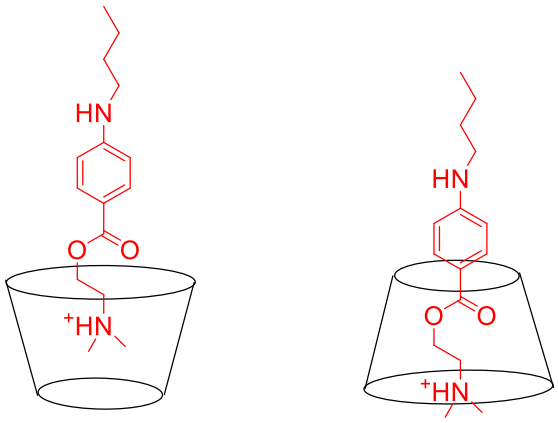

Figure 18: Inclusion complexes of tetracaine with *para*-sulfonatocalix[6]arene (Fernandes *et al.*, 2007).

Topotecan (TPT), a derivative of camptothecin (Figure 19), is a chemotherapy agent used in the treatment of neoplastic diseases that acts as an inhibitor of the topoisomerases. Although it is used to treat many diseases such as ovarian and cervical cancers, it has previously been formulated in the form of its hydrochloride salt due to its low inherent solubility. In order to improve the solubility of TPT without changing its formula, a water-soluble *para*-sulfonatocalix[4]arene was used to encapsulate it within its cavity. The results showed that the solubility was increased compared with the pure drug (Wang *et al*., 2011).

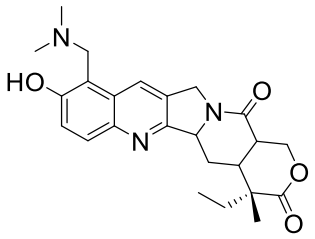

Figure 19: The molecular structure of topotecan (TPT).

Nifedipine, a 1,4-dihydropyridine derivative (Figure 20), is a calcium-channel blocker that is widely used to treat cardiovascular diseases such as high blood pressure, congestive heart failure, and cerebral ischemia. As with many hydrophobic drugs, the highly variable bioavailability of nifedipine in humans is due to its poor water solubility. The water–soluble *para*-sulfonatocalix[n]arenes was used to encapsulate nifedipine in its hydrophobic cavity in order to enhance the solubility of the drug. It was proven that the *para*-sulfonatocalix[n]arene significantly increased the aqueous solubility of nifedipine depending on the size and the concentration of the calix[n]arenes as well as the pH of the solution. Overall, *para*-sulfonatocalix[8]arene improved the solubility of nifedipine the most, followed by *para*-sulfonatocalix[4]arene, while in the presence of *para*-sulfonatocalix[6]arene, the solubility of nifedipine was decreased (Yang & Villiers, 2004).

Furosemide, 5-(aminosulfonyl)-4-chloro-2-((2-furanyl-methyl)amino) benzoic acid (Figure 20), is a loop diuretic that is used orally in the treatment of hypertension, heart failure, renal failure, nephritic syndrome, and cirrhosis. Furosemide is practically insoluble but its solubility increases with an increase in pH. The oral bioavailability of furosemide is very poor due to aqueous solubility at gastrointestinal pH, making solubility the rate-determining step in the gastric absorption of furosemide (Yang & de Villiers, 2004). Several techniques have been used to overcome the poor bioavailability of furosemide and to increase its aqueous

solubility, including cyclodextrin complexation (Ozdemir & Ordu, 1998; Spamer *et al*., 2002; Vlachou & Papaioannou, 2003). The experimental results of those studies showed that furosemide drug molecules are encapsulated into hydrophobic cavity of cyclodextrins and a significant increase in the solubility and dissolution rate of furosemide. Also, the solubilization of the practically water insoluble drug furosemide by host-guest complexes with *para*-sulfonatocalix[n]arenes has been reported. It was proven that the solubility of furosemide was increased significantly when the concentrations of the three *para*-sulfonatocalix[n]arenes (n = 4, 6, or 8) in the aqueous solutions were increased (pH< 4). Overall, *para*-sulfonatocalix[6]arene improved the solubility of furosemide the most followed by *para*-sulfonatocalix[8]arene, while para-sulfonatocalix[4]arene increased the solubility of furosemide the least (Yang & de Villiers, 2004).

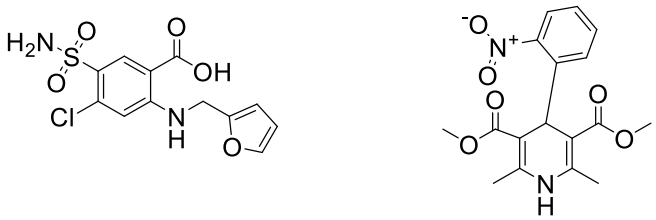

Figure 20: The molecular structures of furosemide and nifedipine.

Platinum–based drugs are used widely in cancer therapy (Kelland, 2007). Carboplatin is a member of the second generation of platinum-based drugs, which are considered to be safer than cisplatin whilst maintaining the same spectrum of activity. Carboplatin has two main limitations: Firstly, its high polarity impedes penetration throughout the membrane of the cell and, secondly, it decomposes readily to inactive complexes by the action of glutathione (γ-glutamylcysteinylglycine) and other proteins which contain methionine or cysteine residues. In order to solve

this problem the formulation can be improved by using vesicles consisting of calix[4]arene-based lipid mimics, which imitate the cell-surface lipids and are a non-toxic host for carboplatin. It is known that calix[n]arenes can aggregate in water to form either micellar as small assemblies or vesicle bilayers as much larger assemblies. The calix[4]arene lipid mimic is prepared by attaching ionisable methyl phosphonic acid groups at the upper rim of a calix[4]arene scaffold and hydrophobic *n*–hexyl groups at the lower rim. Vesicles based on the self-assembly of tetra-*para*-phosphonomethyl calix[4]arene are affective in binding a carboplatin molecule within the cavity of the calix[4]arene lipid mimic. According to Mo and co-workers the results indicated that the 1:1 complex formation of carboplatin with the calix[4]arene lipid mimic significantly increased the anti-cancer efficacy of the drug (Figure 21) (Mo *et al*., 2015).

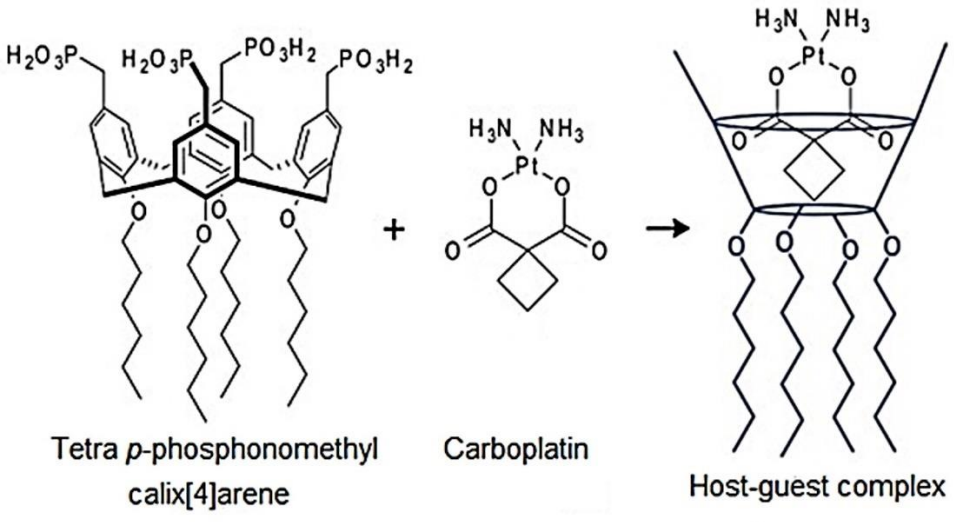

Figure 21: The complex between a calix[4]arene and carboplatin (Mo *et al.*, 2015).

Many studies have reported on the effect of water–soluble *para*-sulfonatocalix[n]arenes on the solubility of drugs (Yang & de Villiers, 2004; Yang *et al*., 2008). In contrast, there is only one study exploring the solubilizing effect of *O*-

phosphorylatocalix[n]arenes that form complexes with neutral molecules by host-guest complexation. *O*-Phosphorylatocalixarene receptors might be useful host molecules as drug-solubilizing agents toward niclosamide, furosemide, and nifedipine (Bayrakci *et al.*, 2012). The water–soluble *para*-phosphonatocalix[n]arene receptors ([n] = 4, 6) were used on the extraction of poorly soluble drug molecules such as nifedipine, niclosamide, and furosemide from the organic phase to the aqueous phase. It has been proven that the size of the *para*-phosphonatocalix[n]arenes affects the extraction rate of these drugs (Bayrakci *et al.*, 2011).

Paclitaxel (PTX) (Figure 22) is a well–known drug commonly used to treat various kinds of cancer including lung, breast and ovarian cancers. What hinders the clinical applications of PTX is its low water solubility, as with most anti–cancer drugs. Therefore, a new formulation was developed to improve the solubility of PTX and decrease its side effects using calix[6]arene hexa-carboxylic acid and calix[8]arene octo-carboxylic acid (Zhao *et al*., 2015). In addition, another study used a *para*-phosphonated calix[4]arene vesicle to load PTX to direct the delivery of the drug to a particular cell as well as increasing its solubility (Mo *et al*., 2016).

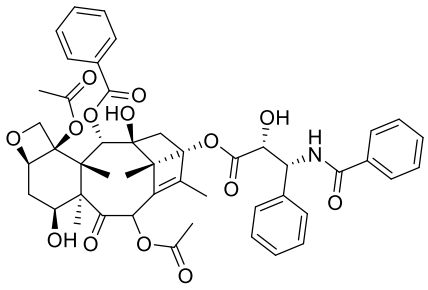

Figure 22: The molecular structure of Paclitaxel (PTX).

Curcumin , derived from the curcuma longa plant, is used in Indian ancient medicine (Aggarwal & Shishodia, 2006). Curcumin behaves as an antioxidant, anti-ischemic, anti-arthritic, and anti–tumour cancer agent *both in vitro* and *in vivo* and has high

pharmacological efficacy with minimal side effects. Although it is used to treat a wide range of human diseases, it was not authorized as a therapeutic agent as a consequence of its poor solubility, low bioavailability and stability (Shukla *et al*., 2008). A number of amphiphilic calix[4]arenes **8**, **9** and **10** designed in the form of phospholipid mimics were developed by attaching head groups such as PO_3H_2 or NMe_3^+ at the upper rim of the calix[4]arenes platform (Figure 23) that can be used as nano-carriers for curcumin delivery. It was established that these compounds, which aggregate in a micellar form are not only effective in delivering curcumin but also have antioxidant properties (James *et al.*, 2013).

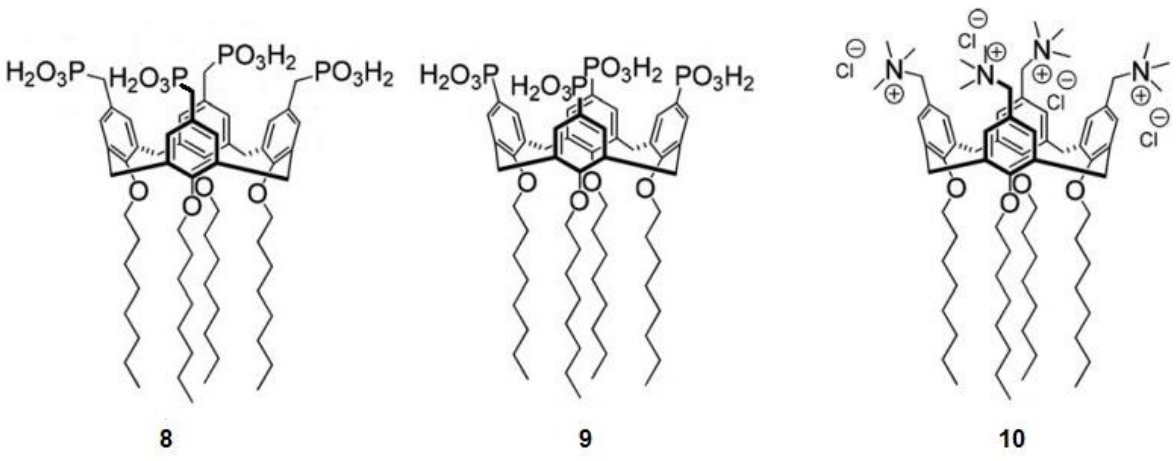

Figure 23: The molecular structure of amphiphilic calix[4]arenes (James *et al*., 2013).

Additionally, *para*-*t*-butylcalix[8]arene has also been used as host molecule for solubilising curcumin: and The host-guest complexes containing curcumin were studied using UV-Vis spectroscopy and the data analysed to determine the association constant. Analysis using the Benesi-Hildebrand method indicated that two modes of complexation of *para*-*t*-butyl calix[8]arene with curcumin are observe, with relative stoichiometries of 1:1 and 4:1 calixarene host: curcumin guest. The 1:1 complex is significantly more stable and is stabilised by hydrogen bonding of the enol

form of curcumin with hydroxyl groups on the lower rim of the *para-t*-butyl calix[8]arene host (Figure 24) (Meenakshi *et al*., 2014).

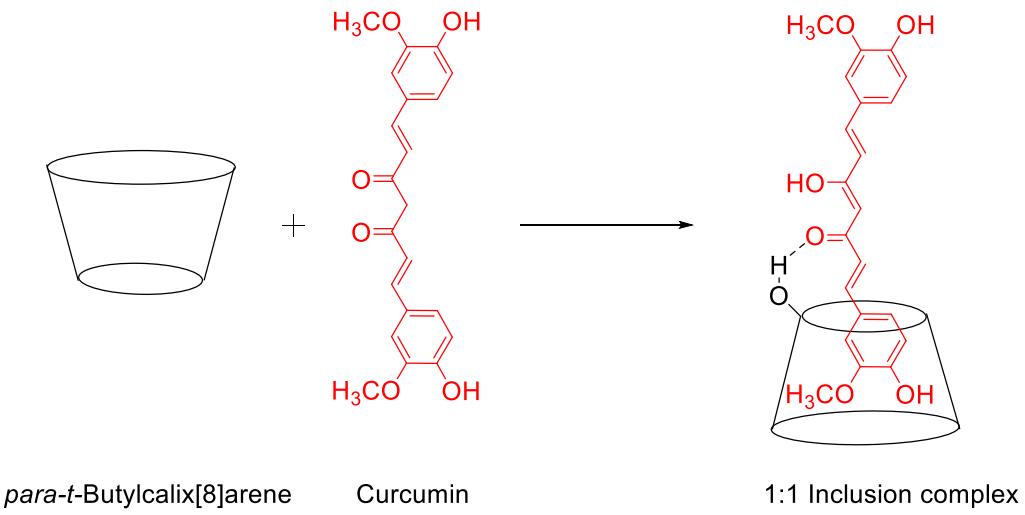

Figure 24: 1:1 Inclusion complex between *para-t*-butyl calix[8]arene and curcumin *(*Meenakshi *et al.*, 2014).

1.5 Calix[4]resorcinarenes and Calix[4]pyrogallolarenes

1.5.1 History and Chemistry of Calix[4]resorcinarenes and Calix[4]pyrogallolarenes

Calix[4]resorcinarenes, non–planar cyclic aromatic tetramers, belong to a class of macrocycles first discovered by Adolf von Baeyer in 1872 and are made by the condensation of resorcinol with aldehydes (Baeyer, 1872; Hogberg, 1980). About a decade later Michael suggested that the products were made by the reaction of equimolar quantities of these components (Timmerman *et al*., 1996). Almost a century later the final structure, based on molecular weight determination was proposed. The structure of calix[4]resorcinarenes was eventually proved by Erdtman using crystallisation techniques (Erdtman &

Hogberg, 1968). In 1994 a widely accepted colloquial name, resorcinarenes, was introduced by Schneider (Schneider & Schneider, 1994), following a series of different names being used such as Hogberg compounds, calix[4]resorcinarenes, resorcinolarenes and octols (Ngodwana, 2012). Figure 25 shows the general structure of calix[4]resorcinarenes when R_1 = H and calix[4]pyrogallolarene when R_1 = OH.

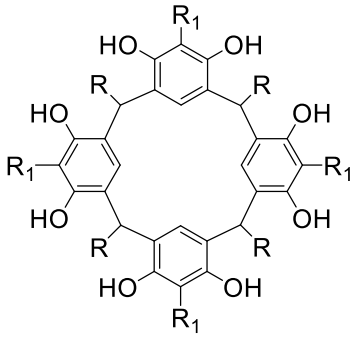

Figure 25: The general structure of a calix[4]resorcinarene and calix[4]pyrogallolarene.

1.5.1.1 Synthesis and Mechanism of Formation of Calix[4]resorcinarene and Calix[4]pyrogallolarene

The most common method for the preparation of calix[4]resorcinarenes and calix[4]pyrogallolarenes is the acid–catalysed condensation between resorcinol or pyrogallol with various aldehydes. The cyclocondensation reaction form the tetrameric product with four aromatic rings connected by substituted methylene groups in reasonable to high yield (Hogberg, 1980) (Scheme 2). Niederl and Vogel described the synthesis process for many calix[4]resorcinarenes as well as confirming the annular tetrameric structure (Niederl & Vogel, 1940; Lake, 2014). In addition, functionalized resorcinol with electron donating groups at their 2-positions, such as 2-alkyl resorcinol, have also been used to prepare *C*-alkyl and *C*-aryl calix[4]resorcinarenes under acidic conditions (Scott & Sherburn, 2017) (Scheme 2).

Resorcinols functionalised with electron withdrawing groups, such as a nitro group (-NO_2), at their 2-positions require basic conditions for condensation (Luce, 2004; Ngodwana, 2012; Sardjono & Rachmawati, 2017). Condensation seems to take place in an irreversible process and the highly stable tetramer is preferred over the pentamer or hexamer, which are not typically observed (Bourgeois & Stoeckli-Evans, 2005).

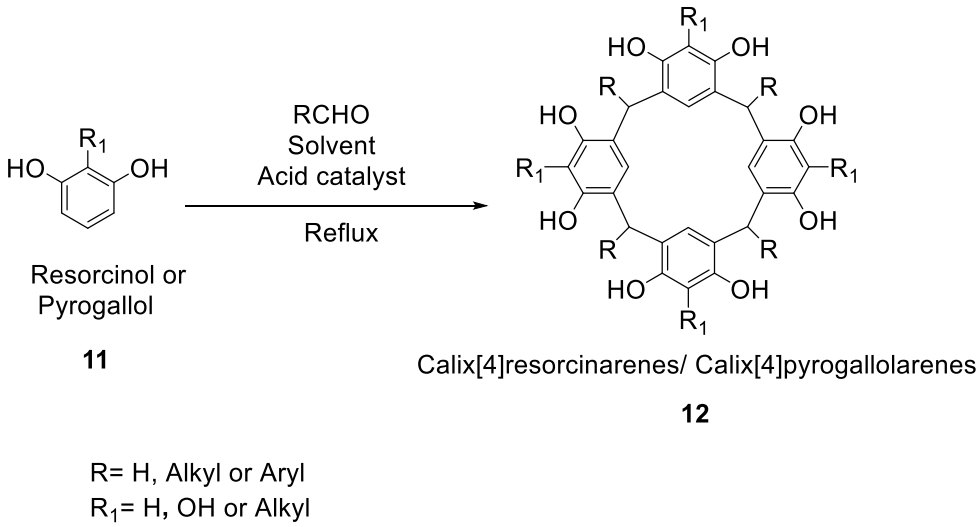

Scheme 2: Acid–catalysed preparation of a calix[4]resorcinarene and calix[4]pyrogalloarene

Well-established structures of the products obtained from the protic-acid catalysed reaction provide evidence to suggest the most likely mechanism of the polycondensation process (Plachkova-Petrova *et al*., 2012). Now the mechanism for the synthesis of calix[4]resorcinarenes proposed by Weinelt and Schneider is accepted and well understood (Moran *et al*., 1991; Weinelt & Schneider, 1991; Jain & Kanaiya, 2011). The reaction follows the following multi-step mechanism illustrated in Scheme 3.

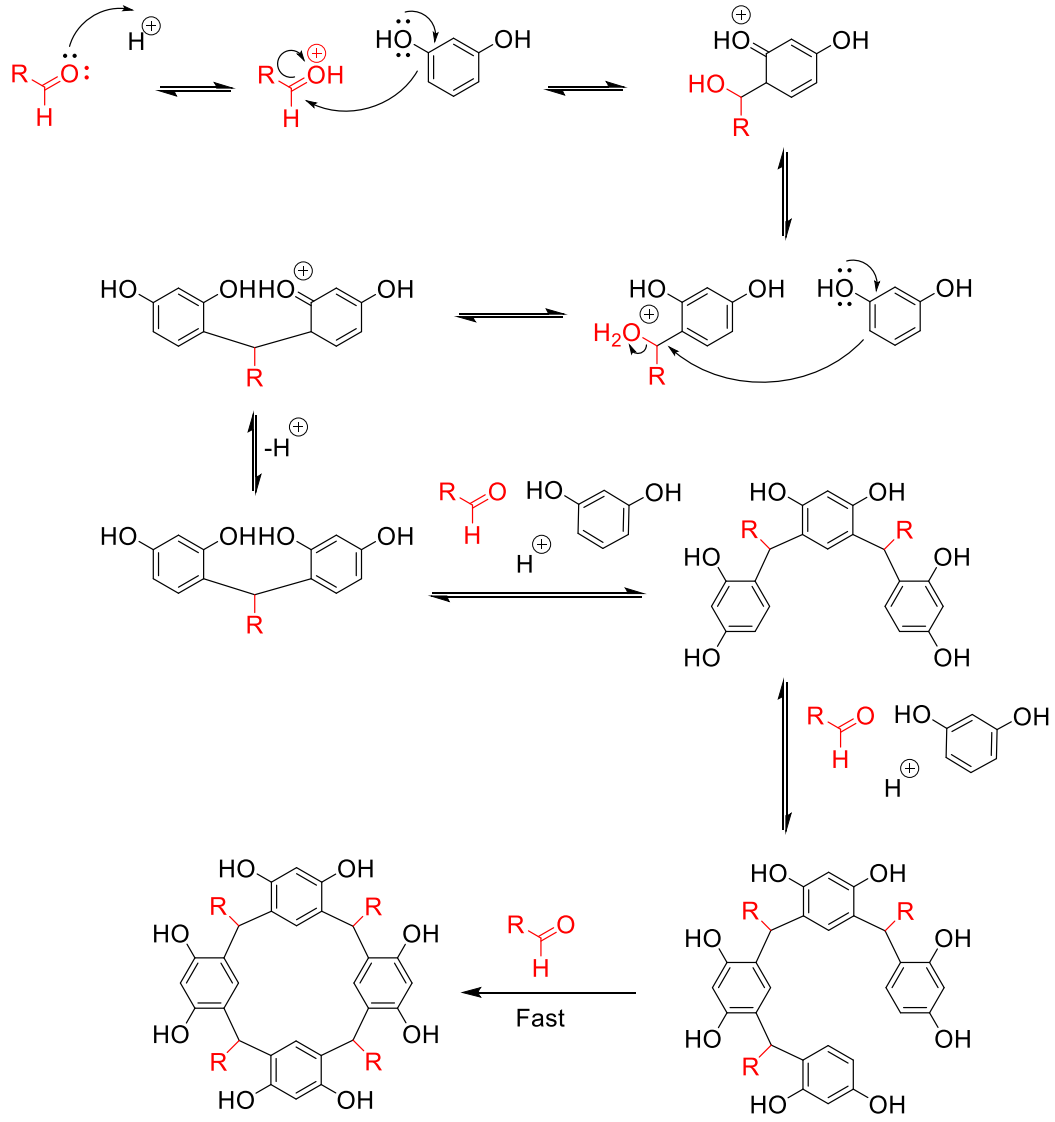

Scheme 3: The mechanism of the preparation of calix[4]resorcinarene under acid condition (Jain & Kanaiya, 2011;Sardjono & Rachmawati, 2017).

1.5.2 Structural Characteristics of Calix[4]resorcinarenes and Calix[4]pyrogallolarenes

The calix[4]resorcinarene and calix[4]pyrogallolarene skeleton have two distinct regions: 1) the upper rim which contains the hydroxyl groups that confer a rigid conformation due to intramolecular hydrogen bonding, and 2) the the lower rim, where residues from the aldehydic starting materials are attached, which can be hydrophilic or lipophilic according to the nature of the aldehydes used.

Calix[4]resorcinarenes possess eight hydroxyl groups at their upper rim, while calix[4]pyrogallolarenes display twelve hydroxyl groups at the upper rim. Several isomeric structures of calix[4]resorcinarenes and calix[4]resorcinarenes can be formed during synthesis. Three factors can govern their stereochemistry: Firstly, the conformation of the macrocyclic ring where five symmetrical conformations can be adopted: crown (C_{4v}), boat (C_{2v}), chair (C_{2h}), diamond (C_s) and saddle (D_{2d}) (Figure 26) (S. Hogberg, 1980; Timmerman *et al.*, 1996; Carey, 2006; Scott & Sherburn, 2017).

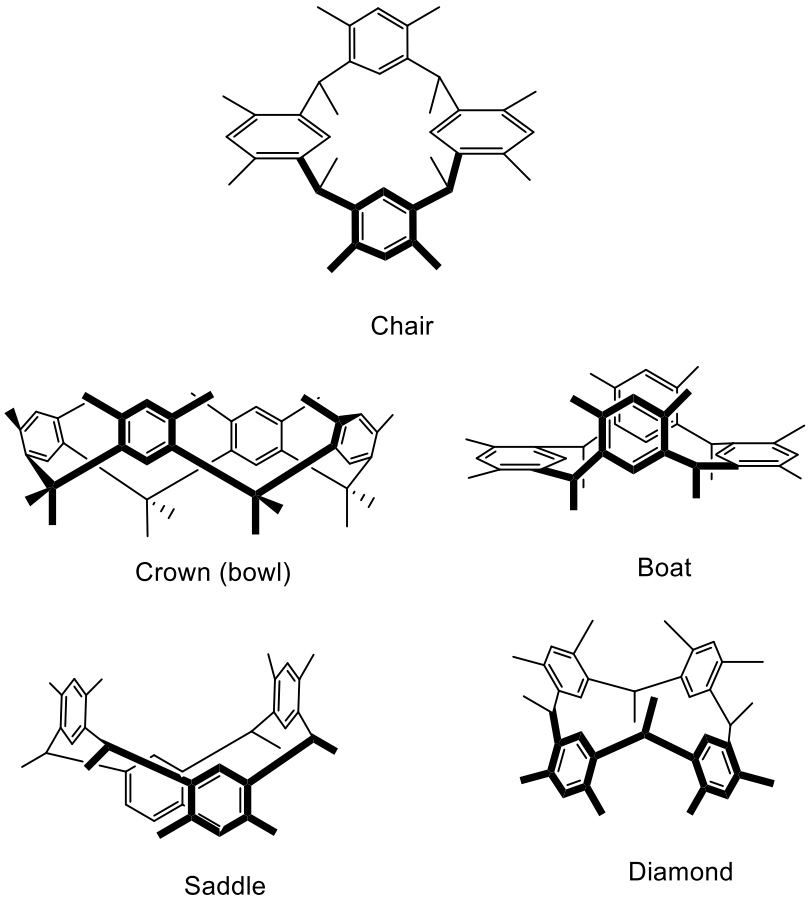

Figure 26: The possible conformations of calix[4]resorcinarenes and calix[4]pyrogallolarenes (Ziaja *et al*., 2016).

The second factor determines the orientation of the substituents at the methylene bridges (Scott & Sherburn, 2017). This gives four possible configurations: *rccc*, where all the substituents face the same direction in a *cis*-relationship to a reference (r) group; *rcct*, where one is in a *trans*-relationship to the other three; *rctt*, where a pair containing the reference group in the opposite direction to the other two groups; and *rtct*, where the reference group is in a *trans*-relationship with the group neighbouring it and in a *cis*-relationship with those opposite to it (Figure 27). The individual stereochemistry of the substituents, which can be either axial or equatorial, is the final factor (Tunstad *et al.*, 1989; Timmerman *et al.*, 1996). Typically, the *rccc* cone conformation is the only isomeric form that results from the acid catalysed condensation of resorcinol and an alkyl aldehyde, while several conformations can be formed from the reaction of resorcinol with aromatic aldehyde, the distribution being dependent upon the thermodynamics of the condensation and duration of the reaction (Carey, 2006).

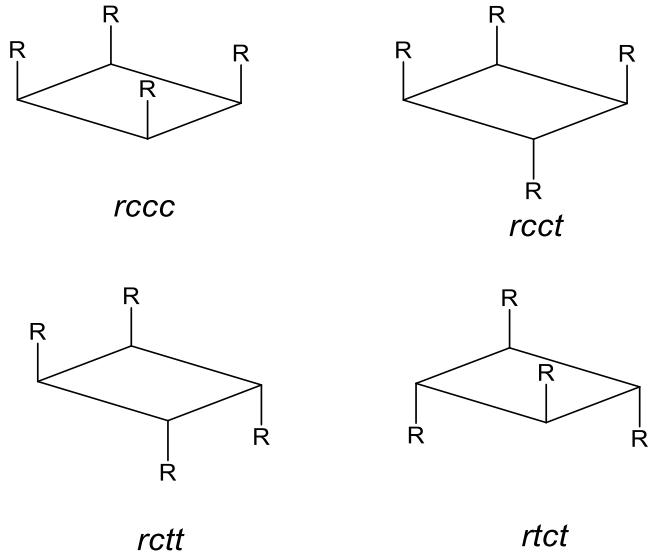

Figure 27: Relative configurations at methylene bridges of calix[4]resorcinarenes and calix[4]pyrogallolarenes.

1.5.3 Functionalization of Calix[4]resorcinarenes and Calix[4]pyrogallolarenes

Calix[4]resorcinarenes and calix[4]pyrogallolarenes are often used as a starting materials to prepare a wide range of compounds because of the ease of their synthesis. Different methods have been developed over the years for the preparation and functionalization of calix[4]resorcinarenes and calix[4]pyrogallolarenes. Modifications to the general structure are made mainly in three positions on the tetrameric structures: Firstly, the lower rim, which can bear residues and functional groups as dictated by the aldehyde selected for use in the synthesis of the calix[4]resorcinarenes and calix[4]pyrogallolarenes. Secondly, the hydroxyl groups at the upper rim of the calix[4]resorcinarenes and calix[4]pyrogallolarenes can be modified by the attachment of different functionalities. Finally, the *ortho* position on each resorcinol ring of a calix[4]resorcinarene can be functionalised (Ngodwana, 2012). In the case of calix[4]pyrogallolarenes, each aromatic ring presents three hydroxyl groups at the upper rim and so *ortho* modification is not possible (Mossine, 2014; Scott & Sherburn, 2017).

1.5.3.1 Lower Rim Functionalization

Functionalization at this position is dependent on the aldehyde used in the initial condensation reaction, since the group attached to the aldehyde functionality appears finally on the lower rim following synthesis. A wide variety of aldehydes have been used successfully, including saturated and unsaturated alkyl aldehydes, aryl aldehydes and those containing a wide variety of functional groups.

1.5.3.2 Upper Rim Functionalization

Like other aromatic compounds, calix[4]resorcinarenes can be subjected to electrophilic substitution reactions, under suitable conditions, at the *ortho* position on their upper rims to provide tetrafunctionalized calix[4]resorcinarenes. Since these positions are activated by the electron donating phenolic groups these compounds are suitable for electrophilic substitution such as bromination. The reaction of calix[4]resorcinarenes **12** with *N*-bromosuccinimide (NBS) provides access to tetrabrominated calix[4]resorcinarenes **13** (Scheme 4). The tetrabromo calix[4]resorcinarenes can act as starting materials for performing further architectural constructions.

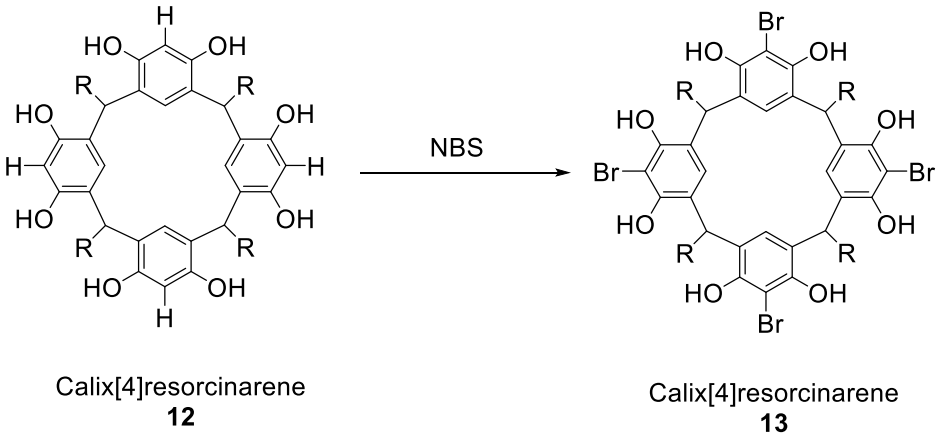

Scheme 4: Calix[4]resorcinarenes functionalised at the upper rim.

The Mannich reaction is another electrophilic substitution reaction which can occur at the *ortho*-position of calix[4]resorcinarenes. Aminomethylation of calix[4]resorcinarenes **12** with primary or secondary amines and formaldehyde readily gives the corresponding tetraoxazines **14** (Scheme 5) (Szumna, 2007). Through this reaction many aminomethylated calix[4]resorcinarenes have been prepared by the acid-catalysed hydrolysis under refluxing conditions of the

corresponding tetraoxazines **14** (Matsushita & Matsui, 1993; Helttunen *et al.*, 2009) gives calix[4]resorcinarene 15 in reasonable yields (Beyeh *et al*., 2012).

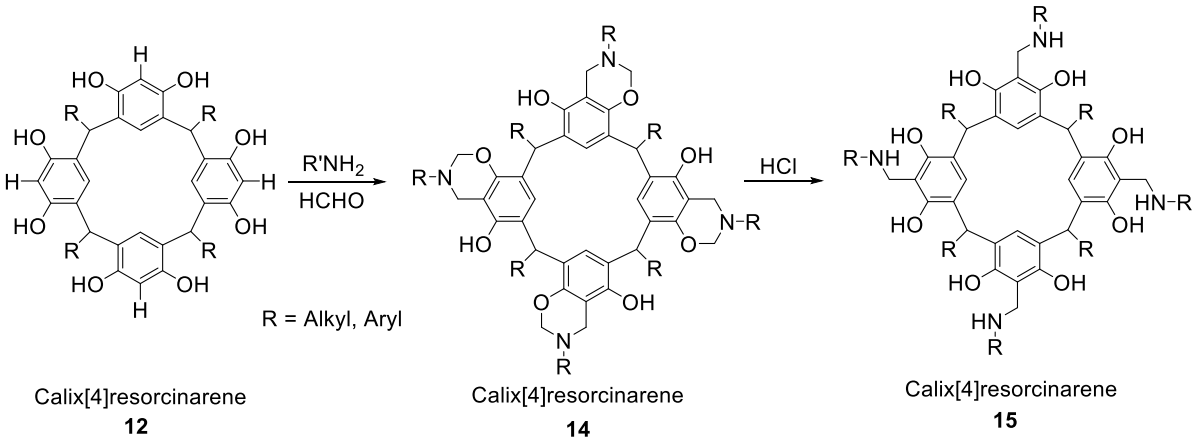

Scheme 5: The Mannich reaction of calix[4]resorcinarenes at the upper rim.

Additionally, the syntheses of aminomethylated calix[4]resorcinarenes using a variety of chiral amines have been has been achieved by using the Mannich reaction. A chiral calix[4]resorcinarene host which contains four proline moieties was reported by Shahgaldian and co–workers (Shahgaldian *et al.*, 2005). Another example of chiral calix[4]resorcinarene modified with L-phenylalanine was presented by Kuberski and Szumna (Kuberski & Szumna, 2009).

1.5.3.3 Reaction of the Hydroxyl Groups

It is known that the presence of the hydroxyl groups in the calix[4]resorcinarene structure plays a key role in the stabilization of the crown conformation, but they can also be exploited in the synthesis of derivatives that possess new physicochemical properties. The eight hydroxyl groups of calix[4]resorcinarenes can be modified with different functional groups, *O*-acylation which results in esters (Fransen & Dutton, 1995; Neda *et al.*, 1998), and *O*-alkylation which, results in ethers (Cometti, 1990) for example (Scheme 6). The octaesters **16** can be obtained as a result of the acylation

of calix[4]resorcinarenes **12** with excess ethylbromoacetate or methylbromoacetate under basic conditions and can subsequently be converted into the corresponding octaacids **17** by hydrolysis. This has been applied to provide calix[4]resorcinarenes which are soluble in aqueous media (Carey, 2006). Aminolysis of octaester **16** with chiral amines and aminoalcohols results in octaamide derivatives **18** (Scheme 6).

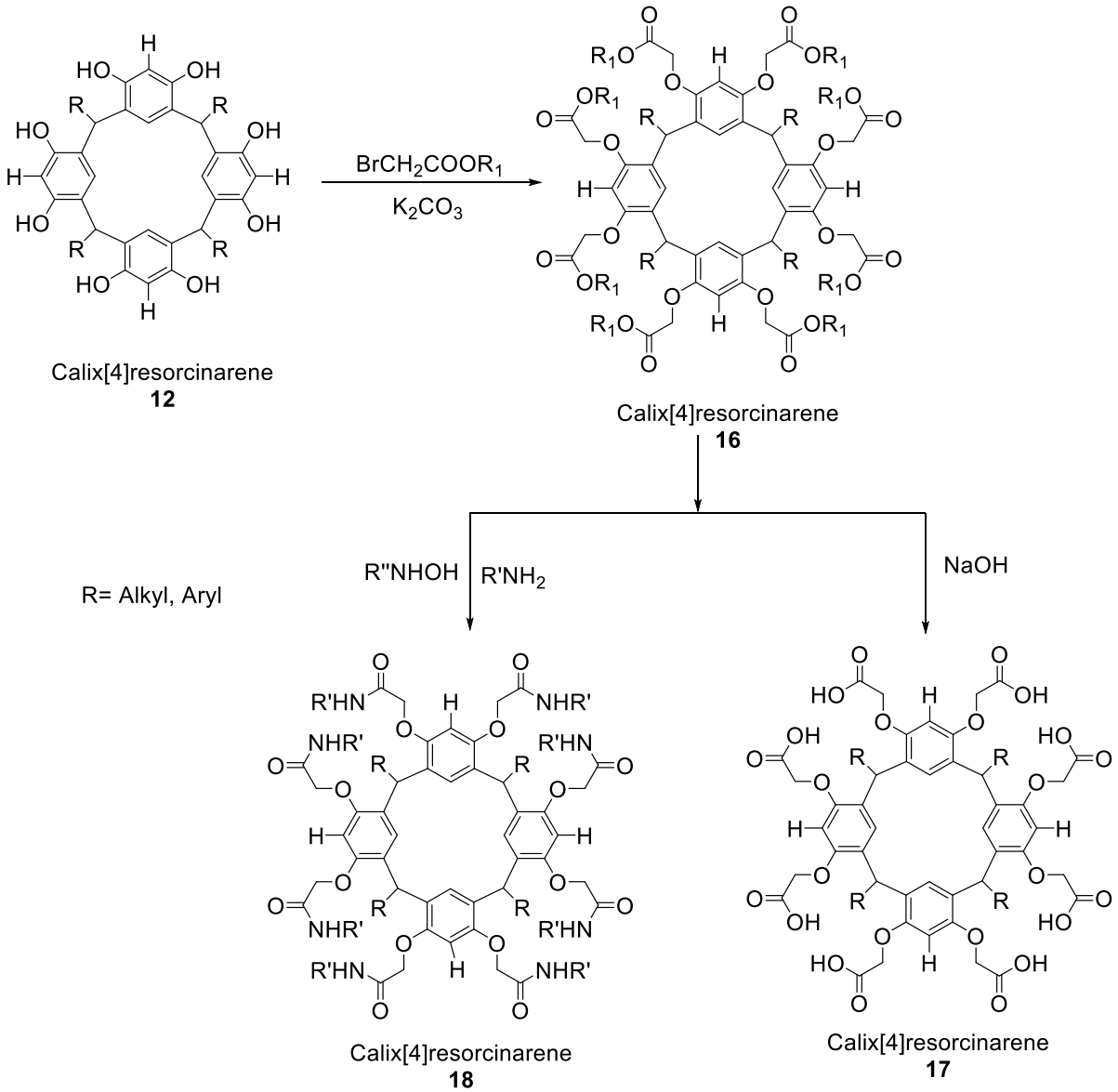

Scheme 6: Calix[4]resorcinarenes functionalised by *o*-acylation at the upper rim followed by the formation of the octaacid and octaamide.

Water soluble calix[4]resorcinarene **22** decorated with eight oligosaccharide groups attached at the upper rim through amide linkages was produced by a multistep procedure (Scheme 7). Reduction of the octaester **16** with $LiAlH_4$ gave the octol **19**, which reacted with phthalimide to give an octaphthalimide **20**. Hydrazinolysis of the phthalimido groups resulted in the corresponding octaamine, **21**, which was subsequently elaborated to give glycocluster **22** (Scheme 7).

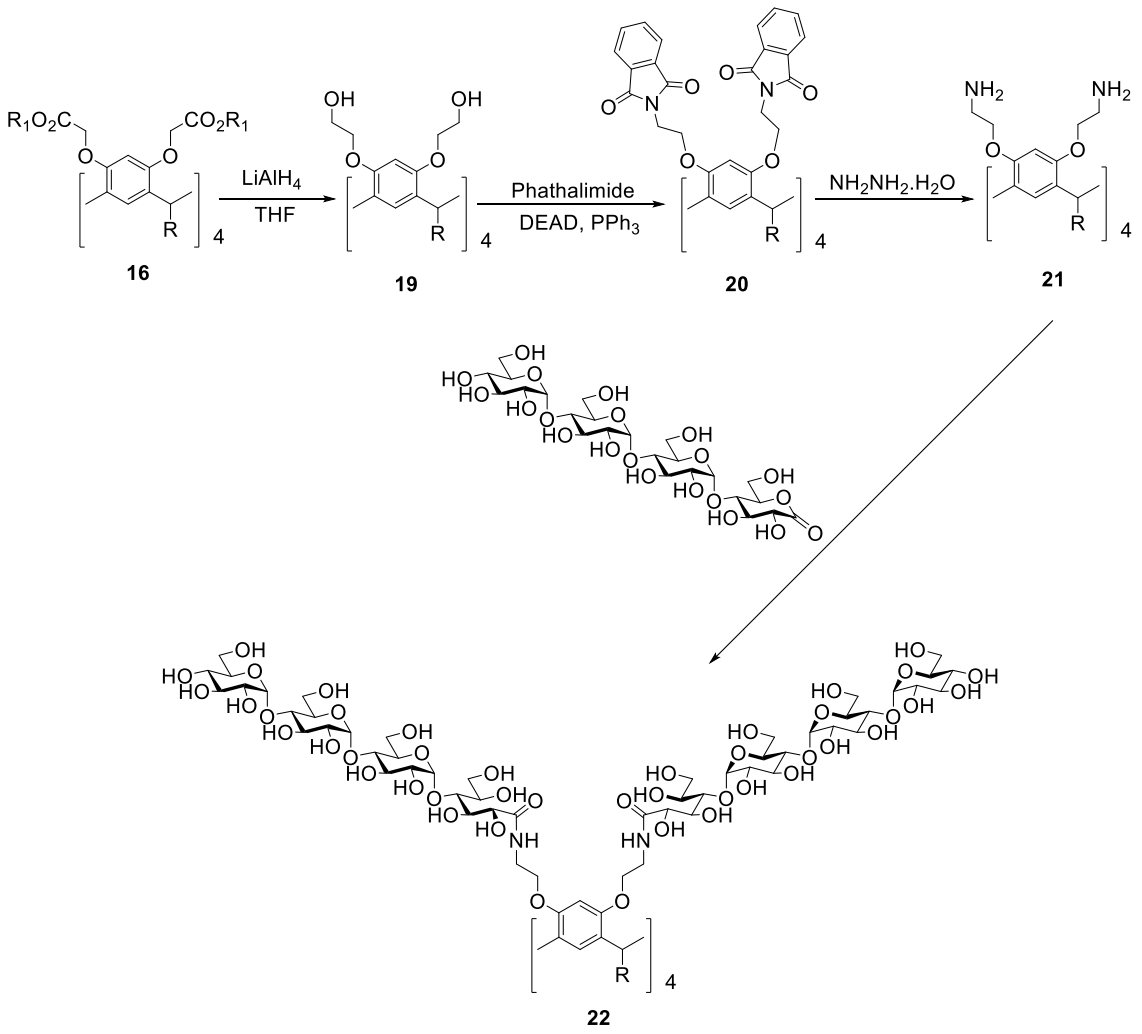

Scheme 7: The formation of a water-soluble calix[4]resorcinarene glycocluster.

1.5.4 Bridged Calix[4]resorcinarenes

Cavitands, a class of macrocycle with an extremely rigid cavity, can be obtained by bridging the hydroxyl groups on the resorcinol rings of a calix[4]resorcinarene under basic conditions using different types of bridging groups such as methylene or heteroatom units, thus allowing the formation of bridged (O-Y-O) rigid calix[4]resorcinarene derivatives **23** (Ngodwana, 2012; Vinodh *et al.*, 2012). The size, shape, rigidity, and other properties of the hydrophobic cavity in cavitands can be adjusted by using different types of bridging and functional groups (Taylor *et al*., 1998). There are four general classifications of cavitands based on the type of bridges in the structure (Kobayashi & Yamanaka, 2014). They are alkylenedioxy (*e.g.* **23a**), dialkylsilicon (*e.g.* **23b**), heterophenylene (*e.g.* **23c**), and phosphoryl bridged cavitands (*e.g.* **23d**) (Scheme 8). Cavitands have an enforced cavity large enough to accommodate different guest molecules, making them excellent molecular receptors and have attracted increasing attention in the field of pharmaceutical science and drug delivery (Cram *et al.*, 1988; Sherman & Cram, 1989; Cram *et al.*, 1992), (Hogberg, 1980; Timmerman *et al.*, 1996).

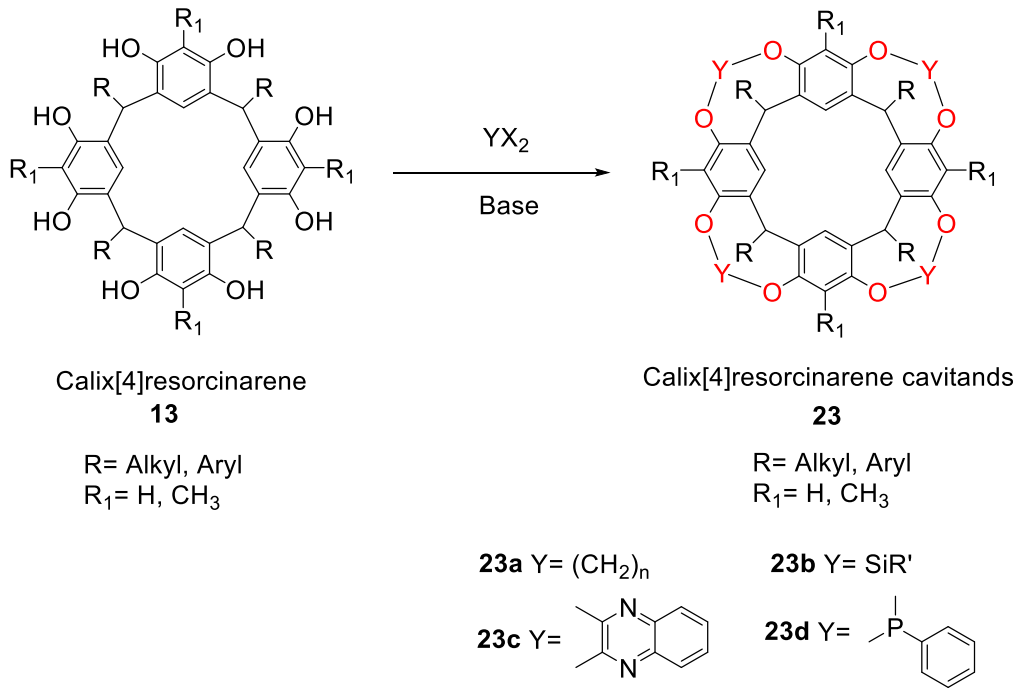

Scheme 8: The synthesis of calix[4]resorcinarene cavitands (Ngodwana, 2012).

In order to prepare cavitand **23a**, the phenolic hydroxyl groups are alkylated with chlorobromomethane, 1,2-dibromoethane, or 1,3-dibromopropane in the presence of anhydrous potassium carbonate or caesium carbonate in different solvents such as dimethyl formamide (DMF), dimethyl acetamide, dimethyl sulfoxide (DMSO) or *N*-methylpirolidinone using a typically general procedure (Pietraszkiewicz *et al.*, 2004). Under suitable conditions, protons *ortho* to the phenolic hydroxyl groups at the upper rim of a calix[4]resorcinarene-based cavitand can be substituted using *N*-bromosuccinamide to give the corresponding tetrabromocavitands (Gruppi *et al*., 2009). A number of derivatives can be formed from the resulting tetrabromocavitands by replacing the bromine atoms with strong nucleophiles, such as thiols or phosphines (Turunen *et al*., 2014).

Cavity expansion can be achieved through the extension of the wall components resulting in the formation of deep cavity cavitands. Deep cavity cavitands possess a cavity that is more elongated and can accommodate a variety of bigger and more

complex guests (Csok *et al*., 2011). In recent years, molecular capsules possessing expanded inner cavities have attracted enormous attention in separation science, drug delivery systems and host-guest recognition (Rudkevich & Rebek, 1999). The depth of the cavity can be increased either by Suzuki cross-coupling reactions, for example (Ma *et al.*, 1998; Schultheiss & Desper, 2006), or by linking the hydroxyl groups of the calix[4]resorcinarenes with 1,4-diazine derivatives (Moran *et al*., 1991).

Calix[4]resorcinarenes have been verified to be a useful scaffold for developing a variety of cavitands and can be modified by attaching polar groups at the upper or the lower rim to make them more soluble in water (Biros *et al.*, 2004; Schramm *et al*., 2007). The deeper cavitands can act as small molecule hosts that accommodate molecular guests selectively, temporarily isolating them from their environment to facilitate solubilization (Moran *et al*., 1982; Schramm *et al*., 2007). The process of molecular encapsulation by more complex cavitands with deep cavities derived from calix[4]resorcinarenes has received a lot of attention (Biros & Rebek, 2007). This can also produce greater control over the properties of the guest molecules by restricting their conformation. Indeed, new forms of isomerism have been observed from the co-encapsulation of multiple guests in the same host (Purse *et al.*, 2008). The characteristics of the inner space of the capsule, such as size and shape, can be adjusted by modifying the bridging and functional groups. Moreover, the modification of calix[4]resorcinarenes with four identical functional groups at the upper rim can offer two main types of derivative: The first is made by incorporating modified bridges between neighbouring hydroxyl groups, such as those that contain aromatic ring-bridge cavitands (Figure 28), to give deep cavitands **24**, and benzal-bridge cavitands **25** and **26** (Cram *et al.*, 1992; Gibb *et al*., 2001). The addition of functional groups at

the *ortho*-position on the resorcinol ring produces another type of derivative **27** (Ebbing *et al.*, 2002).

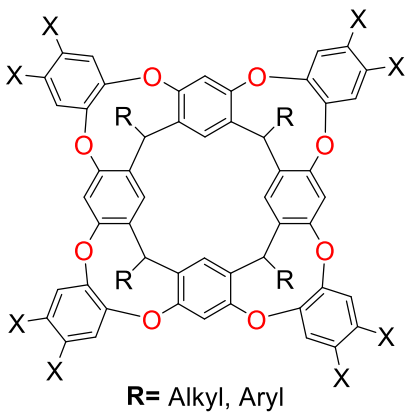

R= Alkyl, Aryl
24a X= Br
24b X= OH
24c X= CH_2Br
24d X= I
24e X= CH_2I

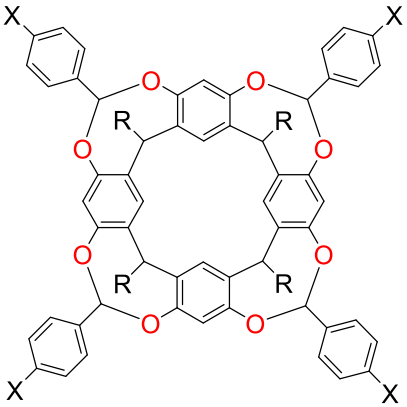

R= Alkyl, Aryl
25a X= Br
25b X= OH
25c X= CH_2Br
25d X= I
25e X= CH_2I

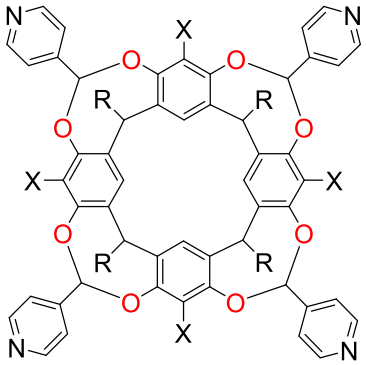

R= Alkyl, Aryl
26a X= Br
26b X= OH
26c X= CH_2Br
26d X= I
26e X= CH_2I

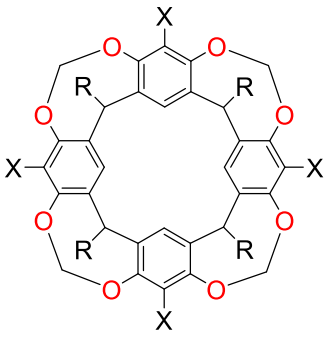

R= Alkyl, Aryl
27a X= Br
27b X= OH
27c X= CH_2Br
27d X= I
27e X= CH_2I

Figure 28: Structures of calix[4]resorcinarene derived cavitands with deep cavities (Kobayashi & Yamanaka, 2014).

1.5.4.1 Water Soluble Cavitands

One of the goals of supramolecular chemistry is the development of specific receptor molecules that are functionally analogous to natural systems. Although a large

number of compounds have been synthesized for this purpose, they have mostly been prepared and demonstrated in organic solvents. Drug delivery, however, requires such molecules to be active in aqueous media. Calix[4]resorcinarene-based cavitands which have the bridged (O-Y-O) structure to confer structural rigidity, have been used widely in the development of water-soluble supramolecular assemblies. The parent cavitands (Y= CH_2, R_1= CH_2Br) are insoluble in water (Oshovsky *et al*., 2007). However, when the upper and lower rims are decorated with charged groups (Gui & Sherman, 2001), saccharide functions (Oshovsky *et al*., 2004), and dendritic oxo substituents (Middel *et al.*, 2002), as examples, the cavitands are now soluble in aqueous media. The upper rim functionalization of tetrabromide cavitands is readily achieved by substitution to give compounds **27c** (Figure 29). Various new synthetic routes have been devised to prepare novel container hosts using tetrabromide cavitands as starting materials due to their easy access as well as relatively facile modification to display other functional groups (Biros & Rebek, 2006).

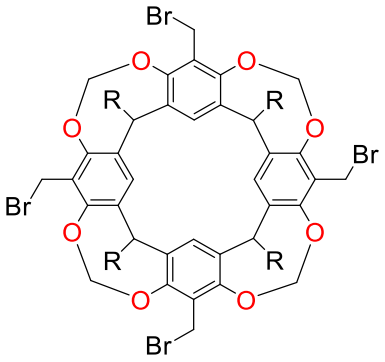

27c

R= Alkyl, Aryl

Figure 29: The general structure of bromomethylated calix[4]resorcinarene-based cavitands.

Novel water-soluble calix[4]resorcinarene-based cavitands were synthesized by the attachment of four viologen units on the upper rim of the calix[4]resorcinarene

platform. The presence of viologen moieties on the upper rim increased the aqueous solubility of the calix[4]resorcinarene as compared to compound **27c**. Compounds **28a-c** possess a highly hydrophobic inner cavity, enabling isolation of a compound with a multiply charged cation and a well-organized structure in which the electron-acceptor properties can be controlled (Kashapov *et al*., 2014). Viologen–calix[4]resorcinarenes **28** with different tail lengths on the lower rim (Scheme 9) exhibited acceptor properties and could electrochemically bind both small donor molecules and bulk macrocyclic compounds (Kashapov *et al.*, 2014; Ziganshina *et al.* , 2007).

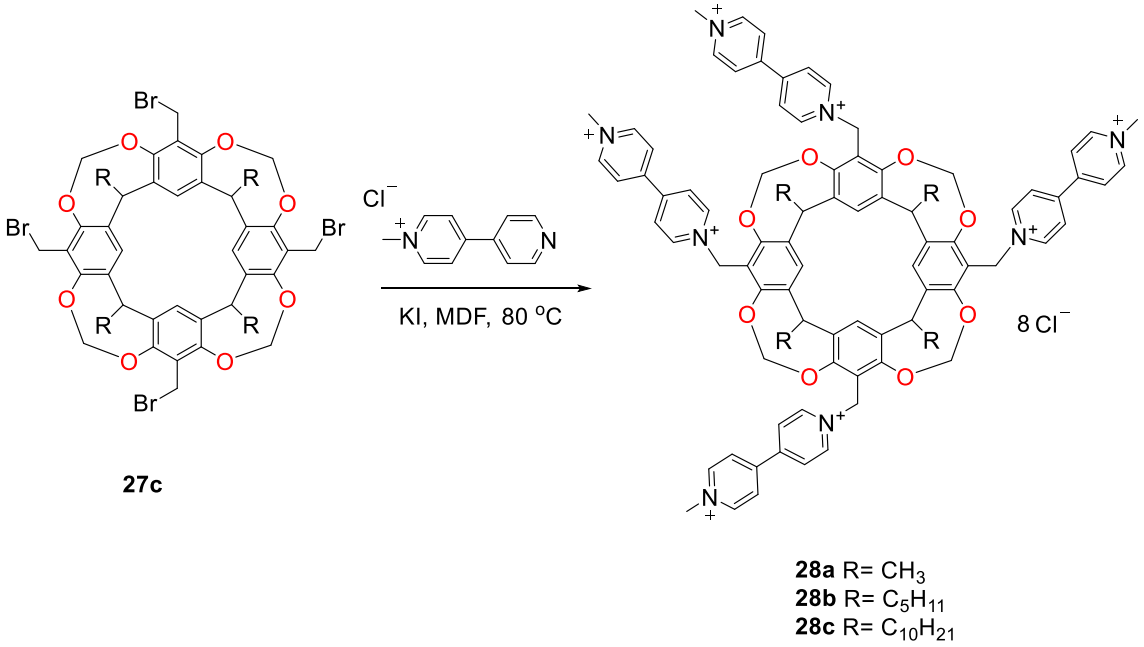

Scheme 9**:** Synthesis of calix[4]resorcinarenes with viologen substituents (Ziganshina *et al*., 2007).

The water-soluble cavitand **29** (Scheme 10), was obtained by reaction of bromomethyl calix[4]resorcinarene-based cavitands with 50 equivalents of pyridine as an amine, giving permanently charged cationic cavitands **29** (Gansey *et al*., 1998).

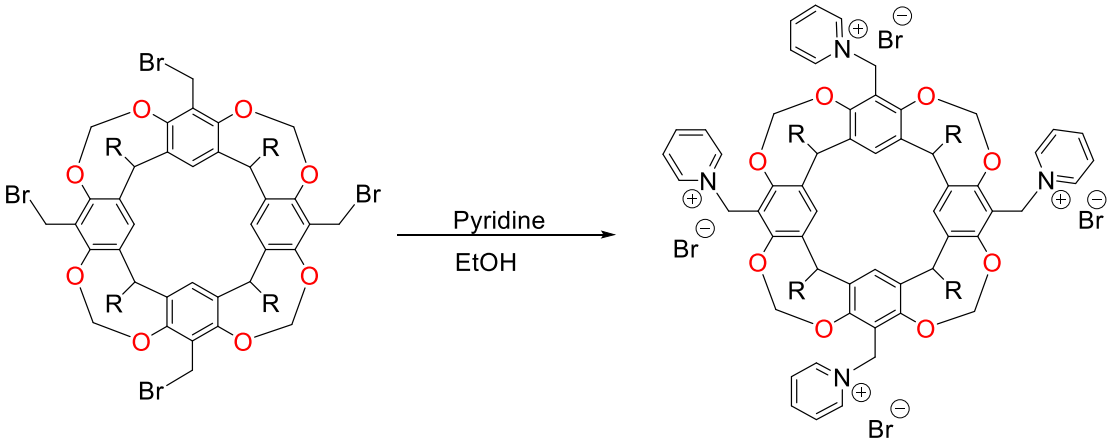

Scheme 10: Synthesis of a water-soluble calix[4]resorcinarene-based cavitand (Gansey *et al*., 1998).

A new water-soluble, anionic calix[4]resorcinarene **32** was synthesized from the known bromomethylcavitand **27c** (Scheme 11). The rigid basket shaped cavity of the water-soluble hosts can selectively accommodate the aromatic portion of pyridinium and quaternary ammonium salts in water (Park & Hong, 2000).

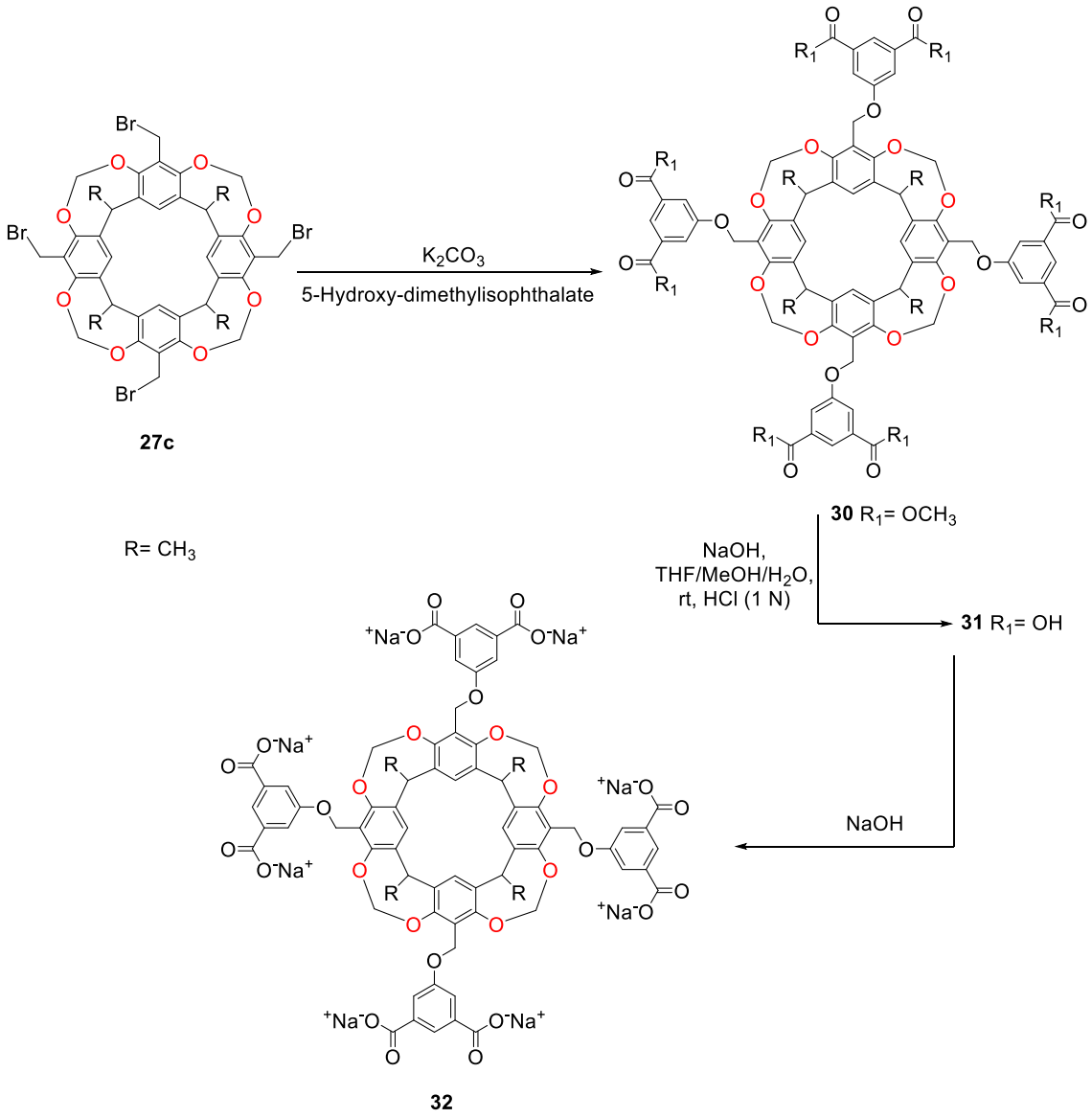

Scheme 11: Synthesis of a water-soluble, anionic calix[4]resorcinarene-based cavitand (Park & Hong, 2000).

1.5.5 Self–organization of Amphiphilic Calix[4]resorcinarenes and Calix[4]pyrogallolarenes in Water

Amphiphiles are a class of molecules that carry both hydrophilic and hydrophobic groups (Jiang *et al*., 2007). When they are dissolved in aqueous solutions, their hydrophilic part prefers to interact with the aqueous phase while the hydrophobic part tries to decrease the free energy of the hydrophilic−hydrophobic interface by

aggregating together to form different assemblies (Lehn, 2002) such as micelles (Chen & Jiang, 2005) or vesicles (Han *et al*., 2004). There are two factors that can determine the characteristics of the formation of assemblies: The repelling and coordinating forces between the different parts of the amphiphile, together with interaction with the surrounding medium (Guo *et al*., 2012; Yao *et al*., 2012). In addition to a wide range of natural amphiphiles, the design and manufacture of synthetic amphiphiles has been a focus of interest due to their importance for day–to–day applications in various fields (Menger, 1991; Lee *et al.*, 2001). Both synthetic and natural amphiphiles have a simple structure with an unprecedented ability to self–assemble, and have applications in the field of pharmacy, pharmaceutics and controlled synthesis of nanomaterials (Ramanathan *et al*., 2013). Synthetic amphiphiles form assemblies in aqueous solution producing small micelles formed at a specific concentration, referred to as the critical micelle concentration (CMC) (Kashapov *et al*., 2011; Voronin *et al*., 2013). In contrast to amphiphilic molecules such as surfactants and amphiphilic block copolymers, there are only a few examples of macrocyclic amphiphiles that have been prepared and used to fabricate supramolecular structures (Yao *et al*., 2012). Not only can they form multidimensional assemblies with well-defined size and shape due to the presence of the hydrophilic and hydrophobic parts on both rims, they can also provide structures based on the self-selectivity of the host-guest interactions (Chen & Jiang, 2011). Among them, the calix[4]resorcinarenes have attracted much attention because of their promising, potential applications (Sun *et al*., 2008).

The use of non-covalent interactions in order to form molecular capsules with new features is still an attractive field in supramolecular chemistry (Conn & Rebek, 1997; Corbellini *et al*., 2003; Corbellini, 2004). Synthetic receptors such as hydrogen-

bonded capsules and open inclusion complexes have enhanced the understanding of chemical and biological recognition and self-assembly. The formation of supramolecular containers for molecular recognition in water is important because most biological processes occur in an aqueous environment (Corbellini *et al*., 2003). Rigid macrocycles such as calix[4]resorcinarenes and calix[4]pyrogallolarenes are promising for building capsular and open inclusion complexes (Kharlamov *et al*., 2013). Studies using calix[4]resorcinarenes and their tetraphenolate derivatives for the complexation of alkyl ammonium cations have indicated that they are capable of interacting with suitably sized ammonium cations as analogues of biologically significant acetylcholine.

1.5.5.1 Calix[4]resorcinarene–based Vesicles

Since the discovery that they can be prepared within the laboratory, vesicles have been the topic of much research in formulation science and supramolecular chemistry. Much like phospholipids, synthetic amphiphiles are capable of forming molecular bilayers enclosing a small aqueous compartment. The molecular host–guest interactions of vesicles have been studied principally using cyclodextrin derivatives (Voskuhl & Ravoo, 2009) but also using cucurbiturils (Lee *et al.*, 2005), calix[n]arenes (Helttunen & Shahgaldian, 2010) and calix[4]resorcinarenes (Tanaka *et al.*, 1999). Deep cavitands that form vesicles and retain their ability to host small guest molecules through hydrophobic interactions in water have been reported (Kubitschke *et al.*, 2012). Vesicles can host hydrophobic guests in the hydrophobic bilayer structure, and the inner aqueous compartment of the vesicles can accommodate hydrophilic guests. Water soluble, neutral cavitands **33** with tetraethylene glycol groups attached at the upper rim of calix[4]resorcinarenes were synthesized by Kubitschke and co-workers (Figure 30). The vesicles assembled from

these deep cavitands were used to host three different types of guest molecules, where small guest molecules were encapsulated within the cavitands, larger hydrophobic guests were accommodated within the vesicle bilayer and hydrophilic molecules were hosted in the inner aqueous compartment (Figure 31). Doxorubicin hydrochloride, a well-known anti-cancer agent, was chosen as a large hydrophilic drug molecule to investigate the ability of these vesicles to encapsulate such molecules within their inner aqueous compartment. The results showed that these vesicles present a promising carrier for drug delivery applications (Kubitschke *et al*., 2012).

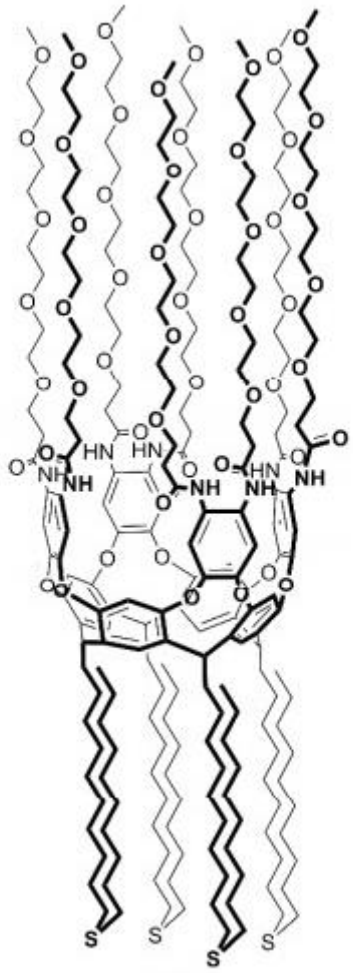

33

Figure 30: Structure of an amphiphilic deep cavitand (Kubitschke *et al.*, 2012).

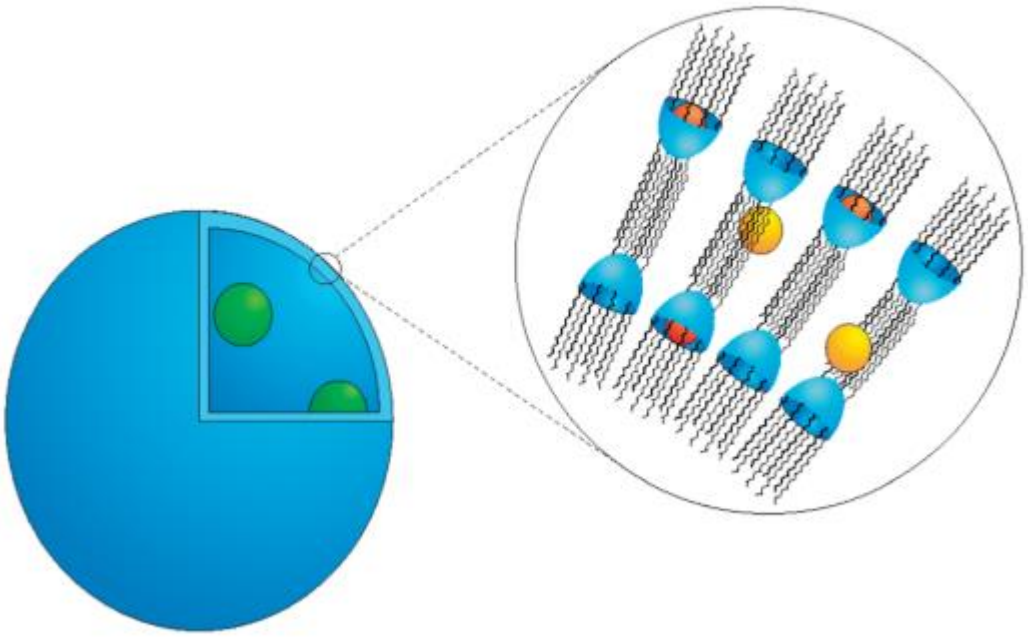

Figure 31: Representation of a vesicle derived from deep cavitand **33**; the small coloured balls represent three different types of guest molecules (Kubitschke *et al*., 2012).

The ability of new aminoacid-substituted calix[4]resorcinarene **34** to dissolve in aqueous media was investigated and the influence of the aminoacid moieties on this solubility was shown. Calix[4]resorcinarene bearing a glycine residue is practically insoluble in water. However, the solubility could be increased with increasing the molecular weight of the amino acid residue, and the behaviour of the compounds in water depended upon whether the calix[4]resorcinarene upper rim was fully deprotonated. The formation of spherical particle aggregates occurs with increasing pH, which probably corresponds to stable multilamellar vesicles. It is evident that vesicular structures can be formed, where the phenyl rings of the macrocycles stack with each other in a face to-face fashion. The aromatic rings and lower rim acts as the tail and the amino acid backbones act as the head groups, respectively, which is

an essential criterion in this case for multilayer structure formation (Kashapov *et al*., 2015) (Figure 32).

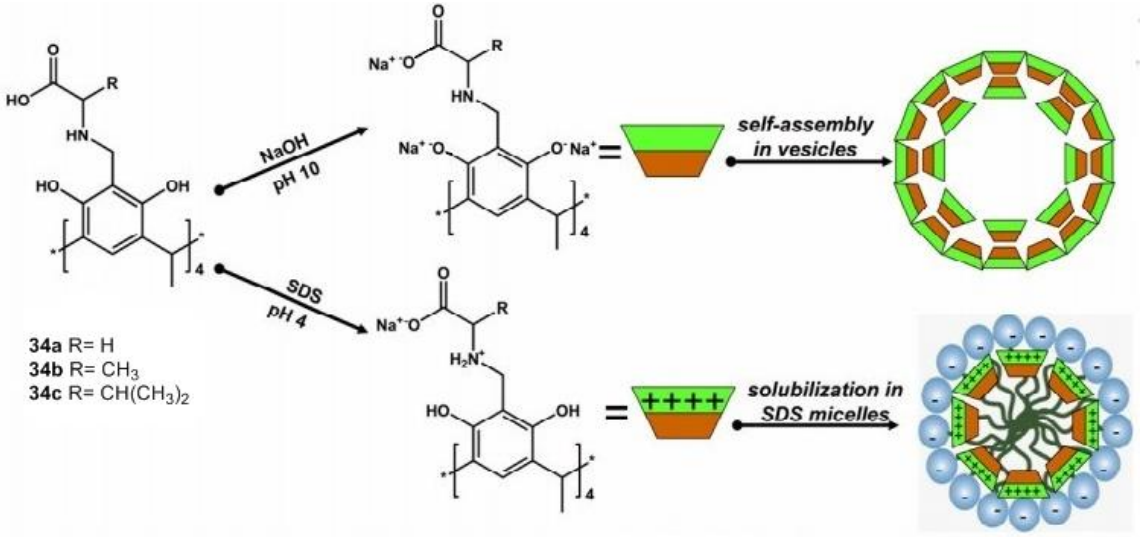

Figure 32**:** An illustration of the structural behaviour of calix[4]resorcinarenes with glycine, D,L-alanine and D,L-valine in aqueous alkaline sodium and sodium dodecyl sulfate (SDS) solutions (Kashapov *et al*., 2015).

1.5.5.2 Micelles

Amphiphilic molecules can be assembled through a spontaneous dynamic process in aqueous solution to form micellar structures that are usually described as occurring when the amphiphilic concentration reaches the CMC. In principle, a conical shape of the amphiphilic molecule is a prerequisite for the formation of small spherical micelles which can only be obtained by controlling the conditions of the self-assembly. Calix[n]arenes and calix[4]resorcinarenes have provided opportunities to achieve this condition. The self-assembly of water soluble calix[4]resorcinarene **35** (Figure 33), a non-ionic amphiphile, which carries extremely large oligosaccharide head groups was studied. Although oligosaccharide groups do not show surfactant properties when surface tension is considered, the clear evidence of their amphiphilic nature is

their aggregation into micellar structures in water. The micelle formation is found to be irreversible even at very low concentrations and the aggregates do not dissociate into monomers. Therefore, in addition to aggregation due to the hydrophobic effect between the lower rim alkyl chains, steep curvature in the shape of the conjugates along with hydrogen bonding between the oligosaccharide chains control the formation of small micelles consisting of few number of molecules instead of lamellar assemblies (Hayashida *et al.*, 2003; Helttunen & Shahgaldian, 2010).

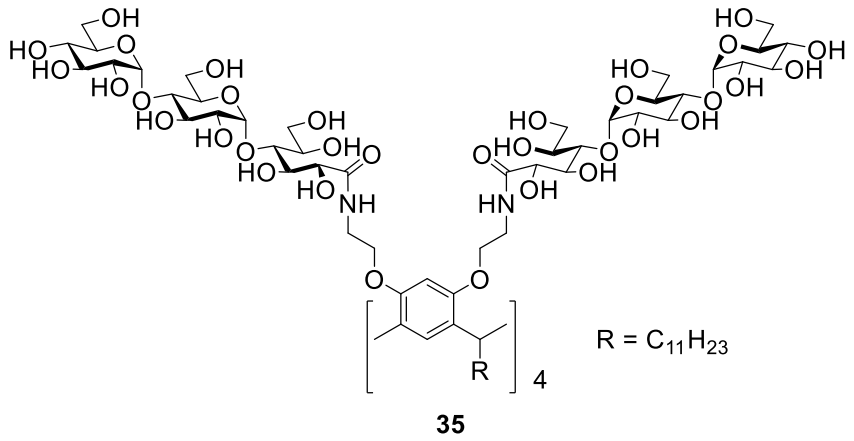

35

Figure 33: Molecular structure of water soluble calix[4]resorcinarene **35** (Helttunen & Shahgaldian, 2010).

Another example of irreversible micellization in water was found with amphiphilic tris(hydroxymethyl)amide calix[4]resorcinarene **36** (Figure 34). The micellization of a mixture of calix[4]resorcinarene **36** and the cationic surfactant cetyltrimethylammonium bromide was studied in water and aqueous dimethylformamide (DMF) solution. The catalytic activity of this system in the hydrolysis of 4-nitrophenyl bis (chloromethyl)phosphinate was also studied. It was shown that the catalytic activity of the mixed systems increased the hydrolysis of phosphoric ester in water compared with a pure amphiphilic calix[4]resorcinarene (Ryzhkina *et al.*, 2004; Helttunen *et al.*, 2009).

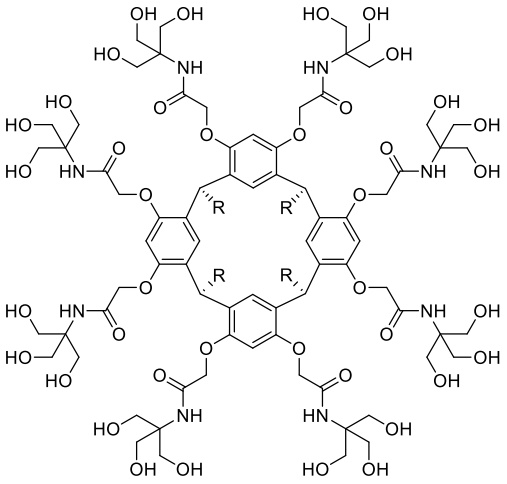

36a R= C_8H_{17}
36b R= $C_{11}H_{23}$

Figure 34: The structure of the tris(hydroxymethyl)amide calix[4]resorcinarenes **36** (Valitova & Konovalov, 2012).

Recently, the self–assembled structure based on calix[4]pyrogallolarene (*2*-hydroxyl calix[4]resorcinarenes) has caught the attention of a number of researchers, as the presence of another phenolic OH group offers by the calix[4]pyrogallolarene additional opportunities for intermolecular bonding. The formulation of large capsules using calix[4]pyrogallolarenes which carry long alkyl chains attached at their lower rim have attracted particular attention. As with calix[4]resorcinarene, these structures form *rccc* isomers (Brown *et al.*, 2006). Water–soluble calix[4]pyrogallolarene **37** (Figure 35) bearing hydrophilic acetylhydrazide groups at the upper rim and hydrophobic alkyl chains at the lower rim was prepared in order to investigate the influence of the aggregation and preorganization of the functional groups (hydrazide) on their reactivity in aqueous medium (Pashirova *et al.*, 2007).

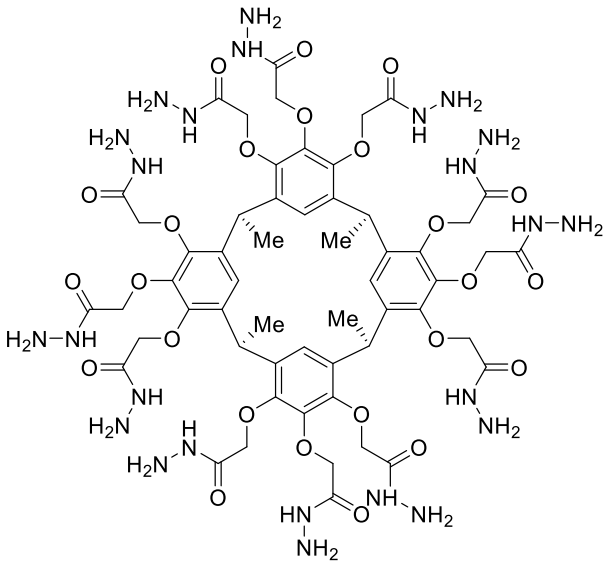

37

Figure 35: The structure of the carbazoylmethyl derivative **37** of calix[4]pyrogallol (Pashirova *et al*., 2007).

1.5.6 Application of Calix[4]resorcinarenes and Calix[4]pyrogallolarenes in Drug Delivery

Research into the use of calix[4]resorcinarenes, cavitands and calix[4]pyrogallolarenes in biomedical applications is still active. This is due to their self-assembly and molecular recognition characteristics, as well as their ability to host different guests by forming various supramolecular assemblies, such as dimeric and hexameric hydrogen-bonded molecular capsules, 1:1 open inclusion complexes and tubular assemblies (Dalgarno *et al.*, 2005; Ahn *et al*., 2014; Beyeh *et al.*, 2014). Therefore, self-assembly of amphiphiles is of great significance in the field of drug delivery in addition to their enormous theoretical interest (Helttunen & Shahgaldian, 2010). Many amphiphilic calix[4]resorcinarenes, modified with chiral moieties have been designed as receptors and have shown their stereo–selective interactions with amino acids (Pru *et al.*, 1998; Shahgaldian *et al.*, 2008). Although chirality plays an

important role in the synthesis and use of drugs, particular stereoisomers of a drug may cause unwanted side effects and may be toxic (Simonyi, 1984). In that case chiral calix[4]resorcinarenes **38** (Figure 36) can be used for hosting these drugs.

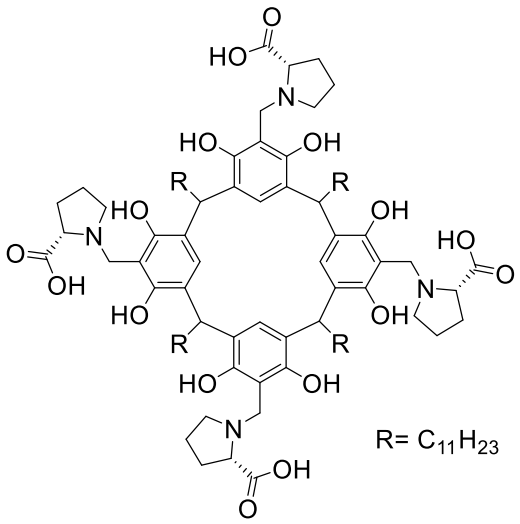

38

Figure 36: Molecular structure of chiral calix[4]resorcinarene **38** (Shahgaldian *et al.*, 2005).

Despite the potential applications of the reversible self–assembly of the macrocycles themselves in various fields including biology, medicine, and materials science, more attention has been paid to the self-assembly of macrocyclic nanomaterials mediated by host–guest interactions (Li & Qi, 2018). Great efforts have been devoted to exploring the well–defined systems of the host-guest complexes to control the targeting and release of drug molecules by enclosing them inside hydrophobic cavities (Biros & Rebek, 2007). A guest is accommodated with the host cavity by non-covalent interactions, which can provide many advantages, such as enhanced solubility, stability and removal of unwanted materials from a mixture (L. Wang *et al.*, 2013; Gangemi *et al.*, 2015). The host–guest complexes assembled using calix[4]resorcinarenes show good potential for use as drug carriers. Indeed, the deep

cavity of the calix[4]resorcinarenes has been shown to accommodate a variety of drugs (Hoskins & Curtis, 2015; Hoskins *et al*., 2016).

Mycophenolate mofetil (MMF), a mycophenolic acid derivative, is a powerful immunosuppressant drug used as a part of standard immunosuppressive chemotherapy treatment regimens without significantly harmful side effects. However, it can cause vomiting, abdominal pain and diarrhoea. The solubility of this hydrophobic drug is 43 µg / mL (Saxena *et al*., 2004). Thus, MMF suffers from poor bioavailibility as a result of its low solubility in aqueous media. The formation of a host-guest complex with *para*-sulfonatocalix[4]resorcinarene which possesses hydrophilic (SO_3^-) groups at the upper rim, can enhance the solubility of this hydrophobic drug. Menon and co–workers investigated the 2:1 complex formation of *para*-sulfonatocalix[4]resorcinarene **39** with MMF (Figure 37) (Menon *et al*., 2011).

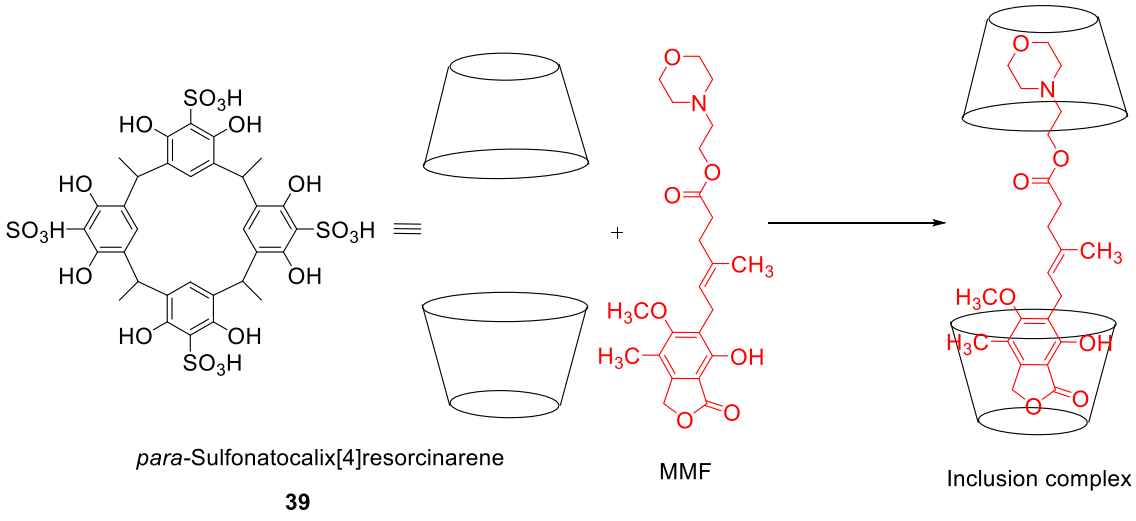

Figure 37: The 2:1 inclusion complex between calix[4]resorcinarene **39** and MMF (Menon *et al*., 2011).

Lamotrigine (LMN) is used to treat or prevent convulsions such as in epilepsy or other seizure disorders. The effective absorption of this drug is limited due to its poor water solubility which may lead to irregular bioavailability. Many researchers have

attempted to improve its effectiveness and efficiency by enhancing the water solubilisation of the drug using cyclodextrin (Shinde *et al.*, 2008; Seridi & Boufelfel, 2011). The promising results obtained from other studies prompted Patel and co-workers to explore the inclusion complex of LMN with *para*-sulfonatocalix[4]resorcinarene **39** (Figure 38) (Patel *et al*., 2013).

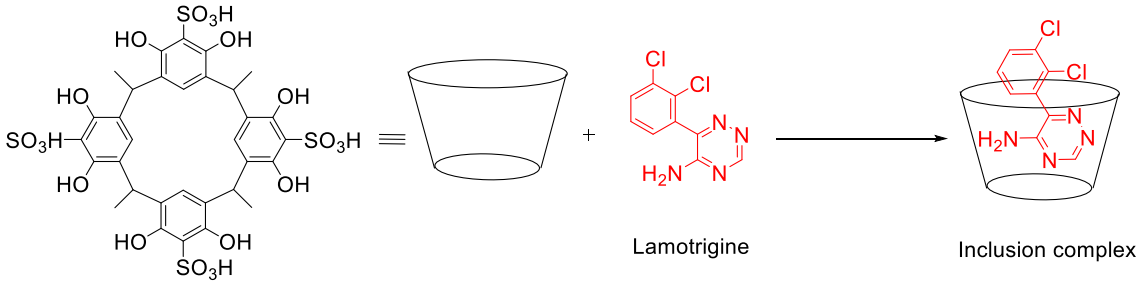

para-Sulfonatocalix[4]resorcinarene

39

Figure 38: 1:1 Inclusion complex of lamotrigine with compound **39** (Patel *et al*., 2013).

As mentioned above, curcumin has potential therapeutic benefits, which are limited as a consequence of its poor solubility. Hence, new technologies for drug solubilization are required to improve the solubility, stability and bioavailability of curcumin. The solubility of curcumin can be improved by hosting it with other compounds that have a good solubility profile. *para*-Sulfonatocalix[4]resorcinarene **39** was chosen as a drug solubilizing agent due to its ease of synthesis as well as its ability to provide anionic binding sites. Water soluble *p*-sulfonato-calix[4]resorcinarene was used to improve the dissolution behaviour of curcumin by Valand and co-workers, who studies the 1:1 host- guest complex of it with curcumin (Figure 39). The hydrophobic cavity of **39** hosted the diketo-lipophilic residue of the symmetrical curcumin molecule (Valand & Menon, 2015).

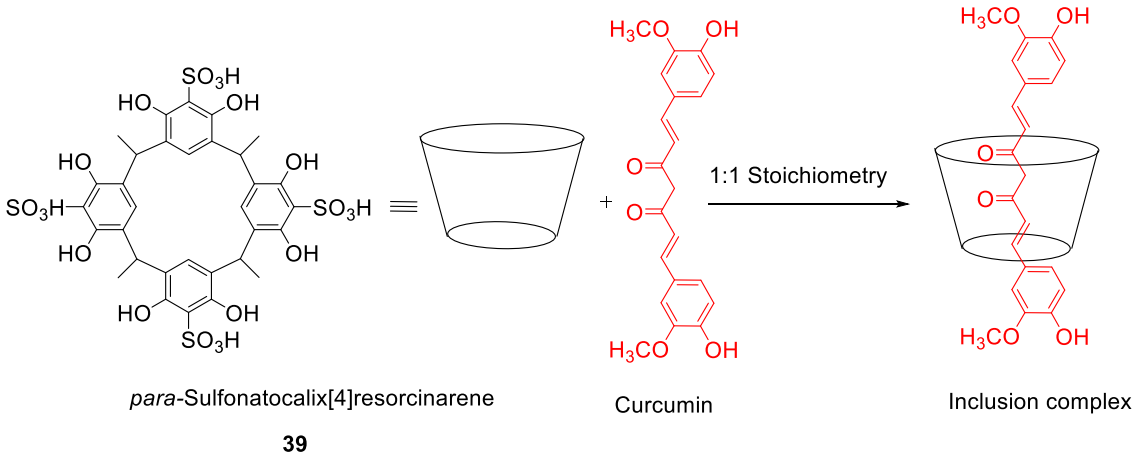

Figure 39: Proposed 1:1 complex of calix[4]resorcinarene **39** with curcumin (Valand & Menon, 2015).

Water–soluble calix[4]resorcinarenes **40** were prepared by adding sulfonate moieties at the upper rim and different length alkyl tails at the lower rim (Figure 40). The hosts possesse a π–electron–rich cavity that is similar to those of other *para*-sulfonatocalix[n]arenes, making it a suitable platform for hosting many aromatic, aliphatic, and cationic guest molecules of different shapes and sizes (Syakaev *et al*., 2012; Pashirova *et al.,* 2014). Such water–soluble sulfonatomethylated calix[4]resorcinarenes **40** can be used to form water–soluble complexes with a variety of hydrophobic drugs (Hoskins *et al*., 2016) because of their high solubility and their capacity for selective bonding with drug molecules.

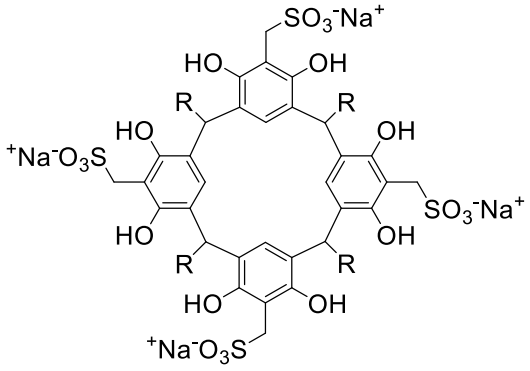

Sulfonatomethylated Calix[4]resorcinarene

40a R= CH_3
40b R= C_4H_9
40c R=C_5H_{11}
40d R= C_7H_{15}
40e R= $C_{10}H_{21}$

Figure 40: Structural formulae of amphiphilic calix[4]resorcinarenes decorated with sulfonate moieties at the upper rim and different alkyl groups at the lower rim (Hoskins *et al*., 2016; Pashirova *et al*., 2014; Syakaev *et al*., 2012).

Desirable drug delivery vehicles will possess the ability to recognise certain molecules selectively as well as transport them across cell membranes (Torchilin, 2012). The transportation across the membrane plays an essential role in the pharmacokinetics of the drug. The big challenge in drug delivery, especially for those drugs able to move through the blood brain barrier, is successful site-targeted delivery (Olivier, 2005). Much work has been done in that direction by creating a benzimidazole cavitand **41** and investigating the host-guest properties of this water-soluble cavitand (Figure 41). Benzimidazole, a water-soluble cavitand, is incorporated in aqueous phosphocholine (PC) micelles, folds in the shape of a vase and acts as a small molecule host that has the ability to isolate hydrophobic guests selectively within its cavity (Biros *et al.*, 2004; Trembleau & Rebek, 2004; Schramm *et al.*, 2007; Javor & Rebek, 2011).

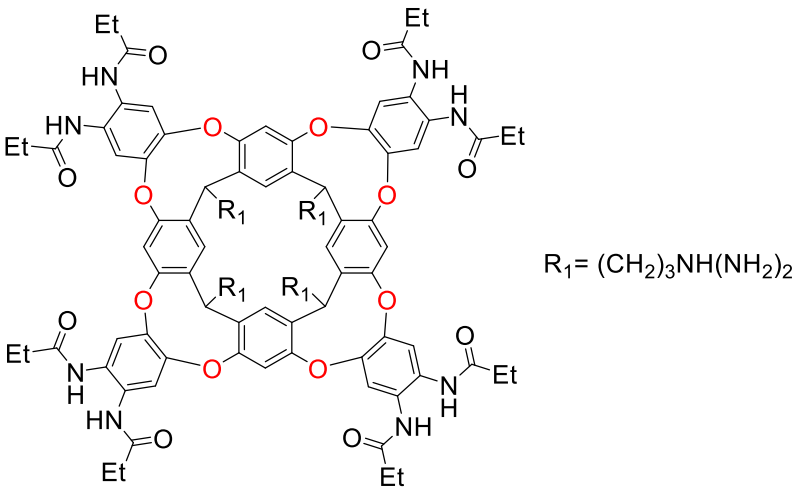

41

Figure 41: The structure of the calix[4]resorcinarene cavitand **41** (Javor & Rebek, 2011).

Solubility can significantly hamper drug delivery. The use of prodrugs as a chemical/biochemical approach aims to overcome this issue. A functional group that confers solubility in aqueous media can be cleaved to give the active drug by enzymatic reaction (Fleisher *et al.*, 1996; Stella & Nti-Addae, 2007). Aminoacid-derived prodrugs are often the best choice since they usually have increased solubility in aqueous media, the drug may be targeted towards a particular site *in vivo,* and they are usually stable (Vig *et al*., 2013). Due to the solubility and stability advantages, aminoacid conjugation provides a new approach in the field of drug and formulation development (Kim *et al*., 2009). A strategy was provided by Kashapov and co-workers to construct a water-soluble form of glycine *C*-methylcalix[4]resorcinarene **42** (Figure 42). Although there are a large number of hydroxyl groups in this compound it is still poorly soluble in water owing to intramolecular hydrogen bonds forming between the hydroxyl groups instead of the hydroxyl groups reacting with the solvent. Its water solubility can be increased by different approaches: first, by the ionization of hydroxyl groups on the

calix[4]resorcinarene under the action of alkali, and, second by exploiting a supramolecular approach, this benefits from the high water solubility of *N*-methylglucamine (Kashapov *et al.*, 2015).

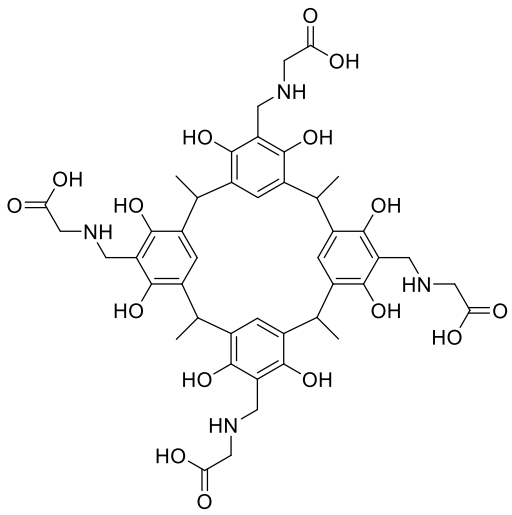

42

Figure 42 : Structure of glycine *C*-methylcalix[4]resorcinarene **42** (Kashapov *et al.*, 2015).

Although solvent particles are often encapsulated in the supramolecular structures, incorporating active pharmaceutical ingredients as guest molecules through a co-crystallizing process is still the main objective in facilitating targeted drug delivery. The biological availability, stability, solubility, and dissolution rates of the active pharmaceutical ingredients can be improved due to the drug co-crystallizing with supramolecular structures (Danylyuk & Suwinska, 2009). Gabapentin (Figure 43), 1-(aminomethyl)-1-cyclohexaneacetic acid, is a γ-aminobutyric acid analogue that is used as an inhibitor of neurotransmitters in the central nervous system. It is a well-known drug widely used to treat epilepsy and neuropathic pain and in the prevention of seizures. As hydrogen bonding plays such an important role in the formation of active pharmaceutical ingredients cocrystals, the use of calix[4]resorcinarenes and calix[4]pyrogallolarenes, with the presence of the upper

rim hydroxyls on the macrocycle, seemed to be a worthwhile choice with gabapentin as both molecules possess hydrogen bond donating and accepting sites. Gabapentin has been shown to from cocrystals with C-hexylcalix[4]resorcinarene, C-propylcalix[4]resorcinarene (Kumari *et al*., 2013), C-butylcalix[4]pyrogallolarene and C-propane-3-ol-calix[4]pyrogallolarenes (Fowler *et al.*, 2011; Spiel *et al.*, 2019).

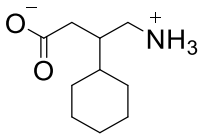

Figure 43: The molecular structure of gabapentin.

One of the strategies for the introduction of hydrophilic groups into the macrocycle in such a way as to decrease its toxicity is the usage of fragments of known biocompatible polymers, such as polyethylene glycol (PEG), polylactic acid and polycaprolactone. Amphiphilic tetraundecylcalix[4]resorcinarene **43**, bearing metoxypolyethylene glycole (mPEG) chains on the upper rim (Figure 44), has been synthesized and used to form nanoconjugates for drug encapsulation such as doxorubicin, naproxen, ibuprofen and quercetin. The obtained conjugate of this amphiphilic exhibits low hemotoxicity and shows promising potential for the use as a supramolecular drug-delivery system (Ermakova *et al*., 2018).

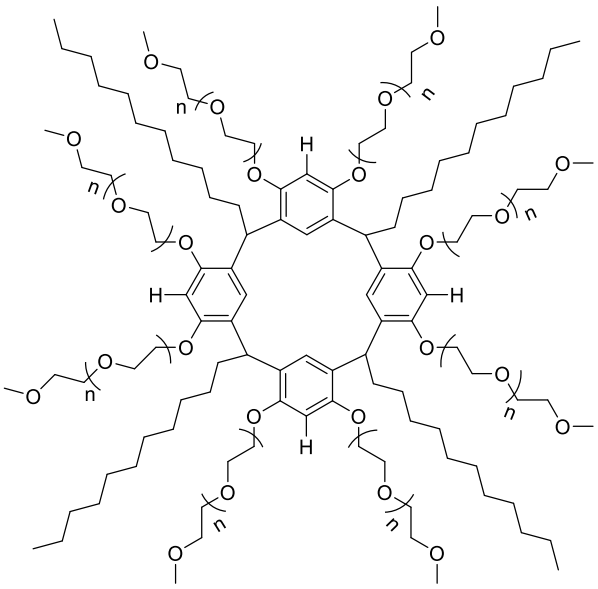

43

Figure 44: Structure of tetraundecylcalix[4]resorcinarene–mPEG conjugate **43** (Ermakova *et al*., 2018).

1.6 Aims and Objectives

The overall aim of this study is to investigate drug delivery for the hydrophobic drugs using novel calix[4]resorcinarene and calix[4]pyrogallolarene nanoparticles as drug carriers. There is clear evidence that calix[4]resorcinarenes and calix[4]pyrogallolarenes can be used for drug delivery, however, the hydrophobic cavity may only play a significant role when a specific drug molecule is present. In essence there is no one calix[4]resorcinarene or calix[4]pyrogallolarene derivative that is capable of acting as a solubilising agent to multiple different drug molecules. The goals were therefore:

- To synthesise four amphiphilic calix[4]resorcinarenes and two calix[4]pyrogallolarenes by attaching hydrophobic and hydrophilic moieties onto the calix[4]resorcinarene and calix[4]pyrogallolarene scaffolds which possess

deep hydrophobic cavities capable of associating with hydrophobic drug molecules of different sizes and physical attributes. These nanocarriers should not be so hydrophobic that they are insoluble in aqueous media themselves so any initial targets would have to bear charged residues.

- To synthesise four aminocalix[4]resorcinarenes by the condensation of calix[4]resorcinarenes with primary amines using the Mannich reaction.
- To synthesise two calix[4]resorcinarene-based cavitand derivatives which possess deep hydrophobic cavities and are soluble in aqueous media.
- To prepare and characterise the self-assemblies formed by the amphiphilic calix[4]resorcinarenes and calix[4]pyrogallolarenes in aqueous media.
- To load the nanocarriers with varied hydrophobic drugs and, hence, to determine the drug loading and the *in vitro* drug release.

In chapter 2, will be described the synthesis of water soluble calix[4]resorcinarenes and calix[4]pyrogallolarenes: resorcinol and 2-substituted resorcinols were chosen as starting material units, along with pentanal and octanal. These were condensed under standard conditions, forming the desired bowl-shape compounds with alkyl groups on the lower rim. The condensation reaction was carried out in ethanol as a solvent, in the presence of concentrated hydrochloric acid. The synthetic procedure for the expected calix[4]resorcinarenes and calix[4]pyrogallolarenes derivatives is summarized in Scheme 12. By using appropriately modified literature procedures (Fransen & Dutton, 1995) calix[4]resorcinarenes **44a-d**, and calix[4]pyrogallolarenes **44e-f** were completely *O*-alkylated through the reaction with methyl bromoacetate, and the resulting octa-esters calix[4]recorcinarenes **45a-d** and dodeca-esters calix[4]pyrogallolarenes, **44e-f** were transformed to the sodium salt derivatives, calix[4]recorcinarenes **46a-d** and calix[4]pyrogallolarenes **46e-f**. Further substitution

in the 2-position of the resorcinol units by Mannich reactions lead to the formation of tetrabenzoxazines (Arnecke *et al*., 1995; Beyeh *et al*., 2010), as described in chapter 4. Various derivatives can be obtained in excellent yields by Mannich reactions with secondary amines. The condensation of each resorcinol unit with the amine and formaldehyde occurs in a selective manner and includes two steps. The first is the usual Mannich aminomethylation, where the primary amine (*N,N*-dimethylethylenediamine or benzyl amine in the work reported here) undergoes ring closure by condensation with a second molecule of formaldehyde and one of the two adjacent hydroxyl groups on the upper rim of calix[4]resorcinarenes **44a and 44b** leading to the formation of the inherently chiral calix[4]resorcinarenes **58a-d**. The second step involves the removal of the *N,O*-acetal bridge producing aminocalix[4]resorcinarenes **59a-d** (Luostarinen *et al*., 2007). Calix[4]resorcinarenes with long-chain aliphatic aldehydes attached at the lower rim are amphiphilic, which means they contain a polar and non-polar region within the same molecule. The solubility of calix[4]resorcinarenes can be adjusted dependent upon the alkyl aldehyde used in the synthesis. The alkyl derivatives of calix[4]resorcinarenes can be made water soluble by adding polar or ionic groups at their upper rim (Helttunen, 2012).

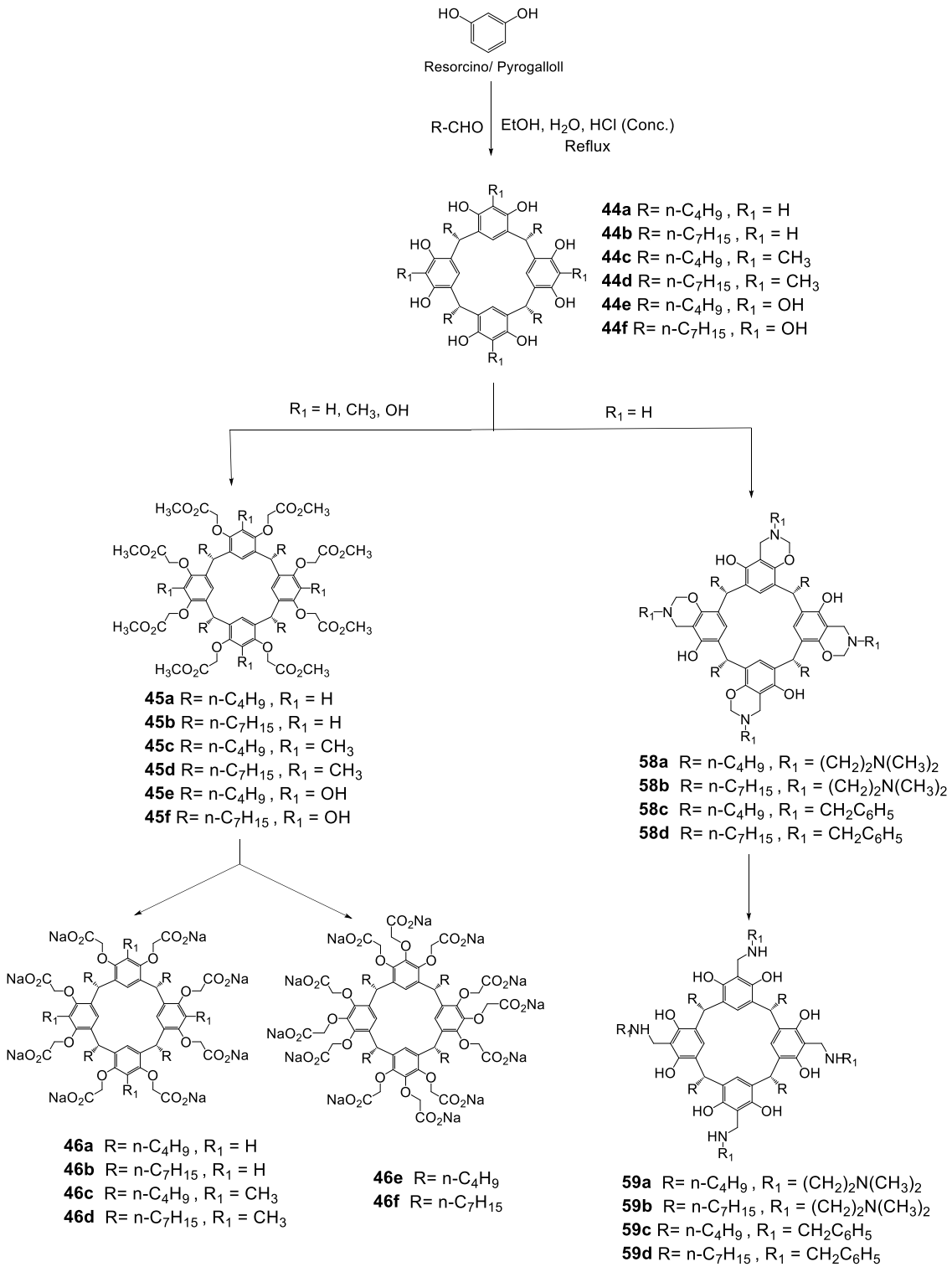

Scheme 12: Preparation of calix[4]resorcinarenes functionalized at the upper rim by *O*-alkylation and by Mannich reaction.

Chapter Two

Synthesis and Characterisation of Calix[4]resorcinarene and Calix[4]pyrogallolarene Nanocarriers and their Aggregation in an Aqueous Environment

2.1 Introduction

Calix[4]resorcinarenes and calix[4]pyrogallolarenes have been used as building blocks in the formation of host-guest complexes in solution. The bowl-shaped crown conformations of calix[4]resorcinarenes and calix[4]pyrogallolarenes have potential as molecular “vessels” for the preparation of polyfunctional host systems. Self-assembly of calix[4]resorcinarenes and calix[4]pyrogallolarenes depends on the nature of the substituents present, the length of any alkyl chains that are attached at the lower rim and the mobility and structure of their upper rim substituents. The solubility of these compounds can be enhanced by introduction of solubilizing groups at positions remote from the cavity.

The aim of this study focuses on the ability of amphiphilic calix[4]resorcinarene octa-sodium salts **46a-d** and calix[4]pyrogallolarene dodeca- sodium salts **46e-f** to form aggregates or ordered assemblies capable of solubilising hydrophobic compounds, especially drug molecules. Several series of calix[4]resorcinarene and calix[4]pyrogallolarene hosts bearing different length lower rim alkyl substituents (C_4 and C_7) were investigated. This chapter covers the synthesis and characterisation of these calix[4]resorcinarene and calix[4]pyrogallolarene ‘nanocarriers’ which possess deep hydrophobic cavities and hydrophobic lower rim environments that are potentially capable of associating with hydrophobic drug molecules of different sizes and physical attributes. Such nanocarriers should not be so hydrophobic that they are insoluble in aqueous media themselves. The amphiphilic nanocarriers were fully characterised using spectroscopy and physico-chemical measurements. Self-assembly and critical aggregation concentration (CAC) measurements of the amphiphilic carriers were carried out by using surface tension measurements, a UV hydrophobic probe and photon correlation spectroscopy (PCS). Aggregates were

characterised using PCS to give particle size, zeta potential and CAC. This can give an indication of their drug loading potential and, hence, vehicles for hydrophobic drug delivery. Their ability to act as drug solubilising agents will be investigated in later chapters, using the same techniques as used for characterisation of target compounds and their aggregation.

2.2 Nuclear magnetic resonance (NMR) spectroscopy

Nuclear magnetic resonance (NMR) spectroscopy is one of the most versatile analytical techniques. It used in research for determining the content and purity of a sample, as well as providing data for molecular structure identification. NMR experiments can be performed on the three main states of matter, liquid, solid, and gas (Polenova *et al.*, 2015). NMR can quantitatively analyse mixtures containing known compounds. With regards to modern pulsed Fourier Transform NMR techniques, there are many variants of NMR experiments, based upon the nucleus being observed and the pulse sequence employed, including: ^{1}H and proton-decoupled ^{13}C one-dimensional spectroscopy; two-dimensional ^{1}H-^{1}H correlation spectroscopy (COSY) which highlights the correlation between protons that are coupled to each other to establish proton connectivity; two-dimensional ^{13}C-^{1}H heteronuclear single quantum coherence (HSQC) spectroscopy to establish direct connectivity of protons to carbons, thereby establishing carbon types, is a C-H correlation experiment which uses detection of signals using an INEPT sequence. It shows higher resolution in the C-dimension than does the related HMQC experiment. Nuclear overhauser effect spectroscopy (NOESY) and rotating frame overhauser effect spectroscopy (ROESY) experiments provide information concerning

proton-proton correlation mediated by dipolar coupling (NOE effect), enabling the identification of protons that are close in space (Molyneux *et al.*, 2019).

2.3 Infrared (IR) spectroscopy

Infrared (IR) Spectroscopy is the analysis of how infrared light interacts with a molecule. IR Spectroscopy measures the vibrations of atoms, and based on this it is possible to determine the functional groups present and bonding in molecules. Generally, stronger bonds and bonds between lighter atoms will vibrate at a high stretching frequency (wavenumber) (EL-Azazy, 2018; Mollaoglu *et al.*, 2018). The infrared portion of the electromagnetic spectrum is usually divided into three regions: the far-IR (FIR, 400–10 cm^{-1}, 25–300 μm); the mid-IR (MIR, 4000–400 cm^{-1}, 2.5–25 μm); the near-IR (NIR, 14,000–4000 cm^{-1}, 0.7–2.5 μm) (Figure 45).

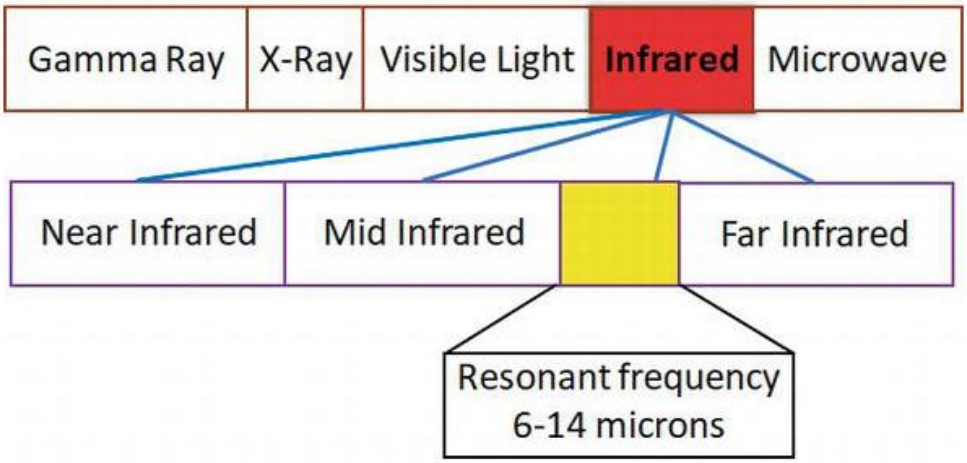

Figure 45: the electromagnetic spectrum showing regions of IR (EL-Azazy, 2018).

2.4 Mass Spectrometry

Mass spectrometry is an instrumental method that chemists use to analyse compounds, which involves ionization of a sample followed by separating and quantitative detection of the charged ions according to their mass/charge (m/z) ratio (Hoffmann & Stroobant, 2007). A number of ionisation methods and detection and analysis techniques are available. The ions produced may be energetically unstable and some will decompose into smaller ions. Only charged species are observed in the mass spectrum so any neutral fragments or free radicals are not observed (Murray *et al.*, 2013).

2.5 Particle Size Analysis of Aggregation

Amphiphilic molecules in aqueous systems have a tendency to form organized assemblies of different shape and size in solutions above a threshold concentration known as the critical aggregation concentration (CAC). Amphiphilic molecules exhibit various states of molecular aggregation, such as spherical and non-spherical micelles, vesicles, and lyotropic liquid crystalline structures, which primarily depends on the molecular structure of the amphiphile. Non-ionic surfactants generally will have much lower CAC values and higher aggregation numbers than that of ionic surfactants, whereas anionic surfactants have slightly lower CAC values than cationic surfactants (Holmberg *et al.*, 2002). Environmental factors such as surfactant concentration, temperature, pH, and ionic strength also have a profound effect on aggregate formation(Fuhrhop & Helfrich, 1993; Mohanty *et al.*, 2007).

2.6 Zeta Potential

One of the key factors that maintain the stability of colloidal systems is electrostatic repulsion resulting from surface charges. According to DLVO electrostatic theory, the stability of emulsions and colloids is a balance between attractive Van der Waals forces and electrical repulsion due to the net surface charge (Derjaguin & Landau, 1941; Verwey & Overbeek, 1948). Zeta potential represents the surface charge of nanoparticles and reflects their long-term stability. Generally, colloid particles are stable at a high value of zeta potential (either positive or negative), typically more than ±30 mV (Gumustas *et al.*, 2017).

2.7 Photon Correlation Spectroscopy in Nanoparticle Size and Zeta Potential Determination

Dynamic light scattering technique (DLS), also known as photon correlation spectroscopy (PCS), is a powerful technique used to determine the hydrodynamic size of particles or macromolecules in solution. When a beam of light passes through the desired solution and hits small particles contained within it, the light scatters in all directions provided the particles are small enough compared to the wavelength of the light used. This scattering of electromagnetic radiation by liquids and solutions can provide information about the particle size and structure. Light scattering results from the differences of refractive index of adjacent components within the mixture caused by some conditions such as random thermal motion, and density and concentration fluctuations. The frequency distribution of the scattered light is broadened more than the incident wave as a result of Brownian motion of components in the solutions and mixtures, known as frequency broadening. The Brownian motion of particles

becomes faster when the size of the particles scattering light are smaller. Such frequency broadening gives rise to the dynamic light scattering. Photon correlation spectroscopy (PCS) has been widely employed for measuring the size and (in some cases) the shapes of nanoparticles in liquids (Wilczura-Wachnik, 2007). One of the recent advances of PCS is the ability for measuring accurate autocorrelation functions covering 12 decades in delay time (i.e. from~12.5 ns to ~104 seconds) that allows the practical application of PCS to study dilute polymer solutions as well as proteins, micelles, emulsions, nanoparticles or colloids (Urban & Schurtenberger, 1998). PCS allows the measurement of particles and aggregates with a hydrodynamic radius of down to 0.5 nm.

The polydispersity index (PDI) is basically a representation of the distribution of size populations within a given sample. The numerical value of PDI ranges from 0.0 for a perfectly uniform sample with respect to the particle size, to 1.0 for a highly polydisperse sample with multiple particle size populations.

2.8 Critical Aggregate Concentration Determination

Aggregates in suspension are characterized by the measurement of turbidity, CAC and aggregate size. The value of the CAC can be determined using a variety of physicochemical methods, including conductivity (Wu et al., 2014), surface tension (Matam et al., 2004) and fluorescence techniques (Domínguez et al., 1997). Dynamic light scattering (DLS) can be used for the characterization of particle size, possible mode of aggregate and charge. Dynamic light scattering (DLS) can be also used to determine the critical micelle concentration (CMC), and study the influence of surfactant concentration and dispersant conditions on micelle size.

2.8.1 Surface Tension

Surface tension is a measure of the cohesive forces between molecules in liquid phase or molecules in solution. In bulk solutions molecules are interacting equally with each other in all directions, but at the surface a net inward force pulls the molecules toward the bulk because such molecules do not have the same environment. When the surface area of an aqueous solution is increased, more molecules of the solute will be at the surface. There are three factors affecting the surface tension: temperature (Vargaftik *et al.*, 1983), pressure and impurities (Jasper, 1972). Surface tension decreases almost linearly with a rise in temperature: The molecular thermal activity is increased with increasing temperature that leads to a decrease in cohesive interaction, which results in a decrease in surface tension. Adding impurities such as amphiphilic surfactants molecules in a pure liquid affects the surface tension. Surfactants reduce the surface tension between two distinct phases, such as water-air or water-oil, due to their amphiphilic nature or surface activity (Burlatsky *et al.*, 2012). In aqueous solution, when some of the water molecules are replaced by the surfactant interaction forces between surfactant and water are less than between two water molecules. This causes a decrease in surface tension (Lauren, 2017). At low surfactant concentration the surfactant molecules arrange on the surface. With increasing concentration of surfactant the number of surfactant molecules on the surface also increases, which causes a decrease in the surface tension of the solution until the surface becomes saturated. At this point the addition of the surfactant molecules will lead to the formation of micelles (Mukerjee, 1971).

2.8.2 Conductivity Methods

Micellar systems are studied traditionally by determining the conductivity of a solution of molecules potentially capable of forming micelles. Conductivity is most often used to determine the critical aggregate concentration (CAC) of ionic micellar systems, which is derived from the plot of conductivity (κ) versus concentration of the ionic surfactant solution, with the point of curvature corresponding to the CAC (Nesmerakk & Nemcova, 2006).

2.8.3 UV Hydrophobic Probes

Methyl orange has been used as a hydrophobic probe to investigate the assembly of surfactant aggregates in an aqueous environment. Methyl orange prefers to localise within the surfactant assemblies when it is exposed to water resulting in a hypsochromic shift of the λ_{max} (the wavelength of maximum UV absorbance) of methyl orange when irradiated with UV light.

2.9 Synthesis and Characterisation of water-soluble Calix[4]resorcinarenes and Calix[4]pyrogallolarenes

2.9.1 Synthetic Strategy

Calix[4]resorcinarene octa-salts **46a-d** and calix[4]pyrogallolarene dodeca-salts **46e-f** and their parent compounds were synthesised using adaptations of established procedures, outlined in Scheme 13. The structures of these compounds were determined using a variety of spectroscopic and spectrometric techniques, including FTIR and NMR spectroscopy, and mass spectrometry. Their physicochemical properties were also investigated using a variety of techniques.

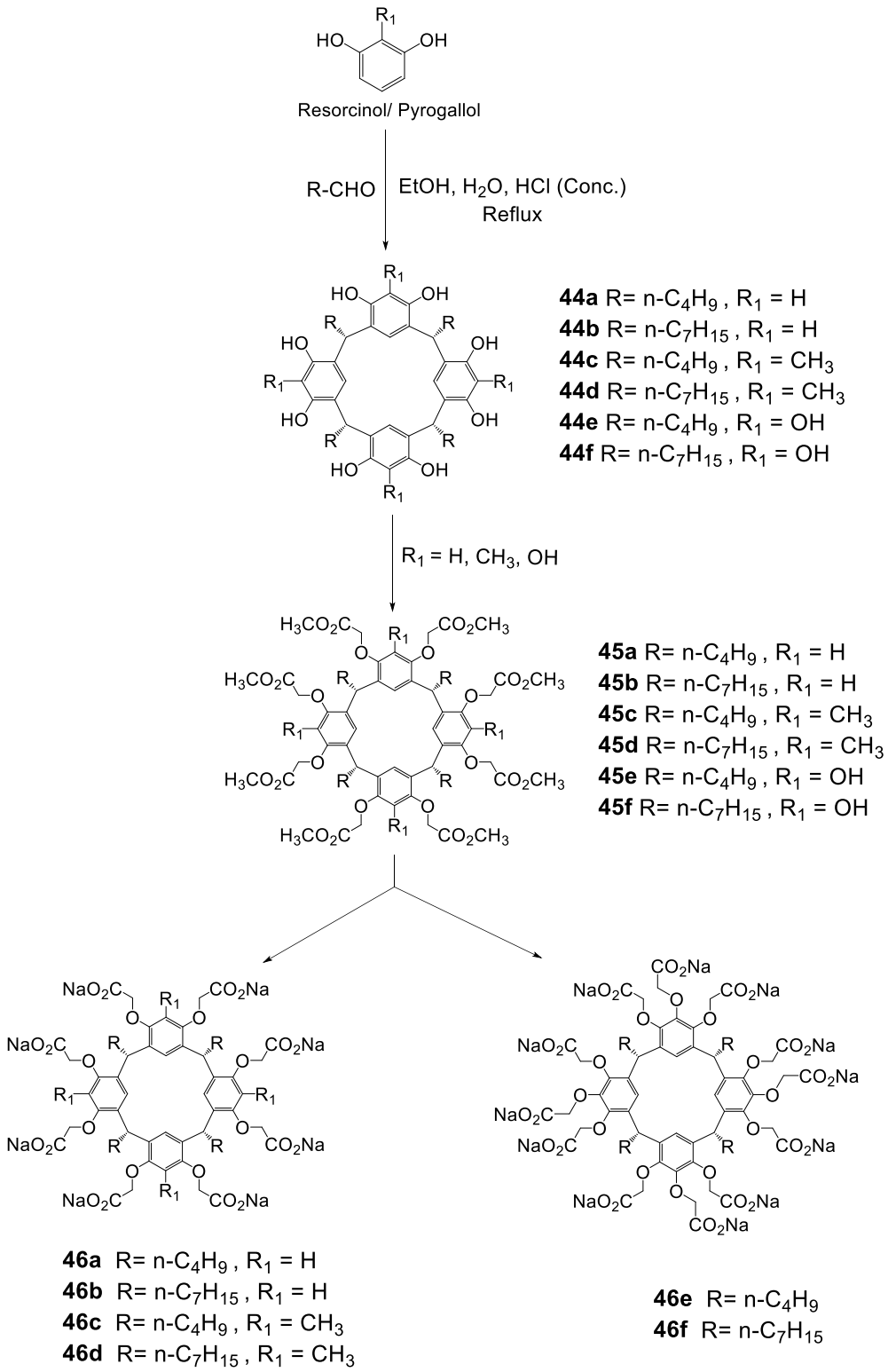

Scheme 13: Preparation of calix[4]resorcinarenes and calix[4]pyrogallolarenes functionalized at the upper rim by *O*-alkylation.

2.9.1.1 Solubility Measurements

The solubility of sodium salts **46a-d** and **46e-f** in distilled water was measured at room temperature (20 ºC). Three replicate measurements were performed and the solubility obtained is the average of these results. The solubility of each compound was obtained by following this procedure: A small amount of each compound was added to 1.0 mL of distilled water, stirring gently until the compound had dissolved. Addition was continued until the aqueous solution was saturated. The solubility can thus be calculated directly.

2.9.1.2 Analysis of Compounds in Aqueous Solution

Dilute solutions (0.1 mg/mL, 1.0 mg/mL, 5.0 mg/mL) of calix[4]resorcinarene octa-sodium salts **46a-d** and calix[4]pyrogallolarene dodeca-sodium salts **46e-f** in deionised water were prepared. The formation of aggregates, which may include ordered self-assembled species, was promoted using probe sonication for 10 minutes. Particle size, size distribution (polydispersity index, PDI), surface charge (zeta-potential) and conductivity measurements were determined using a Zetasizer Nano-ZS photon correlation spectrometer, Malvern Instruments, UK. All measurements were performed in triplicate at 25 °C and an average value was determined.

2.9.1.3 Critical Aggregation Concentration CAC

2.9.1.3.1 UV Hydrophobic Probe

This method was adjusted from that described by Uchegbu (Uchegbu *et al.*, 2001): An aqueous solution of methyl orange (25 µM) in sodium tetraborate buffer (0.02 M, pH 9.4) was prepared to be used as a diluent in the preparation of a series solutions of concentrations (10 mg/mL - 0.0195 mg/mL) of calix[4]resorcinarene octa-salts **46a-**

d and calix[4]pyrogallolarene dodeca-salts **46e-f**. All diluted samples were sonicated using a probe sonicator for 5 minutes using a Soniprep 150 (Wolflabs, Pocklington, UK) to aid the formation of aggregates. After cooling to room temperature the samples were placed in a spectrophotometer (UV-2600 UV-VIS spectrometer (Shimadzu, Germany) to record the UV-visible spectra of the samples from 350 nm to 600 nm in order to identify their maximum absorbance (λ_{max}). The aqueous methyl orange stock solution was used as a control.

2.9.1.3.2 Surface Tension

A series of solutions of particular concentrations (6 mg/mL- 0.00192 mg/mL) of calix[4]resorcinarene octa-salts **46a-d** and calix[4]pyrogallolarene dodeca-salts **46e-f** were made up in deionised water. After sonication for 5 minutes using a probe sonicator and cooling to room temperature, the surface tension was measured using a torsion balance (Torsion Balance Supplies, Weston-super-Mare, UK) calibrated with deionized water at 25 °C. The platinum ring and platform were cleaned before each measurement using ethanol and deionised water to remove any residual deposits. Calibration with deionised water was performed between each measurement to ensure that samples were not contaminated. The measurements for each solution were conducted in triplicate to check for repeatability and to obtain an average value within an error of (≤ ± 1 N/m).

2.9.1.3.3 Conductivity

A series of solutions of particular concentrations (5 mg/mL- 0.0192 mg/mL) of calix[4]resorcinarene octa-salts **46a-d** and calix[4]pyrogallolarene dodeca-salts **46e-f** were made up in deionised water. After sonication for 5 minutes using a probe sonicator and cooling to room temperature, the conductivity was measured using a

photon correlation spectrometer (PCS) on a Zetasizer Nano-ZS, Malvern Instruments, UK. All measurements were performed in triplicate at 25 °C and an average value was determined.

2.10 Results

2.10.1 Synthesis of c-Alkyl Calix[4]resorcinarene octa-sodium Salts and c-Alkyl Calix[4]pyrogallolarenes dodeca-sodium Salts

The first step involved the preparation of calix[4]resorcinarenes **44a-44d** and calix[4]pyrogallolarenes **44e-44f** via acid catalysed condensation and cyclization of resorcinol and its derivatives (2-methyl and 2-hydroxyl (pyrogallol)) with an aldehyde (pentanal and octanal, respectively) in a mixture of refluxing concentrated aqueous hydrochloric acid and ethyl and ethanol using a modification of literature methods (Cram *et al.*, 1988; Tunstad *et al.*, 1989; Timmerman *et al.*, 1996) (Scheme 13). The products were purified by means of recrystallization from acetonitrile. These derivatives were characterized using FTIR spectroscopy, ^{1}H NMR and ^{13}C NMR spectroscopy experiments and mass spectrometry. The spectroscopic data obtained for calix[4]resorcinarenes **44a**-**b** and calix[4]pyrogallolarenes **44e**-**f** agreed with that reported previously elsewhere (Bowley, 2008; Darvish & Khazraee, 2014; Hoskins *et al.*, 2016; Momose & Bosch, 2010; Tunstad *et al.*, 1989). In particular, the FTIR spectrum for **44c** and **44d** showed hydroxyl group stretches at 3384 cm^{-1} (O-H) and 1260 cm^{-1} (C-O), and evidence of the alkyl substituents and the aromatic ring. The ^{1}H NMR spectrum showed resonance signals for the aromatic hydrogen atoms (δ = 7.28 ppm), the methylene bridge fragments (δ = 4.18 ppm) and methyl moieties on the aromatic ring (δ = 1.93 ppm). The attributions of the signals in the ^{13}C NMR

spectra were also determined. It can be assumed that all compounds were obtained in the crown conformation (*rccc* conformation), as evidenced by the ^{1}H NMR spectrum. It is known that the main factor stabilizing the "cone" conformation in parent calix[4]resorcinarene is the existence of intramolecular hydrogen bonds between the resorcinol fragments (Volkmer *et al.*, 2002). Depending on the substituents present on the upper- and lower-rims of calix[4]resorcinarenes and calix[4]pyrogallolarenes, several isomeric forms (*rccc*, *rctt, rcct,* and *rtct*) are accessible for both of them. The *rccc* (c_{4v}) isomer of calix[4]resorcinarenes and calix[4]pyrogallolarenes bearing alkyl substituents at the lower rim are readily accessible from the condensation of aldehydes with the corresponding resorcinol derivative in refluxing ethanolic hydrochloric acid. This conformational preference can be deduced from their ^{1}H NMR spectrum. For example, in calix[4]resorcinarene **44c** with crown conformation, the aromatic proton H_5, the benzylic H_6, and phenolic protons H_7 show as singlets at δ = 1.93, 7.28 and 8.69 ppm, respectively (Figure 46). Clearly we can see that when calix[4]resorcinarenes exist in the crown conformation, the NMR spectra are simplified due to the inherent symmetry of the compounds.

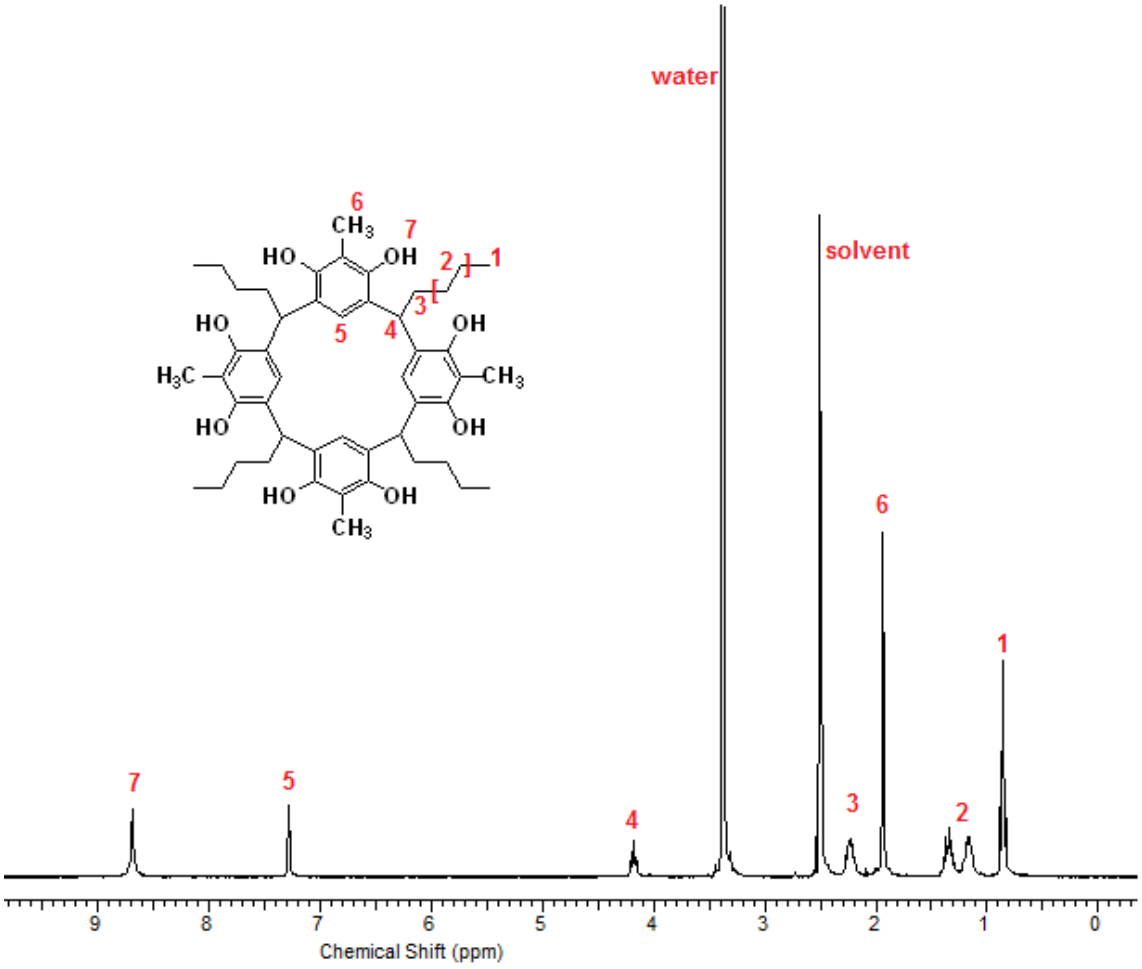

Figure 46: ^{1}H NMR spectrum of calix[4]resorcinarene **44c** in DMSO-d_6 carried out at 300 MHz at 25 °C.

Functionalization of these products on the phenolic hydroxyl groups hydroxyl groups was performed by reacting each compound with methyl bromoacetate in in the presence of potassium carbonate as base to give calix[4]resorcinarene-octacetate **45a-d** and calix[4]pyrogallolarene-dodeca acetate **45e-f** respectively, again following established procedures (Bazzanella *et al.*, 1997; Elidrisi *et al.*, 2015; Gao *et al.*, 2013). The ^{1}H NMR data corresponded to the reference data in the literature (Arduini *et al.*, 1986; Fransen & Dutton, 1995; Podyachev *et al.*, 2009; Zhou *et al.*, 2010; Daschbach *et al.*, 2011). The ^{1}H NMR data of the functionalized **45a-f** were similar to those of **44a-f**, except that **45a-f** showed signals at (δ = 3.8 ppm) and (δ = 4.18 ppm)

for the methylene groups. The substitution of the hydroxyl protons by the carboxymethyl groups could promote a change in the conformation of the calix structure, with a conformer with C_{2v} symmetry appearing in solution (Pod *et al.*, 2003). However, the crown *rccc* conformation was obtained in our study (Harrisc *et al.*, 1991).

Compounds **45a-45f** were then reacted with sodium hydroxide in THF solution to obtain calix[4]resorcinarene octa-sodium salts **46a-d** (Figure 47-50) and calix[4]pyrogallolarene dodeca-sodium salts **46e-f** (Figure 51 and 54). The ^{1}H NMR data of compounds **46a-f** were similar to those of **45a-f**. However, the aromatic proton on C_5 was not clear in the ^{1}H NMR spectra due to H/D exchange in D_2O, in particular for calix[4]pyrogallolarenes **46e-f** (Figure 51 and 53). However, the ^{13}C NMR spectra of these compounds (Figure 52 and 54) showed all the aromatic carbon signals.

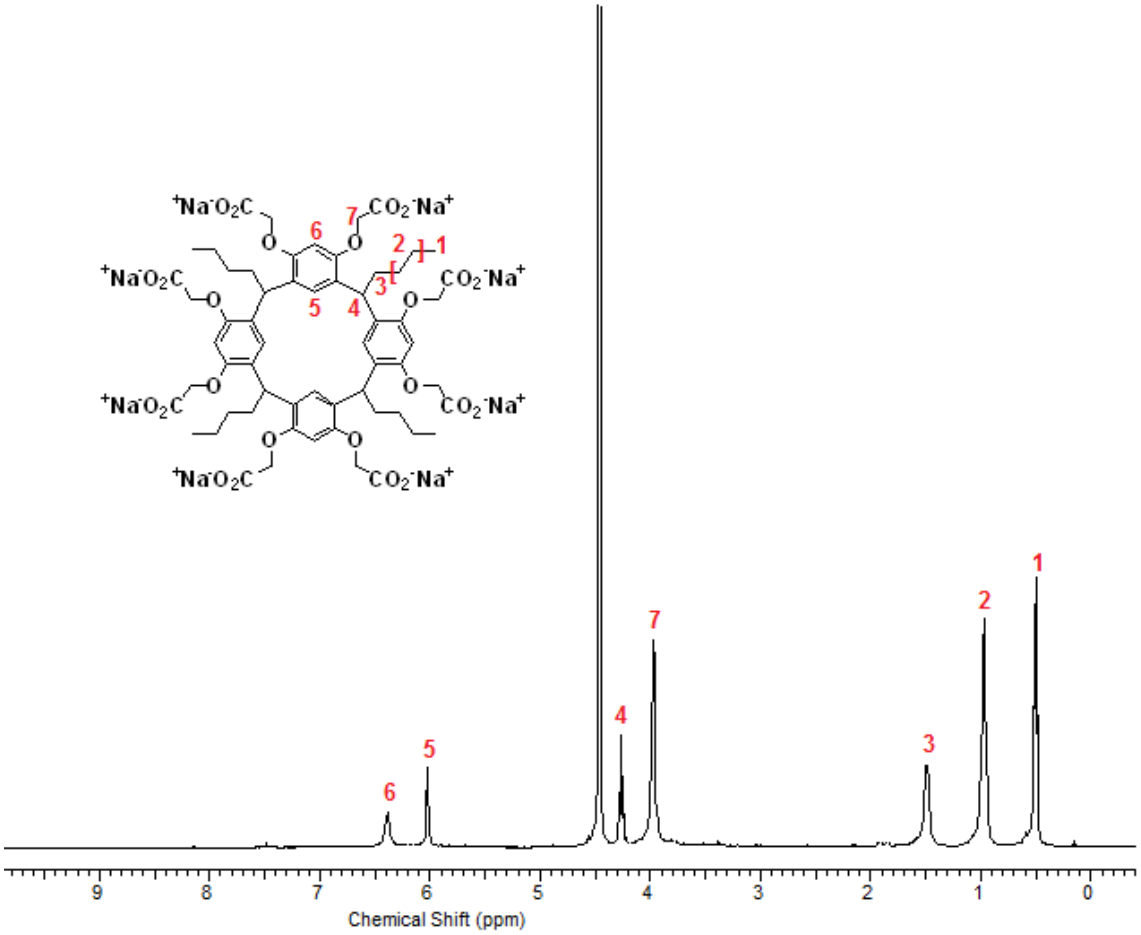

Figure 47: ^{1}H NMR spectrum of calix[4]resorcinarene octa-sodium salt **46a** in D_2O at 300 MHz at 25 °C.

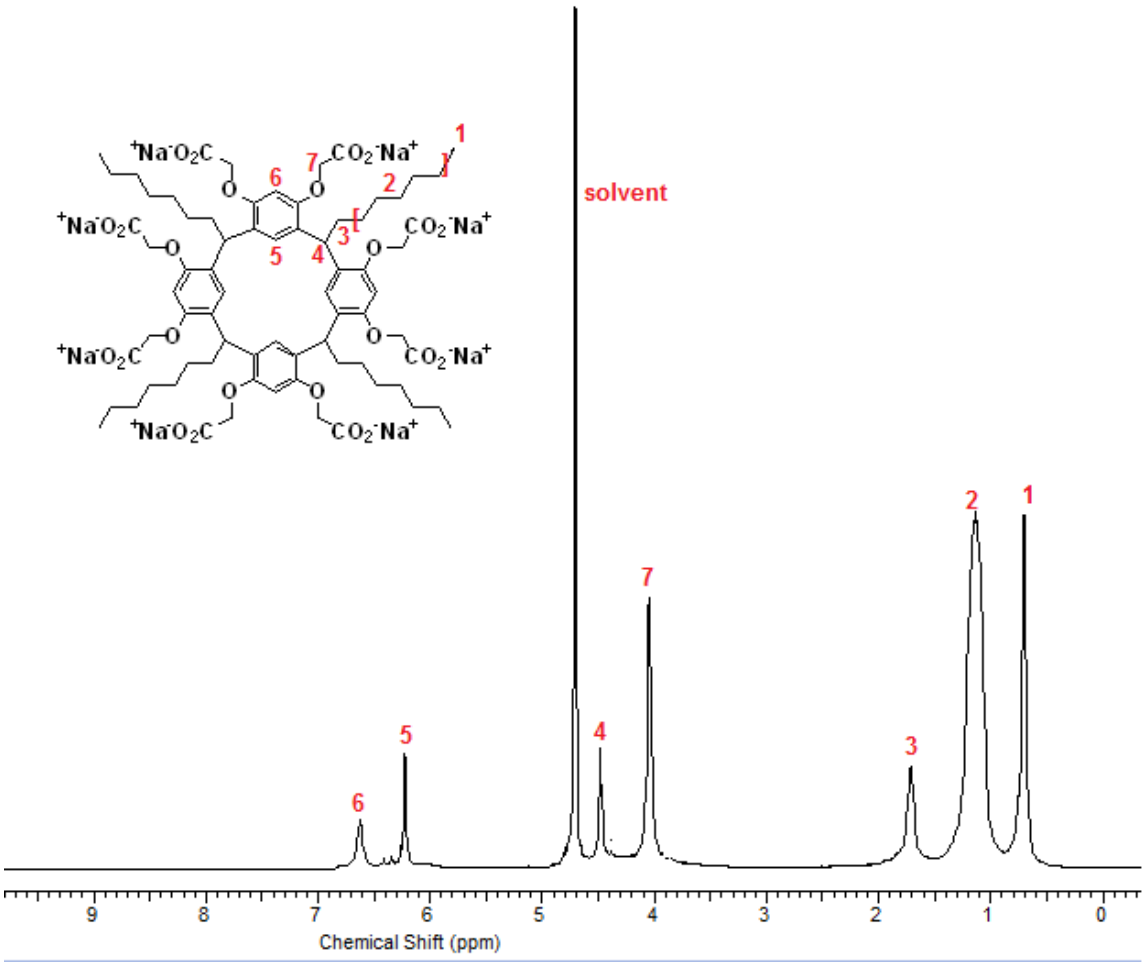

Figure 48: ^{1}H NMR spectrum of calix[4]resorcinarene octa-sodium salt **46b** in D_2O at 300 MHz at 25 °C.

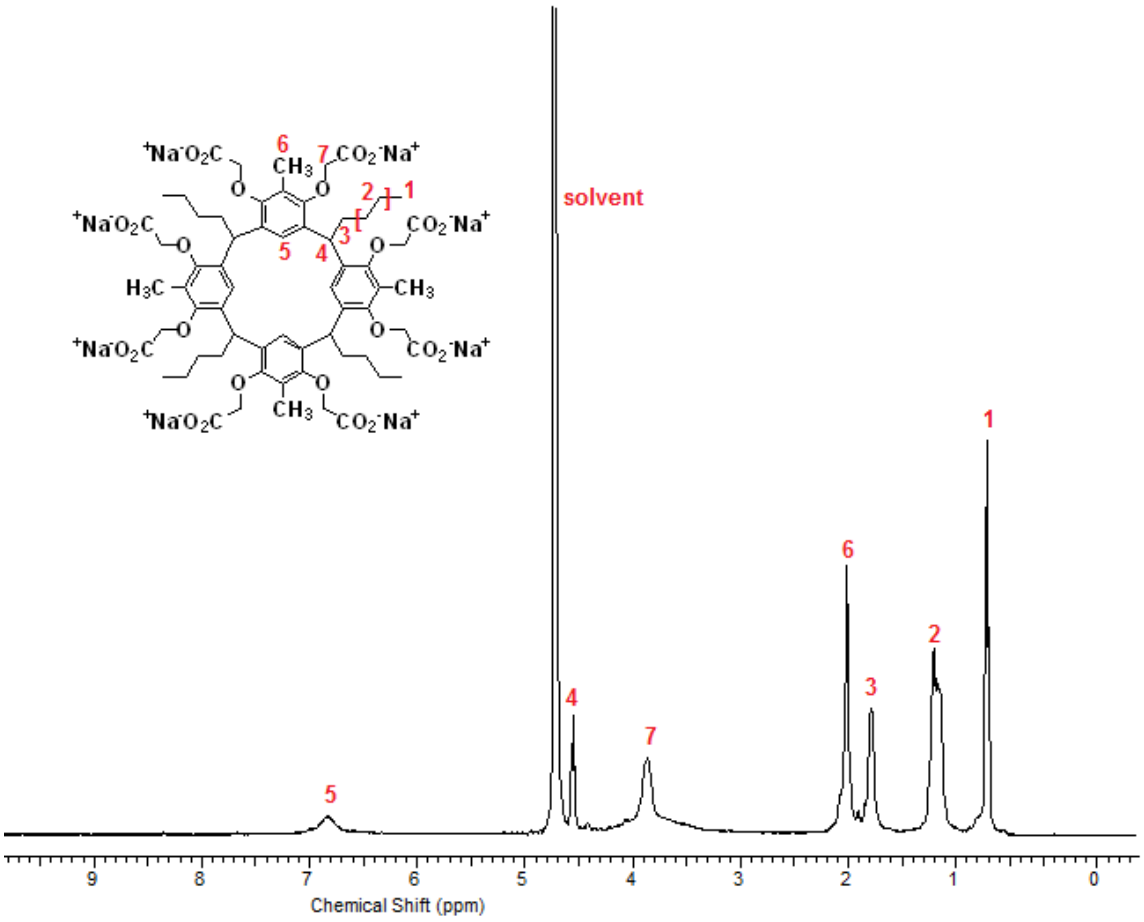

Figure 49: ^{1}H NMR spectrum of calix[4]resorcinarene octa-sodium salt **46c** in D_2O at 300 MHz at 25 °C.

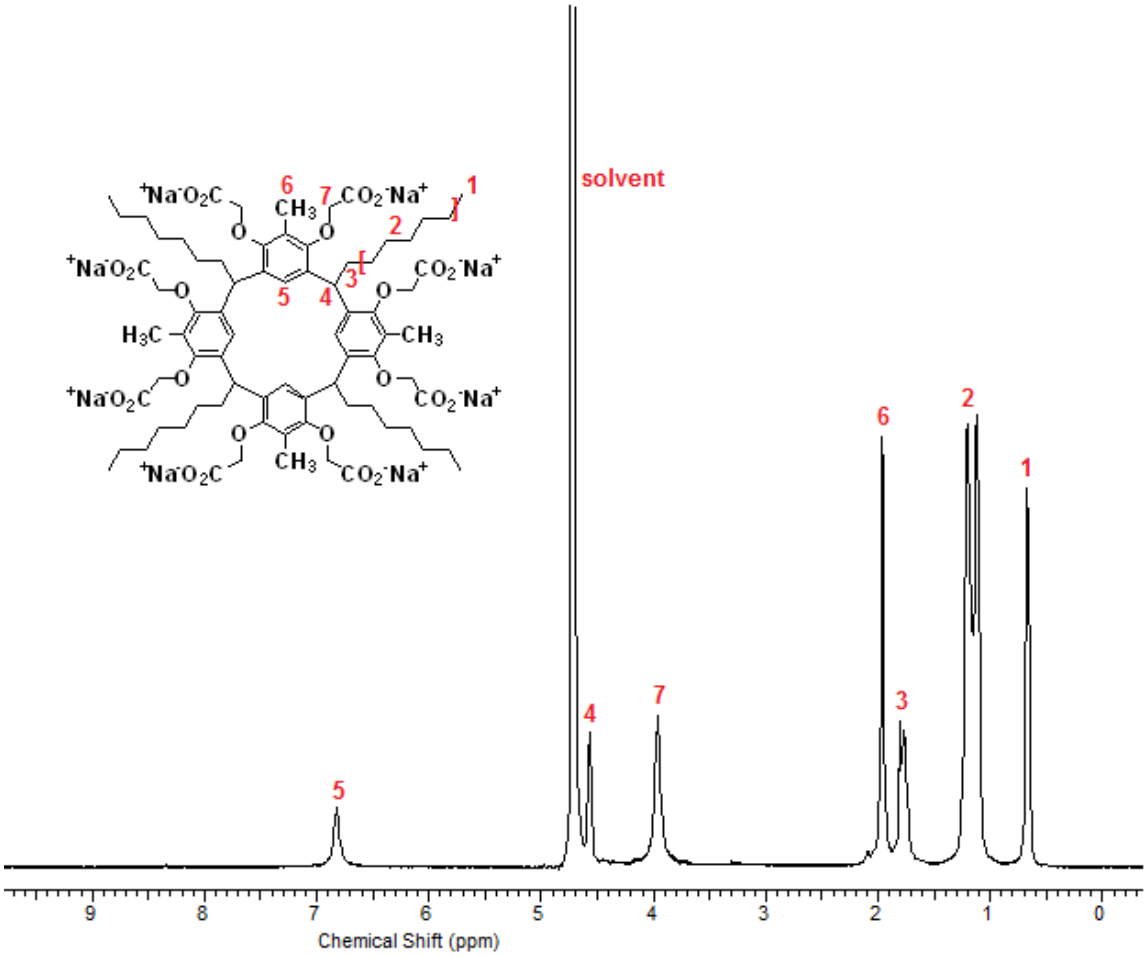

Figure 50: ^{1}H NMR spectrum of calix[4]resorcinarene octa-sodium salt **46d** in D_2O at 300 MHz at 25 °C.

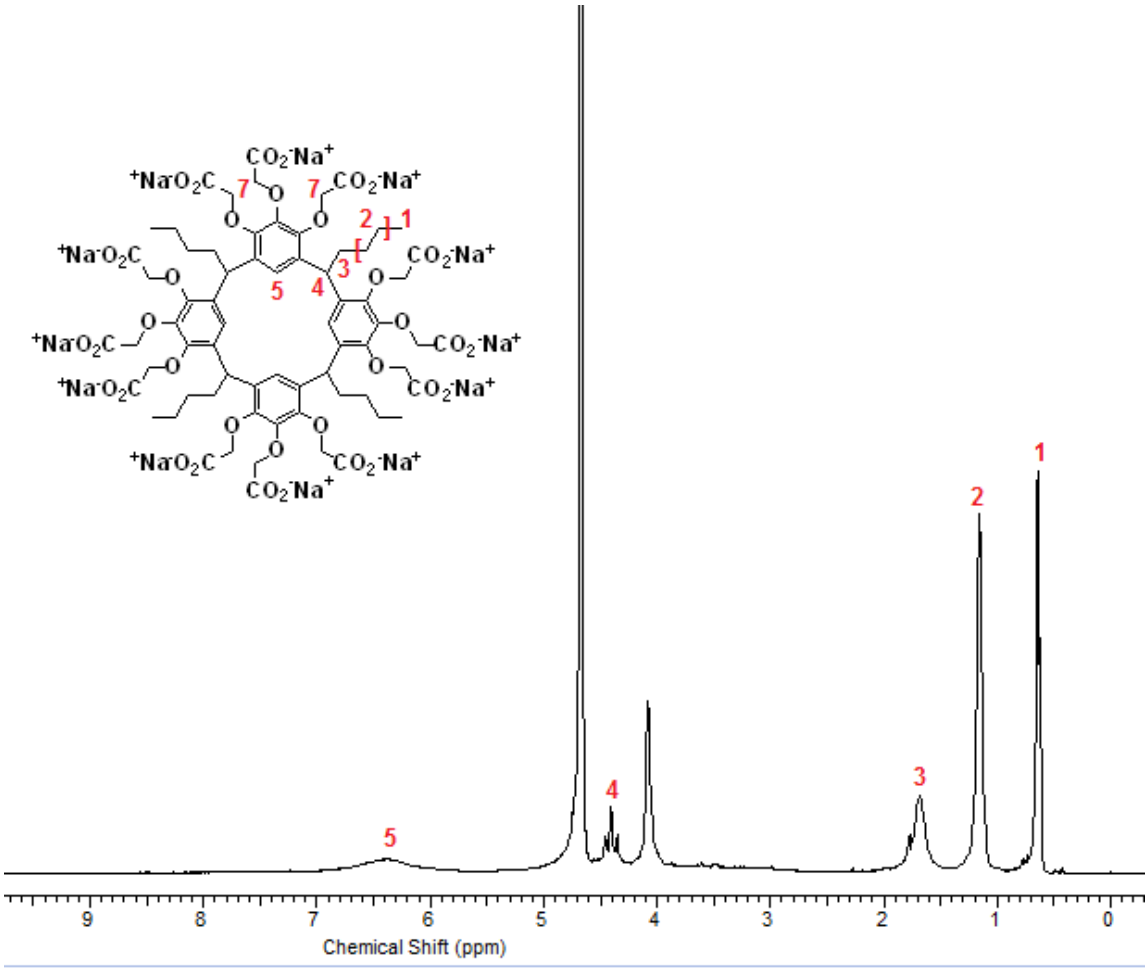

Figure 51: ^{1}H NMR spectrum of calix[4]pyrogallolarene dodeca-sodium salt **46e** in D_2O at 300 MHz at 25 °C.

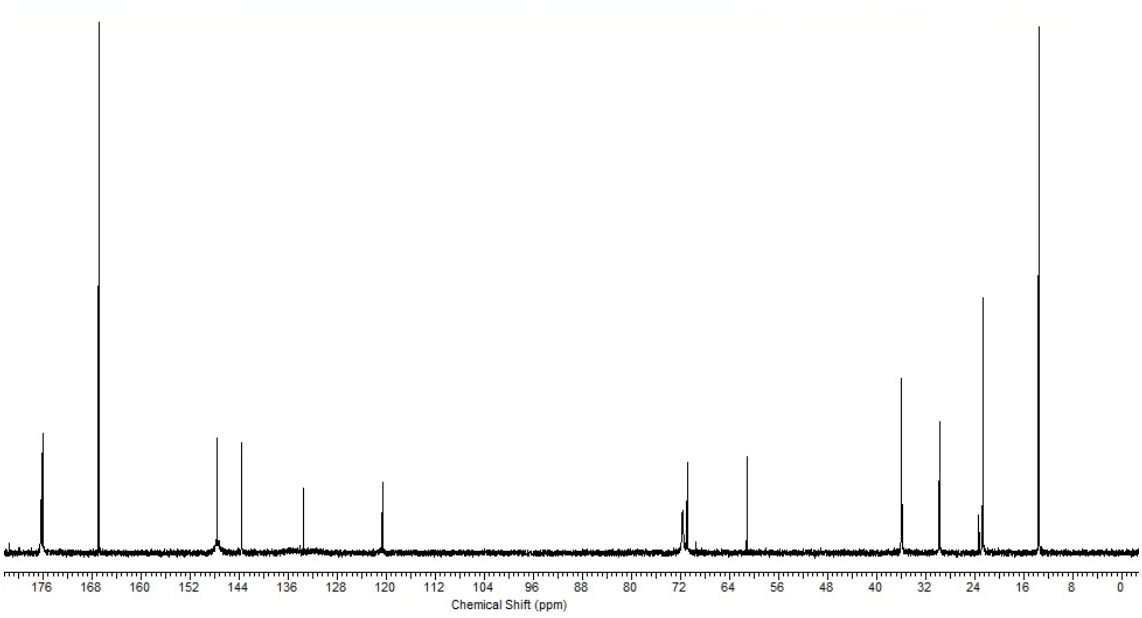

Figure 52: ^{13}C NMR spectrum of calix[4]pyrogallolarene dodeca-sodium salt **46e** in D_2O at 75 MHz at 25 °C.

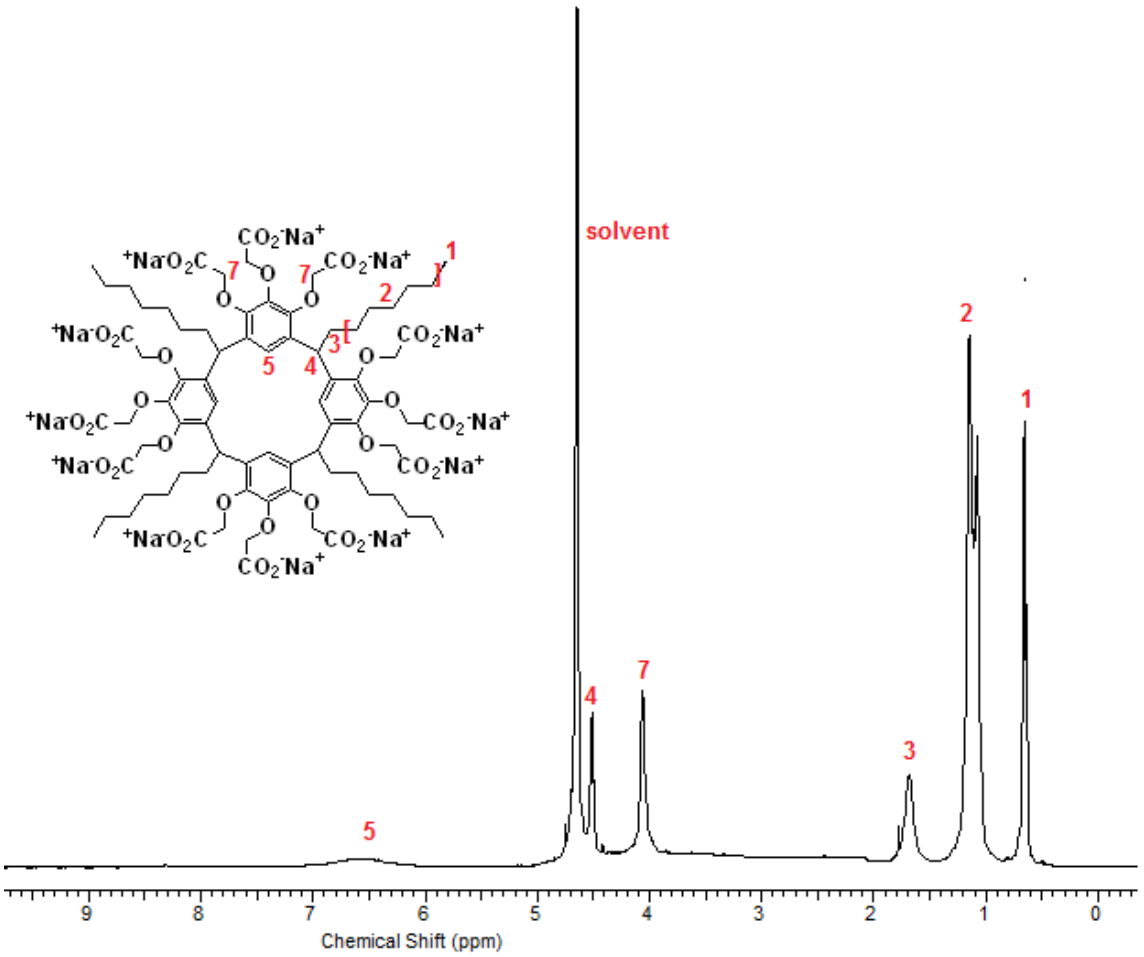

Figure 53: ^{1}H NMR spectrum of calix[4]pyrogallolarene dodeca-sodium salt **46f** in D_2O at 300 MHz at 25 °C.

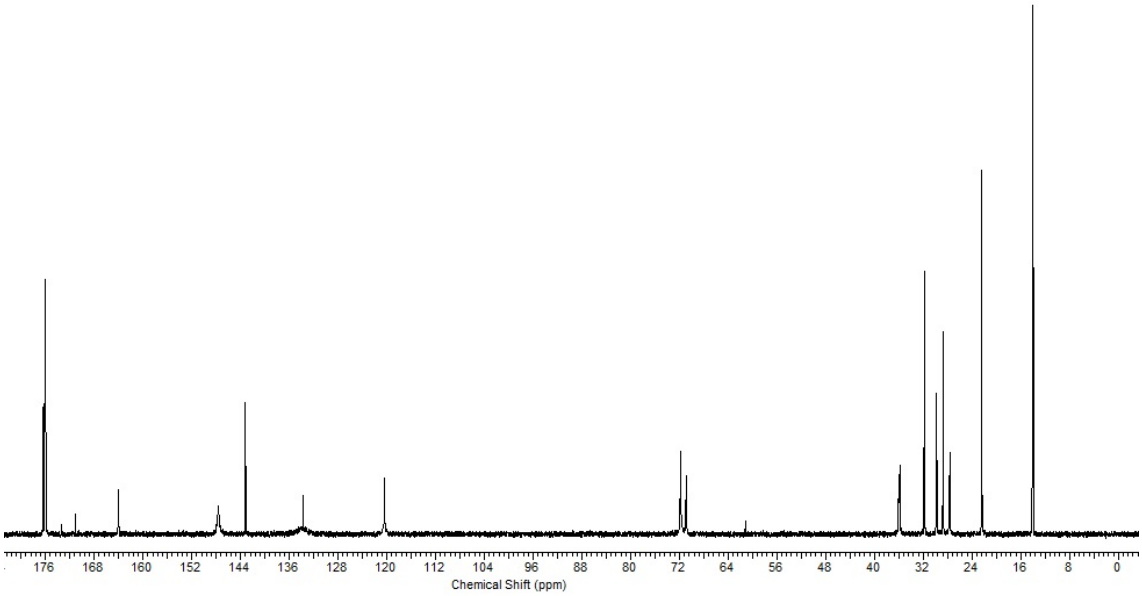

Figure 54: ^{13}C NMR spectrum of calix[4]pyrogallolarene dodeca-sodium salt **46f** in D_2O at 75 MHz at 25 °C.

2.10.2 Solubility

Solubility indicates the maximum amount of a substance that can be dissolved in a solvent at a given temperature. The solubility of all amphiphilic calix[4]resorcinarene salts **46a-d** and calix[4]pyrogallolarene salts **46e-f** in deionised water is greater than 0.5 g/ mL.

2.10.3 Photon Correlation Spectroscopy

2.10.3.1 Particle Size and Zeta Potential

It is known that the ability of amphiphilic calix[4]resorcinarenes to form aggregates depends on the size of their hydrophobic portion, in this case the alkyl residues on the lower rim of calix[4]resorcinarene salts **46a-d** and calix[4]pyrogallolarene salts **46e-f** (Cheipesh *et al.*, 2014; Morozova *et al.*, 2010). The particle size and the zeta potential of aggregates in solutions of calix[4]resorcinarene salts **46a-d** and

calix[4]pyrogallolarene salts **46e-f** at different concentrations (0.1 mg/mL, 1 mg/mL, and 5 mg/mL) of the amphiphiles were determined using dynamic light scattering.

For the carrier **46a**, before filtration of the sample the hydrodynamic radius of aggregates observed decreased as the concentration of carrier **46a** increases, from 221.6 nm at 0.1 mg/mL to 190.7 nm at 1 mg/mL. However, the hydrodynamic radius then increased to 257.7 nm at 5 mg/mL (Table 2). The polydispersity index (PDI), which is an indication of the size distribution of the aggregates observed (Danaei *et al.*, 2018) shows that the mixtures analysed are not homogeneous systems and other, typically larger aggregates are observed (Figure 55) (Ruozi *et al.*, 2005). Note that the sign of the zeta potential is negative for all carriers investigated, confirming the presence of carboxyl groups on the surface of the aggregates formed in solution, and decreases steadily in magnitude to more negative values as the concentration increases. This is to be expected for aggregates that have dense carboxylate functionality on the surface. The zeta-potential of aggregates of compound **46a** ranged from -44 mV to -54 mV which corresponds to stable aggregate systems (Table 2).

Table 2**:** Hydrodynamic radius and polydispersity index analysis for solutions (0.1 mg/mL, 1 mg/mL, and 5 mg/mL) of compound **46a** before filtration. Samples were recorded in triplicate at 25°C.

Compound	Concentration mg/mL	Radius nm (± SD): Percentage occurrence	PDI	Zeta Potential
Calix[4]-resorcinarene **46a**	0.1	221.6 (8.4): 62 % 2767.3 (30.6): 38 %	0.577 (0.049)	-44.5 (1.40)
	1	190.7 (11.6): 93 % 2464 (20.9): 7 %	0.433 (0.105)	-47.6 (0.70)
	5	257.7 (11.5): 75 % 2031 (15): 25 %	0.436 (0.029)	-54.4 (0.46)

The particle size correlation charts for carrier **46a** (Figure 55) shows the self-assemblies formed are not all of uniform size and that two size populations are present in solution. The most significant peak between 191- 258 nm indicates that the majority of the aggregates in solution exist within this size range.

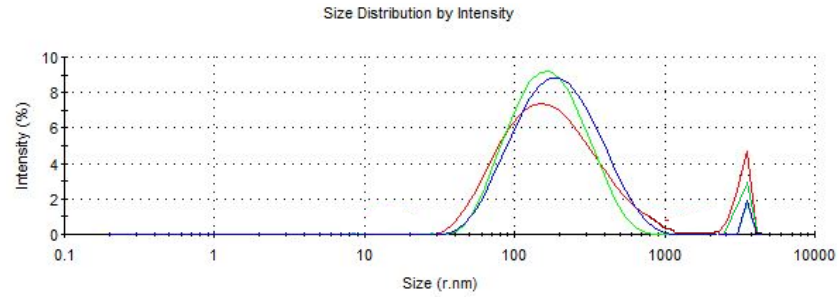

A.

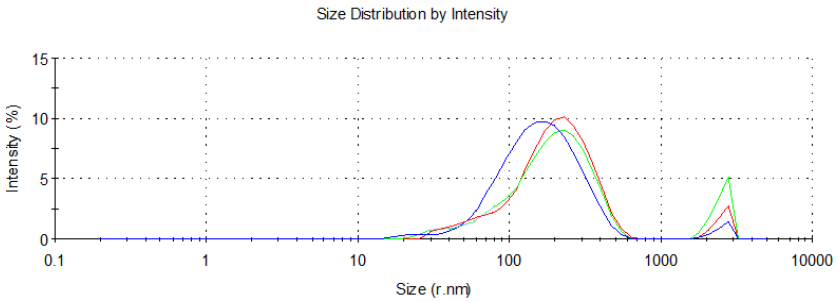

B.

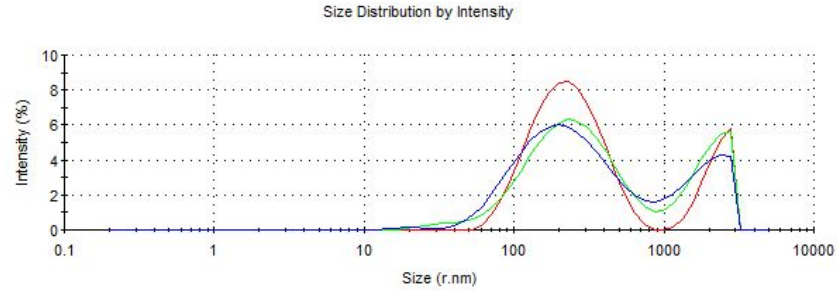

C.

Figure 55: Photon correlation spectroscopy size correlation charts for unfiltered solutions of carrier **46a** with concentrations 0.1 mg/mL (A),1 mg/mL (B) and 5 mg/mL (C) in deionised water (n=3).

In subsequent experiments to determine the solubilisation of poorly-soluble hydrophobic drugs, solutions of the carrier-drug mixture are filtered to remove any insoluble drug. For this reason, all solutions of the calix[4]resorcinarene salts **46a-d** and calix[4]pyrogallolarene salts **46e-f** investigated were also filtered and subsequently analysed. Following filtration, the hydrodynamic radius of the aggregates remaining decreased as the carrier **46a** concentration increased, from

412 nm at 0.1 mg/mL to 293.7 nm at 1 mg/mL. However, further increase in the carrier concentration to 5 mg/mL led to an increase in the size of the aggregates to 373.7 nm. The zeta potential became more negative, from -42 mV to -54 mV, as the carrier concentration increased (Table 3).

Table 3: Hydrodynamic radius and polydispersity index analysis for solutions (0.1 mg/mL, 1 mg/mL, and 5 mg/mL) of compound **46a** following filtration. Samples were recorded in triplicate at 25°C.

Compound	Concentration mg/mL	Radius nm (± SD): Percentage occurrence	PDI	Zeta Potential
Calix[4]-resorcinarene **46a**	0.1	412.3 (12.4): 100 %	0.064 (0.012)	-42.1 (1.40)
	1	293.7 (9.6): 100 %	0.266 (0.028)	-47.6 (0.70)
	5	373.8 (13.5): 100 %	0.233 (0.039)	-54.4 (0.46)

Figure 56 shows the size distribution report for carrier **46a** after filtration. The charts shows that all the aggregates obtained are within a similar size range, with no larger aggregates being observed.

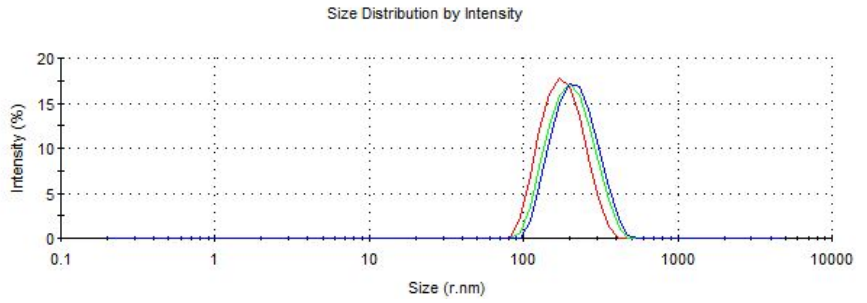

A.

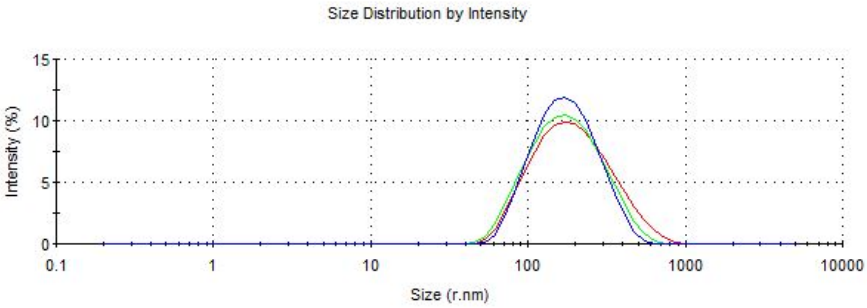

B.

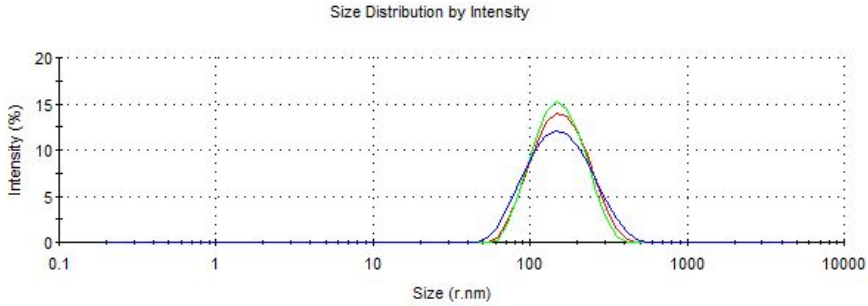

C.

Figure 56: Photon correlation spectroscopy size correlation charts for filtered solutions of carrier **46a** with concentrations 0.1 mg/mL (A),1 mg/mL (B) and 5 mg/mL (C) in deionised water (n=3).

An increase in concentration of carrier **46b** in unfiltered aqueous solution led to an increase in the hydrodynamic radius of the aggregates observed, from 199.8 nm at 0.1 mg/mL to 237.1 nm at 1 mg/mL, while further increasing the concentration to 5 mg/mL led to a decrease in the aggregate size to 173.9 nm (Table 4). The sizing analyses also showed the presence of larger aggregates with hydrodynamic radii of about 2060, 2193 and 2480 nm at concentrations 0.1 mg/mL, 1 mg/mL and 5 mg/mL,

respectively. The zeta potential observed became more negative as the concentration of the carrier **46b** in solution increased.

Table 4: Hydrodynamic radius and polydispersity index analysis for solutions (0.1 mg/mL, 1 mg/mL, and 5 mg/mL) of compound **46b** before filtration. Samples were recorded in triplicate at 25°C.

Compound	Concentration mg/mL	Radius nm (± SD): Percentage occurrence	PDI	Zeta Potential
Calix[4]-resorcinarene **46a**	0.1	199.8 (7.47): 89 % 2060 (24.4): 11 %	0.381 (0.043)	-40.5 (3.40)
	1	237.1 (11.6): 94 % 2193 (20.9): 6 %	0.327 (0.027)	-48.2 (3.07)
	5	173.9 (14.7): 85 % 2480 (40): 15 %	0.498 (0.061)	-55.9 (3.20)

The size correlation charts for carrier **46b** at these concentrations (0.1 mg/mL, 1 mg/mL and 5 mg/mL) show that two sizes of aggregates are observed for each sample (Figure 57).

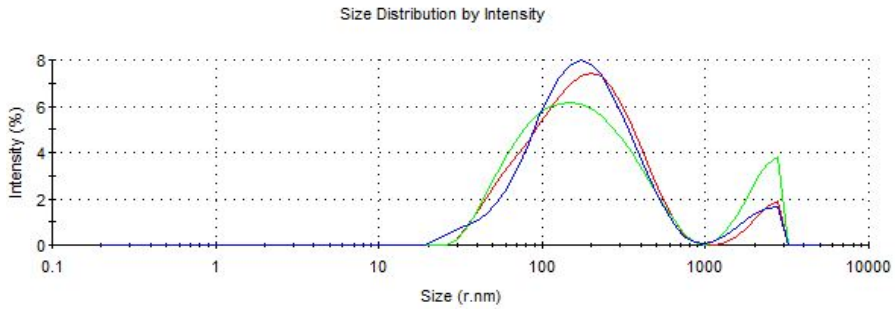

A.

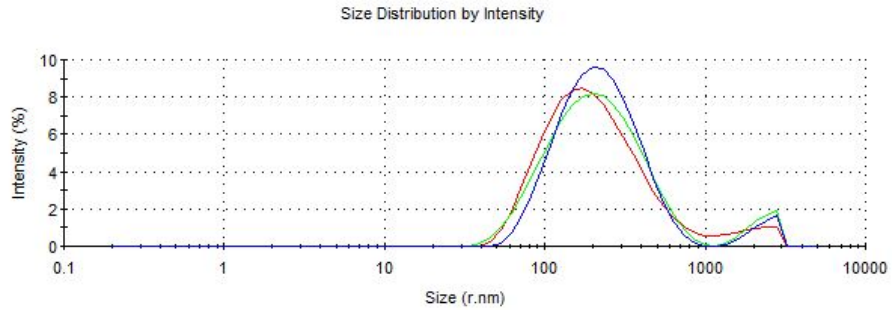

B.

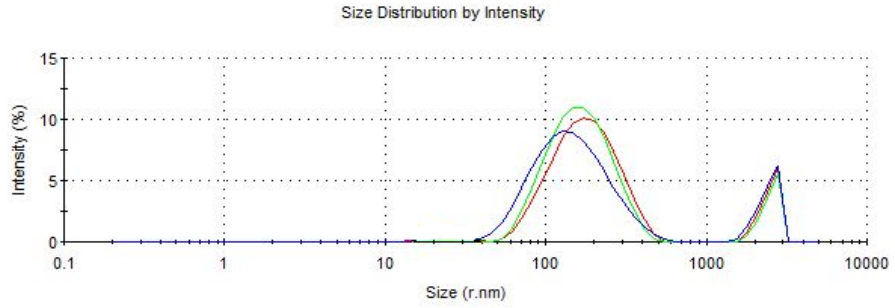

C.

Figure 57: Photon correlation spectroscopy size correlation charts for unfiltered solutions of carrier **46b** with concentrations 0.1 mg/mL (A),1 mg/mL (B) and 5 mg/mL (C) in deionised water (n=3).

The sizes of the particles in individual solutions of carrier **46b** after filtration (Table 4) had hydrodynamic radii of 258 nm at 0.1 mg/ml and 907 nm at 1 mg/ml, respectively. Two sizes of aggregates are observed for the solution with concentration of 0.1 mg/mL. This may indicate that the remaining aggregates of carrier **46b** in the filtered solution re-equilibrate to form larger aggregates with a size of 4752 nm. Upon increasing the concentration of carrier **46b** to 5 mg/mL the size of the aggregates

decreased to 387 nm and some smaller aggregates were also observed. The zeta potential became more negative, from -45 mV to -61 mV, as the carrier concentration increased (Table 5).

Table 5: Hydrodynamic radius and polydispersity index analysis for solutions (0.1 mg/mL, 1 mg/mL, and 5 mg/mL) of compound **46b** following filtration. Samples were recorded in triplicate at 25°C.

Compound	Concentration mg/mL	Radius nm (± SD): Percentage occurrence	PDI	Zeta Potential
Calix[4]-resorcinarene **46b**	0.1	258.7(12.4): 80 % 4752.3 (25.2): 20 %	0.456 (0.06)	-45.3 (0.31)
	1	907.4 (15.6): 100 %	0.361 (0.028)	-53.1 (1.85)
	5	387.2 (10.5): 88 % 5.8 (0.25): 12 %	0.404 (0.039)	-61.0 (2.38)

Figure 58 shows the size distribution reports for solutions of carrier **46b** after filtration. The aggregates in solutions with concentrations of 0.1 mg/mL and 5 mg/mL formed are within the broad range of 50 – 400 nm. At these concentrations two sizes of aggregates are observed (Figure 58A and 58C). Small aggregates of 1– 10 nm were observed for carrier **46b** at concentration 5 mg/mL. At 1 mg/mL the aggregates formed are within the size range of 500-1100 nm. Although this is a relatively large range, only one type of aggregation is present as only one peak is observed (Figure 58B).

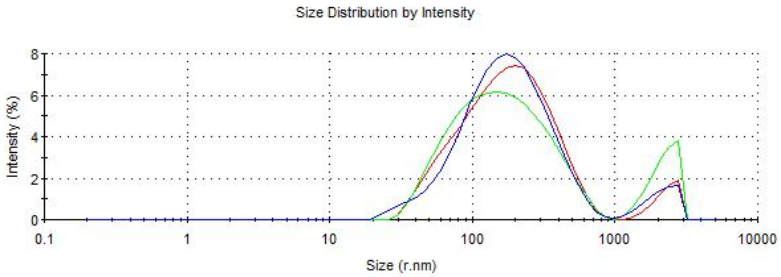

A.

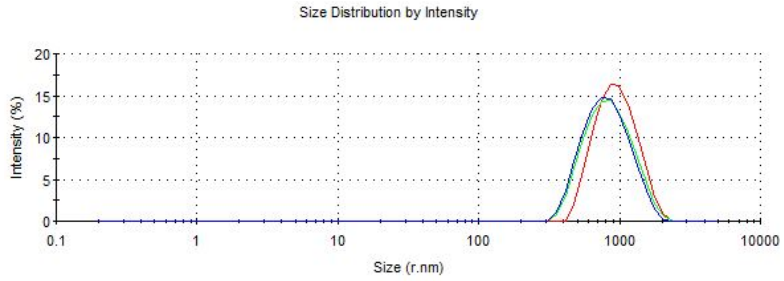

B.

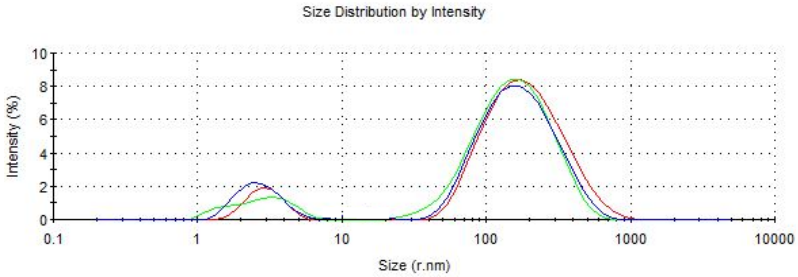

C.

Figure 58: Photon correlation spectroscopy size correlation charts for filtered solutions of carrier **46b** with concentrations 0.1 mg/mL (A),1 mg/mL (B) and 5 mg/mL (C) in deionised water (n=3).

Unfiltered aqueous solutions of carrier **46c** showed the formation of aggregates with hydrodynamic radius of 183.7 nm at a concentration of 0.1 mg/mL. At a concentration of 1 mg/mL, the average size of the aggregates decreased to 99.64 nm. A further increase in concentration resulted in aggregates of mean radius of 204.4 nm (Table 6). The volume distribution indicates the presence of other, larger aggregates at all the concentrations measured. The zeta potential of all solutions of carrier **46c** containing aggregates was within the range -40 to -60.3 mV, corresponding to stable systems.

Table 6: Hydrodynamic radius and polydispersity index analysis for solutions (0.1 mg/mL, 1 mg/mL, and 5 mg/mL) of compound **46c** before filtration. Samples were recorded in triplicate at 25°C.

Compound	Concentration mg/mL	Radius nm (± SD): Percentage occurrence	PDI	Zeta Potential
Calix[4]-resorcinarene **46c**	0.1	183.7 (7.4): 81 % 2186 (24.4): 19 %	0.432 (0.071)	-40.4 (1.39)
	1	99.64 (11.6): 86 % 2434 (20.9): 14 %	0.427 (0.085)	-44.5 (1.37)
	5	204.4 (10.9): 89 % 2253 (40.7): 11 %	0.399 (0.029)	-60.3 (1.99)

The size correlation charts for carrier **46c** at various concentrations before filtration (Figure 59) show that two aggregated systems are formed in each solution. The majority of aggregates observed are within the range 100-204 nm but in all cases much larger aggregates are observed, perhaps due to micelle-type aggregates.

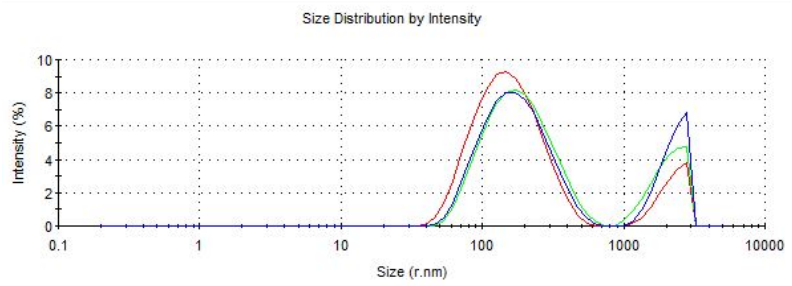

A.

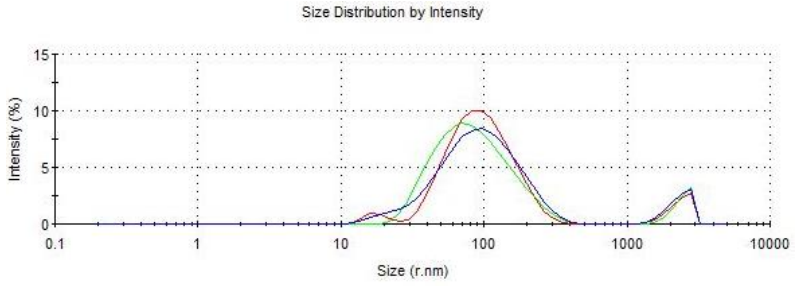

B.

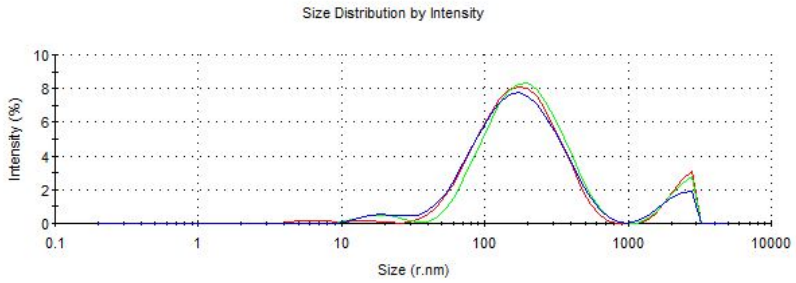

C.

Figure 59: Photon correlation spectroscopy size correlation charts for unfiltered solutions of carrier **46c** with concentrations 0.1 mg/mL (A),1 mg/mL (B) and 5 mg/mL (C) in deionised water (n=3).

Following filtration, the radius of aggregates observed for solutions of concentration 0.1 mg/mL and 1 mg/mL were 198 nm to 141 nm, respectively. For the solution of concentration 5 mg/mL, the size of the aggregates slightly increased to 136 nm. The zeta-potentials obtained for each solution was in the range of -48 to -78 mV, corresponding to stable systems (Table 7).

Table 7: Hydrodynamic radius and polydispersity index analysis for solutions (0.1 mg/mL, 1 mg/mL, and 5 mg/mL) of compound **46c** following filtration. Samples were recorded in triplicate at 25°C.

Compound	Concentration mg/mL	Radius nm (± SD): Percentage occurrence	PDI	Zeta Potential
Calix[4]-resorcinarene **46c**	0.1	198.7 (14.2): 100%	0.203 (0.05)	-43.1 (1.54)
	1	141.4 (10.6): 100 %	0.174 (0.03)	-72.7 (1.56)
	5	136.3 (5.5): 100 %	0.176 (0.01)	-77.9 (1.16)

Figure 60 shows the size distribution reports for solutions of carrier **46c** after filtration. The charts shows that all the aggregates formed are within the size range of 100-200 nm and potentially only one type of aggregate is present.

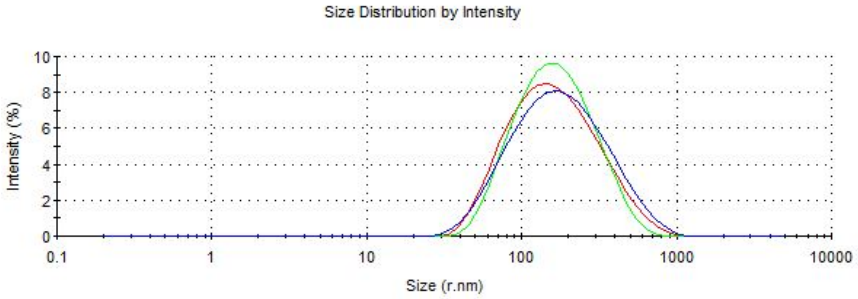

A.

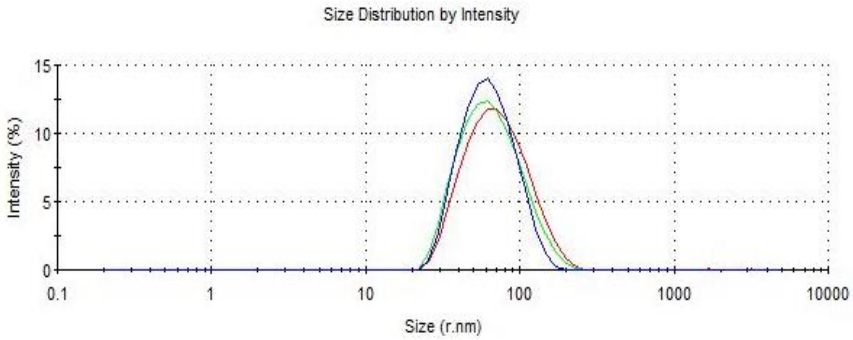

B.

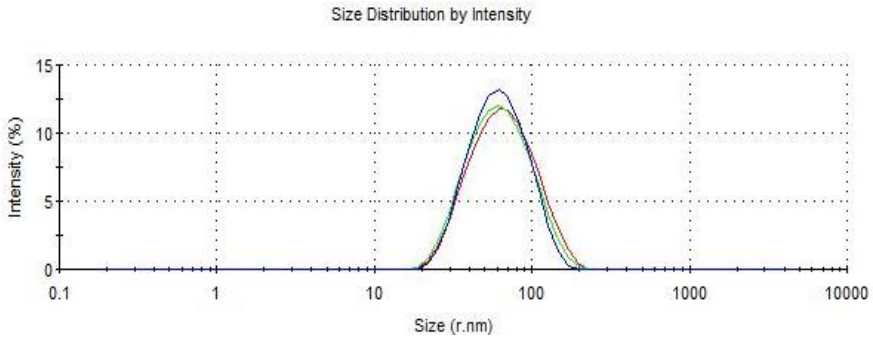

C.

Figure 60: Photon correlation spectroscopy size correlation charts for filtered solutions of carrier **46c** with concentrations 0.1 mg/mL (A),1 mg/mL (B) and 5 mg/mL (C) in deionised water (n=3).

For all unfiltered aqueous solutions of carrier **46d** studied at each concentration, it was observed that the size of aggregates were within the range 190 nm to 238 nm but the aggregates formed were not all of uniform size and that two size populations were present (Table 8). At a concentration of 1 mg/mL the hydrodynamic radius of

the aggregates was 362.4 nm and only one population was observed. As expected, the zeta potential became more negative as the concentration of the carrier solution increased, ranging between -46 to -73 mV which corresponds to stable systems.

Table 8: Hydrodynamic radius and polydispersity index analysis for solutions (0.1 mg/mL, 1 mg/mL, and 5 mg/mL) of compound **46d** before filtration. Samples were recorded in triplicate at 25°C.

Compound	Concentration mg/mL	Radius nm (± SD): Percentage occurrence	PDI	Zeta Potential
Calix[4]-resorcinarene **46d**	0.1	190.8 (7.91): 93 % 2173 (24.4): 7 %	0.345 (0.078)	-45.9 (2.99)
	1	362.4 (31.27): 100%	0.305 (0.060)	-48.8 (2.65)
	5	237.6 (19.9): 95 % 2223 (74.1): 5 %	0.500 (0.029)	-72.9 (0.68)

The size correlation charts for unfiltered solutions of carrier **46d** (Figure 61A and C) show the formation of larger aggregates for carrier concentrations of 0.1 mg/mL and 5 mg/mL. For the solution with concentration 1 mg/mL the aggregates formed are within the size range of 100 – 400 nm and potentially only one type of aggregation is present (Figure 61B).

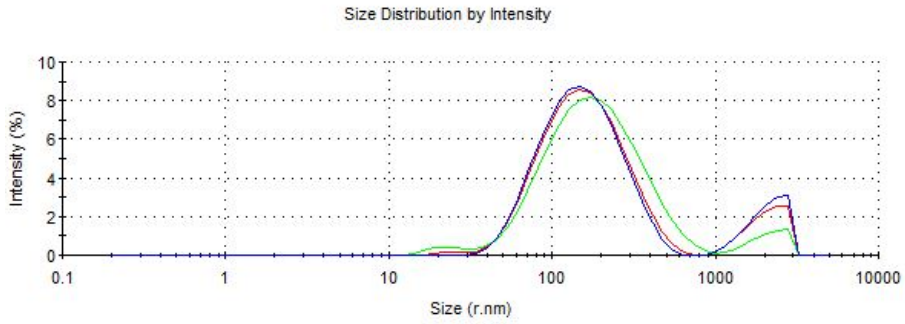

A.

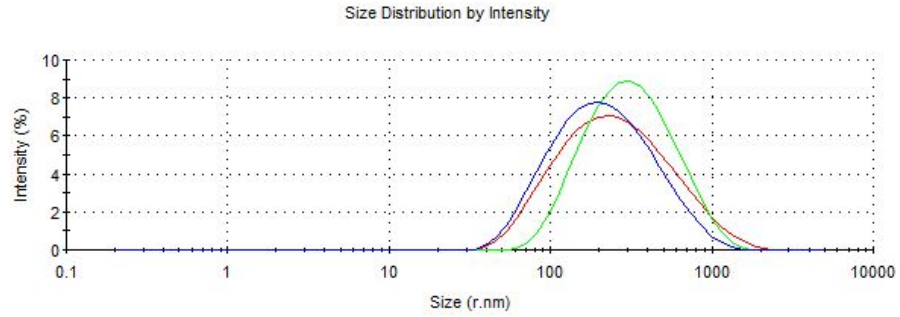

B.

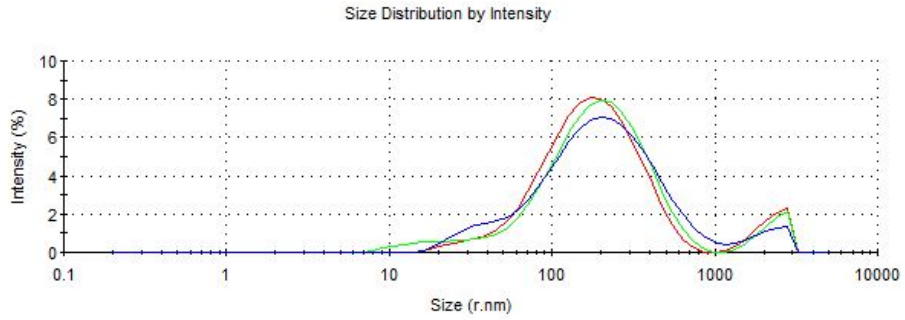

C.

Figure 61: Photon correlation spectroscopy size correlation charts for unfiltered solutions of carrier **46d** with concentrations 0.1 mg/mL (A),1 mg/mL (B) and 5 mg/mL (C) in deionised water (n=3).

Following filtration of solutions of carrier **46d** studied, it was observed for all concentrations that the size of the aggregates formed generally decreased and became more uniform. Larger aggregates were evident in solutions with concentrations of 0.1 mg/mL and 5 mg/mL, which may be due to some equilibration

effect. The zeta potential became more negative with the increase of concentration of the carrier (-48 to -83 mV), corresponding to stable systems (Table 9).

Table 9: Hydrodynamic radius and polydispersity index analysis for solutions (0.1 mg/mL, 1 mg/mL, and 5 mg/mL) of compound **46d** following filtration. Samples were recorded in triplicate at 25°C.

Compound	Concentration mg/mL	Radius nm (± SD): Percentage occurrence	PDI	Zeta Potential
Calix[4]-resorcinarene **46d**	0.1	361.8 (17.2): 83 % 2537.7 (30.1): 7 %	0.232 (0.073)	-47.7 (2.2)
	1	286.6 (10.5): 100 %	0.289 (0.056)	-75.96 (5.4)
	5	212.5 (11.5): 95 % 4755.3 (20.5): 5 %	0.324 (0.036)	-83.1 (2.4)

The size correlation charts for aqueous solutions of carrier **46d** with concentrations of 0.1 mg/mL and 5 mg/mL following filtration (Figure 62A and C) show the presence of two aggregate populations in solution. This indicates that larger aggregates of **46d** are more stable than the corresponding carrier **46c** which displays a shorted alkyl chain on the lower rim. The size correlation chart for carrier **46d** at 1 mg/mL (Figure 62B) shows that aggregates are formed are within the broad size range of 50-300 nm and potentially only one mode of aggregation is present.

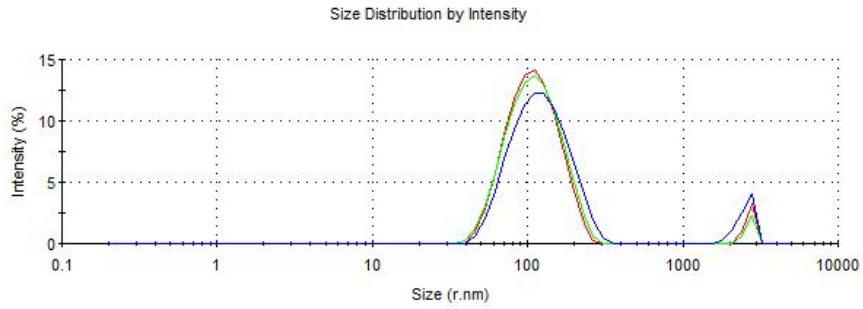

A.

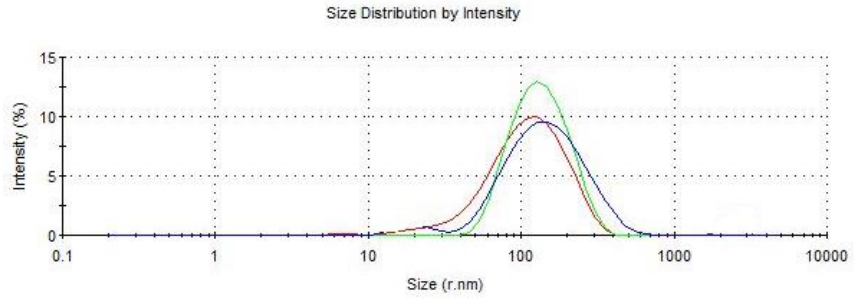

B.

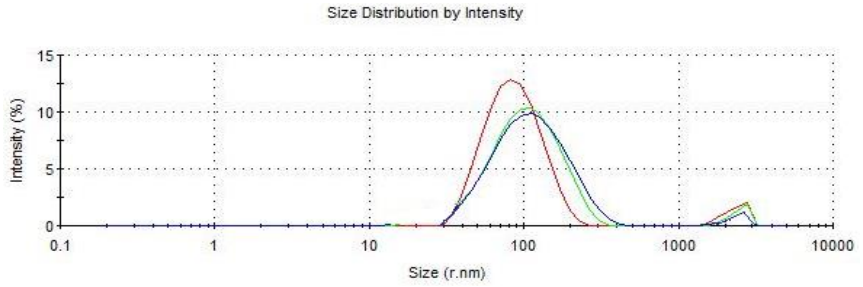

C.

Figure 62: Photon correlation spectroscopy size correlation charts for filtered solutions of carrier **46d** with concentrations 0.1 mg/mL (A),1 mg/mL (B) and 5 mg/mL (C) in deionised water (n=3).

For unfiltered solutions of calix[4]pyrogallolarene **46e**, it was observed that the size of the principal aggregates formed decreased upon increasing the concentration of carrier **46e** in solution from 0.1 mg/mL to 5 mg/mL. At all concentrations studied two sizes of the aggregates were observed, with a significant proportion of larger aggregates with radii greater than 2000 nm being present in each solution. The zeta

potential became more negative as the carrier concentration increased, from -52.9 mV to -77.9 mV (Table 10).

Table 10: Hydrodynamic radius and polydispersity index analysis for solutions (0.1 mg/mL, 1 mg/mL, and 5 mg/mL) of compound **46e** before filtration. Samples were recorded in triplicate at 25°C.

Compound	Concentration mg/mL	Radius nm (± SD): Percentage occurrence	PDI	Zeta Potential
Calix[4]-pyrogallolarene **46e**	0.1	202.5 (16.81): 67% 2181.3 (21.3): 33 %	0.367 (0.092)	-52.9 (2.99)
	1	157.1 (11.14): 94 % 2183 (20.6): 6 %	0.356 (0.055)	-56.2 (2.65)
	5	178.6 (3.35): 84 % 2236 (49.1): 16 %	0.384 (0.034)	-77.9 (0.68)

The size correlation charts for unfiltered solutions of carrier **46e** (Figure 63) clearly show that aggregation occurs at the three concentrations studied, to give species with a hydrodynamic radius of approximately 200 nm and larger supramolecular aggregates in the micron range.

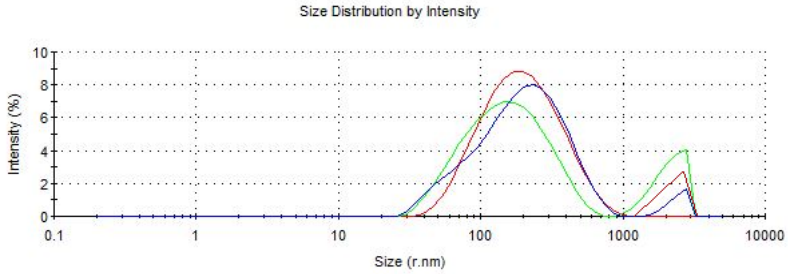

A.

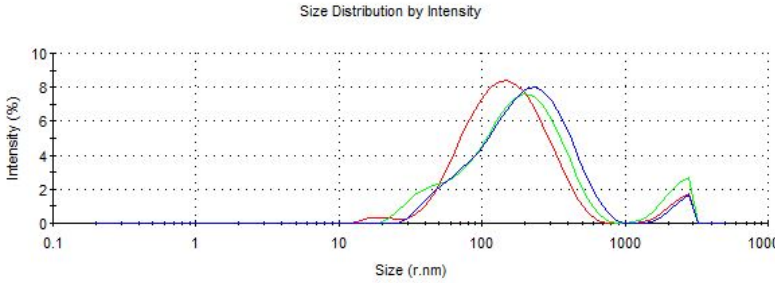

B.

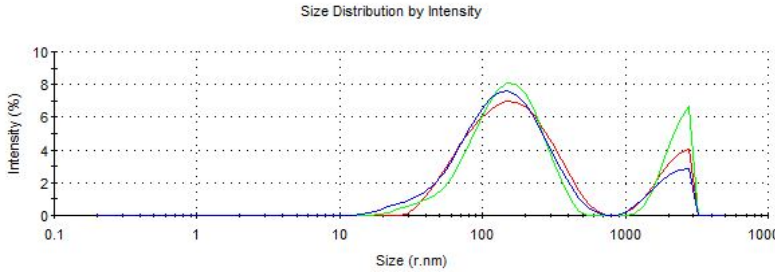

C.

Figure 63: Photon correlation spectroscopy size correlation charts for unfiltered solutions of carrier **46e** with concentrations 0.1 mg/mL (A),1 mg/mL (B) and 5 mg/mL (C) in deionised water (n=3).

Following filtration of the solutions of carrier **46e**, the size of the aggregates increased as the concentration increased from 0.1 mg/mL to 1 mg/mL. At the concentration 5 mg/mL, the mean hydrodynamic radius of the aggregates was 330 nm (Table 11). Of note is that no large supramolecular aggregates were observed at any of the concentrations following filtration.

Table 11: Hydrodynamic radius and polydispersity index analysis for solutions (0.1 mg/mL, 1 mg/mL, and 5 mg/mL) of compound **46e** following filtration. Samples were recorded in triplicate at 25°C.

Compound	Concentration mg/mL	Radius nm (± SD): Percentage occurrence	PDI	Zeta Potential
Calix[4]-pyrogallolarene **46e**	0.1	192.3 (17.6): 100%	0.249 (0.018)	-47.7 (2.2)
	1	267.3 (23.5): 100 %	0.212 (0.038)	-75.96 (5.4)
	5	330.1 (8.5): 100 %	0.306 (0.066)	-83.1 (2.4)

Figure 64 shows the size distribution reports for solutions of carrier **46e** following filtration. As can be seen, only one potential mode of aggregation is observed but the aggregates formed have a broad size range, as indicated by the PDI.

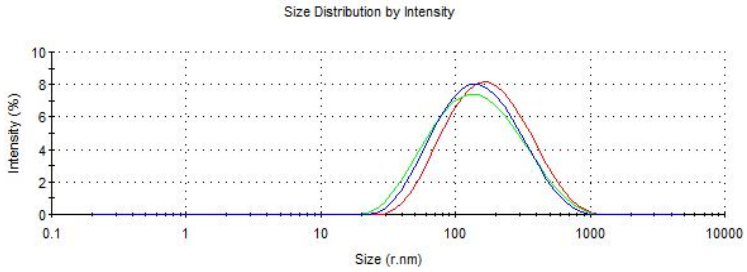

A.

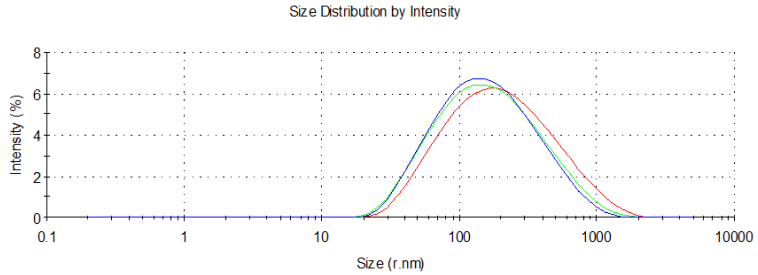

B.

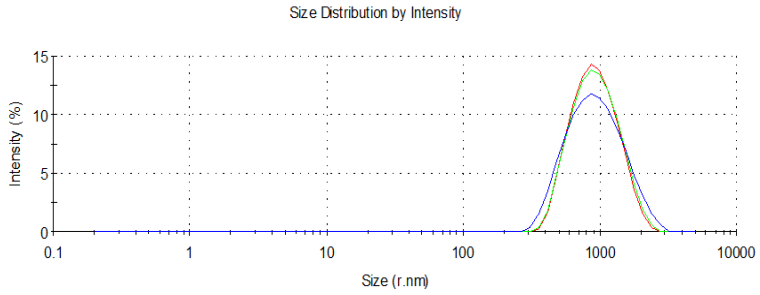

C.

Figure 64: Photon correlation spectroscopy size correlation charts for filtered solutions of carrier **46e** with concentrations 0.1 mg/mL (A),1 mg/mL (B) and 5 mg/mL (C) in deionised water (n=3).

Data obtained from measurement of particle size and zeta potential for carrier **46f** prior to filtration was broadly similar to that for carrier **46e** and, to some extent, carrier **46d**. For all solutions within the concentration range studied, aggregation gave particles with hydrodynamic radius of approximately 180 nm and also supramolecular species with a radius of approximately 2 microns. The zeta potential became more negative from -54 mV to -77.9 mV with increasing concentration of the carrier **46f** solutions (Table 12).

Table 12: Hydrodynamic radius and polydispersity index analysis for solutions (0.1 mg/mL, 1 mg/mL, and 5 mg/mL) of compound **46f** before filtration. Samples were recorded in triplicate at 25°C.

Compound	Concentration mg/mL	Radius nm (± SD): Percentage occurrence	PDI	Zeta Potential
Calix[4]-pyrogallolarene **46f**	0.1	187.9 (12.97): 93% 2290 (56.10): 7 %	0.404 (0.020)	-54.1 (2.99)
	1	340.7 (21.1): 100%	0.361 (0.055)	-61.3 (2.65)
	5	178.6 (3.35): 84 % 2236 (49.1): 16 %	0.384 (0.034)	-77.97 (0.68)

The size correlation charts for carrier **46f** solutions with concentrations 0.1 mg/mL and 5 mg/mL before filtration (Figure 65A and C) show clearly that the aggregates formed are not all of uniform size and that two populations are present in solution. The size correlation chart for carrier **46f** in solution with a concentration of 1 mg/ml (Figure 65B) shows that the aggregates formed are within a broad size range and only one principal mode of aggregation is observed.

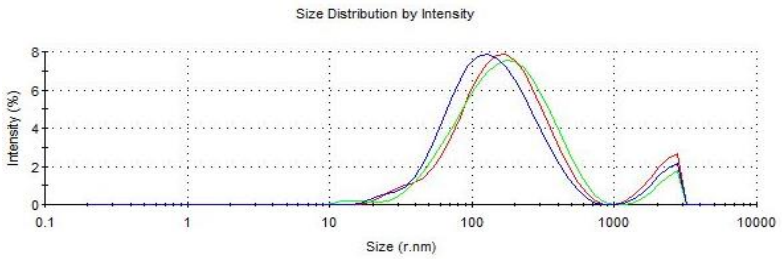

A.

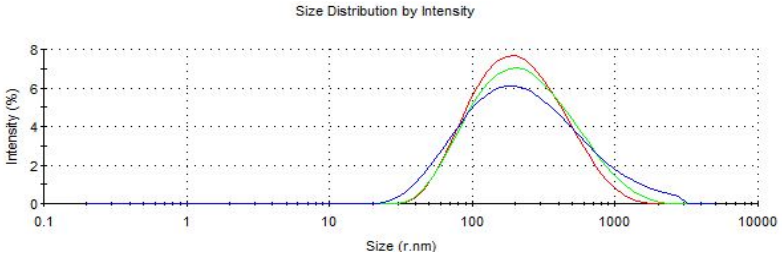

B.

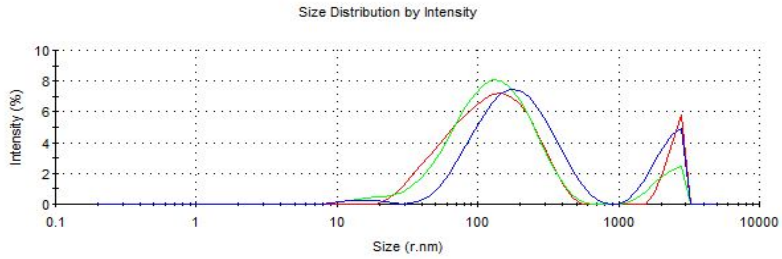

C.

Figure 65: Photon correlation spectroscopy size correlation charts for unfiltered solutions of carrier **46f** with concentrations 0.1 mg/mL (A),1 mg/mL (B) and 5 mg/mL (C) in deionised water (n=3).

Following filtration of the solutions of carrier **46f**, increasing the concentration of carrier 45f from 0.1 mg/mL to 1 mg/mL, it was observed that the size of the aggregates decreased from 401 nm to 340 nm. A further increase in the concentration to 5 mg/mL leads to aggregates with a greater decrease in size to 165 nm. The zeta potential became more negative, from -44 mV to -90 mV, as the carrier concentration in solution increased (Table 13).

Table 13: Hydrodynamic radius and polydispersity index analysis for solutions (0.1 mg/mL, 1 mg/mL, and 5 mg/mL) of compound **46f** following filtration. Samples were recorded in triplicate at 25°C.

Compound	Concentration mg/mL	Radius nm (± SD): Percentage occurrence	PDI	Zeta Potential
Calix[4]-pyrogallolarene **46f**	0.1	401.5 (17.2): 100%	0.188 (0.073)	-43.5 (3.23)
	1	324.3 (10.5): 88 % 4783.7 (30.8): 12%	0.482 (0.006)	-62.9 (0.90)
	5	165.8 (5.7): 100 %	0.383 (0.028)	-90.4 (1.02)

Figure 66 shows the size distribution reports for filtered solutions of carrier **46f**. The charts show that only one population of aggregates are present in all of the solutions studied. This may potentially indicate the existence of only one mode of aggregation for carrier **46f** in filtered solutions.

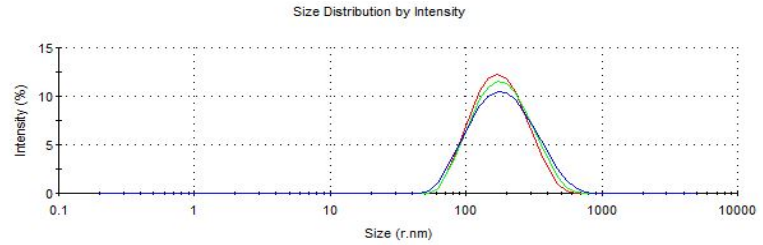

A.

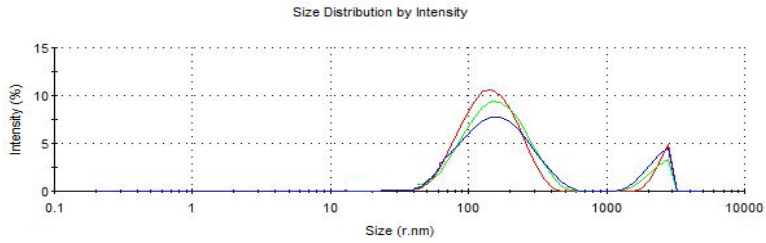

B.

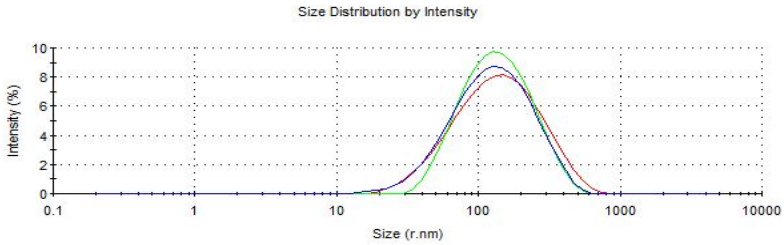

C.

Figure 66: Photon correlation spectroscopy size correlation charts for filtered solutions of carrier **46f** with concentrations 0.1 mg/mL (A),1 mg/mL (B) and 5 mg/mL (C) in deionised water (n=3).

2.10.4 Critical Aggregation Concentration CAC

2.10.4.1 UV Hydrophobic Probe

Methyl orange was used as a hydrophobic probe to investigate whether a hypochromic shift was observed which corresponds to the formation of aggregates of the amphiphilic carriers **46a-f** in solution in an aqueous environment. Thus, the CAC value can be determined for the amphiphilic carriers **46a-f** using ths protocol which is similar to that used for polymer studies (Cheng *et al.*, 2006; Thompson *et al.*, 2008; W. Wang, *et al.*, 2004). A hypochromic shift in λ_{max} (wavelength of maximum

absorbance) values for absorbance in the UV spectra was not observed for all amphiphilic calix[4]resorcinarenes **46a-d** and calix[4]pyrogallolarenes **46e-f** (Figure 67). The λ_{max} for methyl orange in water solution is 465 nm. In the presence of an excess amount of calix[4]resorcinarenes **46a-d** or calix[4]pyrogallolarenes **46e-f**, the λ_{max} decreased to 455 nm. The adsorption is at a lower wavelength than the control, this is likely to be due to the protonation/deprotonation equilibration of the azo group of the methyl orange (Kazakova *et al.*, 2013; Morozova *et al.*, 2010). Due to this, the CAC was determined using direct measurement of the surface tension of solutions of carriers **46a-f**.

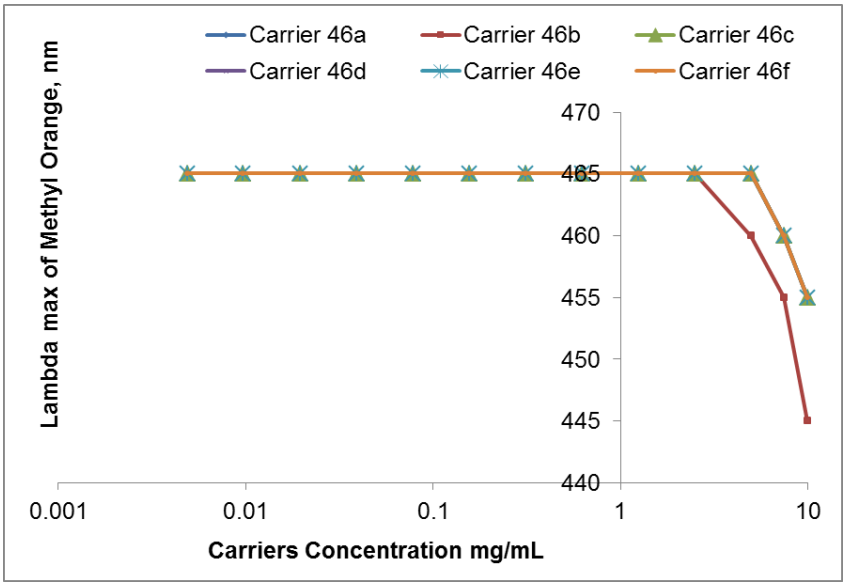

Figure 67: Methyl orange CMC/CAC measurement for the amphiphilic carriers **46a-f**. (Error bars have been omitted for clarity).

2.10.4.2 Surface Tension

The surface activity of all carriers 46a-f was determined by measuring the surface tension of solutions of each carrier in water. This allows estimation of the critical association concentrations (CAC) values for each carrier in aqueous solution (Figure 68-70). These studies can provide evidence of supramolecular architectures in bulk

solution and are often used in amphiphilic polymer characterisation (Hoskins *et al.*, 2012). The CAC values were measured at the point in the graph where a sharp break can be observed in the curves obtained, evidencing the formation of aggregates (Hoskins *et al.*, 2012). In comparison to polymers, calix[n]arenes have well-defined structures that generally do not require further intervention to promote formation of stable aggregates in aqueous environments, though sonication is useful for breaking up larger, insoluble aggregates. In aqueous media, hydrophobic alkyl groups on the lower rim of calix[4]resorcinarenes can promote aggregation due to interaction of the hydrophobic groups and a consequent reduction in Gibbs' energy of the aggregated systems (Hoskins *et al.*, 2016). As shown in Figure 68, the surface tension for carriers **46a** and **46b** decreased gradually with an increase in the carrier concentration. For calix[4]resorcinarene carrier **46a** a break point is evident at a concentration of 0.75 mg/mL, corresponding to the CAC of this carrier. The CAC value for carrier **46b** was observed to be 0.375 mg/mL (Figure 68). The surface tension plots for calix[4]resorcinarenes **46a-d** and calix[4]pyrogallolarenes **46e-f** showed only one point of inflexion and hence only one CAC value for each compound. For all of the carriers **46a-f** the CAC indicates the formation of intermolecular aggregates, since the molecules are unable to form intramolecular aggregates due to their essentially rigid structures (Hoskins *et al.*, 2012). As an example, for calix[4]resorcinarene **46a** (Figure 68) it is assumed that the CAC at 0.75 mg/mL is a result of molecules aggregating by association of their lipophilic chains, forming weak hydrophobic-hydrophobic interactions. Larger supramolecular structures are likely to form with increasing concentrations of the carrier above the CAC value (0.75 mg/mL) as more carrier molecules associate through their hydrophobic residues.

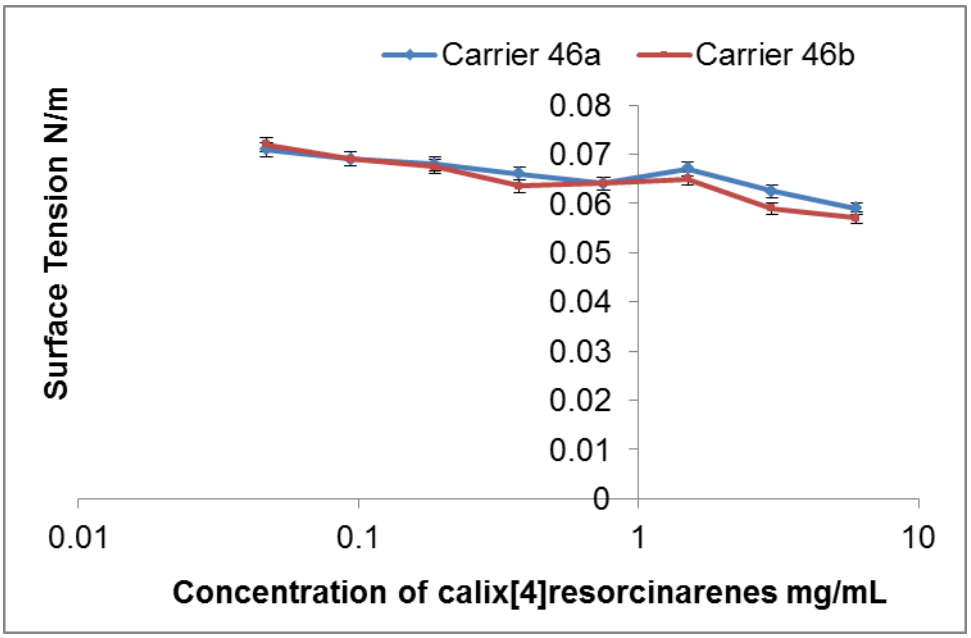

Figure 68: Surface tension of solutions of calix[4]resorcinarenes **46a-b** measured at 20 °C using a torsion balance (n = 3 ± SD).

The surface tension of aqueous solutions containing carriers **46c** or **46d** at various concentrations decreased with the increase in the carrier concentration (Figure 69). The plots were almost identical and a clear break point was observed at a CAC of 1.5 mg/mL, greater than that for both carriers **46a** and **46b**.

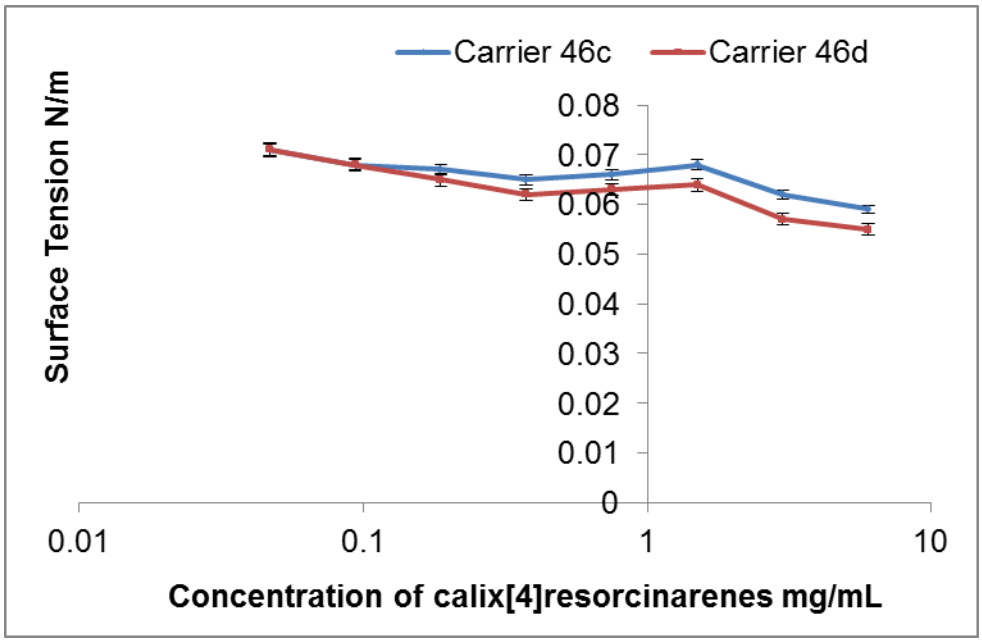

Figure 69: Surface tension of solutions of calix[4]resorcinarenes **46c-d** measured at 20 °C using a torsion balance (n = 3 ± SD).

For calix[4]pyrogallolarenes **46e** and **46f** (Figure 70), again the plots are almost identical with a break point indicating a CAC of 0.75 mg/mL for both compounds.

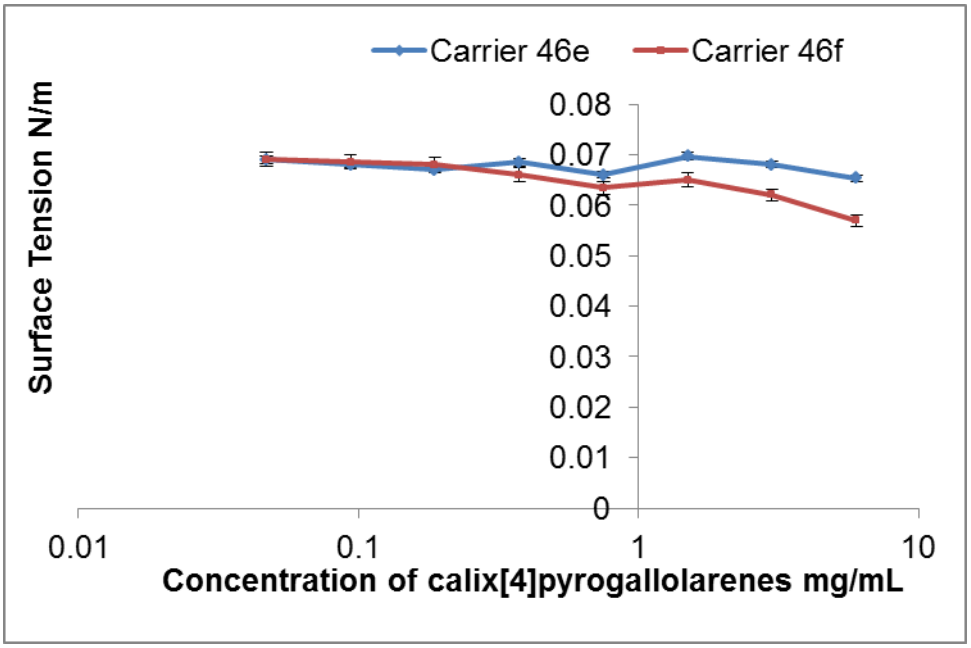

Figure 70: Surface tension of solutions of calix[4]pyrogallolarenes **46e-f** measured at 20 °C using a torsion balance (n = 3 ± SD).

2.10.4.3 Conductivity Measurements

Measurement of the conductivity of a solution of the calix[4]resorcinarene carriers **46a-d** and the calix[4]pyrogallolarene carriers **46e-f** can also be used estimate the CAC for each compound. A plot of conductivity versus concentration dependence for carrier **46a** is linear up to 0.75 mg/mL, but when the concentration of carrier in solution is further increased this result in a decrease in the gradient of the line of best fit (Figure 71). The point at which these two lines intersect is the CAC. Conductivity data for carrier **46a** reveals that the CAC for this compound is 0.92 mg/mL. This method gives a better estimate of the CAC.

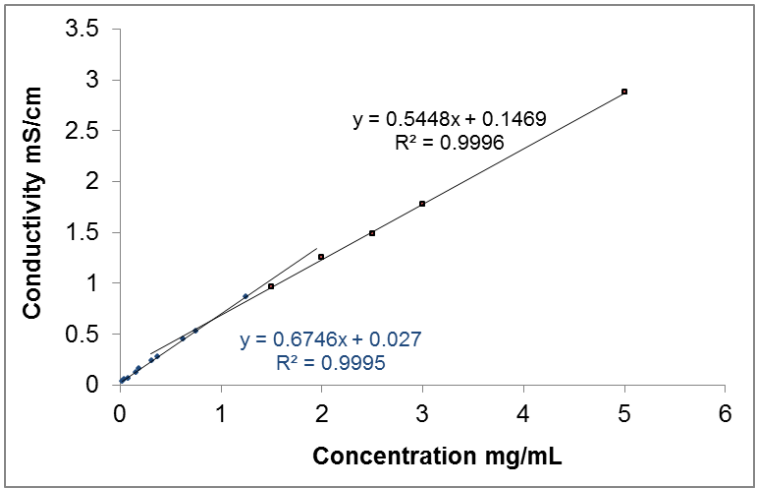

Figure 71: Dependence of the conductivity of solutions of carrier **46a** with varying concentration.

A similar linear dependence for carrier **46b** (Figure 72) is characterized up to 0.75 mg/mL though the gradient of each linear region is less than that observed for carrier **46a**. The intersection and, hence, CAC for carrier **46b** is at 0.76 mg/mL.

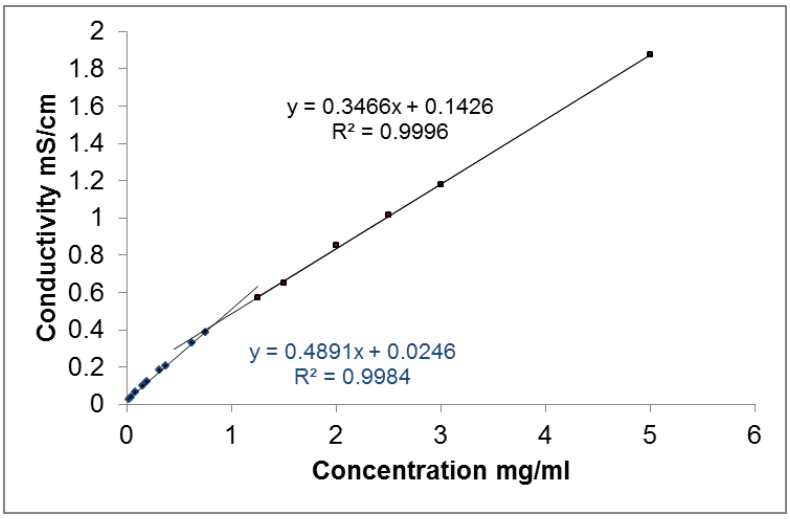

Figure 72: Dependence of the conductivity of solutions of carrier **46b** with varying concentration.

A similar plot for carrier **46c** at various concentrations in aqueous solution (Figure 73) indicates a CAC of 1.52 mg/mL for this compound.

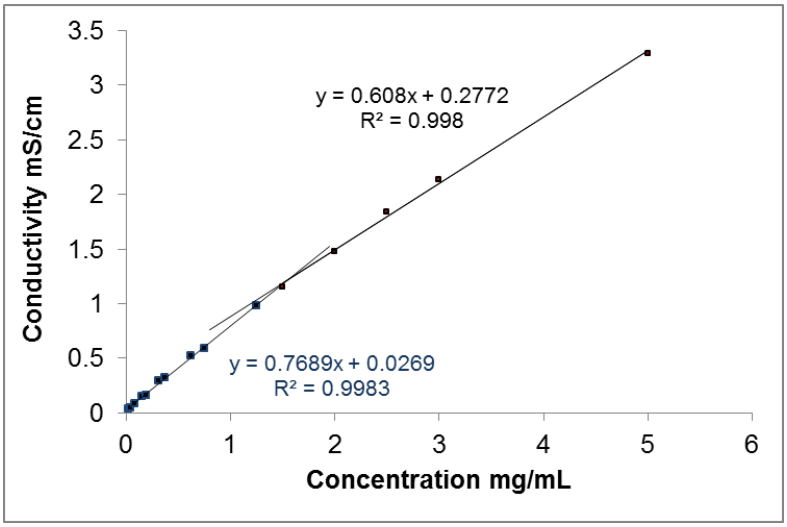

Figure 73: Dependence of the conductivity of solutions of carrier **46c** with varying concentration.

For carrier **46d** at the intersection was observed at a CAC of 1.56 mg/ml (Figure 74). The conductivity plots for carriers **46c** and **46d** give CAC values that are in broad agreement with values determined by surface tension measurements.

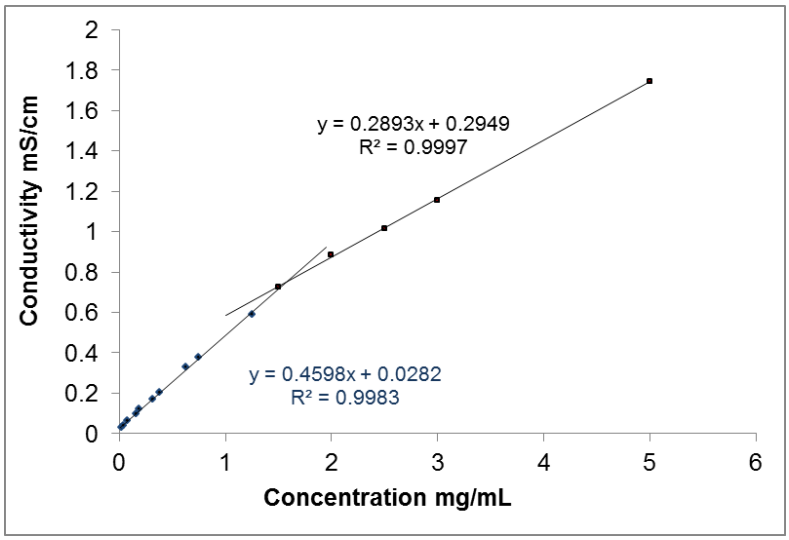

Figure 74: Dependence of the conductivity of solutions of carrier **46d** with varying concentration.

The conductivity versus concentration dependence for calix[4]pyrogallolarene carrier **46e** indicates a CAC value of 1.00 mg/mL (Figure 75).

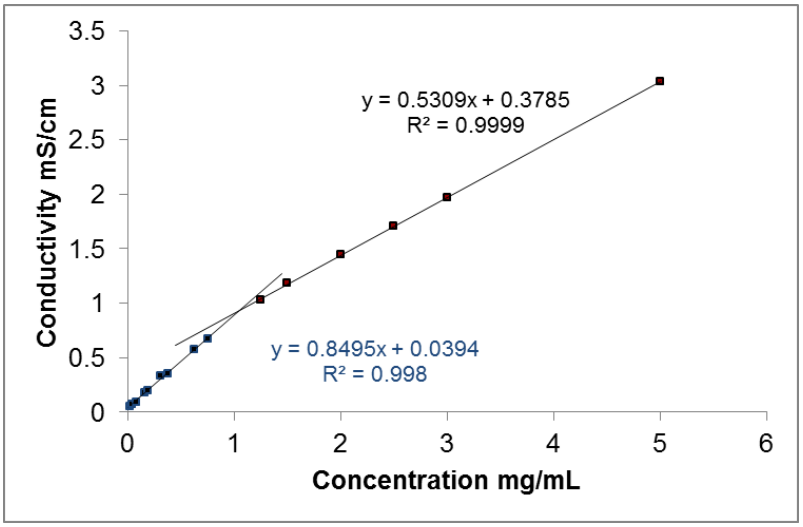

Figure 75: Dependence of the conductivity of solutions of carrier **46e** with varying concentration.

In the case of calix[4]pyrogallolarene carrier **46f** the CAC in aqueous solution was determined to be 0.66 mg/mL (Figure 76).

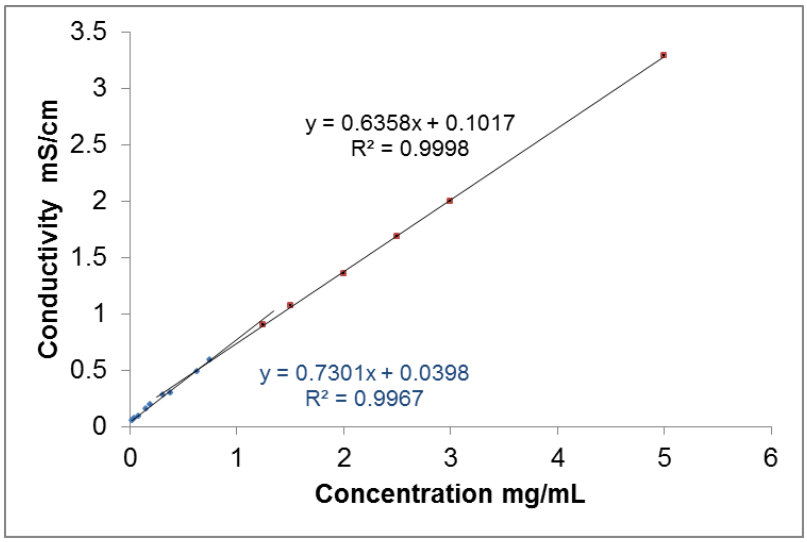

Figure 76: Dependence of the conductivity of solutions of carrier **46f** with varying concentration.

2.11 Discussion

The sodium salts of octa-carboxylated calix[4]resorcinarenes **46a-d** and dodeca-carboxylated calix[4]pyrogallolarenes **46e-f** were prepared using standard methods **(**Figure 77). Each of these amphiphilic compounds, isolated in the *rccc* crown conformation, possess multiple negatively-charged residues on the upper rim of the crown with lower rim alkyl chains containing either four carbon atoms (C_4) or seven carbon atoms (C_7). In each case, the amphiphilic carriers were soluble in aqueous media and practically insoluble in organic solvents due to the presence of anionic groups on their upper rim. These carrier molecules were characterised fully using spectroscopy, spectrometry and physico-chemical measurements.

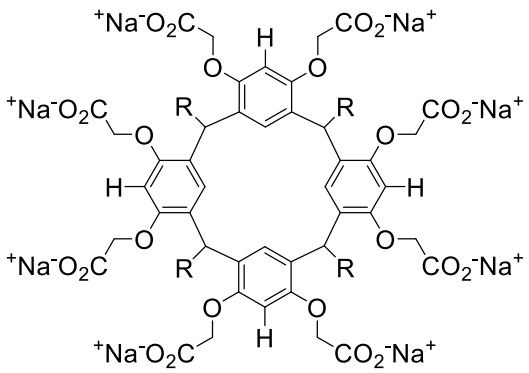

R= C_4H_9 **46a**
R= C_7H_{15} **46b**

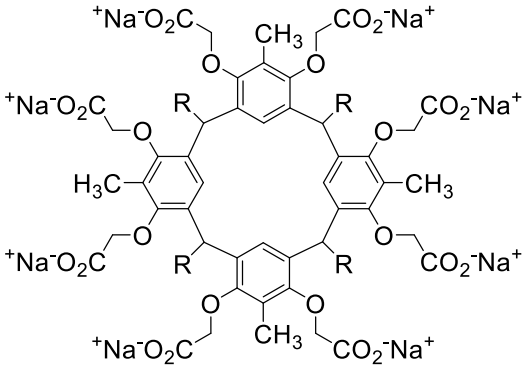

R= C_4H_9 **46c**
R= C_7H_{15} **46d**

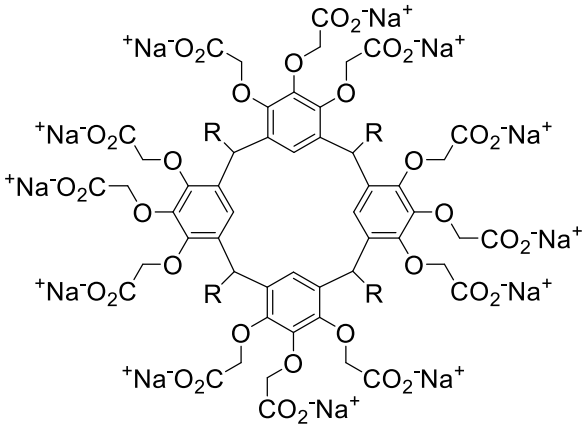

R= C_4H_9 **46e**
R= C_7H_{15} **46f**

Figure 77: Molecular structure of calix[4]resorcinarenes **46a-d** and calix[4]pyrogallolarenes **46e-f**.

The aggregation behaviour of each compound **46a-f** in aqueous solution was examined, in order to compare with any aggregation observed when the carrier molecules interact with other, different hydrophobic compounds, as noted in the Aims and Objectives of this research programme. Carrier molecules **46a-f** were dissolved in water at various concentrations and these solutions were sonicated to disperse the molecules and any aggregates, then allowed to cool and relax to provide an opportunity for aggregates to form. The ability of carriers **46a-f** to self-assemble into

aggregated particulates in aqueous environments was assessed by measurement of the critical aggregation concentration (CAC), particle size and zeta potential of each of the carriers, and the data was compared to related compounds reported in the literature (Mironova *et al.*, 2013; Pashirova *et al.*, 2014; Syakaev *et al.*, 2018).

Experimental observation of the solubility of calix[4]resorcinarenes **46a-d** and calix[4]pyrogallolarenes **46e-f** in deionised water indicated that each carrier molecule exhibited high solubility in aqueous media. It is appropriate to study the aggregation behaviour of the carrier molecules **46a-f** in aqueous solution at concentrations of 0.1 mg/mL, 1 mg/mL and 5 mg/mL because these are typical concentrations used to determine potential as solubilising agents with various drug molecules. However, the protocol for assessing the solubilisation potential requires that solutions containing carrier molecules **46a-f** and the drug being investigated are filtered to remove any undissolved drug. In this case, the aggregation behaviour of each carrier in solution before filtration and following filtration using a 0.45 micron in-line filter.

Results from dynamic light scattering experiments indicate that all of the carrier molecules investigated form aggregates in aqueous solutions, with a similar distribution before and after filtration. For example: the calix[4]resorcinarene-derived carrier **46a** aggregates spontaneously in deionised water to give aggregates that are not uniform in size, as confirmed by the polydispersity index data (Figure 78A). There are also two populations of aggregates present in solution, the larger of which may be due to the formation of micellar-like structures similar to those observed for less structurally complex amphiphilic surfactant molecules. However, these larger supramolecular species are removed by filtration (Figure 78B) and only one potential mode of aggregation is observed. This is most likely to be due to the carrier

molecules associating side-by-side with each other or through a linear end-to-end interaction between molecules.

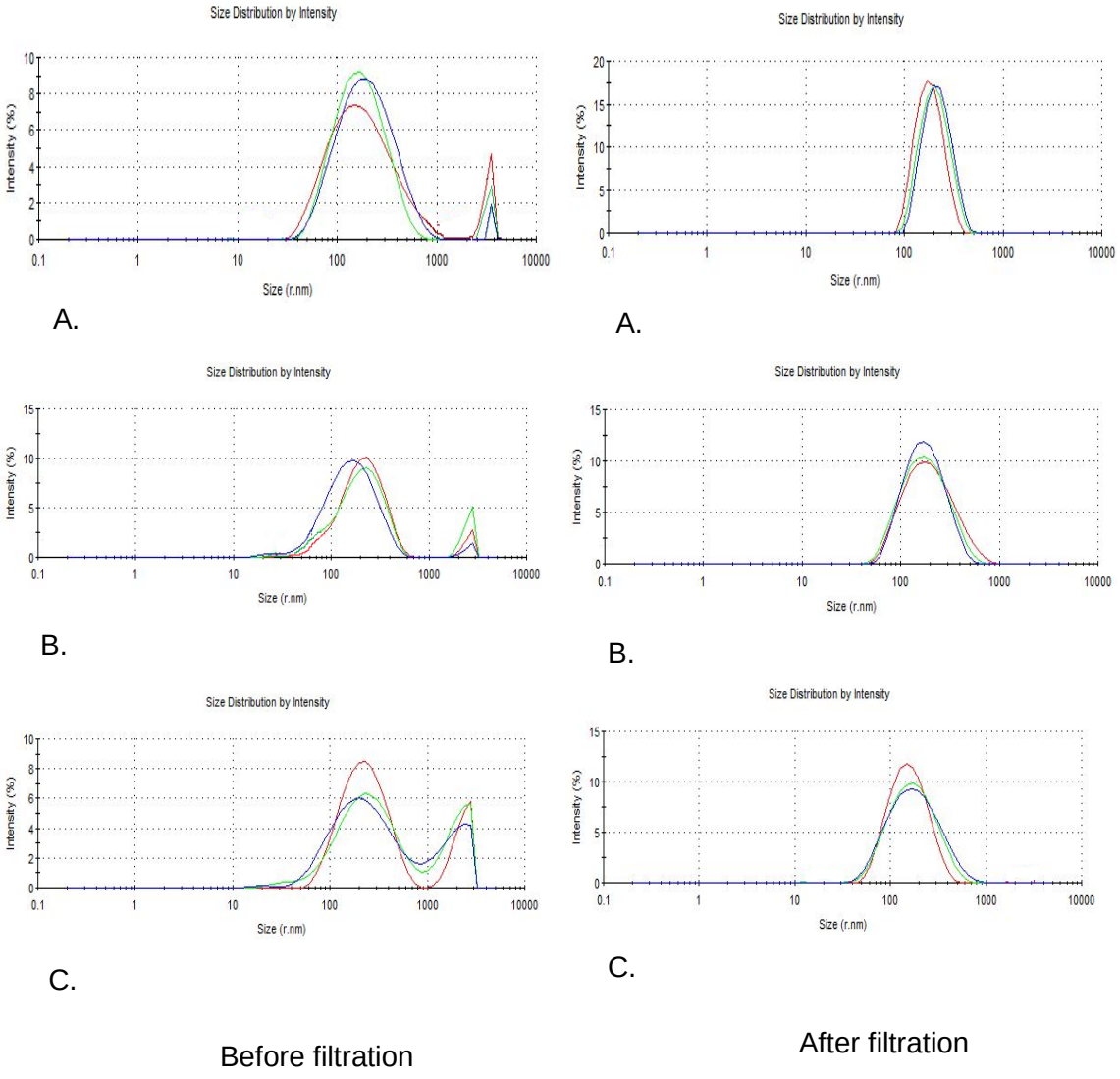

Figure 78: Photon correlation spectroscopy size correlation charts for solutions of carrier **46a** with concentrations 0.1 mg/mL (A),1 mg/mL (B) and 5 mg/mL (C) in deionised water (n=3).

Zeta potential measurements indicate that all aggregates formed by carriers **46a-f** in aqueous solution are stable, with the highest zeta potential values being observed for aggregates formed from solutions containing high concentrations of the carriers. The negative zeta potentials observed are as expected due to the presence of carboxylate anions on the carrier surface.

Carrier molecules **46a**, **46c** and **46e** that display short butyl chains containing only four carbons on their lower rim do not possess the degree of hydrophobicity of carriers **46b**, **46d** and **46f** which display heptyl chains with seven carbons. Thus, it can be anticipated that the mode of formation and stabilisation of aggregates may be different for the C_4 and C_7 derivatives. This could affect the critical aggregation concentration values observed (Hoskins *et al.*, 2016; Mironova *et al.*, 2015, 2013; Syakaev *et al.*, 2008; Syakaev *et al.*, 2012).

The CAC of each calix[4]resorcinarene and calix[4]pyrogallolarene investigated was determined using a methyl orange hydrophobic probe, surface tension measurements and by comparing the conductivity of each carrier in solution. The CAC occurs as a result of two or more molecules or particulates associating together with their lipophilic residues and, hence, forming weak hydrophobic-hydrophobic interactions. Increasing concentrations above the CAC value are likely to form larger aggregates and supramolecular structures as associated molecules combine with others to protect their lipophilic tails from the ‘hostile’ aqueous environment. As the concentration of the molecules in solution increases there can be a change in the mode of aggregation, resulting in the formation of micelles.

The hypochromic shift in the UV absorption of methyl orange allows the CAC to be estimated (Cheng *et al.*, 2006; W. Wang *et al.*, 2004). Amphiphilic *O*-substituted calix[4]resorcinarenes are known to selectively bind many species including azo dyes resulting in increased solubility of the dye and a shift in the UV spectrum (Davis *et al.*, 2009; Kazakova *et al.*, 2013). In this present research, accurate determination of the CAC using methyl orange was not possible for calix[4]resorcinarenes and calix[4]pyrogallolarenes **46a-f**, principally because the method is not sensitive enough to detect the CAC values. Surface tension measurement is a widely

accepted method for the determination of surfactant properties (Maza *et al.*, 1998; Peltonen & Yliruusi, 2000; Komorek & Wilk, 2004). It is reasonable to expect carriers **46a-f** to possess some surfactant properties due to their highly amphiphilic structures. CAC values could be estimated for each carrier investigated using surface tension measurements, by determining the appearance of a point of inflexion in the plot of surface tension against concentration of the solution.

Conductivity measurements provide a more accurate estimation of the CAC. By plotting conductivity of the solution against the concentration of carrier **46a-f** present, the CAC can be determined by observing the point of intersection of linear regions of data and solving for concentration using simultaneous equations. The CAC values for carriers **46a-f** determined using surface tension measurements and analysis of conductivity data are summarized in Table 14. As can be seen, data obtained by conductivity measurements is more precise than that derived from surface tension measurements.

Table 14: Critical Association Concentrations (CAC, mg/mL) measured at 25 °C using a torsion balance and conductivity (n = 3 ± SD).

Carrier molecule	CAC	
	Surface tension	Conductivity
Calix[4]resorcinarene **46a**	0.750 (0.002)	0.92 (0.006)
Calix[4]resorcinarene **46b**	0.375 (0.003)	0.76 (0.005)
Calix[4]resorcinarene **46c**	1.500 (0.0337)	1.52 (0.025)
Calix[4]resorcinarene **46d**	1.500 (0.057)	1.56 (0.036)
Calix[4]pyrogallolarenes **46e**	0.750 (0.005)	1.00 (0.017)
Calix[4]pyrogallolarenes **46f**	0.750 (0.007)	0.66 (0.012)

Analysis of the CAC values for all carriers obtained using conductivity measurements shows some trends. The CAC of carrier **46b** is lower than that for carrier **46a** presumably due to weaker interactions between the hydrophobic C_4 alkyl chains displayed by carrier **46a** as compared to stronger interactions between the longer C_7 alkyl chains displayed by carrier **46b**. A similar trend is observed for the calix[4]pyrogallolarene derivatives: the CAC of carrier **46f** is considerably lower than that for carrier **46e** but this difference will also be affected by the greater number and density of negatively-charged residues present in the aggregates. The repulsion between these dense 'head groups' may promote and end-to-end mode of aggregation. In the case of carriers **46c** and **46d** the difference between their CAC is negligible, which may be the consequence of these molecules possessing and additional hydrophobic group on the upper rim.

2.12 Conclusion

An ideal calix[n]arene acceptor molecule which can be used as a host for hydrophobic drug molecules in aqueous media must both a hydrophobic site to bind the hydrophobic guest and a hydrophilic site in order to solubilize the host molecule in water. Calix[4]resorcinarenes **46a-d** and calix[4]pyrogallolarenes **46e-f** satisfy these criteria. Conceptually, it would also be preferable for the host to be in the *rccc* crown conformation, which is the case for calix[4]resorcinarenes **46a-d** and calix[4]pyrogallolarenes **46e-f**.

The structures of the carrier molecules **46a-f** were determined and their physicochemical properties measured, with a particular emphasis on their aggregation behaviour in aqueous solution. Attempts were made to determine the mode of aggregation for each molecule, particularly using 2-dimensional NMR

experiments, but it was not possible to do this. However, any large micellar assemblies could be removed by filtration.

There is only one example in the literature of a molecule with a similar structure to carriers **46a** and **46b** being investigated using similar methodology to that described here (Ryzhkina *et al.*, 2014). This chapter presents the first systematic investigation into potential drug solubilisation agents based upon calix[4]resorcinarenes and calix[4]pyrogallolarenes. Subsequent chapters will describe how these molecules can be used to solubilise a range of hydrophobic drug molecules.

Chapter Three

Drug Loading and Release Studies of Calix[4]resorcinarene and Calix[4]pyrogallolarene Nanocarrier Formulations

3.1 Introduction

The aim of this study is to investigate the potential of amphiphilic calix[4]resorcinarene octa-sodium salts **46a-d** and calix[4]pyrogallolarenes dodeca-sodium salts **46e-f** as solubilising agents for the formulation of hydrophobic drug molecules. There is considerable interest in the development of such delivery systems, especially those which enable controlled release of the drug (Langer, 1998; Wei *et al.,* 2013). The aqueous solubility of a drug is one of the significant factors to consider when attempting to achieve the desired concentration of drug in the systemic circulation for in order to achieve the required pharmacological response (Jain *et al.*, 2010; Novichkov *et al.*, 2011). Poor water solubility of drugs can affect the efficacy of the drug and the bioavailability. Some drugs also show side effects as a result of their poor aqueous solubility, since they can localise in the adipose tissues and membranes. Several methods have been used to improve the solubility of poorly water-soluble drugs (Chiou *et al.*, 1976) such as salt and polymorph formation (Haleblian & McCrone, 1969), solid dispersion (Chiou & Riegelman, 1971; Serajuddin, 1999), co-precipitation using inert, water-soluble compounds as carriers (Stupak *et al.*, 1974) and formation of inclusion complexes (Kumar *et al.*, 2011; Shinde *et al.*, 2008). By solubilising hydrophobic drugs, agents such as nanocarriers **46a-f** can increase the efficacy and, hence, therapeutic potential of the drugs. This entails lower dosages being required to achieve the desire therapeutic effect and side effects can be minimised (Dekker, 1994; Soppimath *et al.,* 2001). The studies presented in this chapter determined the maximum drug loading capacity of each of the nanocarriers **46a-f**, each of the formulations prepared were characterised and compared to data observed for the carriers alone, and *in vitro* drug release profiles were determined for each formulation.

3.2 Model Hydrophobic Drugs used in this Study

Three model hydrophobic drugs were used in this study: Propofol, prednisolone and tetracaine (Figure 79).

Propofol is a commonly used short acting anaesthetic agent. It has a favourable pharmacokinetic and pharmacodynamic profile (Baker & Naguib, 2005; Sahinovic *et al.,*2018). However poor aqueous solubility (100 µg/mL at 25 °C) and high lipophilicity (log P = 4.16) are a particular challenge for the administration and formulation of propofol (Thompson & Goodale, 2000). The high lipophilicity means that good propofol miscibility can only be achieved in lipophilic substances or organic solvents. Therefore, propofol is formulated in soybean oil (100 mg/mL), in an oil-in-water or lipid-based emulsion (Momot *et al.*, 2003; Baker & Naguib, 2005). Alternative formulations such as microemulsions (Morey *et al.*, 2006), inclusion complexes (Trapani *et al.*, 1998), and polymeric micelles (Ravenelle *et al.*, 2008) have been developed to improve the solubility of propofol.

Prednisolone (PLS) is a corticosteroid most frequently used clinically for the treatment of inflammatory conditions, such as arthritis, and asthma. Prednisolone is slightly soluble in water (215 µg/mL at 25 ºC) and has lipophilic (log P = 1.8), leading to decreased oral bioavailability (Kabasakalian *et al.*, 1966; Teshima *et al.*, 2006). Prednisolone is commonly administered as coated tablets or, more commonly, as a suspension (Teshima *et al.*, 2006). Various other solid dosage formulations have been developed but none offer any significant advance (Spireas & Sadu, 1998). Poor patient compliance is also significant (Ratto *et al.*, 1988). Thus, a new water-soluble formulation is required to increase oral bioavailability, reducing the dosage required and reduce the unfavourable taste associated with the drug.

Tetracaine is an ester-based local anaesthetic. It is a lipophilic drug with an aqueous solubility of 0.555 mg/mL at 25 °C (logP= 3.54), though the drug can be formulated as a salt with a much improved solubility profile. However, in order for tetracaine to exert a therapeutic effect by crossing the skin barrier it must be exist in both neutral and salt forms. Hence, novel formulations are appropriate.

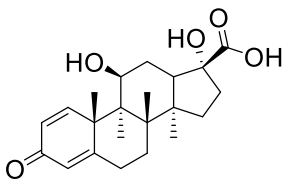

Prednisolone

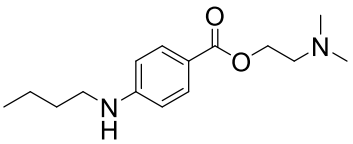

Tetracaine

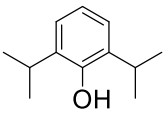

Propofol

Figure 79: The molecular structures of hydrophobic drugs propofol, tetracaine and prednisolone.

Calix[4]resorcinarenes octa- sodium salt **46a-d** and calix[4]pyrogallolarenes dodeca-sodium salt **46e-f** were synthesised as previously described.

3.3 UV-Visible Spectroscopy

UV-Vis spectrophotometry is a quantitative analytical technique based upon the absorption of near-ultraviolet (180–390 nm) or visible (390–780 nm) radiation by chemical species in solution or in the gas phase. The basic principle is the measurement of the intensity of radiation at specific spectral wavelengths which are characteristic to the samples involved. Atoms or molecules can absorb light of certain energies, resulting in a transition from the ground state or a lower-energy excited state to a higher-energy excited state; the wavelength at which this occurs depends upon the bonding of the atom or molecules' electrons. When UV-Visible light is passed through a sample, the light emerging from the sample is then analysed by a

spectrophotometer producing an absorption spectra. In absorption UV-Visible spectroscopy, the absorption is proportional to concentration according to the Beer Lambert law. Calibration curves can be used to predict the concentration of unknown samples (Venkatachalam, 2016).

3.4 High Performances Liquid Chromatography

High performance liquid chromatography (HPLC) is the most common analytical method used in the pharmaceutical industry. HPLC is one of the powerful techniques that allows the isolation, identification and quantitative determination of compounds on the basis of transport of molecules by a mobile phase through a stationary phase, colloquially known as a column. HPLC stationary phases can be chosen from an extremely large selection of commercially available materials. The mobile phase is typically an organic solvent mixed with water and salts, buffers, acids, bases or other additives and organic solvents. HPLC can be used for the separation of almost any mixture of solubilised chemical compounds (Mcpolin, 2003).

3.5 Loading of Hydrophobic Drugs into Nanocarriers

Calix[4]resorcinarene octa- sodium salts **46a-d** and calix[4]pyrogallolarene dodeca-sodium salts **46e-f** solutions of various concentrations (1 mg/mL, 3 mg/mL and 6 mg/mL) were prepared in deionised water and probe sonicated for 10 minutes to ensure dispersion of the carriers and allow any aggregates to form, in a similar manner to that reported in Chapter 2. The drugs being investigated were added separately to the solutions of each carrier. A total of 27 mixtures of each hydrophobic drug with the carriers were investigated. For each of the carrier **46a-f**, various weight ratios were prepared by adding 1:1, 5:1 and 10:1 initial drug: carrier weight ratios. All carriers: drug mixtures were probe sonicated for a further 10 min to ensure maximum

dispersion of the molecules and aggregates present was achieved. Propofol is an oily, viscous liquid but the other drugs used were added in powder form. After cooling to room temperature, the mixtures were filtered using 0.45 µm in-line filters to ensure removed any excess insoluble free drugs, again using the same protocol as in Chapter 2. The resulting solutions were allowed to relax so that aggregates could form.

3.5.1 Determination of Drug Loading Capacity

3.5.1.1 Solubilisation of Propofol

The drug loading capacity of carriers **46a-f** was determined by HPLC. Carrier: propofol samples were filtered using an in-line membrane filter (0.45 µm), and diluted with 1 mL of the mobile phase. The chromatographic analysis was performed a reverse phase RP Zorbax ODS 250 mm × 46 mm × 5 µm (Hichrom, Lutterworth, UK) column, and a mobile phase of methanol: water (80:20, v/v) at a flow rate of, 1 mL/min. The detector was set at λ = 229 nm.The linear peak area-concentration standard curves over the concentration range 80-0.625 µg/mL were used to calculate the quantity of propofol present in the samples. The correlation coefficient obtained was 0.9998. Drug quantification was run in triplicate. The results of HPLC analysis of pure propofol, pure carrier and the corresponding drug: carrier inclusion complex of propofol with carrier are shown in Figure 80. Pure propofol had a retention time of 2.22 minutes and carrier **46a** had a retention time of 0.72 minutes (Figure 80A and B). The chromatogram of the inclusion complex shows peaks attributed to both pure propofol and carrier **46a** at the same retention times, indicating the existence of both propofol as well as carrier in the inclusion complex. Complexation of propofol with the other carriers was carried out and the HPLC results shown in Figures 81-85.

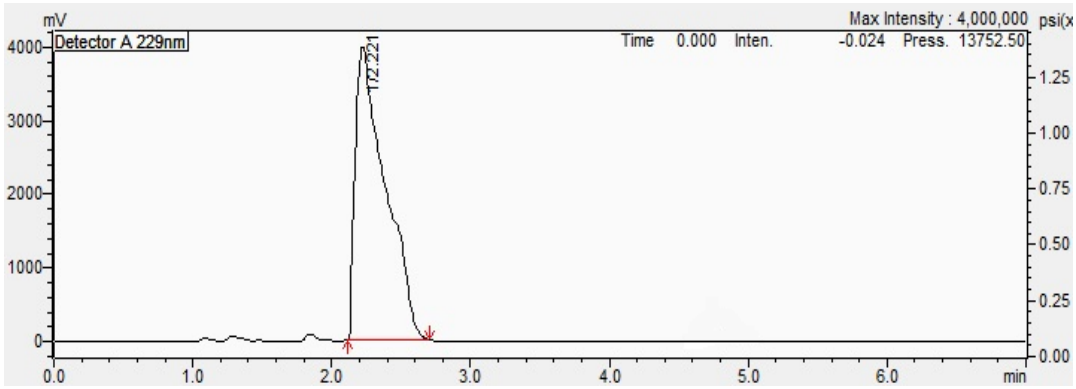

A. Pure Drug (Propofol)

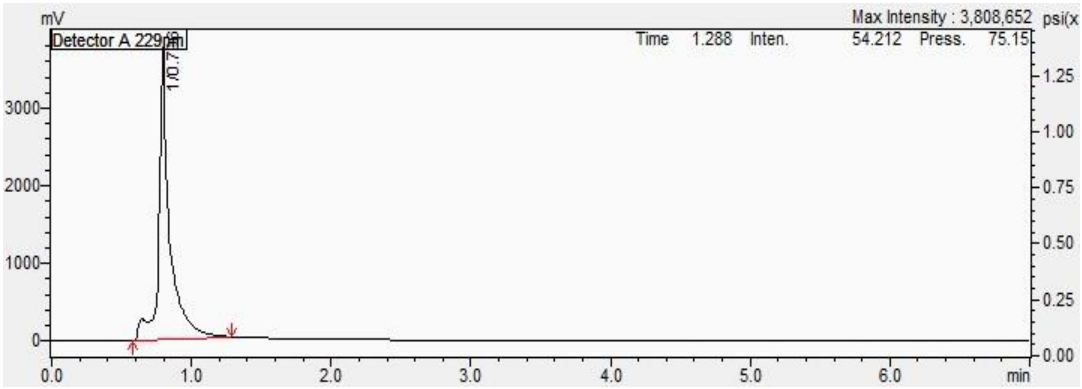

B. Carrier **46a**

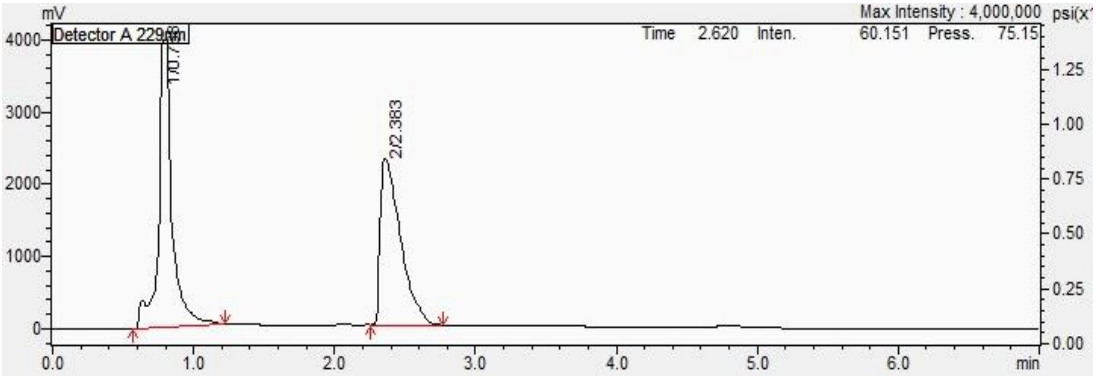

C. Formulation

Figure 80: The HPLC chromatogram of (A) standard pure drug propofol (B) carrier **46a** and (C) carrier: drug formulation.

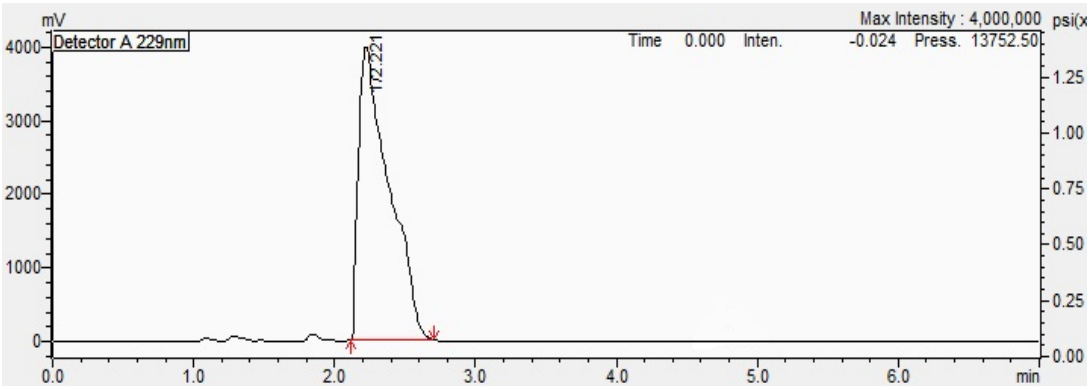

A. Pure Drug (Propofol)

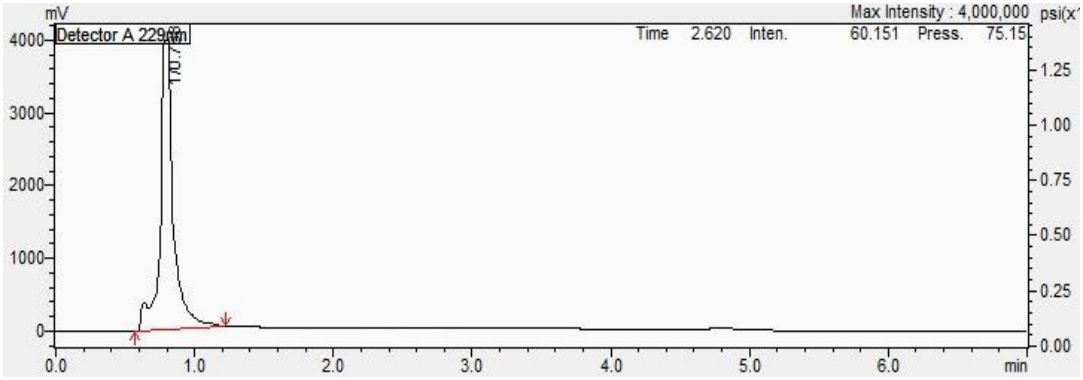

B. Carrier **46b**

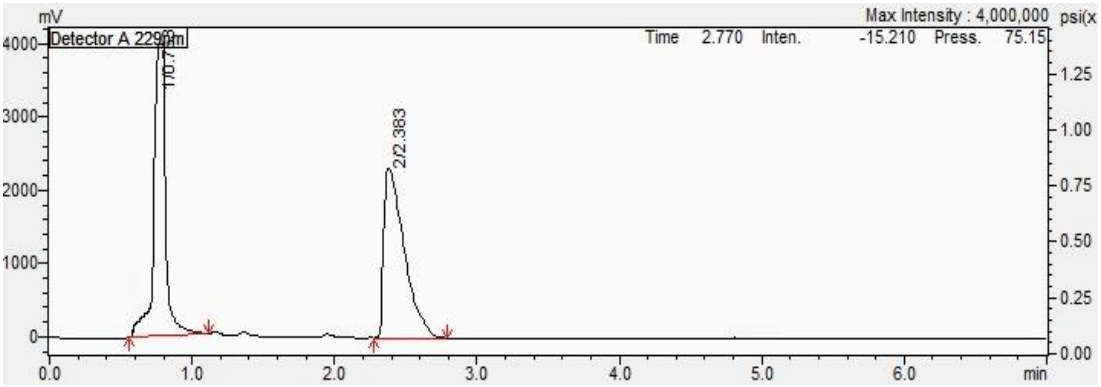

C. Formulation

Figure 81: The HPLC chromatogram of (A) standard pure drug propofol (B) carrier **46b** and (C) carrier: drug formulation.

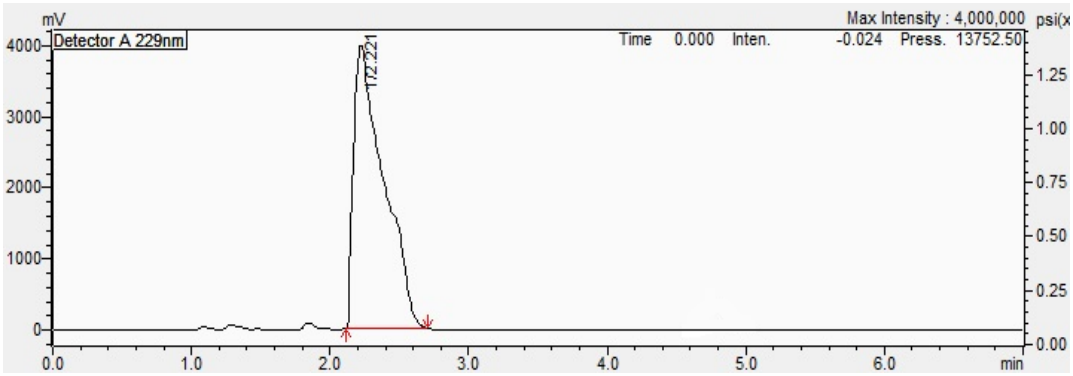

A. Pure Drug (Propofol)

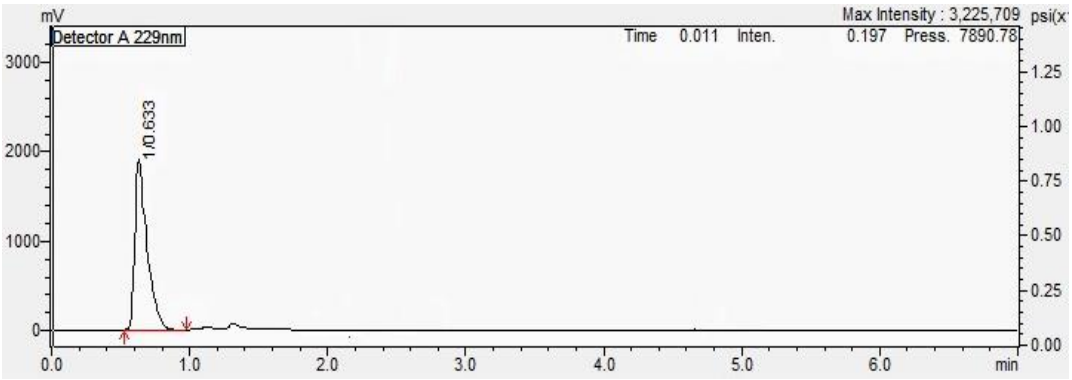

B. Carrier **46c**

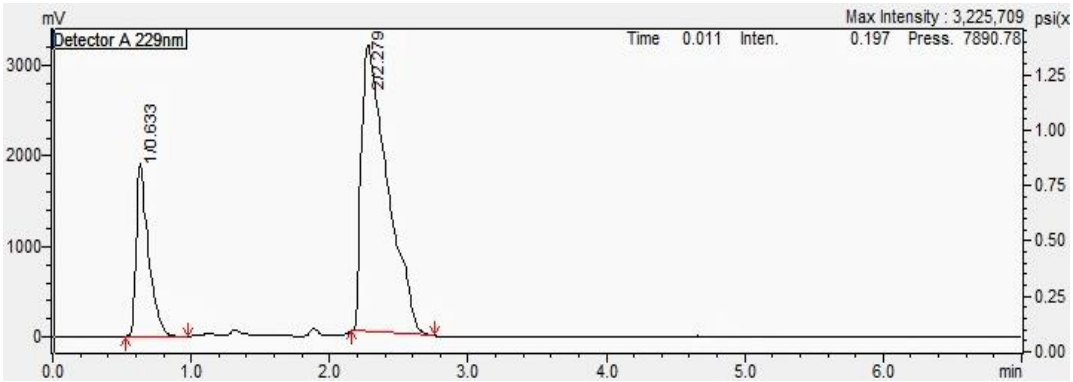

C. Formulation

Figure 82: The HPLC chromatogram of (A) standard pure drug propofol (B) carrier **46c** and (C) carrier: drug formulation.

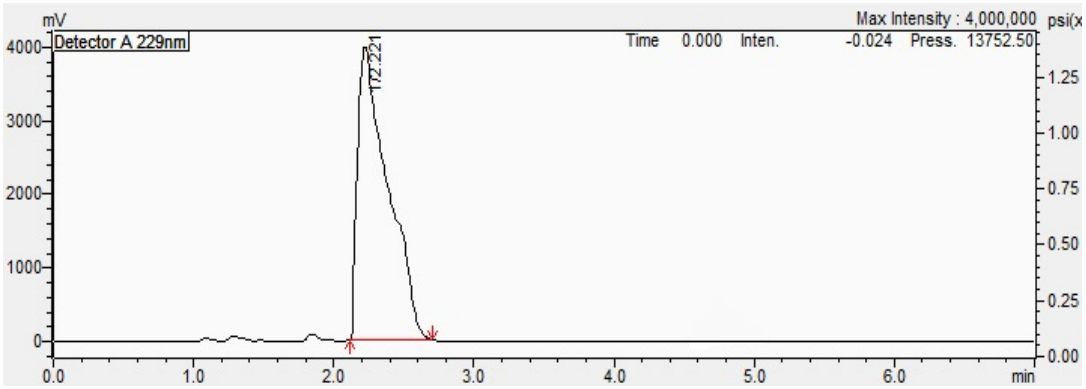

A. Pure Drug (Propofol)

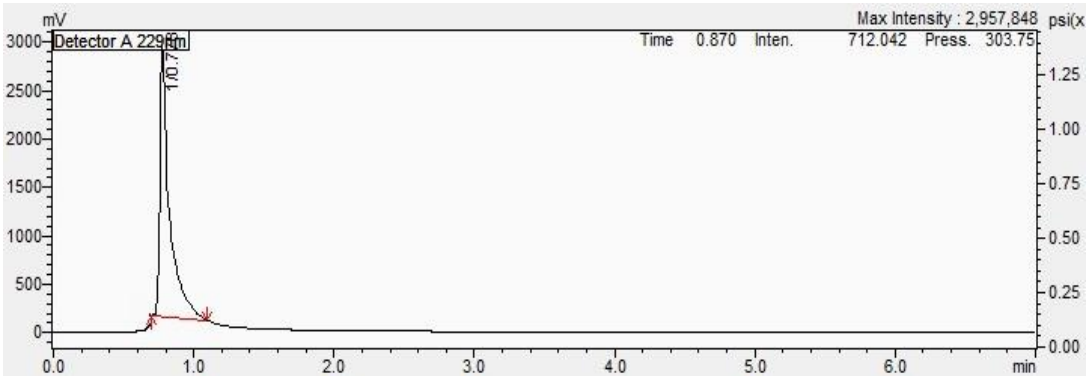

B. Carrier **46d**

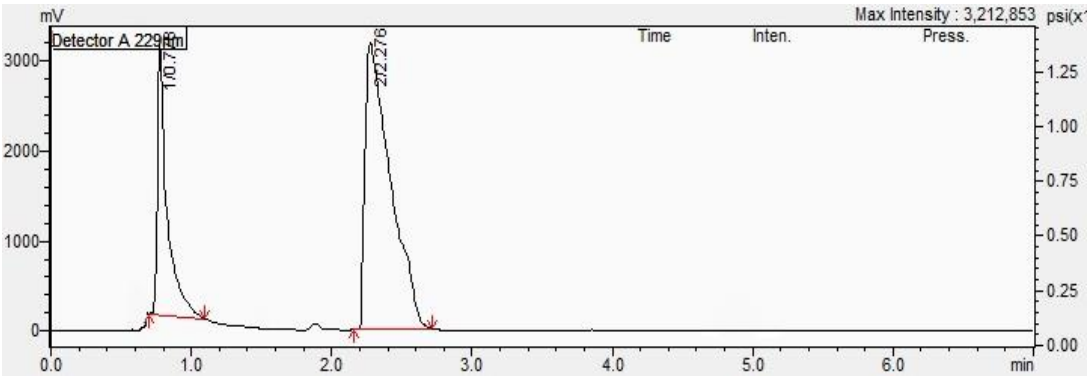

C. Formulation

Figure 83: The HPLC chromatogram of (A) standard pure drug propofol (B) carrier **46d** and (C) carrier: drug formulation.

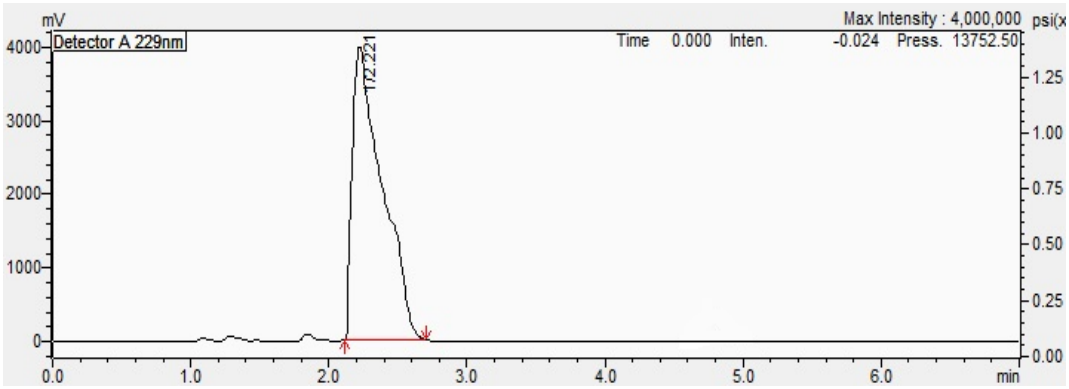

A. Pure Drug (Propofol)

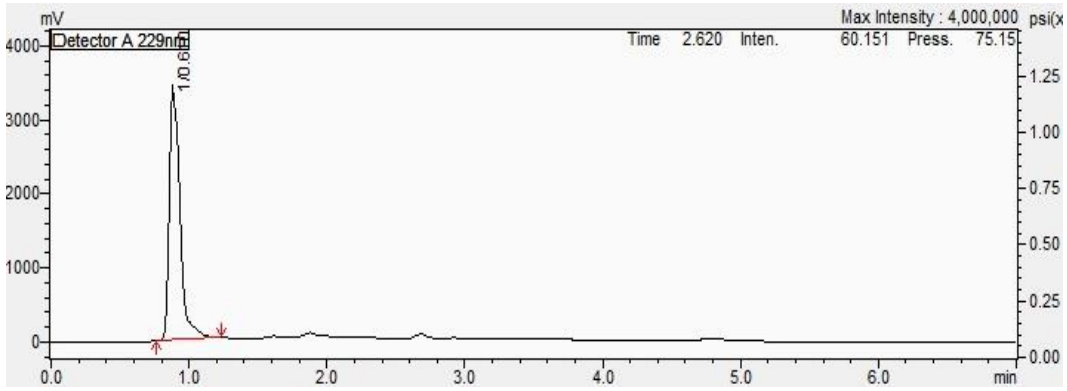

B. Carrier **46e**

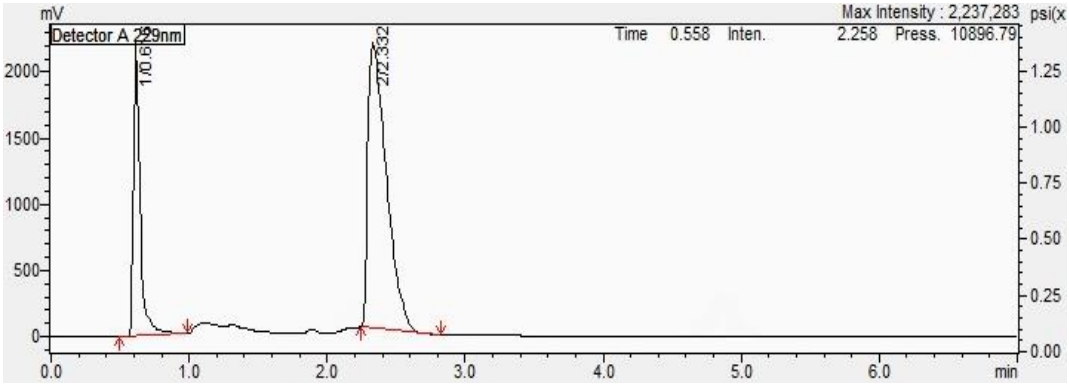

C. Formulation

Figure 84: The HPLC chromatogram of (A) standard pure drug propofol (B) carrier **46e** and (C) carrier: drug formulation.

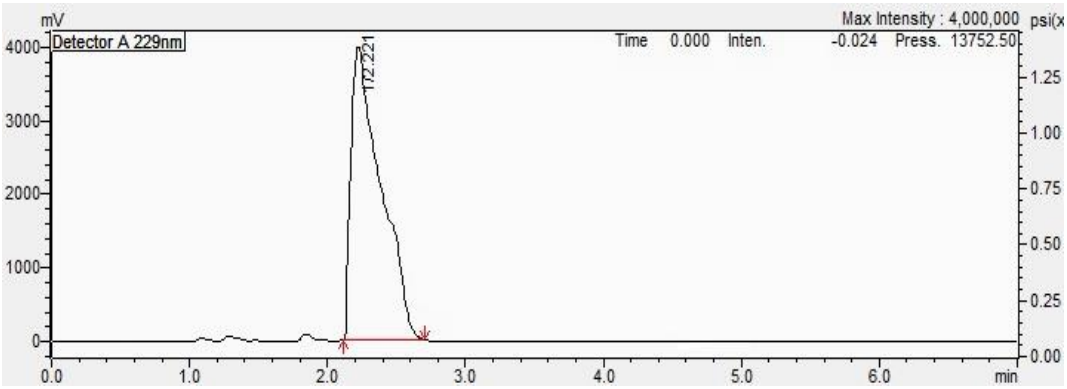

A. Pure Drug Propofol

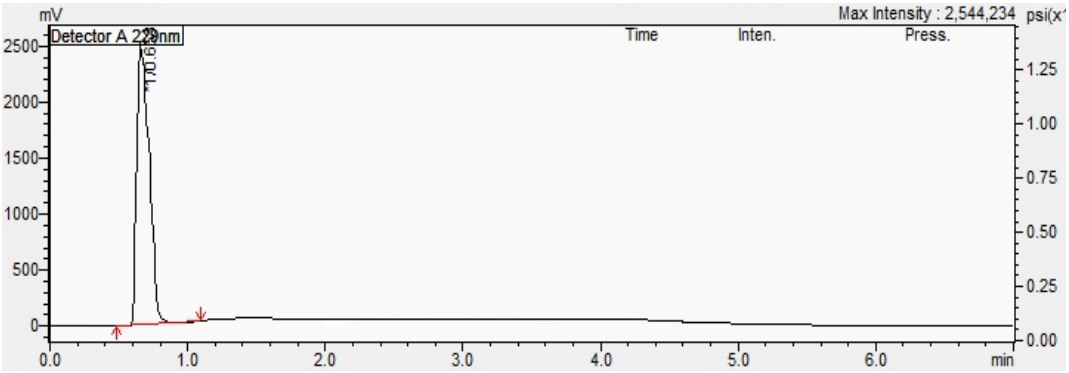

B. Carrier **46f**

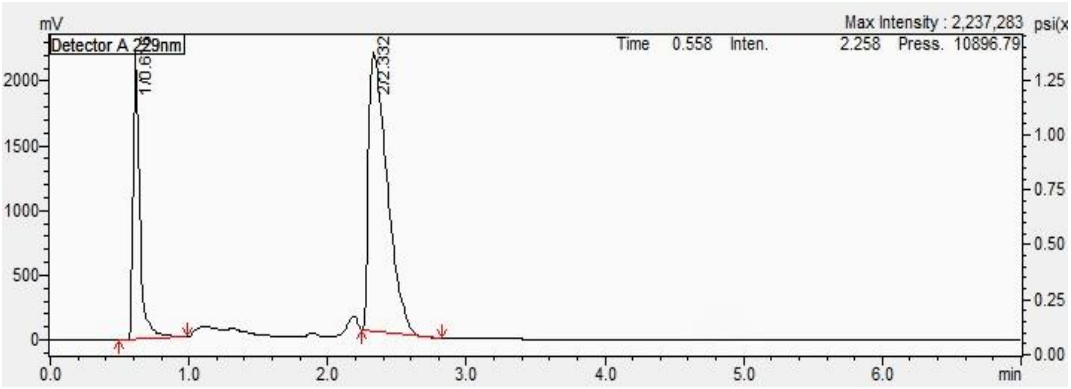

C. Formulation

Figure 85: The HPLC chromatogram of (A) standard pure drug propofol (B) carrier **46f** and (C) carrier: drug formulation.

3.5.1.2 Solubility of Prednisolone (PLS)

The drug loading was measured after filtration of the samples using an in-line membrane filter (0.45 µm) and diluted with 1 mL of the mobile phase

(water/acetonitrile 70: 30, v/v). Prednisolone content was analysed by HPLC using a reverse-phase RP Zorbax ODS 250 mm × 46 mm × 5 µm HPLC column with the mobile phase at flow rate of 1 mL/min and the detector set at λ= 243 nm. The amount of prednisolone contained in the samples was quantified from a standard calibration curve of the free drug (6 µg/mL – 25 µg/mL) with a correlation coefficient of 0.9998. Pure prednisolone (PLS) had a retention time of 3.25 minutes (Figure 86A). The carrier **46a** had a retention time of 0.95 minutes (Figure 86B). The chromatogram of the carrier: drug formulation showing that the same retention times were observed for the pure drug and the carrier is shown in Figure 86C. These results confirm the presence of the drug prednisolone (PLS) as well as carrier **46a** in the formulation. Complexation of prednisolone (PLS) with all carriers was carried out and the HPLC results shown (Figures 87-91).

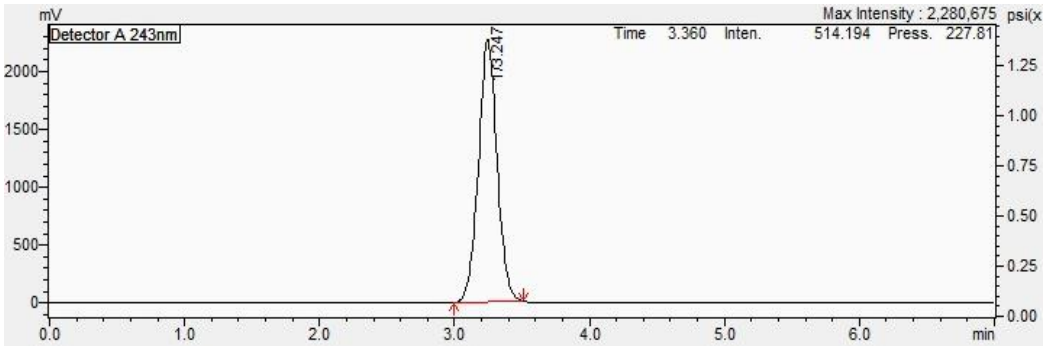

A. Pure Drug Prednisolone (PLS)

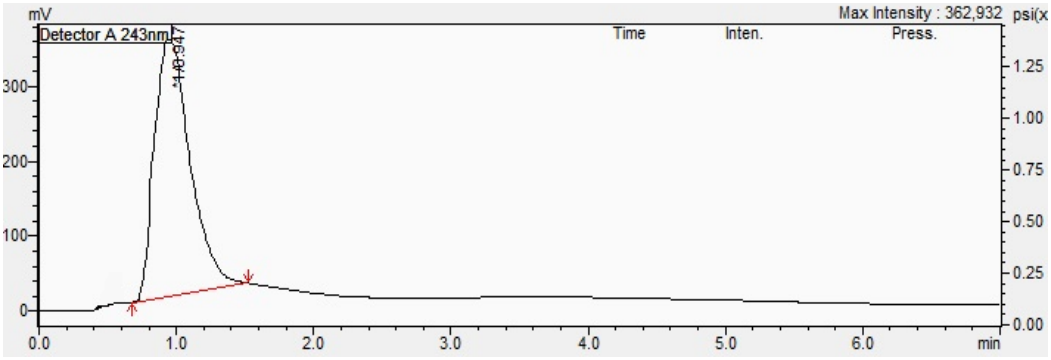

B. Carrier **46a**

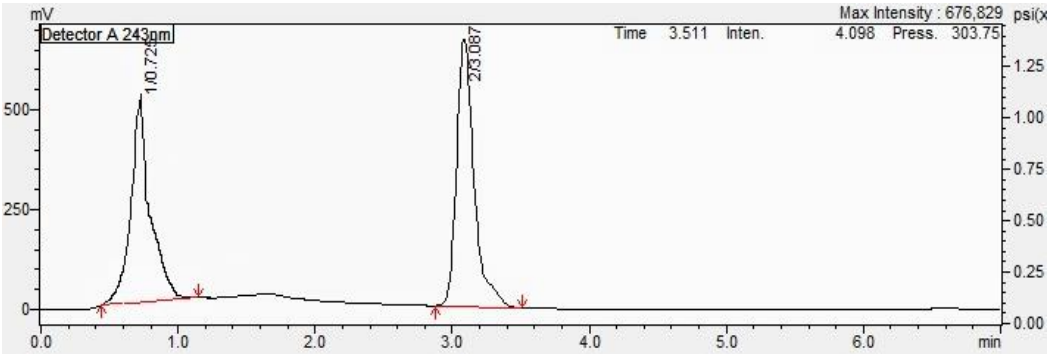

C. Formulation

Figure 86: The HPLC chromatogram of (A) standard pure drug prednisolone PLS (B) carrier **46a** and (C) carrier: drug formulation.

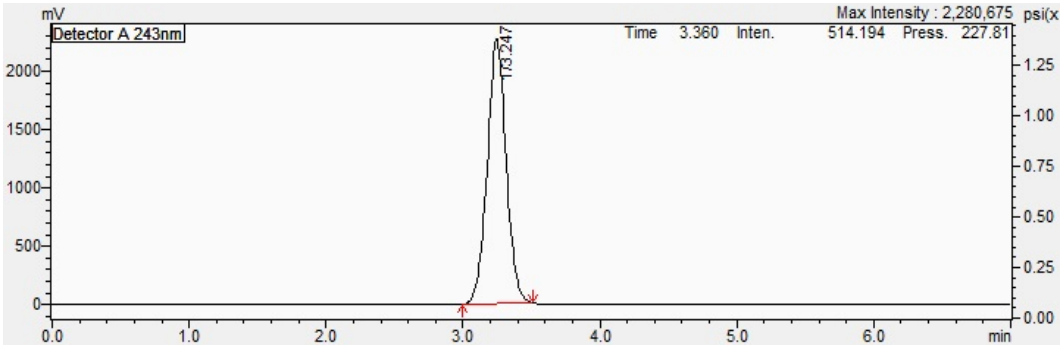

A. Pure Drug Prednisolone (PLS)

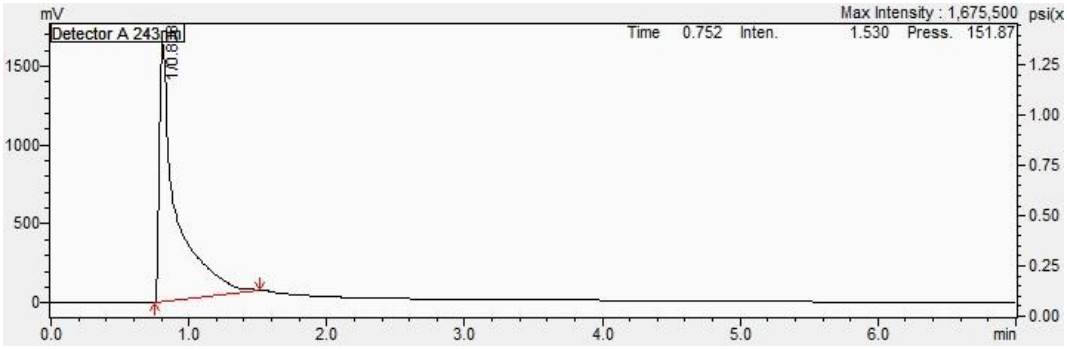

B. Carrier **46b**

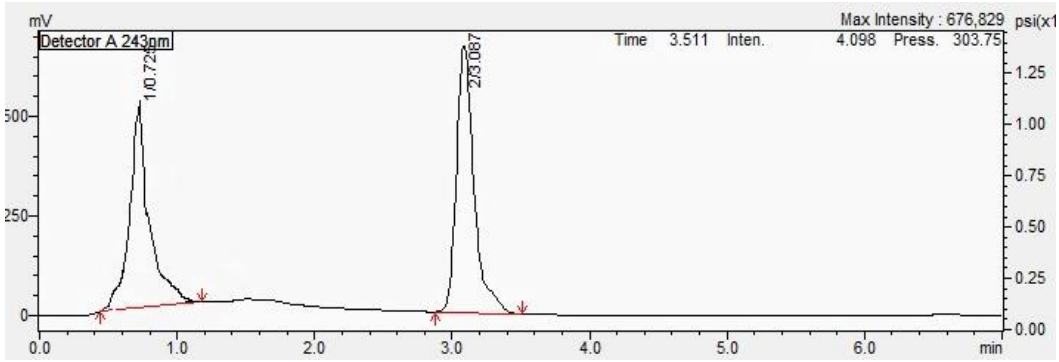

C. Formulation

Figure 87: The HPLC chromatogram of (A) standard pure drug prednisolone PLS (B) carrier **46b** and (C) carrier: drug formulation.

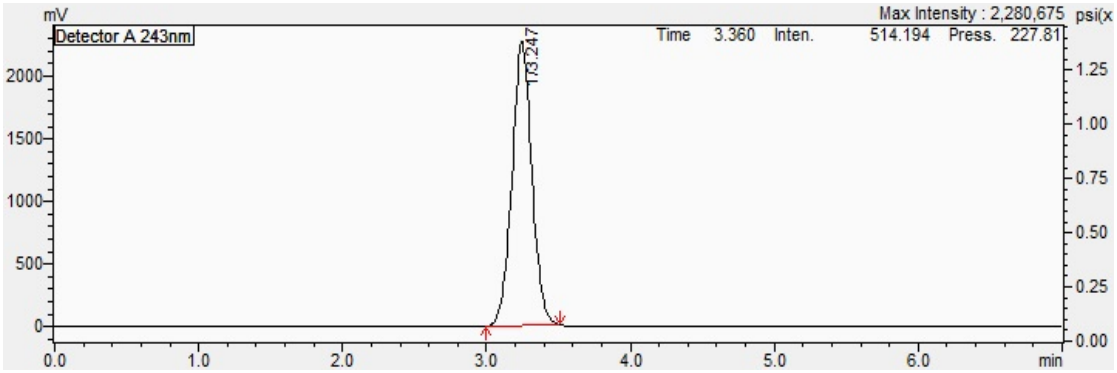

A. Pure Drug Prednisolone (PLS)

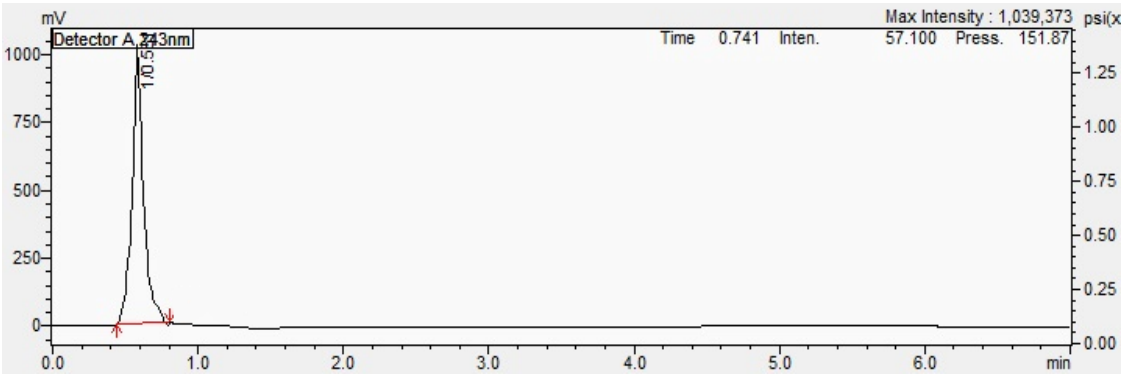

B. Carrier **46c**

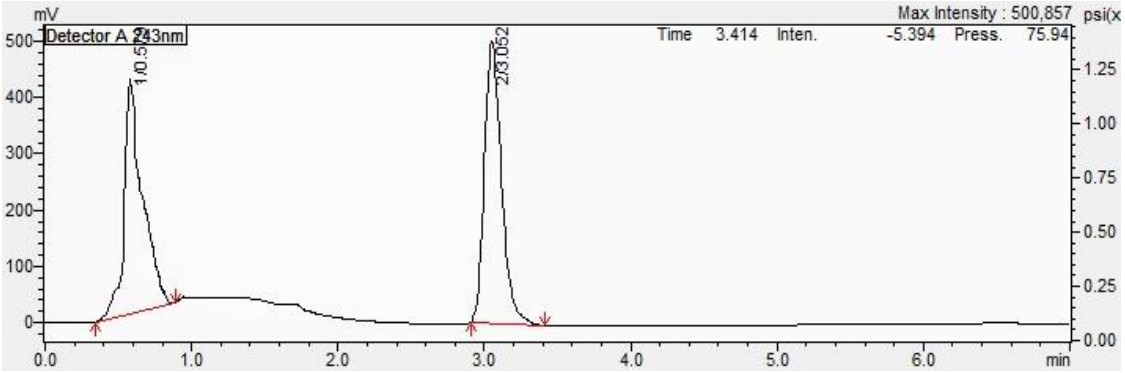

C. Formulation

Figure 88: The HPLC chromatogram of (A) standard pure drug prednisolone PLS (B) carrier **46c** and (C) carrier: drug formulation.

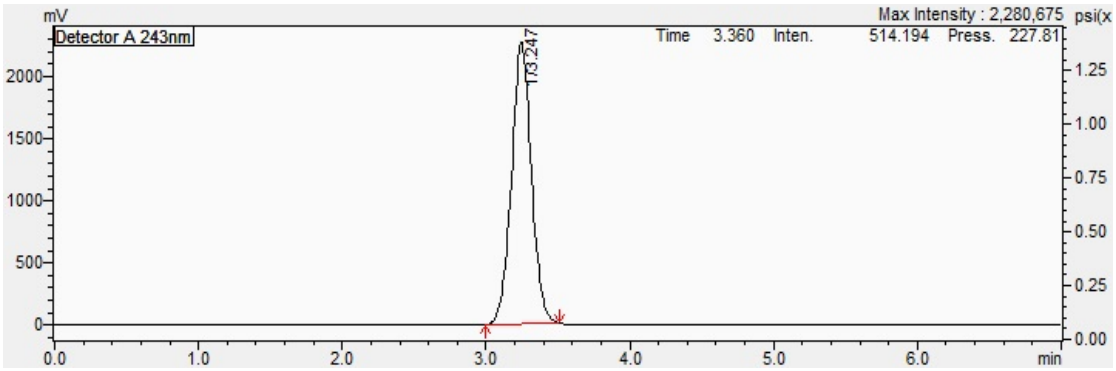

A. Pure Drug Prednisolone (PLS)

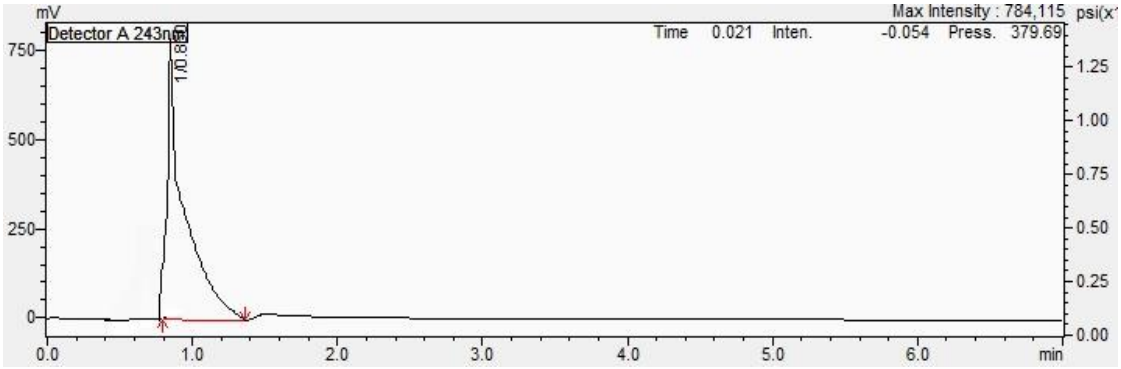

B. Carrier **46d**

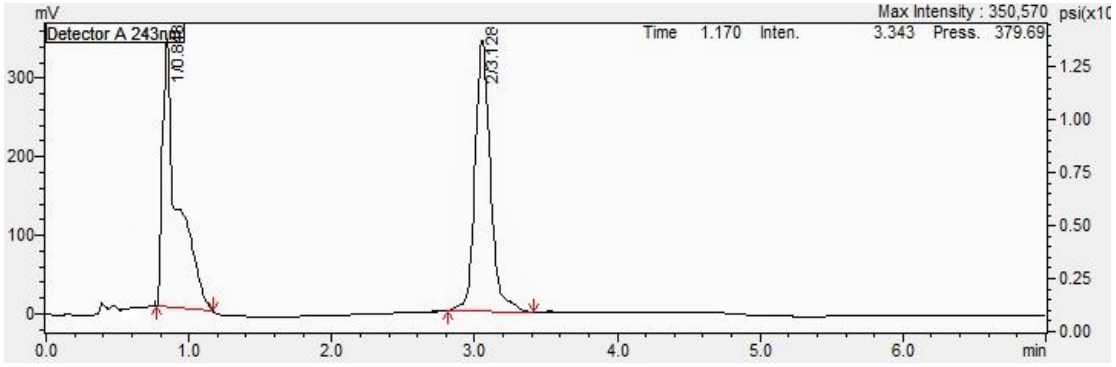

C. Formulation

Figure 89: The HPLC chromatogram of (A) standard pure drug prednisolone PLS (B) carrier **46d** and (C) carrier: drug formulation.

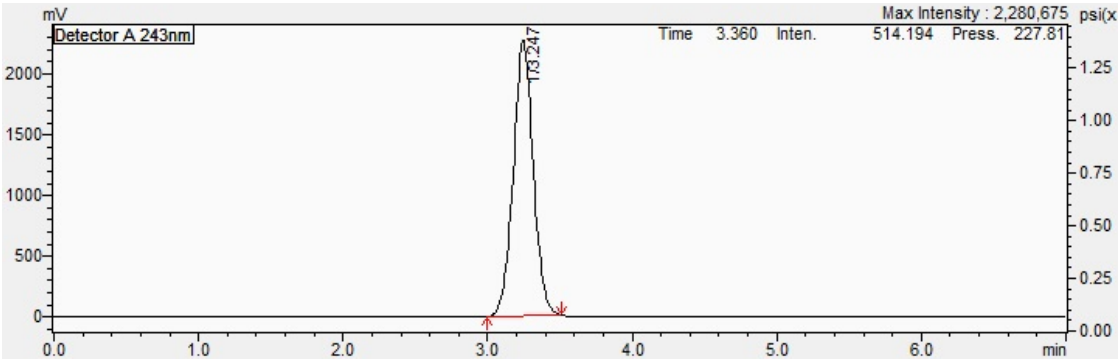

A. Pure Drug Prednisolone (PLS)

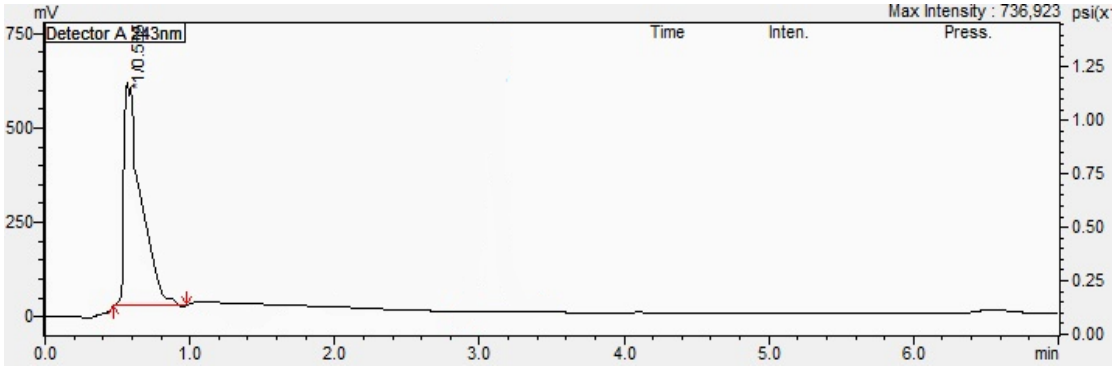

B. Carrier **46e**

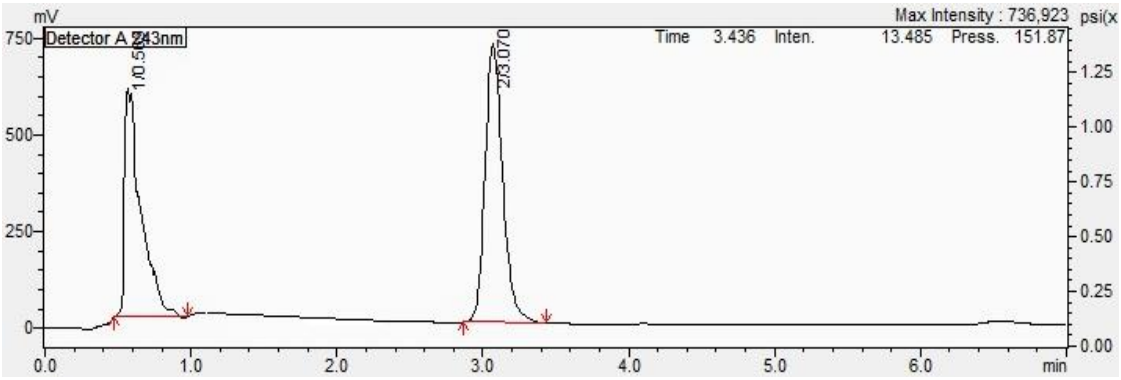

C. Formulation

Figure 90: The HPLC chromatogram of (A) standard pure drug prednisolone PLS (B) carrier **46e** and (C) carrier: drug formulation.

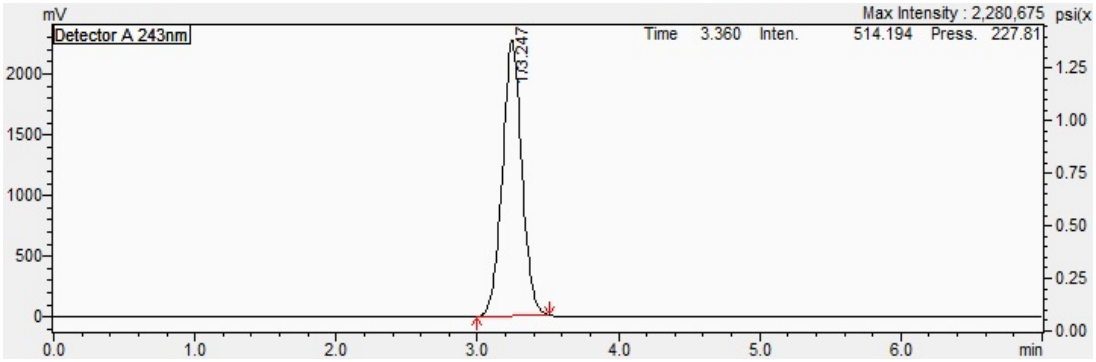

A. Pure Drug Prednisolone (PLS)

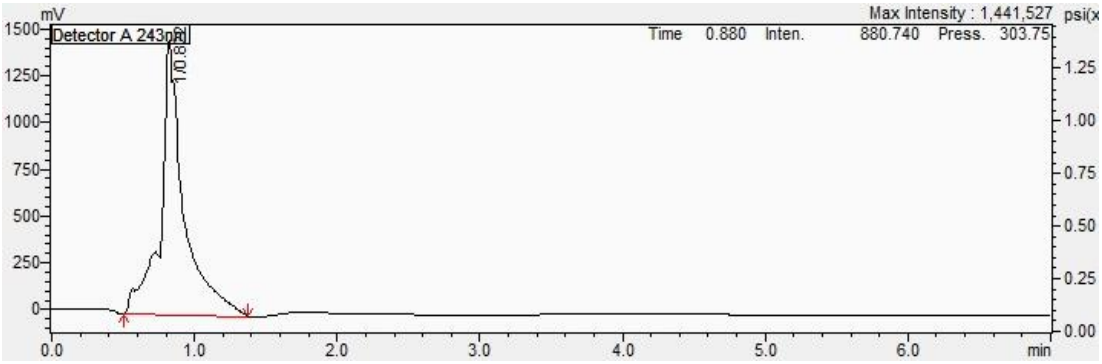

B. Carrier **46f**

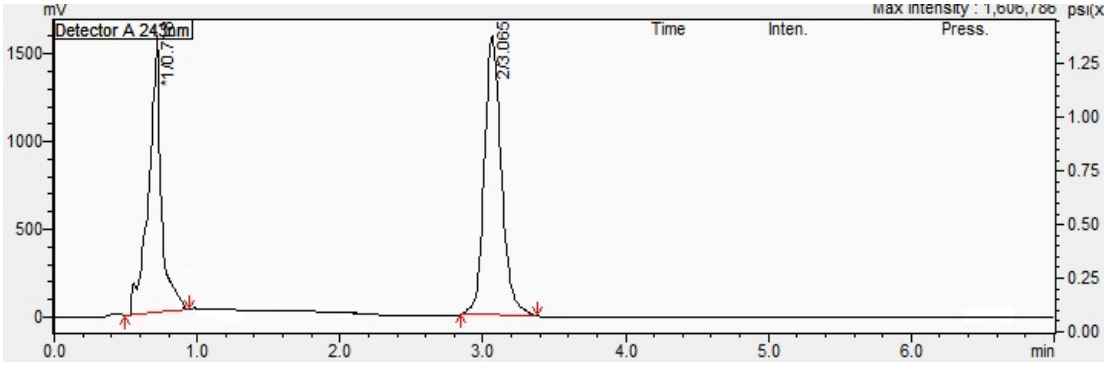

C. Formulation

Figure 91: The HPLC chromatogram of (A) standard pure drug prednisolone PLS (B) carrier **46f** and (C) carrier: drug formulation.

3.5.1.3 Solubility of Tetracaine (TTC)

The total amount of the hydrophobic drug tetracaine loaded solubilised by the calix[4]resorcinarnes **46a-d** and calix[4]pyrogallolarenes **46e-f** was measured by HPLC using a reverse phase RP Zorbax ODS 250 mm × 46 mm × 5 µm HPLC

column, with a flow rate of 1 mL/min and the spectrophotometric detector set at λ = 210 nm. Carrier: tetracaine samples were filtered using an in-line membrane filter (0.45 µm), and diluted with 1 mL of the mobile phase (45: 55, v: v acetonitrile: 45 mM potassium dihydrogen phosphate made up in water and pH adjusted to pH 3 with orthophosphoric acid). Tetracaine content was quantified from a standard calibration curve of the free drug (0.1 µg/mL – 25 µg/mL) with a correlation coefficient of 0.9998. Pure tetracaine (TTC) had a retention time of 1.97 minutes, which corresponds to the protonated species (Figure 92A), whilst that for carrier **46a** was 0.62 minutes for the salt and 4.07 min for the protonated carrier, due to the acidic eluent (Figure 92B). The chromatogram of the formulation (carrier **46a**: TTC) contained the same components (Figure 92C). These results indicated the presence of TTC as well carrier **46a** in the formulation. Complexation of TTC with carrier **46b** was also carried out and the HPLC results shown (Figure 93).

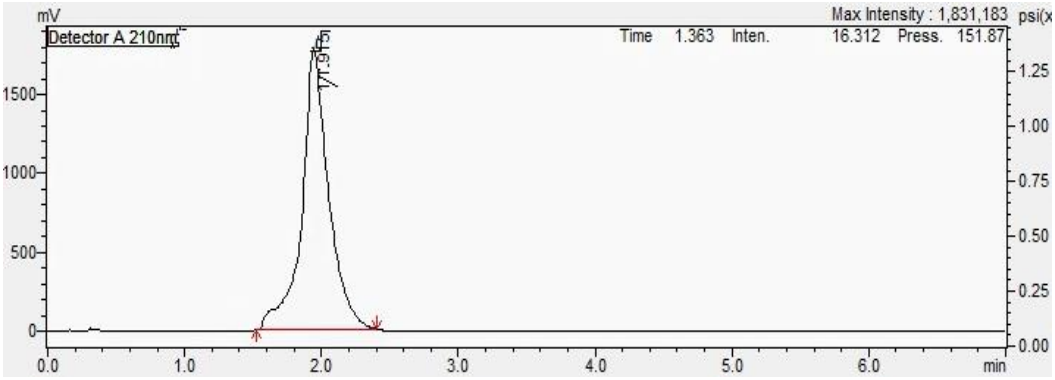

A. Pure Drug Tetracaine (TTC)

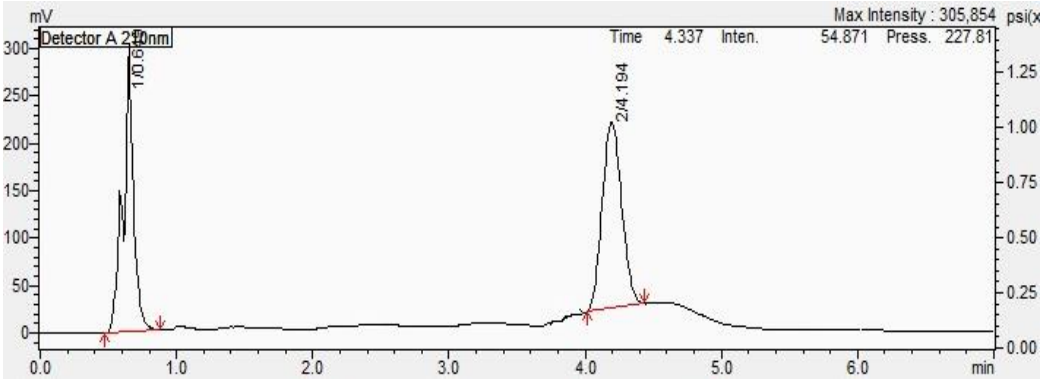

B. Carrier **46a**

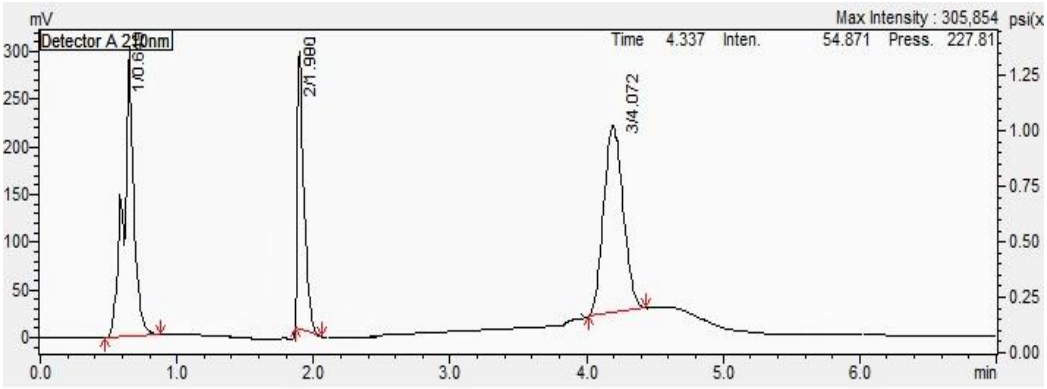

C. Formulation

Figure 92: The HPLC chromatogram of (A) standard pure drug TTC (B) carrier **46a** and (C) carrier: drug formulation.

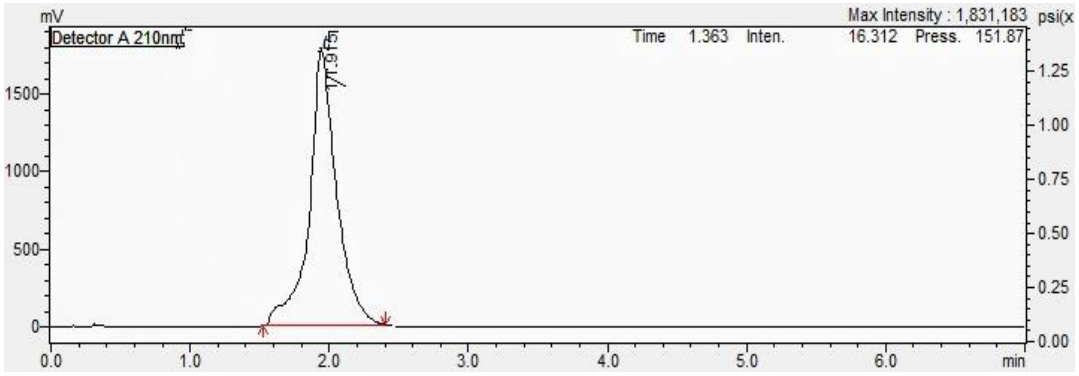

A. Pure Drug Tetracaine (TTC)

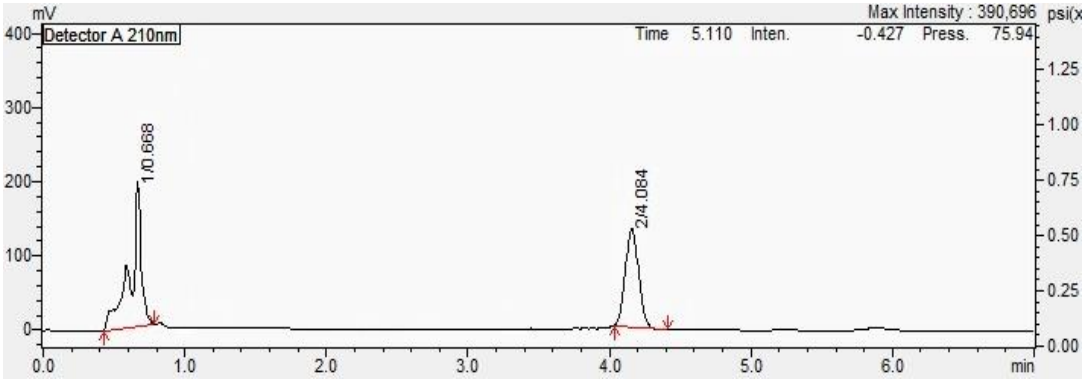

B. Carrier **46b**

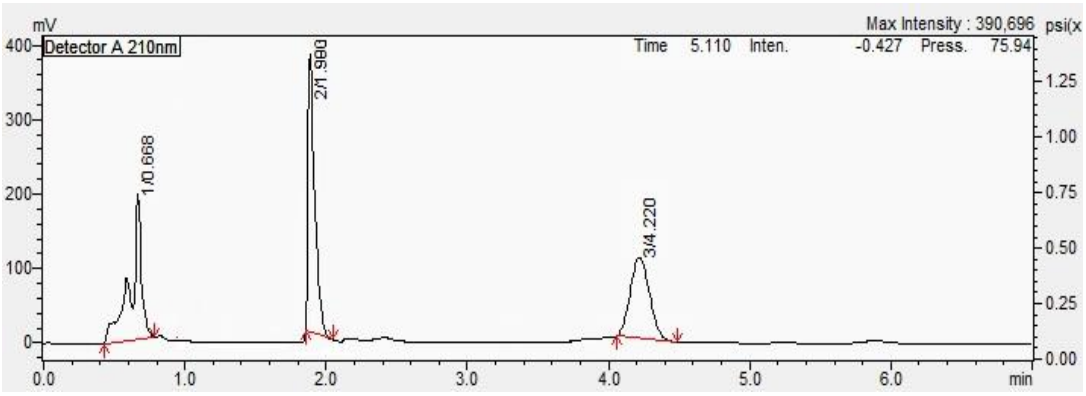

C. Formulation

Figure 93: The HPLC chromatogram of (A) standard pure drug TTC (B) carrier **46b** and (C) carrier: drug formulation.

3.5.2 Particle Size, Zeta Potential and Conductivity Measurements of Aggregate Formed

Particle size and Zeta potential and conductivity measurements were determined for all drug formulations using the Zetasizer instrument, photon correlation spectroscopy (PCS) in particular, as previously described in Chapter Two.

3.5.2.1 FTIR Analysis of Freeze Dried Formulations

Freshly prepared formulations (as described in 3.3.2.3) were freeze-dried. The freeze-dried material was analysed by Fourier Transform Infrared spectroscopy (FTIR). The spectra obtained were compared to spectra of the free drug and unloaded carriers **46a-f**, respectively.

3.5.2.2 UV-Vis Spectroscopy Analysis of Formulations

UV-Vis spectroscopy was used to characterise each of the pure drugs, carriers **46a-f** and all carrier: drug formulations. The λ_{max} of the pure drugs, carriers **46a-f** and carrier: drug formulations were determined within the range 400–700 nm and compared.

3.5.3 *In Vitro* Drug Release

A modification of the method described by Lee was used for this study (Lee *et al.*, 2004): 2 mL volumes of the carrier: drug formulations containing a known quantity of drug under investigation were pipetted into Visking membrane (MW cut off = 12-14 kDaltons), and the drug was released into deionised water (200 mL) at 20 ºC and at 37 ºC with stirring for 120 h. At pre-determined time points (*e.g.*, 5 minutes, 10 minutes, etc.) a 1 mL volume of the release medium was withdrawn and replaced with the same volume of deionised water. The amount of the drug released from

each formulation was determined using HPLC. The cumulative profile of drug release was calculated in respect to drug loading concentration. All experiments were carried out in triplicate.

3.6 Results

3.6.1 Drug Loading Evaluation

3.6.1.1 Propofol Solubilisation

Propofol was loaded into all calix[4]resorcinarene carriers **46a-d** and calix[4]pyrogallolarene carriers **46e-f** aqueous solutions (1 mg/mL, 3 mg/mL and 6 mg/mL) using initial drug: carrier mass ratios of 1:1, 5:1 and 10:1. The maximum loading concentration for each carrier was determined by using HPLC. The amount of propofol solubilised by each of the amphiphilic carriers compared with the intrinsic drug solubility was obtained (Figure 94). It can be seen that as the concentration of the calix[4]resorcinarene carriers **46a-d** and calix[4]pyrogallolarene carriers **46e-f** increased from 1 mg/mL to 6 mg/mL, the amount of drug loading increased and the highest drug loading was achieved at an initial drug: carrier: mass ratio of 10:1. Typically, drug incorporation is affected by the drug feed ratio, thus increased feed ratios result in increased drug content. The results (Figure 94A) demonstrate that the loading capacity of calix[4]resorcinarene **46a**, possessing C_4 alkyl substituents on the lower rim, was about 12 mg/mL compared with 42 mg/mL for carrier **46b** which possesses longer and more hydrophobic C_7 alkyl substituents on the lower rim (Figure 94B). The amphiphilic nanocarrier **46c** with methyl groups attached at the 2-position of the upper rim and C_4 alkyl substituents on the lower rim was able to increase drug solubilisation compared to **46d** C_7 alkyl substituents on the lower rim, as maximum concentrations of 18 mg/mL were achieved with **46c** compared with 35

mg/mL for **46d** (Figure 94C and D). Additionally, for the calix[4]pyrogallolarenes **46e**, bearing twelve polar groups attached to the upper rim and C_4 alkyl substituents on the lower rim, and **46f** with the C_7 alkyl substituents on the lower rim, 15 mg/mL of drug loading was achieved with **46e** compared to 27 mg/mL for **46f** (Figure 94E and F). At all carrier concentrations **46a-f** appeared to load the maximum concentration of propofol at 10:1 drug: carrier initial mass ratio.

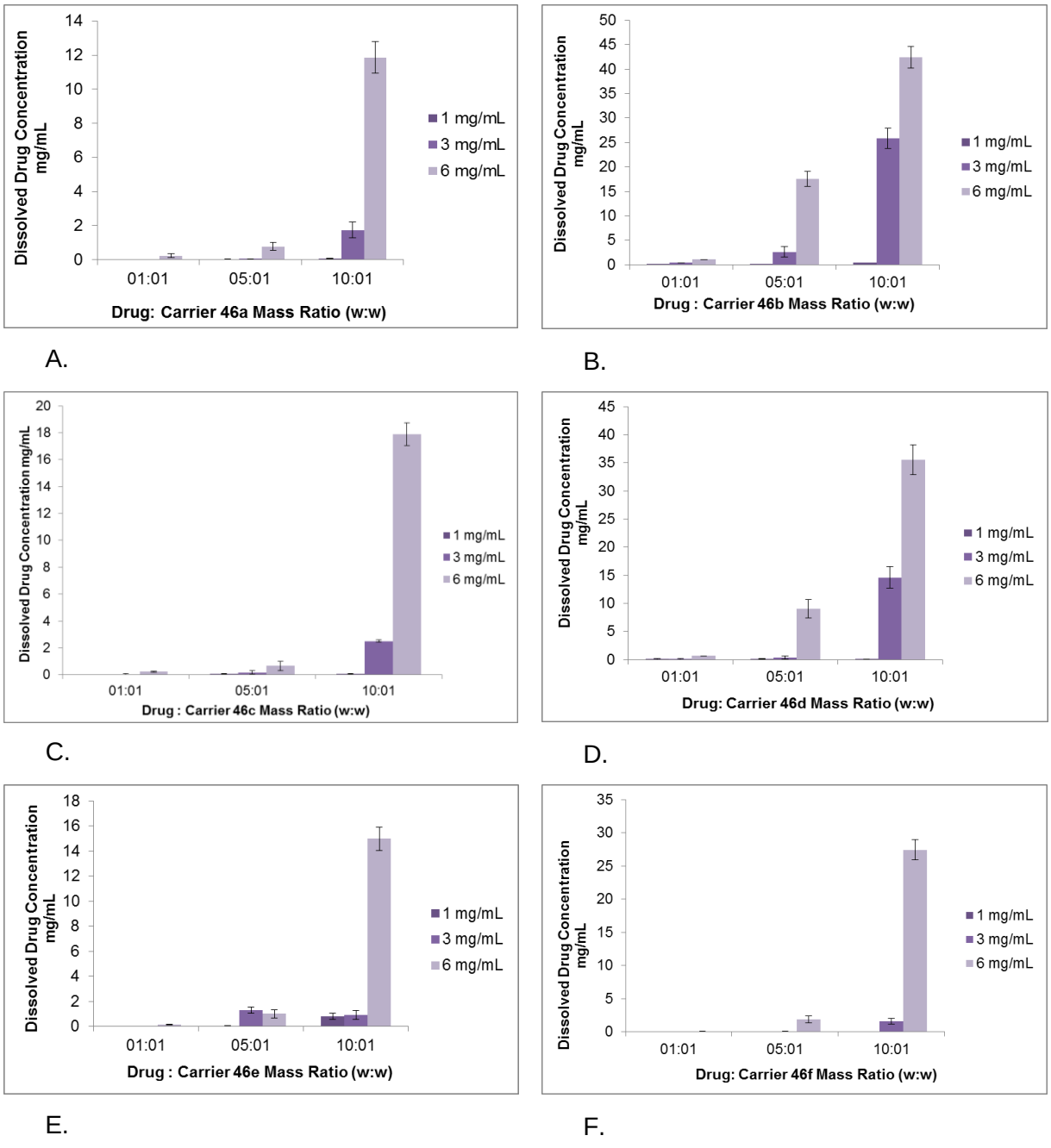

Figure 94: Propofol- loading concentration at three different feed ratios (1:1, 5:1 and 10:1) of drug: carriers (calix[4]resorcinarenes **46a-d** and calix[4]pyrogallolarenes **46e-f**.

3.6.1.2 Prednisolone (PLS) Solubilisation

Similar to the propofol study, nano-aggregates of the carriers with prednisolone were tested at varied concentrations, 1 mg/mL, 3 mg/mL and 6 mg/mL and using 1:1, 5:1 and 10:1 drug: carriers mass loading ratios. Prednisolone is a much larger molecule (molecular weight = 360.444 g/mol) compared to propofol (molecular weight = 178

g/mol), and the structure is much more complex bearing a number of polar residues. As could thus be expected, prednisolone loading did not follow the same trend in comparison with propofol. The results of drug solubilisation within all formulations (mg/mL) at varied excipient (calix[4]resorcinarenes **46a-b** and calix[4]pyrogallolarenes **46e-f** concentrations and initial drug: excipient feed concentration was presented (Figure 95). The results indicated that the highest solubilisation was obtained at the lowest concentration of 1 mg/mL. It was observed that prednisolone loading decreased with increasing carrier concentration. Accordingly, the drug solubilisation at low drug: carrier ratios were greater than at high drug: carrier ratios. The maximum concentration of prednisolone solubilised by each amphiphilic carrier was achieved at 1 mg/mL and 1:1 initial drug: carrier loading ratios, except for calix[4]pyrogallolarene **46e** (Figure 95E) which was at 5:1 initial drug: carrier loading ratio. There was no significant difference in the drug loading at 3 mg/mL and 6 mg/mL. The results showed that calix[4]pyrogallolarene **46a** (Figure 95A), calix[4]resorcinarene **46c** (Figure 95C) and calix[4]resorcinarene **46e** (Figure 95E) increased drug solubility by 1.30 mg/mL, 1.079 mg/mL and 1.038 mg/mL, respectively, when compared with the intrinsic drug solubility. This is not a particularly significant increase. Calix[4]resorcinarene **46a** with C_4 alkyl substituents on the lower rim was capable of solubilising up to 1.30 mg/mL of prednisolone, compared with only 1.05 mg/mL for calix[4]resorcinarene **46b** (Figure 95B).

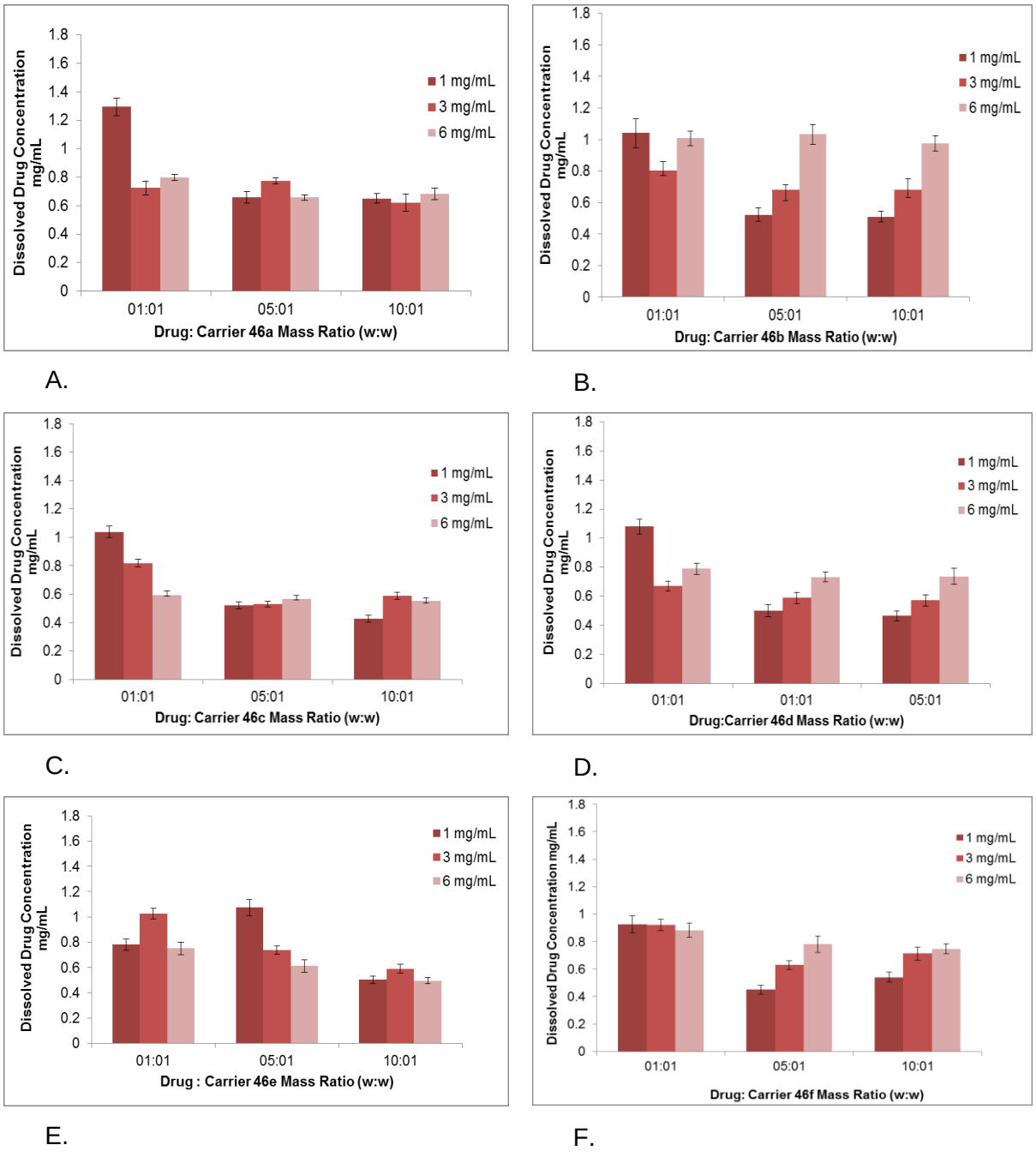

Figure 95: Prednisolone- loading concentration at three different feed ratios (1:1, 5:1 and 10:1) drug: carriers concentrations (calix[4]resorcinarenes **46a-d** and calix[4]pyrogallolarenes **46e-f**).

3.6.1.3 Tetracaine (TTC) Solubilisation

The hydrophobic drug, tetracaine, was loaded with calix[4]resorcinarenes **46a-b** nano-aggregates in aqueous solution (1 mg/mL, 3 mg/mL and 6 mg/mL) using initial

drug: carriers mass ratios of 1:1, 5:1 and 10:1. The amount of solubilised tetracaine ranged from 136 mg/mL to 500 mg/mL with the carriers **46a** and **46b**, respectively. The maximum concentration solubilised by each of the amphiphilic carriers is shown (Figure 96A and B). Both calix[4]resorcinarene **46a** and **46b** demonstrated excellent drug loading capacity and solubilisation of tetracaine (6 mg/mL, at initial drug: carrier loading ratio of 10:1). However, a precipitate was formed in each sample after two days, thus loading with other carriers was not investigated further. In this case it may be necessary to carry out the experiments under different conditions, at different pH values for example, but protonation of tetracaine increases its intrinsic solubility since it has two basic residues that may be protonated easily.

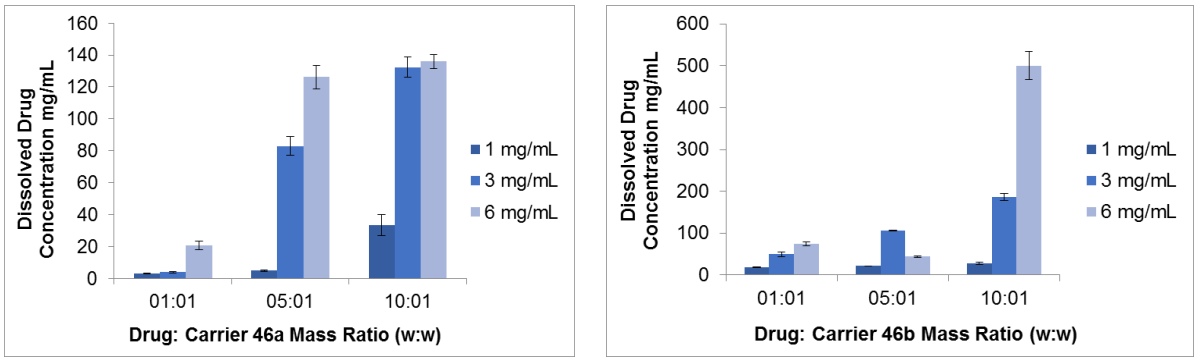

A. B.

Figure 96: Tetracaine- loading concentration at three different feed ratios (1:1, 5:1 and 10:1) for drug: carriers ratios for calix[4]resorcinarene **46a** (A) and calix[4]pyrogallolarene **46b** (B).

3.6.2 UV-Vis Spectroscopy

3.6.2.1 Propofol UV-Vis Spectroscopy

The UV-Vis data of the pure propofol, carrier **46a**, and the inclusion complex are shown in Figure 97. The results show three peaks corresponding to the wavelength of maximum absorption (λ_{max}) at 220, 280 and 275 nm for pure propofol, carrier 46a and the inclusion complex, respectively. The λ_{max} of carrier **46a** was shifted by the

addition of propofol, indicating that there is some interaction between the carrier **46a** and drug molecule. An absorption change was observed with all carriers (Figure 97).

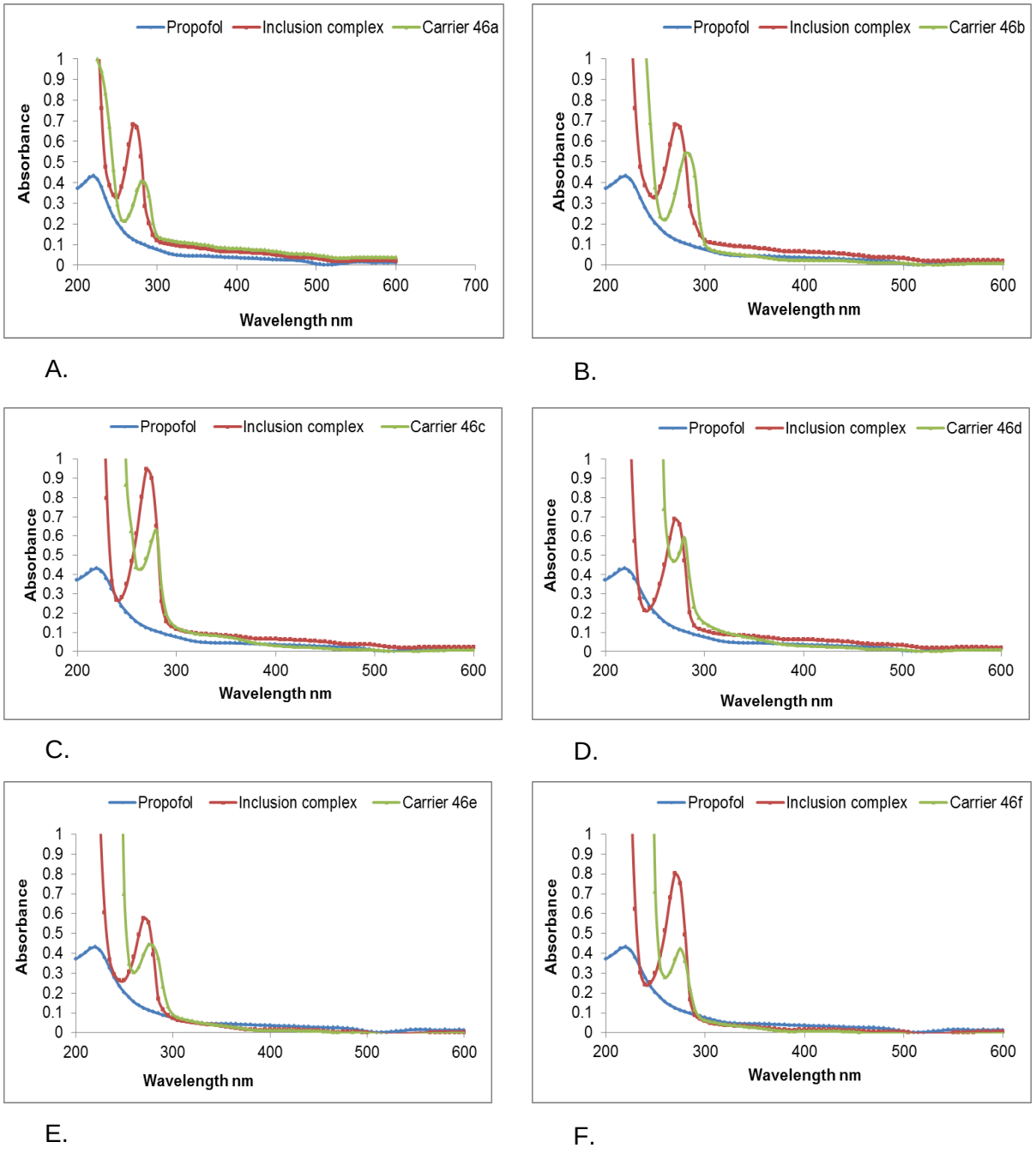

Figure 97: UV-Vis spectra of propofol; inclusion complex and carriers **46a-f**.

3.6.2.2 Prednisolone (PLS) UV-Vis Spectroscopy

The UV-Vis data of the pure prednisolone, carrier **46a**, and the inclusion complex are shown in Figure 98A. The results show three peaks at 240, 280 and 275 nm for pure

prednisolone, carrier **46a** and the inclusion complex, respectively. The λ_{max} of carrier **46a** was altered by the addition of prednisolone. Again, it is clear from the UV–Vis spectra that there is some interaction between the carrier **46a** and drug molecule, demonstrated for other carriers also and significantly so for calix[4]pyrogallolarenes **46e** and **46f**.

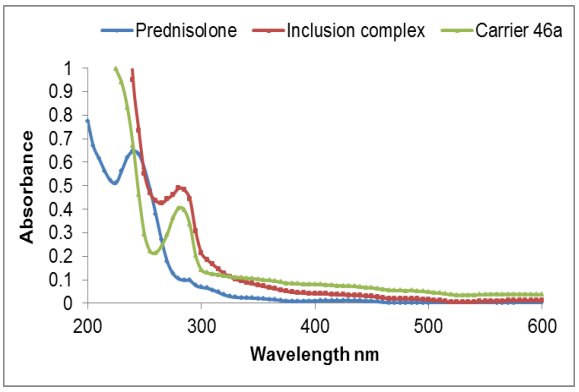

A.

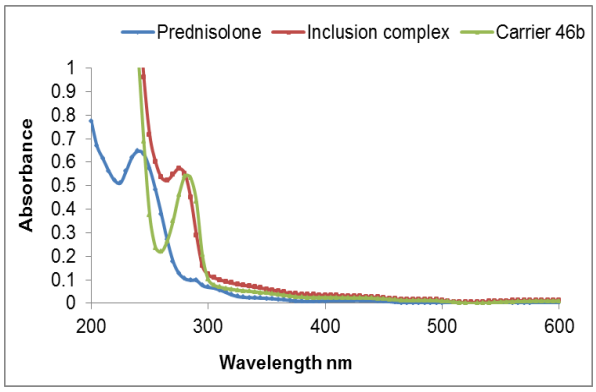

B.

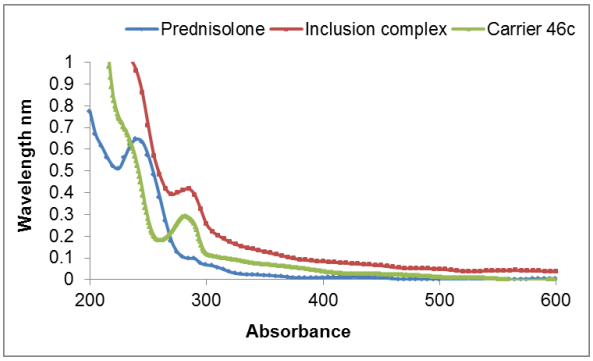

C.

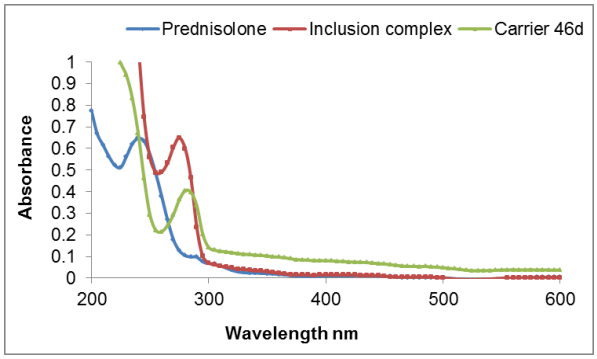

D.

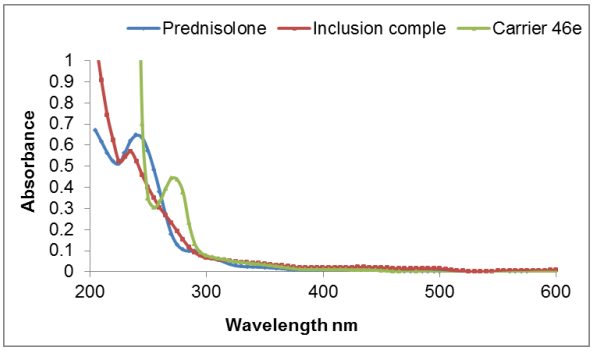

E.

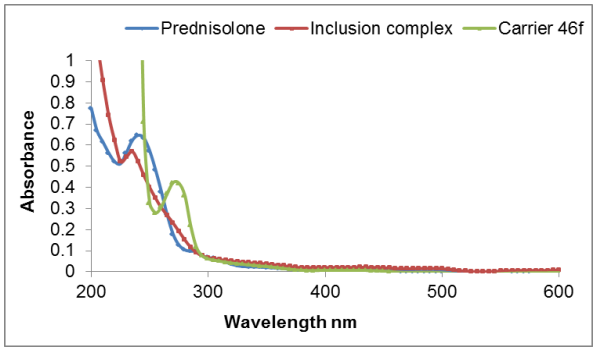

F.

Figure 98: UV-Vis spectra of prednisolone (PLS); inclusion complex and carriers **46a-f**.

3.6.2.3 Tetracaine (TTC) UV-Vis Spectroscopy

The UV-Vis spectra of tetracaine (TTC), carrier **46a** and the corresponding inclusion complex of TTC–carrier **46a** are shown in Figure 99A. The results show three λ_{max} at 300, 280 and 295 nm for pure TTC, carrier **46a** and the inclusion complex, respectively. The λ_{max}) of carrier **46a** was altered by the addition of TTC. Thus, the UV-Vis spectra indicate the formation of an inclusion complex between TTC and carrier **46a**. An absorption change was also observed with carrier **46b** (Figure 99B).

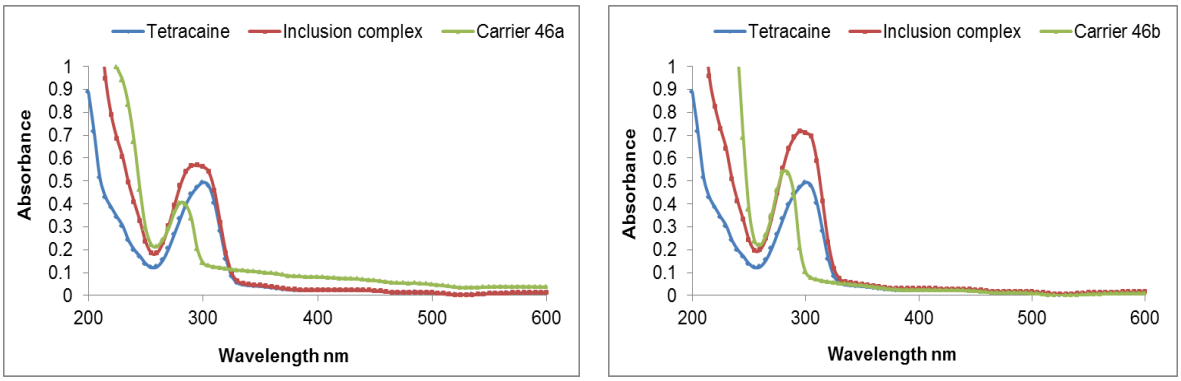

A. B.

Figure 99: UV-Vis spectra of tetracaine (TTC); inclusion complex and carrier **46a** and carrier **46b.**

3.6.3 FTIR Analysis of Freeze Dried Formulations

The FTIR spectra of pure drugs, carrier **46b**, and the inclusion complexes formed are shown in Figures 100-102. In all the IR spectra of the inclusion complex formed with the carrier **46b**, the main bands were found to overlap with the characteristic drug peaks. The FTIR spectra of the inclusion complexes did not show any significant new peaks, demonstrating that no new chemical bonds were formed in the inclusion complex.

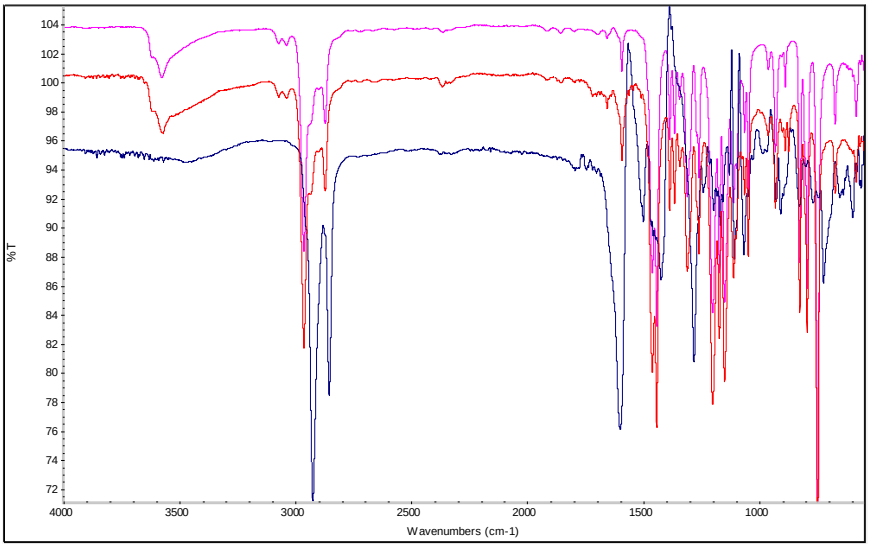

Figure 100: FT-IR spectral analysis of (pink) Propofol (red) inclusion complex (blue) carrier **46b.**

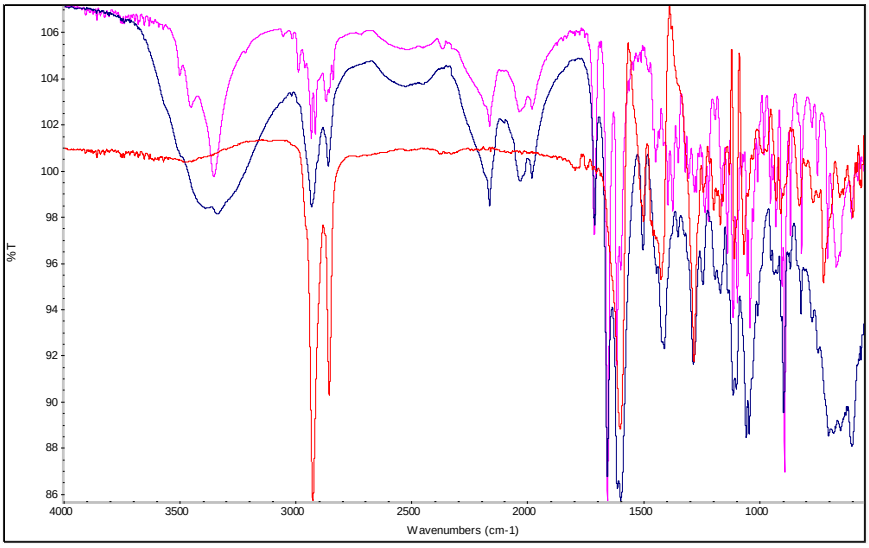

Figure 101: FT-IR spectral analysis of (pink) Prednisolone (blue) inclusion complex (red) carrier **46b**.

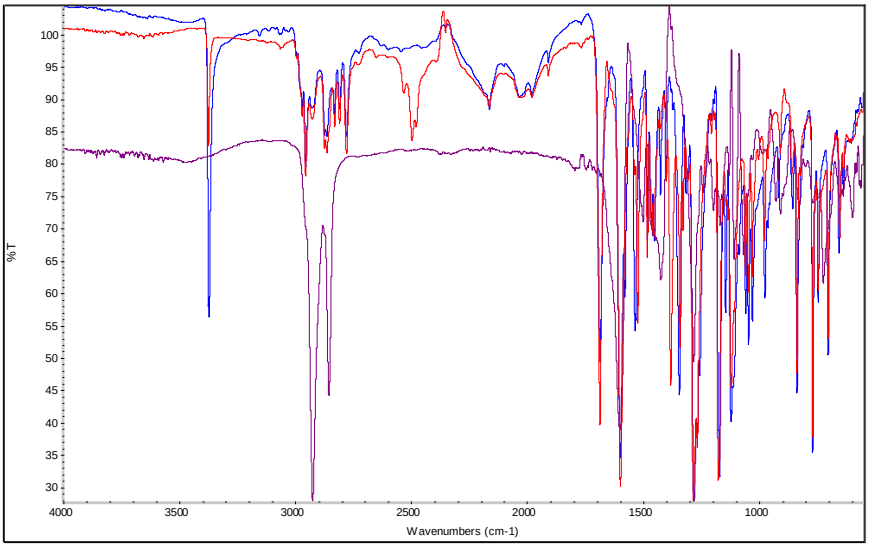

Figure 102: FT-IR spectral analysis of (blue) tetracaine (red) inclusion complex (purple) carrier **46b**.

3.6.4 NMR Analysis of Formulations

The 1D and 2D ^{1}H NMR spectra of formulations of carrier **46b** with each of the three drugs investigated were obtained in order to confirm the presence of the drug within the solubilised formulation and attempt to elucidate the mode of incorporation.

3.6.4.1 Propofol Formulations

A solution containing propofol and carrier **46b** corresponding to an initial carrier concentration of 6 mg/mL and drug: carrier ratio of 1:1 was made up in D_2O. The ^{1}H NMR spectrum and NOESY spectrum of the solution are shown in Figures 103 and 104, respectively.

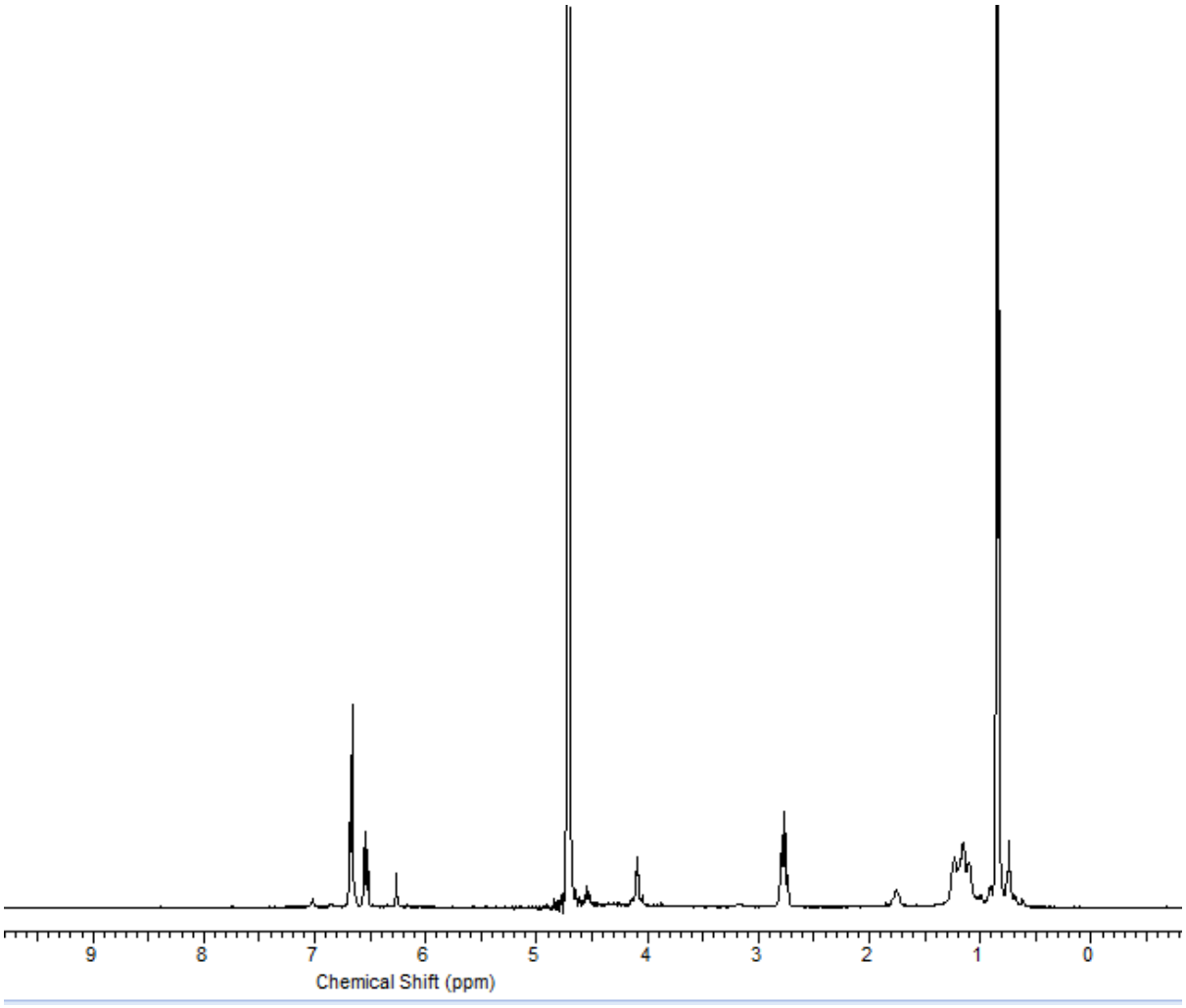

Figure 103: ^{1}H NMR spectrum of a solution of propofol and carrier **46b** corresponding to an initial carrier concentration of 3 mg/mL and drug: carrier ratio of 1:1 in D_2O.

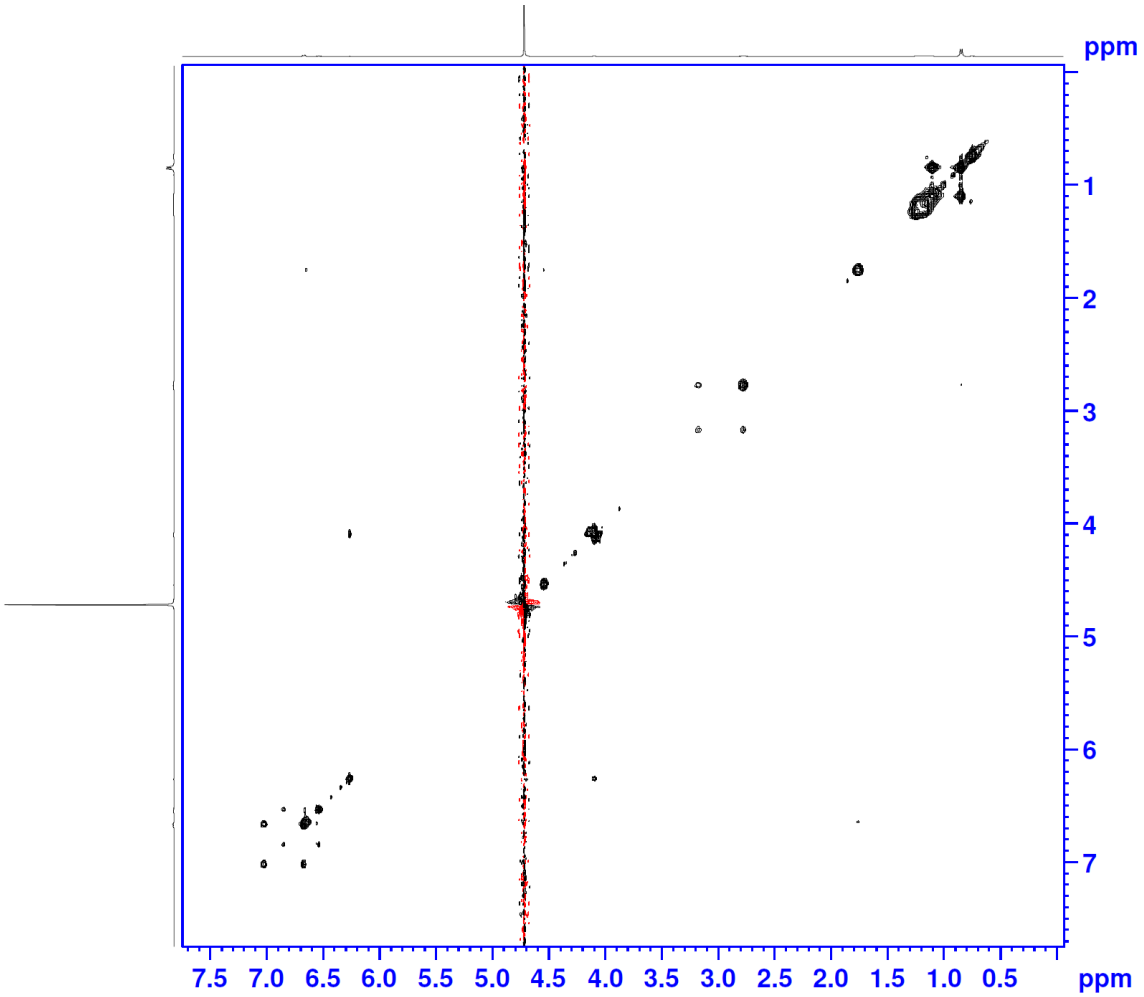

Figure 104: ^{1}H NOESY NMR spectrum of a solution of propofol and carrier **46b** corresponding to an initial carrier concentration of 3 mg/mL and drug: carrier ratio of 1:1 in D_2O.

As can be observed in the ^{1}H NMR spectrum, a significant amount of propofol was solubilised by the carrier **46b**. The carrier molecule can be identified by the presence of signals associated with aromatic protons and the bridgehead protons. However, it appears that the aromatic protons are resonating at higher chemical shifts and the signal associated with the bridgehead protons has become a multiplet, rather than the distinct singlet as observed in the spectrum of pure carrier **46b**.

The ^{1}H NOESY NMR spectrum potentially highlights the interactions through space between protons on the carrier molecule and those on propofol. It is clear that there is an interaction between the protons in the 2-position on the calix[4]resorcinarene carrier (δ = 6.21 ppm) and neighbouring O-CH_2-O protons on the ester substituents (δ = 4.07 ppm). However, there are also interactions evident between aromatic protons that can be attributed to propofol and other aromatic protons tentatively assigned to the carrier: In particular, there is an interaction between the protons in the 3- and 5- positions on propofol and an aromatic proton at δ = 7.05 ppm; this signal has been tentatively assigned to the aromatic 5-position in the carrier **46b**. There are other interactions in the aromatic region also.

3.6.4.2 Prednisolone (PLS) Formulations

A solution containing prednisolone and carrier **46b** corresponding to an initial carrier concentration of 3 mg/mL and drug: carrier ratio of 1:1 was made up in D_2O. The ^{1}H NMR spectrum and NOESY spectrum of the solution are shown in Figures 105 and 106, respectively.

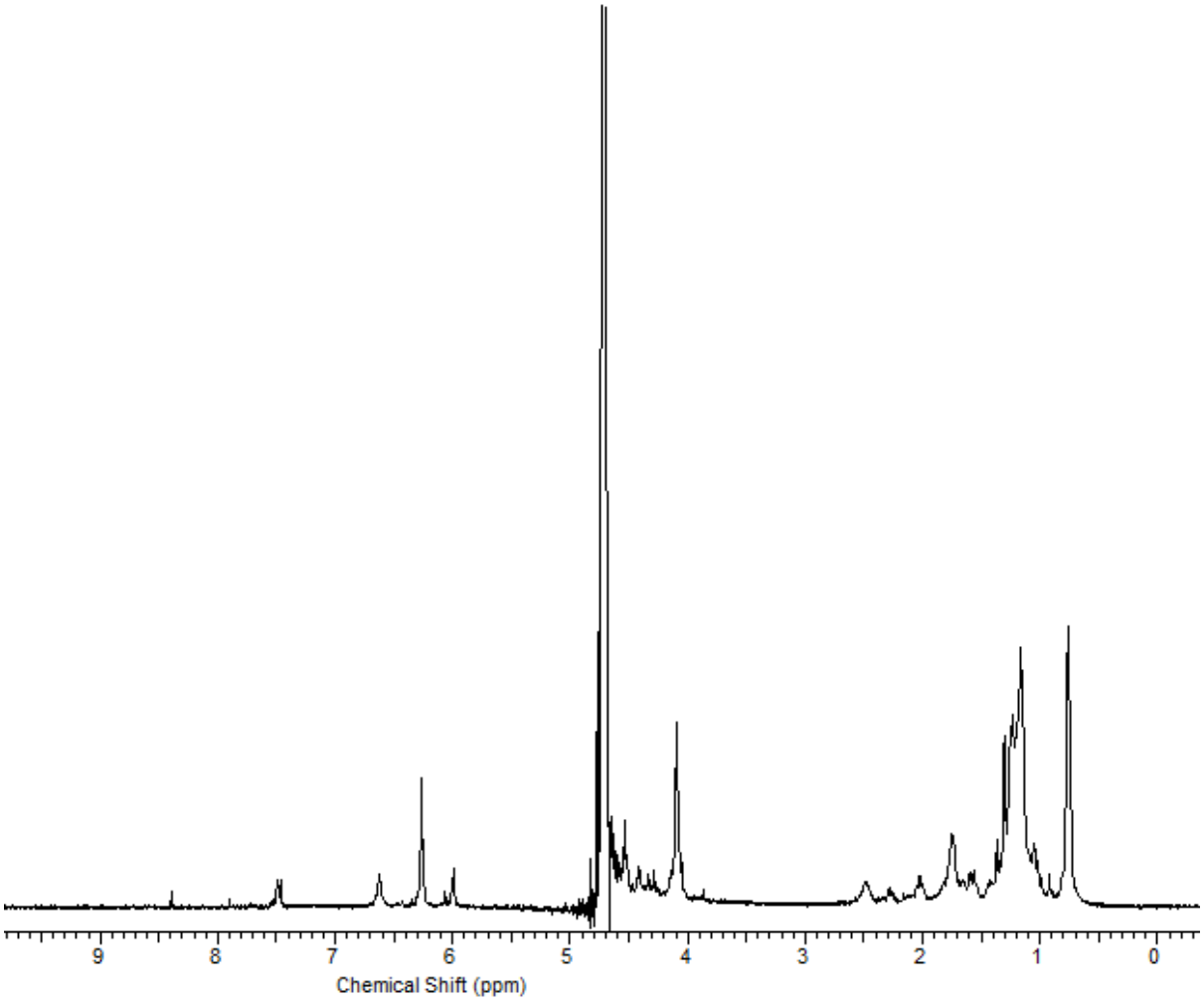

Figure 105: ^{1}H NMR spectrum of a solution of prednisolone and carrier **46b** corresponding to an initial carrier concentration of 3 mg/mL and drug: carrier ratio of 1:1 in D_2O.

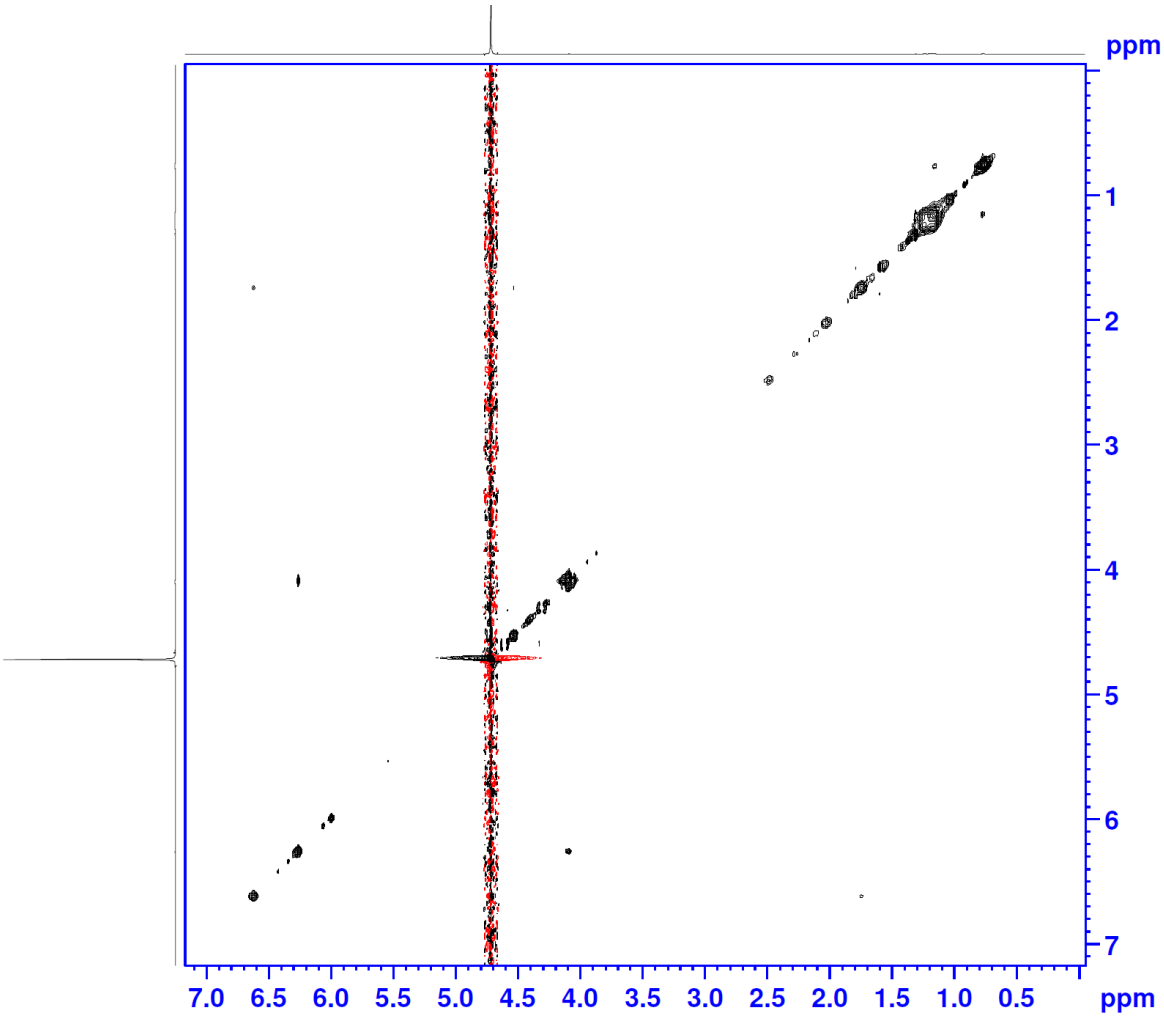

Figure 106: ^{1}H NOESY NMR spectrum of a solution of prednisolone and carrier **46b** corresponding to an initial carrier concentration of 3 mg/mL and drug: carrier ratio of 1:1 in D_2O.

In the case of the ^{1}H NMR spectrum of the solution in D_2O, there is evidence of the presence of prednisolone in the appearance of signals in the aromatic region and elsewhere. However, the NOESY spectrum shows no interactions in addition to those observed for the pure carrier **46b** alone.

3.6.4.3 Tetracaine (TTC) Formulations

A solution containing tetracaine and carrier **46b** corresponding to an initial carrier concentration of 3 mg/mL and drug: carrier ratio of 1:1 was made up in D_2O. The ^{1}H

NMR spectrum and ROESY spectrum of the solution are shown in Figures 107 and 108, respectively.

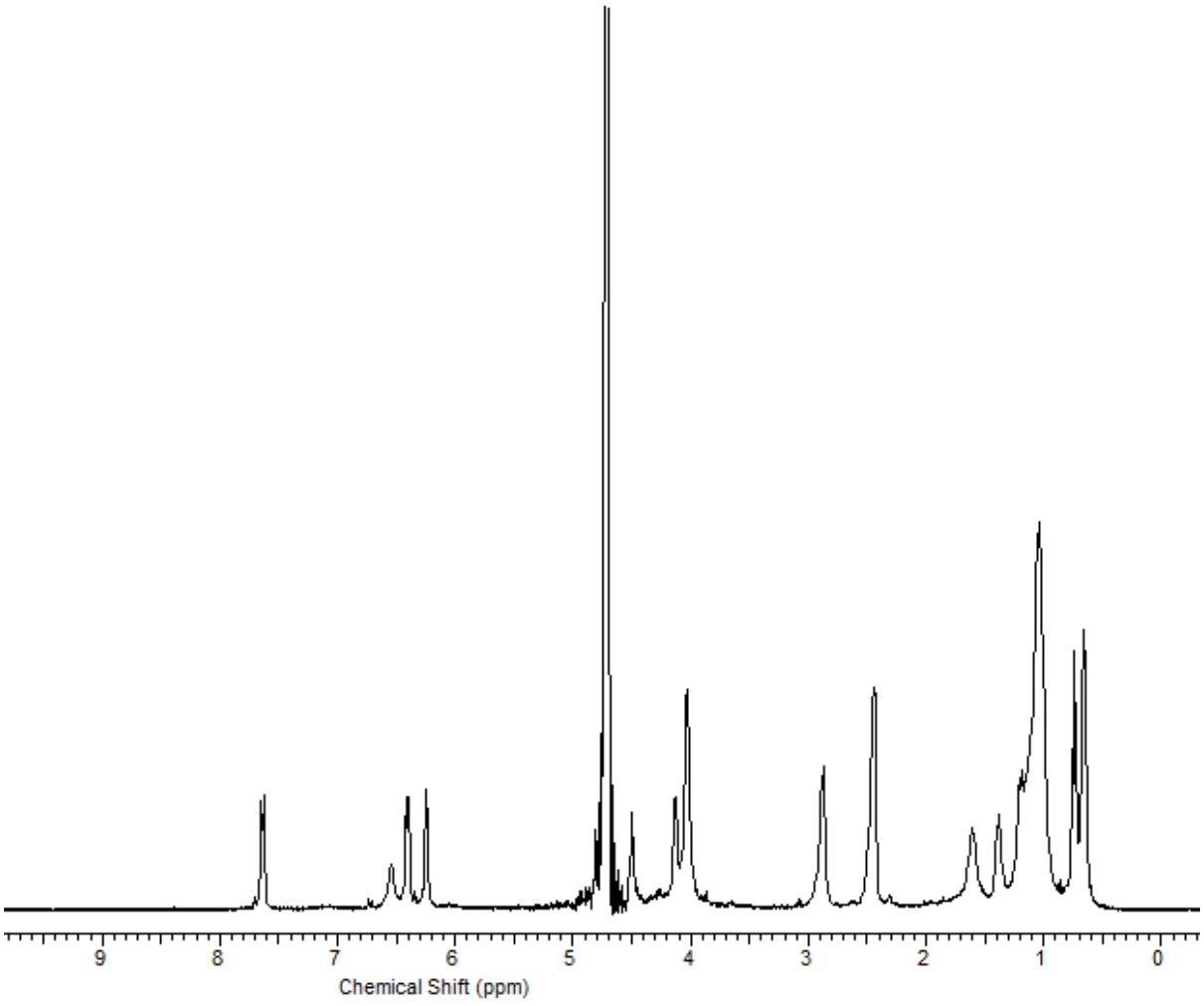

Figure 107: ^{1}H NMR spectrum of a solution of tetracaine and carrier **46b** corresponding to an initial carrier concentration of 3 mg/mL and drug: carrier ratio of 1:1 in D_2O.

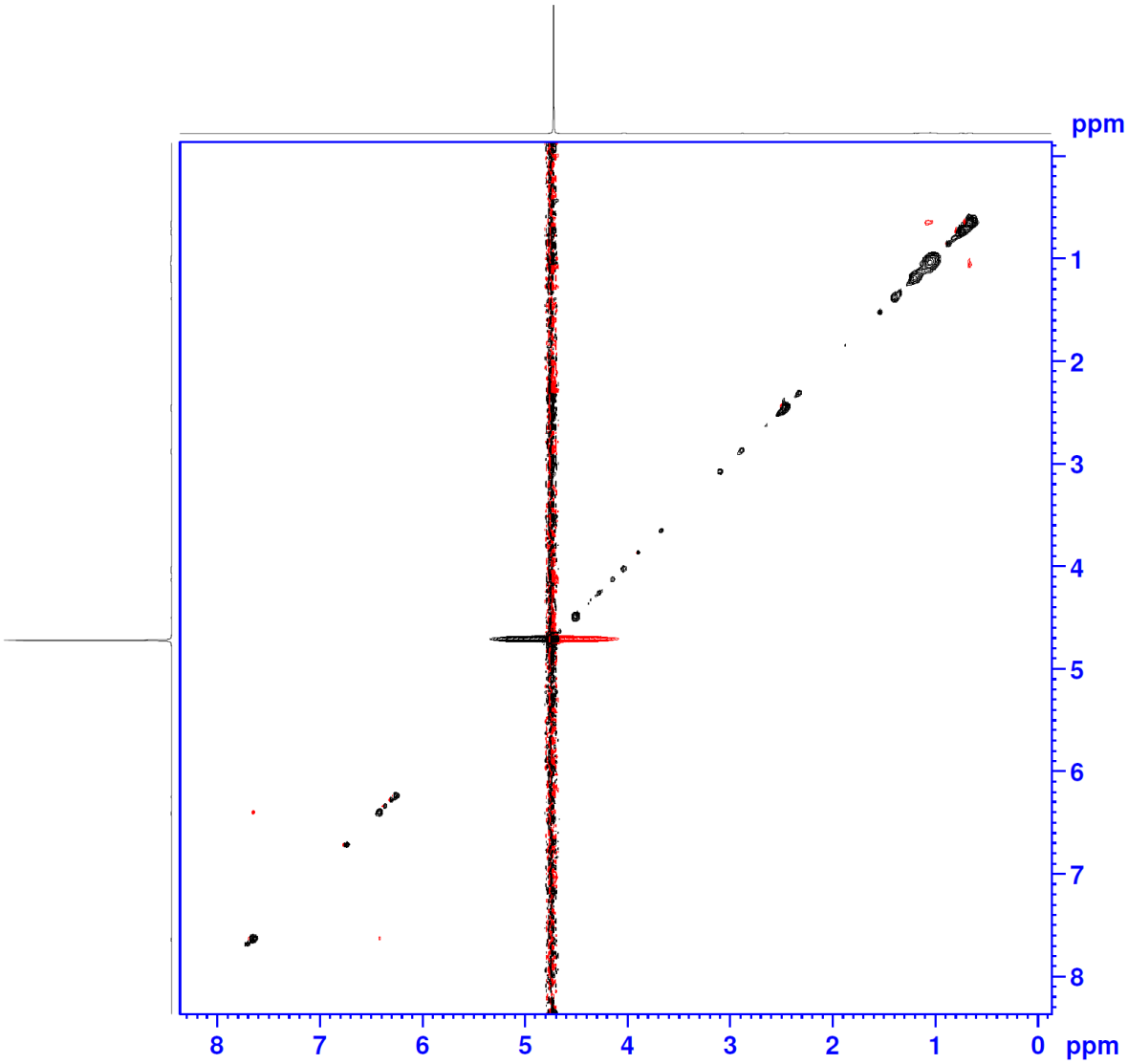

Figure 108: ^{1}H ROESY NMR spectrum of a solution of tetracaine and carrier **46b** corresponding to an initial carrier concentration of 3 mg/mL and drug: carrier ratio of 1:1 in D_2O.

The ^{1}H ROESY NMR spectrum of the solution of carrier **46b** with tetracaine was acquired. As for prednisolone, the 1D and 2D spectra showed the presence of tetracaine in solution but no significant interactions in addition to those observed for the pure carrier **46b** alone were evident. At increased intensity, the ROESY spectrum did show additional interactions that could be attributed to intramolecular interactions of the tetracaine molecule.

3.6.5 Photon Correlation Spectroscopy

3.6.5.1 Size an Aggregate Size and Zeta Potential Measurements

3.6.5.1.1 Propofol Formulations

The hydrodynamic ratio and the zeta potential of aggregates formed in the optimal formulations for each drug were determined by photon correlation spectroscopy, in a similar manner to that described for the carriers **46a-f** in Chapter 2. All the PCS data reported in this chapter is based upon the initial carrier concentrations and drug: carrier feed ratios, and the data returned is for filtered solutions containing the drug: carrier aggregates.

Carrier **46a** alone gave aggregates with a radius of 373.8 nm. Interestingly the pattern of the size measurements seemed to follow the pattern of the drug solubilisation capability. The propofol loaded aggregates had the largest amount of propofol solubilised (11.86 mg/mL) and radius (1769.33 nm) for the highest initial drug: carrier ratio (6 mg/ml, 10:1). Carrier **46a** at initial concentration 3 mg/ml and drug: carrier ratio of 10:1 was only capable of solubilising 1.7 mg/mL of drug g and gave aggregates with a radius of 395 nm, a similar size to that of the free carrier (Table 15).

Table 15: Photon correlation spectrometry size analysis of optimal carrier **46a** formulations at different initial concentrations and initial drug: carrier mass ratio (n=3, ave).

Aggregate	Concentration mg/mL Drug: Carrier Ratio	Size nm (± SD): Percentage occurrence	PDI	Zeta Potential
Carrier **46a** alone	5	373.8 (13.5): 100 %	0.233 (0.039)	-54.4 (0.46)
Propofol-Carrier **46a**	3 (10:1)	395 (13.1): 100 %	0.257 (0.009)	-77.1 (3.1)
	6 (10:1)	1769.3 (23.4): 88 % 188.1 (2.7): 12 %	0.569 (0.093)	-74 (2.6)

The size correlation chart for **46a** formulations (Figure 109) shows the aggregates formed have different hydrodynamic radii depending upon the initial carrier concentrations. Note that two species of aggregates are formed for the initial carrier concentration of 6 mg/mL.

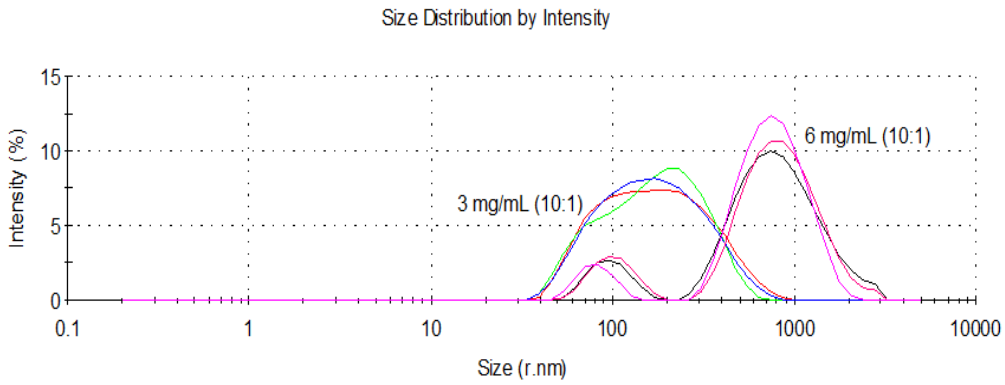

Figure 109: Photon correlation spectroscopy size correlation chart for propofol: carrier **46a** (10:1) at 3 mg/mL and 6 mg/mL in deionised water (n=3, ave).

The hydrodynamic radius of aggregates of pure carrier **46b** was 387 nm, significantly smaller than the drug loaded aggregates at initial concentration of 3 mg/ml and drug: carrier ratio (10:1) (Table 16). The propofol loaded aggregates had the largest amount of propofol solubilised (42 mg/mL) with an aggregate radius of 451 nm for the highest initial drug: carrier ratio (6 mg/ml, 10:1). However, the propofol loaded system with initial carrier concentration of 3 mg/ml and drug: carrier ratio of 10:1 gave aggregates of the greatest size of 1079 nm with solubilisation of 26 mg/mL.

Table 16: Photon correlation spectrometry size analysis of optimal carrier **46b** formulations at different initial concentrations and initial drug: carrier mass ratio (n=3, ave).

Aggregate	Concentration mg/mL Drug: Carrier Ratio	Size nm (± SD): Percentage occurrence	PDI	Zeta Potential
Carrier **46b** alone	5	387.2 (10): 100%	0.404 (0.039)	-80.9 (2.38)
Propofol-Carrier **46b**	3 (1:10)	1079.3(44.3):100%	0.342 (0.058)	-85.7 (0.79)
	6 (1:10)	451.4 (14.1): 100%	0.256 (0.009)	-119 (6.24)

Figure 110 shows the size distribution report for the optimum drug: carrier **46b** formulations. The chart shows that the size of the propofol loaded aggregates at initial carrier concentration of 6 mg/ml appeared to be smaller than the loaded aggregates resulting from the initial concentration of 3 mg/ml. This may indicate a strong interaction in the inclusion complex resulting in a more compact formation of the aggregates.

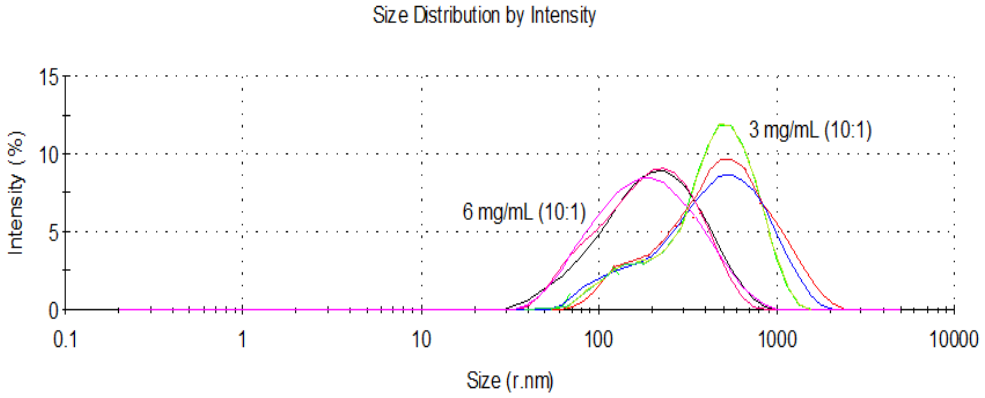

Figure 110: Photon correlation spectroscopy size correlation chart for propofol: carrier **46b** (10:1) at 3 mg/mL and 6 mg/mL in deionised water (n=3, ave).

Carrier **46c** alone gave aggregates with radius of 136 nm. The pattern of the size measurements seemed to follow the pattern of the drug loading capacity (Table 17). The propofol loaded aggregates had the largest amount of propofol solubilised (17.89

mg/mL) and size (1534 nm) for the highest initial carrier: drug ratio (6 mg/ml, 10:1). Aggregates containing propofol at initial carrier concentration of 3 mg/ml and drug:carrier ratio of 10:1 were only capable of solubilising 2.5 mg/mL of drug and the aggregate size also followed this trend, giving aggregates with a radius of 1026 nm.

Table 17: Photon correlation spectrometry size analysis of optimal carrier **46c** formulations at different initial concentrations and initial drug: carrier mass ratio (n=3, ave).

Aggregate	Concentration mg/mL Drug: Carrier Ratio	Size nm (± SD): Percentage occurrence	PDI	Zeta Potential
Carrier **46c** alone	5	136.3 (5.5): 100 %	0.176 (0.01)	-77.97 (1.16)
Propofol-Carrier **46c**	3 (10:1)	1026.2 (37.8):100 %	0.276 (0.007)	-86.2 (6.79)
	6 (10:1)	1534.3 (39.7): 100%	0.256 (0.009)	-64.7 (4.24)

Figure 111 shows the size distribution report for drug: carrier **46c** formulations. The chart shows that the size of the propofol loaded aggregates at 6 mg/ml appeared to be bigger than the loaded aggregates at 3 mg/mL.

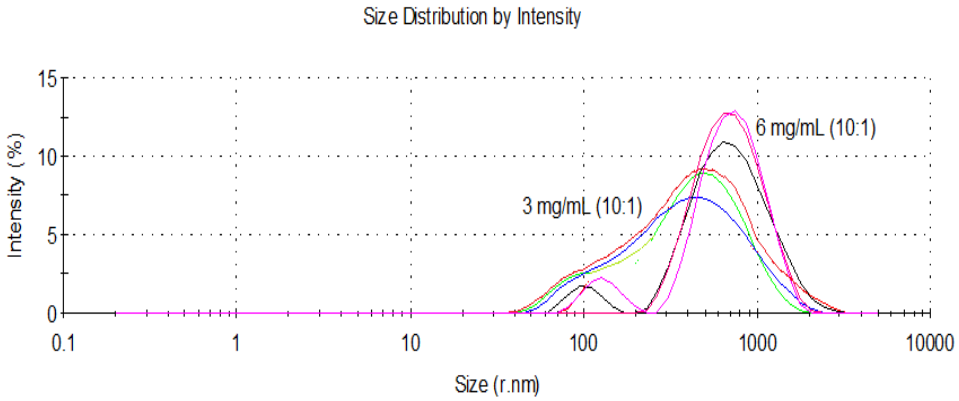

Figure 111: Photon correlation spectroscopy size correlation chart for propofol: carrier **46c** (10:1) at 3 mg/mL and 6 mg/mL in deionised water (n=3, ave).

The size distribution of aggregates of carrier **46d** significantly changed in the presence of propofol: The average radius of the aggregates increased from 212 nm

to 1245 nm for samples with an initial carrier concentration of 3 mg/mL, which also showed another peak at 236 nm. The radius of aggregates derived from of the carrier **46d** with initial concentration of 6 mg/mL was 760 nm, significantly smaller than the drug loaded aggregates from the solutions formed from the initial carrier concentration 3 mg/ml, with some larger aggregates being observed (Table 18).

Table 18: Photon correlation spectrometry size analysis of optimal carrier **46d** formulations at different initial concentrations and initial drug: carrier mass ratio (n=3, ave).

Aggregate	Concentration mg/mL Drug: Carrier Ratio	Size nm (± SD): Percentage occurrence	PDI	Zeta Potential
Carrier **46d** alone	5	212.5 (11.5): 100 %	0.324 (0.036)	-83.1 (2.4)
Propofol-Carrier **46d**	3 (10:1)	1245.7 (40.8): 92 % 236.4 (11.6): 8 %	0.27 (0.037)	-49.4 (4.79)
	6 (10:1)	760.2 (16.8): 94 % 4676.3 (40.7): 6 %	0.29 (0.051)	-107.8 (5.24)

The trend in hydrodynamic radius observed for the carrier **46d** formulations was similar to that observed for carrier **46b** formulations, as shown (Figure 112).

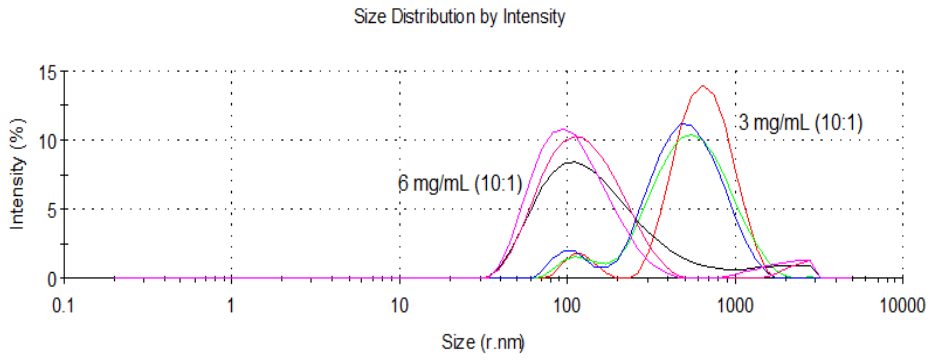

Figure 112: Photon correlation spectroscopy size correlation chart for propofol: carrier **46d** (10:1) at 3 mg/mL and 6 mg/mL in deionised water (n=3, ave).

On loading carrier **46e** with propofol, aggregates formed with a large increase in hydrodynamic radius (Table 19). The size of aggregates formed by the carrier **46e** alone (330 nm) significantly increased to 1427 nm from solutions derived from an initial carrier concentration of 3 mg/mL and drug: carrier ratio of 10:1, whilst solutions with initial concentrations of 6 mg/mL the size of aggregates observed decreased to 200 nm upon encapsulation of the drug. The propofol loaded aggregates derived from solutions with initial concentrations of 6 mg/mL solubilised the largest amount of propofol (15 mg/mL). However, the size of the propofol loaded aggregates appeared to be smaller than the non-loaded aggregates; this suggests strong interactions resulting in a compact formation of the assemblies.

Table 19: Photon correlation spectrometry size analysis of optimal carrier **46e** formulations at different initial concentrations and initial drug: carrier mass ratio (n=3, ave).

Aggregate	Concentration mg/mL Drug: Carrier Ratio	Size nm (± SD): Percentage occurrence	PDI	Zeta Potential
Carrier **46d** alone	5	330.1 (8.5): 100 %	0.306 (0.066)	-47.7 (2.2)
Propofol-Carrier **46e**	3 (10:1)	1426.7 (28.6): 58 % 200.2 (2.8): 30 % 5350.4 (32.8): 12 %	0.813 (0.139)	-78.4 (2. 9)
	6 (10:1)	200.4 (4.8): 92 % 30.3 (3.2): 6 % 4214.7 (20.7): 2 %	0.426 (0.015)	-91.3 (0.24)

The size trend observed for the carrier **46e** formulations was similar to that observed for the formulations derived from carriers **46b** and **46d** as shown (Figure 113). Each of these carriers possess C_7 alkyl substituents on the lower rim. The particle size distribution of carrier **46e** significantly changes in the presence of propofol, with larger aggregates appearing, which leads to an increase of the PDI value.

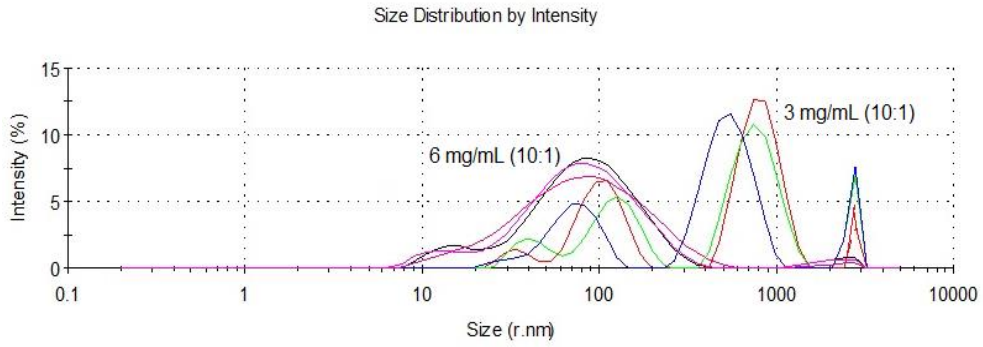

Figure 113: Photon correlation spectroscopy size correlation chart for propofol: carrier **46e** (10:1) at 3 mg/mL and 6 mg/mL in deionised water (n=3, ave).

As shown in the data presented in Table 20, the radius of aggregates of carrier **46f** alone was 166 nm, significantly smaller than the drug loaded aggregates observed for solutions with initial carrier concentrations of 3 mg/ml and 6 mg/ml. The propofol loaded aggregates formed from solutions with initial concentration of 6 mg/mL had the greatest radius of 1291 nm, whereas those for the propofol loaded system formed from solutions with initial concentration of 3 mg/mL had an observed radius of 860 nm.

Table 20: Photon correlation spectrometry size analysis of optimal carrier **46f** formulations at different initial concentrations and initial drug: carrier mass ratio (n=3, ave).

Aggregate	Concentration mg/mL Drug: Carrier Ratio	Size nm (± SD): Percentage occurrence	PDI	Zeta Potential
Carrier **46f** alone	5	165.8 (5.7): 100 %	0.383 (0.028)	-90.4 (1.02)
Propofol-Carrier **46f**	3 (10:1)	860 (9.8):100 %	0.273 (0.047)	-105.3 (2.87)
	6 (10:1)	1290.7 (44.7): 92 % 172.9 (3.6): 8 %	0.407 (0.012)	-87.1 (5.51)

Figure 114 shows the size distribution report for drug: carrier **46f** formulations. As can be observed, the change in hydrodynamic radius of aggregates formed as initial

carrier concentration increases from 3 mg/mL to 6 mg/mL is not particularly significant.

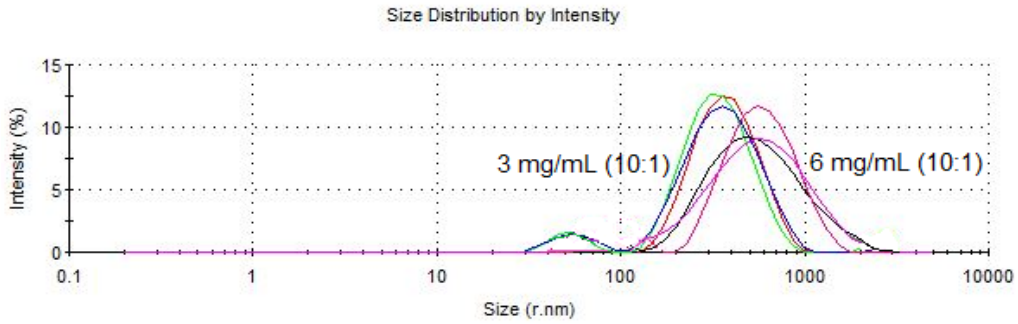

Figure 114: Photon correlation spectroscopy size correlation chart for propofol: carrier **46f** (10:1) at 3 mg/mL and 6 mg/mL in deionised water (n=3, ave).

3.6.5.1.2 Prednisolone (PLS) Formulations

The trend observed in the hydrodynamic radius measurements for prednisolone loaded aggregates seemed to follow the drug loading capability of the carrier **46a**. The prednisolone loaded aggregates derived from a solution containing an initial carrier concentration of 1 mg/mL and a drug: carrier ratio of 1:1 had the largest amount of prednisolone solubilised (1.3 mg/mL) and a radius of 1146 nm with a PDI of 0.082. Aggregates of 46a derived from a solution containing an initial carrier concentration of 3 mg/mL and a drug: carrier ratio of 1:1 had a much more varied size (Table 21).

Table 21: Photon correlation spectrometry size analysis of optimal carrier **46a** formulations at different initial concentrations and initial drug: carrier mass ratio (n=3, ave).

Aggregate	Concentration mg/mL Drug: Carrier Ratio	Size nm (± SD): Percentage occurrence	PDI	Zeta Potential
Carrier **46a** alone	1	293.7 (9.6): 100 %	0.266 (0.028)	-47.6 (0.70)
Prednisolone-Carrier **46a**	1 (1:1)	1146.3 (19.8): 100 %	0.082 (0.005)	-63.7 (1.6)
	3 (1:1)	102.1 (3.7): 68 % 2348 (29.1): 32 %	0.538 (0.125)	-45.3 (1. 4)

Figure 115 shows the size distribution report for drug: carrier **46a** formulations. The chart shows that the size of the prednisolone loaded aggregates at 1 mg/ml appeared to be much better defined than the loaded aggregates at 3 mg/mL. At the higher initial drug concentration two size populations are observed.

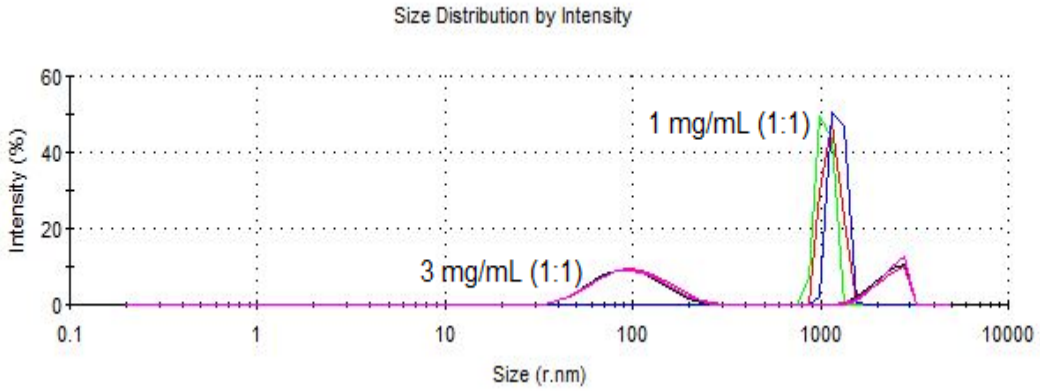

Figure 115: Photon correlation spectroscopy size correlation chart for prednisolone: carrier **46a** (1:1) at 1 mg/mL and 3 mg/mL in deionised water (n=3, ave).

Aggregates of carrier **46b** containing prednisolone derived from solutions containing an initial carrier concentration of 1 mg/mL were only capable of solubilising 1.0 mg/mL of drug and the radius measurement observed was 221 nm, while the aggregates derived from solutions with initial carrier concentration of 3 mg/mL had an

observed radius of 192 nm. The size of the prednisolone loaded aggregates appeared to be smaller than those observed for the non-loaded carrier, suggesting very strong interactions resulting in compact aggregates (Table 22).

Table 22: Photon correlation spectrometry size analysis of optimal carrier **46b** formulations at different initial concentrations and initial drug: carrier mass ratio (n=3, ave).

Aggregate	Concentration mg/mL Drug: Carrier Ratio	Size nm (± SD): Percentage occurrence	PDI	Zeta Potential
Carrier **46b** alone	1	907.4 (15.6): 100 %	0.361 (0.028)	-61.1 (1.8)
Prednisolone-Carrier **46b**	1 (1:1)	220.6 (10.5): 100 %	0.280 (0.020)	-67.4 (1.4)
	3 (1:1)	192. (4.5): 100 %	0.271 (0.010)	-48.8 (0.96)

The size trend observed for the carrier **46b** formulations was different to that observed for carrier **46a** formulations as shown (Figure 116).

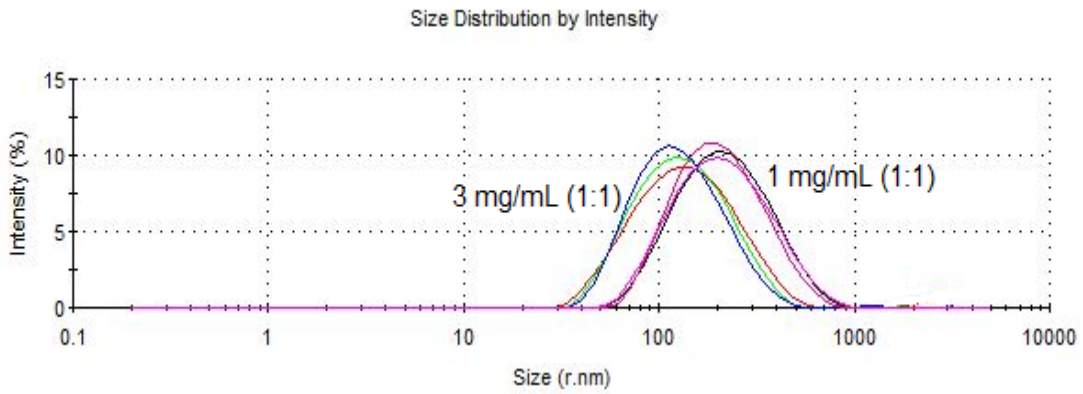

Figure 116: Photon correlation spectroscopy size correlation chart for prednisolone: carrier **46b** (1:1) at 1 mg/mL and 3 mg/mL in deionised water (n=3, ave).

On loading carrier **46c** with prednisolone at 1 mg/ml and 3 mg/ml, both formulations obtained gave a large observed increase in size as compared to the carrier alone (Table 23). This appeared to be a large increase considering the low concentration of

prednisolone encapsulated within the formulations (1.04 mg/mL and 0.82 mg/mL at 1 mg/mL and 3 mg/mL respectively).

Table 23: Photon correlation spectrometry size analysis of optimal carrier **46c** formulations at different concentrations with different initial carrier: drug mass ratio (n=3, ave).

Aggregate	Concentration mg/mL Drug: Carrier Ratio	Size nm (± SD): Percentage occurrence	PDI	Zeta Potential
Carrier **46c** alone	1	141.4 (10.6): 100 %	0.174 (0.03)	-72.7 (1.6)
Prednisolone-Carrier **46c**	1 (1:1)	377.3 (13.1): 100 %	0.078 (0.003)	-48.7 (3.1)
	3 (1:1)	605 (21.4): 94 % 105.8 (3.1): 6 %	0.078 (0.003)	-39 (2.4)

Figure 117 shows the size distribution report for drug: carrier **46c** formulations. The chart clearly shows that the hydrodynamic radius of the prednisolone loaded aggregates derived from solutions containing an initial carrier concentration of 1 mg/mL appeared to be smaller than the loaded aggregates derived from solutions containing an initial carrier concentration of 3 mg/mL.

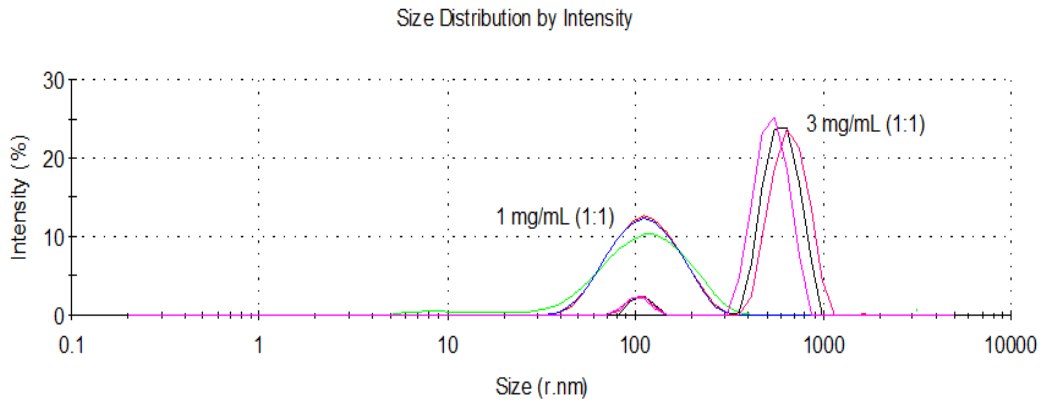

Figure 117: Photon correlation spectroscopy size correlation chart for prednisolone: carrier **46c** (1:1) at 1 mg/mL and 3 mg/mL in deionised water (n=3, ave).

The size of the prednisolone loaded aggregates derived from solutions containing an initial carrier concentration of 1 mg/mL of carrier **46d** appeared to be smaller than the unloaded aggregates (Table 24). However, the size of the prednisolone loaded aggregates increased to 642 nm for formulations derived from solutions containing an initial drug concentration of 3 mg/mL.

Table 24: Photon correlation spectrometry size analysis of optimal carrier **46d** formulations at different concentrations with different initial carrier: drug mass ratio (n=3, ave).

Aggregate	Concentration mg/mL Drug: Carrier Ratio	Size nm (± SD): Percentage occurrence	PDI	Zeta Potential
Carrier **46d** alone	1	286.6 (10.5): 100 %	0.289 (0.056)	-76 (5.4)
Prednisolone-Carrier **46d**	1 (1:1)	276.6 (10.1): 87 % 42.8 (6.3): 13 %	0.663 (0.038)	-75.2 (3.5)
	3 (1:1)	641.5 (36.4): 100 %	0.149 (0.002)	-51 (1.5)

Figure 118 shows that the size of the prednisolone loaded aggregates derived from solutions containing an initial carrier concentration of at 1 mg/mL appeared to be smaller than the loaded aggregates derived from solutions containing an initial carrier concentration of 3 mg/mL.

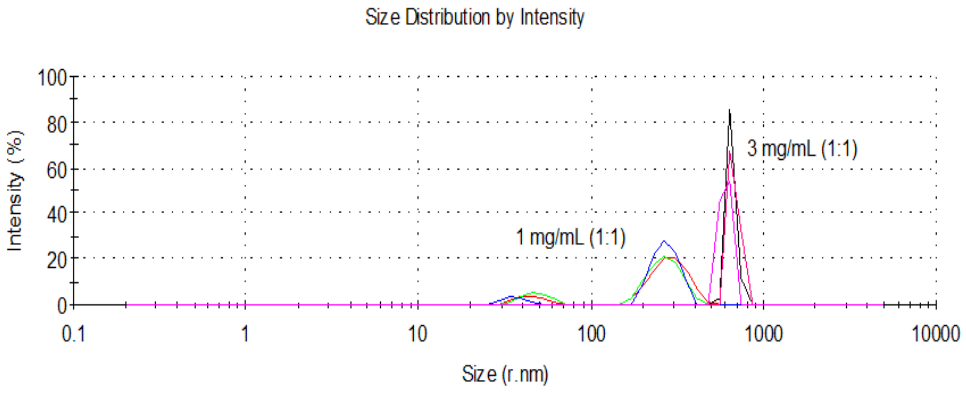

Figure 118: Photon correlation spectroscopy size correlation chart for prednisolone: carrier **46d** (1:1) at 1 mg/mL and 3 mg/mL in deionised water (n=3, ave).

The aggregates formed in formulations containing carrier **46e** from solutions containing a drug: carrier ratio of 5:1 had distinctly different hydrodynamic radii, as can be seen in Table 25. In particular, those derived from solutions containing an initial carrier concentration of 3 mg/mL had a particularly low PDI.

Table 25: Photon correlation spectrometry size analysis of optimal carrier **46e** formulations at different concentrations with different initial carrier: drug mass ratio (n=3, ave).

Aggregate	Concentration mg/mL Drug: Carrier Ratio	Size nm (± SD): Percentage occurrence	PDI	Zeta Potential
Carrier **46e** alone	1	267.3 (23.5): 100 %	0.212 (0.038)	-75.96 (5.4)
Prednisolone-Carrier **46e**	1 (5:1)	117.5 (1.8): 80 % 2478.3 (40.9): 20 %	0.307 (0.051)	-59.1 (1.6)
	3 (5:1)	496.9 (8.3): 100 %	0.186 (0.035)	-56.8 (2.5)

Figure 119 shows that the size of the prednisolone loaded aggregates formed from carrier **46e** vary considerably in hydrodynamic radius with only a doubling of initial carrier concentration.

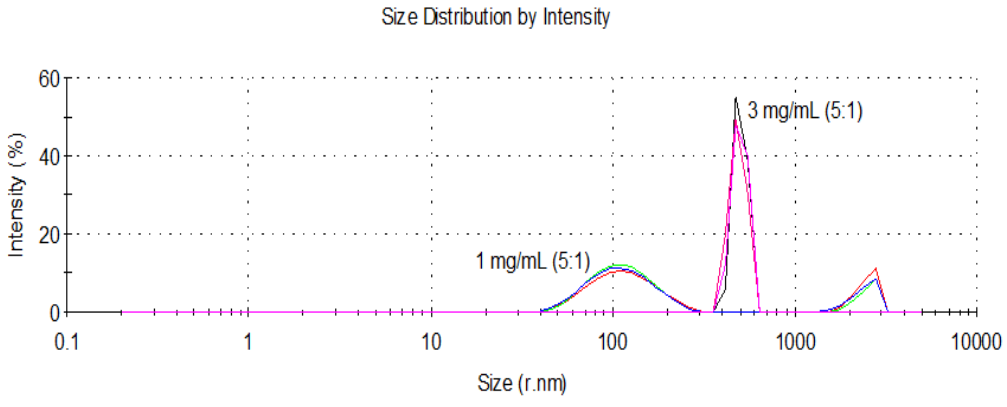

Figure 119: Photon correlation spectroscopy size correlation chart for prednisolone: carrier **46e** (5:1) at 1 mg/mL and 3 mg/mL in deionised water (n=3, ave).

The formulations obtained for carrier **46f** derived from solutions containing an initial carrier concentration of 1 mg/mL loaded with prednisolone gave consistently smaller aggregates than for the prednisolone formulations derived from solutions containing an initial carrier concentration of 3 mg/mL. Both formulations were capable of solubilising the same amount of prednisolone (Table 26).

Table 26: Photon correlation spectrometry size analysis of optimal carrier **46f** formulations at different concentrations with different initial carrier: drug mass ratio (n=3, ave).

Aggregate	Concentration mg/mL Drug: Carrier Ratio	Size nm (± SD): Percentage occurrence	PDI	Zeta Potential
Carrier **46f** alone	1	324.3 (10.5): 88 % 4783.7 (30.8): 12 %	0.482 (0.006)	-62 (1.90)
Prednisolone-Carrier **46f**	1 (1:1)	448.3 (11.8): 69 % 108.3 (5.2): 20 % 2630.7 (40.9): 11 %	0.66 (0.059)	-49.6 (2.7)
	3 (1:1)	457.8 (12.2): 100 %	0.184 (0.093)	-52.2 (1.9)

The size trend observed for the formulations derived from carrier **46f** was similar to the trend observed for the carrier **46e** formulations, as shown (Figure 120). The chart shows that the size of the prednisolone loaded aggregates derived from solutions containing an initial carrier concentration of 3 mg/ml appeared to be bigger than the loaded aggregates derived from solutions containing an initial carrier concentration of 1 mg/mL.

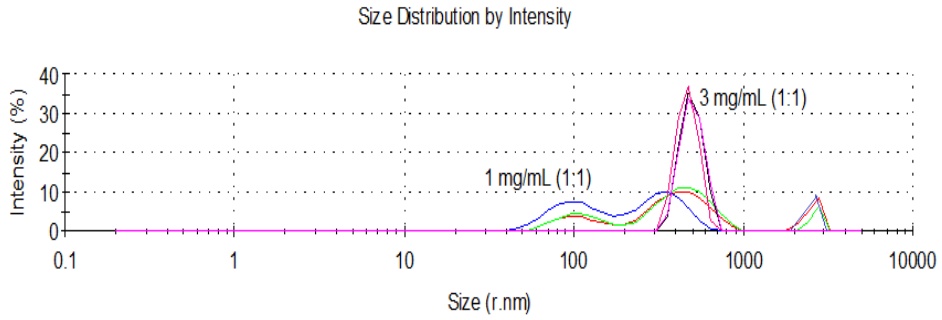

Figure 120: Photon correlation spectroscopy size correlation chart for prednisolone: carrier **46f** (1:1) at 1 mg/mL and 3 mg/mL in deionised water (n=3, ave).

3.6.6 *In Vitro* Drug Release from Nano-aggregates

3.6.6.1 Drug Release at 20 ºC and at 37 ºC

Drug release from the calix[4]resorcinarene drug solubilising carriers **46a-d** and calix[4]pyrogallolarene drug solubilising carriers **46e-f** was studied up to 120 h at two different temperatures. 2 mL of the optimal formulation was deposited in dialysis tubing, which was then placed in a conical glass flask containing 200 mL of gently stirring deionised water in order to obtain sink conditions over 5 days. All the carrier formulations were able to achieve sustained drug release between the period of 48 h to 120 h. Drug release was faster with those carriers possessing C_4 alkyl substituents on the lower rim than those possessing C_7 alkyl substituents on the lower rim, possibly because the drug was loaded within the hydrophobic tail of the carriers. The release of propofol from the carrier formulations is shown in Figure 121.

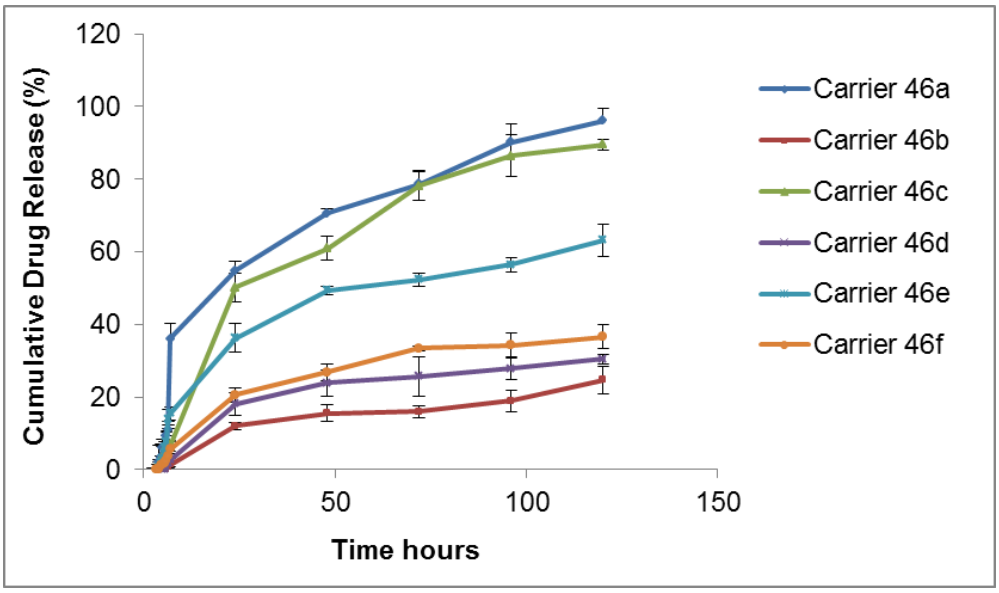

Figure 121: The drug propofol release from the optimal formulations derived from carrier **46a-f** at 20 ºC.

Propofol release from calix[4]resorcinarenes **46a-b** showed different release profiles over 120 h. The release was almost constant upon initial drug release. The release began after 3.5 h and 55 % of propofol was released after 24 h. After 120 h the drug was completely released from carrier **46a**. Propofol was released after 5 h from carrier **46b**,only 12 % was released after 24 h, and 25 % had been released after 96 h. (n=3, ±SD).

Propofol release from formulations derived from calix[4]resorcinarenes **46c-d** showed a different profile. Carrier **46c** had only released 7 % of the drug in the first 7 h and after 24 h 50 % of the drug was released. The drug was steadily released until 90 % of the drug was released at 96 h. On the other hand only 2 % was released from the formulation derived from carrier **46d** in the first 7 h and after 24 h 24 % of the drug was released. The release continued steadily until 30 % of the drug was released at 96 h. For calix[4]pyrogallolarene **46e**, the initial release occurred in the first 4 h and 36 % of the drug was released after 24 h. The drug was steadily released until 63 %

was released at 120 h. For calix[4]pyrogallolarene **46f**, the initial release was at 4 h. Then the drug was steadily released until 20 % of the drug was released at 24 h. After 120 h 36 % of drug release had occurred. Interestingly, no significant differences in the release rate were noticed for all carriers **46a-f** between 20 ºC and at 37 ºC.

Prednisolone release was measured for all formulations over 120 h (Figure 122). For carrier **46a**, the initial release occurred in the first 2.5 h and accounts for 12 % of the total drug content 1.3 mg. After 3 h, 24 % of the drug was releasedand 100 % of the drug was released at 24 h. The release profile for prednisolone was tested at 37 ºC, and a significant difference was found between these two temperatures. The drug release rate at 37 ºC was much faster, with about 59 % of prednisolone released in 3.5 h, and the drug release was complete after 5.5 h. The amphiphilic carrier **46b** had only released 11 % of prednisolone in the first 4 h at 20 ºC. After 6 h 55 % of the drug had been released and the drug release was almost complete after 48 h. At 37 ºC only 4.3 % of prednisolone was released in the first 2 h and approximately 44 % was released within 4.5 h. Major drug release was observed within 7 h reaching 86 % and the drug release was almost complete after 48 h.

Calix[4]resorcinarene **44c** released 3 % of the drug after 3 h at 20 ºC, compared with 29 % released after 3 h at 37 ºC. After 96 h only a total of 82 % of the drug being released at 20 ºC, whereas the drug had been completely released after 24 h at 37 ºC. The release data for calix[4]resorcinarene **46d** showed that only 2 % of prednisolone was released after 4 h and after 48 h 32 % of the drug content had been released at 20 ºC. In contrast, the major drug release was observed in the first 5 h of 47 % at 37 ºC. The release continued steadily until after 48 h the drug was completely released.

In the case of calix[4]pyrogallolarene **46e** the initial release occurs in the first 2.5 h representing 3 % of the total drug content at 20 ºC and at the end of 48 h the total release was 55 %. The initial release was observed in the first 2 h at 37 ºC and the drug release was complete after 48 h. As observed with carrier **46e**, there is a significant difference in the drug release of carrier **46f** at 37 ºC compared with the data at 20 ºC. At 20 ºC, only 48 % of prednisolone was released after 48 h. In contrast, 98 % were released at the end of 48 h at 37 ºC.

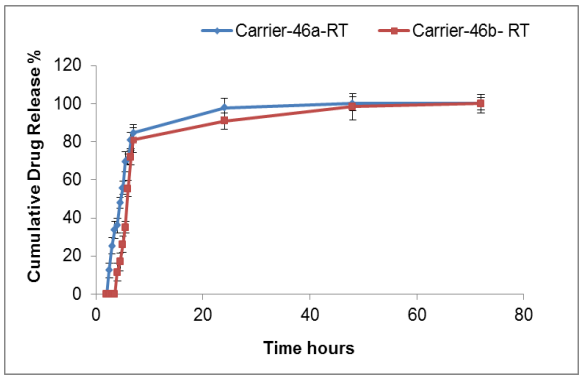

Calix[4]resorcinarenes **46a-b**

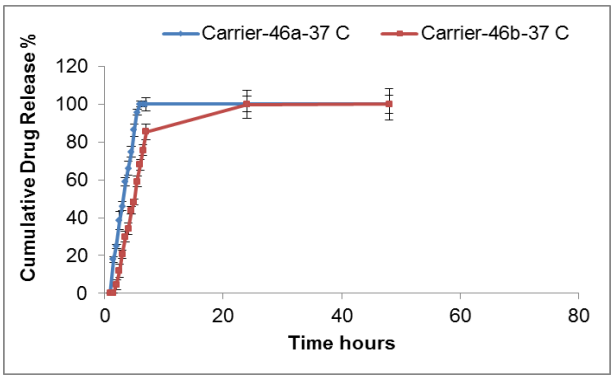

Calix[4]resorcinarenes **46a-b**

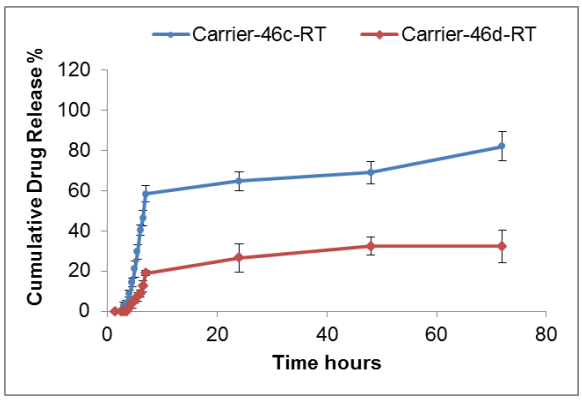

Calix[4]resorcinarenes **46c-d**

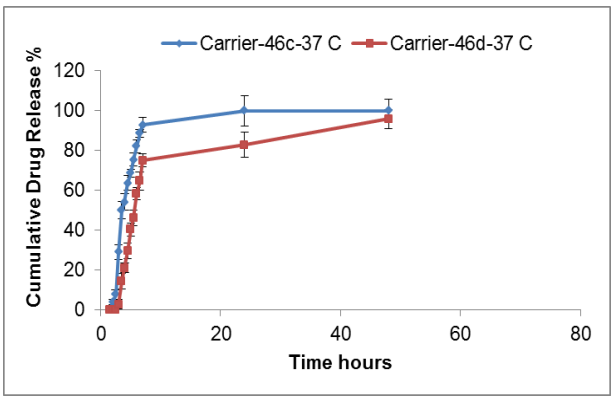

Calix[4]resorcinarenes **46c-d**

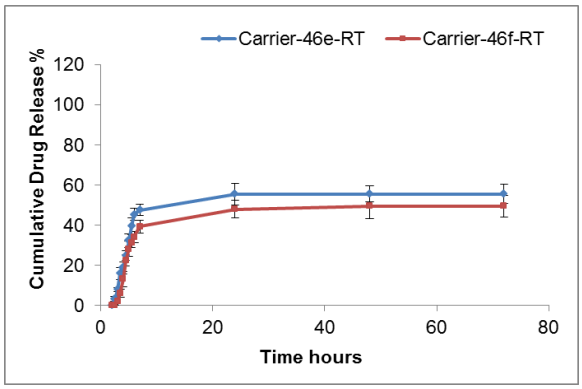

Calix[4]pyrogallolarenes **46e-f**

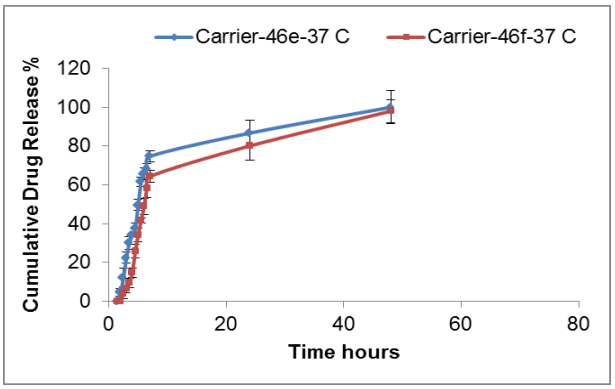

Calix[4]pyrogallolarenes **46e-f**

A. Prednisolone percentage released from the amphiphilic carriers 44a-f at 20 ºC

B. Prednisolone percentage released from the amphiphilic carriers 44a-f at 37 ºC

Figure 122: The *in vitro* release profiles of prednisolone.

3.7 Discussion

The solubilisation of model hydrophobic drugs propofol, prednisolone and tetracaine, each with different hydrophobicity by calix[4]resorcinarenes **46a-d** and calix[4]pyrogallolarenes **46e-f** (Figure 77) was studied in an effort to improve the solubility and observed the dissolution rate of these drugs from the resulting formulations. The drug loading capacity of these amphiphilic carriers possessing either C_4 or C_7 alkyl substituents on the lower rim was compared.

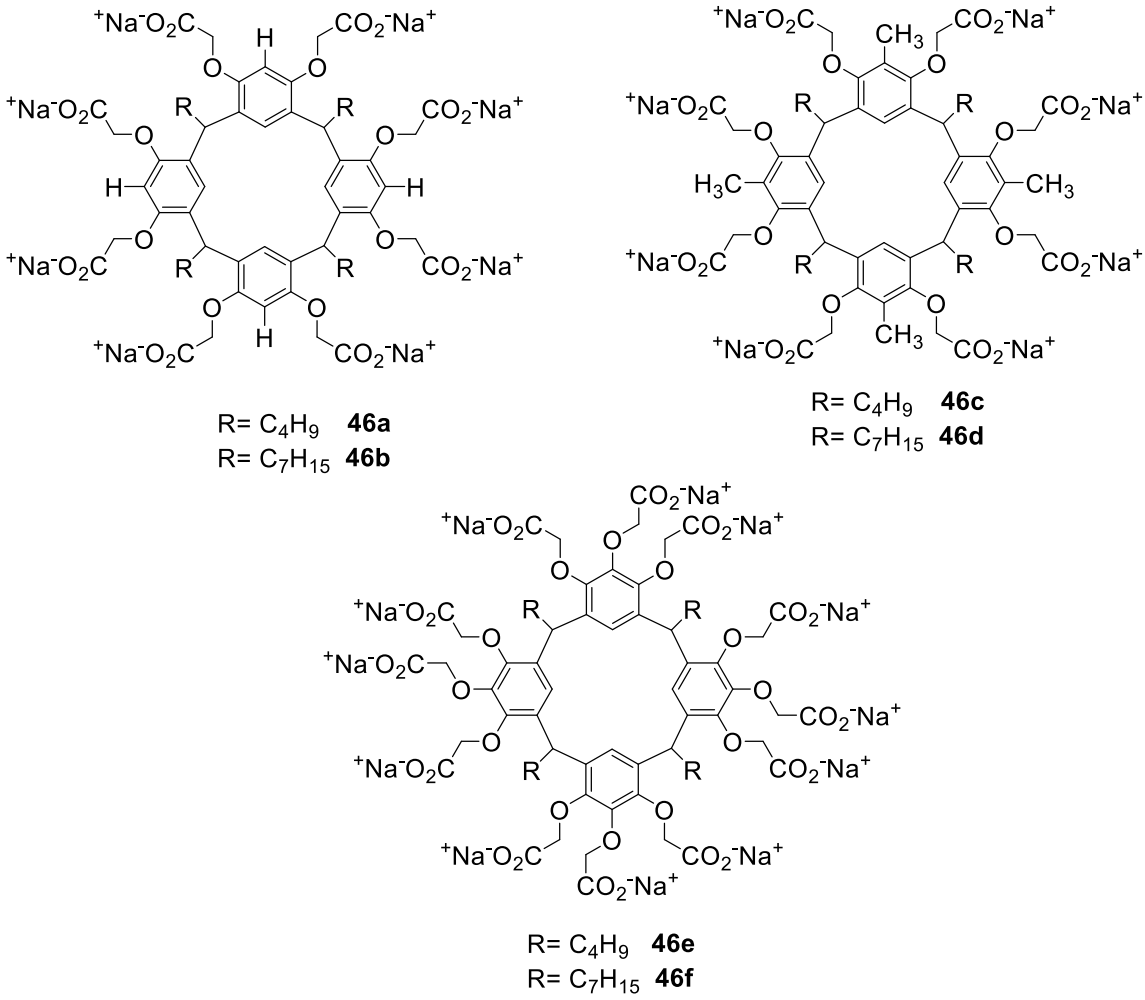

Figure 77: Molecular structure of calix[4]resorcinarenes **46a-d** and calix[4]pyrogallolarenes **46e-f** derivatives.

The ability of a carrier to load different drugs with differing efficiency will depend on a variety of factors: The structural properties of drugs being loaded have an impact on drug loading capacity (Fahmy *et al.,* 2019). Planar (flat) structures of drugs cotaining aromatic rings have the ability to stack closely together, allowing higher concentrations to become encapsulated within aggregated formulations. Large drug molecules with higher molecular weight and perhaps more rigid structures introduce strong steric hindrance which makes it more difficult to accommodate the drug molecules in high concentration, meaning solubilisation efficiency is decreased.

The solubility of drugs in solutions is usually quantified as log P (the negative logarithm of the partition coefficient). Log P is used to describe a molecule's hydrophobicity. Drugs with high log P values indicate the ability of a molecule to mix with an oily phase rather than aqueous media (Zhang *et al.,* 2009). Thus, a high value for log P means the drug has a higher affinity for the hydrophobic regions of the potential solubilising agent, resulting in increased loading of the hydrophobic drug (increased solubilisation). Moreover, poor aqueous solubility of lipophilic drugs impacts the dissolution rate. The more lipophilic the drug molecule, the greater affinity it will have for the hydrophobic regions of the carrier-drug aggregates.

In order to choose the appropriate excipient as a carrier for drug solubilisation, it is important to compare between more than one carrier to select the ideal candidate for an optimal formulation. In the case of calix[4]resorcinarenes and calix[4]pyrogallolarenes, a number of factors such as hydrophobicity, molecular weight and architecture of the drug being solubilised play an important role in characterising the drug carrier and mode of incorporation in aggregates formed (Morozova *et al.*, 2018; Syakaev *et al.,* 2018).

Propofol has a log P value of 4.16 and is thus highly insoluble in aqueous media. Figure 123 shows that with propofol the highest drug loading content for carriers **46a-f** was obtained from solutions containing an initial carrier concentration of 6 mg/mL and an initial drug: carrier loading ratio of 10:1. All the carriers proved to be excellent in the solubilisation of propofol and it was observed that the high initial carrier concentration achieved the greatest solubilisation. The aqueous solubility of propofol was increased by 27.44 mg/mL, 35.59 mg/mL, and 42.41 mg/mL with the carrier **46f**, carrier **46d** and carrier **46b** respectively. Calix[4]resorcinarnes **46b-d** and calix[4]pyrogallolarenes **46f** with possessing C_7 alkyl substituents on the lower rim exhibited the highest drug loading capacity taking all data into consideration, forming larger aggregates capable of drug solubilisation in particular. This indicated that the drug might be accommodated within the alkyl chains. The low molecular weight (MW = 178 g/mol) of propofol allows the molecules to fit closely together without much steric hindrance thus maximising the concentrations being encapsulated. However, the results cannot confirm the mechanism for binding of such hydrophobic drugs with aggregated amphiphilic carriers (Shinkai *et al.*, 1986; Ghosh& Nau, 2012).

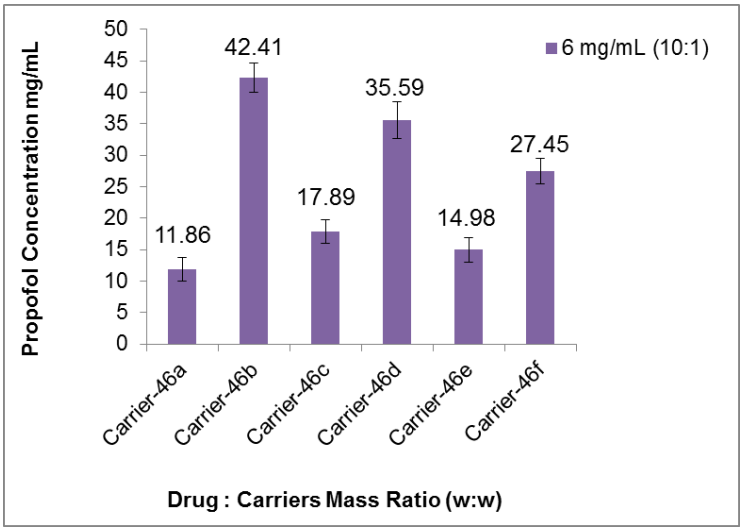

Figure 123: Maximum propofol concentration solubilised by calix[4]resorcinarenes **46a-d** and calix[4]pyrogallolarenes **46e-f**.

The chemical structure of prednisolone (MW = 360 g/mol), is more bulky and inflexible thus hindering close proximity of the molecules by stacking. The prednisolone solubility with all formulations was significantly lower than that with propofol. From the initial drug loading studies, where the effect of the chain length was investigated, a trend of increasing excipient concentration and initial drug: excipient feed concentration with reducing drug loading was noted with the bulky molecular weight drug, prednisolone (Figure 124) shows the highest incorporation. The loading capacity of prednisolone entrapped with carrier **46e**, carrier **46c** and carrier **46a** was 27 %, 26 % and 32 %, respectively, when compared with the intrinsic drug solubility (Figure 124). Interestingly, carrier **46a** and carrier **46e** with the short alkyl chains on the lower rim were capable of solubilising more prednisolone compared to carrier **46b** and carrier **46f** possessing the long C_7 alkyl chains. As previously mentioned, prednisolone is a bulky molecule, thus the drug loading was reduced probably due to steric hindrance from the drug. Optically, before filtration of the crude formulations derived from carriers possessing the C_7 alkyl chains appear to be more opaque and solubilise greater drug content compared to those possessing the shorter C_4 alkyl chains. It is assumed that the aggregates formed from these more hydrophobic carriers exceeded the maximum cut-off for the 0.45 μm filter and hence could not pass through, resulting in an observed reduction of drug concentration and, hence, solubilising potential. In the case of prednisolone, for the carriers possessing C_4 alkyl chains may apparently form simple drug: carrier aggregates. On the other hand, as it is clear from (Figure 124) drug loading of carrier **46d** with long C_7 alkyl chains is higher than carrier **46c** possessing short C_4 alkyl chains; this result is rational based on the steric hindrance of the methyl group on the carrier **46c-d** upper rim. Thus, the incorporation of prednisolone might be within the

tail instead. Furthermore, for the carrier-drug formulation, drug solubility was increased with increased initial feed ratios of 5:1 drug: carrier. The rationale for this is the presence of an extra carboxyl group on the upper rim of the calix[4]pyrogallolarenes **46e-f** which may form additional non-covalent interactions or confer increased solubility on the aggregates.

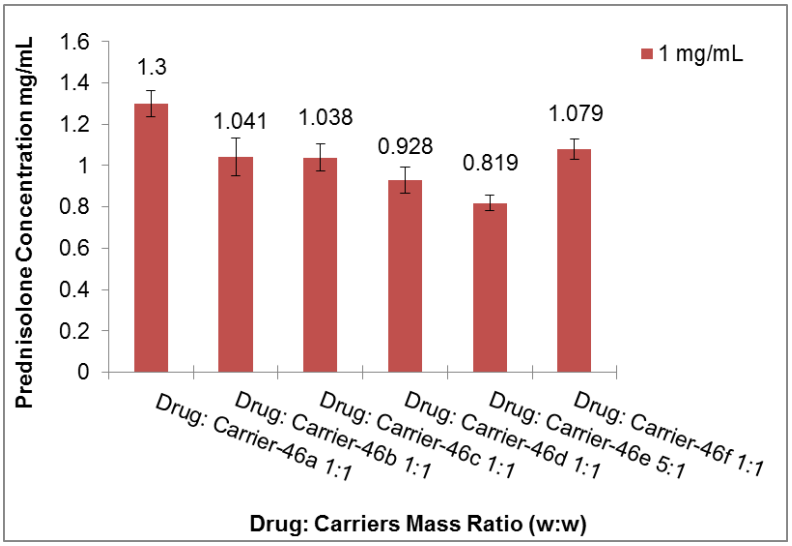

Figure 124: Maximum prednisolone concentration solubilised by calix[4]resorcinarenes octa-sodium salt **46a-d** and calix[4]pyrogallolarenes dodeca-sodium salt **46e-f**.

The results of DLS analysis confirmed the trend observed as the particle size distribution of the aggregates formed significantly changes in the presence of the drug molecules. In the case of propofol the averaged size of the self-assemblies formed increased for all carriers (Figure 125 and 126). Also, a trend was observed in which the size of the aggregates formed increased as the drug loading capacity for the carriers increased, typified by the carriers **46a** and **46c** possessing short C_4 aliphatic chains on the lower rim. However, the average aggregate size was decreased with increased drug loading capacity for the carriers **46b** and **46d** possessing longer C_7 aliphatic chains on the lower rim. The effects of drugs on the zeta potential of the carrier were studied. It is obvious that the drug loading capacity

has an effect on the zeta potential: in all cases, an increase in the drug loading capacity led to less negative values of the zeta potential.

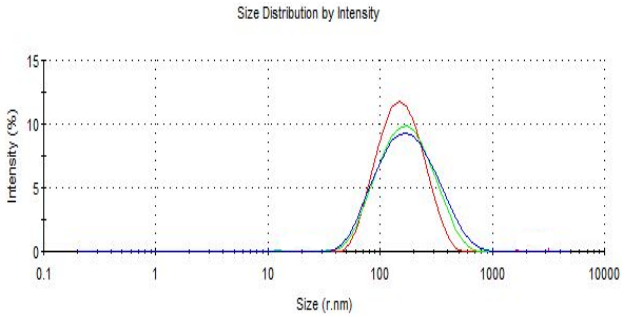

A. Carrier **46a** alone

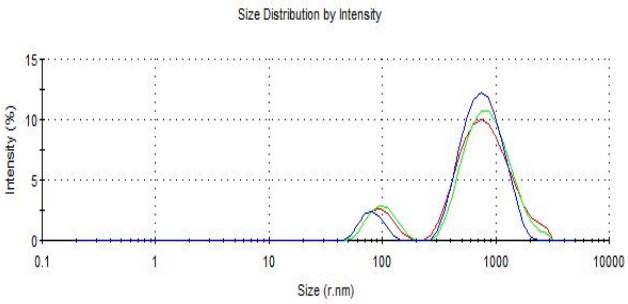

B. Propofol: Carrier **46a** 6mg/mL (10:1)

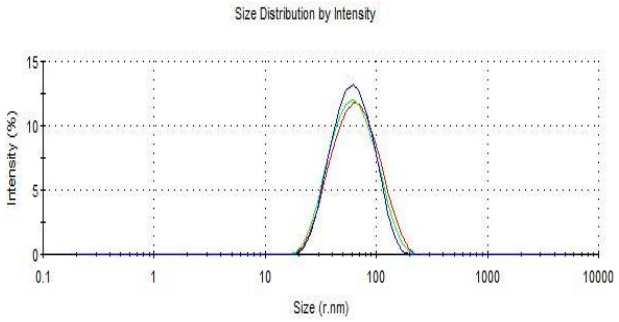

C. Carrier **46c** alone

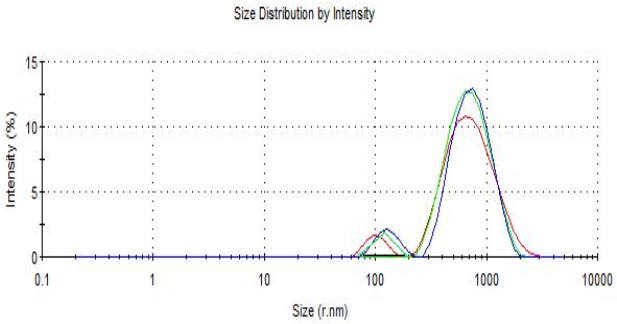

D. Propofol: Carrier **46c** 6 mg/ml (10:1)

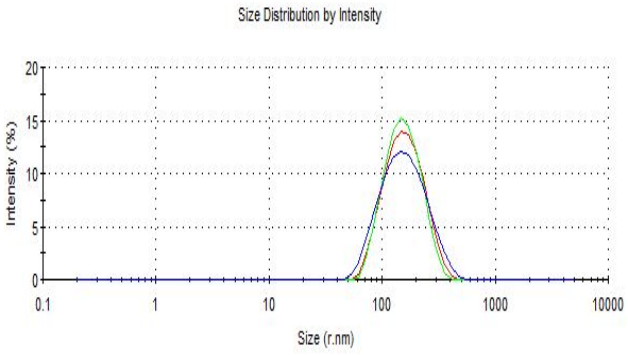

E. Carrier **46e** alone

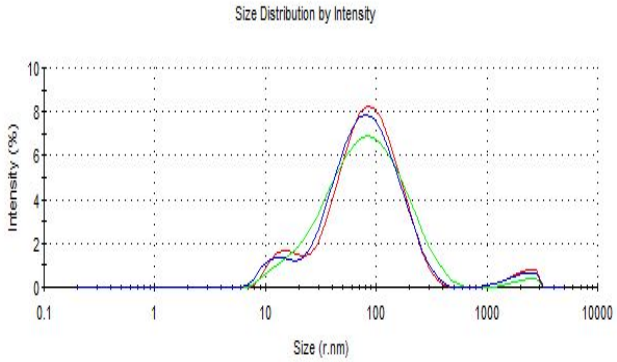

F. Propofol: Carrier **46e** 6 mg/mL (10:1)

Figure 125: Photon correlation spectroscopy size correlation chart for carrier with short chains and drug: carrier formulation in deionised water (n=3, ave).

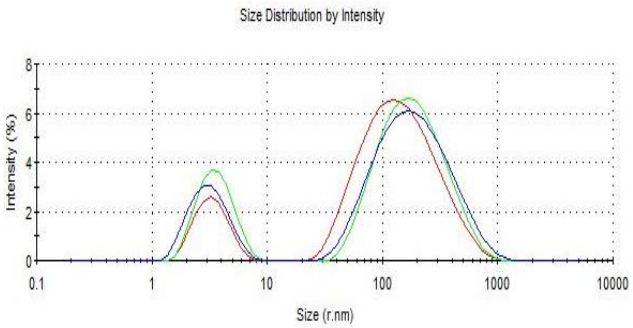

A. Carrier **46b** alone

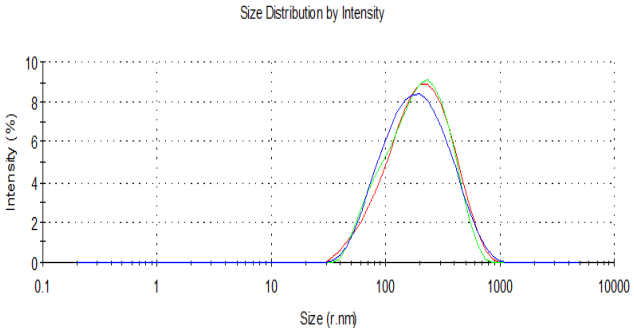

B. Propofol: Carrier **46b** 6 mg/mL (10:1)

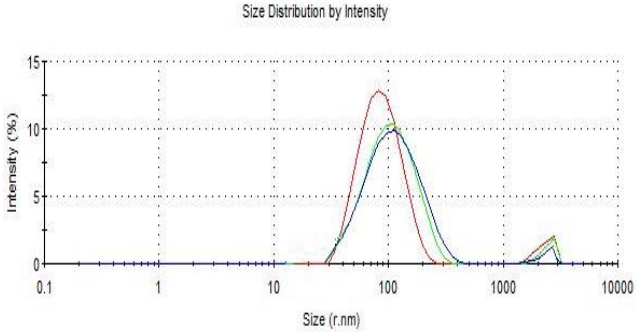

C. Carrier **46d** alone

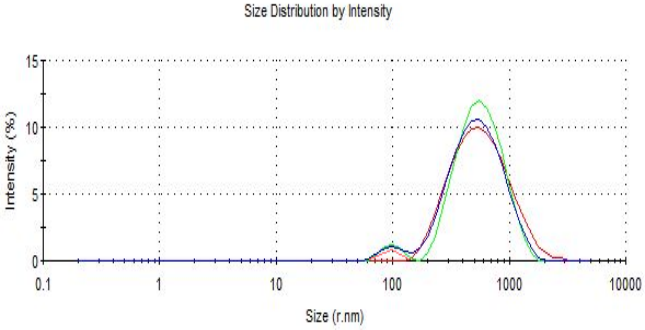

D. Propofol: Carrier **46d** 6 mg/mL (10:1)

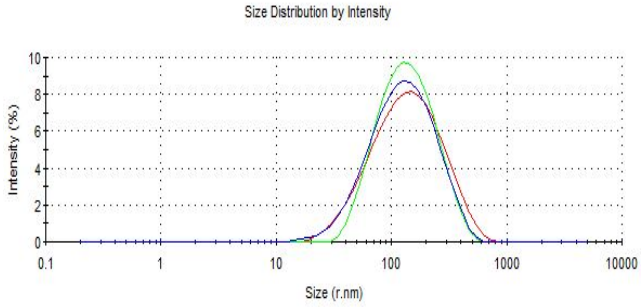

E. Carrier **46f** alone

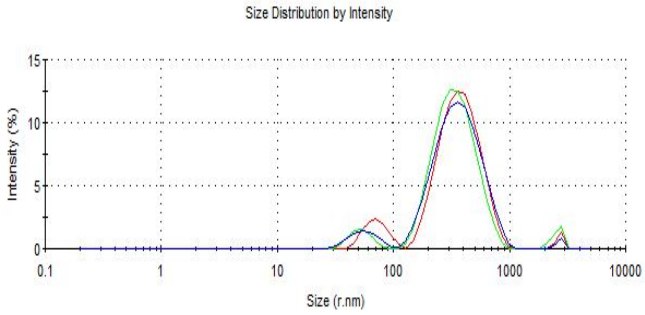

F. Propofol: Carrier **46f** 6 mg/mL (10:1)

Figure 126: Photon correlation spectroscopy size correlation chart for carrier with long chains and drug: carrier formulation in deionised water (n=3, ave).

The aggregates formed from formulations loaded with prednisolone were obviously different from the corresponding propofol formulations. Carriers with short alkyl chains on the lower rim gave aggregates with a large and well-defined hydrodynamic radius (Figure 127). This behaviour is different from the aggregates formed with

carriers possessing long alkyl chains (Figure 128). In the case of carriers **46e** and **46f**, varying aggregation was observed in prednisolone formulations, due potentially to the extra carboxyl groups at the upper rim

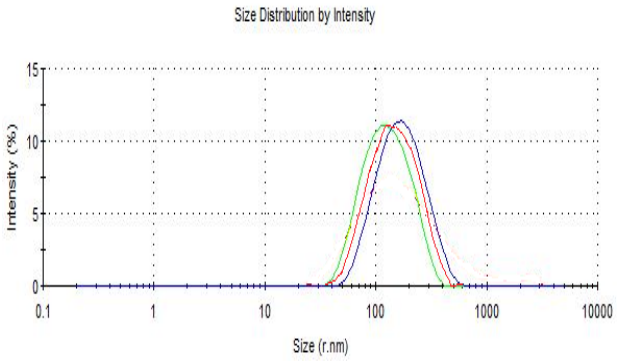

A. Carrier **46a** alone

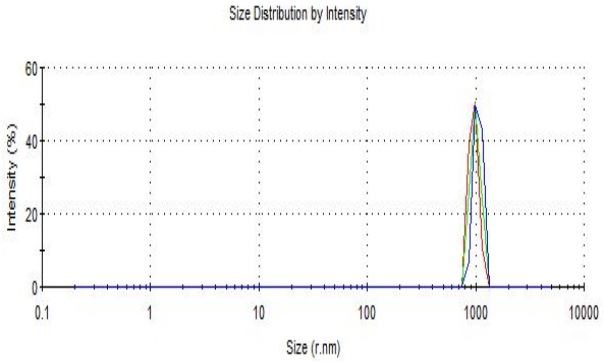

B. PLS-carrier **46a** 1 mg/mL (1:1)

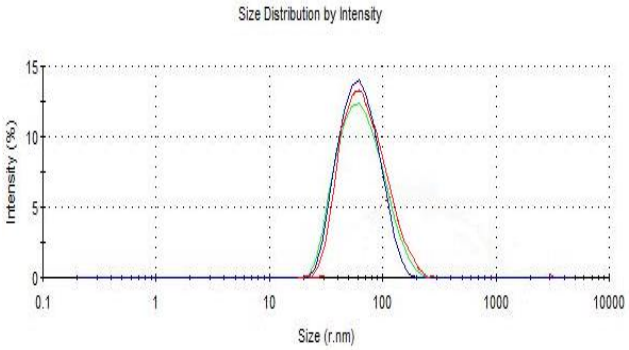

C. Carrier **46c** alone

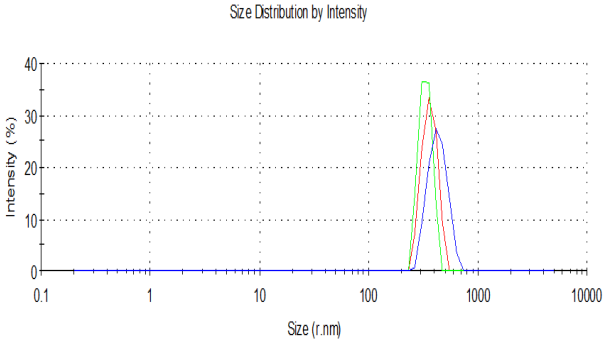

D. PLS-carrier **46c** 1 mg/mL (1:1)

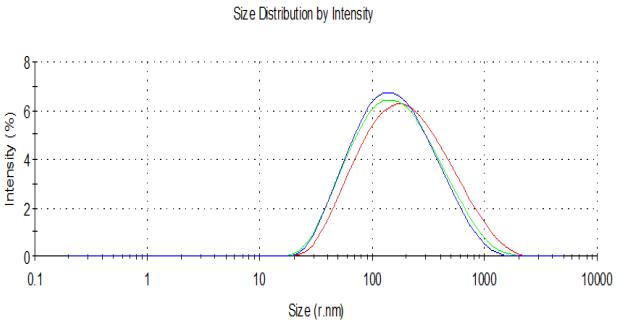

E. Carrier **46e** alone

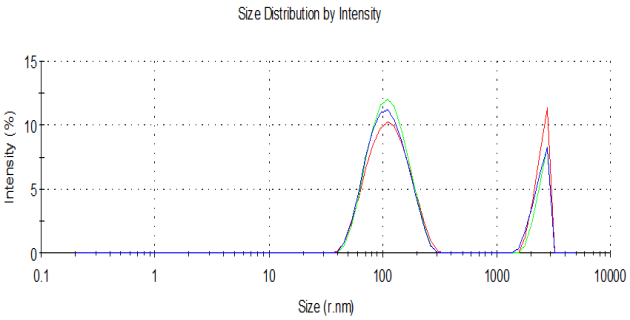

F. PLS-carrier **46e** 1 mg/mL (5:1)

Figure 127: Photon correlation spectroscopy size correlation chart for carrier with short chains and drug: carrier formulation in deionised water (n=3, ave).

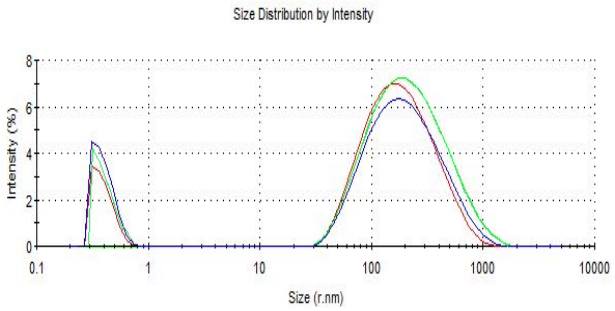

A. Carrier **46b** alone

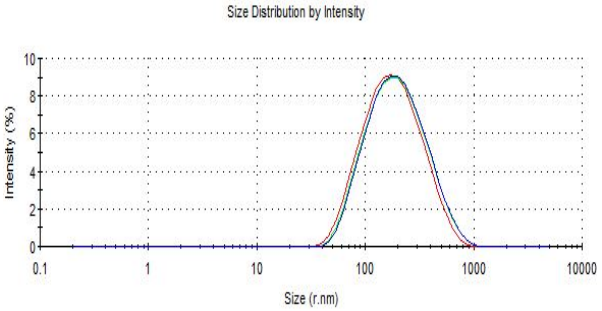

B. PLS-carrier **46b** 1 mg/mL (1:1)

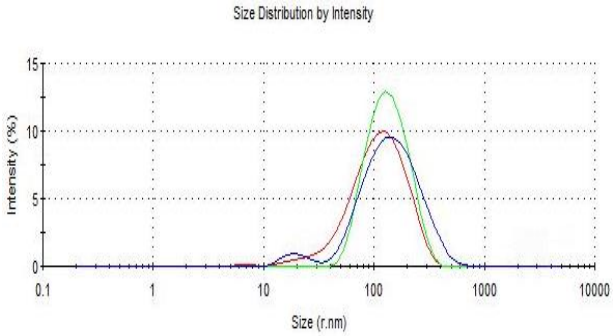

C. Carrier **46d** alone

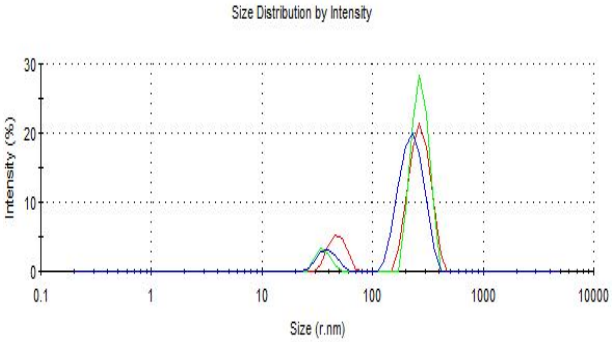

D. PLS-carrier **46d** 1 mg/mL (1:1)

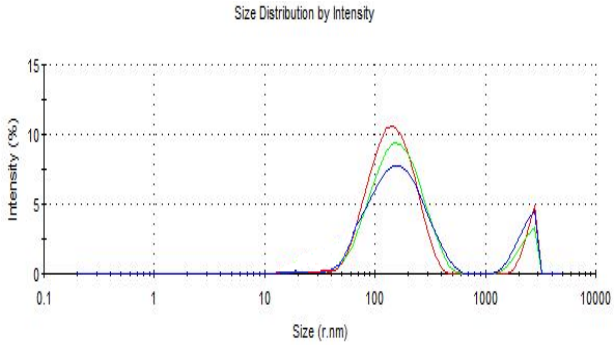

E. Carrier **46f** alone

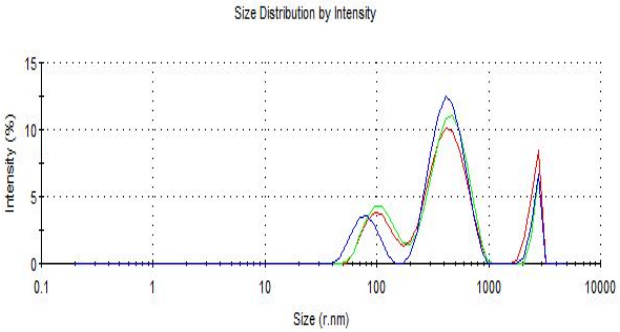

F. PLS-carrier **46f** 1 mg/mL (5:1)

Figure 128: Photon correlation spectroscopy size correlation chart for carrier with long chains and drug: carrier formulation in doubly distilled water (n=3, ave).

Analysis of the formulations obtained by solubilising propofol, prednisolone and tetracaine with calix[4]resorcinarene carrier **46b** gave some insight as to the possible mode of association within the drug:carrier complexes. In each case a solution was made of the drug and carrier in D_2O, corresponding to an initial drug concentration of

3 mg/mL and a drug: carrier ratio of 1:1. Significant interaction between propofol and carrier **46b** was observed, particularly in the NOESY spectrum which highlighted the proximity of propofol molecules to the aromatic protons in the 5-position on the calix[4]resorcinarene annulus. In addition, the signal assigned to the bridgehead protons was observed to be a multiplet in the drug: carrier solution, possibly indicating that the incorporation of propofol into the alkyl residues on the lower rim of the carrier can induce a conformational change: the presence of increased amounts of propofol may force the calix[4]arene to form the *rccc* boat conformation, due to the strong hydrophobic association effect. This will require further investigation to confirm. In summary, NMR data for the propofol: carrier **46b** complex indicates that the propofol is located within the alkyl chains on the lower rim of the carrier.

In the cases of prednisolone and tetracaine, no significant information concerning the mode of association could be discerned. This observation was expected for prednisolone; since the drug loading was very low and the drug molecule is very polar so was not anticipated to associate with the lower rim substituents. However, it was envisaged that tetracaine may associate with the alkyl substituents. It is important to note here that tetracaine becomes protonated at approximately pH 8 and pH 4, due to the presence of two basic centres in the drug molecule. A solution of carrier **46b** with concentration of 3 mg/mL has pH 7.65, and the pH of a tetracaine: carrier **46b** solution with the corresponding initial drug concentration and drug: carrier ratio of 1:1 is 9.43. This indicates the potential for an ionic interaction between tetracaine and the carrier **46b** at this concentration, which would not be evident in NMR spectra. Also, there is evidence in the literature that tetracaine is capable of self-association in solution, which may complicate the situation further (Cai *et al.,* 2016).

In vitro drug release profiles of the amphiphilic carriers **46a-f** were studied with the two model drugs propofol and prednisolone, each with differing physicochemical properties. Increasing evidence suggests that a drugs' intrinsic aqueous solubility can impact drug release rate (D'Souza, 2014; Wang *et al.,* 2009; Zhao *et al.,* 2015). Hence, the release profile was expected to be slow. Aqueous solubility of these hydrophobic drugs was determined to be 0.1 mg/mL (propofol) and 0.22 mg/mL (prednisolone) respectively. The release data for all the carriers confirm the above statement, as propofol with less aqueous solubility than prednisolone shows a much lower release profile. This trend was mostly observed over 3 days for the two drugs.

Figure (129 A) shows the drug release from the carriers possessing short alkyl chains on the lower rim: propofol is released from carrier **46a** with only about 70 % after 48 h compared with 97 % for prednisolone. For carrier **46c**, propofol shows lower release profile with 60 % being released after 48 h compared with 68 % for prednisolone. Additionally, carrier **46e** had only released 55 % of prednisolone compared with 49 % of propofol. This trend was also observed in the release from the carriers with the long alkyl chains over this time period (Figure 129 B). For carrier **46b** propofol showed a much lower release profile with only 16 % being released after 48 h compared with 90 % for prednisolone. The fastest drug released from the carrier **46d** self-assemblies was prednisolone with 32 % followed by the propofol with only 24 %. It can be seen from (Figure 129 B) for carrier **46f**, the percentage drug released of prednisolone is 48 % compared to 34 % for propofol.

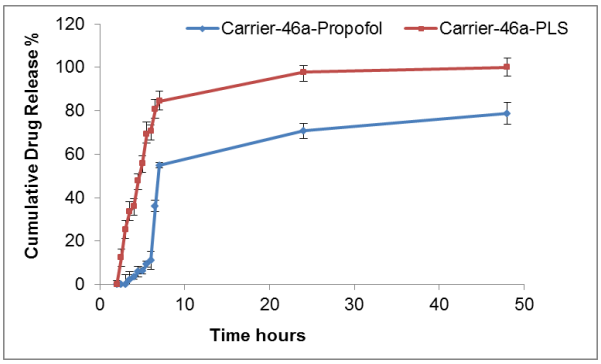

Calix[4]resorcinarene **44a**

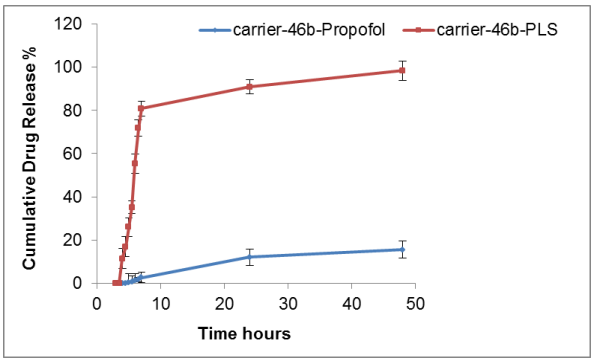

Calix[4]resorcinarene **46b**

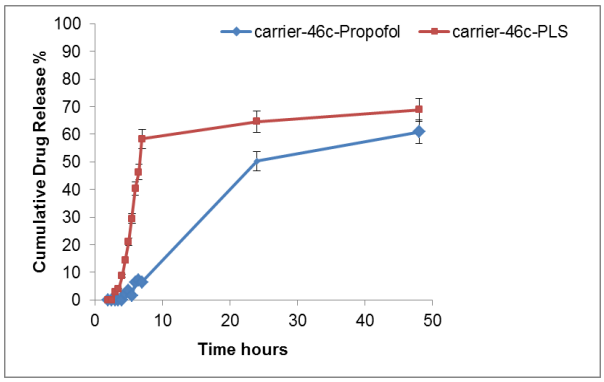

Calix[4]resorcinarene **46c**

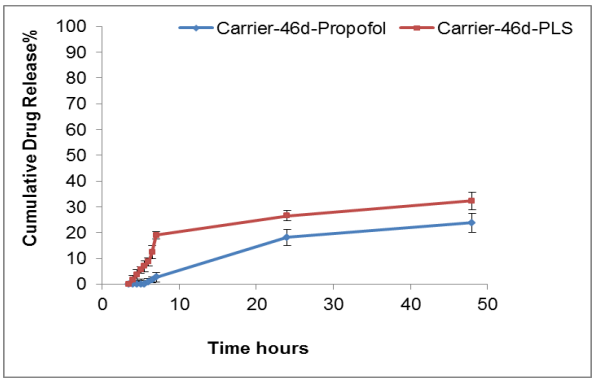

Calix[4]resorcinarene **46d**

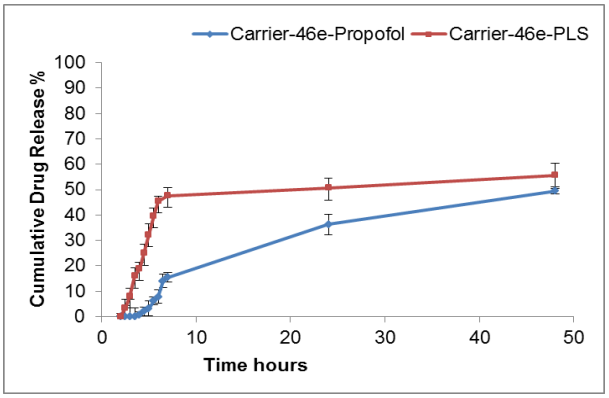

Calix[4]resorcinarene **46e**

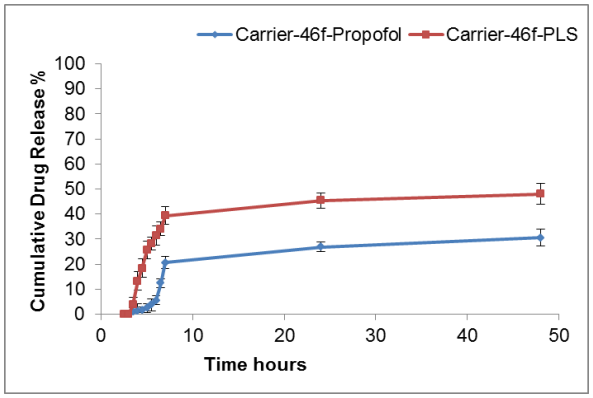

Calix[4]resorcinarene **46f**

A. *In vitro* release of propofol and prednisolone (PLS) from the short chained carrier formulations

B. *In vitro* release of propofol and prednisolone (PLS) from the long chained carrier formulations

Figure 129: Comparison of the release profiles rate of propofol and prednisolone over 48 h at 20 ºC.

Intrinsic hydrophobicity of nano-aggregates is a key determinant of the drug release rate. In this study, the rate of drug release depends on the length of the alkyl chain

displayed on the lower rim and is the greatest for both of the drugs from the carriers which possess the short alkyl chains. Consequently, propofol encapsulated in carrier **46a** with the shorter, less lipophilic C_4 chain is released faster (79 % after 72 h) than when held in the more lipophilic structure of the carrier **46b** (16 % after 72 h) (Figure 130).

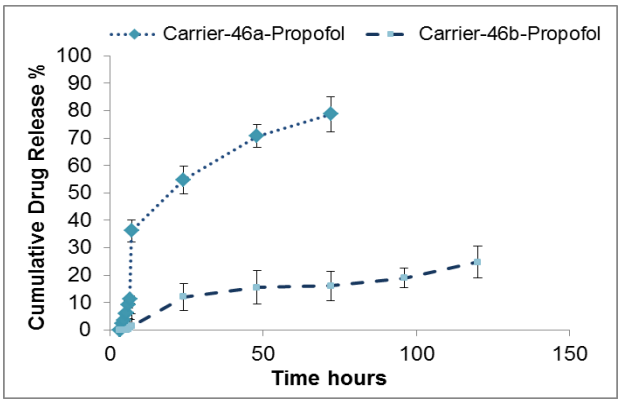

Calix[4]resorcinarenes **44a-b**

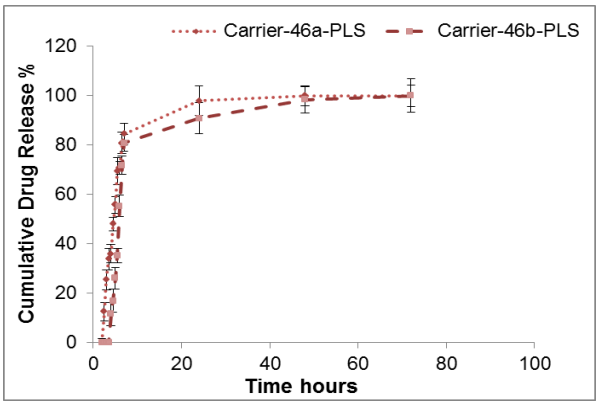

Calix[4]resorcinarenes **46a-b**

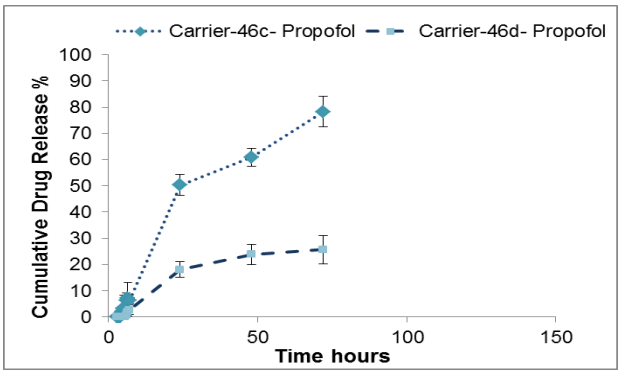

Calix[4]resorcinarenes **46c-d**

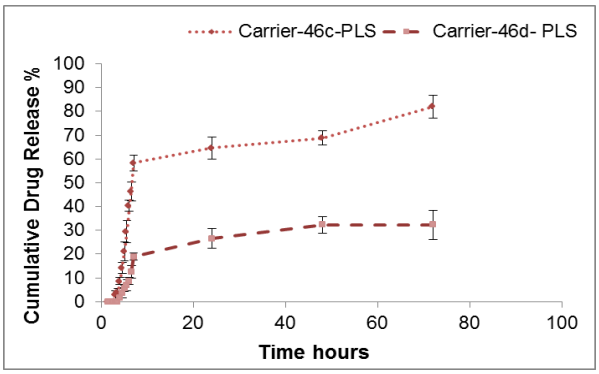

Calix[4]resorcinarenes **46c-d**

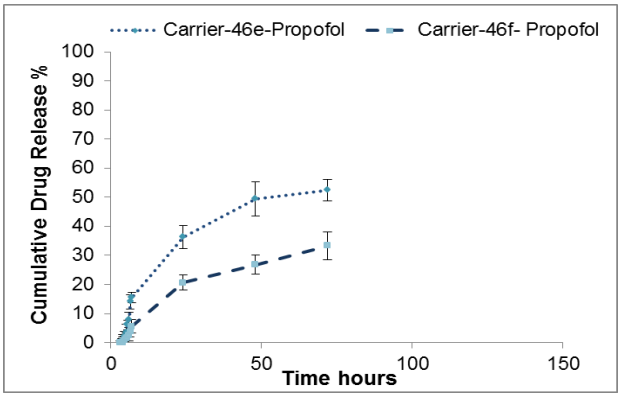

Calix[4]pyrogallolarenes **46e-f**

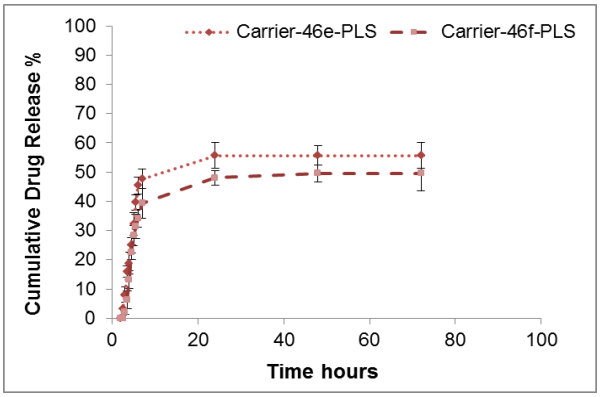

Calix[4]pyrogallolarenes **46e-f**

A. *In vitro* propofol release from both the short and long chained carrier formulations at 20 ºC

B. *In vitro* prednisolone release from both the short and the long chained carrier formulation at 20 ºC

Figure 130: Comparison of the drugs release profile rate between the long and short chain carriers over (72 h) at 20 ºC.

Among several drug formulations, a sustained release formulation with low release rate is favoured more than rapid release. Strategies to control drug release have significant advantages, including reduced local toxicity and increased *in vivo* half-life (D'Souza, 2014; Hoskins *et al.,* 2016; Zhao *et al.,* 2015). From this aspect, drug formulations containing calix[4]resorcinarene carriers which possess C_7 alkyl chains on the lower rim may be more desirable than those formulations derived from calix[4]resorcinarene carriers which possess shorter C_4 alkyl substituents, since they have increased stability under sink conditions.

Analysis of all the evidence gathered provides some insight into aggregate formation and the mode of interaction between the model drugs investigated and nanocarriers **46a-f**.

In solutions derived from an initial carrier concentration of 6 mg/mL and drug:carrier ratio of 10:1, ropofol forms aggregates with carriers **46a** and **46c** that have varying hydrodynamic radius including larger aggregates in the micron (>1000 nm) range. Carrier **46e** does behave differently which is most likely due to it possessing twelve carboxylate residues on the upper rim. However, the drug loading capacity of these carriers for propofol is lower than the loading capacities for carriers **46b**, **46d** and **46f**. Calix[4]resorcinarenes **46b** and **46d** and calix[4]pyrogallolarene **46f** possess longer C_7 alkyl chain residues on the lower rim and all form aggregates with propofol that have a consistent hydrodynamic radii in the range 500-700 nm. The data suggest two different modes of aggregation dependent upon the lower rim substituents; none of the data obtained suggests the presence of micellar structures in the filtered solutions.

Figure 131 shows the potential aggregation of carriers **46a** and **46c** with propofol: the short alkyl chains on the lower rim are able to accommodate a limited amount of

propofol, due to the lower hydrophobicity of the alkyl region. However, more propofol can be accommodated within the spaces between carrier molecules. There is a size limit for this aggregation mode which is in the micron range, beyond which the aggregates become less stable.

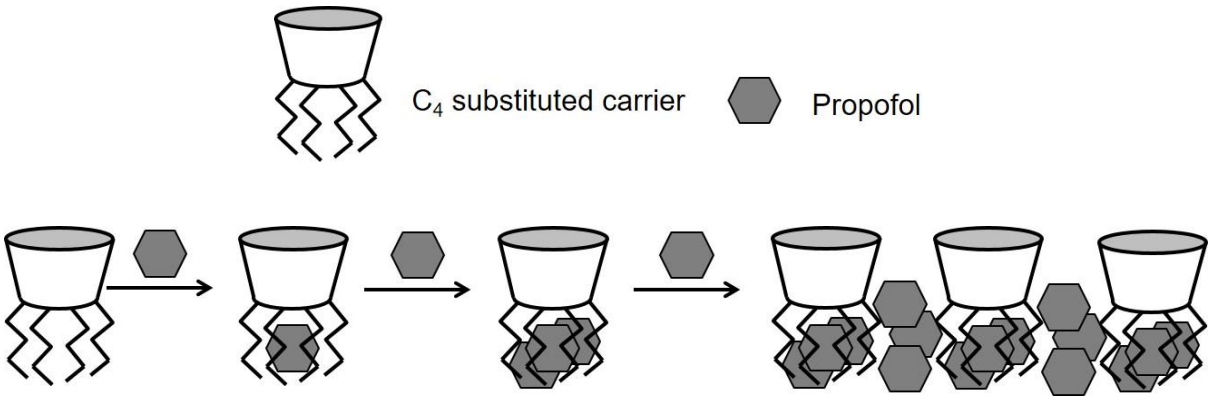

Figure 131: Potential mode of aggregation of propofol with carriers **46a** and **46c.**

Figure 132 shows the potential aggregation of carriers **46b**, **46d** and **46f** with propofol: the longer alkyl chains on the lower rim are able to accommodate more propofol due to the higher hydrophobicity of and increased flexibility within the alkyl region. There is also a size limit for this aggregation mode which is in the sub-micron range, in fact the size of the aggregates decreases as drug loading increases. This may be due to the van der Waals interactions between propofol and the alkyl pendants on the lower rim, which will increase as more propofol was loaded thus pulling the carrier molecules closer together.

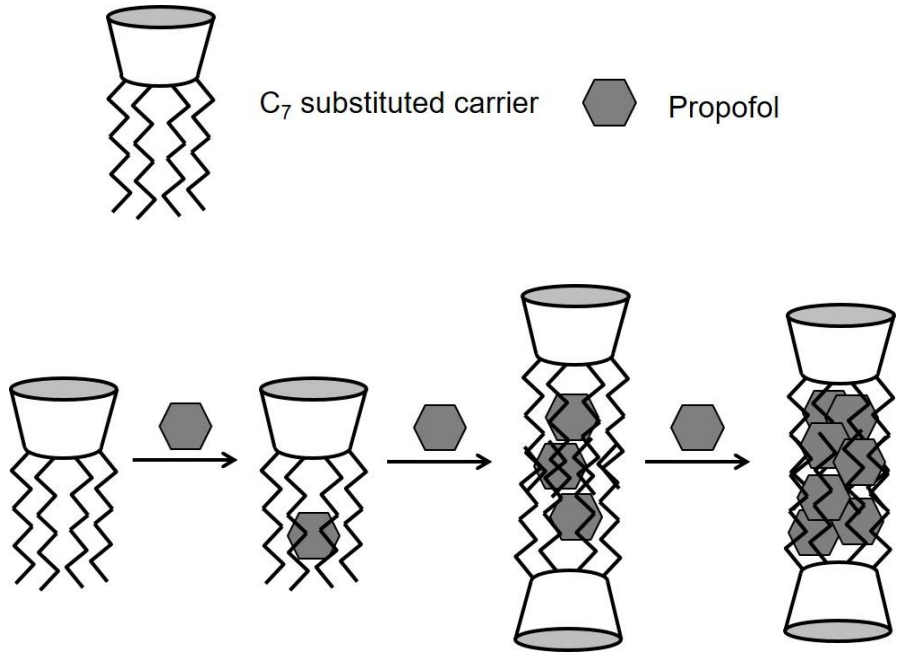

Figure 132: Potential mode of aggregation of propofol with carriers **46b**, **46d** and **46f**.

In the case of prednisolone, the drug loading observed for all carriers **46a-f** was very low and the drug was released much more quickly than in systems containing propofol. Whilst there was an indication from the UV-Visble spectra that there is some interaction with the carrier molecules, there was no significant change observed in the NMR spectra. Taking all of these factors into account, the forces holding prednisolone in drug: carrier aggregates are assumed to be weak and the proposed mode of association of prednisolone within the aggregates formed reflects this (Figure 133)

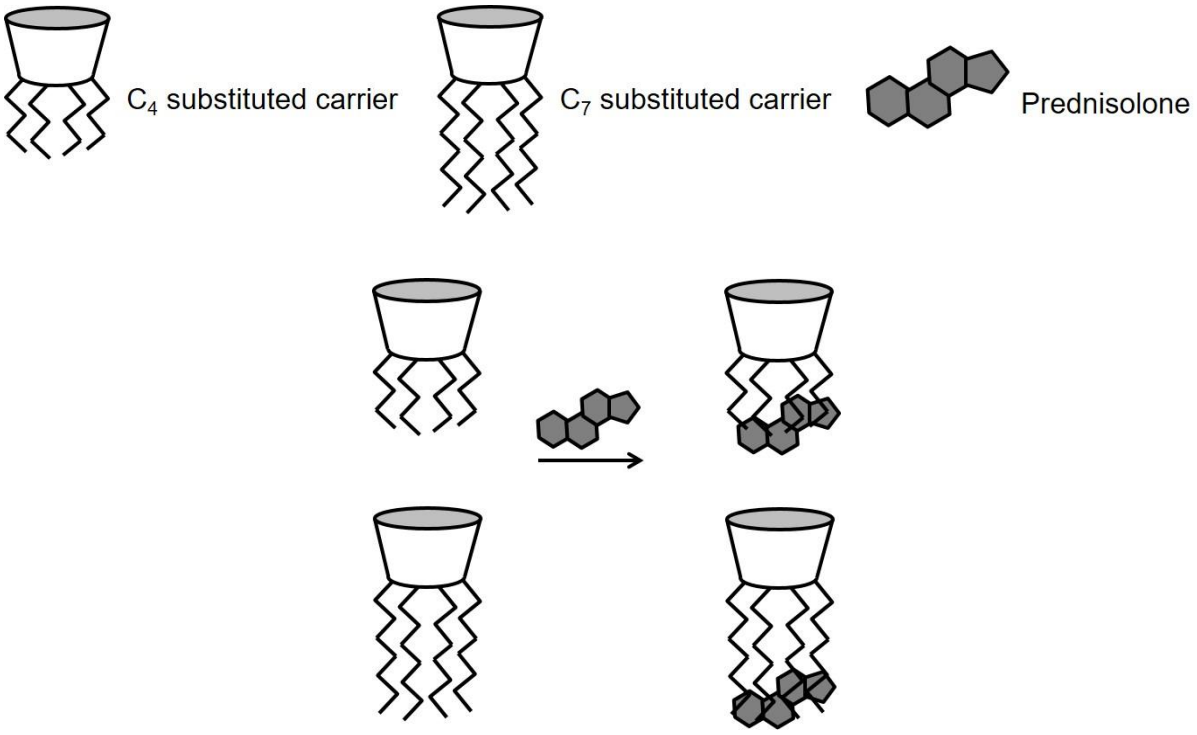

Figure 133: Potential mode of aggregation of prednisolone with carriers **46a-f**.

The drug loading observed for tetracaine with carriers **46a-b** was considerable. However, there was little indication from UV-Vis, FTIR and NMR spectroscopy to support any proposed mode of association in the aggregated formed. It is clear from pH measurements that there is a significant change in pH when tetracaine is loaded into the carriers, providing some evidence for an electrostatic or ionic interaction. There is literature precedence that tetracaine is capable of self-association in aqueous media. A significant observation is that a crystalline precipitate forms in solutions containing drug: carrier aggregates after a few days. At this stage, it is hard to propose any meaningful mode of association, beyond speculation that there is formation of ion pairs in aqueous solution. Further work on this system is required.

3.8 Conclusion

In conclusion, the incorporation of hydrophobic substrates into the aggregates of the carrier depends on the substrate structure and includes the interaction with both hydrophobic and hydrophilic residues of the macrocyclic molecules as well as with the aromatic platform of the macrocycle.

Interestingly, all of the formulations studied significantly improved the aqueous solubility and dissolution rate of both of the hydrophobic drugs tested (propofol and prednisolone), indicating that these amphiphilic carriers can be used as drug solubilising agents. This was not the case for the hydrophobic drug, tetracaine: the formulations with this drug formed a precipitate after two days so in this case it may be necessary to carry out the experiments under different conditions, at different pH values for example. The capability of the calix[4]resorcinarenes and calix[4]pyrogallolarenes used to encapsulate the hydrophobic drugs varied with the types of hydrophobic pendant group attached to the lower rim and the nature of the drug. The difference in drug encapsulation ability between the two drugs is possibly due to differences in molecular weight, size and polarity. Also aggregation plays crucial roles in the binding properties of amphiphilic carriers. Among the carriers assessed in this study, carrier **46b** (Figure 123 and 124) showed the highest solubilisation potential for hydrophobic drugs. Efficient binding of the substrates with this amphiphilic carrier is achieved due to their significant aggregation (Mironova *et al.*, 2013; Morozova *et al.*, 2018; Syakaev *et al.*, 2012). The *in vitro* drug release profiles showed controlled release of the hydrophobic drugs from the novel formulations: for calix[4]resorcinarenes **46b** and **46d** and calix[4]pyrogallolarene **46f** bearing the longer C_7 alkyl chains, the drug release ranged from 48–120 h.

Additionally, the impact of temperature on the formation of inclusion complexes was explored in this study. However, above all this there is definitely a need to investigate toxicology, stability and *in vivo* toxicity before the clinical relevance of these systems can be explored further. Stability can become a limiting factor in drug encapsulation possibilities, thus it is the intended subject of future samples analysis.

Chapter Four

Drug Loading and Release Studies of Calix[4]resorcinarene and Calix[4]pyrogallolarene Nanocarrier Formulations of 2,4-dimethoxy-*N*-(4-phenylbutyl)benzamide

4.1 Introduction

The amide bond occurs widely in both naturally occurring and synthetic compounds (Figure 134) (Taoufik *et al.*, 2018; Williams *et al.,* 2003). Amide bonds constitute the backbone of biologically crucial proteins and are also found in some of the most versatile and widely used synthetic polymers (Andrea *et al.*, 2015; Cheng *et al.*, 2018) and drugs (Baker *et al.*, 2007; Berliner *et al.*, 2011). It is noteworthy that the amide bond is found in up to 25 % of clinically available drugs and in two-thirds of drug candidates, therefore amides clearly play an important role in the pharmaceutical field (Ghose *et al.*, 1999; Carey *et al.*, 2006; Chaudhari *et al.*, 2011; Lundberg *et al.*, 2014). The amide bond is neutral, stable and has both hydrogen-bond accepting and donating properties (Montalbetti & Falque, 2005; Raut & Shirote, 2012; Pragna *et al.*, 2015).

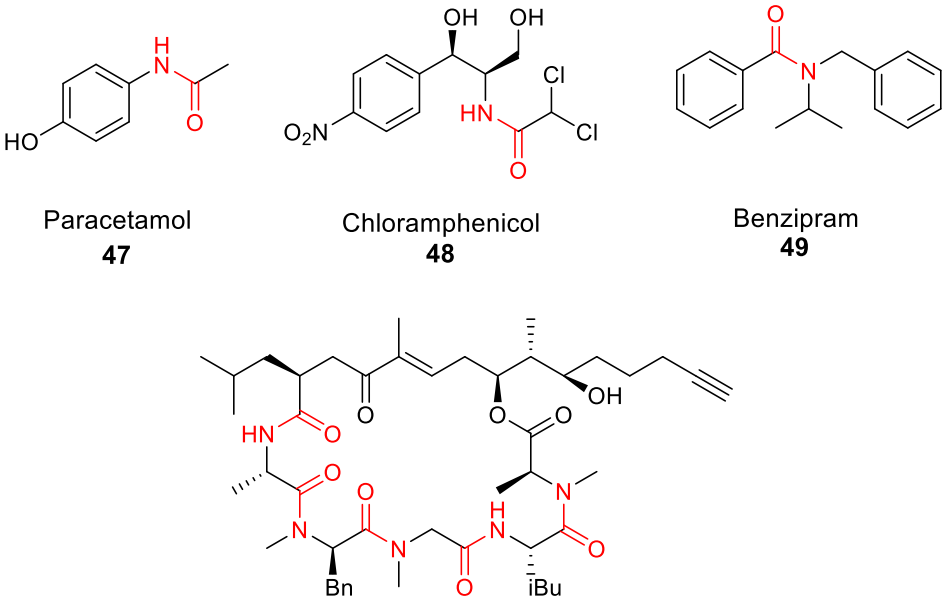

Figure 134: Amide bonds in drug molecules (**47**-**49**) and natural products (**50**) (Allen, 2012).

Amide bonds are typically formed by using two main strategies: Amides can be obtained from the reaction of amines and pre-activated carboxylic acid derivatives, such as acyl halides, anhydrides or active esters (Humphrey & Chamberlin, 1997; Hu *et al.*, 2016; Cheng *et al.*, 2018). Alternatively, stoichiometric amounts of coupling reagents such as carbodiimides or phosphonium or uranium salts can be used to activate and condense a carboxylic acid with amine (Han & Kim, 2004; Valeur & Bradley, 2009; Magano & Dunetz, 2011).

Where amide bonds are formed through the condensation of a carboxylic acid and an amine the only by-product of the reaction would be water (Scheme 14) (Allen *et al.*, 2012; Lanigan *et al.*, 2013; Lundberg *et al.*, 2014; Leggio *et al.*, 2017).

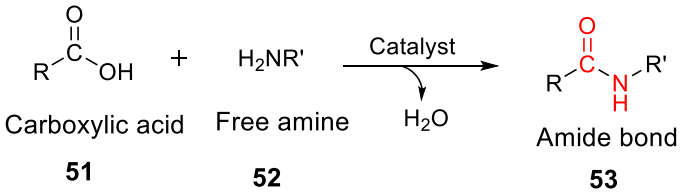

Scheme 14: General equation for direct amide condensation.

The ideal approach would involve direct condensation of a carboxylic acid and amine in the presence of a catalyst because it would be cost-effective with water as the only by-product, and thus a very high atom economy is obtained (Arnold *et al.*, 2006; Berliner *et al.*, 2011; Krause *et al.*, 2016; Cheng *et al.*, 2018).

Direct amidation between carboxylic acids and amines is possible by thermal or catalytic methods and generally requires a high temperature, but is a low yielding process. In order to reduce the amount of reagents or reactant required, or reduce thermal degradation of the product, a low temperature is required for any reaction (Arnold *et al.*, 2008). Although asymmetric induction processes are generally regarded as being more efficient at lower temperatures, since the effects of small

differences in energy between diastereoisomeric transition states are amplified, there are an increasing number of examples where this is not the case and improved asymmetric induction can be obtained at higher temperatures (Enders *et al.*, 1998; Wang *et al.*, 2007). This may also be appropriate for amide bond synthesis using chiral starting materials.

In general, traditional approaches for amide synthesis produce large amount of undesired derivatives, thus increasing the difficulty and cost of isolating the desired amide product (Han & Kim, 2004; Al-Warhi *et al.*,2012). Although the classical methods are used widely for preparing amides in the pharmaceutical industry, new synthetic efforts have been made in order to obtain amides directly from carboxylic acids without using any coupling reagent (Charville *et al.*, 2011). The primary motive in the development of new methods is waste minimization, leading to a more eco-friendly or green process (Carey *et al.*, 2006; Dunn *et al.*, 2007; Roughley & Jordan, 2011; Andrea *et al.*, 2015).

The formation of amides by reaction of carboxylic acids and amines using a stoichiometric amount of dicyclohexyl carbodiimide (DCC) is commonly used in the laboratory, following the mechanism shown in Scheme 15 (Clayden *et al.*, 2012)

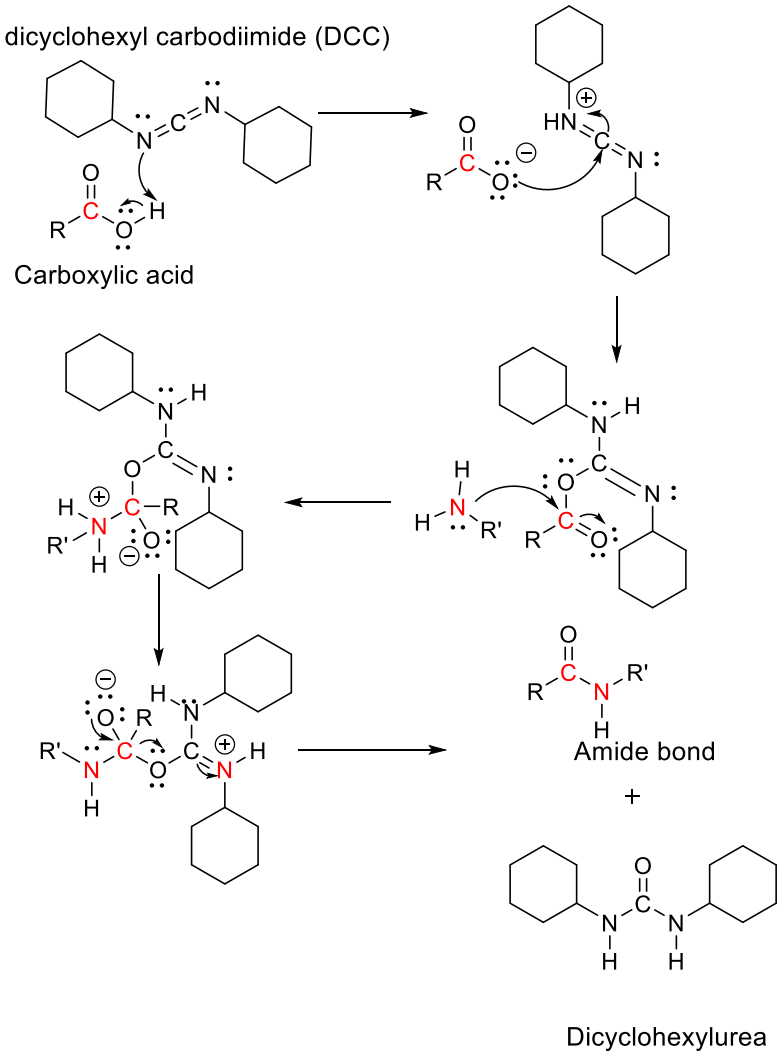

Scheme 15: The mechanism of amide bond formation using DCC (Clayden *et al.*, 2012).

4.1.1 The Uses of Benzamide Derivatives in Medicinal Chemistry and their Pharmacological Potential

Benzamides are aromatic amides, derived from the reaction of an amine with a benzoic acid derivative. Benzamides have attracted considerable attention over the past few decades in pharmacological applications. Benzamides bearing a halogen substituent on the aryl ring and quinoxaline amide derivatives show great promise in anti-tumor, anti-inflammatory, anti-oxidant, analgesic and anti-viral chemotherapy. It was also reported that substituted benzamides have an anti-convulsive,

hypoglycaemic, anti-arrhythmic and have fungicidal activity (Kolev *et al.*, 2013; Robinson *et al*., 2015; Mohan & Sreenivasa, 2016). The effects of adding different substituents on benzamides either by aliphatic, aromatic or heteroaromatic systems were investigated; in an effort to improve the biological activity of benzamide (Figure 135) (Asif, 2016; Oliveira *et al.*, 2019; Robinson *et al.*, 2015; Shelke *et al.*, 2019).

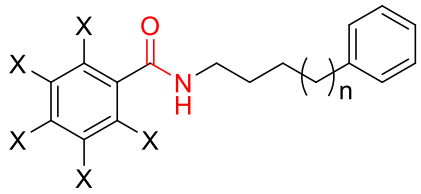

Amides bearing a halogen substitution

54

X= F, Cl, Br
n= 1, 2, 3, ...

Figure 135: The structure of a benzamide derivative with different substituents (Robinson *et al.*, 2015; Shelke *et al.*, 2019).

This chapter describes the synthesis and characterisation of a model drug-like molecule, 2,4-dimethoxy-*N*-(4-phenylbutyl) benzamide (LO9 **57**): LO9 **57** bears similarities to known benzamide derivatives of general structure **54** that have been shown to have activity against cancer cell lines and has itself been shown to be more active than those compounds reported in the literature (Robinson *et al.*, 2015). This chapter also highlights investigations into the formulation of LO9 **57** with amphiphilic calix[4]resorcinarenes **46a-d** and calix[4]pyrogallolarenes **46e-f**: These carrier molecules have been shown to act as drug solubilising agents for drug loading and release of model drugs and so were challenged with LO9 **57**, which is insoluble in aqueous media. The maximum loading capacity for LO9 **57** of each of the carriers was assessed and optimal formulations characterised using a number of analytical

techniques, including photon correlation spectroscopy (PCS). As for the drug loading, *in vitro* drug release profiles were determined by HPLC.

4.2 Preparation of LO9 57 and Formulations and Characterisation Methods used

LO9 **57** was successfully prepared using a standard protocol described in the literature (Robinson *et al.*, 2015). 2,4-Dimethoxybenzoic acid **55** was reacted with 4-phenylbutylamine **56** in the presence of a stoichiometric amount of dicyclohexylcarbodiimide (DCC) in DCM (Scheme 16). After the reaction was complete the urea by-product was removed by filtration and the desired LO9 **57** was obtained in 70% yield as a white solid following chromatography. The product was analysed using a variety of spectroscopic methods.

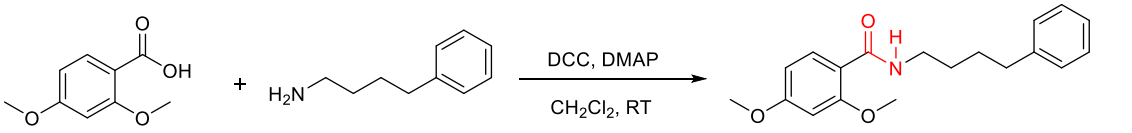

2,4-Dimethoxybenzoic acid **55**

4-phenylbutyl amine **56**

2,4-dimethoxy-*N*-(4-phenylbutyl)benzamide LO9 **57**

Scheme 16: Synthesis of model drug analogue LO9 **57**

4.2.1 Drug Incorporation Studies

Solutions of calix[4]resorcinarenes **46a-d** and calix[4]pyrogallolarenes **46e-f** (1 mg/mL, 3 mg/mL and 6 mg/mL) were prepared in deionised water and probe sonicated for 10 min to ensure aggregation. For each carrier **46a-f**, formulations with LO9 **57** were prepared containing various weight ratios by adding 1:1, 5:1 and 10:1 initial drug: excipient weight ratios. All solutions containing mixtures of LO9 **57** with a

carrier were probe sonicated for a further 10 min to ensure maximum drug loading was achieved. After cooling to room temperature, the solutions were filtered using 0.45 µm syringe filters to ensure any excess free drug was removed.

4.2.2 Determination of Drug Loading Capacity

The drug loading capacity of each carrier **46a-f** for LO9 **57** was measured after filtration of the samples (0.45 µm) and dilution with the mobile phase [(water (0.05 % TFA)/ acetonitrile (0.05 % TFA) (50: 50 v/v)] (Arnold *et al.*, 2006). The amount of LO9 **57** contained in aggregates present in the formulations was determined by analysing the drug content in the aqueous solution by high-performance liquid chromatography (HPLC) (Shimadzu Prominence) over a RP Zorbax ODS 250 mm × 46 mm × 5 µm HPLC column (Hichrom, Lutterworth, UK) with the mobile phase at flow rate of 1 mL/min a detector wavelength set at λ =255 nm. HPLC analysis of pure LO9 **57** (A), carrier **46a** (B) and inclusion complex (C) showed is shown in Figure 136. The retention time of carrier **46a** was 1.04 min and that for LO9 **57** was 3.74 min (Figure 136). These same retention times were observed in analyses of the inclusion complexes formed. Hence, it can be concluded from the HPLC analysis that LO9 **57** was present in inclusion complexes. Complexation of LO9 **57** with other carriers was carried out and the HPLC results were shown (Figure 137-141). The content of LO9 **57** contained in the aggregates was quantified from the standard calibration curve of the free drug (6 µg/mL – 25 µg/mL) with a correlation coefficient of 0.9998.

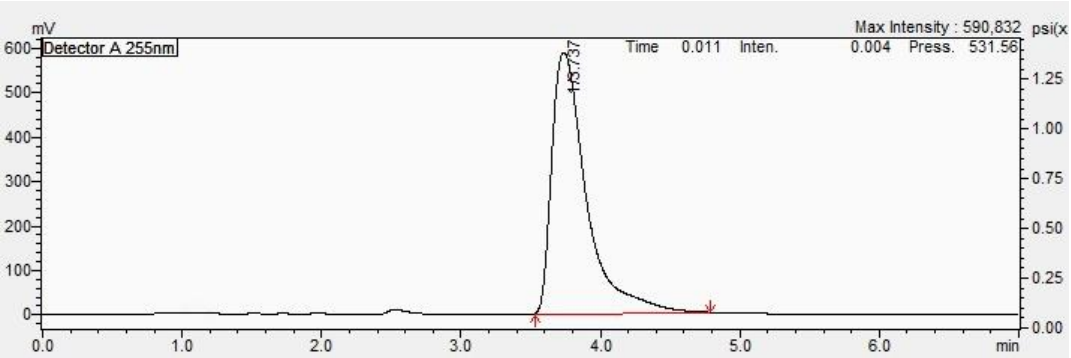

A. Pure Drug LO9 **57**

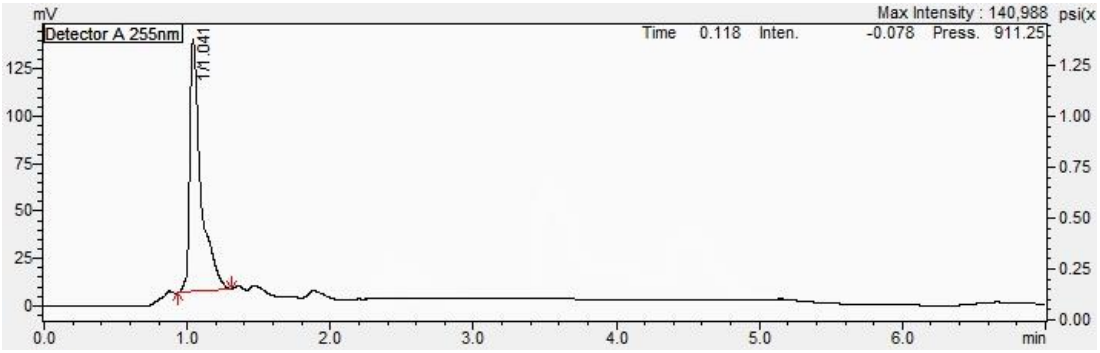

B. Carrier **46a**

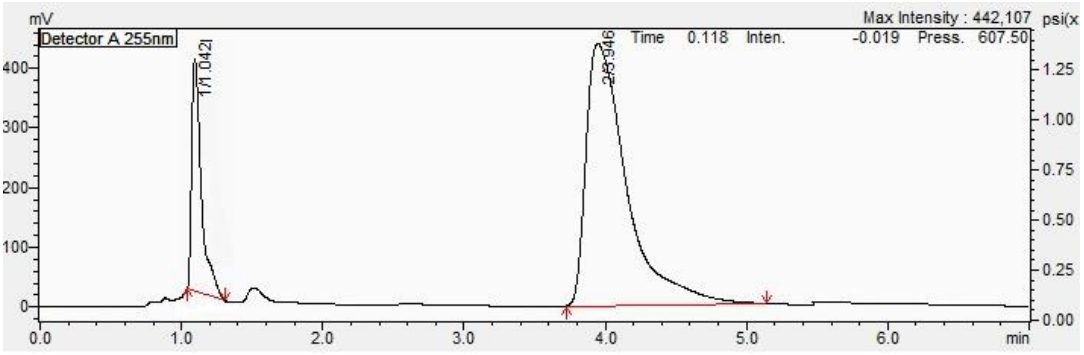

C. Inclusion complex

Figure 136: The HPLC chromatogram of (A) standard pure drug LO9 **57** (B) carrier **46a** and (C) carrier: drug formulation.

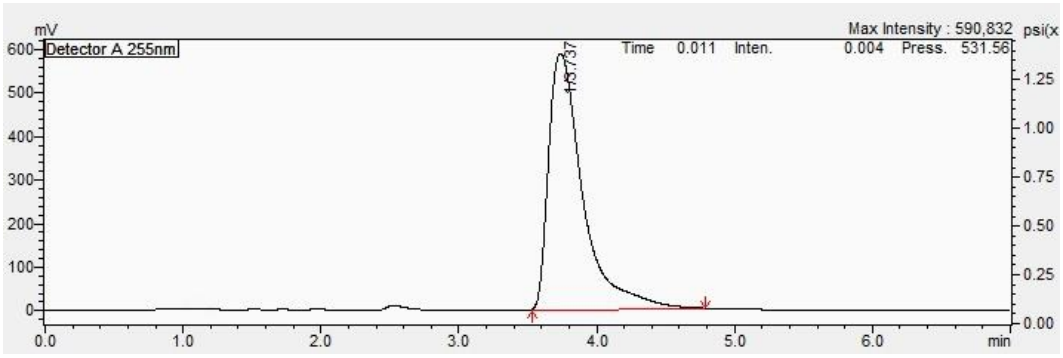

A. Pure Drug LO9 **57**

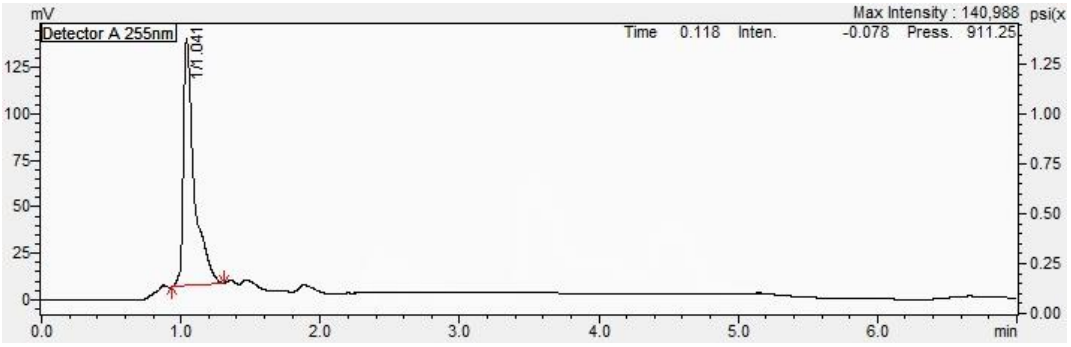

B. Carrier **46b**

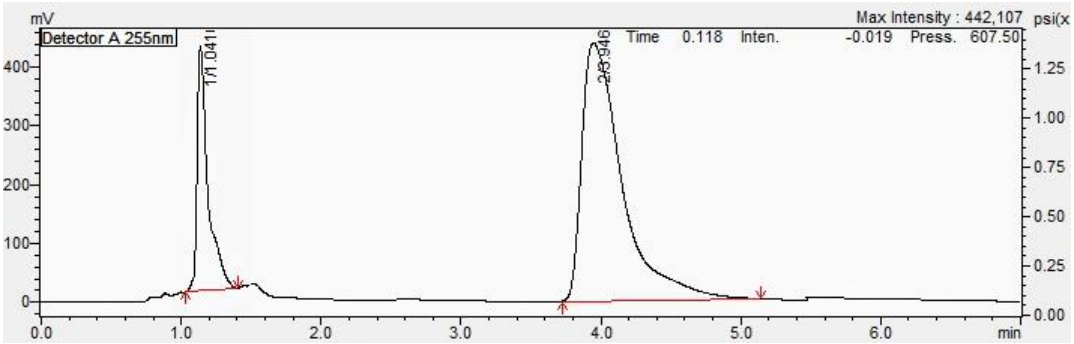

C. Inclusion complex

Figure 137: The HPLC chromatogram of (A) standard pure drug LO9 **57** (B) carrier **46b** and (C) carrier: drug formulation.

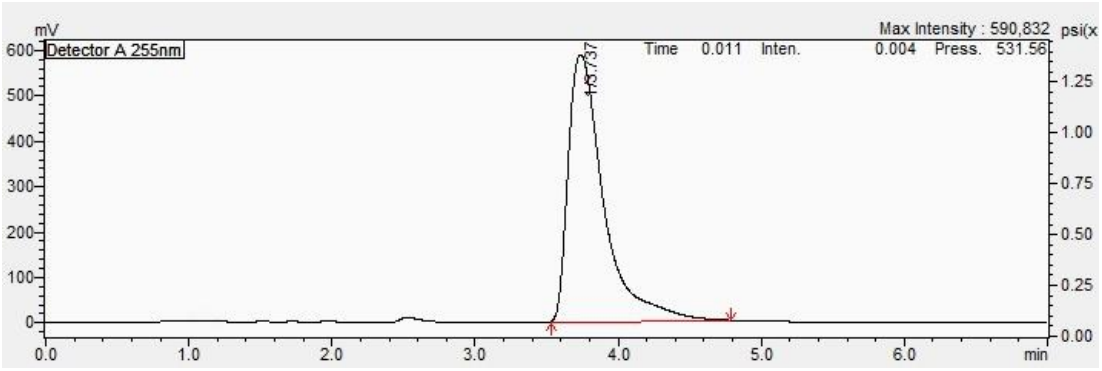

A. Pure Drug LO9 **57**

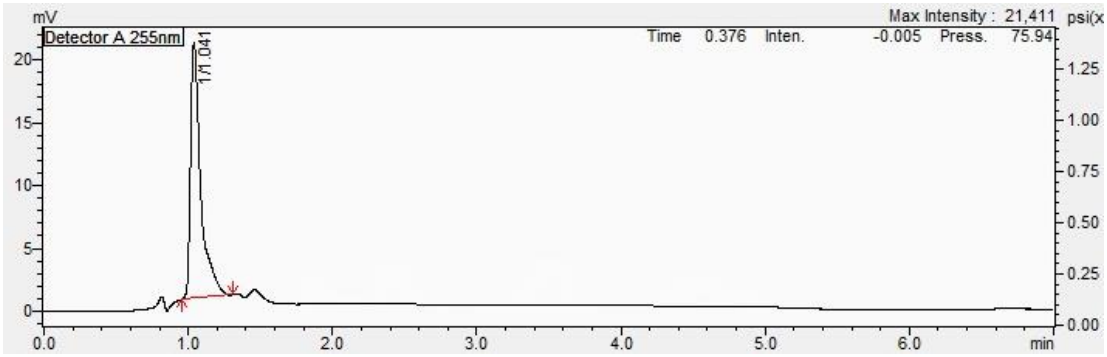

B. Carrier **46c**

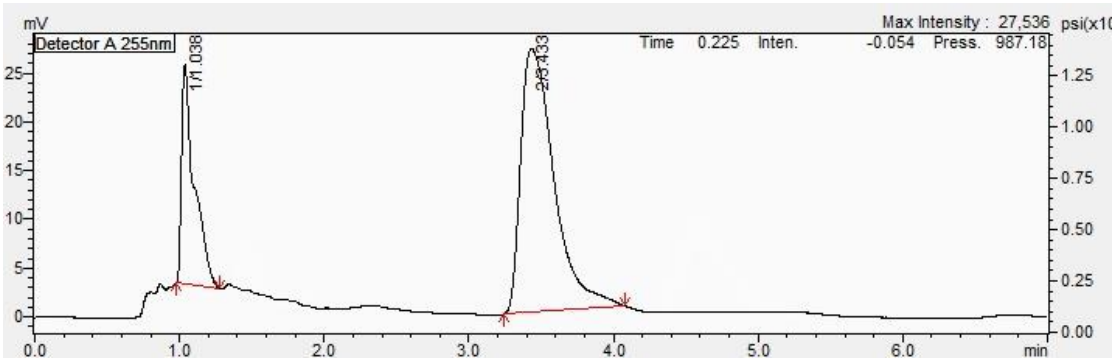

C. Inclusion complex

Figure 138: The HPLC chromatogram of (A) standard pure drug LO9 **57** (B) carrier **46c** and (C) carrier: drug formulation.

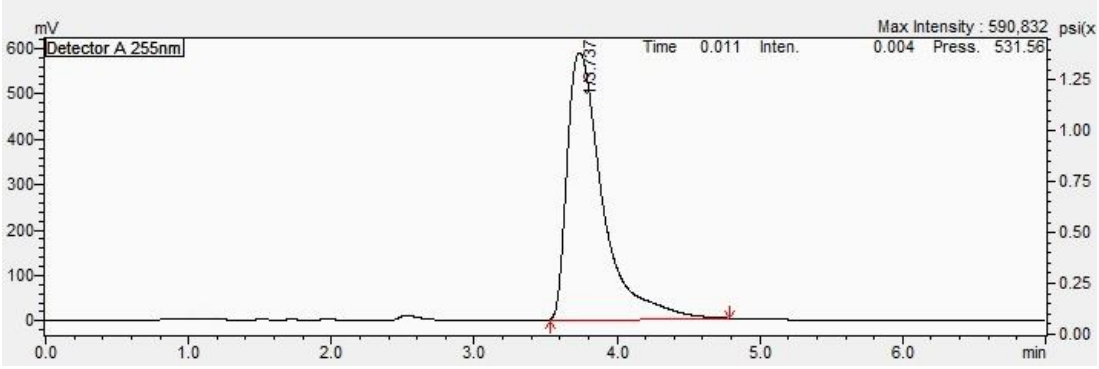

A. Pure Drug LO9 **57**

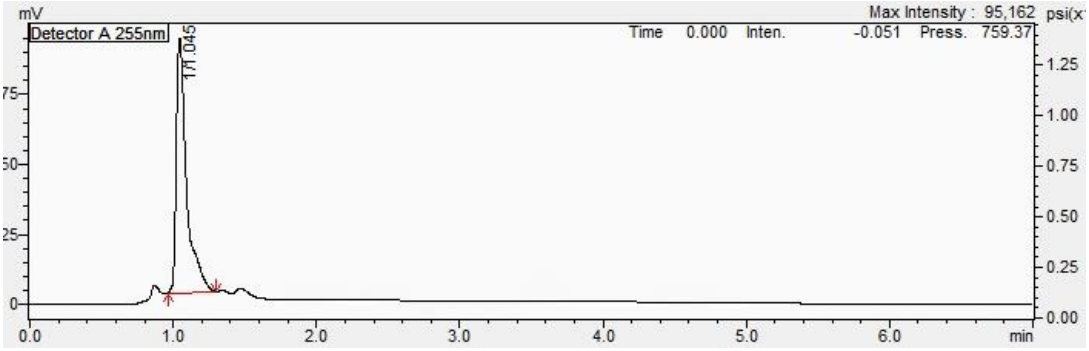

B. Carrier **46d**

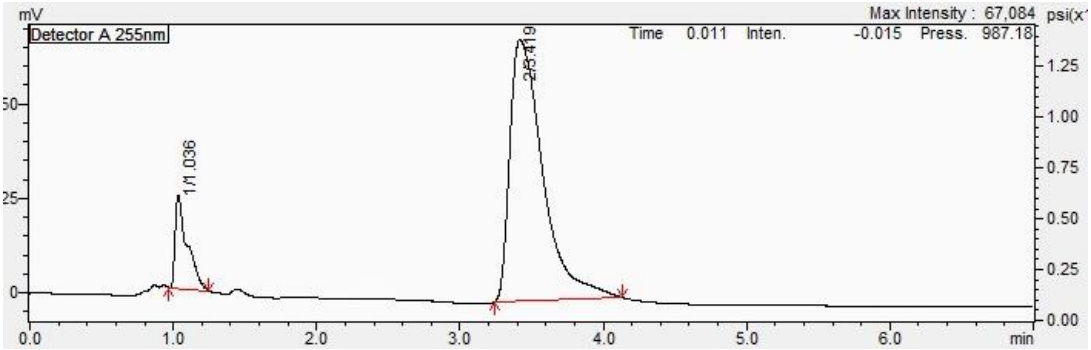

C. Inclusion complex

Figure 139: The HPLC chromatogram of (A) standard pure drug LO9 **57** (B) carrier **46d** and (C) carrier: drug formulation.

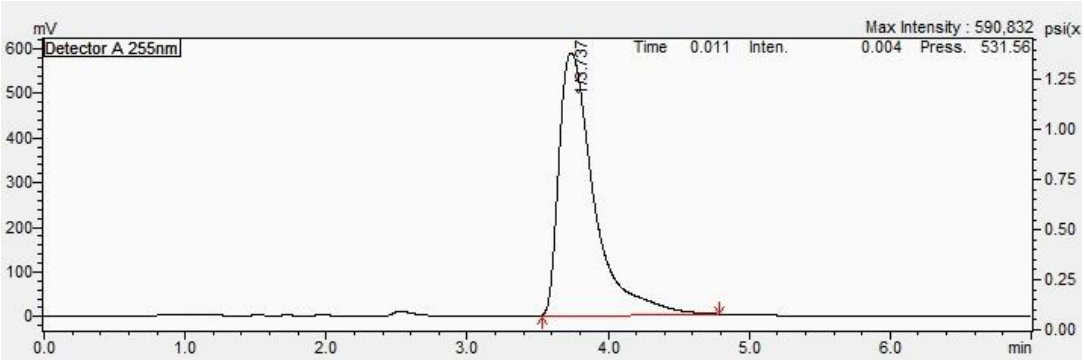

A. Pure Drug LO9 **57**

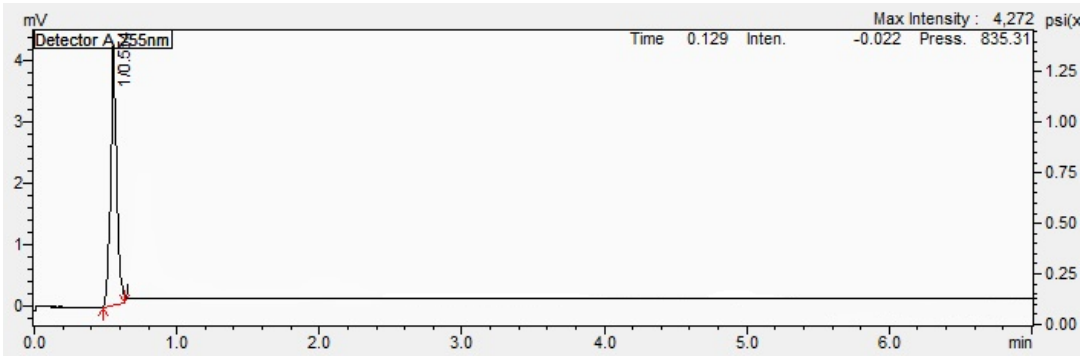

B. Carrier **46e**

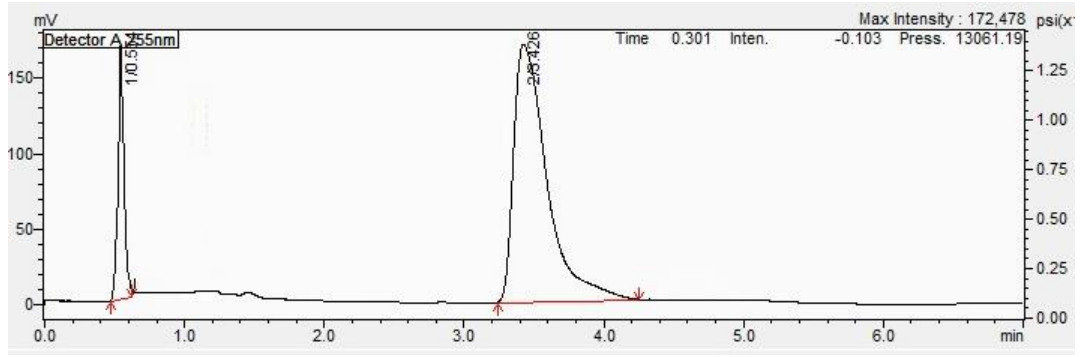

C. Inclusion complex

Figure 140: The HPLC chromatogram of (A) standard pure drug LO9 **57** (B) carrier **46e** and (C) carrier: drug formulation.

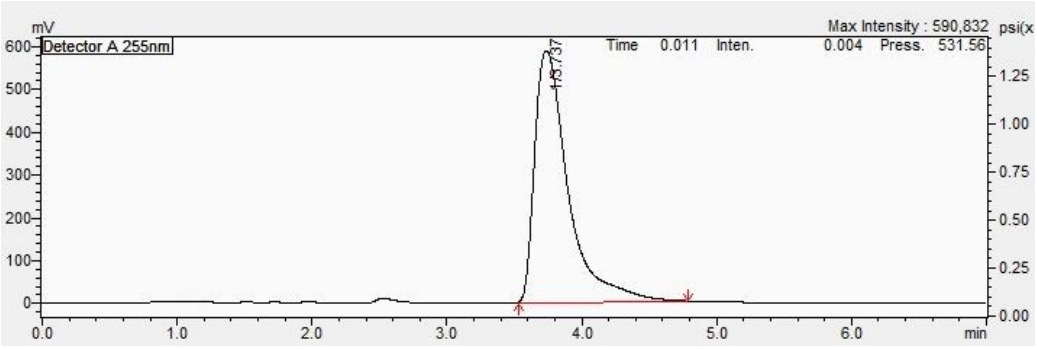

A. Pure Drug LO9 **57**

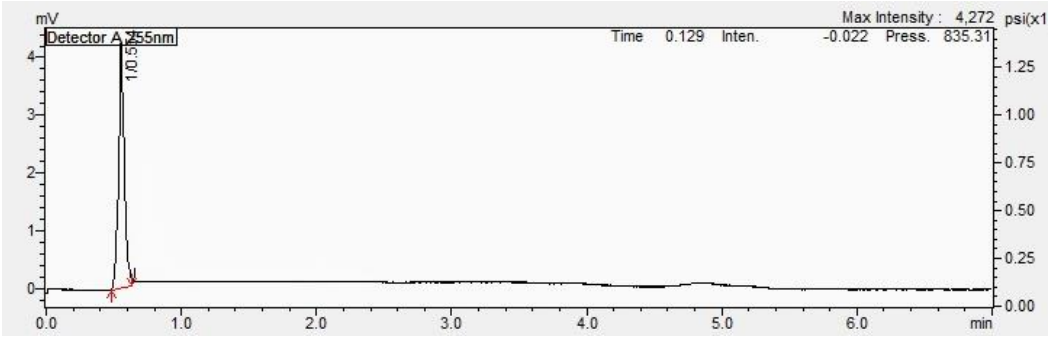

B. Carrier **46f**

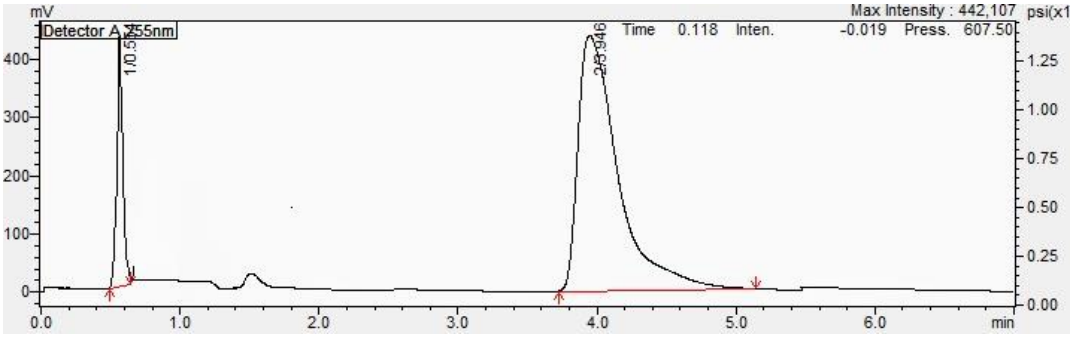

C. Inclusion complex

Figure 141: The HPLC chromatogram of (A) standard pure drug LO9 **57** (B) carrier **46f** and (C) carrier: drug formulation.

4.2.3 Spectroscopic Analysis of the Formulation

UV-Vis, FTIR and NMR spectroscopy was used to analyse each of the carrier: LO9 **57** formulations using methods as described in Chapter 3.

4.2.4 Particle Size and Zeta Potential Measurement using Photon Correlation Spectroscopy.

Optimal formulations of calix[4]resorcinarenes **46a-d** and calix[4]pyrogallolarenes **46e-f** with LO9 **57** (6 mg/mL, 10:1) in deionised water were prepared. The formation of aggregates was promoted using probe sonication. Hydrodynamic radii, size distribution (polydispersity index, PDI) and zeta-potential measurements were conducted using a photon correlation spectrometer (PCS) on a Zetasizer Nano-ZS, Malvern Instruments, UK. All measurements were performed in triplicate at 25 °C and an average value was determined.

4.2.5 *In Vitro* Drug Release Studies

An *in vitro* release study was conducted over a 2-week period under sink conditions in order to determine the extent and rate of LO9 **57** released from the formulations. According to the method of Lee and co-workers (Lee *et al.*, 2004), 2 mL of each formulation was deposited into a dialysis bag with molecular weight cut off of 12-14 kDa. The dialysis bag was immersed in 200 mL of deionised water which was kept at a constant temperature with stirring for 2 weeks. At predetermined time intervals (*e.g.*, 5 min, 10 min etc.), aliquots (1 mL) of the release medium was taken and replaced by fresh deionised water. To determine the impact of temperature on drug release, the studies were also performed at 37 ºC. The LO9 **57** content in the medium was measured by HPLC as described above. The cumulative release was reported as the percentage of the actual amount of drug present in the drug-loaded samples.

4.3 Results

4.3.1 Characterization of LO9 57

LO9 **57** was characterised using ^{1}H and ^{13}C NMR spectroscopy, and FTIR spectroscopy. The data corresponded to that acquired in previous studies within the laboratory at Keele University (Omotaje, 2013).

4.3.1.1 Fourier Transform Infrared Spectroscopy (FTIR) of LO9 57

The FTIR spectrum of LO9 **57** is shown in Figure 142.

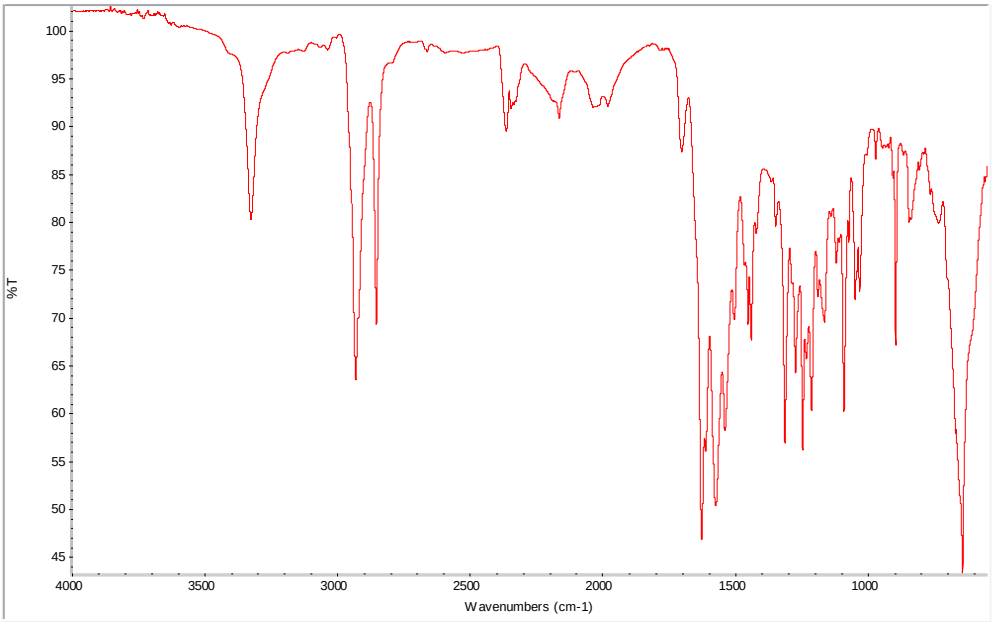

Figure 142: FTIR spectrum of LO9 **57**

4.3.1.2 Nuclear Magnetic Resonance (NMR) of LO9 57

The ^{1}H NMR and ^{13}C NMR spectrum of LO9 **57** is shown in Figure 143 and 144.

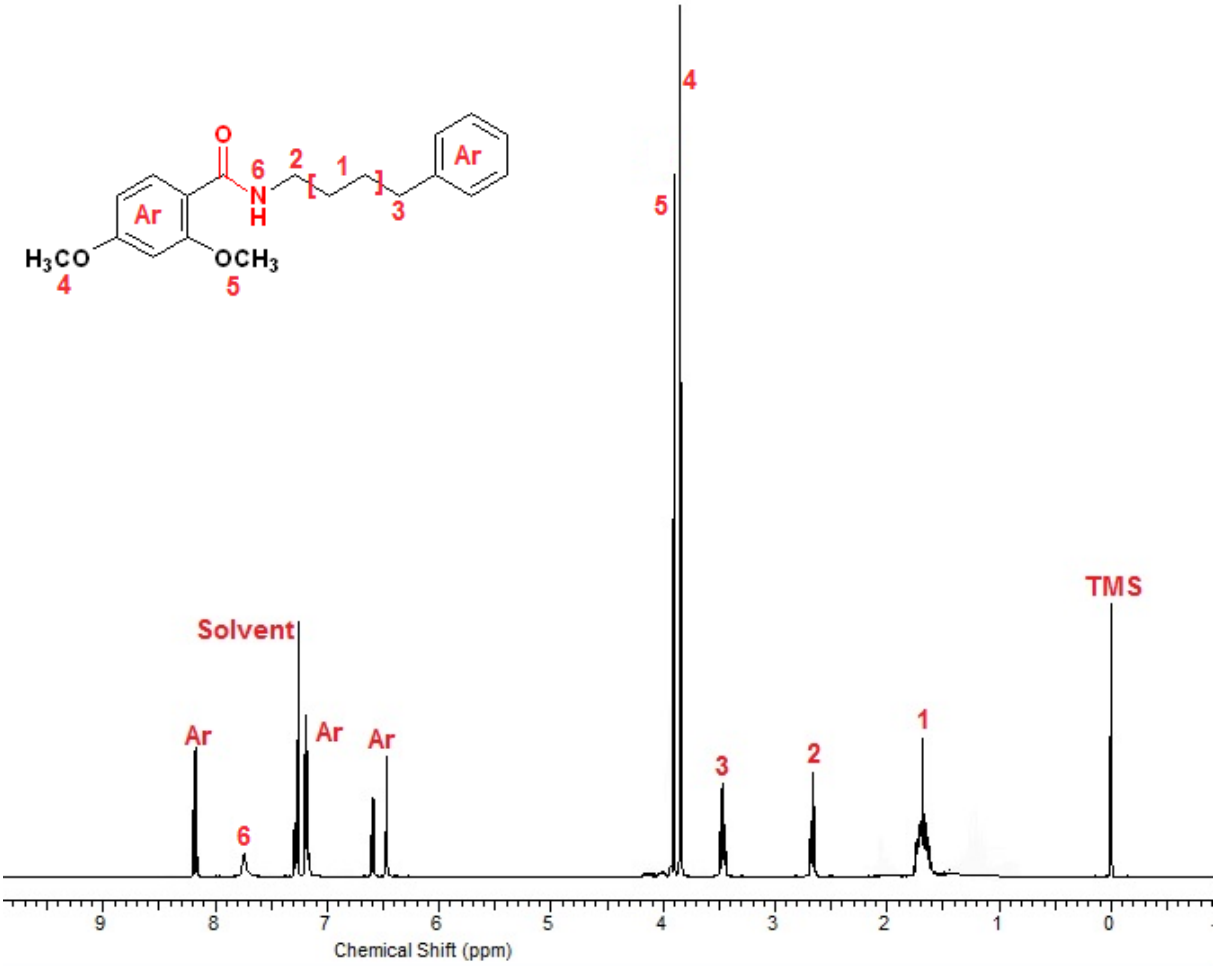

Figure 143: ^{1}H NMR spectrum of LO9 **57** in $CDCl_3$ solution at 25 °C.

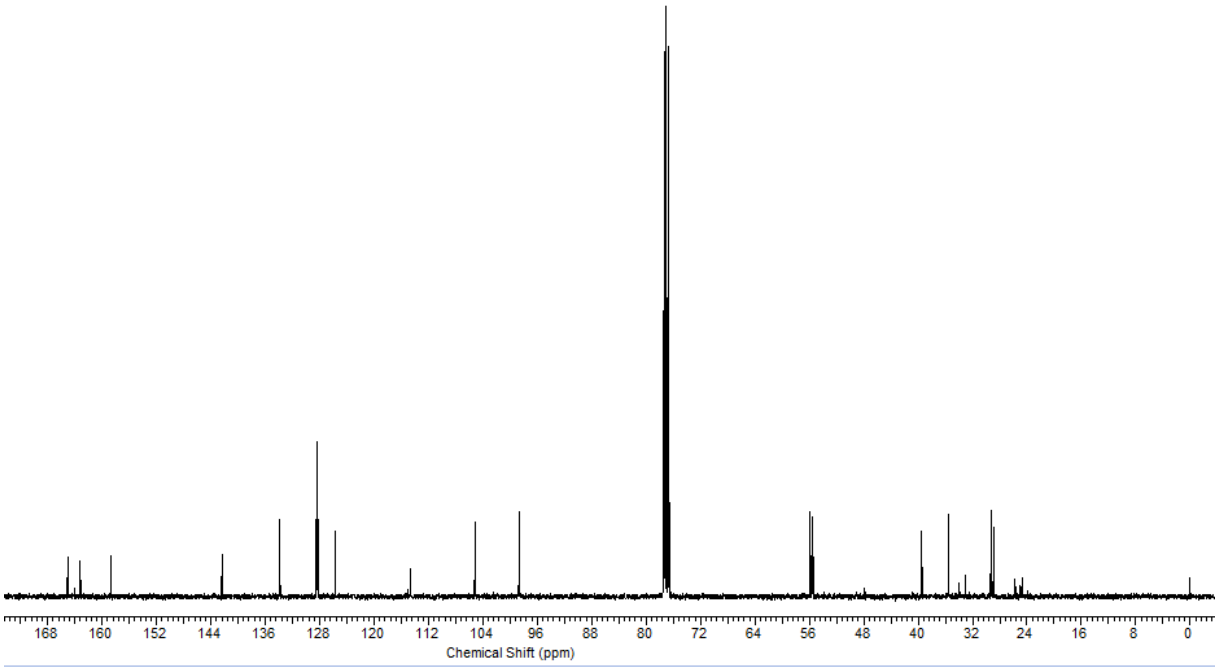

Figure 144: ^{13}C NMR spectrum of LO9 **57** in $CDCl_3$ solution at 25 °C.

4.3.2 Determination of Drug Loading Capacity for LO9 57

Hydrophobic drug candidate LO9 **57** was loaded into all carrier molecules **46a-f** in aqueous solution (1 mg/mL, 3 mg/mL and 6 mg/mL) using initial drug: carrier mass ratios of 1:1, 5:1 and 10:1. The maximum loading capacity for each carrier was determined by using HPLC. The retention time for LO9 **57** was 3.74 min. The concentration of LO9 **57** solubilised by each of the amphiphilic carriers compared with the intrinsic drug solubility is shown (Figure 145). It can be seen that, as the concentration of the excipient (calix[4]resorcinarene and calix[4]pyrogallolarenes) increased from 1 mg to 6 mg, the values of drug loading increased and the highest drug loading was achieved at for the formulation derived from an initial drug: carrier mass ratio of 10:1. In general, drug incorporation is affected by the drug feed ratio, thus increased feed ratios result in increased drug content. The amount of LO9 **57** solubilised with carrier **46a**, (6 mg/mL) increased from 2 mg/mL to 4 mg/mL when the

initial drug: carrier was changed from 1:1 to 5:1, respectively. The maximum loading concentration of 54 mg/mL was achieved in a solution derived from an initial drug: carrier mass ration of 10:1(Figure 145A). The more hydrophobic carrier **46b** showed an interesting change in drug loading profile. The aggregates encapsulated the highest LO9 **57** concentration at an initial drug: carrier ratio of 10:1. This was observed for all carrier concentrations (1 mg/mL, 3 mg/mL and 6 mg/mL). In a solution derived from an initial carrier concentration of 6mg/mL, the optimal LO9 **57** loading was achieved with 555.6 mg/mL at 10:1 drug: carrier ratio (Figure 145B).

At lower carrier concentrations (1 mg/mL and 3 mg/mL) both carriers **46c** and **46d** appeared to load the maximum concentration of LO9 **57** at in solutions derived from an initial drug: carrier feed ratio of 10:1. At 3 mg/mL, these carriers improved the aqueous solubility up to 7 mg/mL and 14.5 mg/mL, respectively. At higher carrier concentration (6mg/mL, at initial drug: carrier loading ratio of 10:1) the optimal LO9 **57** loading was achieved of 50.2 mg/mL and 73.9 mg/mL, respectively (Figure 145C and D).

The optimal LO9 **57** formulations with calix[4]pyrogallolarenes **46e**-**f** (Figure 145F) were at an initial carrier concentration of 6 mg/mL and drug: carrier ratio of 10:1. Loading of the carrier **46e** (Figure 145E) was notably poor compared with carrier **46f**, with 1.5 and 238 mg/mL of drug being solubilised respectively. It was clearly observed that there was no significant change in LO9 **57** solubilisation efficiency when the weight ratio of LO9 **57** to amphiphilic carriers was 1:1, suggesting that to acquire the best LO9 **57** solubilisation, the ratio of amphiphilic carriers: LO9 **57** was fixed at 10:1(w: w), and the weight ratio of LO9 **57** and the carrier should be 6 mg.

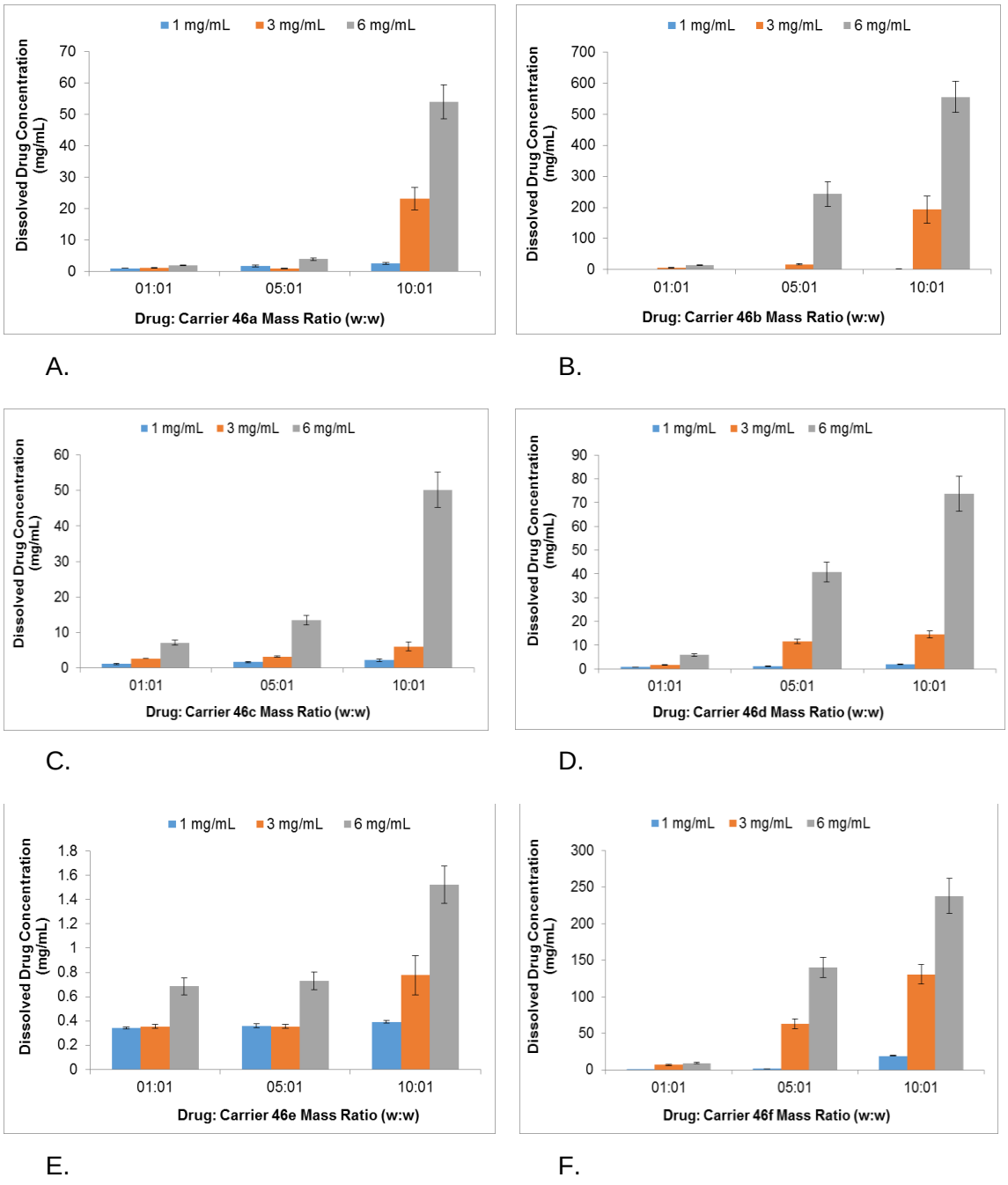

Figure 145: LO9 **57** loading concentration at three different initial drug: carrier feed ratios (1:1, 5:1 and 10:1) for calix[4]resorcinarenes **46a-d** and calix[4]pyrogallolarenes **46e-f**.

4.3.2.1 UV-Vis Analysis of LO9 57 Formulations

The UV-Vis data for LO9 **57**, carrier **46a**, and the corresponding inclusion complex are shown in Figure 146A. The results show an absorbance at 290 nm for LO9 **57**, at 280 nm corresponding to the λ_{max} for carrier **46a** and at 282 nm corresponding to the

λ_{max} for the inclusion complex. The wavelength of maximum absorption (λ_{max}) of LO9 **57** at ~250 nm was not visible in the spectrum of the inclusion complex. This indicates the successful formation of an inclusion complex between LO9 **57** and carrier **46a**. A similar result was obtained with carrier **46b** (Figure146B).

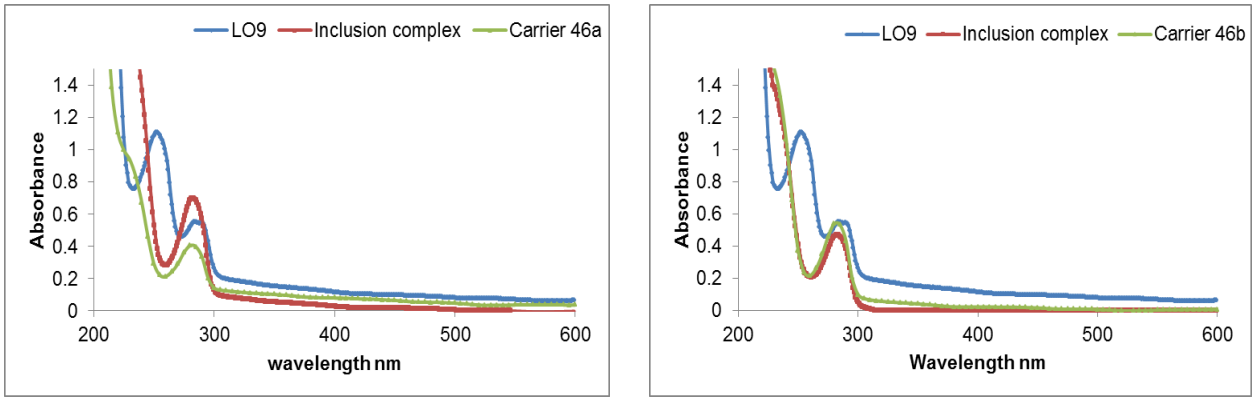

A. B.

Figure 146: UV-Vis spectra of LO9 **57**, carrier and the corresponding inclusion complex.

The UV-Vis data for inclusion complexes formed by carriers **46c** and **46d** are shown in Figure 147. As above, there is a significant change in the data observed when LO9 **57** is loaded in to the individual carrier solutions, indicating some distinct interaction with the carriers that results in the 'masking' of LO9 **57**.

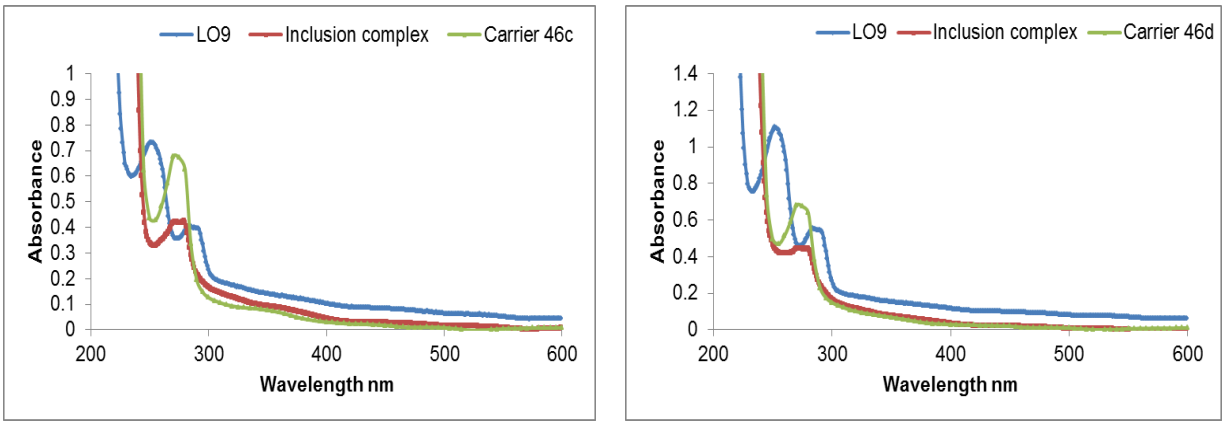

A. B.

Figure 147: UV-Vis spectra of LO9 **57**, carrier and the corresponding inclusion complex.

The UV-Vis data of LO9 **57**, carrier **46e-f**, and the corresponding inclusion complexes are shown in Figure 148. The results are similar to those for all the other carriers **46a-d** screened; there is no absorbance in the spectra of the inclusion complexes that can be attributed directly to LO9 **57**. This may be due to the degree of drug loading within the carriers screened based upon the initial carrier concentrations and initial drug: carrier ratios.

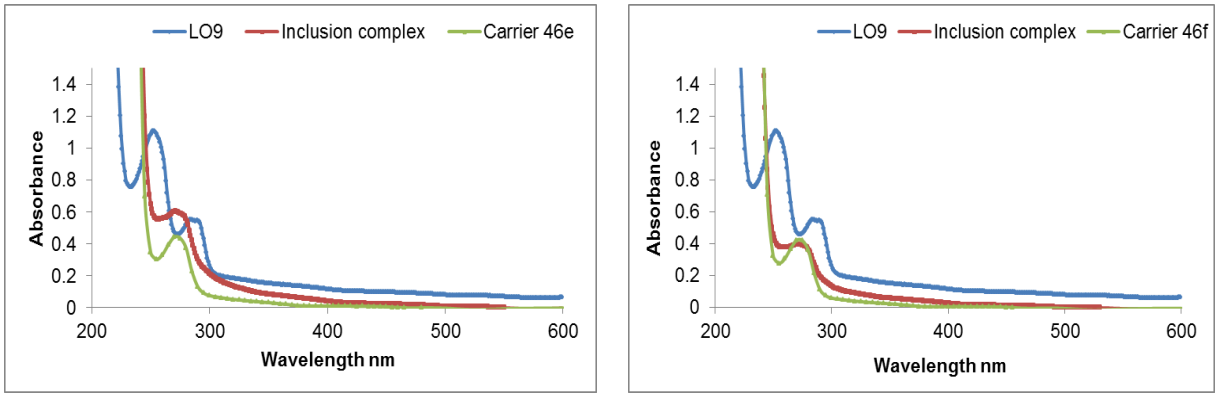

A. B.

Figure 148: UV-Vis spectra of LO9 **57**, carrier and the corresponding inclusion complex.

4.3.2.2 FTIR Analysis of Freeze-dried Formulations

The FTIR data for LO9 **57**, carriers **46a-b**, and the corresponding inclusion complexes are shown in Figure 149 and 150. The FTIR spectra of the inclusion complexes contained signals that were found to overlap with the characteristic peaks for LO9 **57**, perhaps due to the association of the drug with the carriers. Notably, the FTIR spectra of the inclusion complexes did not show any new peaks, demonstrating that no new chemical bonds were formed in the formulation process.

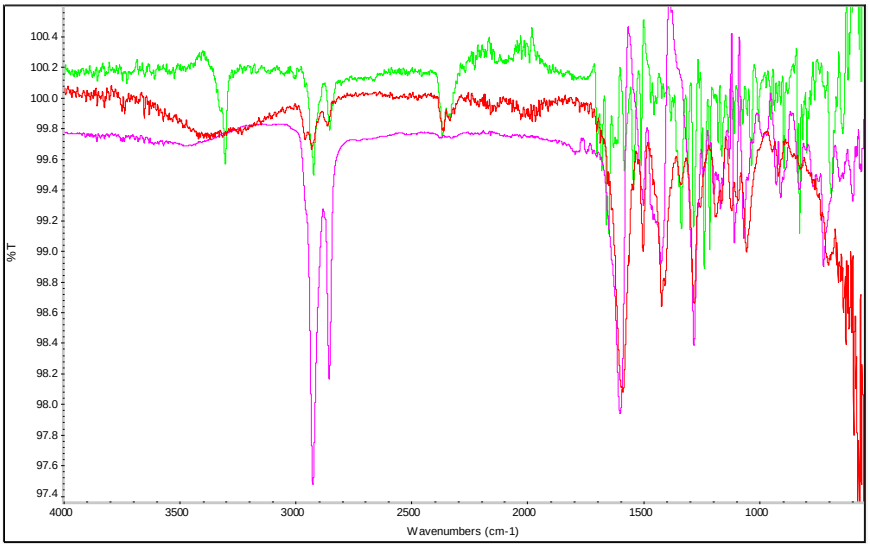

Figure 149: FTIR spectral analysis of (green) LO9 **57** (red) inclusion complex (pink) carrier **46a**.

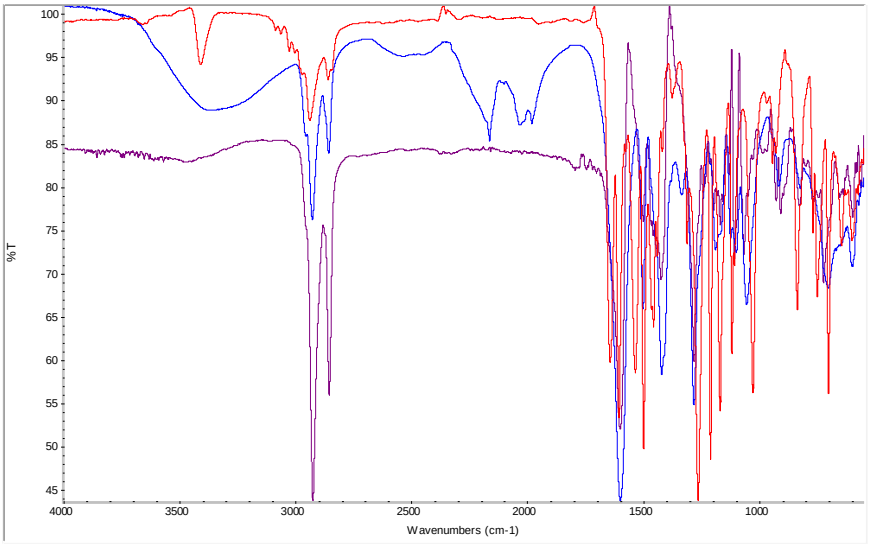

Figure 150: FTIR spectral analysis of (red) LO9 **57** (blue) inclusion complex (purple) carrier **46b**.

4.3.2.3 Nuclear Magnetic Resonance (NMR) Analysis of Formulations

LO9 **57** has a cLog P value of 3.77 and is not soluble to any extent in aqueous media, but NMR spectroscopy confirms it is solubilised when associated with the host **46b** in water. Figure 151 shows the ^{1}H NMR spectrum obtained from a 1:1 mixture of the calix[4]resorcinarene **46b** and LO9 **57** in D_2O solution, corresponding

to an initial carrier concentration of 3 mg/mL. As can be seen, there is clear evidence for the presence of LO9 **57** in solution. There are also some clear changes in chemical shift for protons attached to the calix[4]resorcinarene carrier, most notably in the aromatic region for the protons assigned to the 5-position in the calix of carrier **46b**. As for the model drugs examined in Chapter 3, a change in chemical shift of these protons is likely to indicate that there is close interaction between the hydrophobic residue of LO9 **57** and the lower rim substituents of host **46b**.

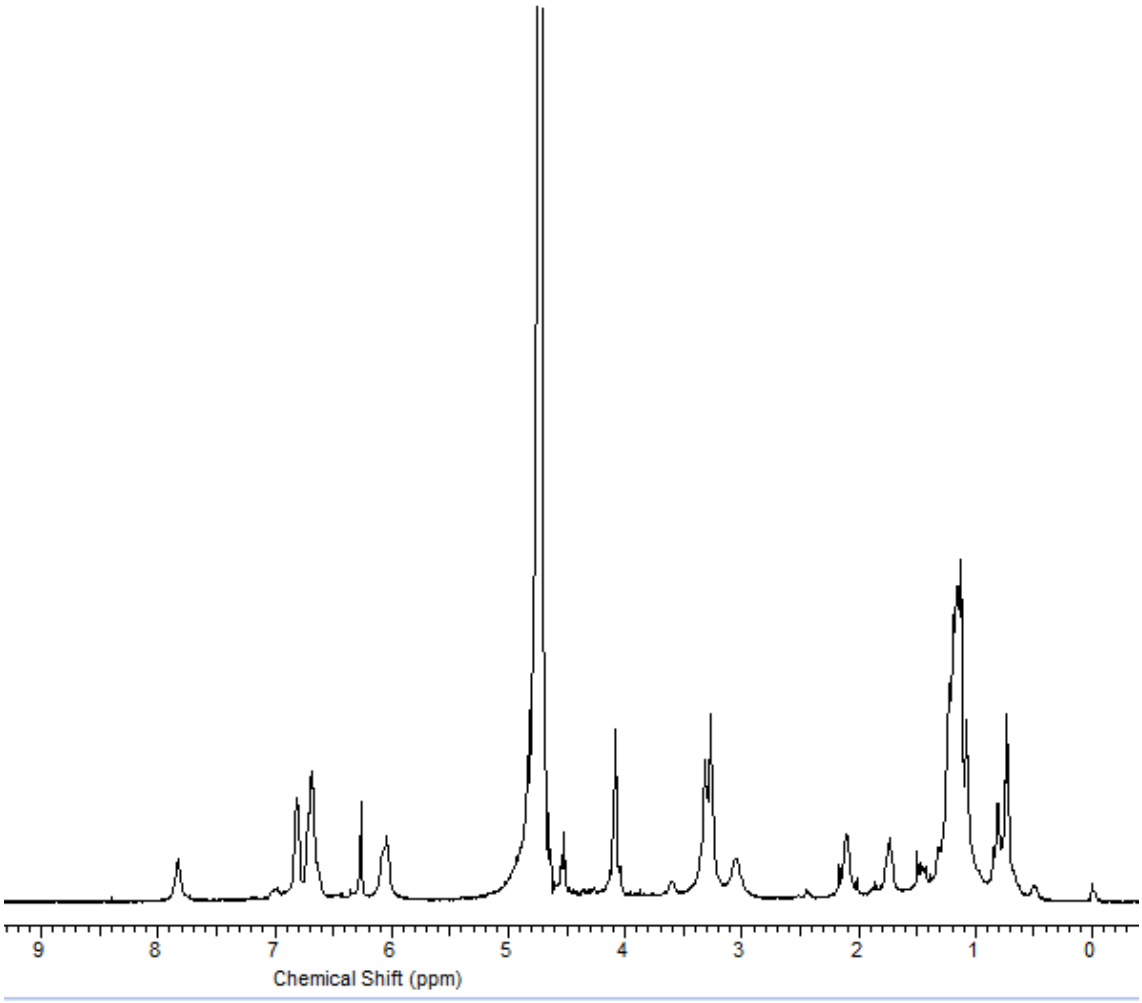

Figure 151: Expansion of the ^{1}H NMR of the host-guest formulation of carrier **46b:** LO9 **57** (1:1) in D_2O carried out at 300 MHz at 25 °C.

A solution containing LO9 **57** and carrier **46a** corresponding to an initial carrier concentration of 6 mg/mL and drug: carrier ratio of 1:1 was made up in D_2O. The NOESY NMR spectrum of the solution is shown in Figure 152.

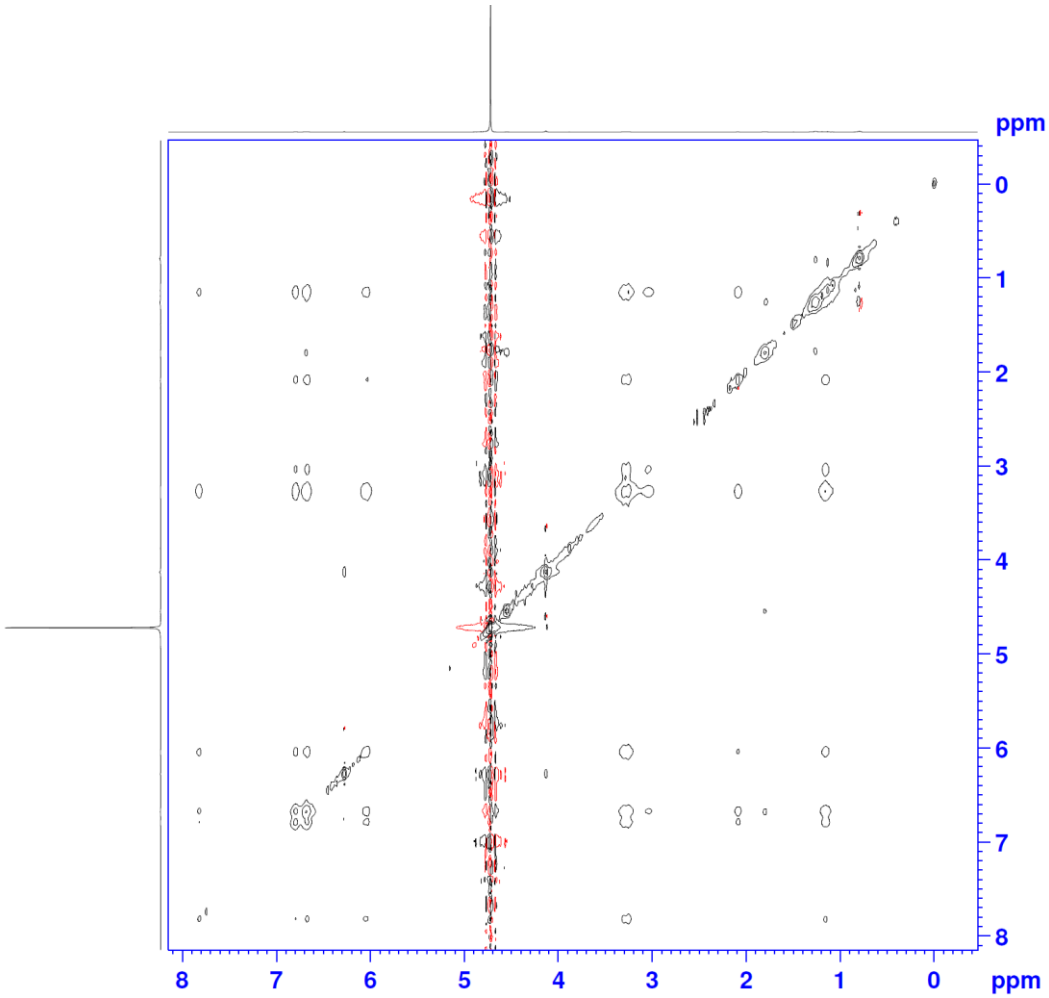

Figure 152: ^1H NOESY NMR spectrum of a solution of LO9 **57** and carrier **46a** corresponding to an initial carrier concentration of 6 mg/mL and drug: carrier ratio of 1:1 in D_2O.

The NOESY NMR spectrum of the LO9 **57** formulation with carrier **46a** showed the expected enhancements due to interactions of protons in the 2-position on the calix[4]resorcinarene calix and methylene groups on the carboxylate substituents. There were significant enhancements in the signals assigned to the alkyl chains on the lower rim of the carrier, associated with resonances in the aromatic region

tentatively assigned to the unsubstituted aryl group of LO9 **57**. This indicates that there is a very close association between this non-polar residue and the C_4 alkyl substituents on the carrier **46a**.

A solution containing LO9 **57** and carrier **46b** corresponding to an initial carrier concentration of 6 mg/mL and drug: carrier ratio of 1:1 in D_2O was also examined using a NOESY NMR experiment. The NOESY NMR spectrum of the solution is shown in Figure 153.

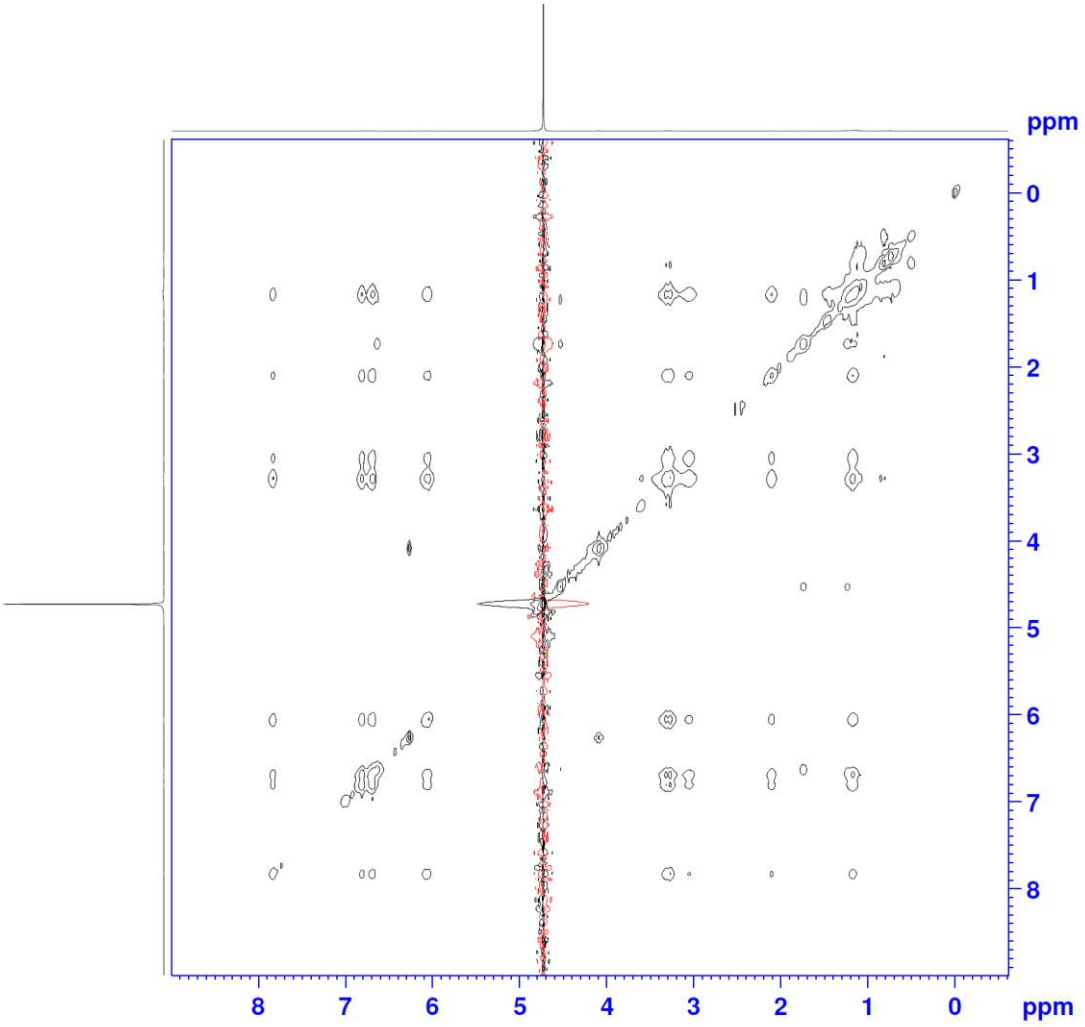

Figure 153: ^{1}H NOESY NMR spectrum of a solution of LO9 **57** and carrier **46b** corresponding to an initial carrier concentration of 6 mg/mL and drug: carrier ratio of 1:1 in D_2O.

As before, the NOESY NMR spectrum of the LO9 **57** formulation with carrier **46b** also showed the expected enhancements due to intramolecular interactions within the carrier. Significant enhancements in the signals assigned to the alkyl chains on the lower rim of the carrier were also observed, again associated with resonances tentatively assigned to the unsubstituted aryl group of LO9 **57**. This provided further evidence of a very close association between this non-polar reside and the C_7 alkyl substituents on the carrier **46b**.

4.3.2.4 Particle Size and Zeta Potential Measurement using Photon Correlation Spectroscopy

Particle size measurements were determined for filtered drug formulations (initial carrier concentration 6 mg/mL, drug: carrier ratio 10:1) using photon correlation spectroscopy (PCS) and the protocol described in Chapter 3. All measurements were performed in triplicate at 25 °C and the mean values were reported. The polydispersity index (PDI), which is an indication of the quality of the data with respect to the size distribution (Danaei *et al.*, 2018) was measured.

On loading carriers **46a** and **46b** with LO9 **57**, aggregates that were significantly larger than those observed for the carriers alone were formed (Table 27). Carrier **46a** gave aggregates with a hydrodynamic radius of 1851 nm whilst carrier **46b** gave aggregates with radius of 685 nm and much larger aggregates with a radius of 4768 nm. The low polydispersity index (PDI) indicates the presence of dimensional homogeneous systems for the optimal drug formulation of LO9 **57**-carrier **46a** (Ruozi *et al.*, 2005). However, the PDI of the formulation with carrier **46b** indicated that the self-assemblies formed are not all of uniform size and confirmed that several size populations were present in solution. Negative zeta potentials were obtained for the

formulations, confirming the presence of carboxyl groups on the surface of the aggregates formed (Table 27).

Table 27: Hydrodynamic radius and polydispersity index analysis for aqueous formulations of LO9 **57** and carriers **46a** and **46b**. Samples recorded in triplicate at 25 °C.

Aggregate	Concentration mg/mL Drug: Carrier Ratio	Size nm (± SD): Percentage occurrence	PDI	Zeta Potential
LO9 **57**-Carrier **46a**	6 (10:1)	1527 (33.6): 100 %	0.195 (0.042)	-31.4 (2.56)
LO9 **57**-Carrier **46b**	6 (10:1)	684.9 (15.2): 80 % 4763.7 (49.4): 20%	0.615 (0.077)	-30.8 (1.45)

Figure 154A shows the size distribution report for the LO9 **57**: carrier **46a** formulation. Only one broad group of aggregates was observed with a hydrodynamic radius just in the micron range. However, the size correlation chart for the LO9 **57**: carrier **46b** formulation (Figure 154B) shows that two size populations are present in solution, perhaps indicating two modes of aggregation. The group of aggregates with hydrodynamic radius of 4763 nm are within the size range for the formation of micellar-type supramolecular structures.

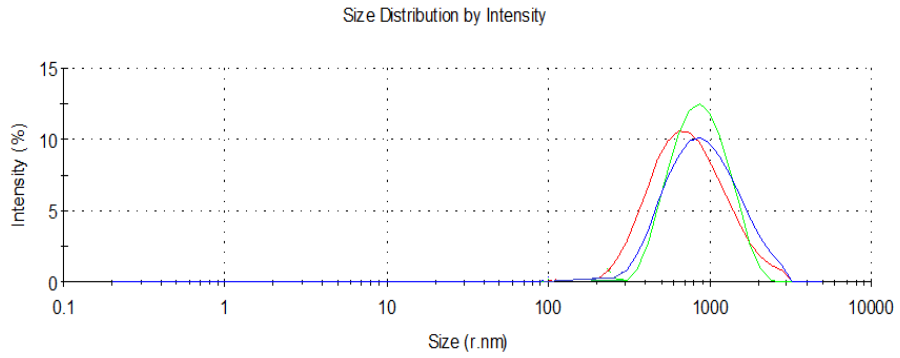

A.

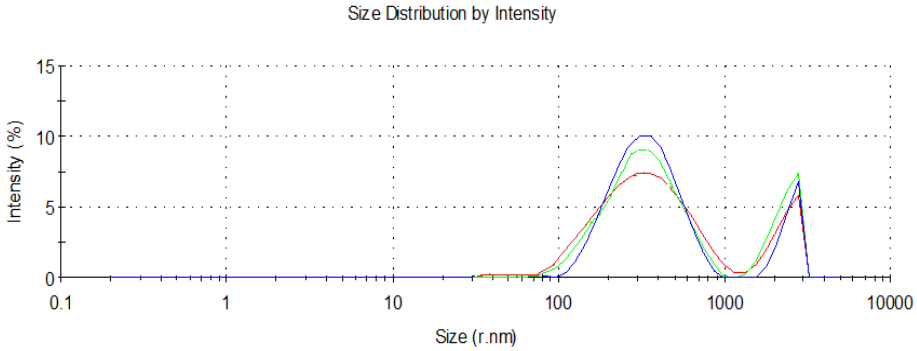

B.

Figure 154: Photon correlation spectroscopy size correlation chart for LO9 **57**: carrier **46a** and **46b** formulations in deionised water (n=3, ave).

In the case of carriers **46c** and **46d** the hydrodynamic radius of the aggregates formed seemed to follow the drug loading capability of the carriers. The formulation with carrier **46d** contained the largest amount of LO9 **57** solubilised (70 mg/mL) and had the largest radius (2674 nm), whereas the formulation with carrier **46c** solubilised 50 mg/mL of LO9 **57** and gave aggregates with a radius of 279 nm. Zeta potential values with a negative value greater than -30 mV were observed (Table 28).

Table 28: Hydrodynamic radius and polydispersity index analysis for aqueous formulations of LO9 **57** and carriers **46c** and **46d**. Samples recorded in triplicate at 25 °C.

Aggregate	Concentration mg/mL Drug: Carrier Ratio	Size nm (± SD): Percentage occurrence	PDI	Zeta Potential
LO9 **57**-carrier **46c**	6 (10:1)	278.5 (3.4): 92 % 4516.7 (19.6): 8 %	0.300 (0.036)	- 40.6 (2.2)
LO9 **57**-carrier **46d**	6 (10:1)	2673.7 (20.6): 83 % 451.2 (7.1): 17 %	0.483 (0.024)	- 33.4 (1.6)

The size correlation chart for the LO9 **57**: carrier formulations containing carriers **46c** and **46d** are shown in Figure 155. Two size populations are clearly formed by both carriers in solution.

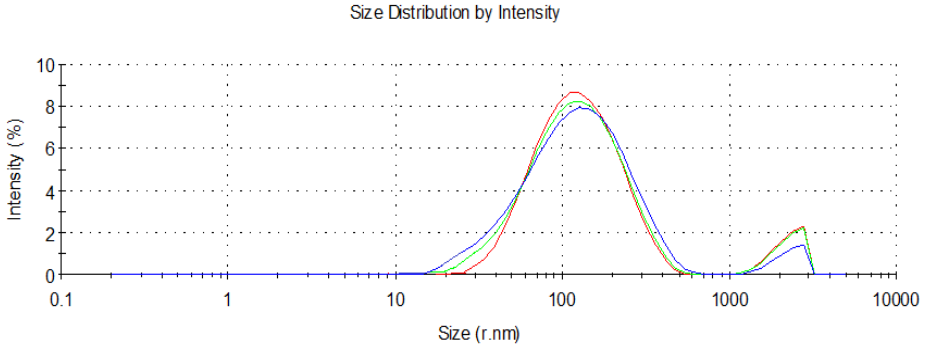

A.

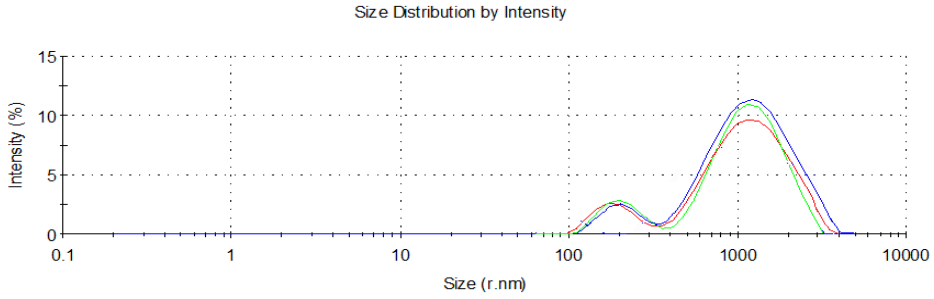

B.

Figure 155: Photon correlation spectroscopy size correlation chart for LO9 **57**: carrier **46c** and **46d** formulations in deionised water

Carrier **46e** was only capable of solubilising 1.5 mg/mL of LO9 **57** and gave aggregates with a hydrodynamic radius of only 210 nm (Table 29). However, carrier **46f** solubilised 238 mg/mL of LO9 **57** and gave aggregates of the formulation with significantly higher radius. Again, the larger aggregates observed were in the range expected for micellar-type structure.

Table 29: Hydrodynamic radius and polydispersity index analysis for aqueous formulations of LO9 **57** and carriers **46e** and **46f**. Samples recorded in triplicate at 25 °C.

Aggregate	Concentration mg/mL Drug: Carrier Ratio	Size nm (± SD): Percentage occurrence	PDI	Zeta Potential
LO9 **57**-carrier **46e**	6 (10:1)	210.1 (11.4): 83 % 92.1 (8.6): 17 %	0.300 (0.036)	- 45.6 (2.4)
LO9 **57**-carrier **46f**	6 (10:1)	1137.3 (25.1): 80 % 5134 (37.8): 18 %	0.453 (0.049)	- 36.7 (1.6)

The data observed for the formulation derived from carrier **46f** was similar to that observed for carrier **46b** (Figure 156).

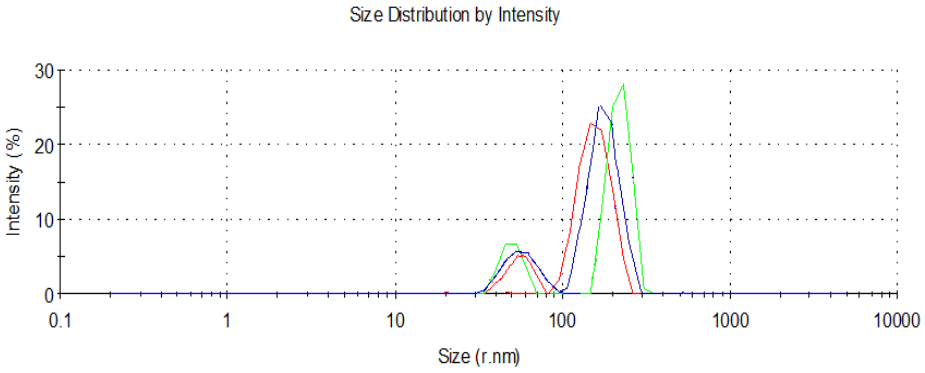

A.

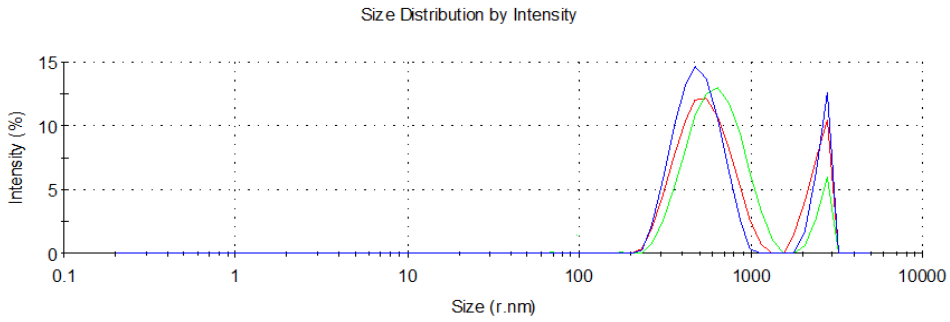

B.

Figure 156: Photon correlation spectroscopy size correlation chart for LO9 **57**: carrier **46e** and **46f** formulations in deionised water.

4.3.3 *In Vitro* Drug Release from Nanoaggregates

The cumulative release rate of LO9 **57** from the various formulations containing calix[4]resorcinarenes **46a-d** and calix[4]pyrogallolarenes **46e-f** was studied for up to 2 weeks at 37 ^{0}C and at 20 ºC in deionized water under sink conditions. Figure 157 shows the drug release from all formulations investigated. The initial release was consistent for all formulations over 7 h. However, drug release from carrier **46e** was fast and finished within 25 min. Drug release was faster from the carriers possessing C_4 alkyl chains in the lower rim than those with C_7 alkyl chains. This release behaviour may be explained by the drug being located predominantly within the hydrophobic tail of the carriers.

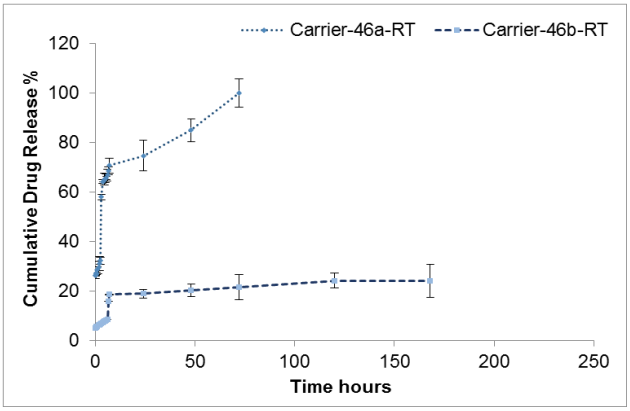

Calix[4]resorcinarene **46a-b**

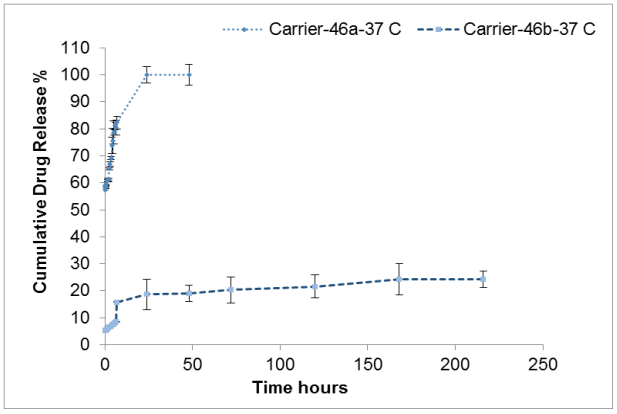

Calix[4]resorcinarene **46a-b**

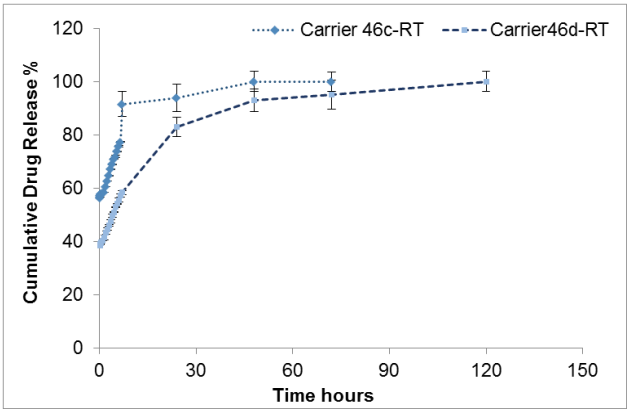

Calix[4]resorcinarene **46c-d**

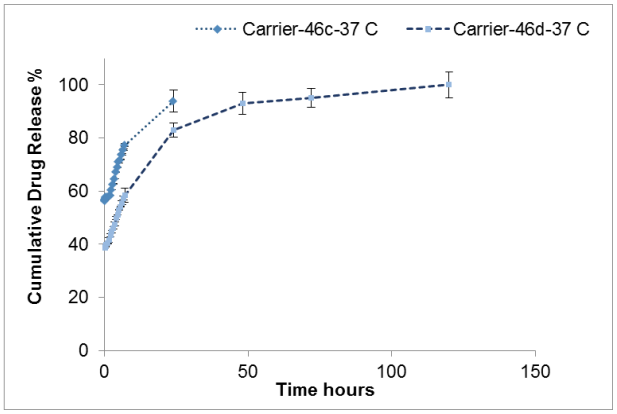

Calix[4]resorcinarene **46c-d**

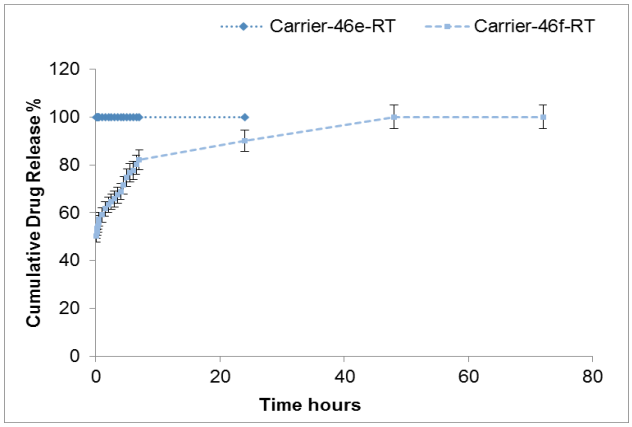

Calix[4]pyrogallolarene **46e-f**

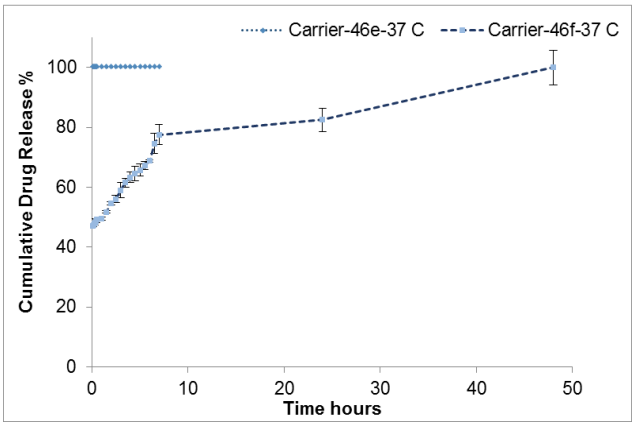

Calix[4]pyrogallolarene **46e-f**

A. LO9 **57** percentage released from the amphiphilic carriers at 20 ºC

B. LO9 **57** percentage released from the amphiphilic carriers at 37 ºC

Figure 157: *In vitro* drug release from all formulations at two different temperatures (n=3, ± SD), (Error bars have been omitted for clarity).

On closer analysis, each carrier **46a-f** had a slightly different release profile, though the data for release at 20 ºC and at 37 ^{0}C was broadly similar. Carrier **46a** discharged the drug payload more rapidly than carrier **46b**.The total amount of drug released from the formulations after 1 h was approximately 29 % and 6 % for carriers **46a** and **46b**, respectively. After 24 h carrier **46a** had released 75 % of the drug compared with only 18 % for carrier **46b**. Release from the formulation with **46a** continued steadily until 72 h, after which all of the drug was completely released, compared with only 20 % for the formulation with carrier **46b**. Carrier **46b** showed a more sustained release profile over the 2 week period.

The total amount of the drug released from the formulations with carrier **46c** and **46d** after 1 h was approximately 62 % and 21 %, respectively. After 24 h the formulation with carrier **46c** had released 93 % of drug compared with 83 % of the formulation with carrier **46d**. After 48 h the drug had been completely released from carrier **46c**, with the release profile showing a consistent release over a 48 h period. The release observed for carrier **46d** continued steadily until the drug was completely released after 120 h.

All of the drug was released from the formulation containing calix[4]pyrogallolarene **46e** was released after 25 min. On the other hand, the amount of drug released from calix[4]pyrogallolarene **46f** was relatively small initially, reaching a cumulative release of 28 % in 7 h. Sustained drug release from the carrier **46f** was observed over 2 weeks.

4.4 Discussion

A number of amphiphilic calix[4]resorcinarenes **46a-d** and calix[4]pyrogallolarenes **46e-f** have been used to solubilise the drug candidate LO9 **57** (Figure 158). LO9 **57**

has a cLog P of 3.77 and is virtually insoluble in aqueous media. LO9 **57** differs from the model drugs described in Chapter 3, in that it has two distinctly different regions in the molecule: the phenylbutyl moiety is non-polar and obviously hydrophobic, whereas the benzamide residue is more polar and potentially less hydrophobic.

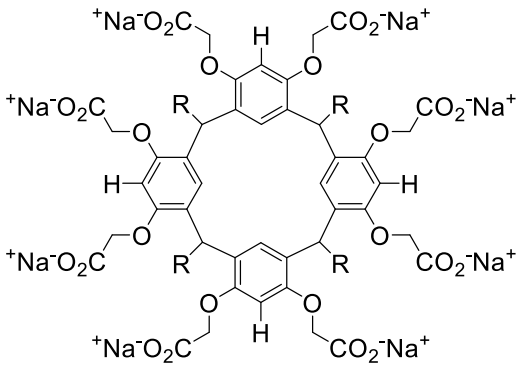

R= C_4H_9 **46a**
R= C_7H_{15} **46b**

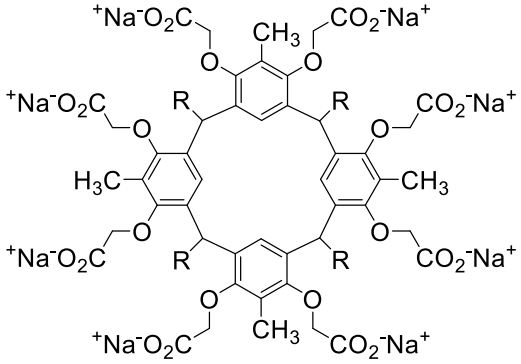

R= C_4H_9 **46c**
R= C_7H_{15} **46d**

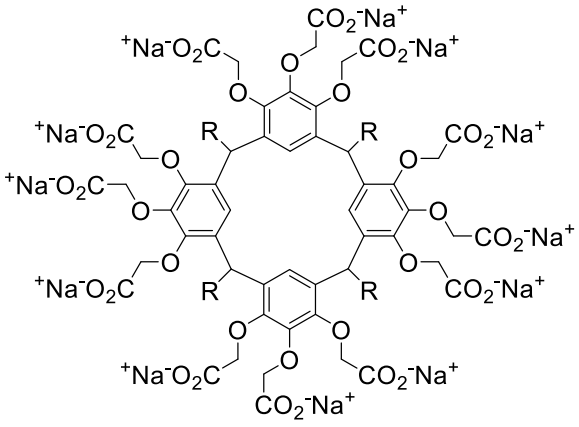

R= C_4H_9 **46e**
R= C_7H_{15} **46f**

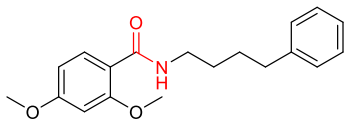

57

Figure 158: Molecular structure of LO9 57, calix[4]resorcinarenes **46a-d** and calix[4]pyrogallolarenes **46e-f**.

To find an optimal loading ratio of LO9 **57** to amphiphilic calix[4]resorcinarenes **46a-b** and calix[4]pyrogallolarenes **46e-f** which allowed for the best solubilisation, a series

of formulations was prepared with different initial weight ratios of LO9 **57** to amphiphilic carriers (1:1, 5:1, 10:1). It was observed that the loading capacity of the carrier solution was affected by the initial ratio of drug to carrier (w/w). Accordingly, the final optimized formulations of LO9 **57** had an initial carrier concentration of 6 mg/mL and a drug: carrier ratio of 10:1 (Figure 159).

The results demonstrate that the maximum loading capacity using these optimum formulation parameters with carrier **46a** which bears C_4 alkyl residues on the lower rim is approximately 54 mg/mL, compared to 556 mg/mL for the formulation with carrier **46b** which bears C_7 alkyl residues on the lower rim. Amphiphilic carrier **46c** bearing methyl groups attached at the 2-position of calix[4]resorcinarene calix and C_4 alkyl residues on the lower rim was able to solubilise 50 mg/mL of LO9 **57,** compared to carrier **46d** which possesses C_7 alkyl residues which solubilised 74 mg/mL. Carrier **46e**, which possesses twelve polar groups attached to the upper rim and C_4 alkyl lower rim substituents could solubilise only 2 mg/mL of LO9 **57**, compared to carrier **46f** which could solubilise 237 mg/mL. These observations are significant because they are reflected in the aggregate sizing experiments, indicating that larger aggregates are capable of greater drug solubilisation (Hoskins *et al.*, 2016; Syakaev *et al.*, 2018). As noted above, all carriers appeared to load the maximum concentration of LO9 **57** in formulations made with a 10:1 initial drug: carrier mass ratio.

For those carriers which were able to solubilise significantly large amounts of LO9 **57**, it can be anticipated that there would be numerous aggregates present in the formulation, resulting in a higher degree of solubilisation. However, much increased solubilisation may be achieved if the aggregates themselves were significantly larger also. With increased drug loading there is a larger driving force for hydrophobic

encapsulation within a lipophilic core of supramolecular assemblies due to much increased van der Waals interactions as more drug molecules are solubilised. Maximum solubilisation of LO9 **57** was observed with carriers **46b** and **46f** (Figure 159), each of which possesses C_7 alkyl chains on the lower rim. This indicates that association of LO9 **57** with aggregated amphiphilic carriers might occur in the hydrophobic region of the carrier substituents (Morozova *et al.*, 2018; Shalaeva *et al.* , 2018; Syakaev *et al.*, 2018).

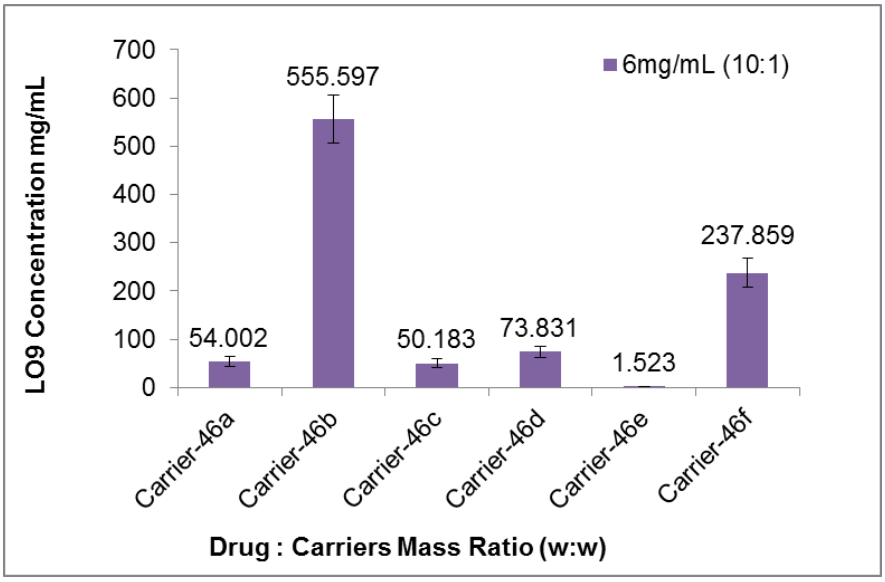

Figure 159: Maximum LO9 **57** concentration solubilised by calix[4]resorcinarenes **46a-d** and calix[4]pyrogallolarenes **46e-f.**

The size, size distribution and zeta potential of the optimal formulations were characterized by photon correlation spectrometry (PCS) (Figure 160). The aggregates formed in each formulation were not all of uniform size and two size populations were present in solution for the majority of formulations. All of the formulations were filtered before analysis to remove any free drug that had not been solubilised. The filters used would also be expected to remove any large aggregates formed in the initial formulation stages. Thus, especially for carriers **46b** and **46f**

which showed the highest drug loading, there must have been some equilibration following filtration to give thermodynamically stable large aggregates within the micron range. These correspond to the region associated with micellar-type structures. All formulations had zeta potentials in the range of -31 to -45 mV. In general, the zeta potential is greater for highly charged particles that are small in radius. I this work, the zeta potentials observed are indicative of larger particles that have a more diffuse surface change. This also provides evidence for larger supramolecular aggregates being formed.

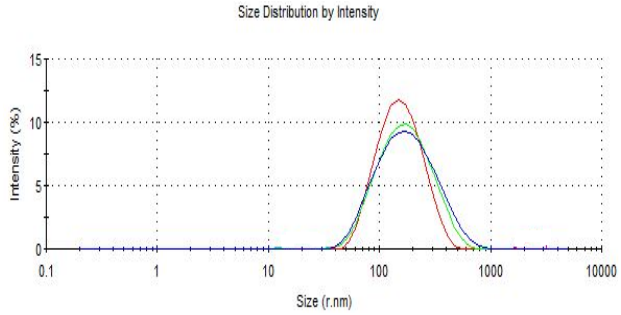

A. Carrier **46a** alone

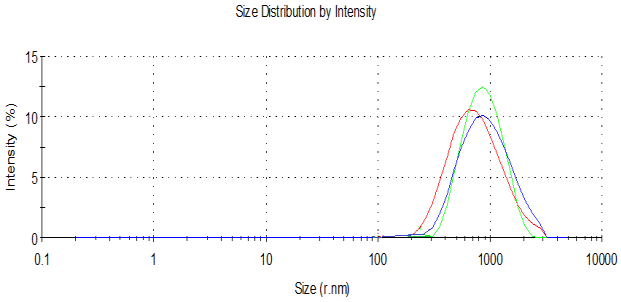

B. LO9 **57**: Carrier **46a** 6 mg/mL (10:1)

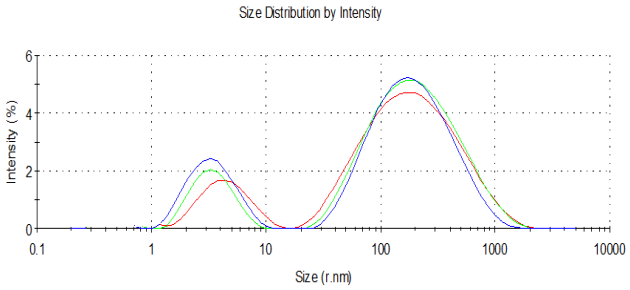

C. Carrier **46b** alone

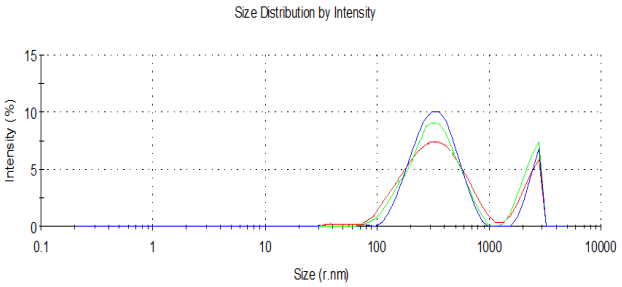

D. LO9 **57**: Carrier **46b** 6 mg/mL (10:1)

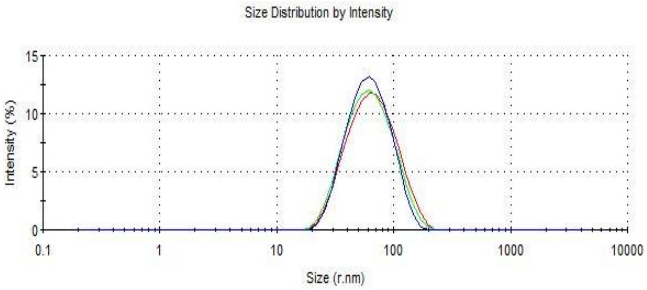

E. Carrier **46c** alone

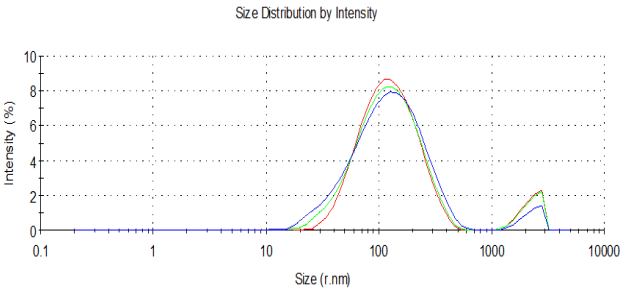

F. LO9 **57**: Carrier **46c** 6 mg/ml (10:1)

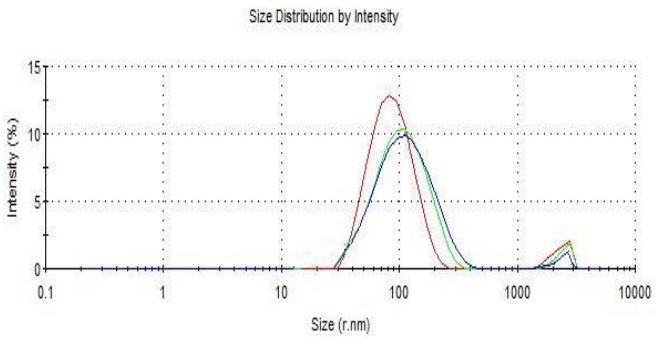

G. Carrier **46d** alone

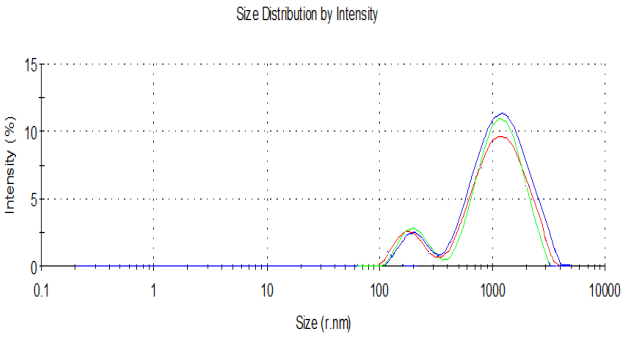

H. LO9 **57**: Carrier **46d** 6 mg/ml (10:1)

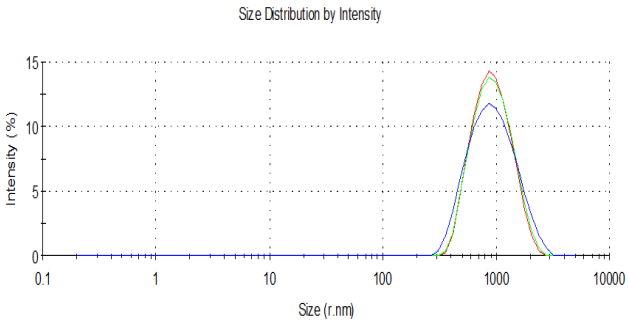

I. Carrier **46e** alone

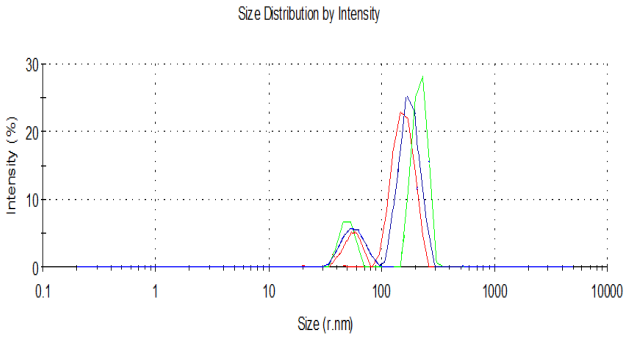

J. LO9 **57**: Carrier **46e** 6 mg/mL (10:1)

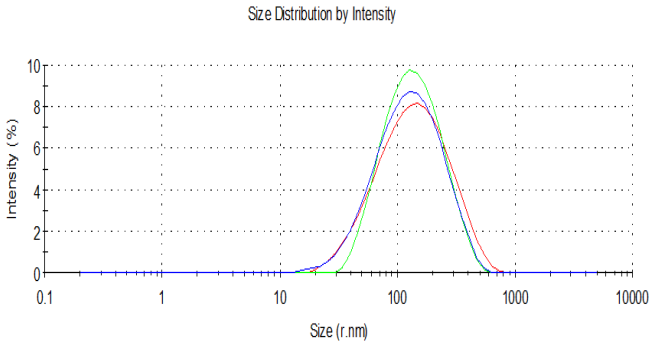

K. Carrier 46f alone

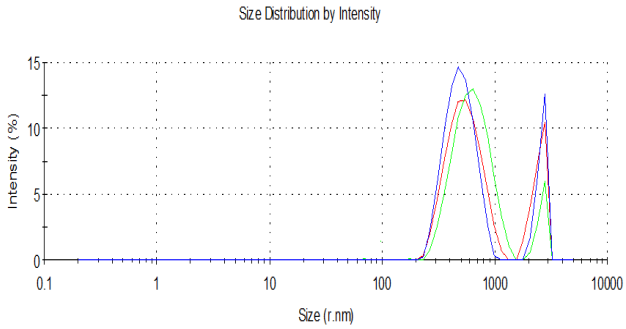

L. LO9 57: Carrier 46f 6 mg/mL (10:1)

Figure 160: Photon correlation spectroscopy size correlation charts for the carrier and drug: carrier formulation in doubly distilled water (n=3, ave).

The *in vitro* release of LO9 **57** from the formulations is shown in Figure 161. Within the range investigated, the length of the alkyl chains attached to the lower rim of the carriers **46-a-f** and the drug loading affected the rate of the drug release from the carrier formulations (Figure 161A and B) (X. Wang *et al.*, 2009; D'Souza, 2014; Zhao *et al.*, 2015). The formulations differed significantly with regard to the percentage drug release at any sampling time. These studies concluded that the formulations derived from calix[4]resorcinarene **46b**, calix[4]resorcinarene **46d** and calix[4]pyrogallolarene **46f** achieve sustained LO9 **57** release over various time periods up to 2 week at 20 ºC. Each of these carriers possesses C_7 alkyl substituents on the lower rim. However, for carriers **46a** and **46c** which have shorter alkyl

substituents, the release continued steadily until the drug was completely released after 72 h. the much faster drug release observed for carrier **46e** may be a consequence of the much lower drug loading capacity of the carrier.

A slower, sustained release of LO9 **57** from carriers **46b** and **46f** again indicate that the drug is internalised in a larger, more structurally organised supramolecular structure.

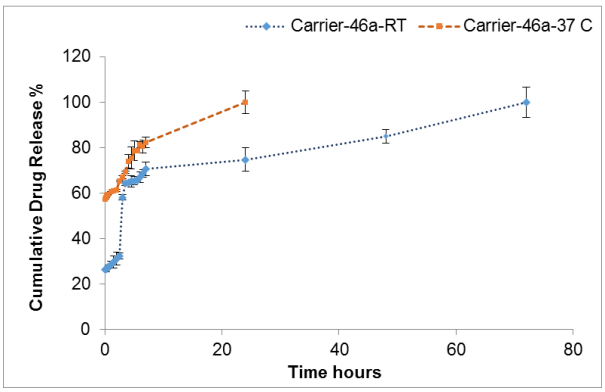

Calix[4]resorcinarene **46a**

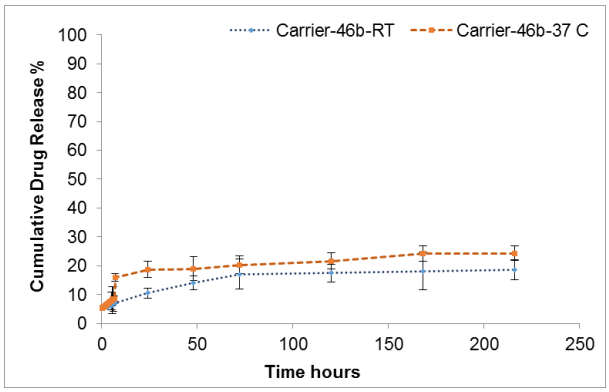

Calix[4]resorcinarene **46b**

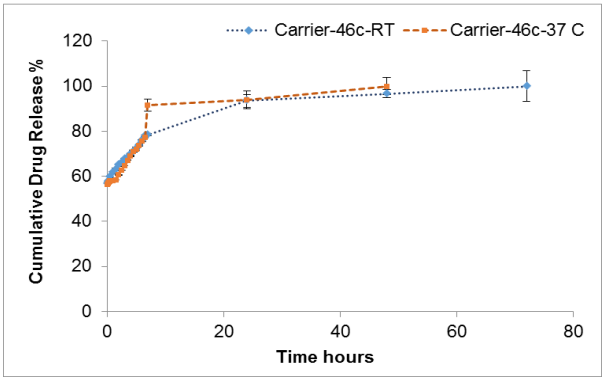

Calix[4]resorcinarene **46c**

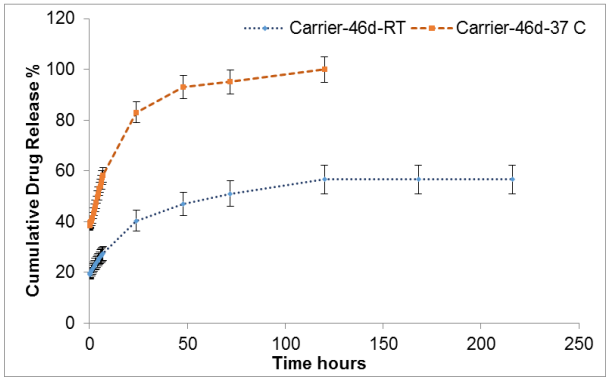

Calix[4]resorcinarene **46d**

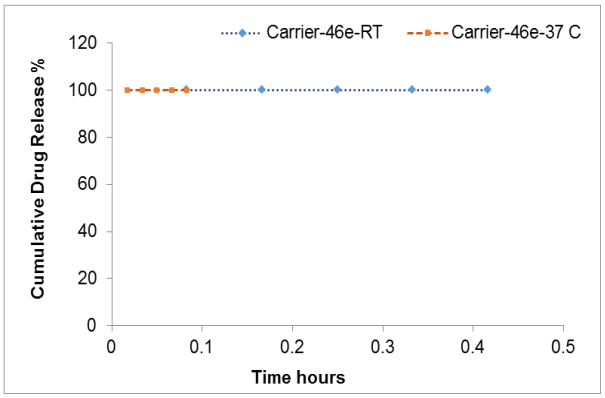

Calix[4]pyrogallolarene **46e**

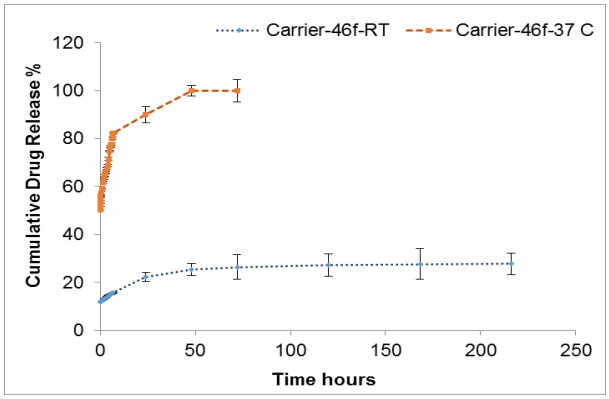

Calix[4]pyrogallolarene **46f**

A. *In vitro* release of LO9 **57** from the short chained carrier formulations

B. *In vitro* release LO9 **57** from the long chained carrier formulations

Figure 161: The drug drug-like molecule LO9 **57** release from the carriers' formulations at 37 ºC and at 20 ºC (Error bars have been omitted for clarity).

The effect of temperature on the *in vitro* release of LO9 **57** from the formulations was also investigated. Drug release profiles for the formulations at 37 ºC are presented in Figure 161. The release of LO9 **57** from all carriers **46a-f** was significantly higher at 37 ºC than at 20 ºC, especially so for those carriers possessing C_4 alkyl substituents on their lower rim.

Notably, however, carrier **46b** showed similar release patterns at both temperatures: drug release from the carrier **46b** was found to be 19 % and 24 % of the encapsulated drug in the first day and after 5 days, respectively, which was almost the same at 20 ºC. Advantageously, the release profile showed a consistent release over the 2 week period at both temperatures. The rational explanation of the slow drug release at all the time points might be that LO9 **57** is localized in the inner core of larger aggregates.

Interestingly, it was observed that drug release from carrier **46f** started with an initial burst, followed by a consistent release over a 24 h period, with the drug being completely released after 48 h, which was much faster than the release at 20 ºC. Advantageously, the release profile again showed a consistent release over the 2 weeks period at 20 ºC.

Based upon all of the data acquired for the solubilisation of LO9 **57** by calix[4]resorcinarenes **46a-d** and calix[4]pyrogallolarenes **46e-f**, it can be concluded that the hydrophobicity of the carriers, especially that presented by the lower rim environment, plays a significant part in the solubilisation. This is particularly true for molecules like LO9 **57** which possess polar and non-polar regions that are well separated.

Large supramolecular structures are likely to form as increased numbers of the carrier molecules come together. The hydrophobic tails are capable of drug solubilisation but will also interact in such a way as to minimize their contact with the aqueous environment, while the hydrophilic heads remain on the outer surface in order to maximize their contact with the aqueous environment (Hoskins *et al.*, 2016).

In the case of carriers **46a**, **46c** and **46e** which possess C_4 alkyl substituents on the lower rim, they form large aggregates in the micron range but which have hydrodynamic radii that are too small to indicate the formation of micellar-type structures. It is proposed that these carriers form aggregates that are diffuse and vary in size but which are not particularly stable, hence the low drug solubilisation and high release rates observed (Figure 162).

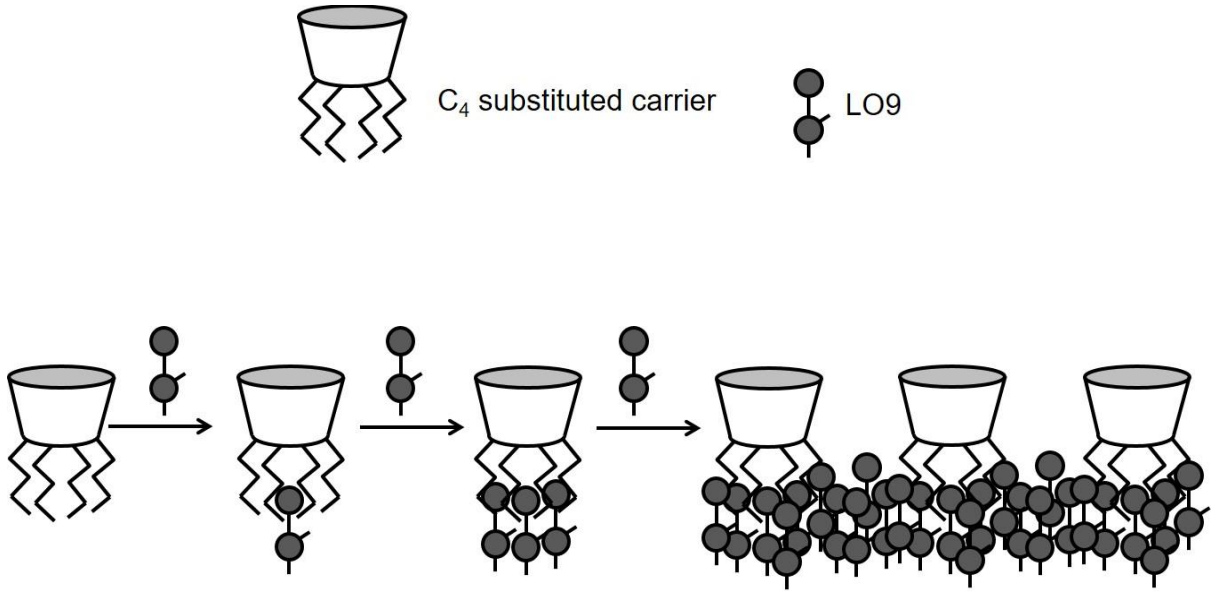

Figure 162: Potential mode of aggregation of LO9 **57** with carriers **46a**, **46c** and **46e**.

Carriers which possess C_7 alkyl substituents on the lower rim, especially carriers **46b** and **46f**, appear to form very large aggregates with hydrodynamic radii in the range indicative of the formation of micellar-type structures. It is proposed that these carriers with C_7 substituents form smaller aggregates which, in the presence of

increased amounts of LO9 **57**, come together and assemble into much larger micelles with the more polar residues of LO9 **57** facing into the interior of the supramolecular structure (Figure 163).

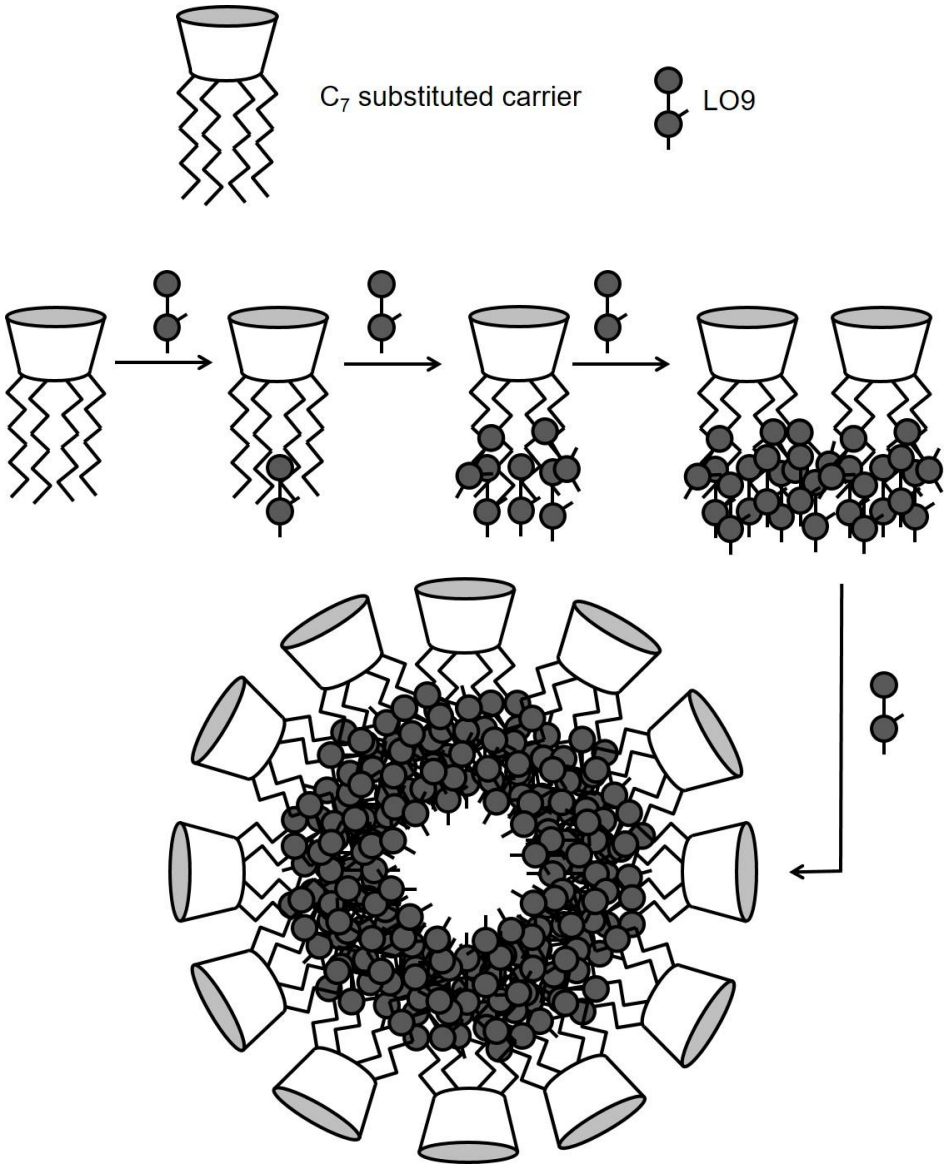

Figure 163: Potential mode of aggregation of LO9 **57** with carriers **46b** and **46f**.

4.5 Conclusion

The work presented in this chapter highlights that amphiphilic calix[4]resorcinarene and calix[4]pyrogallolarene salts **46a-f** are effective solubilizing agents for the

hydrophobic drug LO9 **57**. There are few reports devoted to the solubilisation of hydrophobic substrates by amphiphilic calix[4]resorcinarenes (Morozova *et al.*, 2010; Syakaev *et al.*, 2018). However, the advantages offered by the calix[4]resorcinarene platform include the ability to optimize structural parameters of the molecules to provide the necessary physical and chemical properties required to develop a solubilizing agent. Among the carriers assessed in this study, calix[4]resorcinarene **46b** showed the greatest potential as a solubilising agent.

It is important to consider both drug release and carrier biodegradation when developing a nanoparticulate delivery system. In general, the drug release rate depends on: drug solubility, environmental conditions such as temperature, drug location within the nanoparticle, and the size of the nanoparticles (Caldorera-moore *et al.*, 2011; Morozova *et al.*, 2017).

In vitro release profiles showed that all of the nanocarriers bearing a C_7 alkyl chain on the lower rim achieved sustained release between 48–120 h. However, toxicology, stability and *in vivo* studies were not explored in this study and require to be further investigated, in order to establish the clinical relevance of these systems. Stability can become a limiting factor in drug encapsulation, thus it is the intended subject of future samples analysis. Additionally, electron microscopy can be used to confirm the formation of micellar structures in stable formulations formed from carriers **46b** and **46f**.

Chapter Five

Synthesis and Characterization of C-alkyl Substituted Calix[4]resorcinarenes and their Derivatives

5.1 Introduction

The chemistry and applications of, calix[n]arenes, calix[4]resorcinarenes and calix[4]pyrogallolarenes have been the focus of much research, as can be deduced by the number of publications over recent years. Calix[4]arenes prefer the formation of a thermodynamically stable cone conformer, however the stability of the host–guest complexes of these host molecules is hampered by the inherent flexibility of the calix (Maerz, 2011). Calix[4]resorcinarenes have eight hydroxyl groups at the upper rim that provide a greater degree of rigidity through increased intramolecular hydrogen bonding. Calix[4]resorcinarenes have properties that can help to stabilize guest complexation, allowing the formation of supramolecular assemblies (Power *et al.*, 2007; Dalgarno *et al.*, 2009; Kulikov *et al.*, 2009).

The initial focus of the work reported in this thesis was to attach different functional groups on the upper rim of calix[4]resorcinarenes, principally by functionalization either on the 2-position of the calix (*ortho* to the phenolic OH groups) in order to make new classes of drug solubilisation agents (Scheme 17). Synthetic modifications of the calix[4]resorcinarene upper rim can be categorised: This includes electrophilic substitution of the aromatic ring by Mannich reaction leading to the formation of tetrabenzoxazines (Arnecke *et al.*, 1995; Beyeh *et al.*, 2010). Various derivatives can be obtained in excellent yields by Mannich reactions with primary and secondary amines. The condensation of each resorcinol unit with the amine and formaldehyde occurs in two steps. The first is the usual Mannich aminomethylation, where the amine (*N,N*-dimethylethylenediamine or benzyl amine as reported in this Chapter) formed undergoes ring closure by condensation with a second molecule of formaldehyde and anadjacent hydroxyl group on the upper rim of calix[4]resorcinarenes **44a** and **44b** leading to the formation of the inherently chiral

calix[4]resorcinarenes **58a-d**. The second step involves the removal of the *N,O*-acetal bridge to deliver aminocalix[4]resorcinarenes **59a-d** (Luostarinen *et al.*, 2007). A second category of reactions, also investigated in this Chapter, includes bridging adjacent hydroxyl groups on the upper rim of the calix[4]resorcinarene to prepare the corresponding cavitand, which can be further modified with different functional groups. Bridging the adjacent hydroxyl groups in the calix[4]resorcinarenes **44c-d** by a methylene groups gives “simple cavitands” **60a-b**. Reaction with *N*-bromosuccinimide (NBS) results in tetrabromomethyl cavitands **61a-b**, which can be further modified by replacing of bromo atoms with solubilizing groups.

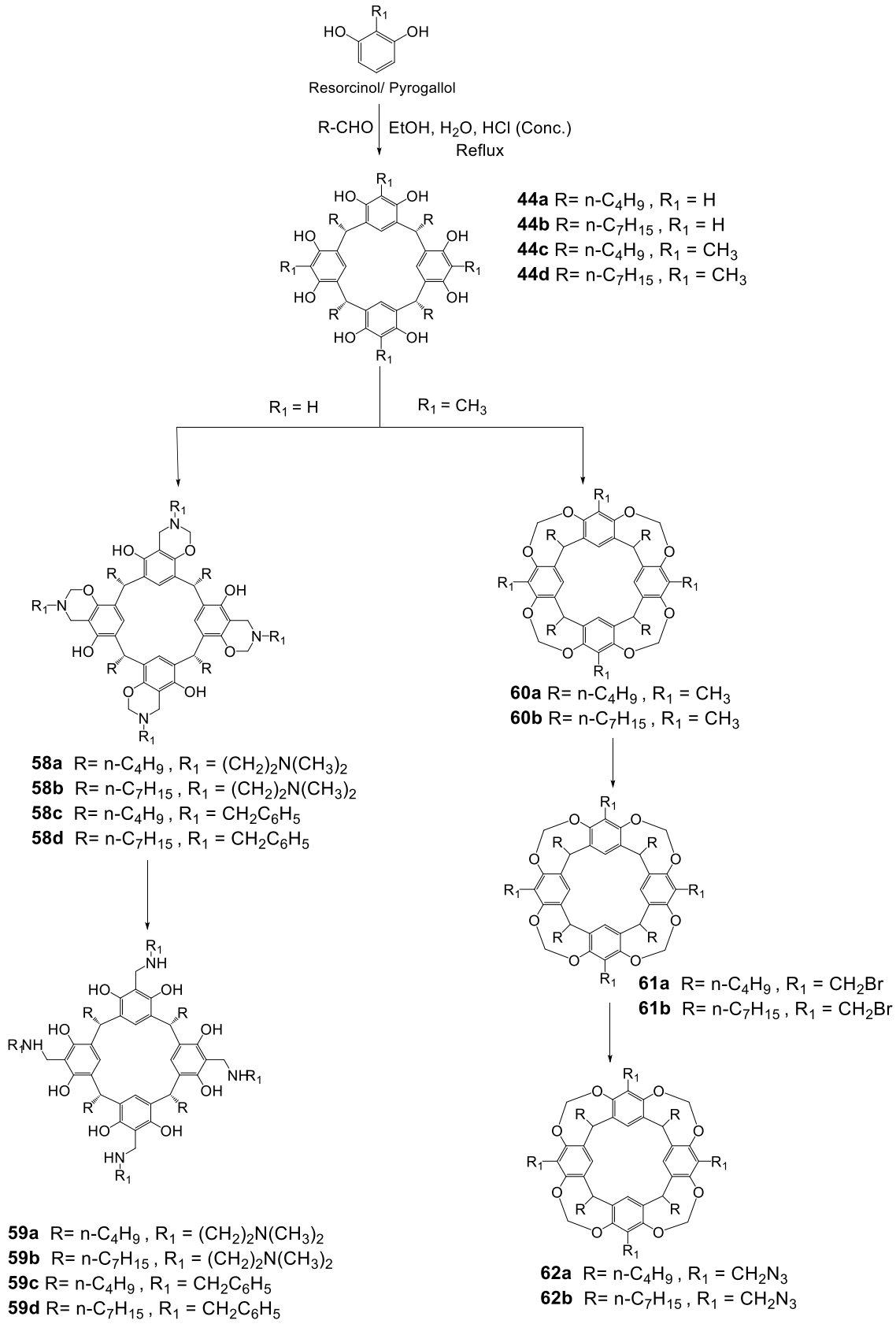

Scheme 17: Preparation of functionalized calix[4]resorcinarenes at the upper rim by *O*-bridging reactions and Mannich reactions.

This Chapter describes efforts to prepare calix[4]resorcinarenes for use as drugs carriers by functionalisation on the upper rim of the calix. The targets possess deeper cavities potentially capable of associating with hydrophobic drug molecules of different sizes and physical attributes. They also possess alkyl groups on the lower rim, which have already been shown in previous Chapters to play an important role in drug solubilisation. The drug solubilisation carriers should not be so hydrophobic that they are insoluble in aqueous media themselves, so the goal was to make calix[4]resorcinarene deivatives with charged residues on the upper rim.

Calix[4]resorcinarenes with four methyl groups at the 2-position of the resorcinol rings **44c** and **44d** were chosen as a platform to prepare deep-cavity cavitands. The upper rim of these cavitands can be further modified with hydrophobic residues, which may allow the insertion of a drug guest that will be more or less surrounded by the walls of the host. It is known that a charge present on the upper rim influences the binding properties of cavitands in aqueous media. The aim of the study presented here was to develop amphiphilic cavitands that have potential to act as nano-sized solubilisation agents for hydrophobic drugs. Notably, the calix[4]resorcinarene precursors used possessed alkyl chain substituents on the lower rim of varied length (C_4 and C_7), as were used in previous chapters.

5.2 Results

A series of calix[4]resorcinarene derivatives modified at the upper rim were synthesized to provide potential solubilising agents for hydrophobic drugs in aqueous solution.

5.2.1 Synthesis of Aminocalix[4]resorcinarenes 58a-b and 59a-b

Aminocalix[4]resorcinarenes **58a-d** were prepared in two steps from calix[4]resorcinarenes **44a-b** started materials, in a manner similar to that described previously in the literature (Airola *et al.*, 1997; Shivanyuk *et al.*, 2000; Beyeh *et al.*, 2010; Beyeh, *et al.*, 2012) (Scheme 17). These derivatives were characterized using FT-IR, ^{1}H-NMR, and ^{13}C NMR spectroscopy. Compounds **58b** and **59b** had been previously prepared by other authors (Kharitonova, Burilov, Pudovik, & Konovalov, 2003). The presence of hydroxyl and secondary amino groups in compounds **58a** and **59a** appeared in their FTIR spectra by a broad band at 3167 cm^{-1} and 3329 cm^{-1}, respectively. The ^{1}H NMR spectrum for compound **58a** showed resonances at δ = 4.92 ppm (NCH_2O), δ = 3.89 ppm (NCH_2Ar), and at δ = 2.24 ppm ($-N(CH_3)_2$), which match the reference data (Burilov *et al.*, 2001). Chemical shifts of the closely related compound **59a** (Figure 164) were the same as compound **58a** except for the signal (NCH_2O), as reported.

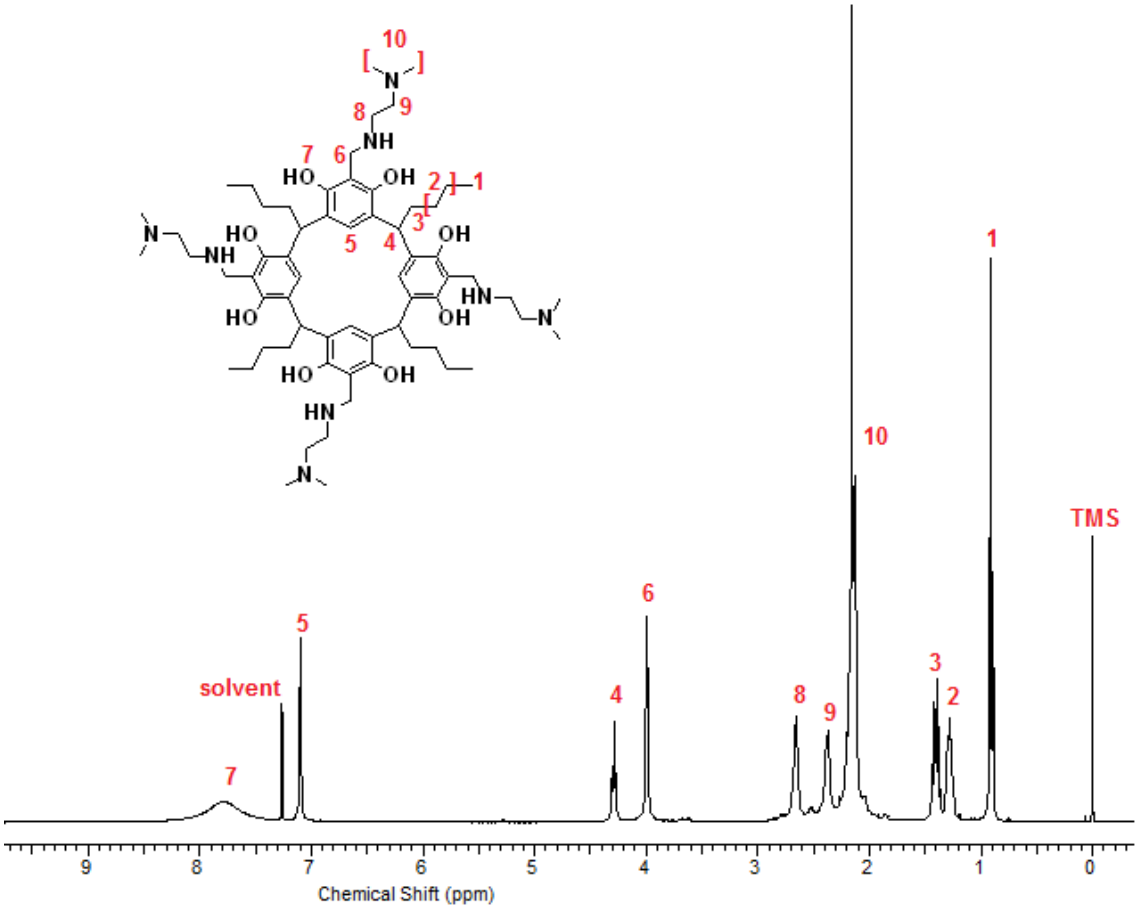

Figure 164: ^{1}H NMR spectrum of aminocalix[4]resorcinarene **59a** in $CDCl_3$ carried out at 300 MHz at 25 °C.

5.2.2 Synthesis of Aminocalix[4]resorcinarenes 58c-d and 59c-d

Mannich condensation reaction between benzylamine and calix[4]resorcinarenes **44a** and **44b** in the presence of excess formaldehyde resulted in tetra benzoxazines **58c-d**, following an established procedure (Airola *et al.*, 1997; Pan *et al.*, 2015). The structure of compounds **58c-d** was confirmed by FTIR, ^{1}H NMR and ^{13}C NMR spectroscopic data. Hydroxyl and secondary amino groups for compound **58c-d** are evidenced in the FTIR spectra by a broad band at 3353–3464 cm^{-1} and 3362 cm^{-1} respectively. The ^{1}H NMR spectrum for compound **58c** showed signals at δ = 4.90 ppm (NCH_2O), at δ = 4.05 ppm (Ar-CH_2-N), and at δ = 3.71 ppm (NCH_2-Ar) , which

match the reference data (Airola *et al.*, 1997; Beyeh *et al.*, 2006; Burilov *et al.*, 2001; Luostarinen *et al.*, 2007). The ^{1}H NMR spectrum for compound **58d** followed a similar pattern. Chemical shifts of the closely related compounds **59c** (Figure 165) and **59d** (Figure 166) were the same as compounds **58c** and **58d**, except for the signal attributed to the (NCH_2O) group.

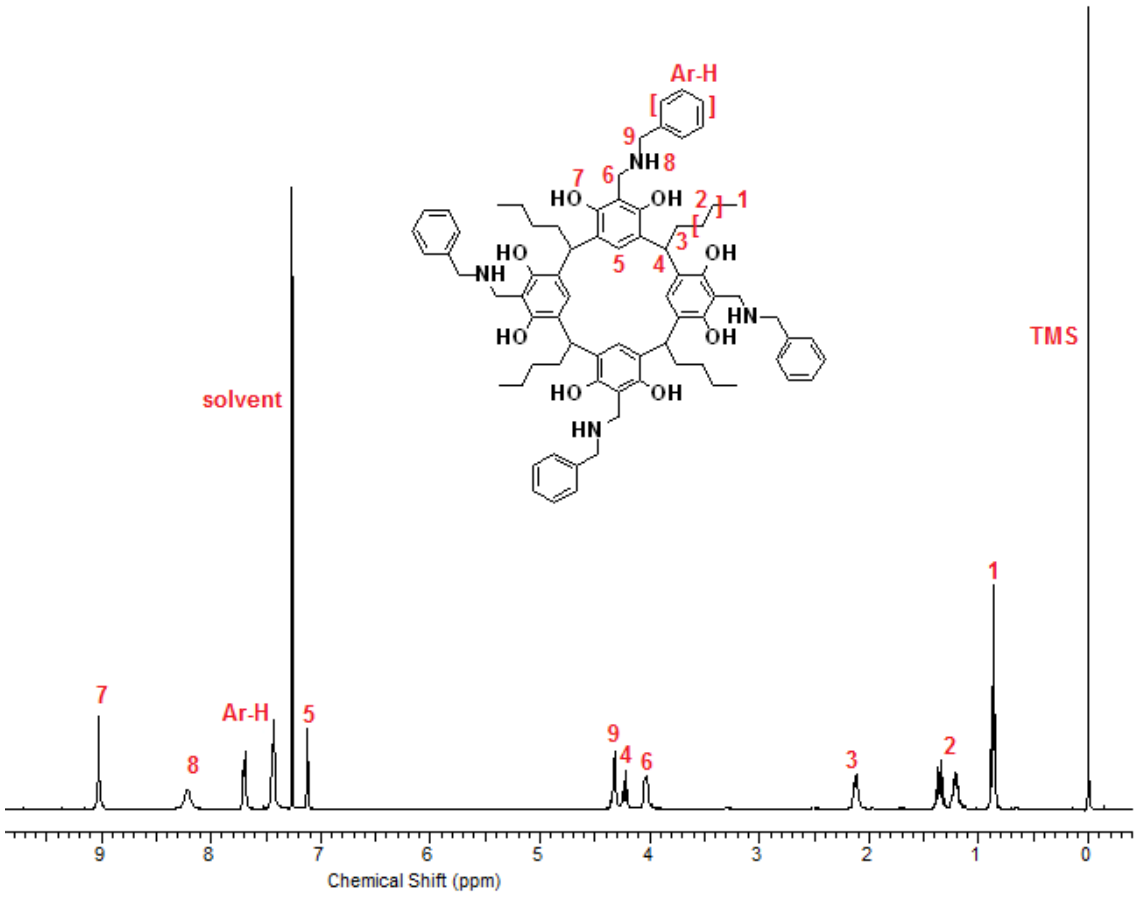

Figure 165: ^{1}H NMR spectrum of aminocalix[4]resorcinarene **59c** in $CDCl_3$ carried out at 300 MHz at 25 °C.

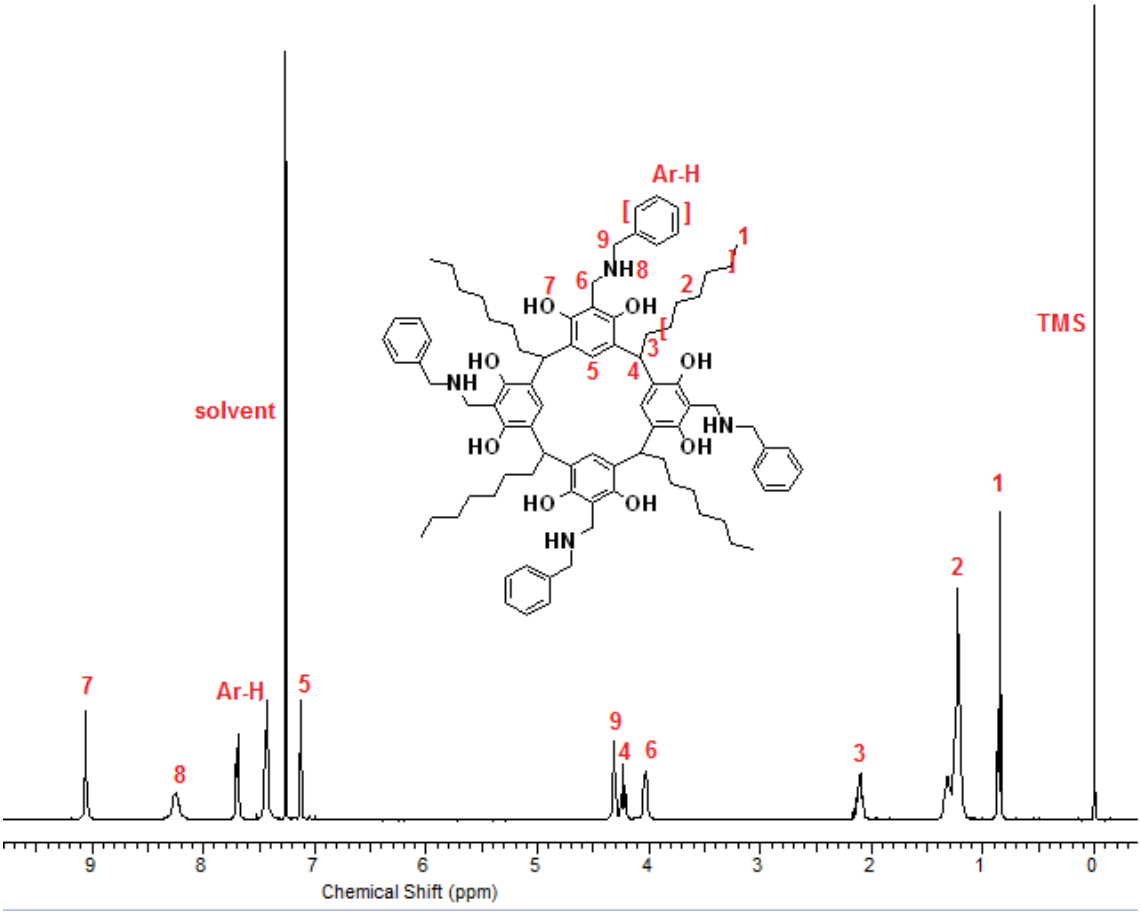

Figure 166: ^{1}H NMR spectrum of aminocalix[4]resorcinarene **59d** in $CDCl_3$ carried out at 300 MHz at 25 °C.

Removal of the *N*-benzyl groups can be achieved by catalytic hydrogenolysis (Ina *et al.*, 1996; Page *et al.*, 1999). The hydrogenolysis step to remove the four methylbenzyl groups of **59c-d** using a palladium (5 %) on carbon catalyst supported on carbon was unsuccessful and led to a mixture of products. Further work is required on this step to prepare the desired compounds for further study as solubilising agents.

5.2.3 Synthesis of Bridge Calix[4]resorcinarenes

The characteristic bowl shape of the calix[4]resorcinarenes can be rigidified into a crown conformation by bridging the hydroxyl groups of adjacent rings. The bridging

reaction to prepare cavitands is known to be low yielding. In addition, the sparing solubility of these macrocycles in organic solvents requires large quantities of solvent to purify the products by column chromatography.

In an effort to obtain solubilising agents with a more rigid structure, a series of cavitands were synthesised and characterized.

5.2.4 Synthesis of Cavitands 60a-b

The rigid bowl shape calix[4]resorcinarene-based cavitands **60a-b** were synthesized by reacting **44c-d** with bromochloromethane, which introduced methylene bridges between the four sets of adjacent oxygens (Cram *et al.*, 1988; Sorrell & Pigge, 1993). The ^{1}H NMR spectrum of **60a**-**b** (Figure 167 and 168) shows the characteristic signals for the cavitand aromatic protons and doublets for the outer bridge protons (OCH_2O) at δ = 5.94 ppm, and the inner bridge protons (OCH_2O) at δ = 4.28 ppm, which matches the reference data (Cram *et al.,* 1988; Moussaoui *et al.,* 2017). ^{1}H NMR spectra of cavitands **60a-b** showed that they exist as cone conformers.

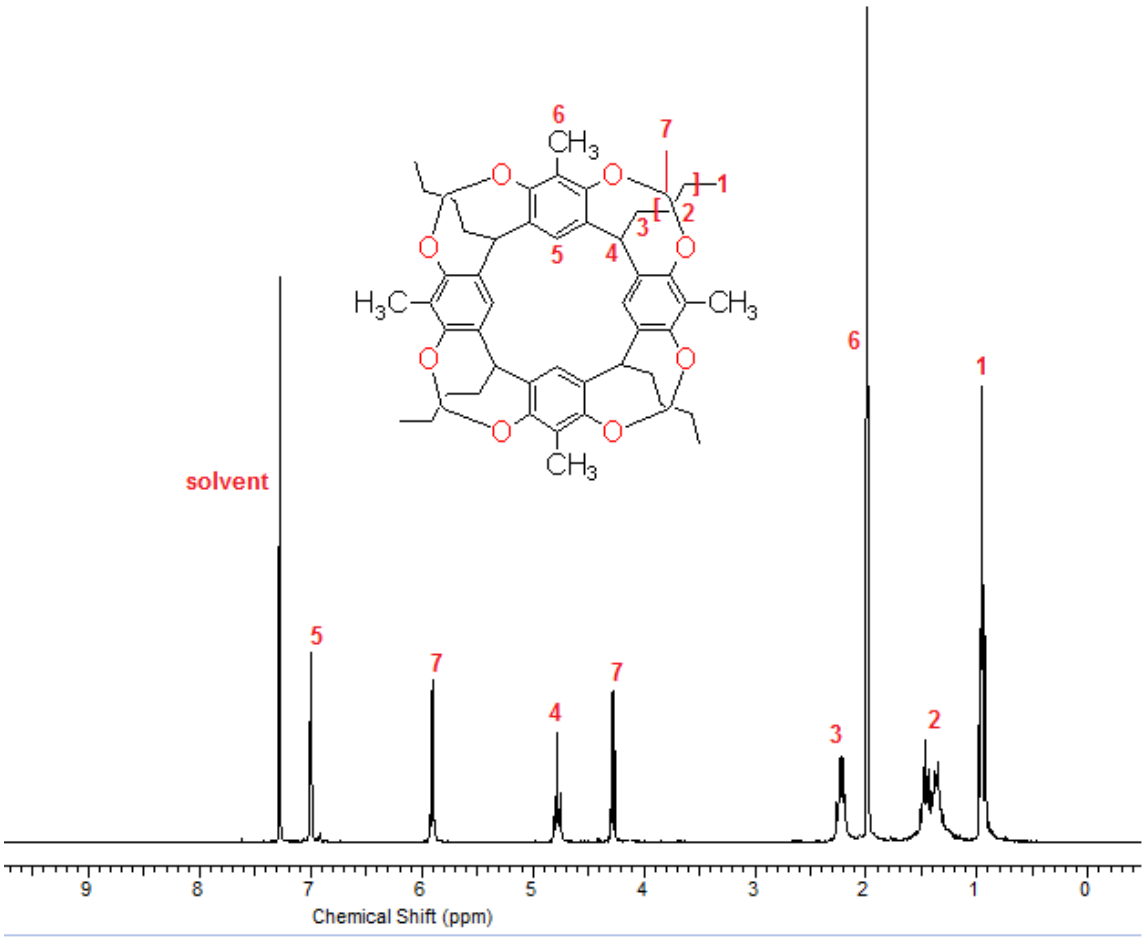

Figure 167: ^{1}H NMR spectrum of calix[4]resorcinarene **60a** in $CDCl_3$ carried out at 400 MHz at 25 °C.

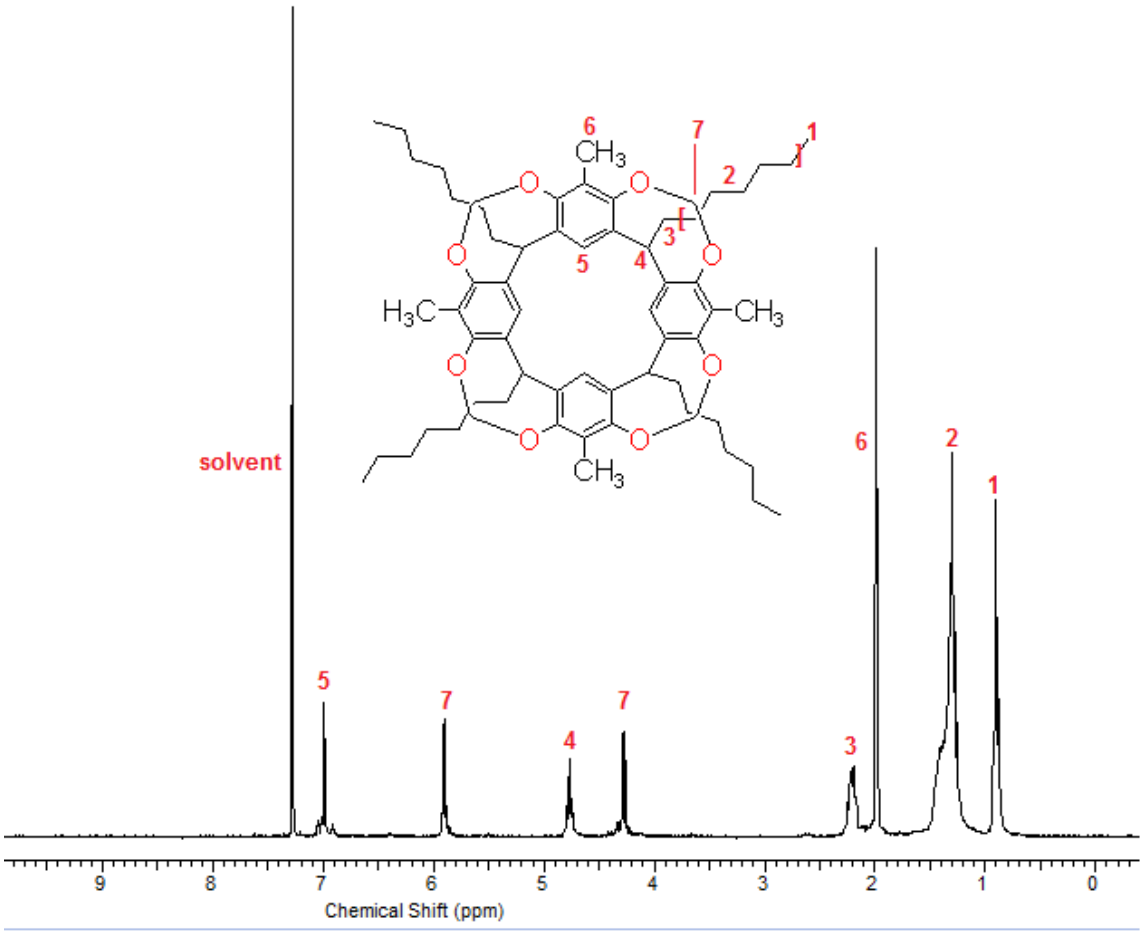

Figure 168: ^{1}H NMR spectrum of calix[4]resorcinarene **60b** in $CDCl_3$ carried out at 400 MHz at 25 °C.

5.2.4.1 Synthesis of Calix[4]resorcinarenes Cavitands 61a-b

Tetra(bromomethyl)cavitands **61a-b** were easily obtained from bromination of cavitands **60a-b** using *N*-bromosuccinimide (NBS) as a source of bromine, in refluxing dimethyl sulfoxide (DMSO) using a modification of literature methods (Boerrigter *et al.*, 1997). The structure of **61a-b** was confirmed from the ^{1}H NMR down-field shifts of the outer bridge protons (δ = 6.05 ppm), inner bridge protons (δ = 4.58 ppm) and the aromatic protons, due to the introduction of the bromine atoms, which matches the reference data (Sorrell & Pigge, 1993; Boerrigter *et al.*, 1996; Boerrigter *et al.*, 1997). ^{1}H NMR spectra of cavitands **61a-b** (Figure 169 and 170)

showed that they exist as cone conformers of structurally rigid cavitands **60a-b**. The bromination takes place through a free radical mechanism in the presence of NBS as initiator and as a source of bromine (Thapa, 2009). The advantage of NBS is that it provides a low-level concentration of bromine (Carey & Sundberg, 1998). The electron-rich methyl groups on the upper rim between two donor alkoxy functions are the most reactive sites towards the radical reaction since the generated radicals are stabilized by the adjacent electron donating groups.

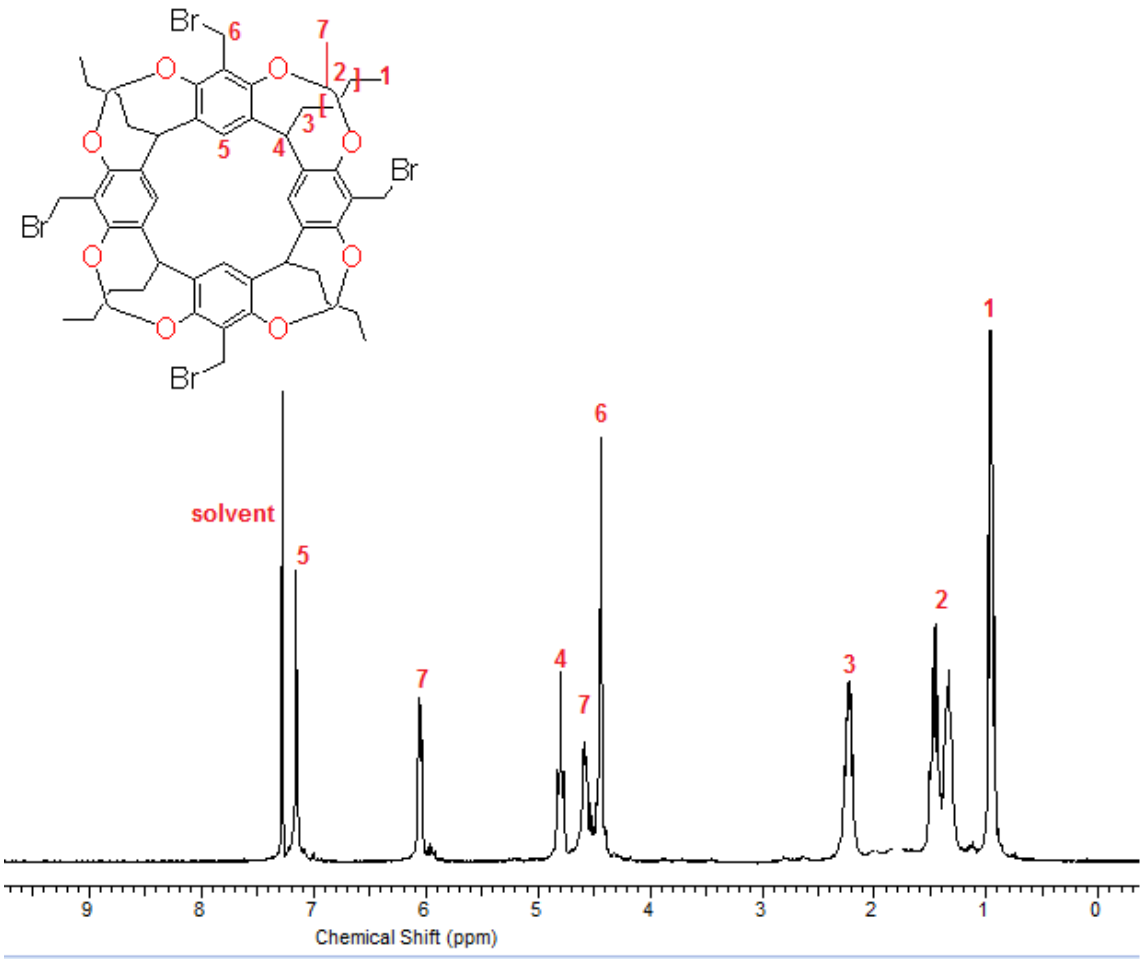

Figure 169: ^{1}H NMR spectrum of calix[4]resorcinarene **61a** in $CDCl_3$ carried out at 400 MHz at 25 °C.

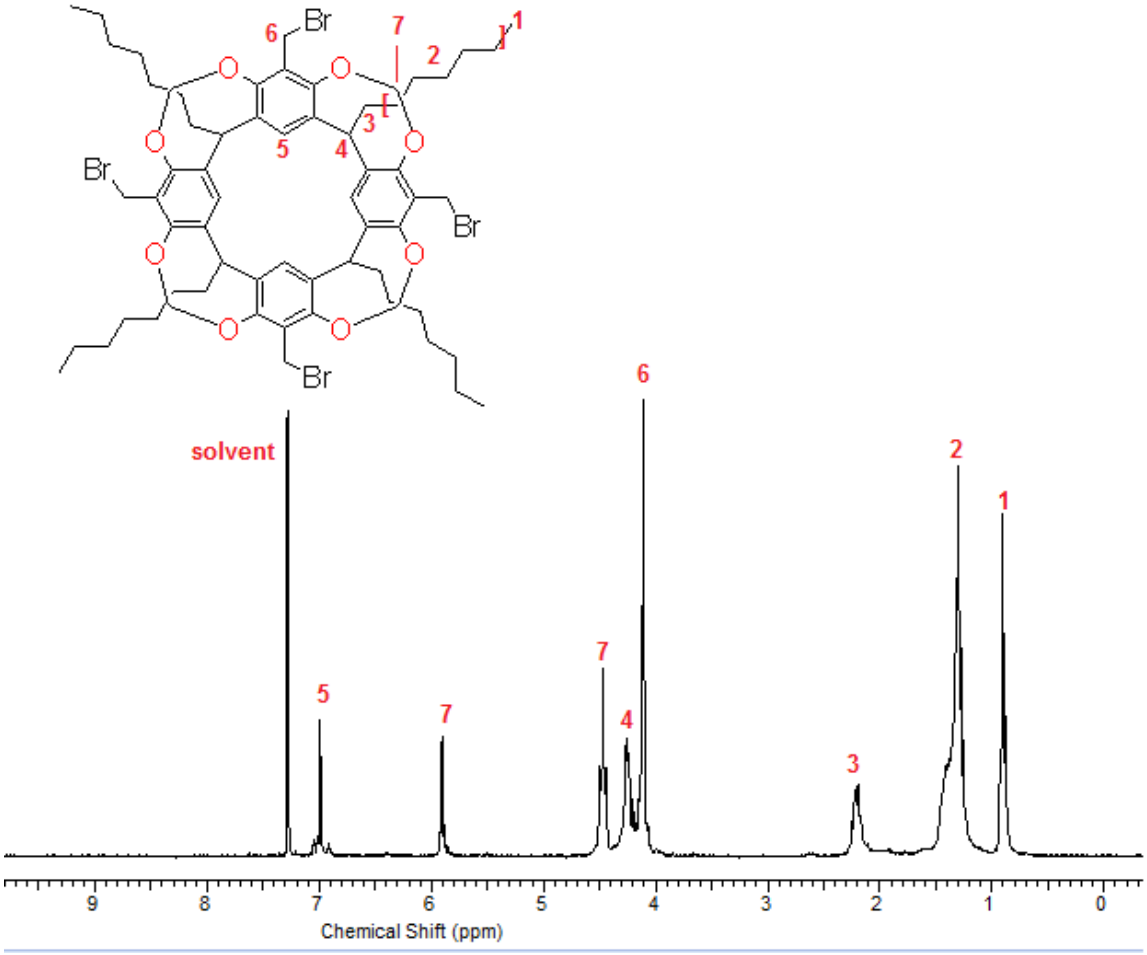

Figure 170: ^{1}H NMR spectrum of aminocalix[4]resorcinarene **61b** in $CDCl_3$ carried out at 400 MHz at 25 °C.

5.2.4.2 Synthesis of Calix[4]resorcinarenes Cavitands 62a-b

Cavitands **62a-b** were synthesised by reaction of the precursors with sodium azide (NaN_3). This substitution requires a solvent with a high dielectric constant in order to dissociate NaN_3. The ^{1}H NMR spectra confirmed the success of this reaction. The ^{1}H NMR spectra of the cavitands **62a-b** (Figure 171 and 172) exhibits characteristic signals at δ = 4.33 ppm for the Ar-CH_2N_3 methylene protons (Moussaoui *et al.,* 2017).

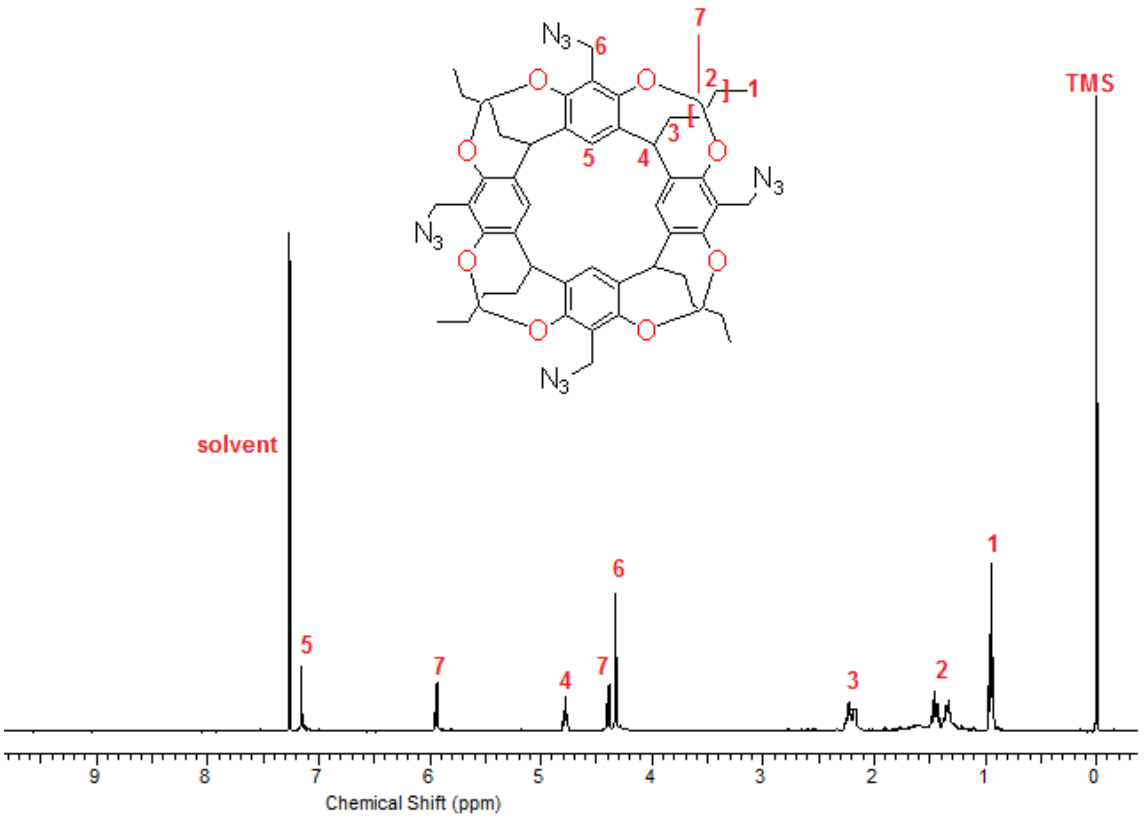

Figure 171: ^{1}H NMR spectrum of calix[4]resorcinarene **62a** in $CDCl_3$ carried out at 300 MHz at 25 °C.

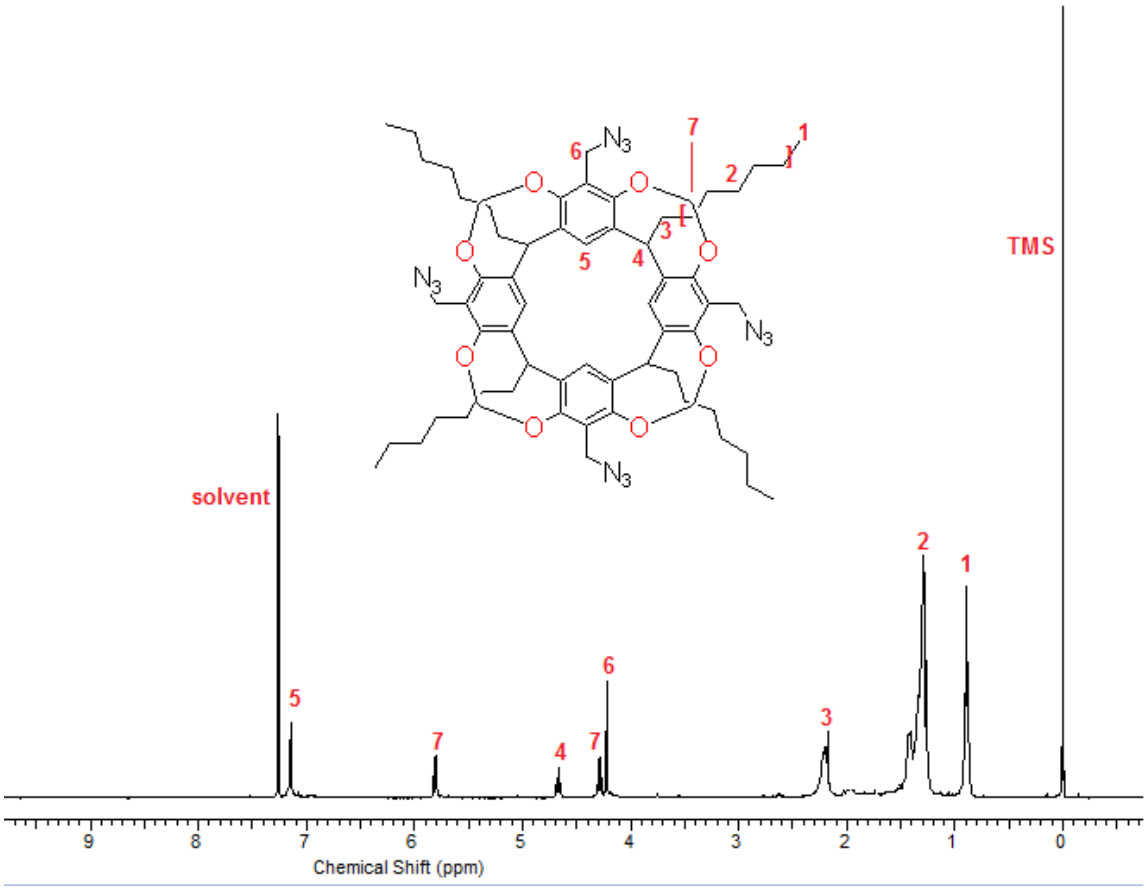

Figure 172: ^{1}H NMR spectrum of calix[4]resorcinarene **62b** in $CDCl_3$ carried out at 300 MHz at 25 °C.

There are two traditional ways to introduce amino group into the aromatic scaffolds of calix[4]resorcinarene derivatives: either by nitration of cavitands, followed by reduction of the nitro group with common reducing agents (Tunstad *et al*., 1989), or by formation of an azo compound followed by reduction with $Na_2S_2O_4$ (Jain & Kanaiya, 2008; Jayswal *et al.,* 2008). Tetra-amino calix[4]resorcinarene derivative can serve as key intermediates for further functionalization to obtain calix[4]resorcinarenes with specific receptor properties. The catalytic reaction of the azido cavitand derivatives **62a-b** to give the corresponding amines was not pursued as other aspects of the research were prioritised.

5.3 Discussion

The first step in this project's strategy was to modify the upper rim of calix[4]resorcinarene **44a-b** with aminomethyl fragments residues in the 2-positions. This was successful (Scheme 17) to give compounds **58a-d** by Mannich reaction of the calix[4]resorcinarene starting materials with *N,N*-dimethylenediamine and benzyl amine. The structure of compounds **58a-d** was confirmed by spectroscopic data, and the formation of a single isomer can be concluded from the ^{1}H NMR spectrum. The ^{1}H NMR spectra for compounds **58a** and **58c** show one singlet for the phenolic protons H_7 and the benzene aromatic protons H_5, one triplet for the methylene bridging protons H_4 and one pair of doublets for each pair of diastereotopic protons H_6 of the Ar-CH_2 and H_8 of the N-CH_2-O groups in the benzoxazine rings (Figure 173 and 174). All the other protons give signals, which are compatible with a single type of each of these residues.

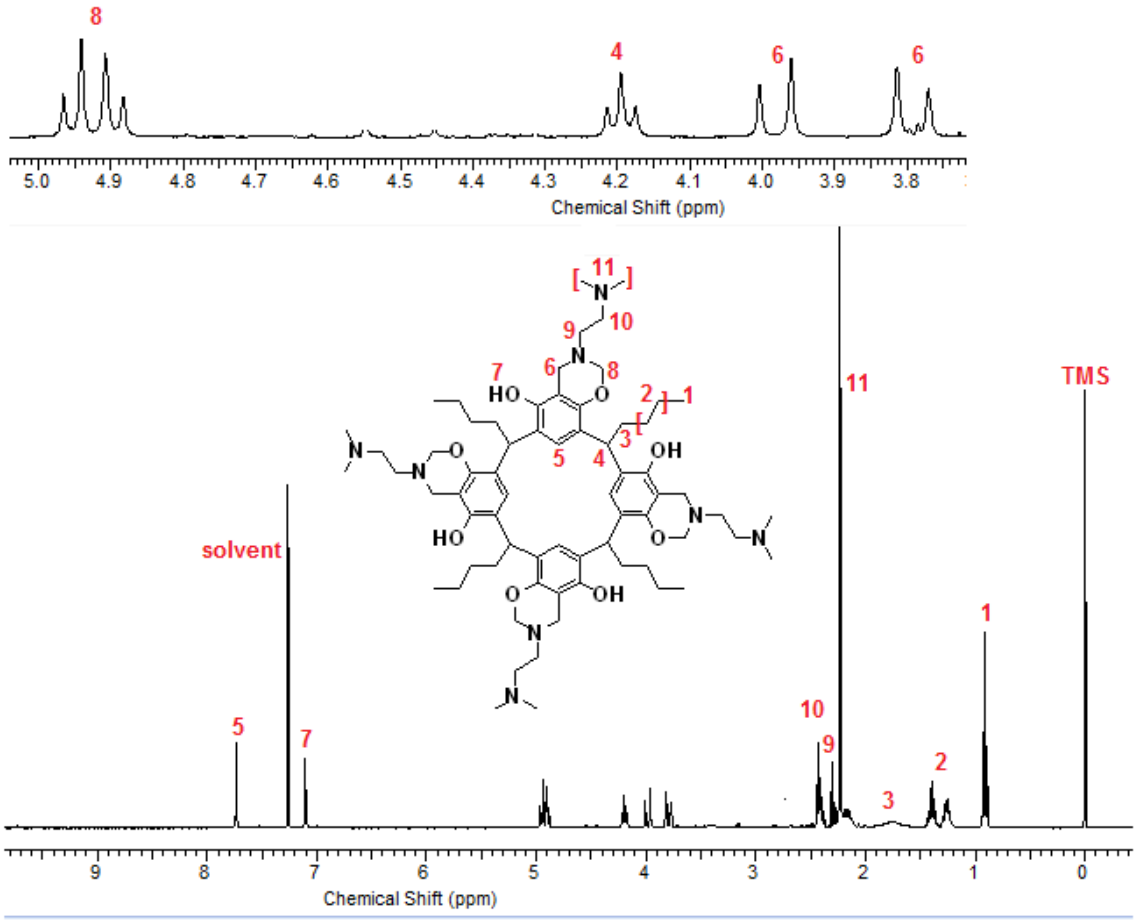

Figure 173: ^{1}H NMR spectrum of calix[4]resorcinarene **58a** in $CDCl_3$ carried out at 300 MHz at 25 °C.

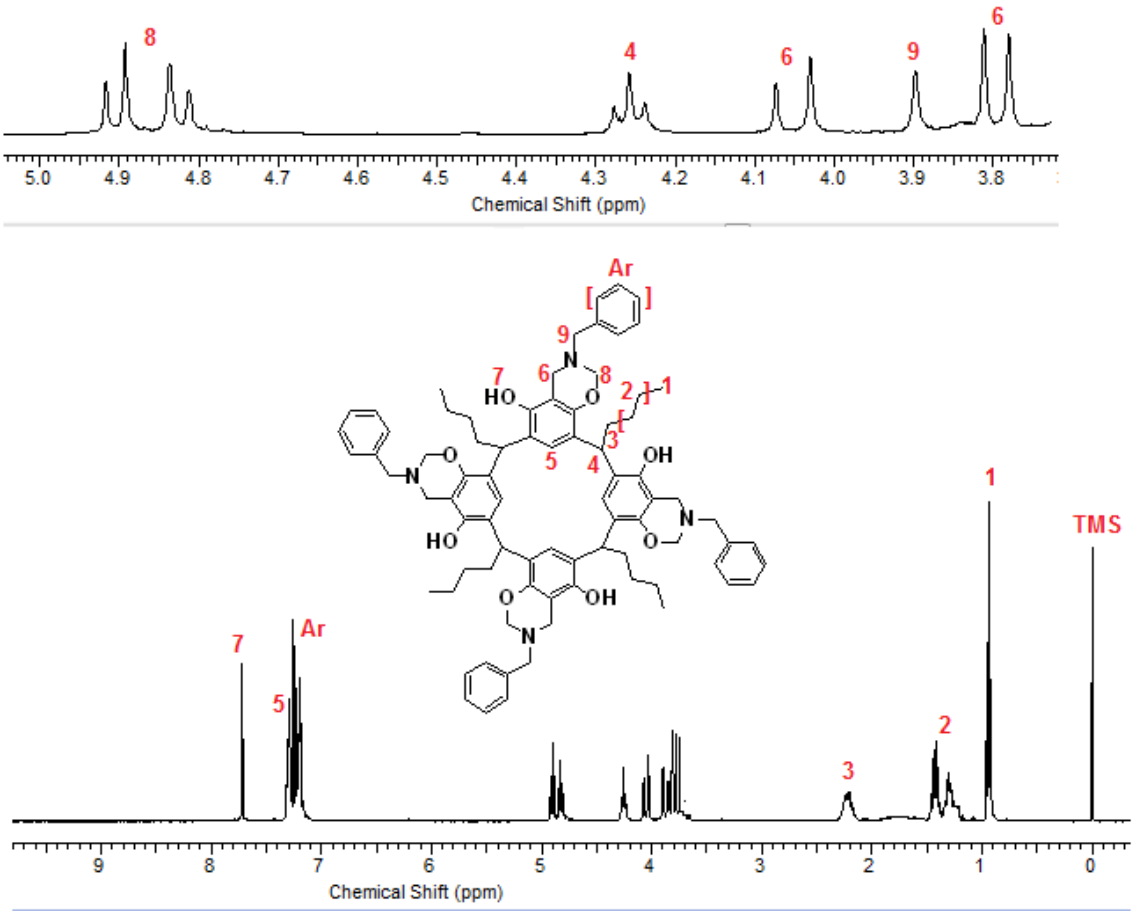

Figure 174: ^{1}H NMR spectrum of calix[4]resorcinarene **58c** in $CDCl_3$ carried out at 300 MHz at 25 °C.

The acid-catalyzed cleavage of the oxazine rings readily transformed tetraoxazines **58a-b** into the corresponding tetraammonium salts **59a-b**, which is soluble in water. However, compounds **59c-d** need the removal of the *N*-benzyl groups to produce tetraammonium salts. The ^{1}H NMR spectra of compound **58a** in $CDCl_3$ contains one set of signals for the phenolic protons H_7 and the aromatic protons H_5, one triplet for the methylene bridging protons H_4, which is in keeping with the C_{4v}-symmetrical crown conformation (Figure 173).

The adjacent hydroxyl groups in compound **44c-d** were bridged with methylene groups. The bridged calix[4]resorcinarenes **60a-b** were characterized using NMR

spectrometry in $CDCl_3$. The ^1H NMR spectrum for all bridged calix[4]resorcinarenes (cavitands) show the disappearance of the phenolic protons H_7 and the presence of two new doublets around (δ = 4.28 and 5.90 ppm) for the inner and outer hydrogen of the newly formed methylene bridge, respectively, as typified in ^1H NMR spectrum of compound **60a** (Figure 175). These two doublet peaks represent H_{7in} methyelene proton pointing inside of the cavitand cavity and H_{7out} methylene proton pointing outside of the cavitand cavity.

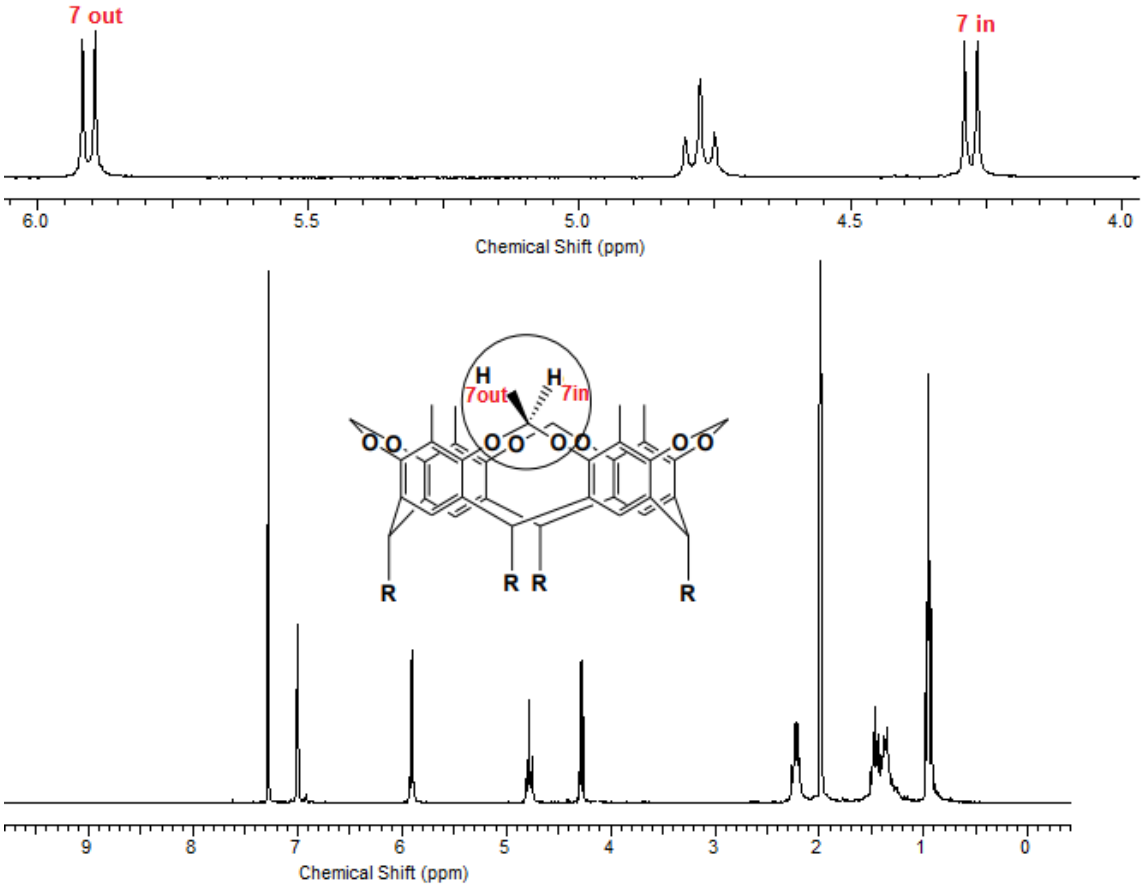

Figure 175: ^1H NMR spectrum of calix[4]resorcinarene **60a** in $CDCl_3$ carried out at 400 MHz at 25 °C.

Radical bromination on the methyl group at the 2-position of the calix[4]resorcinarene ring was successfully achieved for both compounds **60a-b**. Both products **61a-b** were characterized by NMR spectrometry in $CDCl_3$. Both ^1H NMR spectra show the downfield shifting of the benzylic H_6 proton from δ = 1.98 ppm to δ = 4.44 ppm (Figure 169).

Tetraazido cavitands **62a-b** was synthesized from compounds **61a-b**, respectively, via a nucleophilic substitution with sodium azide (NaN_3). Both products were characterized by ^1H and ^{13}C NMR spectrometry in $CDCl_3$. From the ^1H NMR spectrum (Figure 171 and 172) we see that the benzylic proton H_6 slightly shifted from δ = 4.44 ppm to around δ = 4.33 ppm and in the ^{13}C NMR spectra (Figure 176) and (Figure 177) we can see the presence of the benzylic carbon at δ = 45.1 ppm.

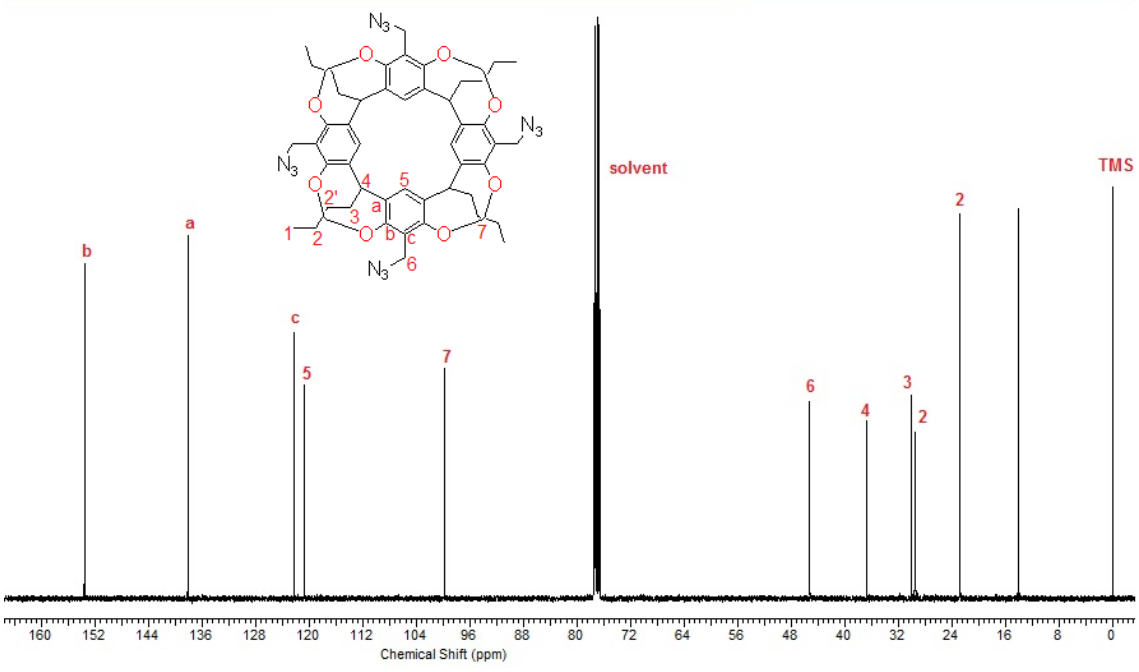

Figure 176: ^{13}C NMR spectrum of calix[4]resorcinarene **62a** in $CDCl_3$ carried out at 100 MHz at 25 °C.

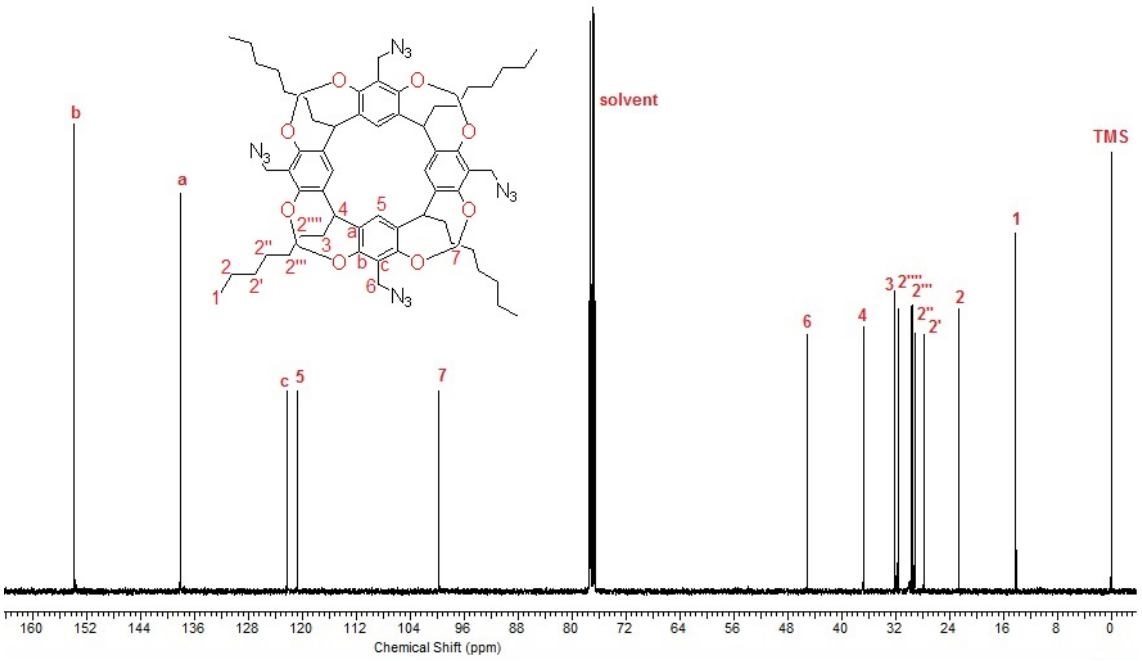

Figure 177: ^{13}C NMR spectrum of calix[4]resorcinarene **62b** in $CDCl_3$ carried out at 100 MHz at 25 °C.

5.4 Conclusion

Whilst it is widely appreciated that calix[4]esorcinarenes plays a central role in the field of host-guest chemistry, making them soluble in aqueous media would be a fundamental step toward their successful application in the challenging field of drug solubilisation. Amphiphilic calix[4]resorcinarenes can be easily prepared, as reported in Chapter 2. Their upper rim is available for further functionalization to improve binding affinity and selectivity. The vase-like shape of these compounds possesses cavities which can potentially host a variety of molecular guests. Additionally, water-soluble deep-cavity calix[4]resorcinarene-based cavitands have been used to study self-assembly driven by the hydrophobic effect. These systems have given rise to numerous novel chemical phenomena and have potential use in drug delivery.

According to the primary goal of the work described in this thesis, calix[4]resorcarenes **44a-d** with *rccc* configuration were successfully synthesised following an established procedure (Tunstad *et al.*, 1989). Subsequently, the parent calix[4]resorcarenes **44a-b** were used to synthesis water-soluble tetraamino functionalized calix[4]resorcinarenes **59a-b**. However, the removal of benzyl protecting groups found in aminocalix[4]resorcinarenes **59c-d** using catalytic hydrogenation was unsuccessful, leading to a mixture of products. Further work is required on this step to prepare the desired products. However, calix[4]resorcinarenes **44c-d** were used to prepare compounds which might be exploited further to design compounds of biological importance. It must be noted here, though, that polyamines have been shown to damage cell membranes which may prove useful for drug delivery but may also give undesirable toxicology profiles for the carriers.

Cavitands **60a-b** were synthesised in four simple steps (Scheme 17). Subsequently calix[4]resorcinarenes **44c-d** were rigidified through bridging the neighbouring hydroxyl groups on the resorcinol rings to give cavitands **60a-b**. Tetrabromomethyl cavitands **61** were then easily obtained from the reaction of **60** with *N*-bromosuccinimide (NBS) in refluxing dimethyl sulfoxide (DMSO) and can be further functionalized to give various hosts. Tetrabromo cavitands **61**can act as starting materials for producing further derivatives with selective functionalization patterns due to the reactivity of the bromide and its easy replacement with other functional groups. Thus these cavitands can be used as building blocks in order to produce series of potential drug solubilising agents that have interesting properties. Furthermore, cavitands **62** containing terminal nitrogen atoms were prepared. In future investigations these molecules will provide key intermediates for the synthesis

of therapeutic delivery vectors. However, the catalytic reduction of the azide derivatives **62** to give the corresponding amines was not pursued as other aspects of the research were prioritised.

Chapter Six

General Conclusion & Future Work

6.1 General conclusion

In this thesis, unfunctionalised calix[4]resorcinarenes **44a-d** and calix[4]pyrogallolarenes **44e-f** bearing alkyl chain substituents varying lengths (C_4 and C_7) on the lower rim have been successfully synthesized and modified with hydrophilic carboxyl groups to produce novel water-soluble octa-carboxylated calix[4]resorcinarenes **46a-d** and dodeca-carboxylated calix[4]pyrogallolarenes **46e-f**, which possess multiple charged residues. Also, calix[4]resorcarenes **44a-b** were successfully used to prepare four aminocalix[4]resorcinarenes **58a-b** and **59a-b**. However, the removal of protecting groups from aminocalix[4]resorcinarenes **59a-b** using catalytic hydrogenation was unsuccessful leading to a mixture of products. The related calix[4]resorcinarene based cavitands **62c-d** containing terminal nitrogen atoms on the upper rims were synthesised using calix[4]resorcinarenes **44c-d** as a starting material. As the azide functional group offers opportunity for further synthetic manipulations, in future investigations these molecules will provide a key intermediate in the synthesis of therapeutic drug delivery vehicles. However, the catalytic reduction of the azide derivatives **62c-d** to give the corresponding amines was not pursued as other aspects of the research, as detailed in Chapters 2, 3 and 4 were prioritised.

In the aqueous environment all the amphiphilic calix[4]resorcinarenes **46a-d** and calix[4]pyrogallolarenes **46e-f** were capable of forming aggregates with potential for the incorporation of hydrophobic drug entities. These compounds formed drug-loaded aggregates with three model hydrophobic drugs (propofol, prednisolone, and tetracaine), giving host-guest complexes in aqueous solution which had various properties dependent upon the lower rim alkyl substituent, the number of the hydrophilic carboxylate groups and the drug structural and physicochemical

properties. Increasing the length of the hydrophobic alkyl substituent of calix[4]resorcinarenes **46a-d** and calix[4]pyrogallolarenes **46e-f** from butyl (C_4) to heptyl (C_7) led to an apparent difference in aggregation and receptor properties towards the hydrophobic drugs in aqueous solutions. The self-aggregation of carriers **46a-f** in aqueous environments and their ability to act as drug solubilising agents have been determined.

It was observed that the calix[4]resorcinarenes **46b**, **46d** and calix[4]pyrogallolarene **46f** with the C_7 alkyl chains showed higher drug loading and solubilisation capacities for both propofol and tetracaine compared to the calix[4]resorcinarenes **46a**, **46c** and calix[4]pyrogallolarene **46e** with the shorter C_4 alkyl chains. This indicated that the drug might be accommodated within the hydrophobic alkyl region on the lower rim. The NMR experiments showed that there is some interaction between propofol and tetracaine and the calix[4]resorcinarenes **46a-b**. However, it is not yet clear for tetracaine whether this is a hydrophobic interaction between the carrier and the drug or a formation of an ionic complex. Further experiments are required to determine this, including analysis of the precipitate formed.

It is difficult to control the self-assembly of molecules in water due to the small size, polarity, and hydrogen bond donating and accepting properties of water which attenuate most non-covalent interactions (Jordan *et al.*, 2019). The data obtained showed that the size of the self-assemblies formed increased as the concentration of the amphiphilic carriers increased. This indicates that supramolecular structures are indeed formed at higher concentrations, in agreement with the surface tension (Hoskins *et al.*, 2016; Morozova *et al.*, 2017; Syakaev *et al.*, 2018). Negative zeta potentials with values greater than -30 mV demonstrate the presence of carboxyl groups on the aggregate surfaces and confirm the stability of the complexes formed.

Moreover, the aggregate size appeared to be dependent on both the length of the alkyl chain and degree of drug loading. The diameter of drug-loaded carriers was significantly larger than that of drug-free carriers. There are two reasons for this; when drug is added into self-assemblies formed by amphiphilic carriers, very often it inserts into a large core of a supramolecular structure, resulting in core expansion with associated increased hydrophobic stabilisation of the lipophilic chains. Otherwise it may be due to addition of further molecular units forming even larger supramolecules. Overall this formation of stabilised supramolecular structures may enhance the applicability of these technologies to a variety of drug molecules.

The amphiphilic calix[4]resorcinarenes **46a**, **46d** and calix[4]pyrogallolarenes **46e-f** were loaded with three model hydrophobic drugs (propofol, prednisolone and tetracaine). The capability of the host molecules to encapsulate the hydrophobic drugs varied with the types of hydrophobic pendant group and drug. Among the carriers assessed in this study, calix[4]resorcinarene **46b**, which possesses the longer C_7 alkyl chains on the lower rim, showed the highest drug solubilisation capacities for propofol (42 mg/mL). This indicates that propofol might be incorporated into the long chains of the carrier. The calix[4]resorcinarene **46d** and calix[4]pyrogallolarene **46f** were shown to be excellent universal drug solubilisers, with a 35.6 mg/mL and 27 mg/mL increase in aqueous propofol solubility observed, respectively. Overall it was observed that for all formulations, higher initial carrier concentrations achieved greatest solubility of propofol. However, calix[4]resorcinarene **46b**, which possesses the shorter C_4 alkyl substituents, showed the highest drug solubilisation capacity for prednisolone (1.2 mg/mL). Interestingly, the short chained calix[4]resorcinarene **46c** and calix[4]pyrogallol[4]arene **46e** were capable of solubilising more prednisolone compared with the long chained carriers (1

mg/mL and 1.1 mg/mL, respectively), albeit very low loading. The resultant formulations possessed extremely low excipient: drug ratios making them very efficient systems for drug release, though again the drug loading was not significantly high. Interestingly, all of the formulations significantly improved the solubilisation of both propofol and prednisolone, indicating that these amphiphilic carriers can be used as drug solubilisers. This achievement, however, was difficult to meet with the hydrophobic drug, tetracaine: The formulations with this drug precipitated after two days so, in this case, it may be necessary to carry out the experiments under different conditions, at different pH values for example, if the delivery of tetracaine is to be pursued. The optimal formulations differ in size for both propofol and prednisolone. This might be due to the varying architectures of both the drugs and the amphiphilic calix[4]resorcinarnes and calix[4]pyrogallolarenes, and their ability to associate and shield each other from the aqueous environment. The formulations were shown to achieve sustained release of both propofol and prednisolone for up to 48 – 120 h. Additionally, the impact of temperature on drug release was explored in this study.

Model drug analogue LO9 **57** was synthesized and its solubilization by aqueous solutions of carboxylated calix[4]resorcinarene and calix[4]pyrogallolarene carriers **46a-f** of different hydrophobicity was studied. The data consistently showed that the macrocycles solubilize the model drug analogue LO9 **57** with the probable incorporation of its structure into the hydrophobic part of the hosts, most likely on the lower rim of the macrocycles. The change of length of the hydrophobic substituent chains on the macrocycles from C_4 to C_7 leads to a significant increase of loading capacity for LO9 **57**. Other derivatives of LO9 **57** which served as breast cancer inhibitors were prepared and identified by another group (Robinson *et al.*, 2015). The

self-assemblies of the calix[4]resorcinarene **46b** and calix[4]pyrogallolarene **46f** with the long alkyl chains formed in aqueous media were able to load significantly high concentrations of LO9 **57** compared to the others carriers. Modified calix[4]resorcinarene **46b** and calix[4]pyrogallolarene **46f** enhanced the aqueous solubility of LO9 **57** by 556 mg/mL and 240 mg/mL, respectively. This indicated that the drug might be accommodated within the hydrophobic inner core of a micellar-type structure (Figure 178).

The architectures of both the drugs and the modified calix[4]resorcinarenes and calix[4]pyrogallolarenes also play a significant role in the sizes of the optimal formulations and their ability to accommodate and shield each other from the aqueous environment. Results showed that the formulations can achieve sustained *in vitro* release of the drugs up to 48–120 h. Additionally, the impact of temperature in the formation of inclusion complexes was explored in this study.

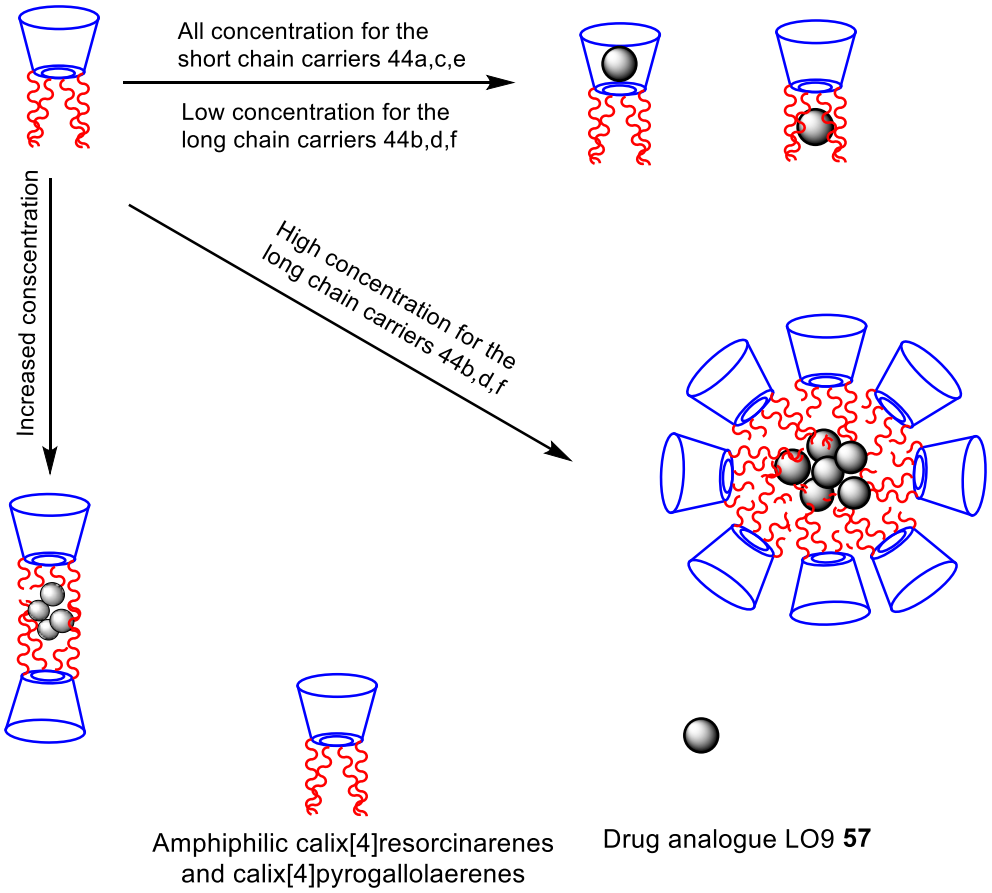

Figure 178: Possible drug- loaded carriers and aggregation mechanisms of carriers calix[4]resorcinarenes and calix[4]pyrogallolalarenes with LO9 **57**

6.2 Future Work

Regardless of all the advantages of using nanoparticles for drug delivery, there is always the opportunity for further improvement in this area. The creation of synthetic receptors for the binding of guests in water with the amphiphilic calix[4]resorcinarenes **46a-d** and calix[4]pyrogallolarenes **46e-f** was achieved and it would be useful to investigate the other synthetic calix[4]resorcinarene derivatives **48a-b** and **55c-d** which can be developed further in order to prepare receptors that possess both a high affinity and a high selectivity for the binding of a range of guests in water. In addition to the nature and length of the alkyl chains attached at the lower

rim of calix[4]resorcinarene platform, the mobility and structure of their upper rim can affect the self-assembly of calix[4]resorcinarenes. Although other forms of water soluble calix[4]resorcinarenes **59a-b** have been synthesised in these studies, the effect of aggregation of these specific carrier excipients and, more interestingly, their interactions with hydrophobic drugs, are unknown.

This work reports a possible ideal formulation with the amphiphilic carriers **46a-f** to enhance the dissolution of hydrophobic drugs, in this case propofol, prednisolone and LO9 **57**, indicating that these amphiphilic carriers can be used as drug solubilisers. However, our understanding of what factors control the formation of the drug complexes with calix[4]resorcinarenes and calix[4]pyrogallolarenes and the location of the drug incorporation is limited. It would be useful to investigate these novel formulations in the solid phase further using X-ray diffraction, differential scanning calorimetry, and scanning electron microscopy techniques. Also, drug loading mechanisms need to be explained to learn how these molecules interact with the hydrophobic drugs. To better understand the molecular mechanism of interaction in supramolecular co-associates at the molecular level, it is important to use NMR spectroscopy, especially fourier transform pulsed-gradient spin—echo (FT-PGSE) NMR. It is a powerful and versatile tool for the study of the structural behavior of all components in supramolecular associate (Stilbs, 1987; Furo, 2005; Pesce & Wiley, 2012). Dissolution enhancement has only briefly been witnessed of a poorly soluble drug, in this case of tetracaine. Further experience is thus required to determine this phenomenon, particularly analysis of the precipitate formed.

Looking towards biological applications, these formulations need to be screened against cytotoxicity assays and applied to appropriate cell lines with highly

differentiated types of cells in preparations for this formulation to be used in *in vivo* studies and to check its cytotoxic effect against animal models such as mice.

The work presented in this thesis details efforts towards a significant enhancement for the formulation of hydrophobic drugs. The rate of drug release from calix[4]resorcinarene and calix[4]pyrogallolarene formulations might lead towards *in vivo* biological applications. Interestingly, all of these formulations significantly improved the aqueous solubility and dissolution of hydrophobic drugs tested (propofol, prednisolone and LO9 **57**), indicating that these amphiphilic carriers can be used as drug solubilisers. In addition, it has been confirmed that sustained drug release can be achieved over a range of temperatures based on the amphiphilic carriers and desired release profile.

Chapter Seven

Experimental Details

7.1 Materials, Analytical Techniques and Methods

7.1.1 Materials

Resorcinol (98 %), 2-methyl resorcinol (98 %), 2-hydroxy resorcinol (pyrogallol) (98 %), potassium carbonate anhydrous, *N*,*N*-dimethylethylenediamine, benzyl amine, potassium iodide, *N*-bromosuccinimide (NBS), dimethyl sulfoxide (DMSO), dicyclohexylcarbodiimide (DCC) and all aldehydes (pentanal and octanal) were purchased from Alfa Aesar. Methanol, ethanol, acetone tetrahydrofuran (THF), and dichloromethane (DCM) solvents were purchased from VWR Chemicals. Sodium hydride, palladium (5 %) on carbon, methyl bromoacetate, bromochloromethane (CH_2BrCl), azobisisobutyronitrile (AIBN), 2,4-dimethoxybenzoic acid, 4-phenylbutyl amine, 4-dimethylamino pyridine (DMAP), methyl orange and trifluoroacetic acid (TFA) were purchased from Sigma Aldrich. Sodium hydroxide, magnesium sulfate, hydrochloric acid, HPLC grade acetonitrile, ethyl acetate and petroleum ether solvents were purchased from Fisher Scientific. 1,2 Dichloroethane was purchased from BDH. Molecular sieves 4 Å, 8 to 12 mesh were purchased from ACROS; they were activated by heating at 60 ºC under reduce pressure (0.1 mmgH). All analytical agents were used without further purification, except acetone which was dried over molecular sieves 4 Å, 8 to 12 mesh. 0.45µm GDX PVDF filters were purchased from Whatman, UK. Dialysis Bags were purchased from Medicell Co., UK.

7.1.2 Analytical Techniques

Mass Spectra

Mass spectra were performed on a Waters Xevo G2-S QTof Mass Spectrometer or a ThermoFisher LTQ Orbitrap XL ETD Hybrid Ion Trap-Orbitrap Mass Spectrometer using electrospray ionisation in either positive or negative ion mode by the National Mass Spectrometry Facility, Swansea University Medical School, Park Campus, Swansea, UK.

Fourier Transform Infrared Spectroscopy (FTIR)

FTIR was carried out using a NICOLET iS5 fitted with an iD5 ATR laminated diamond crystal tip (Thermo Scientific™, UK).

Nuclear Magnetic Resonance (NMR)

^{1}H and ^{13}C nuclear magnetic resonance (NMR) spectra were obtained using a 300 MHz Bruker Spectrospin DPX 300 Spectrometer and a 400 MHz Bruker Ascend 400 spectrometer. Multiplicities were recorded as singlets peaks (s), broad peaks (br), doublets (d), triplets (t) and multiplets (m). All NMR samples were carried out in deuterated solvents. ^{1}H and ^{13}C NMR shifts were reported in parts per million (ppm) relative to tetramethylsilane (TMS) or relative to an internal standard setting in the NMR instrument software. Coupling constants (*J*-values) are reported in Hertz (Hz).

Thin Layer Chromatography (TLC)

Analytical thin-layer chromatography was performed by using the pre-coated silica gel plates (0.20 mm) were purchased from VWR Chemicals, thin layer chromatography (TLC) was conducted, and examined under UV light. Column chromatography in silica gel was performed using Geduran Si 60 (40-63 µm) from

VWR Chemicals. The minimum amount of silica was used to pre-absorbed samples. By using the hand bellows pressure was introduced.

Sonication Probe

Aggregates of the carrier were formed by probe sonication using a Sonication Probe Soniprep 150 (Wolflabs, Pocklington, UK).

Photon correlation spectrometer (PCS)

The size, zeta, polydispersity index and the conductivity measurements were carried out using a photon correlation spectrometer (PCS) on a Zetasizer Nano-ZS, Malvern Instruments, UK. UV-visible (UV-2600 UV-VIS (NIR) spectrometer (Shimadzu, Germany).

Torsion balance

The surface tension of the carrier solutions were measured using a torsion balance (Torsion Balance Supplies, Weston-super-Mare, UK).

High-performance liquid chromatography (HPLC)

The total amount of the hydrophobic drug loaded into the nanoparticles and the content of the drug released was determined using high-performance liquid chromatography (HPLC) (Perkin Elmer Flexar LC Auto Sampler) and (Shimadzu Prominence).

Melting Point

The melting point of compounds was determined using a Stuart (SMP30) and are uncorrected.

pH Meter

The pH of an aqueous solution of the carrier was measured using a HANNA pH meter.

UV-Visible Spectroscopy

The hydrophobic drug, the carrier and the formulation solution was analysed in a Varian Cary 50 Bio UV-Vis spectrophotometer (64 scans) over a wavelength range of 400-700 nm (1 nm, stepwise) and recorded the maximum absorbance at (200-800 nm) and the wavelength maxima (λ_{max}) was determined.

7.1.3 Methods

7.1.3.1 Synthesis of Alkyl Calix[4]resorcinarenes and Calix[4]pyrogallolarenes

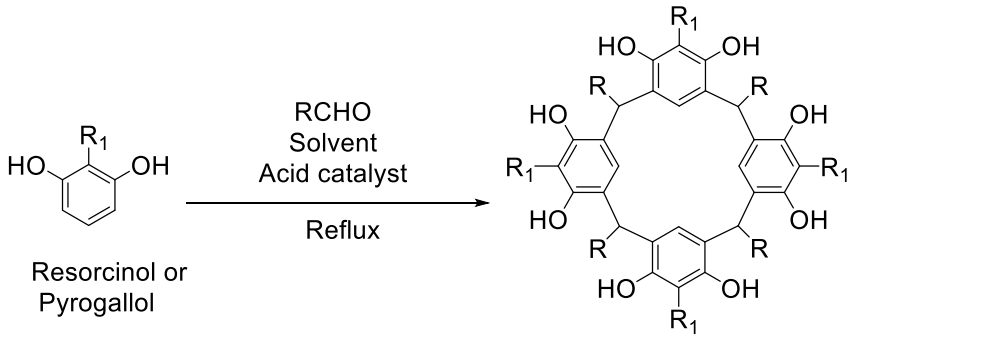

Resorcinol or Pyrogallol

11

R= C_4H_9, C_7H_{15}
11a R_1= H
11c R_1= CH_3
11e R_1= OH

Calix[4]resorcinarenes/ Calix[4]pyrogallolarenes

44a R= C_4H_9; R_1= H
44b R= C_7H_{15}; R_1= H
44c R= C_4H_9; R_1= CH_3
44d R= C_7H_{15}; R_1= CH_3
44e R= C_4H_9; R_1= OH
44f R= C_7H_{15}; R_1= OH

Scheme 18: The acid–catalysed condensation of resorcinol **11** with an aldehydes (pentanal and octanal**)** to prepare calix[4]resorcinarene **44**.

General procedures for the synthesis of the calix[4]resorcinarenes:

1. Stirred solution of resorcinol **11** (100 mmol) in absolute ethanol (50 mL) and concentrated hydrochloric acid (15 mL) was combined in a dropwise manner with a solution of an aldehyde (100 mmol) in ethanol (25 mL) over a 0.5 h period at 5 °C. The reaction solution was warmed slowly to 25 °C and then heated under reflux for 24 h at 78 °C (Scheme 18). Subsequently, the clear solution turned cloudy and a precipitate separated over time. The resulting mixture was allowed to cool to room temperature then the flask reaction was placed in an ice-bath and distilled water (50 mL) was added to the mixture until precipitation of the desired compound was completed. The resulting precipitation was filtered using a Buchner funnel, washed with distilled water and dried in a vacuo oven at 60 °C.
2. To a solution of resorcinol **11** (100 mmol) and an aldehyde (100 mmol) in 75 mL of absolute ethanol, was carefully added 12.5 mL of concentrated hydrochloric acid. The reaction solution was warmed slowly to 25 °C and then heated under reflux for 4 h at 105 °C (Scheme 18). Subsequently, the clear solution turned cloudy and a precipitate separated over time. The resulting mixture was allowed to cool to room temperature then the flask reaction was placed in an ice-bath and distilled water (50 mL) was added to the mixture until precipitation of the desired compound was completed. The resulting precipitation was filtered using a Buchner funnel, washed with distilled water and dried in a vacuo oven at 60 °C and identified.

7.1.3.2 Synthesis of Calix[4]resorcinarene 44a

Procedure 1; resorcinol **11a** (11.01 g, 100 mmol) and pentanal (8.61 g, 100 mmol); giving a pale yellow solid in (13.62 g, 94 % yield); m.p. (330-331 °C) (Tunstad *et al.*,

1989). FTIR (cm^{-1}): 3467 (OH group), 2956 (Ar-CH), 2905 (C-H aliphatic), 1615 and 1506 (C=C aromatic),1375 (-CH_3), 1260 (C-O); ^{1}H NMR (300 MHz, acetone-d_6), δ (ppm): 0.9 (12H, t; *J* = 7 Hz, CH_3), 1.29-1.35 (16H, $(CH_2)_2$), 2.30 (8H, q; *J* = 7.7 Hz, CH-$\underline{CH_2}$), 4.3 (4H, t; *J* = 7.6 Hz, -CH bridge), 6.24 (4H, s, Ar-H *ortho* to OH), 7.58 (4H, s, Ar-H *meta* to OH), 8.51 (8H, s, OH); ^{13}C NMR (75 MHz, acetone-d_6), δ (ppm): 14.6, 23.4, 31.3, 33.9, 34.3, 103.1, 124.4, 124.5, 151.9 (Tunstad *et al.*, 1989). ESI-MS for $C_{44}H_{56}O_8$: m/z 711.3897 $(M-H)^-$. Observed: m/z 711.3904; the desired compound did not need any further purification.

7.1.3.3 Synthesis of Calix[4]resorcinarene 44b

Procedure 1; resorcinol **11a** (11.01 g, 100 mmol) and octanal (12.82 g, 100 mmol); giving a yellow solid in (16.49 g, 91 % yield); m.p. (300-301 °C) (Macarov, 2018). FTIR (cm^{-1}): 3209 (OH group), 2923 (Ar-CH), 2855 (C-H aliphatic), 1616 and 1506 (C=C aromatic), 1456 (-CH_3), 1169 (C-O); ^{1}H NMR (300 MHz, acetone-d_6), δ (ppm): 0.89-0.91 (12H, m, CH_3), 1.38-1.41 (40H, m, $(CH_2)_5$), 2.29-2.31 (8H, m, CH-$\underline{CH_2}$), 4.29 (4H, t; *J* = 7.8 Hz, -CH bridge), 6.25 (4H, s, Ar-H *ortho* to OH), 7.55 (4H, s, Ar-H *meta* to OH), 8.66 (8H, s, OH); ^{13}C NMR (75 MHz, acetone-d_6), δ (ppm): 14.4, 23.4 30.3, 30.4, 30.5, 30.7, 32.7, 34.3, 103.7, 125.2, 125.4, 152.6; ESI-MS for $C_{56}H_{80}O_8$: m/z 879.5775 $(M-H)^-$. Observed: m/z 879.5782; the solid product did not need any further purification.

7.1.3.4 Synthesis of Calix[4]resorcinarene 44c

Procedure 2; 2-methyl resorcinol **11c** (12.41 g, 100 mmol) and pentanal (8.61 g, 100 mmol); giving a light orange solid in (18.19 g, 95 % yield); m.p. (290-291 ºC); FTIR (cm^{-1}): 3384 (OH group), 2928-2861 (C-H aliphatic), 1615 and 1473 (C=C aromatic), 1337 (-CH_3), 1260 (C-O), 735-770 (Ar-CH_3); ^{1}H NMR (300 MHz, DMSO-d_6), δ (ppm):

0.86 (12H, t; *J* = 7.3 Hz, CH_3), 1.26-1.31 (16H, m, $(CH_2)_2$),1.93 (12H, s, Ar-CH_3), 2.19-2.23 (8H, m, CH-$\underline{CH_2}$), 4.18 (4H, t; *J* = 7.8 Hz, -CH bridge), 7.28 (4H, s, Ar-H, *meta* to OH), 8.69 (8H, s, Ar-OH); ^{13}C NMR (75 MHz, DMSO-d_6), δ (ppm): 10.3, 14.2, 22.1, 30.3, 32.6, 34.1, 111.5, 121.2, 124.8, 148.9; ESI-MS for $C_{48}H_{64}O_8$: m/z 767.4523 $(M-H)^-$. Observed: m/z 767.4507; the material did not need any further purification.

7.1.3.5 Synthesis of Calix[4]resorcinarene 44d

Procedure 2; 2-methyl resorcinol **11c** (12.41 g, 100 mmol) and octanal (12.82 g, 100 mmol); giving a yellow powder in (21.97 g, 94 % yield); m.p.(284-285 ºC)); FTIR (cm^{-1}): 3383 (OH group), 2923 (Ar-CH), 2854 (C-H aliphatic), 1611 and 1473 (C=C aromatic),1261 (-CH_3), 1261 (C-O), 894 (ArCH_3); ^{1}H NMR (300 MHz, DMSO-d_6), δ (ppm): 0.85 (12H, t; *J* = 7.3 Hz, CH_3), 1.29-1.35 (40H, m, $(CH_2)_5$), 1.93 (12H, s, Ar-CH_3), 2.27-2.31 (8H, m, CH-$\underline{CH_2}$), 4.17 (4H, t; *J* = 7.9 Hz, -CH bridge), 7.22 (4H, s, Ar-H, *meta* to OH), 8.69 (8H, s, Ar-OH); ^{13}C NMR (75 MHz, DMSO-d_6), δ (ppm): 10.2, 14.2, 22.1, 28.4, 29.4, 29.6, 31.8, 33.6, 34.7, 112.1, 121.2, 125.2, 149.5 (Castillo-aguirre *et al.*, 2017; Cram *et al.*, 1988). ESI-MS for $C_{60}H_{88}O_8$: m/z 935.6401 $(M-H)^-$. Observed: m/z 935.6414; the solid product was suitable to be used for next reactions without any additional purification.

7.1.3.6 Synthesis of Calix[4]pyrogallolarene 44e

Procedure 1; 2-hydroxyl resorcinol (pyrogallol) **11e** (12.61 g, 100 mmole) and pentalnal (8.61 g, 100 mmol); giving a light pink solid in (13.15 g, 68 % yield); m.p. (293-294 °C); FTIR (cm^{-1}): 3420, 3100 (OH group), 2924 (C-H aliphatic), 1472 (C=C aromatic), 1296 (C-O), 874; ^{1}H NMR (300 MHz, acetone-d_6), δ (ppm): 0.90 (12H, t; *J* = 7.2 Hz, CH_3), 1.35-1.41 (16H, m, $(CH_2)_2$), 2.29 (8H, q; *J* = 7.6 Hz, CH-$\underline{CH_2}$), 4.34

(4H, t; *J* = 7.8 Hz, -CH bridge), 7.13 (4H, s, Ar-H *meta* to OH), 7.32 (4H, br.s, OH), 8.13 (8H, br.s, Ar-OH); ^{13}C NMR (75 MHz, acetone-d_6), δ (ppm): 13.5, 22.3, 30.2, 32.5, 33.9, 113.3, 124.7, 132.5, 138.9; (Gerkensmeier *et al.*, 1999). The material was suitable to be used for next reactions without any additional purification.

7.1.3.7 Synthesis of Calix[4]pyrogallolarene 44f

Procedure 1; 2-Hydroxyl resorcinol (pyrogallol) **11e** (12.61 g, 100 mmol) and octanal (12.82 g, 100 mmol); giving a dark purple powder in (17.46 g, 74 % yield); m.p. (272-273 °C); FTIR (cm^{-1}): 3383 (OH group), 2923-2854 (C-H aliphatic), 1611 and 1473 (C=C aromatic), 1456, 1336, 1280, (C-O), 894; ^{1}H NMR (300 MHz, acetone-d_6), δ (ppm): 0.91 (12H, t; *J* = 7.1 Hz, CH_3), 1.38-1.42 (40H, m, $(CH_2)_5$), 2.18-2.29 (8H, m, CH-$\underline{CH_2}$), 4.34 (4H, t; *J* = 7.9 Hz, -CH bridge), 7.12 (4H, s, Ar-H *meta* to OH), 7.27 (4H, br.s, Ar-OH), 8.16 (8H, s, OH); ^{13}C NMR (75 MHz, acetone-d_6), δ (ppm): 14.4, 23.4, 30.5, 30.6, 30.7, 32.7, 33.9, 35.0, 114.4, 125.7, 133.7,140.1 (Gerkensmeier *et al.*, 1999). The material was suitable to be used for next reactions without any additional purification.

7.1.4 Modification of Calix[4]resorcinarenes 44 (Elidrisi *et al.*, 2015; Fransen & Dutton, 1995).

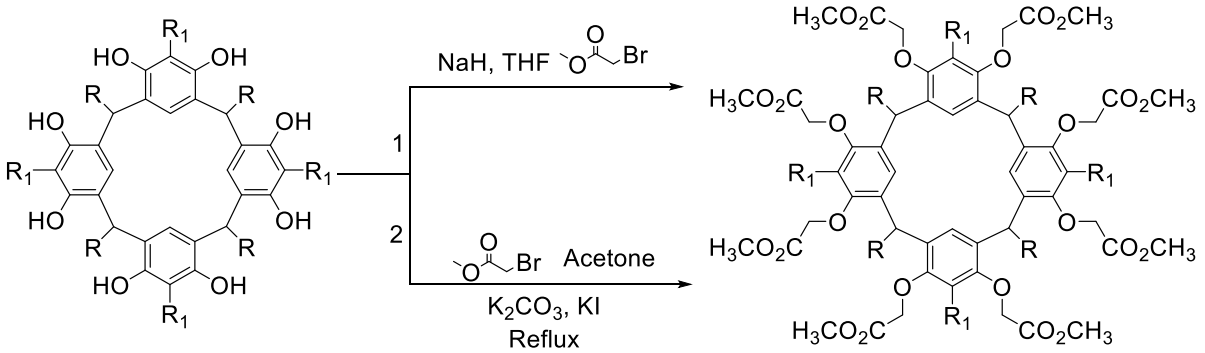

Calix[4]resorcinarene

44a R= n-C_4H_9, R_1= H
44b R= n-C_7H_{15}, R_1= H
44c R= n-C_4H_9, R_1= CH_3
44d R= n-C_7H_{15}, R_1= CH_3
44e R= n-C_4H_9, R_1= OH
44f R= n-C_7H_{15}, R_1= OH

Calix[4]resorcinarene-octa-ester

45a R= n-C_4H_9, R_1= H
45b R= n-C_7H_{15}, R_1= H
45c R= n-C_4H_9, R_1= CH_3
45d R= n-C_7H_{15}, R_1= CH_3
45e R= n-C_4H_9, R_1= CO_2CH_3
45f R= n-C_7H_{15}, R_1= CO_2CH_3

Scheme 19: Synthesis of octa-ester calix[4]resorcinarenes **45a-d** and dodeca-ester calix[4]pyrogallolarenes **45e-f**.

General procedures for alkylation of alkyl calix[4]resorcinarenes and calix[4]pyrogallolarenes:

1. A suspended solution of sodium hydride (3.42 g, 86 mmol); free from mineral oil by washing with petroleum ether (bp 40-60 °C) (15 mL × 3) in dry THF (15 mL) was stirred at room temperature under a nitrogen atmosphere. A solution of compounds **44a-d** (4 mmol) in dry THF (20 mL) was added slowly to the suspension solution and stirred at room temperature for at least 1 h under a nitrogen atmosphere. Methyl bromoacetate (13.12 g, 86 mmol) was added to the mixture and heated to reflux for 24 h under nitrogen atmosphere (Scheme 19). After cooling to room temperature the solvent was removed under reduced pressure. The residue was taken up in dichloromethane (DCM) (100 mL) and washed with water (100 mL × 3). The organic

layers were collected and dried over magnesium sulfate ($MgSO_4$), filtered and the solvent was removed under reduced pressure.

2. To a stirred suspension of compounds **44a-f** (4 mmol), anhydrous potassium carbonate (5.52 g, 40 mmol), and a catalytic amount of potassium iodide (0.03 g, 0.2 mmol) in anhydrous acetone (120 mL), methyl bromoacetate (4.90 g, 32 mmol) was added in one portion at room temperature. The mixture was stirred and heated to reflux under nitrogen atmosphere for 48 h (Scheme 19). After removed acetone, the residue was suspended in sodium thiosulfate aqueous solution (5 %, 30 mL) for 0.5 h, and then extracted with dichloromethane (20 mL × 3). The organic extract was dried over magnesium sulfate, filtered and concentrated to (15 mL). The product was precipitated upon the addition of cold ice methanol.

7.1.4.1 Synthesis of Calix[4]resorcinarene 45a

Procedure 1; clix[4]resorcinarene **44a** (2.85 g, 4 mmol); giving light brown like solid in (5 g, 91 % yield); m.p. (85-86 ºC); FTIR (cm^{-1}): 2955, 2927, 2820, 1754, 1727, 1609, 1580, 1495, 1435, 1497,1207,1176,1129; ^1H NMR (300 MHz, $CDCl_3$), δ (ppm): 0.91 (12H, br.s, CH_3), 1.30-1.39 (16 H, m, $(CH_2)_2$), 1.90-1.93 (8H, m, CH-$\underline{CH_2}$), 3.72 (24H, s, OCH_3), 4.44 (16H, s, Ar-O-CH_2), 4.69 (4H, t; *J* = 7.2 Hz, -CH bridge), 6.47 (4H, s, Ar-H), 6.7 (4H, s, Ar-H); ^{13}C NMR (75 MHz, $CDCl_3$), δ (ppm): 14.5, 23.6, 31.2, 34.5, 36.5, 52.0, 52.7, 67.2, 101.1, 126.7, 128.2, 155.5, 170.3; ESI-MS for $C_{69}H_{90}O_{24}$: m/z 1306.6010 $(M+NH_4)^+$. Observed: m/z 1306.6028.

Procedure 2; calix[4]resorcinarene **44a** (2.85 g, 4 mmol); giving a yellow powder in (4.12 g, 80 % yield); m.p. (85-86 ºC); FTIR (cm^{-1}): 2945, 2927, 2830, 1754, 1727, 1609, 1584, 1499, 1435, 1305, 1176,1122; ^1H NMR (300 MHz, $CDCl_3$), δ (ppm): 0.87 (12H, t; *J* = 7.3 Hz, CH_3), 1.31-1.35 (16 H, m, $(CH_2)_2$),1.86 (8H, q; *J* = 6.7 Hz, CH-

$\underline{CH_2}$), 3.76 (24H, s, OCH_3), 4.28 (16H, s, Ar-O-CH_2), 4.59 (4H, t; *J* = 7.3 Hz, -CH bridge), 6.21 (4H,s, Ar-H), 6.61 (4H, s, Ar-H); ^{13}C NMR (75 MHz, $CDCl_3$), δ (ppm): 14.1, 22.9, 30.2, 34.2, 35.7, 51.9, 67.2, 100.8, 126.6, 128.6, 154.5, 169.8.

7.1.4.2 Synthesis of Calix[4]resorcinarene 45b

Procedure 1; calix[4]resorcinarene **44b** (3.53 g, 4 mmol); giving a viscous brown solid in (6 g, 96 % yield); m.p. (101-102 ºC); FTIR (cm^{-1}): 2925, 2970, 2852, 1758, 1731, 1610, 1587, 1504, 1436, 1177, 1126, 1081; ^{1}H NMR (300 MHz, $CDCl_3$), δ (ppm): 0.87 (12H, t; *J* = 6.5 Hz, CH_3), 1.33-1.37 (40H, m, $(CH_2)_5$),1.86-1.90 (8H, m, CH-$\underline{CH_2}$), 3.73 (24H, s, OCH_3), 4.59 (16H, s, Ar-O-CH_2), 4.69 (4H, t; *J* = 7.3 Hz, -CH bridge), 6.21 (4H, s, Ar-H), 6.61 (4H, s, Ar-H); ^{13}C NMR (75 MHz, $CDCl_3$), δ (ppm): 13.5, 22.5, 30.4, 31.7, 31.9, 32.8, 34.6, 35.6, 51.1, 66.4, 100.4, 126.1, 127.7, 145.7, 169.4; ESI-MS for $C_{81}H_{114}O_{24}$: m/z 1474.7887 $(M+NH_4)^+$. Observed: m/z 1474.7894 (Fransen & Dutton, 1995).

Procedure 2; calix[4]resorcinarene **44b** (3.53 g, 4 mmol); giving a yallow powder in (5.82 g, 93 % yield); m.p. (101-102 ºC); FTIR (cm^{-1}): 2925, 2950, 2825, 1758, 1731, 1610, 1587, 1504, 1436, 1286, 1176, 1129, 1004; ^{1}H NMR (300 MHz, $CDCl_3$), δ (ppm): 0.85 (12H, br.s, CH_3), 1.27-1.30 (16H, m, $(CH_2)_5$), 1.80-1.85 (8H, m, CH-$\underline{CH_2}$), 3.75 (24H, s, OCH_3), 4.28 (16H, s, Ar-O-CH_2), 4.57 (4H, t; *J* = 7.2 Hz, -CH bridge), 6.21 (4H, s, Ar-H), 6.61 (4H, s, Ar-H); ^{13}C NMR (75 MHz, $CDCl_3$), δ (ppm): 14.1, 23.4, 30.4, 31.8, 31.9, 32.0, 34.5, 35.7, 51.9, 67.2, 101.4, 126.9, 128.3, 155.5; (Fransen & Dutton, 1995; R. Zhou *et al*., 2010).

7.1.4.3 Synthesis of Calix[4]resorcinarene 45c

Procedure 1; calix[4]resorcinarene **44c** (3.53 g, 4 mmol); giving an off-white powder in (4.35 g, 76 % yield); m.p. (124-125 ºC); FTIR (cm^{-1}): 2954, 2940, 2890, 1759,

1738, 1599, 1495, 1435, 1380, 1283,1200,1109; ^{1}H NMR (400 MHz, $CDCl_3$), δ (ppm): 0.91 (12H, br.s, CH_3), 1.19-1.27 (16H, m, $(CH_2)_2$), 1.81-1.86 84 (8H, m, CH-$\underline{CH_2}$), 2.06 (12H, s, Ar-CH_3), 3.73 (24H, s, OCH_3), 4.16 (16H, s, Ar-O-CH_2), 4.39 (4H, t; *J* = 7.1 Hz, -CH bridge), 6.38 (4H, s, Ar-H); ^{13}C NMR (100 MHz, $CDCl_3$), δ (ppm): 9.9, 13.6, 22.6, 28.4, 34.9, 37.9, 51.6, 54.6, 70.5, 123.7, 124.5, 133.6, 135.9, 154.1, 169.3

Procedure 2; calix[4]resorcinarene **44c** (3.53 g, 4 mmol); giving white crystals in (3.89 g, 68 % yield); m.p. (124-125 ºC); FTIR (cm^{-1}): 2954, 2940, 2890, 1759, 1738, 1599, 1495, 1435, 1380, 1283,1200,1109; ^{1}H NMR (400 MHz, $CDCl_3$), δ (ppm): 0.90 (12H, br.s, CH_3), 1.34-1.37 (16H, m, $(CH_2)_2$),1.89-1.91 (8H, m, CH-$\underline{CH_2}$), 2.13 (12H, s, Ar-CH_3), 3.80 (24H, s, OCH_3), 4.19 (16H, s, Ar-O-CH_2), 4.50 (4H, t; *J* = 7.1 Hz, -CH bridge), 6.48 (4H, s, Ar-H); ^{13}C NMR (100 MHz, $CDCl_3$), δ (ppm): 10.0, 14.1, 22.9, 30.6, 31.8, 34.9, 51.9, 69.4, 123.5, 124.5, 133.8, 153.8, 169.3; ESI-MS for $C_{72}H_{96}O_{24}$: m/z 1362.6636 $(M+NH_4)^+$. Observed: m/z 1362.6637

7.1.4.4 Synthesis of Calix[4]resorcinarene 45d

Procedure 1; calix[4]resorcinarene **44d** (3.08 g, 4 mmol); giving a white powder in (5 g, 77 % yield); m.p. (89-90 ºC); FTIR (cm^{-1}): 2925, 2853, 1754, 1436, 1382, 1202, 1111, 1074, 981; ^{1}H NMR (400 MHz, $CDCl_3$), δ (ppm): 0.84 (12H, t; *J* = 6.3 Hz , CH_3), 1.22-1.32 (40H, m, $(CH_2)_5$), 1.87-1.88 (8H, m, CH-$\underline{CH_2}$), 2.13 (12H, s, Ar-CH_3), 3.76 (24H, s, OCH_3), 4.22 (16H, s, Ar-O-CH_2), 4.46 (4H, t; *J* = 6.9 Hz, -CH bridge), 6.44 (4H, br.s, Ar-H); ^{13}C NMR (100 MHz, $CDCl_3$), δ (ppm): 9.9, 14.1, 22.7, 28.5, 29.45, 30.0, 32.1, 35.2, 38.0, 51.9, 69.4, 123.5, 124.5, 133.8, 153.7, 169.3; ESI-MS for $C_{84}H_{120}O_{24}$: m/z 1530.8513 $(M+NH_4)^+$. Observed: m/z 1530.8524

Procedure 2; calix[4]resorcinarene **44d** (3.08 g, 4 mmol); giving an off-white powder in (5.6 g, 86 % yield); m.p. (89-90 ºC); FTIR (cm^{-1}): 2925, 2853, 1754, 1436, 1382,

1202, 1111, 1074, 981; ^{1}H NMR (400 MHz, $CDCl_3$), δ (ppm): 0.88 (12H, t; *J* = 5.9 Hz, CH_3), 1.28-1.34 (40H, m, $(CH_2)_5$), 1-85-1.90 (8H, m, CH-$\underline{CH_2}$), 2.16 (12H, s, Ar-CH_3), 3.79 (24H, s, OCH_3), 4.18 (16H, s, Ar-O-CH_2), 4.49 (4H, t; *J* = 6.5 Hz , -CH bridge), 6.47 (4H, br.s, Ar-H); ^{13}C NMR (100 MHz, $CDCl_3$), δ (ppm): 10.2, 14.1, 22.7, 28.0, 29.4, 29.9, 32.0, 35.2, 38.0, 51.9, 69.3, 123.5, 124.5, 133.8, 154.5, 169.2

7.1.4.5 Synthesis of Calix[4]pyrogallolarene 45e

Procedure 2; calix[4]pyrogallolarenes **44e** (3.11 g, 4 mmol); giving a white powder in (4.67 g, 71 % yield); m.p. (104-105 ºC); R_f (0.36) (ethyl acetate: petroleum ether 3:1 v/v); FTIR (cm^{-1}): 2954, 2830, 1750, 1435, 1384, 1205,1150, 1083, 891; ^{1}H NMR (400 MHz,, $CDCl_3$), δ (ppm): 0.88 (12H, t; *J* = 6.2 Hz, CH_3), 1.30-1.34 (16H, br.s, $(CH_2)_2$), 1.83-1.84 (8H, m, CH-$\underline{CH_2}$), 3.74 (36H, s, OCH_3), 4.58 (24H, s, Ar-OCH_2), 4.63 (4H, t; *J* = 7.2 Hz, -CH bridge), 6.43 (4H, br.s, Ar-H); ^{13}C NMR (100 MHz, $CDCl_3$), δ (ppm): 14.0, 22.6, 30.9, 34.9, 37.1, 51.6, 60.7, 69.9, 121.5, 133.9, 143.1, 147.9, , 169.5; ESI-MS for $C_{80}H_{104}O_{36}$:m/z 1658.6651 $(M+NH_4)^+$. Observed: m/z 1658.6669

7.1.4.6 Synthesis of Calix[4]pyrogallolarene 45f

Procedure 2; Calix[4]pyrogallolarenes **44f** (3.78 g 4 mmol); givind an off-white powder in (4.23 g, 58 % yield); m.p. (64-65 ºC); FTIR (cm^{-1}): 2926, 2855, 1754, 1436, 1204, 1110, 1084, 892; ^{1}H NMR (400 MHz, $CDCl_3$), δ (ppm): 0.89 (12H, t; *J* = 6 Hz, CH_3), 1.27-1.31 (40H, m, $(CH_2)_5$), 1.78-1.82 (8H, m, CH-$\underline{CH_2}$), 3.74 (36H, s, $COOCH_3$), 4.52 (4H, t; *J* = 7.2 Hz, -CH bridge), 4.62 (24H, s, Ar-O-CH_2), 6.43 (4H, br.s, Ar-H); ^{13}C NMR (100 MHz, $CDCl_3$), δ (ppm): 14.1, 22.7, 28.1, 29.4, 29.9, 32.0, 35.2, 37.1, 52.2, 60.7, 69.6, 121.5, 143.1, 147.9, 169.5; ESI-MS for $C_{92}H_{128}O_{36}$: m/z 1826.8529 $(M+NH_4)^+$. Observed: m/z 1826.8560

7.1.5 Synthesis of Calix[4]resorcinarenes Octa-Sodium Salt 46a-d and Calix[4]pyrogallolarenes Dodeca-Sodium Salt 46e-f.

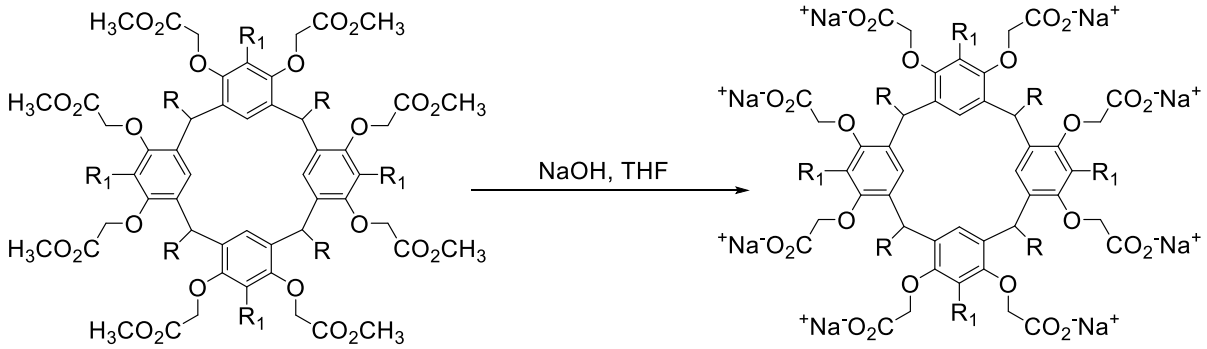

45a R= C_4H_9, R_1= H
45b R= C_7H_{15}, R_1=H
45c R= C_4H_9, R_1= CH_3
45d R= C_7H_{15}, R_1= CH_3
45e R= C_4H_9, R_1= $CH_2CO_2CH_3$
45f R= C_7H_{15}, R_1= $CH_2CO_2CH_3$

46a R= C_4H_9, R_1= H
46b R= C_7H_{15}, R_1=H
46c R= C_4H_9, R_1= CH_3
46d R= C_7H_{15}, R_1= CH_3
46e R= C_4H_9, R_1= CH_2CO_2Na
46f R= C_7H_{15}, R_1= CH_2CO_2Na

Scheme 20: The synthesis of calix[4]resorcinarene-octa-sodium and calix[4]pyrogallolarene dodeca-sodium

General procedure for the synthesis of calix[4]resorcinarenes octa-sodium and calix[4]pyrogallolarenes dodeca-sodium

A solution of calix[4]resorcinarene **45a-d** and calix[4]pyrogallolarenes **45e-f** (3 mmol) in dry THF (20 mL) was stirred at room temperature for 15 min followed by the addition of an aqueous solution of sodium hydroxide (75 mmol, 1 M solution.). The reaction mixture was stirred overnight at ambient temperature (Scheme 20). After which time a light yellowish solution was formed, and the product was precipitated upon the addition of acetone. The excess of sodium hydroxide was destroyed by careful addition of acetone and water and the solvent evaporated under reduced the pressure. The product was dried in freeze dryers**.**

7.1.5.1 Synthesis of Calix[4]resorcinarene 46a

Calix[4]resorcinarene **45a** (3.86 g, 3 mmol); giving a light brown powder in (2.53 g, 86 % yield); m.p. (>300 ºC); FTIR (cm^{-1}): 2926, 2855, 1754, 1436, 1204,1110, 1084, 892; ^{1}H NMR (400 MHz, D_2O), δ (ppm): 0.74 (12H, t; *J* = 7 Hz, CH_3), 1.17-1.21 (16H, m, $(CH_2)_2$), 1.75-1.83 (8H, m, CH-$\underline{CH_2}$), 4.02 (16H, s, Ar-O-CH_2COONa), 4.49 (4H, t; *J* = 6.8 Hz, -CH bridge), 6.21 (4H, br.s, Ar-H), 6.63 (4H, s, Ar-H); ^{13}C NMR (100 MHz, D_2O), δ (ppm): 13.5, 22.7, 29.7, 31.7, 35.1, 68.9, 100.8, 126.6, 128.5,154.7, 177.1

7.1.5.2 Synthesis of Calix[4]resorcinarene 46b

Calix[4]resorcinarene **53b** (4.36 g, 3 mmol); affording a prown powder in (4.71 g, 98 % yield); m.p. (>300 ºC); FTIR (cm^{-1}): 2928, 2852, 1754, 1430, 1206,1120, 1086; ^{1}H NMR (400 MHz, D_2O), δ (ppm): 0.64 (12H, br.s, CH_3), 1.09-1.20 (40H, m, $(CH_2)_5$), 1.66-1.70 (8H, m, CH-$\underline{CH_2}$), 4.01 (16H, br.s, Ar-O-CH_2COONa), 4.45 (4H, t; *J* = 7.2 Hz, -CH bridge), 6.14 (4H, br.s, Ar-H), 6.55 (4H, s, Ar-H); ^{13}C NMR (100 MHz, D_2O), δ (ppm): 13.5, 22.7, 29.7, 30.4, 31.7, 31.7, 31.9, 35.1, 68.9, 103.7, 125.2, 125.4, 154.7, and 177.1

7.1.5.3 Synthesis of Calix[4]resorcinarene 46c

Calix[4]resorcinarene **45c** (4.8 g, 4 mmol); giving a light yellow powder in (4.00 g, 95 % yield); m.p. (>300 ºC), FTIR (cm^{-1}): 2930, 2840, 1750, 1430, 1201, 1112, 1084; ^{1}H NMR (400 MHz, D_2O), δ (ppm): 0.71 (12H, t; *J* = 6.4 Hz,CH_3), 1.18-1.21 (16H, m, $(CH_2)_2$), 1.76-1.78 (8H, m, CH-$\underline{CH_2}$), 2.01 (12H, br.s, Ar-CH_3), 3.87 (16H, s, Ar-O-CH_2COONa), 4.55 (4H, t; *J* = 7.2 Hz, -CH bridge), 6.82 (4H, s, Ar-H); ^{13}C NMR (100 MHz, D_2O), δ (ppm): 10.1, 13.5, 22.4, 29.9, 36.2, 36.4, 71.4, 124.9, 124.1, 153.8, 176.6.

7.1.5.4 Synthesis of Calix[4]resorcinarene 46d

Calix[4]resorcinarene **45d** (5.4 g, 3 mmol); giving a yellow powder in (5.4 g, 96 % yield); m.p. (300> ºC); FTIR (cm^{-1}): 2935, 2848, 1752, 1433, 1205, 1116, 1086, 980; ^{1}H NMR (400 MHz, D_2O), δ (ppm): 0.67 (12H, br.s, CH_3), 1.16-1.25 (40H, m, $(CH_2)_5$), 1.76-1.80 (8H, m, CH-$\underline{CH_2}$), 1.96 (12H, br.s, Ar-CH_3), 4.00 (16H, br.s, Ar-O-CH_2COONa), 4.56 (4H, t; *J* = 7.2 Hz, -CH bridge), 6.81 (4H, br.s, Ar-H); ^{13}C NMR (100 MHz, D_2O), δ (ppm): 9.8, 14.0, 22.4, 28.1, 28.8, 29.9, 31.8, 36.2, 36.8, 71.7, 153.8,176.4

7.1.5.5 Synthesis of Calix[4]pyrogallolarene 46e

Calix[4]pyrogallolarenes **45e** (5.86 g, 4 mmol); giving a white powder in (5.4 g, 92 % yield); m.p. (>300 ºC); FTIR (cm^{-1}): 2957, 2160, 1602, 1432, 1205, 1032, 863, 686; ^{1}H NMR (400 MHz, D_2O), δ (ppm): 0.68 (12H, br.s, CH_3), 1.17-1.22 (16H, m, $(CH_2)_2$), 1.69-1.73 (8H, m, CH-$\underline{CH_2}$), 4.06 (24H, s, Ar-O-CH_2COONa), 4.56-4.59 (4H, m, -CH bridge), 6.81 (4H, br.s, Ar-H,); ^{13}C NMR (100 MHz, D_2O), δ (ppm): 22.7, 29.8, 36.0, 36.2, 71.0, 143.8, 168.4, 176.2

7.1.5.6 Synthesis of Calix[4]pyrogallolarene 46f

Calix[4]pyrogallolarenes **45f** (6.46 g, 3 mmol); giving white powder in (5 g, 77 % yield); m.p. (>300 ºC); FTIR (cm^{-1}): 2924, 2160, 1599, 1417, 1340, 1057, 878, 652; ^{1}H NMR (400 MHz, D_2O), δ (ppm): 0.61 (12H, br.s, CH_3), 1.10-1.25 (16H, m, $(CH_2)_5$), 1.66-1.72 (8H, m, CH$\underline{CH_2}$), 4.04 (24H, s, Ar-O-CH_2COONa), 4.49 (4H, t; *J* = 7.2 Hz, -CH bridge), 6.49 (4H, br.s, Ar-H); ^{13}C NMR (100 MHz, D_2O), δ (ppm): 22.2, 27.2, 28.6, 29.8, 31.8, 35.3, 35.9, 70.8, 72.6, 143.2, 166.4, 176.36

7.1.6 Synthesis of Model Drug Analogue LO9 57

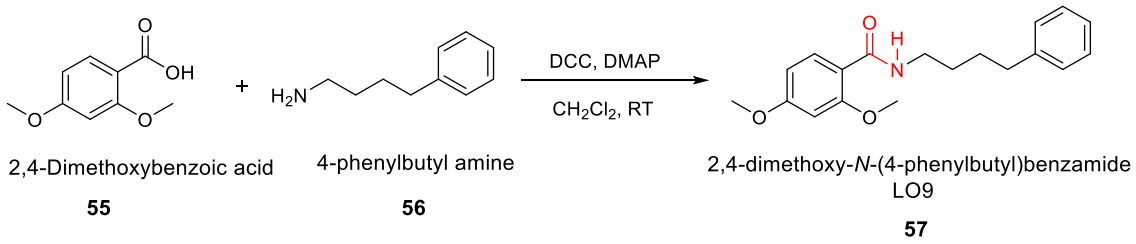

2,4-Dimethoxybenzoic acid **55**

4-phenylbutyl amine **56**

2,4-dimethoxy-*N*-(4-phenylbutyl)benzamide LO9 **57**

Scheme 21: Synthesis of model drug analogue LO9 **57**

A solution of 2,4-dimethoxybenzoic acid **55** (1.09 g, 6 mmol) in dichloromethane (40 mL) was stirred at room temperature. To this mixture was added 4-phenylbutylamine **56** (0.895 g, 6 mmol) in one portion followed by dicyclohexylcarbodiimide (DCC), (1.238 g, 6 mmol) and 4-dimethylaminopyridine (DMAP), (50 mg, 0.4 mmol). The reaction mixture was stirred at room temperature for 72 h (Scheme 21). TLC conducted during the course of the reaction; after the completion of the reaction a white precipitate was formed, and then the reaction mixture was filtered. The filtrate was distilled off under reduced pressure on the rotary evaporator to remove dichloromethane. The resulting yellow solid was subjected to column chromatography (SiO_2; (ethyl acetate: petroleum ether 1:1 v/v; R_f= 0.44)) affording 2,4-dimethoxy-*N*-(4-phenylbutyl)benzamide as a colourless crystals LO9 **57** (1.32 g, 70 % yield); m.p. (80-81 ºC); FTIR (cm^{-1}): shows common peaks relating to the N-H stretch of the amide at 3322 cm^{-1}, 2926 cm^{-1}, and 2849 cm^{-1}. Other peaks identified at 1571 cm^{-1} were due to the C-C in the aromatic ring, 1623 cm^{-1} for the C=O stretch; further C=C stretches were also identified at 1435 cm^{-1}, 1242, 1044 cm^{-1}; The ^1H NMR spectrum of LO9 **57** was acquired as a solution in $CDCl_3$ and showed characteristic signals at δ (ppm) = 1.69 (4H, m, 2 × CH_2), 2.67 (2H, t; *J* = 7.4 × (2) Hz, $ArCH_2$), 3.47 (2H, m, CH_2N), 3.85 (3H, s, OCH_3), 3.90 (3H, s, OCH_3), 6.47 (1H, d;

J = 2.3 Hz, Ar-H), 6.59 (1H, br.s, Ar-H), 7.18-7.20 (3H, m, Ar-H), 7.28-7.30 (2H, m, Ar-H), 7.75 (1H, br.s, CONH), 8.18 (1H, d; *J* = 8.8 Hz, Ar-H), ^{13}C NMR (75 MHz, $CDCl_3$), δ (ppm): 28.9, 29.3, 35.6, 39.5, 55.5, 125.8, 126.9, 128.3, 128.9, 133.0, 133.9, 142.2, 158.7, 163.1, 164.0, 165 (Kunishima *et al.*, 2001; Arnold *et al.*, 2006; Holzschneider *et al.*, 2019).

7.1.7 Modification of Calix[4]resorcinarenes 44a-b to Prepare Aminocalix[4]resorcinarenes 58a-d (Shivanyuk & Rebek, 2001).

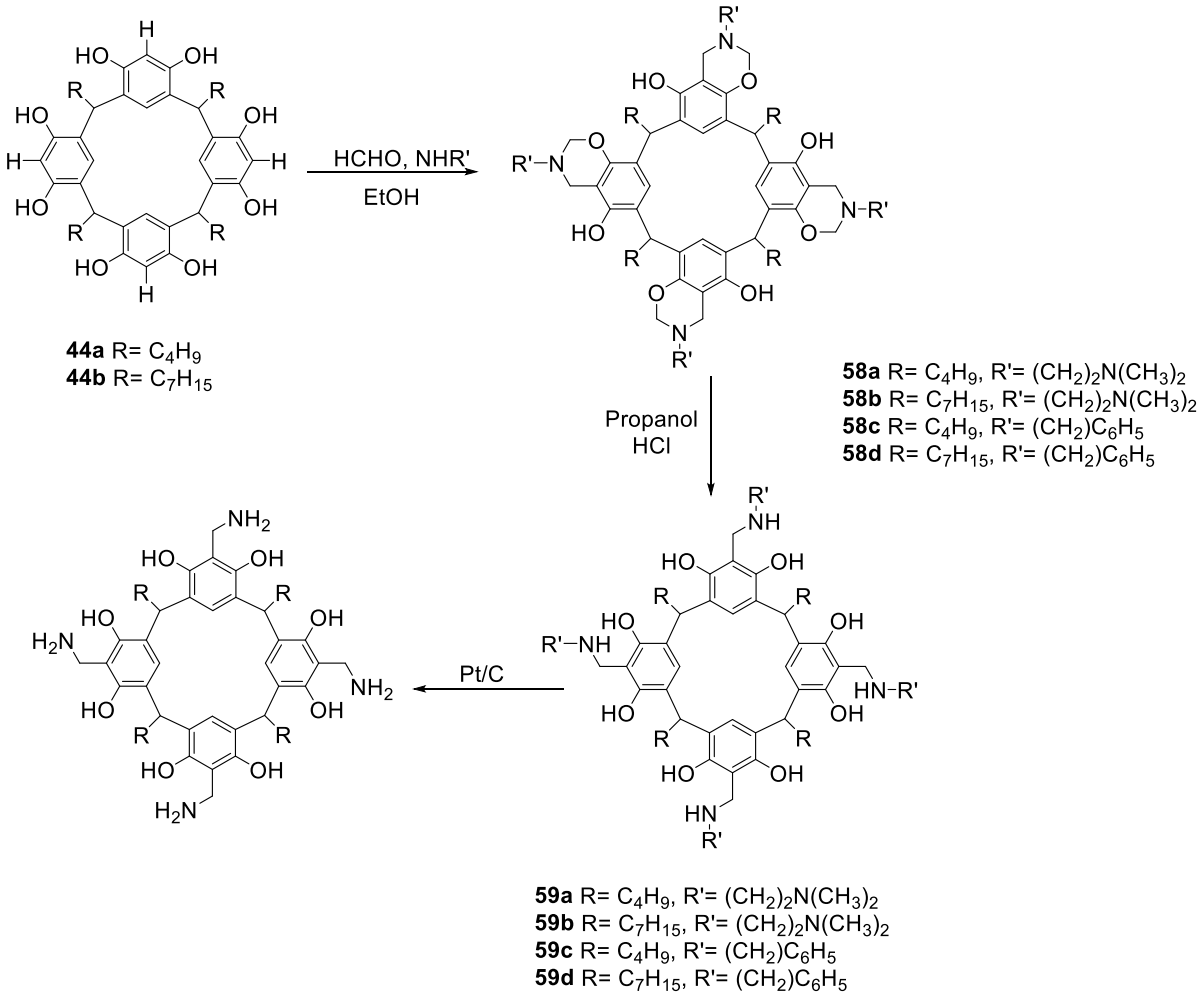

Scheme 22: Synthesis of aminocalix[4]resorcinarene.

cis Isomers **44a-b** are subject to further modification in 2-position of the resorcinol units using the Mannich reaction to prepare the aminocalix[4]resorcinarene in two steps. First of all tetrabutyl calix[4]resorcinarene **44a** and tetraheptyl calix[4]resorcinarene **44b** were transformed to tetrabenzoxazines **58a-d** by the condensation with primary amines (*N,N*-dimethylethylenediamine or benzyl amine) and an excess of formaldehyde in ethanol using a known procedure, the condensation leads to the formation of benzoxazine rings. The second step including the removal of the *N,O*-acetal bridge to produce **59a-d.**

General procedure for the synthesis of tetraoxazines 58

To a stirred solution of calix[4]resorcinarene **44** (5.5 mmol) in ethanol (50 mL), formaldehyde (37 %, 10 mL, 40 mmol) was added slowly followed by dropwise addition of amine (40 mmol). Then the mixture reaction was stirred at room temperature for 24 h (Scheme 22). The crude product was treated with acetonitrile. The precipitate that formed was filtered off and washed with acetonitrile (10 mL) dried in vacuo oven at 60 ºC for 24 h.

7.1.7.1 Synthesis of Calix[4]resorcinarene 58a

Calix[4]resorcinarene **44a** (3.92 g, 5.5 mmol); *N,N*-dimethylethylenediamine (3.526 g, 40 mmol); affording a brown powder in (4.86 g, 76 % yield); m.p. (85-86 ºC); FTIR (cm^{-1}): 3167 (OH), 2924-2857 (C-H aliphatic), 1595 and 1558 (C=C aromatic), 1457 ,1375 ($-CH_3$), 1218 (C-N), 1124 (CO); ^{1}H NMR (300 MHz, $CDCl_3$) δ (ppm): 0.91 (12H, t; *J* = 7.3 Hz, CH_3), 120-1.25 (16H, m, $(CH_2)_2$), 1.35-1.40 (8H, m, $CH\text{-}\underline{CH_2}$), 2.24 (24H, s, $N(CH_3)_2$), 2.43 (8H, t; *J* = 6.8 Hz, $\underline{CH_2}N(CH_3)_2$), 2.55 (8H, t; *J* = 6.7 Hz, $\underline{CH_2}CH_2N(CH_3)_2$), 3.89 (8H, s, NCH_2Ar), 4.2 (4H, t; *J* = 7.3 Hz, -CH bridge), 4.92 (8H, s, NCH_2O), 7.1 (4H, s, Ar-OH), 7.74 (4H, br.s, Ar-H *meta* to OH); ^{13}C NMR (75 MHz,

$CDCl_3$), δ (ppm): 14.2, 22.7, 30.3, 32.7, 33.3, 44.8, 45.7, 45.8, 46.5, 50.7, 57.8, 108.4, 121.1, 123.5, 124.3, 147.9, 149.6

7.1.7.2 Synthesis of Calix[4]resorcinarene 58b

Calix[4]resorcinarene **44b** (4.85 g, 5.5 mmol); *N,N*-dimethyethylenediamine (3.53 g, 40 mmol); giving a brown powder in (5.52 g, 76 % yield); m.p. (75-76 ºC) (Kharitonova *et al*., 2003). FTIR (cm^{-1}): 3194 (OH), 2923-2852 (C-H aliphatic), 1595 and 1462 (C=C aromatic), 1353, 1260 (-CH_3), 1124 (CO), 1083 (C-N), 948; ^{1}H NMR (300 MHz, $CDCl_3$), δ (ppm): 0.89 (12H, t; *J* = 7.2 Hz, CH_3), 1.28-1.33 (40H, m, $(CH_2)_5$), 1.66-1.72 (8H, m, CH-$\underline{CH_2}$), 2.24 (24H, s, $N(CH_3)_2$), 2.42 (8H, t; *J* = 6.9 Hz, $\underline{CH_2}N(CH_3)_2$), 2.85 (8H, t; *J* = 6.7 Hz, $\underline{CH_2}CH_2N(CH_3)_2$), 3.89 (8H, s, NCH_2Ar), 4.19 (4H, t; *J* = 7.3 Hz, -CH bridge), 4.92 (8H, s, NCH_2O), 7.1 (4H, s, Ar-OH), 7.73 (4H, s, Ar-H *meta* to OH); ^{13}C NMR (75 MHz, $CDCl_3$), δ (ppm): 14.1, 22.7, 28.1, 29.4, 29.7, 31.9, 32.7, 33.6, 45.7, 45.8, 45.8, 46.6, 49.3, 49.6, 50.7, 57.6, 57.8, 58.0, 108.4, 121.1, 123.5, 124.3, 147.9, 149.6 (Kharitonova *et al.*, 2003).

7.1.7.3 Synthesis of Calix[4]resorcinarene 58c

Calix[4]resorcinarene **44a** (3.92 g, 5.5 mmol); benzylamine (4.29 g, 40 mmol); giving a pink powder in (6.4 g, 94 % yield); m.p. (102-103 ºC); FTIR (cm^{-1}): 3467 (OH group), 3353 (OH), 2925-2860 (C-H aliphatic), 1601 and 1494 (C=C aromatic), 1455, 1375 (-CH_3), 1135 (CO). 12241050 (C-N); ^{1}H NMR (300 MHz, $CDCl_3$), δ (ppm): 0.94 (12H, t; *J* = 7.3 Hz, CH_3), 2.20-2.23 (16H, m, $(CH_2)_2$), 2.20-2.25 (8H, m, CH-$\underline{CH_2}$), 3.71 (8H, d; *J* = 7.1 Hz, NCH_2Ar), 4.05, 3.8 (each 4H, d; *J* = 7.2 Hz, $ArCH_2N$), 4.26 (4H, t; *J* = 7.8 Hz, -CH bridge), 4.82, 4.9 (each 4H, d; *J* = 7.3 Hz, NCH_2O), 7.20 (20H, m, benzyl-H), 7.30 (4H, br.s, Ar-H *meta* to OH), 7.72 (4H, s, Ar-OH); ^{13}C NMR (75 MHz, $CDCl_3$), δ (ppm): 14.2, 22.7, 30.3, 32.7, 33.4, 46.6, 55.8, 57.0, 58.5, 108.5,

121.3, 123.7, 124.4, 127.1, 127.3, 128.2, 128.9, 129.0, 137.8, 138.4, 148.0 149.8; the desired compound did not need any further purification.

7.1.7.4 Synthesis of Calix[4]resorcinarene 58d

Calix[4]resorcinarene **44b** (4.85 g, 5.5 mmol); benzylamine (4.29 g, 40 mmol); giving a pink powder in (8.02 g, 89 % yield); m.p. (70-71 ºC); FTIR (cm^{-1}): 3362 (OH), 2923-2854 (C-H aliphatic), 1601 and 1471 (C=C aromatic), 1348,(-CH_3), 1225 (CN), 1055 (C-O), 881; ^{1}H NMR (300 MHz, $CDCl_3$), δ (ppm): 0.94 (12H, t; *J* = 7.3 Hz, CH_3), 1.35-1.43 (40H, m, $(CH_2)_5$), 2.22-2.26 (8H, m, CH-$\underline{CH_2}$), 3.72 (8H, d; *J* = 12.2 Hz, NCH_2Ar), 4.05, 3.79 (each 4H, d; *J* = 7.1 Hz, $ArCH_2N$), 4.26 (4H, t; *J* = 7.8 Hz, -CH bridge), 4.9, 4.84 (each 4H, d; *J* = 9.2 Hz, OCH_2N), 7.20 (20H, m, benzyl-H), 7.29 (4H, br.s, Ar-H *meta* to OH), 7.72 (4H, s, Ar-OH); ^{13}C NMR (75 MHz, $CDCl_3$), δ (ppm): 14.18, 22.7, 28.1, 29.4, 29.6, 31.9, 32.7, 33.7 , 46.5, 55.7, 57.0, 58.5, 108.5, 121.3, 123.7, 124.4, 127.1, 127.3, 128.2, 128.9, 129.00, 137.8, 138.4, 148.0, 149.8; the desired compound did not need any further purification.

General procedure of aminocalix[4]resorcinarene 59

To a solution of tetrabezoxazine **58** (3 mmol) in propanol (50 mL), concentrated hydrochloric acid (21 mL) and water (10 mL) were added. The mixture was heated to reflux for 4 h (Scheme 22). After the removal of water and formaldehyde by azeotropic distillation, the remaining propanol was evaporated, ethanol and toluene (1:1) were added and solvents were evaporated in vacuo. The crude product was treated with acetonitrile, filtered off, washed with acetonitrile and dried in vacuo oven at 60 ºC for 24.

7.1.7.5 Synthesis of Calix[4]resorcinarene 59a

Tetrabezoxazine **58a** (3.34 g, 3 mmol); giving a yellowish powder in (3 g, 90 % yield); m.p. (120-121 ºC); FTIR (cm^{-1}): 3329 (OH and NH), 2927-2859 (C-H aliphatic), 1600 (C=C aromatic), 1469 (-CH methine bridge),1303 (-CH3), 1186 (C-N), 983; ^{1}H NMR (300 MHz, $CDCl_3$), δ (ppm): 0.91 (12H, t; *J* = 7.2 Hz, CH_3); 1.28-1.32 (16H, m, $(CH_2)_2$); 1.40-1.44 (8H, m, CH-$\underline{CH_2}$); 2.17 (24H, s, $N(CH_3)_2$), 2.37 (8H, br.s, $\underline{CH_2}N(CH_3)_2$), 2.66 (8H, br.s, $\underline{CH_2}CH_2N(CH_3)_2$); 3.99 (8H, s, NCH_2Ar), 4.29 (4H, t; *J* = 7.8 Hz, -CH bridge), 7.1 (4H, s, Ar-OH), 7.78 (4H, Ar-H meta to OH); ^{13}C NMR (75 MHz, $CDCl_3$), δ (ppm): 14.2, 22.8, 30.5, 30.9, 33.1, 33.5, 45.2, 45.5, 45.8, 57.5, 108.7, 121.8, 124.2, 151.7

7.1.7.6 Synthesis of Calix[4]resorcinarene 59b

Tetrabezoxazine **58b** (3.85 g, 3 mmol); giving a pink powder in (2.63 g, 68 % yield); m.p. (135-136 ºC); FTIR (cm^{-1}): 3319 (OH and NH), 2953-2852 (C-H aliphatic), 1601 (C=C aromatic), 1467, 1301 (-CH_3), 1190 (C-N), 904; ^{1}H NMR spectrum (300 MHz, $CDCl_3$), δ (ppm): 0.91 (12H, t; *J* = 7.2 Hz, CH_3), 1.28-1.33 (16H, m, $(CH_2)_5$), 1.42-1.44 (8H, m, CH-$\underline{CH_2}$), 2.17 (24H, s, $N(CH_3)_2$), 2.37 (8H, br.s, $\underline{CH_2}N(CH_3)_2$), 2.66 (8H, br.s, $\underline{CH_2}CH_2N(CH_3)_2$), 3.99 (8H, s, NCH_2Ar), 4.29 (4H, t; *J* = 7.8 Hz, -CH bridge), 7.1 (8H, s, Ar-OH), 7.78 (4H, ArH *meta* to OH); ^{13}C NMR (75 MHz, $CDCl_3$), δ (ppm): 14.2, 21.7, 27.3, 28.4, 29.9, 30.9, 32.4, 32.5, 44.2, 44.4, 44.7, 45.1, 56.8, 107.7, 120.7, 123.0, 151.7 (Kharitonova *et al.*, 2003).

7.1.7.7 Synthesis of Calix[4]resorcinarene 59c

Tetrabezoxazine **58c** (3.71 g, 3 mmol); giving a pink powder in (2.63 g, 68 % yield); m.p. (180-181 ºC); FTIR (cm^{-1}): 3319 (OH and NH), 2953-2852 (C-H aliphatic), 1601 (C=C aromatic), 1467, 1301 (-CH_3), 1190 (C-N), 904; ^{1}H NMR spectrum (300 MHz,

$CDCl_3$), δ (ppm): 0.91 (12H, t; *J* = 7.2 Hz, CH_3), 1.20-1.25 (16H, m, $(CH_2)_2$), 1.42-1.45 (8H, m, CH-$\underline{CH_2}$), 4.05, 3.8 (each 4H, d; *J* = 7.2 Hz, $ArCH_2N$), 4.26 (4H, t; *J* = 7.8 Hz, -CH bridge), 7.20 (20H, m, benzyl-H), 8.23 (4H, br.s, NH_2^+), 9.01 (8H, s, Ar-OH); ^{13}C NMR (75 MHz, $CDCl_3$), δ (ppm): 14.2, 21.7, 27.3, 28.4, 29.9, 30.9, 32.4, 32.5, 44.2, 44.4, 44.7, 45.1, 56.8, 107.7, 120.7, 123.0, 151.7

7.1.7.8 Synthesis of Calix[4]resorcinarene 59d

Tetrabezoxazine **58d** (4.22 g, 3 mmol); giving a pink powder in (3.41 g, 73 % yield); m.p. (189-190 ºC); FTIR (cm^{-1}): 3300 (OH and NH), 2927-2800 (C-H aliphatic), 1602 and 1558 (C=C aromatic), 1474, 1456 (-CH_3), 1212 (C-N); ^1H NMR (300 MHz, $CDCl_3$), δ (ppm): 0.94 (12H, t; *J* = 7.3 Hz, CH_3), 1.26-135 (16H, m, $(CH_2)_5$), 2.13-2.16 (8H, m, CH-$\underline{CH_2}$), 4.04 (8H, br.s, N$\underline{CH_2}$-benzyl), 4.23 (4H, t; *J* = 7.8 Hz, -CH bridge), 4.31 (8H, br.s, N$\underline{CH_2}$Ar), 7.14 (4H, s, Ar-H *meta* to OH), 7.34 (12H, d; *J* = 6.6 Hz, benzyl-H), 7.7 (8H, d; *J* = 6.2 Hz, benzyl-H), 8.22 (4H, br.s, NH_2^+), 9.08 (8H, s, Ar-OH), ^{13}C NMR (75 MHz, $CDCl_3$), δ (ppm): 14.1, 22.6, 30.1, 32.4, 34.3, 42.2, 52.0, 108.6, 124.7, 126.4, 129.1, 129.5, 129.7, 130.6, 150.2

General procedure for removing the benzyl group from the aminocalix[4]resorcinarenes 59c-d.

Calix[4]resorcinarene **59c and 59d** (1 mmol), was dissolved in ethanol (20 mL) followed by the addition of 0.3 g of Pt/C (5 %).The mixture was stirred at room temperature under nitrogen atmosphere for 72 h. The mixture was then filtered over celite and the collected solvent was evaporated using a rotary evaporator affording a crude product. Further work is needed on this step to purify the product.

7.1.8 Synthesis of Calix[4]resorcinarene Cavitands

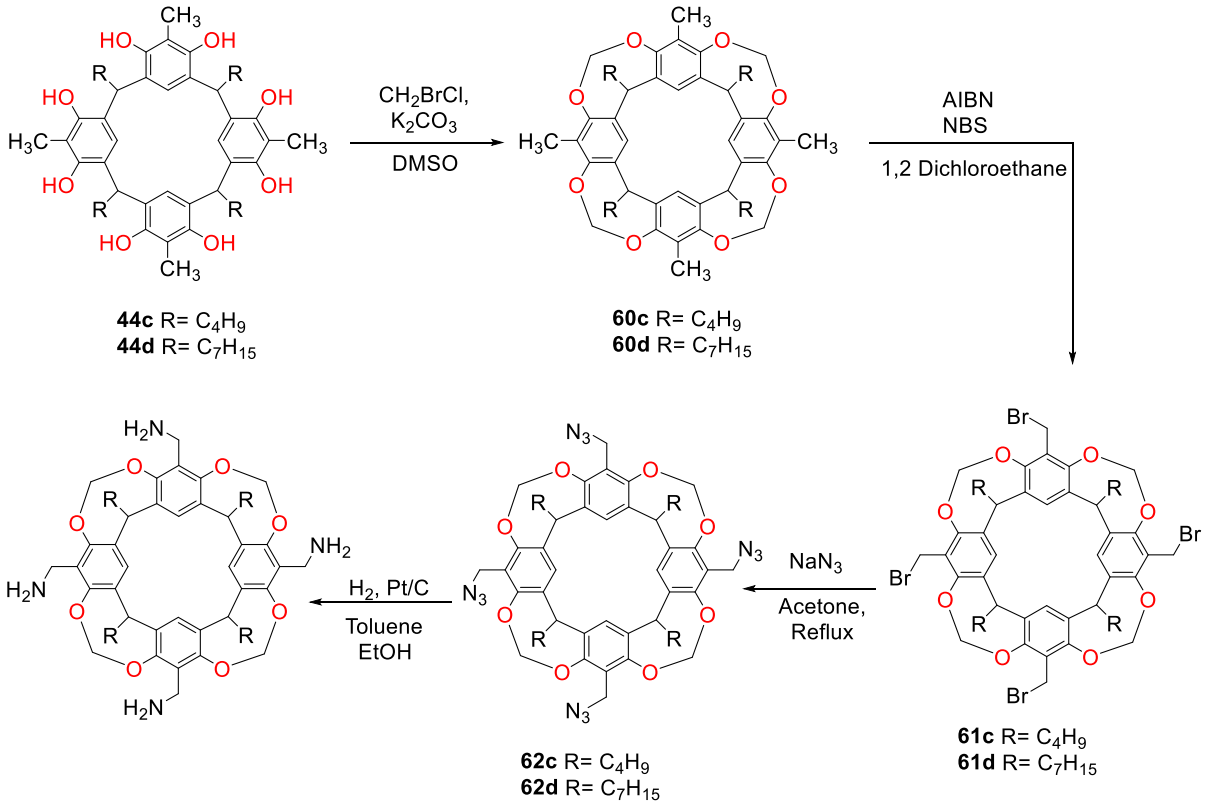

Scheme 23: The bridging reaction of hydroxyl groups in calix[4]resorcinarene **44c-d** to form calix[4]resorcinarene cavitands**.**

General procedure of synthesis of cavitand 60 (Donald, Tunstad, & Knobler, 1992).

To a solution of calix[4]resorcinarene **44c** (10 mmol) in (40 mL) dry dimethyl sulfoxide (DMSO) was added, in a sealed tube with potassium carbonate (22.12 g). Then bromochloromethane (CH_2BrCl) (4.6 mL, 68.6 moles) was added to the tube and sealed under nitrogen at room temperature. The reaction mixture was sealed and immersed in preheated oil bath 80 ºC and stirred for 24 h (Scheme 23). Subsequently, the reaction mixture turned dark brown over the time. The resulting mixture was quenched with (250 mL) water and acidified with (2 N) hydrochloric acid

until (pH = 2) was reached then extracted with (200 mL × 2) of dichloromethane (DCM). The collected organic layers were washed with water (100 mL × 2) and dried over anhydrous magnesium sulphate and filtered. After solvent removal under a vacuum, the residual, crude compound was purified by column chromatography (ethyl acetate: petroleum ether 1:3).

7.1.8.1 Synthesis of Calix[4]resorcinarene 60a

Calix[4]resorcinarene **44c** (7.96 g, 10 mmol); giving a yellow powder in (3.25 g, 40 % yield); m.p. (296-297 ºC); FTIR (cm^{-1}): 2927-2869 (C-H aliphatic), 1461 (C=C aromatic), 1429, 1374 (-CH_3), 972; ^{1}H NMR (400 MHz, $CDCl_3$), δ (ppm) = 0.95 (12H, t; *J* = 7.1 Hz, CH_3), 1.34-1.45 (16H, m, $(CH_2)_2$), 1.99 (12 H, s, Ar-CH_3), 2.22-2.26 (8 H, m, CH-$\underline{CH_2}$), 4.28 (4 H, d; *J* = 7 Hz, inner OCH_2O), 4.78 (4H, t; *J* = 8.1 Hz, -CH bridge), 5.9 (4 H, d; *J* = 7 Hz, outer OCH_2O), 7.00 (4H, s, Ar-H); ^{13}C NMR (100 MHz, $CDCl_3$), δ (ppm): 10.4, 14.2, 22.8, 29.73, 30.1, 36.9, 98.5, 117.6, 121.2, 137.9, 153.2

7.1.8.2 Synthesis of Calix[4]resorcinarene 60b

Calix[4]resorcinarene 44d (9.37 g, 10 mmole); giving a yellow powder in (6 g, 64 % yield); m.p. (169-170 ºC); FTIR (cm^{-1}): 2923-2855 (C-H aliphatic), and 1456 (C=C aromatic), 1429, 1374 (-CH_3), 97; 1H NMR (400 MHz, $CDCl_3$), δ (ppm) = 0.91(12H, t; J = 7.2 Hz, CH_3), 1.25-1.41 (40H, m, $(CH_2)_5$), 1.98 (12H, s, Ar-CH_3), 2.16-2.25 (8H, m, CH-$\underline{CH_2}$), 4.27 (4H, d; J = 7 Hz, inner OCH_2O), 4.77 (4H, t; J = 8.1 Hz, -CH bridge), 5.9 (4 H, d; J = 7 Hz, outer OCH_2O), 7.00 (4H, s, Ar-H); ^{13}C NMR (75 100 MHz, $CDCl_3$), δ (ppm): 10.4, 14.2, 22.7, 27.9, 29.4, 29.84, 30.12, 31.89, 36.96, 98.51, 117.57, 123.61, 137.9, 153.2

7.1.9 Bromination of Calix[4]resorcinarene Cavitands 60

General procedure of Synthesis of cavitand 61

Calix[4]resorcinarene cavitand **60** (1.5 mmol) was dissolved in 1,2 dichloroethane (100 mL) with a catalytic amount of azobisisobutyronitrile (AIBN) flowed by the addition of *N*-bromosuccinimide (NBS) (2.0822 g) in a portion wise. The mixture was stirred under nitrogen for three hours under reflux. After that time extra catalytic amount of azobisisobutyronitrile (AIBN) and *N*-bromosuccinimide (NBS) (0.30 g) were added to the mixture and stirred for further 24 h at room temperature (Scheme 23). TLC conducted during the course of the reaction; after the completion of the reaction, the solvent was removed under reduced pressure by flash evaporator. The precipitation was dissolved in absolute ethanol (150 mL) and stirred for 2 h. Water (100 mL) was poured into the mixture and the precipitate was collected by filtration and dried in vacuo. The crude was purified over silica gel column chromatography (SiO_2; using (ethyl acetate: petroleum ether 1:9 v/v).

7.1.9.1 Synthesis of Calix[4]resorcinarene Cavitand 61a

Calix[4]resorcinarene cavitand **60a** (1.23 g, 1.5 mmol); giving a yellowish powder in (1.21 g, 86 % yield); m.p. (299-300º C); FTIR (cm^{-1}): 2923-2855 (C-H aliphatic), 1456 (C=C aromatic), 1429, 1374 (-CH_3), 97; ^{1}H NMR (400 MHz, $CDCl_3$), δ (ppm) = 0.96 (12H, t; *J* = 7.2 Hz, CH_3), 1.44-1.50 (16H, m, $(CH_2)_2$), 2.20-2.24 (8H, m, CH-$\underline{CH_2}$), 4.44 (8H, s, Ar-CH_2Br), 4.58 (4 H, d; *J* = 6.4 Hz, inner OCH_2O), 4.79 (4H, t; *J* = 7.9 Hz, -CH bridge), 6.05 (4 H, d; *J* = 7 Hz, outer OCH_2O), 7.16 (4H, s, Ar-H); ^{13}C NMR (100 MHz, $CDCl_3$), δ (ppm): 14.2, 22.8, 23.0, 29.7, 31.1, 36.8, 99.1, 120.9, 124.7, 138.1, 158.53

7.1.9.2 Synthesis of Calix[4]resorcinarene Cavitand 61b

Calix[4]resorcinarene cavitand **60b** (1.46 g, 1.5 mmol); giving a yellowish powder in (1.21 g, 86 % yield); m.p. (110-111 ºC); FTIR (cm^{-1}): 2923-2855 (C-H aliphatic), and 1455 (C=C aromatic), 1431, 1374 (-CH_3), 970; ^{1}H NMR (300 MHz, $CDCl_3$), δ (ppm): 0.90 (12H, t; *J* = 6.8 Hz, CH_3), 1.30-1.60 (40H, m, $(CH_2)_5$), 2.23 (8 H, m, CH-$\underline{CH_2}$), 4.44 (8H, s, Ar-CH_2Br), 4.58 (4 H, d; *J* = 6.6 Hz, inner OCH_2O), 4.81 (4H, t; *J* = 6.8 Hz, -CH bridge), 6.05 (4 H, d; *J* = 6.6 Hz, outer OCH_2O), 7.15 (4H, s, Ar-H); ^{13}C NMR (75 MHz, $CDCl_3$), δ (ppm):14.1, 14.2, 22.7, 25.60, 27.3, 29.4, 29.7, 30.1, 31.8, 36.8, 99.1, 120.9, 124.5, 153.5, 171.2

7.1.10 Modification of Calix[4]resorcinarene Cavitands 61 (Moussaoui *et al.*, 2017).

General procedure of Synthesis of cavitand 62

To a solution of tetramethylbromocalix[4]resorcinarenes cavitand **61** (2.4 mmol) in (80 mL) of acetone, (0.9 g,15 mmol) of sodium azide NaN_3 was subsequently added. The mixture was stirred and refluxed for 3 h (Scheme 23). TLC conducted during the course of the reaction; after the completion of the reaction, the mixture was filtered over celite and the collected solution was evaporated under reduced pressure.

7.1.10.1 Synthesis of Calix[4]resorcinarene Cavitand 62a

Calix[4]resorcinarene **61a (**2.72 g, 2.4 mmol); giving as a brown solid in (1.01 g, 43 % yield); m.p. (105-106 ºC); FTIR (cm^{-1}): 2923-2855 (C-H aliphatic), 1733 and 1455 (C=C aromatic), 1431 (-CH methane bridge), 1374 (-CH_3), 970; ^{1}H NMR (300 MHz, $CDCl_3$), δ (ppm): 0.95 (12H, t; *J* = 6.8 Hz, CH_3), 1.32-1.47 (16H, m, $(CH_2)_2$), 2.20-2.25 (8H, m, CH-$\underline{CH_2}$), 4.33 (8H, s, CH_2N_3), 4.39 (4H, d; *J* = 7.1 Hz, inner OCH_2O), 4.77 (4H, t; *J* = 7.2 Hz, -CH bridge), 5.94 (4 H, d; *J* = 7.1 Hz, outer OCH_2O), 7.16

(4H, s, Ar-H); ^{13}C NMR (75 MHz, $CDCl_3$), δ (ppm): 14.1, 29.4, 30.9, 36.8, 45.1, 99.7, 120.8, 122.3, 138.1, 153.7

7.1.10.2 Synthesis of Calix[4]resorcinarene Cavitand 62b

Calix[4]resorcinarene **61b** (4.97 g, 2.4 mmol); giving a brown solid in (2 g, 73 % yield); m.p. (112-113 ºC); FTIR (cm^{-1}): 2923-2855 (C-H aliphatic), 1733 and 1455 (C=C aromatic), 1431 (-CH methane bridge), 1374 ($-CH_3$), 970; ^{1}H NMR (300 MHz, $CDCl_3$), δ (ppm): 0.90 (12H, t; *J* = 6.7 Hz, CH_3), 1.21-1.47 (40H, m, $(CH_2)_5$), 2.23-2.28 (8H, m, CH-$\underline{CH_2}$), 4.44 (8H, s, Ar-CH_2N_3), 4.58 (4H, d; *J* = 6.9 Hz, inner OCH_2O), 4.81 (4H, t; *J* = 7 Hz, -CH bridge), 6.05 (4 H, d; *J* = 6.9 Hz, outer OCH_2O), 7.15 (4H, s, Ar-H); ^{13}C NMR (75 MHz, $CDCl_3$), δ (ppm): 14.1, 27.7, 29.3, 30.14, 30.9, 31.9, 50.8, 99.2, 120.9, 124.5, 153.5

7.1.11 Modification of Calix[4]resorcinarene Cavitands 62 (Moussaoui *et al.*, 2017).

The catalytic reduction of the calix[4]resorcinarene cavitands **62a-b** to give the corresponding aminocalix[4]resorcinarene cavitands was not pursued as other aspects of the research were prioritised.

References

References

Aggarwal, B. B., & Shishodia, S. (2006). Molecular targets of dietary agents for prevention and therapy of cancer. *Biochem Pharmacol*, *71*(10), 1397–1421.

Agrawal, Y. K., Pancholi, J. P., & Vyas, J. M. (2009). Design and Synthesis of calixarene. *J. Sci. Ind. Res.*, *68*, 745–768.

Ahmed, M., Morrel, E. M., & Clemente, E. (2001). Bioavailability and pharmacokinetics of a new liquid prednisolone formulation in comparison with two commercially available liquid prednisolone products. *Curr Ther Res Clin Exp*, *62*(7), 548–556.

Ahn, S., Park, T. J., & Choe, J. (2014). mPW1PW91 Calculated Structures and IR Spectra of the Conformational Stereoisomers of C-Cyanophenyl Pyrogallol[4]arene. *Bull. Korean Chem. Soc.*, *35*(5), 1323–1328.

Ahuja, N., Katare, O. P., & Singh, B. (2007). Studies on dissolution enhancement and mathematical modeling of drug release of a poorly water-soluble drug using water-soluble carriers. *Eur. J. Pharm. Biopharm.*, *65*(1), 26–38.

Airola, K., Bohmer, V., Paulus, E. F., Rissanen, K., Schmidt, C., Thondorf, I., & Vogt, W. (1997). Selective derivatisation of resorcarenes: 1. The regioselective formation of tetra-benzoxazine derivatives. *Tetrahedron*, *53*(31), 10709–10724.

Akkus, G. U., Aslan, S., Taktak, F. F., & Memon, S. (2008). Synthesis and selective extractant properties of a calixarene thioether derivative and its oligomeric analogue. *Turk J Chem*, *32*(5), 635–643.

Al-Warhi, T., Al-Hazimi, H. M. A., & El-Faham, A. (2012). Recent development in

peptide coupling reagents. *J. Saudi Chem. Soc.*, *16*(2), 97–116.

Aliabadi, H. M., & Lavasanifar, A. (2006). Polymeric micelles for drug delivery. *Expert Opin. Drug Deliv*, *3*(1), 139–162.

Allen, C. L. (2012). *Catalytic Approaches to the Synthesis of Amide Bonds*. Bath University.

Allen, C. L., Chhatwal, A. R., & Williams, J. M. J. (2012). Direct amide formation from unactivated carboxylic acids and amines. *Chem. Commun.*, *48*(5), 666–668.

Allen, C., Maysinger, D., & Eisenberg, A. (1999). Nano-engineering block copolymer aggregates for drug delivery. *Colloids Surf B Biointerfaces*, *16*, 3–27.

Andrea, O.-P., Alejandra, H.-S., & Diego, G.-S. (2015). Direct amidation of carboxylic acids with amines under microwave irradiation using silica gel as a solid support. *Green Chem.*, *17*(5), 3157–3163.

Angelini, G., Ketzler, J. T., & Coursin, D. B. (2001). Use Of Propofol And Other Nonbenzodiazepine Sedatives In The Intensive Care Unit. *Crit. Care Clin.*, *17*(4), 863–880.

Arduini, A., Pochini, A., Reverberi, S., Ungaro, R., Anreetti, G. D., & Ugozzoli, F. (1986). The preparation and properties of a new lipophilic sodium selective ether ester ligand derived from p-t-butylcalix[4]arene. *Tetrahedron*, *42*(7), 2089–2100.

Arimura, T., Kawabata, H., Matsuda, T., Muramatsu, T., Satoh, H., Fujio, K., Shinkai, S. (1991). New Water-Soluble Host Calixarenes Bearing Chiral Substituents. *J. Org. Chem.*, *56*(1), 301–306.

Arnecke, R., Bohmer, V., Vogt, W., & Paulus, E. F. (1995). Regioselective Formation

of Dissymmetric Resorcarene Derivatives with C4-Symmetry. *J. Am. Chem. Soc.*, *117*(11), 3286–3287.

Arnold, K., Davies, B., Giles, R. L., Grosjean, C., Smith, G. E., & Whiting, A. (2006). To catalyze or not to catalyze? Insight into direct amide bond formation from amines and carboxylic acids under thermal and catalyzed conditions. *Adv. Synth. Catal.*, *348*(7–8), 813–820.

Arnold, K., Davies, B., Hérault, D., & Whiting, A. (2008). Asymmetric direct amide synthesis by kinetic amine resolution: A chiral bifunctional aminoboronic acid catalyzed reaction between a racemic amine and an achiral carboxylic acid. *Angew. Chem., Int. Ed.*, *47*(14), 2673–2676.

Arnott, G. E. (2017). Inherently Chiral Calixarenes: Synthesis and Applications. *Chem. - A Eur. J.*, *24*(8), 1744–1754.

Arora, V., Chawla, H. M., & Singh, S. P. (2007). Calixarenes as sensor materials for recognition and separation of metal ions. *ARKIVOC*, *ii*, 172–200.

Asif, M. (2016). Modern Chemistry & Applications Pharmacological Potential of Benzamide Analogues and their Uses in Medicinal Chemistry. *Mod Chem. Appl*, *4*(4), 7–10.

Athar, M., & Das, A. J. (2014). Therapeutic nanoparticles : State-of-the-art of nanomedicine. *Adv.Mater. Rev.*, *1*(1), 25–37.

Bader, H., Ringsdorf, H., & Schmidt, B. (1984). Watersoluble polymers in medicine. *Die Angewandte Makromolekulare Chemie*, *123*(1), 457–485.

Baeyer, A. (1872). Ueber die Verbindungen der Aldehyde mit den Phenolen. *Ber.*

Dtsch. Chem. Ges., *5*(1), 280–282.

Baker, D. D., Chu, M., Oza, U., & Rajgarhia, V. (2007). The value of natural products to future pharmaceutical discovery. *Nat. Prod. Rep.*, *24*(6), 1225–1244.

Baker, M. T., & Naguib, M. (2005). propofol: The Challenges of Formulation. *Anesthesiology*, *103*(4), 860–876.

Bayrakci, M., Ertul, S., & Yilmaz, M. (2011). Transportation of Poorly Soluble Drug Molecules from the Organic Phase to the Aqueous Phase by Using Phosphorylated Calixarenes. *J. Chem. Eng. Data*, *56*, 4473–4479.

Bayrakci, M., Ertul, S., & Yilmaz, M. (2012). Phase Solubility Studies of Poorly Soluble Drug Molecules by Using *O*-Phosphorylated Calixarenes as Drug-Solubilizing Agents. *J. Chem. Eng. Data*, *57*(1), 233–239.

Bazzanella, A., Morbel, H., Bachmann, K., Milbradt, R., Bohmer, V., & Vogt, W. (1997). Highly efficient separation of amines by electrokinetic chromatography using resorcarene-octacarboxylic acids as pseudostationary phases. *J. Chromatogr. A*, *792*, 143–149.

Becker, D. E. (2013). Basic and Clinical Pharmacology of Glucocorticosteroids. *Anesth Prog*, *60*(1), 25–32.

Berliner, M. A., Dubant, S. P. A., Makowski, T., Ng, K., Sitter, B., Wager, C., & Zhang, Y. (2011). Use of an iridium-catalyzed redox-neutral alcohol-amine coupling on kilogram scale for the synthesis of a GlyT1 inhibitor. *Org. Process Res. Dev.*, *15*(5), 1052–1062.

Beyeh, N. Kodiah, Cetina, M., Lofman, M., Luostarinen, M., Shivanyuk, A., &

Rissanen, K. (2010). Hydrogen bond-stabilised N -alkylammonium resorcinarene halide cavitands. *Supramol. Chem.*, *22*(11–12), 737–750.

Beyeh, N. Kodiah, Cetina, M., & Rissanen, K. (2012). Binding modes of nonspherical anions to N-alkylammonium resorcinarenes in the solid state. *Cryst. Growth Des.*, *12*(10), 4919–4926.

Beyeh, N Kodiah, Goth, M., Kaufmann, L., Schalley, C. A., & Rissanen, K. (2014). The Synergetic Interplay of Weak Interactions in the Ion-Pair Recognition of Quaternary and Diquaternary Ammonium Salts by Halogenated Resorcinarenes. *Eur. J. Org. Chem.*, 80–85.

Beyeh, Ngong K, Fehe, D., Luostarinen, M., Schalley, A., & Rissanen, K. (2006). Synthesis of Chiral Resorcinarene-based Hosts and a Mass Spectrometric Study of Their Chemistry in Solution and the Gas Phase. *J Incl Phenom Macrocycl Chem*, *56*, 381–394.

Biros, S. M., & Rebek, J. (2006). Structure and binding properties of water-soluble cavitands and capsules. *Chem. Soc. Rev.*, *36*(1), 93–104.

Biros, S. M., Ullrich, E. C., Hof, F., Trembleau, L., & Rebek, J. (2004). Kinetically Stable Complexes in Water: The Role of Hydration and Hydrophobicity. *J. AM. CHEM. SOC.*, *126*(9), 2870–2876.

Boerrigter, H., Verboom, W., & Reinhoudt, D. N. (1997). Novel Resorcinarene Cavitand-Based CMP(O) Cation Ligands: Synthesis and Extraction Properties. *J. Org. Chem.*, *62*(21), 7148–7155.

Boerrigter, H., Verboom, W., Van Hummel, G. J., Harkema, S., & Reinhoudt, D. N. (1996). Selective functionalization of resorcinarene cavitands; single crystal X-

ray structure of a distally functionalized cavitand. *Tetrahedron Lett.*, *37*(29), 5167–5170.

Bohmer, V. (1995). Calixarenes, Macrocycles with (Almost) Unlimited Possibilities. *Angew. Chem., Int. Ed.*, *34*(7), 713–745.

Bourgeois, J. M., & Stoeckli-Evans, H. (2005). Synthesis of new resorcinarenes under alkaline conditions. *Helv. Chim. Acta*, *88*(10), 2722–2730.

Bowley, N. (2008). *Synthetic and Structural Studies of Calix[4]pyrogallolarenes Towards Biological Applications*. Requirements of Nottingham Trent University, 219.

Brown, P. O., Enright, D., & Ripmeester, J. A. (2006). Resorcinarene configuration and inclusion behaviour : Isolation of a guest free form of pyrogall[4]arene. *Cryst Eng Comm*, *8*, 381–383.

Burilov, A. R., Bashmakova, N. I., Nikolaeva, I. L., Pudovik, M. A., & Konovalov, A. I. (2001). Aminomethylated Calix[4]resorcinolarenes Having NH Groups. *Russ. J. Gen. Chem.*, *71*(3), 480–481.

Burlatsky, S. F., Atrazhev, V. V, Dmitriev, D. V, Sultanov, V. I., Timokhina, E. N., Ugolkova, E. A., Vincitore, A. (2012). Surface tension model for surfactant solutions at the critical micelle concentration. *J. Colloid Interface Sci.*, *393*, 151–160.

Butterworth, J. F., & Strichartz, G. R. (1990). Molecular mechanisms of local anesthesia: A Review. *Anesthesiology*, *72*, 711–734.

Cai, X. J., Patel, T., Woods, A., Mesquida, P., & Jones, S. A. (2016). Investigating

the influence of drug aggregation on the percutaneous penetration rate of tetracaine when applying low doses of the agent topically to the skin. *Int. J. Pharm.*, *502*(1–2), 10–17.

Caldorera-moore, M. E., Liechty, W. B., & Peppas, N. A. (2011). Responsive Theranostic Systems: Integration of Diagnostic Imaging Agents and Responsive Controlled Release Drug Delivery Carriers. *Acc. Chem. Res*, *44*(10), 1061–1070.

Carey, F. A., & Sundberg, R. J. (1998). *Advanced Organic Chemistry-Part B: Reactions and Synthesis* (Fifth Edit).

Carey, J. S., Laffan, D., Thomson, C., & Williams, M. T. (2006). Analysis of the reactions used for the preparation of drug candidate molecules. *Org. Biomol. Chem.*, *4*(12), 2337–2347.

Carey, S. (2006). *The Synthesis and Medicinal Applications of Pyrogallol[4] arenes*.

Casnati, A., Fabbi, M., Pelizzi, N., Pochini, A., Sansone, F., Ungaro, R., Tarzia, G. (1996). Synthesis, antimicrobial activity and binding properties of calix[4]arene based vancomycin mimics. *Bioorganic Med. Chem. Lett.*, *6*(22), 2699–2704.

Castillo-aguirre, A., Rivera-monroy, Z., & Maldonado, M. (2017). Selective *O*-Alkylation of the Crown Conformer of Tetra(4-hydroxyphenyl)calix[4]resorcinarene to the Corresponding Tetraalkyl Ether. *Molecules*, *22*, 1660.

Chalam, K. V., Murthy, R. K., Agarwal, S., Gupta, S. K., & Grover, S. (2009). Comparative efficacy of topical tetraVisc versus lidocaine gel in cataract surgery. *BMC Ophthalmology*, *9*(7), 1–4.

Charville, H., Jackson, D. A., Hodges, G., Whiting, A., & Wilson, M. R. (2011). The Uncatalyzed Direct Amide Formation Reaction–Mechanism Studies and the Key Role of Carboxylic Acid H-Bonding. *Eur. J. Org. Chem.*, *30*, 5981–5990.

Chaudhari, P. S., Salim, S. D., Sawant, R. V., & Akamanchi, K. G. (2011). Sulfated Tungstate: A New Solid Heterogeneous Catalyst for Amide Synthesis. *ChemInform*, *42*(6), 1.

Chawla, H. M., & Srinivas, K. (1996). Synthesis of new chromogenic calix[4]arenes bridged at the upper rim through bisazobiphenyl linkages. *J. Org. Chem.*, *61*(24), 8464–8467.

Cheipesh, T. A., Zagorulko, E. S., Mchedlov-petrossyan, N. O., Rodik, R. V, & Kalchenko, V. I. (2014). The difference between the aggregates of short-tailed and long-tailed cationic calix[4]arene in water as detected using fluorescein dyes. *J. Mol. Liq.*, *193*, 232–238.

Chen, D., & Jiang, M. (2005). Strategies for Constructing Polymeric Micelles and Hollow Spheres in Solution via Specific Intermolecular Interactions, *38*(6), 494–502.

Chen, G., & Jiang, M. (2011). Cyclodextrin-based inclusion complexation bridging supramolecular chemistry and macromolecular self-assembly. *Chem. Soc. Rev.*, *40*(5), 2254–2266.

Chen, H., Khemtong, C., Yang, X., Chang, X., & Gao, J. (2010). Nanonization strategies for poorly water-soluble drugs. *Drug Discov Today*, *00*(00).

Chen, Y. C., Lo, C. L., & Hsiue, G. H. (2013). Multifunctional nanomicellar systems for delivering anticancer drugs. *J Biomedi Mater Res A*, *102*(6), 2024–2038.

Cheng, L., Ge, X., & Huang, L. (2018). Direct amidation of non-activated phenylacetic acid and benzylamine derivatives catalysed by NiCl2. *R. Soc. Open Sci.*, *5*(2), 1–9.

Cheng, W. P., Gray, A. I., Tetley, L., Le, T., Hang, B., Scha, A. G., & Uchegbu, I. F. (2006). Polyelectrolyte Nanoparticles with High Drug Loading Enhance the Oral Uptake of Hydrophobic Compounds. *Biomacromolecules*, *7*(5), 1509–1520.

Chiou, Win L., Chen, S. -J, & Athanikar, N. (1976). Enhancement of dissolution rates of poorly water-soluble drugs by crystallization in aqueous surfactant solutions I: Sulfathiazole, prednisone, and chloramphenicol. *J. Pharm. Sci.*, *65*(11), 1702–1704.

Chiou, Win Loung, & Riegelman, S. (1971). Pharmaceutical Applications of Solid Dispersion Systems. *J. Pharm. Sci.*, *60*(9), 1281–1302.

Chutimaworapan, S., Ritthidej, G. C., Yonemochi, E., Oguchi, T., & Yamamoto, K. (2000). Effect of Water-Soluble Carriers on Dissolution Characteristics of Nifedipine Solid Dispersions. *Drug Dev Ind Pharm*, *26*(11), 1141–1150.

Clayden, J., Greeves, N., & Warren, S. (2012). *Organic Chemistry* (Second Edi). Oxford Unvirsity Press.

Coleman, A. W., Jebors, S., Cecillon, S., Perret, P., Garin, D., Marti-Battle, D., & Moulin, M. (2008). Toxicity and biodistribution of para-sulfonato-calix[4]arene in mice. *New J. Chem.*, *32*(5), 780–782.

Cometti, G. (1990). New Bowl-Shaped Columnar Liquid Crystals. *J. Chem. Soc., Chem. Commun.*, *2*, 163–165.

Conn, M. M., & Rebek, J. (1997). Self-Assembling Capsules. *Chem. Rev.*, *97*, 1647–1668.

Corbellini, F. (2004). *Molecular capsules based on ionic interactions*. University of Twente, 175.

Corbellini, F., Costanzo, L. Di, Crego-calama, M., Geremia, S., & Reinhoudt, D. N. (2003). Guest Encapsulation in a Water-Soluble Molecular Capsule Based on Ionic Interactions. *J. Am. Chem. Soc.*, *1*, 9946–9947.

Cram, D. J., Choi, H.-J., Bryan, J. A., & Knobler, C. B. (1992). Solvophobic and Entropic Driving Forces for Forming Velcraplexes, Which Are Four-Fold, Lock-Key Dimers in Organic Media's2. *J. Am. Chem. Soc.*, *114*(20), 7748–7765.

Cram, D. J., & Cram, J. M. (1994). *Container Molecules and their Guests*. (J. Fraser Stoddart, Ed.). England: RSC, Cambridge, 85-130.

Cram, D. J., Karbach, S., Kim, H. E., Knobler, C. B., Maverick, E. F., Ericson, J. L., & Helgeson, R. C. (1988). Host-Guest Complexation. 46. Cavitands as Open Molecular Vessels Form Solvates. *J. Am. Chem. Soc.*, *110*(7), 2229–2237.

Cram, D. J., Karbach, S., Kim, Y. H., Baczynskyj, L., Marti, K., Sampson, R. M., & Kalleymeyn, G. W. (1988). Host-guest complexation. 47. Carcerands and carcaplexes, the first closed molecular container compounds. *J. Am. Chem. Soc.*, *110*(6), 2554–2560.

Csok, Z., Kegl, T., Parkanyi, L., Varga, A., Kunsagi-, S., & Kollar, L. (2011). Facile , high-yielding synthesis of deepened cavitands : a synthetic and theoretical study. *Supramol. Chem.*, *23*(10), 710–719.

Cui, J., Uzunova, V. D., Guo, D. S., Wang, K., Nau, W. M., & Liu, Y. (2010). Effect of lower-rim alkylation of p-sulfonatocalix[4]arene on the thermodynamics of host-guest complexation. *Eur. J. Org. Chem.*, (9), 1704–1710.

D'Souza, S. (2014). A Review of In Vitro Drug Release Test Methods for Nano-Sized Dosage Forms. *Adv Pharm*, *304757*, 1–12.

Dalgarno, S. J., Szabo, T., Siavosh-Haghighi, A., Deakyne, C. A., Adams, J. E., & Atwood, J. L. (2009). Exploring the limits of encapsulation within hexameric pyrogallol[4]arene nano-capsules. *Chem.Commun.*, *7345*(11), 1339–1341.

Dalgarno, S. J., Tucker, S. A., Bassil, D. B., & Atwood, J. L. (2005). Fluorescent Guest Molecules Report Ordered Inner Phase of Host Capsules in Solution. *Science*, *309*, 2037–2040.

Danaei, M., Dehghankhold, M., Ataei, S., Hasanzadeh Davarani, F., Javanmard, R., Dokhani, A., Mozafari, M. R. (2018). Impact of particle size and polydispersity index on the clinical applications of lipidic nanocarrier systems. *Pharmaceutics*, *10*(57), 1–17.

Danylyuk, O., & Suwinska, K. (2009). Solid-state interactions of calixarenes with biorelevant molecules. *Chem. Commun.*, (39), 5799–5813.

Darvish, F., & Khazraee, S. (2014). Molecular iodine: An efficient and environment-friendly catalyst for the synthesis of calix[4]resorcinarenes. *C. R. Chimie*, *17*(9), 890–893.

Daschbach, M. M., Kulikov, O. V, Long, E. F., & Gokel, G. W. (2011). Pyrogallol[4] arenes Show Highly Variable Amphiphilic Behavior at the Air – Water Interface Dependent Upon Side Chain Length and Branching. *Chem. Eur. J.*, *17*, 8913–

8921.

Davis, F., Faul, F. J., & Higson, S. P. J. (2009). Calix[4]resorcinarene–surfactant complexes : formulation, structure and potential sensor applications. *Soft. Matter*, *5*, 2746–2751.

de Lima, R., De Jesus, M., Cereda, C., Tofoli, G. R., Cabeca, L. F., Mazzaro, I., De Paula, E. (2012). Improvement of tetracaine antinociceptive effect by inclusion in cyclodextrins. *J Drug Target*, *20*(1), 85–96.

de Paula, E., Cereda, C., Tofoli, G., Franz-Montan, M., Fraceto, L., & de Araujo, D. (2010). Drug Delivery Systems for Local Anesthetics. *Recent Pat Drug Deliv Formuln*, *4*(1), 23–34.

Dekker, M. (1994). *Colloidal Drug Delivery Systems*. (J. K. Ed, Ed.), *new york,* 219-342.

Derjaguin, B., & Landau, L. (1941). Theory of the stability of strongly charged lyophobic sols and of the adhesion of strongly charged particles in solutions of electrolytes Acta Phys. *Acta Physicochim*, *14*, 633–662.

Domínguez, A., Fernández, A., Gonzalez, N., Iglesias, E., & Montenegro, L. (1997). Determination of critical micelle concentration of some surfactants by three techniques. *J. Chem. Educ.*, *74*(10), 1227–1231.

Donald, J., Tunstad, M., & Knobler, B. (1992). C- and Z-Shaped Ditopic Cavitands, Their Binding Characteristics, and Monotopic Relatives'. *J. Org. Chem.*, *57*(2), 528–535.

Duncan, R. (2006). Polymer conjugates as anticancer nanomedicines. *Nat. Rev.*

Cancer, *6*, 688–701.

Duncan, R., Edward, K., & Avenue, V. I. I. (2003). The Dawning Era Of Polymer Therapeutics. *Nat. Rev. Drug Disc.*, *2*, 347–360.

Dunn, P. J., Constable, D. J. C., Hayle, J. D., Humphrey, G. R., Leazer, J. J. L., Linderman, R. J., Zhang, T. Y. (2007). Key green chemistry research areas—a perspective from pharmaceutical manufacturers. *Green Chem.*, *9*(5), 411–420.

Ebbing, M. H. K., Villa, M.-J., Valpuesta, J.-M., Prados, P., & de Mendoza, J. (2002). Resorcinarenes with 2-benzimidazolone bridges: self-aggregation, self-assembled dimeric capsules, and guest encapsulation. *PNAS*, *99*(8), 4962–4966.

EL-Azazy, M. (2018). Introductory Chapter : Infrared Spectroscopy-A Synopsis of the Fundamentals and Applications. In *Infrared Spectroscopy-Principles, Advances, and Applications* (pp. 1–10).

Elidrisi, I., Bhatt, P. V, Govender, T., Kruger, H. G., & Maguire, G. E. . (2015). Synthesis and NMR elucidation of novel octa-amino acid resorcin[4]arenes derivatives. *South African J. Chem.*, *68*, 27–38.

Enders, D., Gielen, H., Runsink, J., Breuer, K., Brode, S., & Boehn, K. (1998). Diastereoselective Synthesis of Chiral (Triazolinylidene)rhodium Complexes Containing an Axis of Chirality. *Eur. J. Inorg. Chem.*, *7*, 913–919.

Erdtman, H. and, & Hogberg, S. (1968). Cyclooligomeric Phenol-Aldehyde Condensation Products I. *Tetrahedron Lett.*, *9*(14), 1679–1682.

Ermakova, A. M., Morozova, J. E., Shalaeva, Y. V., Syakaev, V. V., Gubaidullin, A.

T., Voloshina, A. D., Konovalov, A. I. (2018). Nanoconjugates of a calixresorcinarene derivative with methoxy poly(ethylene glycol) fragments for drug encapsulation. *Beilstein J. Nanotechnol.*, *9*(1), 2057–2070.

Espanol, E. S., & Villamil, M. M. (2019). Calixarenes: Generalities and their role in improving the solubility, biocompatibility, stability, bioavailability, detection, and transport of biomolecules. *Biomolecules*, *9*(90), 1–15.

Fahmy, S. A., Brußler, J., Alawak, M., El-Sayed, M. M. H., Bakowsky, U., & Shoeib, T. (2019). Chemotherapy based on supramolecular chemistry: A promising strategy in cancer therapy. *Pharmaceutics*, *11*(6), 1–16.

Farokhzad, O. C., & Langer, R. (2009). Impact of Nanotechnology on Drug Delivery. *ACS Nano*, *3*(1), 16–20.

Fernandes, R. A., & Mulay, S. V. (2014). Chiral cups (calixarenes) via Dotz benzannulation. *Synth.*, *46*(14), 1836–1846.

Fernandes, S. A., Cabeca, L. F., Marsaioli, A. J., & Paula, E. de. (2007). Investigation of tetracaine complexation with beta-cyclodextrins and p -sulphonic acid calix[6] arenes by noe and PGSE NMR, and PGSE NMR. *J Incl Phenom Macrocycl Chem*, *57*, 395–401.

Fleisher, D., Bong, R., & Stewart, B. H. (1996). Improved oral drug delivery: Solubility limitations overcome by the use of prodrugs. *Adv. Drug Deliv. Rev.*, *19*(2), 115–130.

Fowler, D. A., Tian, J., Barnes, C., Teat, J., & Atwood, J. L. (2011). Cocrystallization of C -butyl pyrogallol[4]arene and C -propan-3-ol pyrogallol[4]arene with gabapentin. *Cryst. Eng. Comm.*, *13*, 1446–1449.

Fransen, J. R., & Dutton, P. J. (1995). Cation binding and conformation of octafunctionalized calix[4]resorcinarenes. *Can. J. Chem.*, *73*, 2217–2223.

Fuhrhop, J., & Helfrich, W. (1993). Fiuld and Solid Fibers Made of Lipid Molecular Bilayers. *Chem. Rev.*, *93*, 1565–1582.

Furo, I. (2005). NMR spectroscopy of micelles and related systems. *J. Mol. Liq.*, *117*(1–3), 117–137.

Gaeta, C., Martino, M. and, & Neri, P. (2006). Conformational templation in a singly bridged calix[7]arene derivative induced by alkali metal cations. *Org. Lett.*, *8*(20), 4409–4412.

Gallagher, J. F., Ferguson, G., Bohmer, V., & Kraft, D. (1994). Self inclusion in a calix[5]arene structure; structure of the cone conformer of a pentahydroxy-p-tert-butylcalix[5]arene. *Acta Cryst.*, *C50*(1), 73–77.

Gangemi, C. M. A., Pappalardo, A., & Sfrazzetto, G. T. (2015). Applications of supramolecular capsules derived from resorcin[4]arenes, calix[n]arenes and metallo-ligands: from biology to catalysis. *RSC Adv.*, *5*(64), 51919–51933.

Gansey, M. H. B. G., Bakker, F. K. G., Geurts, H. P. M., Feiters, M. C., Verboom, W., & Reinhoudt, D. N. (1998). Water-Soluble Resorcin[4]arene Based Cavitands. *Tetrahedron Lett.*, *39*, 5447–5450.

Gao, C., Wang, Y., Gou, P., Cai, X., Li, X., Zhu, W. and, & Shen, Z. (2013). Synthesis and Characterization of Resorcinarene-Centered Amphiphilic A8B4 Miktoarm Star Copolymers Based on Poly(e-caprolactone) and Poly(ethylene glycol) by Combination of CROP and “Click” Chemistry. *Polym. Chem.*, *51*, 2824–2833.

Garbo, G. M., & Morgan, A. R. (1988). Delivery systems for hydrophobic drugs. *J. Photochem. Photobiol.*, *1*(4), 494–495.

Gerkensmeier, T., Iwanek, W., Agena, C., Fröhlich, R., Kotila, S., Näther, C., & Mattay, J. (1999). Self-Assembly of 2 , 8 , 14 , 20-Tetraisobutyl-5 , 11, 17, 23-tetrahydroxyresorc[4]arene. *Eur. J. Org. Chem.*, *9*, 2257–2262.

Ghose, A. K., Viswanadhan, V. N., & Wendoloski, J. J. (1999). A knowledge-based approach in designing combinatorial or medicinal chemistry libraries for drug discovery. 1. A qualitative and quantitative characterization of known drug databases. *J. Comb. Chem.*, *1*(1), 55–68.

Ghosh, I., & Nau, W. M. (2012). The strategic use of supramolecular pKa shifts to enhance the bioavailability of drugs. *Adv. Drug Deliv. Rev.*, *64*(9), 764–783.

Gibb, C. L. D., Stevens, E. D., & Gibb, B. C. (2001). C-H...X-R (X = Cl, Br, and I) hydrogen bonds drive the complexation properties of a nanoscale molecular basket. *J. Am. Chem. Soc.*, *123*(24), 5849–5850.

Gong, J., Chen, M., Zheng, Y., Wang, S., & Wang, Y. (2012). Polymeric micelles drug delivery system in oncology. *J Control Release*, *159*(3), 312–323.

Grady, T., Harris, S. J., Smyth, M. R., Diamond, D., & Hailey, P. (1996). Determination of the enantiomeric composition of chiral amines based on the quenching of the fluorescence of a chiral calixarene. *Anal. Chem.*, *68*(21), 3775–3782.

Gruppi, F., Boccini, F., Elviri, L., & Dalcanale, E. (2009). Self-assembly of a cavitand-based heteronuclear coordination cage. *Tetrahedron*, *65*(35), 7289–7295.

Gui, X., & Sherman, J. C. (2001). Host-guest binding of simple cavitands in water. *Chem. Commnun.*, 2680–2681.

Gumustas, M., Sengel-Turk, C. T., Gumustas, A., Ozkan, S. A., & Uslu, B. (2017). *Effect of Polymer-Based Nanoparticles on the Assay of Antimicrobial Drug Delivery Systems*. *Multifunctional Systems for Combined Delivery, Biosensing and Diagnostics*. Corum, Turkey: Elsevier Inc, 67-108.

Guo, D.-S., & Liu, Y. (2014). Supramolecular Chemistry of *p*-Sulfonatocalix[n]arenes and Its Biological Applications. *Acc. Chem. Res.*, *47*, 1925–1934.

Guo, D. S., Wang, K., & Liu, Y. (2008). Selective binding behaviors of *p*-sulfonatocalixarenes in aqueous solution. *J Incl Phenom Macrocycl Chem*, *62*, 1–21.

Guo, D. S., Wang, K., Wang, Y. X., & Liu, Y. (2012). Cholinesterase-responsive supramolecular vesicle. *J. Am.Chem. Soc.*, *134*(24), 10244–10250.

Gutsche, C. D. (1983). Calixarenes. *Acc. Chem. Res*, *16*(5), 161–170.

Gutsche, C. D. (1998). *Calixarenes Revisited*. (J. Fraser Stoddart, Ed.), *RSC*. RSC.

Gutsche, C. D. (2008). *Calixarenes - an introduction*. (J. Fraser Stoddard, Ed.) (2nd Editio, Vol. 34). RSC.

Gutsche, C. D., & Bauer, L. J. (1985). Calixarenes. 13. The conformational properties of calix[4]arenes, calix[6]arenes, calix[8]arenes, and oxacalixarenes. *Am. Chem. Soci.*, *107*(21), 6052–6059.

Hagan, S. A., Coombes, A. G. A., Garnett, M. C., Dunn, S. E., Davies, M. C., Illum, L., & Davis, S. S. (1996). Polylactide-Poly(ethylene glycol) Copolymers as Drug

Delivery Systems .1. Characterization of Water Dispersible Micelle-Forming Systems. *Langmuir*, *12*(4), 2153–2161.

Haleblian, J., & McCrone, W. (1969). Pharmaceutical Applications of Polymorphism. *J. Pharm. Sci.*, *58*(8), 911–929.

Han, F., He, X., Huang, J., Li, Z., & Wang, Y. (2004). Surface Properties and Aggregates in the Mixed Systems of Bolaamphiphiles and Their Oppositely Charged Conventional Surfactants. *J. Phys. Chem. B 2004*, *108*, 5256–5262.

Han, S., & Kim, Y. (2004). Recent development of peptide coupling reagents in organic synthesis. *Tetrahedron*, *60*(672), 2447–2467.

Harrisc, S. J., Owens, M., Ferguson, G., & Estate, I. (1991). Chemically Modified Calix[4]arenes. Regioselective Synthesis of 1,3-(Distal) Derivatives and Related Compounds. X-Ray Crystal Structure of a Diphenol- Dinitrile. *J. Chem. Soci. Perkin Trans*, *3*, 2–3.

Haskell, R., Wong, B., & Hasen, J. (1984). A double-blind, randomized clinical trial of methylprednisolone in status asthmaticus. *Arch Intern Med*, *143*, 1324–1327.

Hassen, W. M., Martelet, C., Davis, F., Higson, S. P. J., Abdelghani, A., Helali, S., & Jaffrezic-Renault, N. (2007). Calix[4]arene based molecules for amino-acid detection. *Sens. Actuator B-Chem.*, *124*(1), 38–45.

Hayashida, O., Mizuki, K., Akagi, K., Matsuo, A., Kanamori, T., Nakai, T., … Aoyama, Y. (2003). Macrocyclic Glycoclusters . Self-Aggregation and Phosphate-Induced Agglutination Behaviors of Calix[4]resorcarene-Based Quadruple-Chain Amphiphiles with a Huge Oligosaccharide Pool. *J. Am. Chem. Soc.*, *25*, 594–601.

Helttunen, K. (2012). *Exploring The Self-Assembly Of Resorcinarenes: From Molecular Level Interactions To Mesoscpic Structures*. University of Jyvaskyla.

Helttunen, K., Prus, P., Luostarinen, M., & Nissinen, M. (2009). Interaction of aminomethylated resorcinarenes with rhodamine B. *New J. Chem.*, *33*(5), 1148–1154.

Helttunen, K., & Shahgaldian, P. (2010). Self-assembly of amphiphilic calixarenes and resorcinarenes in water. *New J. Chem.*, *34*, 2704–2714.

Hoffmann, de E., & Stroobant, V. (2007). *Mass Spectrometry Principles and Applications* (Third Edit). John Wiley & Sons, 489.

Hogberg, A. G. S. (1980). Two Stereoisomeric Macrocyclic Resorcinol-Acetaldehyde Condensation Products. *J. Org. Chem*, *45*(10), 4498–4500.

Hogberg, S. (1980). Stereoselective Synthesis and DNMR Study of Two 1,8,15,22-T etraphenyl [I4]metacyclophan-3,5,10,12,17,19,24,26-octolss. *J. Am. Chem. Soc.*, *102*(19), 6046–6050.

Holmberg, K., Bo, J., Kronberg, B., & Lindman, B. (2002). *Surfactants And Polymers In Aqueous Solutions*. *IEEE Electrical Insulation Magazine* (Second Edi, Vol. 14). John Wiley & Sons.

Holzschneider, K., Häring, A. P., & Kirsch, S. F. (2019). 2 , 2-Diazido-1 ,2-diarylethanones : Synthesis and Reactivity with Primary Amines. *Eur. J. Org. Chem.*, *2*(I), 1–9.

Horter, D., & Dressman, J. B. (1997). Influence of physicochemical properties on dissolution of drugs in the gastrointestinal tract. *Adv. Drug Deliv. Rev.*, *25*(96),

3–14.

Hoskins, C., & Curtis, A. D. M. (2015). Simple Calix[n]arenes and Calix[4]resorcinarenes as Drug Solubilizing Agents. *J Nanomed Res*, *2*(3), 1–8.

Hoskins, C., Lina, P. K. T., Tetleyb, L., & Cheng, W. P. (2012). Novel fluorescent amphiphilic poly(allylamine) and their supramacromolecular self-assemblies in aqueous media. *Polym. Adv. Technol*, *23*(3), 710–719.

Hoskins, C., Yang, N., Li, T., Zhang, P. P., Chen, X., Hu, X., & Zhang, W. (2016). Investigation into Drug Solubilisation Potential of Sulfonated Calix[4]resorcinarene. *J Nanomed Res*, *7*(2), 1–6.

Hu, L., Xu, S., Zhao, Z., Yang, Y., Hu, L., Xu, S., Wang, C. (2016). Ynamides as racemization-free coupling reagents for amide and peptide synthesis Ynamides as racemization-free coupling reagents for amide and peptide synthesis. *J. Am. Chem. Soc.*, *138*(40), 13135–13138.

Hu, Q., Tang, G., & Chu, P. K. (2014). Cyclodextrin-Based Host−Guest Supramolecular Nanoparticles for Delivery : From Design to Applications. *Acc. Chem. Res.*, *47*, 2017–2025.

Humphrey, J. M., & Chamberlin, A. R. (1997). Chemical Synthesis of Natural Product Peptides : Coupling Methods for the Incorporation of Noncoded Amino Acids into Peptides. *Chem. Rev.*, *97*(95), 2243–2266.

Hussein, Y. H. A., & Youssry, M. (2018). Polymeric micelles of biodegradable diblock copolymers: Enhanced encapsulation of hydrophobic drugs. *Materials*, *11*(5), 2–26.

Imam, T. H. (2013). Propofol-Related Infusion Syndrome : Role of Propofol in Medical Complications of Sedated Critical Care Patients. *Perm J*, *17*(2), 85–87.

Ina, H., Ito, M., & Kibayashi, C. (1996). Enantioselective Total Synthesis of the Macrocyclic Spermidine Alkaloid (-) -Oncinotine. *J. Org. Chem.*, *61*(8), 1023–1029.

Jain, P., Goel, A., Sharma, S., & Parmar, M. (2010). Solubility Enhancement Techniques With Special Emphasis On Hydrotrophy. *IJPPR*, *1*(1), 34–45.

Jain, V K, & Kanaiya, P. H. (2011). Chemistry of calix[4]resorcinarenes. *Russ. Chem. Rev.*, *80*(1), 75–102.

Jain, Vinod K, & Kanaiya, Æ. P. H. (2008). Diazo reductive : a new approach to the synthesis of novel ‘“ upper rim ”’ functionalized resorcin[4]arene Schiff-bases. *J Incl Phenom Macrocycl Chem*, *62*, 111–115.

James, E., Eggers, P. K., Harvey, A. R., Dunlop, S. a, Fitzgerald, M., Stubbs, K. a, & Raston, C. L. (2013). Antioxidant phospholipid calix[4]arene mimics as micellular delivery systems. *Org. Biomol. Chem.*, *11*(36), 6108–6112.

Jasper, J. J. (1972). The Surface Tension of Pure Liquid Compounds Content. *J Phys Chem Ref Data*, *1*(4), 841–1010.

Javor, S., & Rebek, J. (2011). Activation of a Water-Soluble Resorcinarene Cavitand at the Water À Phosphocholine Micelle Interface. *J. Am. Chem. Soc.*, *133*, 17473–17478.

Jayswal, K. P., Patel, J. R., Patel, V. B., & Patel, M. H. (2008). A New Approach Towards Synthesis of Some Novel “ Upper Rim ” Functionalized

Calix[4]resorcinarene Schiff-bases. *Acta Chem. Slov*, *55*, 302–307.

Jiang, B. P., Guo, D. S., Liu, Y. C., Wang, K. P., & Liu, Y. (2014). Photomodulated fluorescence of supramolecular assemblies of sulfonatocalixarenes and tetraphenylethene. *ACS Nano*, *8*(2), 1609–1618.

Jiang, Y., Wang, Y., Ma, N., Wang, Z., Smet, M., Zhang, X., & Leu, V. (2007). Reversible Self-Organization of a UV-Responsive PEG-Terminated Malachite Green Derivative : Vesicle Formation and Photoinduced Disassembly. *Langmuir*, (23), 4029–4034.

Jones, M., & Leroux, J. (1999). Polymeric micelles-a new generation of colloidal drug carriers. *Eur. J. Pharm. Biopharm.*, *48*(2), 101–111.

Jones, M., Leroux, J., Lukyanov, A. N., Torchilin, V. P., Atanase, L. I., & Riess, G. (2004). Self-assembly of block and graft copolymers in organic solvents: An overview of recent advances. *Polymers*, *10*(2), 1273–1289.

Jordan, J. H., Wishard, A., Mague, J. T., & Gibb, B. C. (2019). Binding properties and supramolecular polymerization of a water-soluble resorcin[4]arene. *Org. Chem. Front*, *0*(0), 0.

Jose, P., & Menon, S. (2007). Lower-rim substituted calixarenes and their applications. *Bioinorg. Chem. Appl.*, 1–16.

Kabanov, A. V., Chekhonin, V. P., Alakhov, V. Y., Batrakova, E. V., Lebedev, A. S., Melik-Nubarov, N. S., Kabanov, V. A. (1989). The neuroleptic activity of haloperidol increases after its solubilization in surfactant micelles. *FEBS Letters*, *258*(2), 343–345.

Kabanov, A. V., Batrakova, E. V., Melik-Nubarov, N. S., Fedoseev, N. A., Dorodnich, T. Y., Alakhov, V. Y., Kabanov, V. A. (1992). A new class of drug carriers: micelles of poly(oxyethylene)-poly(oxypropylene) block copolymers as microcontainers for drug targeting from blood in brain. *J Control Release*, *22*(2), 141–157.

Kabasakalian, P., Britt, E., & Yudis, M. D. (1966). Solubility of some steroids in water. *J Pharm Sci*, *55*(6), 642–642.

Kadam, S. V., Shinkar, D. M., & Saudagar, R. B. (2013). Review On Solubility Enhancement Techniques. *Int J Pharm Bio Sci*, *3*(3), 462–475.

Kaddu, R., Bhattacharya, D., Metriyakool, K., & Thomas, R. (2002). Propofol compared with general anesthesia for pediatric GI endoscopy : Is propofol better ? *Gastrointest. Endosc.*, *55*(1), 27–32.

Karthauser, Z. (2013). *A New Approach to Drug Delivery : Non- Peptidic , High Load Macrocyclic Alternatives to Cell Penetrating Peptides*. Unversity of East Anglia, 234.

Kashapov, R. R., Kharlamov, S. V, Sultanova, E. D., Mukhitova, R. K., Kudryashova, Y. R., Zakharova, L. Y., Konovalov, A. I. (2014). Controlling the Size and Morphology of Supramolecular Assemblies of Viologen–Resorcin[4]arene Cavitands. *Chem. Eur. J.*, *20*, 14018–14025.

Kashapov, R. R., Pashirova, T. N., Kharlamov, S. V, Ziganshina, A. Y., Ziltsova, E. P., Lukashenko, S. S., Konovalov, A. I. (2011). Novel self-assembling system based on resorcinarene and cationic surfactant. *Phys. Chem.*, *13*, 15891–15898.

Kashapov, R. R., Ya, L., Saifutdinova, M. N., Kochergin, Y. S., Gavrilova, E. L., &

Sinyashin, O. G. (2015). Construction of a water-soluble form of amino acid C-methylcalix[4]resorcinarene. *J. Molecular Liquids*, *208*, 58–62.

Kashapov, R. R., Zakharova, L. Y., Saifutdinova, M. N., Gavrilova, E. L., & Sinyashin, O. G. (2015). Self-assembly strategies for improving the water solubility of new amino acid calix[4]resorcinarenes. *Tetrahedron Lett.*, *56*(19), 2508–20511.

Kataoka, K., Kwon, G. S., Yokoyama, M., Teruo, O., & Yasuhisa, S. (1993). Block copolymer micelles as vehicles for drug delivery. *J Control Release*, *24*(1–3), 119–132.

Kazakova, E., Morozova, J., Mironova, D., Syakaev, V., Muslinkina, L., & Konovalov, A. (2013). Influence of amidoammonium calix[4]resorcinarenes on methyl orange protolytic equilibrium: Supramolecular indicator systems. *Supramol. Chem.* Taylor & Francis.

Kelland, L. (2007). The resurgence of platinum-based cancer chemotherapy. *Nature Reviews. Cancer*, *7*(8), 573–584.

Khadka, P., Ro, J., Kim, H., Kim, I., Tae, J., Kim, H., Lee, J. (2014). An approach to improve drug solubility , dissolution and bioavailability. *Asian J Pharm Clin Res*, *9*(6), 304–316.

Kharitonova, N. I., Burilov, A. R., Pudovik, M. A., & Konovalov, A. I. (2003). Aminomethylated calix[4]resorcinolarenes with NH groups on the upper rim of the molecule. *Russ.Chem.Bull.,Int.Ed.*, *52*(3), 725–727.

Kharlamov, S. V, Kashapov, R. R., Pashirova, T. N., Zhiltsova, E. P., Lukashenko, S. S., Ziganshina, A. Y., Konovalov, A. I. (2013). A Supramolecular Amphiphile Based on Calix[4]resorcinarene and Cationic Surfactant for Controlled Self-

Assembly. *J. Phys. Chem C*, *117*, 20280–20288.

Kiick, K. L. (2007). Polymer Therapeutics. *Science*, *1182*(5842), 1182–1183.

Kim, K., Selvapalam, N., Ko, Y. H., Park, K. M., Kim, D., & Kim, J. (2007). Functionalized cucurbiturils and their applications. *Chem. Soc. Rev.*, *36*(2), 267–279.

Kim, M. K., Park, K. su, Yeo, W. seok, Choo, H., & Chong, Y. (2009). In vitro solubility, stability and permeability of novel quercetin-amino acid conjugates. *Bioorganic Med. Chem.*, *17*(3), 1164–1171.

Kimizuka, N., Kawasaki, T., Hirata, K., & Kunitake, T. (1998). Supramolecular membranes. Spontaneous assembly of aqueous bilayer membrane via formation of hydrogen bonded pairs of melamine and cyanuric acid derivatives. *J. Am. Chem. Soc.*, *120*(17), 4094–4104.

Kipp, J. E. (2004). The role of solid nanoparticle technology in the parenteral delivery of poorly water-soluble drugs. *Int. J. Pharm.*, *284*(1–2), 109–122.

Kobayashi, K., & Yamanaka, M. (2014). Self-assembled capsules based on tetrafunctionalized calix[4]resorcinarene cavitands. *Chem. Soc. Rev.*, *44*, 449–466.

Koh, K. N., Araki, K., Ikeda, A., Otsuka, H., & Shinkai, S. (1996). Reinvestigation of calixarene-based artificial-signaling acetylcholine receptors useful in neutral aqueous (water/methanol) solution. *J. Am. Chem. Soc.*, *118*(4), 755–758.

Komorek, U., & Wilk, K. A. (2004). Surface and micellar properties of new nonionic gemini aldonamide-type surfactants. *J. Colloid Interface Sci.*, *271*, 206–211.

Krause, T., Baader, S., Erb, B., & Gooßen, L. J. (2016). Atom-economic catalytic amide synthesis from amines and carboxylic acids activated in situ with acetylenes. *Nat. Commun.*, *7*, 1–7.

Kuberski, B., & Szumna, A. (2009). A self-assembled chiral capsule with polar interior, *1*(15), 1959–1961.

Kubitschke, J., Javor, S., & Jr, J. R. (2012). Deep cavitand vesicles–multicompartmental hosts. *Chem. Commun.*, *48*, 9251–9253.

Kulikov, O. V., Daschbach, M. M., Yamnitz, C. R., Rath, N., & Gokel, G. W. (2009). Self-assembled, cogged hexameric nanotubes formed from pyrogallol[4]arenes with a unique branched side chain. *Chem. Commun.*, (48), 7497–7499.

Kulling, D., Fantin, A. C., Biro, P., Bauerfeind, P., & Fried, M. (2001). Safer colonoscopy with patient-controlled analgesia and sedation with propofol and alfentanil. *Gastrointest. Endosc.*, *54*(1), 1–7.

Kumar, A., Sahoo, S. K., Padhee, K., Pal, P., Kochar, S., Satapathy, A., & Pathak, N. (2011). Review on Solubility Enhancement Techniques for Hydrophobic Drugs. *IJCP*, *3*(30), 1–7.

Kumari, H., Zhang, J., Erra, L., Barbour, L. J., Deakyne, C. A., & Atwood, J. L. (2013). Cocrystals of gabapentin with C-alkylresorcin[4]arenes. *CrystEngComm*, *15*(20), 4045–4048.

Kunishima, M., Kawachi, C., Hioki, K., Terao, K., & Tani, S. (2001). Formation of carboxamides by direct condensation of carboxylic acids and amines in alcohols using a new alcohol- and water- soluble condensing agent : DMT-MM. *Tetrahedron*, *57*, 1551–1558.

Kuroda, Y., Ogawa, M., Nasu, H., Terashima, M., Kasahara, M., Kiyama, Y., Nakagawa, T. (1996). Locations of local anesthetic dibucaine in model membranes and the interaction between dibucaine and a Na^+ channel inactivation gate peptide as studied by ^2H- and ^1H-NMR spectroscopies. *Biophys J*, *71*(3), 1191–1207.

Kwon, G., Naito, M., Yokoyama, M., Okano, T., Sakurai, Y., & Kataokatfs, K. (1993). Micelles based on AB block copolymers of poly(ethylene oxide) and poly(beta-benzyl L-aspartate) Micelles Based on AB Block Copolymers of Poly(ethylene oxide) and Poly(ß-benzyl L-aspartate). *Langmuir*, *9*(4), 945–949.

Lacy, J., Embleton, J., Berkshire, Corporation, R. P. S., & Troy, M. (1997). Delivery systems for hydrophobic drugs. *U. s. Patent*, *1*(4), 494–495.

Lake, J. C. C. (2014). *Molecular encapsulation in kinetically trapped, Hydrogen-bonded pyrogallolarene hexamers*. University of Denver, 193.

Langer, R. (1998). Drug delivery and targeting. *Nature*, *392*, 5–10.

Lanigan, R. M., Starkov, P., & Sheppard, T. D. (2013). Direct synthesis of amides from carboxylic acids and amines using $B(OCH_2CF_3)_3$. *J. Organic Chem.*, *78*(9), 4512–4523.

Lauren, S. (2017). *Surface and interfacial tension*.

Lavasanifar, A., Samuel, J., & Kwon, G. S. (2002). Poly(ethylene oxide)-block-poly(L-amino acid) micelles for drug delivery. *Adv. Drug Deliv. Rev.*, *54*, 169–190.

Lee, H., Park, K. M., Jeon, Y. J., Kim, D., Oh, D. H., Kim, H. S., Kim, K. (2005). Vesicle Formed by Amphiphilc Cucurbit[6]uril : Versatile , Noncovalent

Modification of the Vesicle Surface , and Multivalent Binding of Sugar-Decorated Vesicles to Lectin. *J. Am. Chem. Soc.*, *127*, 5006–5007.

Lee, J., Cho, E. C., & Cho, K. (2004). Incorporation and release behavior of hydrophobic drug in functionalized poly(D,L-lactide)-block-poly(ethylene oxide) micelles. *J Control Release*, *94*(2–3), 323–335.

Lee, M., Cho, B., & Zin, W. (2001). Supramolecular Structures from Rod−Coil Block Copolymers. *Chem. Rev.*, *101*, 3869–3892.

Lee, W. Y., Park, C. J., Shin, T. J., Yum, K. W., Yoon, T. G., Seo, K. S., & Kim, H. J. (2009). Only tetracaine and not other local anaesthetics induce apoptosis in rat cortical astrocytes. *Br. J. of Anaesth.*, *103*(5), 719–725.

Leggio, A., Bagalà, J., Belsito, E. L., Comandè, A., Greco, M., & Liguori, A. (2017). Formation of amides: One-pot condensation of carboxylic acids and amines mediated by TiCl4. *Chem. Cent. J.*, *11*(1), 1–12.

Lehn, J.-M. (1987). Supramolecular Chemistry-Scope and Perspectives Molecules-Supramolecules-Molecular Devices. *ChemInform*, *34*(17).

Lehn, J.-M. (1988). Supramolecular Chemistry Concepts and Perspectives. *J Incl Phenom Macrocycl Chem*, *6*(4), 351–396.

Lehn, J. M. (2002). Toward self-organization and complex matter. *Science*, *295*, 2400–2403.

Li, D., & Qi, L. (2018). Self-assembly of inorganic nanoparticles mediated by host-guest interactions. *Curr. Opin. Colloid Interface Sci.*, *35*, 59–67.

Li, J., & Loh, X. J. (2008). Cyclodextrin-based supramolecular architectures:

Syntheses, structures, and applications for drug and gene delivery. *Adv. Drug Deliv. Rev.*, *60*(9), 1000–1017.

Li, S. Y., Xu, Y. W., Liu, J. M., & Su, C. Y. (2011). Inherently chiral calixarenes: Synthesis, optical resolution, chiral recognition and asymmetric catalysis. *Int. J. Mol. Sci.*, *12*(1), 429–455.

Li, Z. (1996). *Synthesis and Properties of Calix[4]naphthalenes*. Memorial University of Newfoundland.

Liu, Y., Guo, D. S., Zhang, H. Y., Ma, Y. H., & Yang, E. C. (2006). The structure and thermodynamics of calix[n]arene complexes with dipyridines and phenanthroline in aqueous solution studied by microcalorimetry and NMR spectroscopy. *J. Phys. Chem. B*, *110*(7), 3428–3434.

Liu, Z., Robinson, J. T., Sun, X., & Dai, H. (2008). PEGylated Nanographene Oxide for Delivery of Water-Insoluble Cancer Drugs. *J. Am. Chem. SOC*, *130*(33), 10876–10877.

Liversidge, M. E. M., & Liversidge, G. G. (2008). Drug Nanoparticles : Formulating Poorly Water-Soluble Compounds. *Toxicol. Pathol.*, *36*, 43–48.

Lukyanov, A. N., & Torchilin, V. P. (2004). Micelles from lipid derivatives of water-soluble polymers as delivery systems for poorly soluble drugs. *Adv. Drug Deliv. Rev.*, *56*(9), 1273–1289.

Lundberg, H., Tinnis, F., Selander, N., & Adolfsson, H. (2014). Catalytic amide formation from non-activated carboxylic acids and amines. *Chem. Soc. Rev.*, *43*(8), 2714–2742.

Luostarinen, M., Nissinen, M., Nieger, M., Shivanyuk, A., & Rissanen, K. (2007). Regioselective acylation of aminoresorcinarenes. *Tetrahedron*, *63*, 1254–1263.

Ma, S., Rudkevich, D. M., & Rebek, J. (1998). " Deep-Cavity " Resorcinarenes Dimerize through Hydrogen Bonding and Self-Inclusion. *J. Am. Chem. Soc.*, *120*(9), 4977–4981.

Ma, X., & Zhao, Y. (2015). Biomedical Applications of Supramolecular Systems Based on Host−Guest Interactions. *Chem. Rev.*, *115*(15), 7794–7839.

Macarov, C. A. (2018). *Investigation of Resorcin[4]arenes Upper Rim Functionalization by*. University of East Anglia, 168.

Maerz, A. K. (2011). *Synthesis and characterization of host-guest complexes : Metal-organic nanocapsules using aryl-substituted pyrogallol[4]arenes*. University of Missouri-Columbia.

Magano, J., & Dunetz, J. R. (2011). Large-Scale Applications of Transition Metal-Catalyzed Couplings for the Synthesis of Pharmaceuticals. *Chem. Rev.*, *111*(3), 2177–2250.

Masayuki, Y., Mizue, M., Noriko, Y., Teruo, O., Yasuhisa, S., Kazunori, K., & Shohei, I. (1990). Polymer micelles as novel drug carrier: Adriamycin-conjugated poly(ethylene glycol)-poly(aspartic acid) block copolymer. *J Control Release*, *11*(1–3), 269–278.

Mata, J., Varade, D., Ghosh, G., & Bahadur, P. (2004). Effect of tetrabutylammonium bromide on the micelles of sodium dodecyl sulfate. *Colloids Surf. A Physicochem. Eng. Asp.*, *245*(1–3), 69–73.

Matsushita, Y. ichi, & Matsui, T. (1993). Synthesis of aminomethylated calix[4]resorcinarenes. *Tetrahedron Lett*, *34*(46), 7433–7436.

Maza, A. De, Coderch, L., Gonzalez, P., & Parra, J. L. (1998). Subsolubilizing alterations caused by alkyl glucosides in phosphatidylcholine liposomes. *J. Control. Release*, *52*, 159–168.

McMahon, G., O'Malley, S., Nalan, K., & Diamond, D. (2003). Important calixarene derivatives – their synthesis and applications. *Arkivoc*, *vii*(7), 23–31.

Mcpolin, O. (2003). *An introduction to HPLC for Pharmaceutical Analysis*. *San Jose State University*. MTS, 148.

Meenakshi, C., Jayabal, P., & Ramakrishnan, V. (2014). Molecular recognition of curcumin (Indian Ayurvedic medicine) by the supramolecular probe, p-t-butyl calix(8)arene. *Spectrochim Acta A Mol Biomol Spectrosc*, *127*, 172–176.

Mellet, C. O., Fernández, J. M. G., & Benito, J. M. (2011). Cyclodextrin-based gene delivery systems. *Chem. Soc. Rev.*, *40*(3), 1586–1608.

Meng, F., Zhong, Z., & Feijen, J. (2009). Stimuli-Responsive Polymersomes for Programmed Drug Delivery. *J. Am. Chem. Soc.*, *10*(2), 198–208.

Menger, B. F. M. (1991). Groups of Organic Molecules That Operate Collectively. *Angew. Chem. Int. Ed. Engl.*, *30*, 1086–1099.

Menon, S. K., Mistry, B. R., Joshi, K. V., Modi, N. R., & Shashtri, D. (2012). Evaluation and solubility improvement of Carvedilol: PSC[n]arene inclusion complexes with acute oral toxicity studies. *J. Incl. Phenom. Macrocycl Chem.*, *73*(1–4), 295–303.

Menon, S. K., Modi, N. R., Mistry, B., & Joshi, K. (2011). Improvement of some pharmaceutical properties of mycophenolate mofetil (MMF) by para sulphonatocalix[4]resorcinarene inclusion complex. *J Incl Phenom Macrocycl Chem*, *70*(1–2), 121–128.

Middel, O., Verboom, W., & Reinhoudt, D. N. (2002). Water-Soluble Cavitands ⁷⁄₈ Synthesis , Solubilities and Binding Properties. *Eur. J. Org. Chem.*, 2587–2597.

Mironova, D. A., Muslinkina, L. A., Morozova, J. E., Shalaeva, Y. V, Kazakova, E. K., Kadyrov, M. T., Konovalov, A. I. (2015). Complexes of tetramethylensulfonatocalix[4]resorcinarene aggregates with methyl orange: Interactions with guests and driving force of color response. *Colloids Surf. A Physicochem. Eng. Asp.*, *468*, 339–345.

Mironova, D. A., Muslinkina, L. A., Syakaev, V. V, Morozova, J. E., Yanilkin, V. V, Konovalov, A. I., & Kh, E. (2013). Crystal violet dye in complexes with amphiphilic anionic calix[4]resorcinarenes : Binding by aggregates and individual molecules. *J. Colloid Interface Sci.*, *407*, 148–154.

Mo, J., Eggers, P. K., Chen, X., Ahamed, M. R. H., Becker, T., Yong Lim, L., & Raston, C. L. (2015). Shear induced carboplatin binding within the cavity of a phospholipid mimic for increased anticancer efficacy. *Scientific Reports*, *5*, 1–9.

Mo, J., Eggers, P. K., Yuan, Z. X., Raston, C. L., & Lim, L. Y. (2016). Paclitaxel-loaded phosphonated calixarene nanovesicles as a modular drug delivery platform. *Scientific Reports*, *6*, 1–12.

Mohanty, A., Patra, T., & Dey, J. (2007). Salt-Induced Vesicle to Micelle Transition in Aqueous Solution of Sodium *N*-(4-n-Octyloxybenzoyl)-L-valinate. *J. Phys. Chem.*

B, *111*, 7155–7159.

Mollaoglu, A. D., Ozyurt, I., & Severcan, F. (2018). Applications of Infrared Spectroscopy and Microscopy in Diagnosis of Obesity. In *Infrared Spectroscopy - Principles, Advances, and Applications* (pp. 1–22).

Molyneux, R. J., Beck, J. J., Colegate, S. M., Edgar, J. A., Gaffield, W., Gilbert, J., Mcconnell, L. L. (2019). Guidelines for unequivocal structural identification of compounds with biological activity of significance in food chemistry (IUPAC Technical Report). *Pure & Appl. Chem.*, *91*(8), 1417–1437.

Momose, A. A., & Bosch, E. (2010). Serendipity in the crystallization of a series of C-alkylcalix[4] resorcinarenes from alcoholic solvents. *Cryst. Growth Des.*, *10*(9), 4043–4049.

Momot, K. I., Kuchel, P. W., Chapman, B. E., Deo, P., Whittaker, D., Poloxamer, F., & Poloxamer, F. (2003). NMR Study of the Association of Propofol with Nonionic Surfactants. *Langmuir*, *19*(6), 2088–2095.

Montalbetti, C. A. G. N., & Falque, V. (2005). Amide bond formation and peptide coupling. *Tetrahedron*, *61*(46), 10827–10852.

Moran, J., Karbach, S., & Cram, D. (1982). Cavitands: synthetic molecular vessels. *J. Am. Chem. Soc.*, *104*(21), 5827.

Moran, J. R., Ericson, J. L., Dalcanale, E., Bryant, J. A., Knobler, C. B., & Cram, D. J. (1991). Vases and Kites as Cavitands. *J. Am. Chem. Soc.*, *113*(15), 5707–5714.

Morey, T. E., Modell, J. H., Hon, D., Shekhawat, D., Klatt, B., Thomas, G. P., Dennis, D. M. (2006). Anesthetic Properties of a Propofol Microemulsion in Dogs.

Anesthesia & Analgesia, *103*(4), 883–886.

Morozova, Ju E, Syakaev, V. V, Shalaeva, Y. V, Ermakova, A. M., Nizameev, I. R., Kadirov, M. K., Antipin, I. S. (2017). Unusual nanosized associates of carboxycalix[4]resorcinarene and cetylpyridinium chloride: the macrocycle as a glue for surfactant micelles. *Soft Matter*, *13*, 2004–2013.

Morozova, Julia E., Kazakova, E. K., Mironova, D. A., Shalaeva, Y. V., Syakaev, V. V., Makarova, N. A., & Konovalov, A. I. (2010). Investigation of tetramethylenesulfonated calix[4]resorcinarene interactions with azo dyes in aqueous solution. *J. Phys. Chem. B*, *114*(41), 13152–13158.

Morozova, Julia E, Syakaev, V. V, Shalaeva, Y. V, Ermakova, A. M., Nizameev, I. R., Kadirov, M. K., & Konovalov, A. I. (2018). Nanoassociates of amphiphilic carboxy-calixresorcinarene and cetylpyridinuim chloride : The search of optimal macrocycle / surfactant molar ratio. *Colloids and Surfaces A*, *553*, 569–577.

Mossine, A. (2014). *Understanding The Self-Assembly Process And Behavior Of Metal-Seamed Pyrogallol[4]arene Nanocapsules*. University of Missouri-Columbia In, 365.

Moussaoui, S. A., Damaj, Z., Wehbie, M., Rostaing, S. P., & Karamé, I. (2017). Alternative and Eco-Friendly Synthesis of Tetrakis(Aminomethyl)Calix-[4]-Resorcinarene. *Int. J. Org. Chem.*, *07*(04), 403–411.

Mukerjee, P. (1971). *Critical micelle concentrations of aqueous surfactant systems*. (K. J. Mysels, Ed.). North Carolina, 36-227.

Murray, K. K., Boyd, R. K., Eberlin, M. N., Langley, G. J., Li, L., & Naito, Y. (2013). Definitions of terms relating to mass spectrometry. *Pure Appl. Chem.*, *85*(7),

1515–1609.

Murtaza, G., Khan, S. A., Najam-ul-Haq, M., & Hussain, I. (2014). Comparative evaluation of various solubility enhancement strategies for furosemide. *Pak. J. Pharm. Sci.*, *27*(4), 963–973.

Nagabandi, V. kumar, Ramarao, T., & Jayaveera, K. N. (2011). LIQUISOLID Compacts: A Novel Approach to Enhance Bioavailability of Poorly Soluble Drugs. *Int J Pharm Bio Sci*, *1*(3), 89–102.

Nagarajan, R. (1997). Solubilization by amphiphilar aggregates. *Curr Opin Colloid Interface Sci*, *2*(3), 282–293.

Nagarajan, R., & Ganesh, K. (1989). Block Copolymer Self-Assembly in Selective Solvents: Theory of Solubilization in Spherical Micelles. *Macromolecules*, *22*, 4312–4325.

Neda, I., Siedentop, T., Vollbrecht, A., Thönnessen, H., Jones, P. G., & Schmutzler, R. (1998). A New Synthesis of Tetrakis(C-methyl)octakis(hydroxyethyl)calix[4]resorcinarene. *Z. Naturforsch*, *53 b*, 841–848.

Nesmerakk, K., & Nemcova, I. (2006). Determination of critical micelle concentration by electrochemical means. *Analytical Letters*, *39*(6), 1023–1040.

Ngodwana, L. (2012). *Selective distal functionalization of resorcinarenes via an ortholithiation approach*. University of Stellenbosch, 104.

Niederl, J., & Vogel, H. (1940). Aldeyde-Resorcinol Condensations. *J. Am. Chem. Soc.*, *62*, 2512.

Nimse, S. B., & Kim, T. (2013). Biological applications of functionalized calixarenes. *Chem. Soc. Rev.*, *42*(1), 366–386.

Novichkov, D. N., Ermilov, A. N., Kovalenko, A. Y., Ovcharov, I. V., Ornat, E. K., Roganov, I. S., & Safonov, V. A. (2011). Hydrotropy: A Promising tool for solubility Enhancement. *IJDDR*, *3*(2), 26–33.

Oliveira, P. J., Alcaro, S., Ortuso, F., & Uriarte, E. (2019). Benzoic acid-derived nitrones : A new class of potential acetylcholinesterase inhibitors and neuroprotective agents. *Eur. J. Med. Chem.*, *174*, 116–129.

Olivier, J. (2005). Drug Transport to Brain with Targeted Nanoparticles. *NeuroRx*, *2*(1), 108–119.

Oshovsky, G. V., Reinhoudt, D. N., & & Verboom, W. (2007). Supramolecular Chemistry in Water. *Angew. Chem., Int. Ed.*, *46*(14), 2366–2393.

Oshovsky, Gennady V, Verboom, W., Fokkens, R. H., & Reinhoudt, D. N. (2004). Anion Complexation by Glycocluster Thioureamethyl Cavitands : Novel ESI-MS-Based Methods for the Determination of K a Values. *Chem. Eur. J.*, *10*, 2739–2748.

Owen, S. C., Chan, D. P. Y., & Shoichet, M. S. (2012). Polymeric micelle stability. *Nano Today*, *7*(1), 53–65.

Ozdemir, N., & Ordu, S. (1998). Improvement of Dissolution Properties of Furosemide by Complexation with p-Cyclodextrin. *Drug Dev. Ind. Pharm.*, *24*(1), 19–25.

Paclet, M. H., Rousseau, C. F., Yannick, C., Morel, F., & Coleman, A. W. (2006). An

absence of non-specific immune response towards para-sulphonato-calix[n] arenes. *J Incl Phenom Macrocycl Chem*, *55*, 353–357.

Page, P. C. B., Heaney, H., Sampler, E. P., & Le, L. (1999). The First Enantioselective Syntheses of Axially Chiral Enantiomerically Pure Calix[4]resorcinarene Derivatives We report here our preliminary work that is designed to address the enantioselective synthesis of axially chiral , enantiomerically pure , c. *J. Am.Chem. Soc.*, *121*(8), 6751–6752.

Pan, F., Beyeh, N. K., & Rissanen, K. (2015). Concerted halogen-bonded networks with N-alkyl ammonium resorcinarene bromides: From dimeric dumbbell to capsular architectures. *J. Am.Chem. Soc.*, *137*(32), 10406–10413.

Panchal, J. G., Patel, R. V., & Menon, S. K. (2010). Preparation and physicochemical characterization of carbamazepine (CBMZ): Para-sulfonated calix[n]arene inclusion complexes. *J Incl Phenom Macrocycl Chem*, *67*(1–2), 201–208.

Park, S. J., & Hong, J. (2000). The cooperative effect of electrostatic and hydrophobic forces in the complexation of cationic molecules by a water-soluble resorcin[4]arene derivative. *Tetrahedron Lett.*, *41*, 8311–8315.

Pashirova, T. N., Leonova, M. V., Podyachev, S. N., S. N. Sudakova, L. Ya. Zakharova, L. A. Kudryavtseva, A., & Konovalov, A. I. (2007). Effect of structural preorganization on the reactivity of carbazoylmethyl derivatives of pyrogallol and calix[4]pyrogallol. *Russ. Chem. Bull.*, *56*(12), 2394–2399.

Pashirova, Tatiana N, Gibadullina, E. M., Burilov, A. R., Kashapov, R. R., Zhiltsova, E. P., Syakaev, V. V, Konovalov, A. I. (2014). Amphiphilic O-functionalized calix[4]resocinarenes with tunable structural behavior. *RSC Adv.*, *4*(1), 9912–

9919.

Pashirova, Tatiana N, Ziganshina, A. Y., Sultanova, E. D., Lukashenko, S. S., Kudryashova, Y. R., Zhiltsova, E. P., Konovalov, A. I. (2014). Supramolecular systems based on calix[4]resorcine with mono-, di-, and tetracationic surfactants: Synergetic structural and solubilization behavior. *Colloids Surf. A*, *448*, 67–72.

Pastor, A., & Martinez-Viviente, E. (2008). NMR spectroscopy in coordination supramolecular chemistry: A unique and powerful methodology. *Coord. Chem. Rev.*, *252*(21–22), 2314–2345.

Patel, M. B., Valand, N. N., Modi, N. R., Joshi, K. V, Harikrishnan, U., Kumar, S. P., … Menon, K. (2013). Effect of p-sulfonatocalix[4]resorcinarene (PSC[4]R) on the solubility and bioavailability of a poorly water soluble drug lamotrigine (LMN) and computational investigation. *RSC Advances*, *3*, 15971–15981.

Patton, D. E., Westt, J. W., Catterallt, W. A., & Goldin, A. L. (1992). Amino Acid Residues Required for Fast Na^+-Channel Inactivation : Charge Neutralizations and Deletions in the III-IV Linker. *Proc. Natl. Acad. Sci. USA*, *89*(22), 10905–10909.

Peltonen, L. J., & Yliruusi, J. (2000). Surface Pressure , Hysteresis , Interfacial Tension , and CMC of Four Sorbitan Monoesters at Water–Air, Water–Hexane , and Hexane–Air Interfaces. *J. Colloid Interface Sci.*, *6*, 1–6.

Perret, F., & Coleman, A. W. (2011). Biochemistry of anionic calix[n]arenes. *Chem. Commun*, *47*(26), 7303–7319.

Pesce, W. J., & Wiley, P. B. (2012). *Analytical Methods in Supramolecular Chemistry, Volume 1 & 2: Second Edition*. (C. A. Schalley, Ed.), *Analytical Methods in*

Supramolecular Chemistry (Second Edi, Vol. 1–2).

Pietraszkiewicz, M., Prus, P., & Pietraszkiewicz, O. (2004). Synthesis of novel , boron-containing cavitands derived from calix[4]resorcinarenes and their molecular recognition of biologically important polyols in Langmuir films. *Tetrahedron*, *60*, 10747–10752.

Plachkova-Petrova, D., Petrova, P., Miloshev, S., & Novakov, C. (2012). Optimization of reaction conditions for synthesis C-tetramethylcalix[4]resorcinarene. *Bulgarian Chem. Commu.*, *3*(3), 208–215.

Pod, S. N., Mustafina, A. R., & Habicher, W. D. (2003). Complex formation of O carboxymethylcalix[4] resorcinolarene with alkaline metal and ammonium ions. *Russ.Chem.Bull.,Int.Ed.*, *52*(1), 73–77.

Podyachev, S. N., Sudakova, S. N., Syakaev, V. V., Burmakina, N. E., Shagidullin, R. R., Morozov, V. I., Konovalov, A. I. (2009). Synthesis and properties of potassium salts of per O carboxymethyl calix[4] pyrogallols and their complexes with Cu^{2+} , Fe^{3+} , and La^{3+}. *Russ. Chem. Bull.*, *58*(1), 80–88.

Polenova, T., Gupta, R., & Goldbourt, A. (2015). Magic Angle Spinning NMR Spectroscopy: A Versatile Technique for Structural and Dynamic Analysis of Solid-Phase Systems. *Anal. Chem.*, *87*, 5458–5469.

Power, N. P., Dalgarno, S. J., & Atwood, J. L. (2007). Guest and ligand behavior in zinc-seamed pyrogallol[4]arene molecular capsules. *Angew. Chem. Int. Ed.*, *46*(45), 8601–8604.

Pragna, T., Dhaval, H., & Jayesh, M. (2015). Synthesis and Characterization of Aroylhydrazino Derivatives of Pharmacologically Activepyrimidine-5-Carbonitrile.

Int. Lett. Chem. Phys. Astron., *39*, 129–135.

Pratten, M., Lloyd, J., Hörpel, G., & Ringsdorf, H. (1985). Micelle-forming block copolymers: Pinocytosis by macrophages and interaction with model membranes. *Makromol. Chem.*, *186*(4), 725–733.

Prus, P., Pietraszkiewicz, M., & Bilewicz, R. (1998). Monolayers of Chiral Calix[4]Resorcinarenes: Surface Pressure and Surface Potential Studies. *Supramol. Chem.*, *10*(2), 17–25.

Purse, B. W., Butterfield, S. M., Ballester, P., & Shivanyuk, A. (2008). Interaction Energies and Dynamics of Acid–Base Pairs Isolated in Cavitands. *J. Org. Chem.*, *73*(17), 6480–6488.

Qin, Z., Guo, D.-S., Gao, X.-N., & Liu, Y. (2014). Supra-amphiphilic aggregates formed by p-sulfonatocalix[4]arenes and the antipsychotic drug chlorpromazine. *Soft Matter*, *10*, 2253–2263.

Ramanathan, M., Shrestha, L. K., Mori, T., Ji, Q., Hill, J. P., & Ariga, K. (2013). Amphiphile nanoarchitectonics: From basic physical chemistry to advanced applications. *Phys. Chem. Chem. Phys.*, *15*(26), 10580–10611.

Ratto, D., Alfaro, C., Sipsey, J., Glovsky, M. M., & Sharma, O. P. (1988). Are Intravenous Corticosteroids Required in Status Asthmaticus? *JAMA*, *260*(4), 527–529.

Raut, K. T., & Shirote, P. J. (2012). Synthesis and characterization of novel amide derivatives of nitro-imidazole. *Der Pharma Chemica*, *4*(4), 1435–1439.

Ravenelle, F., Vachon, P., Sneyd, J. R., Garrec, D. Le, Gori, S., Lessard, D., Pl, P.

(2008). Anaesthetic effects of propofol polymeric micelle : a novel water soluble propofol formulation. *Br J Anaesth*, *101*(2), 186–193.

Reinhoudt, D. N. (1992). Application of supramolecular chemistry in the development of ion-selective chemfets. *Sens. Actuators, B*, *6*(1–3), 179–185.

Robinson, E., Leung, E., Matuszek, A. M., Krogsgaard-Larsen, N., Furkert, D. P., Brimble, M. A., Reynisson, J. (2015). Virtual screening for novel Atg5-Atg16 complex inhibitors for autophagy modulation. *MedChemComm*, *6*(1), 239–246.

Roughley, S. D., & Jordan, A. M. (2011). The Medicinal Chemist ' s Toolbox : An Analysis of Reactions Used in the Pursuit of Drug Candidates †. *J. Med. Chem.*, *54*(10), 3451–3479.

Rudkevich, D. M., & Rebek, J. (1999). Deepening Cavitands. *Eur. J. Org. Chem.*, 1991–2005.

Ruozi, B., Tosi, G., Forni, F., Fresta, M., & Vandelli, M. A. (2005). Atomic force microscopy and photon correlation spectroscopy: Two techniques for rapid characterization of liposomes. *Eur. J. Pharm. Scie.*, *25*(1), 81–89.

Ryzhkina, I. S., Kiseleva, Y. V., Mishina, O. A., Masagutova, E. M., Sergeeva, S. Y., Sudakova, S. N., Konovalov, A. I. (2014). Highly diluted solutions of amphiphilic derivatives of calix[4] resorcinols : self organization and physicochemical properties. *Russ.Chem.Bull.,Int.Ed.*, *63*(6), 1399–1408.

Saharan, V. A., Kukkar, V., Kataria, M., Gera, M., & Choudhury, P. K. (2009). Dissolution Enhancement of Drugs. Part I: Technologies and Effect of Carriers. *Int J Health Res*, *2*(2), 107–124.

Sahinovic, M. M., Struys, M. M. R. F., & Absalom, A. R. (2018). Clinical Pharmacokinetics and Pharmacodynamics of Propofol. *Clin Pharmacokinet*, *57*(12), 1539–1558.

Sansone, F., Barboso, S., Casnati, A., Fabbi, M., Pochini, A., Ugozzoli, F., & Ungaro, R. (1998). Synthesis and Structure of Chiral Cone Calix[4]arenes Functionalized at the Upper Rim with L -Alanine Units. *Eur. J. Org. Chem.*, 897–905.

Sardjono, R. E., & Rachmawati, R. (2017). Green Synthesis of Oligomer Calixarenes. In H. S. Iyad Karamé (Ed.), *Green Chemical Processing and Synthesis* (p. 160). BoD–Books on Demand.

Savic, R., Eisenberg, A., & Maysinger, D. (2006). Block copolymer micelles as delivery vehicles of hydrophobic drugs. *J Drug Target*, *14*(6), 343–355.

Savjani, K. T., Gajjar, A. K., & Savjani, J. K. (2012). Drug Solubility: Importance and Enhancement Techniques. *ISRN Pharmaceutics*, *2012*, 1–10.

Saxena, S., Virmani, S., Singh, K., & Malhotra, K. (2004). Mycophenolate mofetil in the treatment of nephrotic syndrome. *Indian J Nephrol*, *14*, 15–17.

Schneider, H. J., & Schneider, U. (1994). The Host-Guest Chemistry of Resorcinarenes [1]. *J. Inclusion Phenom. Mol. Recognit. Chem.*, *19*, 67–68.

Schramm, M. P., Hooley, R. J., & Rebek, J. (2007). Guest recognition with micelle-bound cavitands. *J. Am. Chem. Soc.*, *129*(31), 9773–9779.

Schultheiss, N., & Desper, J. (2006). C-Pentyltetra(3-pyridyl) cavitand : A Versatile Building Block for the Directed Assembly of Hydrogen-Bonded Heterodimeric Capsules. *Organic Letters*, *8*(12), 2607–2610.

Scott, M. P., & Sherburn, M. S. (2017). Resorcinarenes and Pyrogallolarenes. In *Reference Module in Chemistry, Molecular Sciences and Chemical Engineering* (Vol. 1, p. 160). Elsevier Ltd.

Sdira, S. Ben, Felix, C., Giudicelli, M. B., Vocanson, F., Perrin, M., & Lamartine, R. (2005). Synthesis, structure and anion binding properties of lower rim α-hydroxyamide calix[4]arene derivatives. *Tetrahedron Lett.*, *46*(34), 5659–5663.

Serajuddin, A. T. M. (1999). Solid Dispersion of Poorly Water-Soluble Drugs : Early Promises , Subsequent Problems , and Recent Breakthroughs. *J. Pharm. Sci.*, *88*(10), 1059–1066.

Seridi, L., & Boufelfel, A. (2011). Molecular modeling study of Lamotrigine/β-cyclodextrin inclusion complex. *Journal of Molecular Liquids*, *158*(2), 151–158.

Shah, V. P., & Amidon, G. L. (2014). A Theoretical Basis for a Biopharmaceutic Drug Classification : The Correlation of In Vitro Drug Product Dissolution and In Vivo Bioavailability. *AAPS J*, *12*(3), 413–420.

Shahgaldian, P., Gualbert, J., Aïssa, K., & Coleman, A. W. (2003). A study of the freeze-drying conditions of calixarene based solid lipid nanoparticles. *Eur. J. Pharm. Biopharm.*, *55*(2), 181–184.

Shahgaldian, P., & Pieles, U. (2006). Cyclodextrin Derivatives as Chiral Supramolecular Receptors for Enantioselective Sensing. *Sensors*, *6*, 593–615.

Shahgaldian, P., Pieles, U., & Hegner, M. (2005a). Enantioselective recognition of phenylalanine by a chiral amphiphilic macrocycle at the air-water interface: A copper-mediated mechanism. *Langmuir*, *21*(14), 6503–6507.

Shahgaldian, P., Pieles, U., & Hegner, M. (2005b). for Enantioselective Recognition by a Chiral amphiphilic Calix-resorcinarene at the Air- water Interface : Mechanism. *Langmuir*, *21*(20), 6503–6507.

Shahgaldian, P., Sciotti, M. A., & Pieles, U. (2008). Amino-substituted amphiphilic calixarenes: Self-assembly and interactions with DNA. *Langmuir*, *24*(16), 8522–8526.

Shalaeva, Y. V, Morozova, J. E., Saifina, A. T. G. A. F., & Ermakova, V. V. S. A. M. (2018). Gold nanoparticles , capped by carboxy-calix[4]resorcinarenes : effect of structure and concentration of macrocycles on the nanoparticles size and aggregation. *J. Incl. Phenom. Macrocyl. Chem.*, *0*(0), 0.

Shelke, R. N., Pansare, D. N., Pawar, C. D., Khade, M. C., Jadhav, V. N., Deshmukh, S. U., Thopate, S. R. (2019). Synthesis and anticancer evaluation of new benzenesulfonamides. *Eur. Chem. Bull*, *8*(1), 1–6.

Sherman, J. C., & Cram, D. J. (1989). arcerand Interiors Provide a New Phase of Matter. *J. Am. Chem. Soc.*, *111*(7), 4528–4529.

Shinde, V. R., Shelake, M. R., Shetty, S. S., Chavan-Patil, A. B., Pore, Y. V., & Late, S. G. (2008). Enhanced solubility and dissolution rate of lamotrigine by inclusion complexation and solid dispersion technique. *J. Pharm. Pharmacol.*, *60*(9), 1121–1129.

Shinkai, S., Mori, S., Tsubaki, T., Sone, T., & Manabe, O. (1984). New water-soluble host molecules derived from calix[6]arene. *Tetrahedron Lett.*, *25*(46), 5315–5318.

Shinkai, Seiji, Araki, K., Matsuda, T., Nishiyama, N., Ikeda, H., Takasu, I., & Iwamoto,

M. (1990). NMR and Crystallographic Studies of a *p*-Sulfonatocalix[4]arene-Guest Complex. *J. Am. Chem. SOC*, *112*(25), 9053–9058.

Shinkai, Seiji, & Ikeda, A. (1997). Novel Cavity Design Using Calix[n]arene Skeletons: Toward Molecular Recognition and Metal Binding. *Chem. Rev.*, *97*, 1713–1734.

Shinkai, Seiji, Mori, S., Koreishi, H., Tsubaki, T., & Manabe, O. (1986). Hexasulfonated Calix[6]arene Derivatives : A New Class of Catalysts, Surfactants, and Host Molecules. *J. Am.Chem. Soc.*, *108*(14), 2409–2416.

Shivanyuk, A, & Rebek, J. (2001). Reversible encapsulation by self-assembling resorcinarene subunits. *PNAS*, *98*(14), 7662–7665.

Shivanyuk, Alexander, Spaniol, T. P., Rissanen, K., Kolehmainen, E., & Bohmer, V. (2000). Hydrogen-bonded analogues of cavitands. *Angew. Chem. Int. Ed.*, *39*(19), 3497–3500.

Shukla, P. K., Khanna, V. K., Ali, M. M., Khan, M. Y., & Srimal, R. C. (2008). Anti-ischemic effect of curcumin in rat brain. *Neurochem. Res.*, *33*(6), 1036–1043.

Simoes, S. M., Figueiras, A. R., Veiga, F., & Concheiro, A. (2014). Polymeric micelles for oral drug administration enabling locoregional and systemic treatments. *Expert Opin. Drug Deliv*, *12*(2), 1–22.

Simonyi, M. (1984). On chiral drug action. *Med Res Rev*, *4*(3), 359–413.

Singh, R., & Jr, J. W. L. (2009). Nanoparticle-based targeted drug delivery. *Exp. Mol. Pathol.*, *86*(3), 215–223.

Sirit, A., & Yilmaz, M. (2009). Chiral calixarenes. *Turk J Chem*, *33*(2), 159–200.

Soppimath, K. S., Aminabhavi, T. M., Kulkarni, A. R., & Rudzinski, W. E. (2001). Biodegradable polymeric nanoparticles as drug delivery devices. *J. Control. Release*, *70*, 1–20.

Sorrell, T. N., & Pigge, F. C. (1993). A Convenient Synthesis of Functionalized Cavitands via Free-Radical Bromination. *J. Org. Chem.*, *58*(14), 784–785.

Spamer, E., Muller, D. G., Wessels, P. L., & Venter, J. P. (2002). Characterization of the complexes of furosemide with 2-hydroxypropyl-b-cyclodextrin and sulfobutyl ether-7-bcyclodextrin. *Eur. J. Pharm. Scie.*, *16*, 247–253.

Spiel, P. D., Sikligar, K., Baker, G. A., Kelley, S. P., & Atwood, J. L. (2019). Cocrystallization of C-Propyl Pyrogallol[4]arene and the Pharmaceutical Gabapentin. *J. Chem. Crystallogr.*, *49*(2), 119–124.

Spireas, S., & Sadu, S. (1998). Enhancement of prednisolone dissolution properties using liquisolid compacts. *Int J Pharm*, *166*(2), 177–188.

St. Luce, N. N. (2004). *Synthesis, Characterization and Study of Novel Reagents for the Detection of Saccharides and Amino Acids*. Graduate Faculty of the Agricultural and Mechanical College, 221.

Steed, J. W., & Atwood, J. L. (2009). *Supramolecular Chemistry* (2nd Edi). A John Wiley & Sons, Ltd., Publication.

Stella, V. J., & Nti-Addae, K. W. (2007). Prodrug strategies to overcome poor water solubility. *Adv. Drug Deliv. Rev.*, *59*(7), 677–694.

Stilbs, P. (1987). Fourier Pulsed-Gradient Studies of Molecular Diffusion. *Prog. NMR Spectrosc.*, *19*, 1–45.

Stupak, E. I., Rosenberg, H. A., & Bates, T. R. (1974). Biopharmaceutical and Physicochemical Studies on Reserpine-Polyvinylpyrrolidone Coprecipitates. *J. Pharmacokinet Biopharm.*, *2*(6), 512–523.

Sultan, S. S. (2014). Patient-controlled sedation with propofol/remifentanil versus propofol/alfentanil for patients undergoing outpatient colonoscopy, a randomized , controlled double-blind study. *Saudi J Anaesth*, *8*(1), s36-40.

Sun, B. Y., Yan, C., Yao, Y., Han, Y., & Shen, M. (2008). Self-Assembly and Metallization of Resorcinarene Microtubes in Water. *Adv. Funct. Mater.*, *18*, 3981–3990.

Syakaev, V. V., Mustafina, A. R., Elistratova, J. G., Latypov, S. K., & Konovalov, A. I. (2008). Head-to-tail Aggregates of Sulfonatomethylated Calix[4]resorcinarene in Aqueous Solutions. *Supramol. Chem.*, *20*(5), 453–460.

Syakaev, V. V, Kazakova, E. K., Morozova, J. E., Shalaeva, Y. V, Latypov, S. K., & Konovalov, A. I. (2012). Guest controlled aggregation of amphiphilic sulfonatomethylated calix[4]resorcinarenes in aqueous solutions. *J. Colloid Interface Sci.*, *370*(1), 19–26.

Syakaev, V. V, Morozova, J. E., Andrei, V., Shalaeva, Y. V, Ermakova, A. M., Voloshina, D., Konovalov, A. I. (2018). Solubilization of azo-dye-modified isatin derivative by amphiphilic carboxyresorcinarenes: the effect of macrocycle structure on the supramolecular association. *Colloids and Surfaces A: Physicochem. Eng. Aspects*, *0*(0), 0.

Szumna, A. (2007). Cyclochiral conformers of resorcin[4]arenes stabilized by hydrogen bonds. *Org. Biomol. Chem.*, *5*(9), 1358–1368.

Tanaka, Y., Miyachi, M., & Kobuke, Y. (1999). Selective Vesicle Formation from Calixarenes, *645*(4), 504–506.

Taoufik, A., Halima, B., Masson-makdissi, J., Newman, G., Halima, T. Ben, Masson-makdissi, J., & Newman, S. G. (2018). Nickel-Catalyzed Amide Bond Formation from Methyl Esters. *Angew. Chem. Int. Ed.*, *57*, 12925 –12929.

Tauran, Y. (2014). *Calix[n]arenes in nano bio-system*. University Claude Bernard-Lyon1,289.

Tauran, Y., Brioude, A., Kim, B., Perret, F., & Coleman, A. W. (2013). Anionic calixarene-capped silver nanoparticles show species-dependent binding to serum albumins. *Molecules*, *18*(5), 5993–6007.

Taylor, P., Dalcanale, E., Jacopozzi, P., Ugozzoli, F., & Mann, G. (1998). Synthesis and Configurational Analysis of Mixed-bridged Phosphate Cavitands Synthesis and Configurational Analysis of Mixed-bridged Phosphate Cavitands. *Supramol. Chem.*, *9*, 305–316.

Teshima, M., Fumoto, S., Nishida, K., Nakamura, J., Ohyama, K., Nakamura, T., Sasaki, H. (2006). Prolonged blood concentration of prednisolone after intravenous injection of liposomal palmitoyl prednisolone. *J Control Release*, *112*(3), 320–328.

Thapa, R. (2009). *Regioselectivity in Free Radical Bromination of Unsymmetrical Dimethylated Pyridines*. Miami University, 56.

Thompson, C. J., Ding, C., Qu, X., Yang, Z., & Uchegbu, I. F. (2008). The effect of polymer architecture on the nano self-assemblies based on novel comb-shaped amphiphilic poly (allylamine). *Colloid Polym Sci*, *286*(13), 1511–1526.

Thompson, K. A., & Goodale, D. B. (2000). The Recent Development of Propofol. *Intensive Care Med*, *26*, 400–404.

Timmerman, P., Verboom, W., & Reinhoult, D. N. (1996). Resorcinarenes. *Tetrahedron*, *52*(8), 2663–2704.

Torchilin, V P. (2004). Targeted polymeric micelles for delivery of poorly soluble drugs. *CMLS, Mol. Life. Sci.*, *61*, 2549–2559.

Torchilin, Vladimir P. (2012). Multifunctional nanocarriers. *Adv. Drug Deliv. Rev.*, *64*(SUPPL.), 302–315.

Trapani, G., Latrofa, A., Franco, M., Lopedota, A., Sanna, E., & Liso, G. (1998). Inclusion Complexation of Propofol with 2-Hydroxypropyl-cyclodextrin. Physicochemical, Nuclear Magnetic Resonance Spectroscopic Studies, and Anesthetic Properties in Rat. *J. Pharm. Sci.*, *87*(4), 2–6.

Trembleau, L., & Rebek, J. J. (2004). Interactions between a surfactant and cavitand in water blur distinctions between host and guest. *Chem. Commun.*, 58–59.

Tunstad, L. M., Sherman, J. C., Helgeson, R. C., Weiser, J., Knobler, C. B., Cram, D. J., … Tucker, J. A. (1989). Host-Guest Complexation. 48. Octol Building Blocks for Cavitands and Carcerands. *J. Org. Chem.*, *54*(6), 1305–1312.

Turunen, L., Beyeh, N. K., Pan, F., Valkonen, A., & Rissanen, K. (2014). multivalent halogen bond donors. *Chem. Commnun.*, *50*, 15920–15923.

Uchegbu, I. F., Sadiq, L., Arastoo, M., Gray, A. I., Wang, W., Waigh, R. D., & Schätzleinä, A. G. (2001). Quaternary ammonium palmitoyl glycol chitosan - A new polysoap for drug delivery. *Int J Pharm*, *224*(1–2), 185–199.

Uekama, K., Hirayama, F., & Irie, T. (1998). Cyclodextrin Drug Carrier Systems. *Chem. Rev.*, *98*(5), 2045–2076.

Ukhatskaya, E. V., Kurkov, S. V., Matthews, S. E., & Loftsson, T. (2013). Encapsulation of drug molecules into Calix[n]arene Nanobaskets. Role of Aminocalix[n]arenes in biopharmaceutical field. *J. of Pharm.Sci.*, *102*(10), 3485–3512.

Urban, C., & Schurtenberger, P. (1998). Characterization of Turbid Colloidal Suspensions Using Light Scattering Techniques Combined with Cross-Correlation Methods. *J Cholloid Interface Sci*, *158*(1), 150–158.

Valand, N. N., & Menon, M. B. P. and S. K. (2015). Curcumin-*p*-sulfonatocalix[4]resorcinarene (*p*-SC[4]R)interaction:thermo-physicochemistry, stabilityandbiologicalevaluation. *RSC Adv.*, *5*, 8739–8752.

Valeur, E., & Bradley, M. (2009). Amide bond formation : beyond the myth of coupling reagents. *Chem. Soc. Rev.*, *38*(2), 606–631.

Valitova, Y. N., & Konovalov, A. A. I. (2012). Low Concentration Aqueous Solutions of an Amphiphilic Calix[4]resorcinarene Derivative : Self Organization , Physicochemical Properties , and Biological Activity under Common and Hypoelectromagnetic Conditions. *Dokl Phys Chem*, *447*(1), 193–199.

Vargaftik, N. B., Volkov, B. N., & Voljak, L. D. (1983). International Tables of the Surface Tension of Water. *J Phys Chem Ref Data*, *12*(3), 817–820.

Vemula, V. R., Lagishetty, V., & Lingala, S. (2010). Solubility Enhancement Techniques. *Int. J Pharm Sci Rev Res*, *5*(1), 41–51.

Venkatachalam, S. (2016). UV/VIS Spectroscopy. In *Ultraviolet and visible spectroscopy studies of nanofillers and their polymer nanocomposites. Elsevier B.V,* (pp. 130–157).

Ventola, E. (2006). *Host-Guest Chemistry of Resorcarene Derivatives Studied by ESI-FTICR Mass Spectrometry*. University of Joensuu Finland, 52.

Ventola, E., Pirskanen, A., & Vainiotalo, P. (2005). Noncovalent complex formation of tetratosylated resorcarene with aromatic, aliphatic, and cyclic alkyl ammonium ions: A mass spectrometric study of complex properties. *Rapid Commun. Mass Spectrom.*, *19*(21), 3159–3165.

Verwey, E. J. W., & Overbeek, J. T. G. (1948). *Theory of the stability of lyophobic colloids. The interaction of solparticles havingand electron double layer*. (E. Amsterdam, Ed.), 197.

Vig, B. S., Huttunen, K. M., Laine, K., & Rautio, J. (2013). Amino acids as promoieties in prodrug design and development. *Adv. Drug Deliv. Rev.*, *65*(10), 1370–1385.

Vinodh, M., Alipour, F. H., Mohamod, A. A., & Al-Azemi, T. F. (2012). Molecular assemblies of porphyrins and macrocyclic receptors: Recent developments in their synthesis and applications. *Molecules*, *17*(10), 11763–11799.

Vlachou, M., & Papaioannou, G. (2003). Preparation and Characterization of the Inclusion Complex of Furosemide with Hydroxypropyl-Cyclodextrin. *J. Biomater. Appl.*, *17*, 197–206.

Volkmer, D., Fricke, M., & Mattay, J. (2002). Oriented crystallization of calcite single crystals grown underneath monolayers of tetracarboxyresorc[4]arenes. *Cryst.*

Eng. Comm., *4*(52), 288–295.

Voronin, M. A., Gabdrakhmanov, D. R., Khaibullin, R. N., Yu, I., Kataev, V. E., Idiyatullin, B. Z., … Konovalov, A. I. (2013). Novel biomimetic systems based on amphiphilic compounds with a diterpenoid fragment : Role of counterions in self-assembly. *J Cholloid Interface Sci*, *405*, 125–133.

Voskuhl, J., & Ravoo, B. J. (2009). Molecular recognition of bilayer vesicles. *Chem. Soc. Rev.*, *38*(2), 495–505.

Wang, B. Y., Yan, Y., Cui, J., Hosta-rigau, L., Heath, J. K., & Nice, E. C. (2010). Encapsulation of Water-Insoluble Drugs in Polymer Capsules Prepared Using Mesoporous Silica Templates for Intracellular Drug Delivery. *Adv. Mater.*, *22*(38), 4293.

Wang, G. S., Zhang, H. Y., Ding, F., & Liu, Y. (2011). Preparation and characterization of inclusion complexes of topotecan with sulfonatocalixarene. *J. Incl. Phenom. Macrocyl. Chem.*, *69*(1–2), 85–89.

Wang, K., Guo, D. S., Zhang, H. Q., Dong, L., Zheng, X. L., & Yu, L. (2009). Highly effective binding of viologens by p-sulfonatocalixarenes for the treatment of viologen poisoning. *J. Med. Chem.*, *52*(20), 6402–6412.

Wang, L., Li, L. L., Fan, Y. S., & Wang, H. (2013). Host-guest supramolecular nanosystems for cancer diagnostics and therapeutics. *Adv. Mater.*, *25*(28), 3888–3898.

Wang, W., Qu, X., Gray, A. I., Tetley, L., & Uchegbu, I. F. (2004). Self-Assembly of Cetyl Linear Polyethylenimine To Give Micelles, Vesicles, and Dense Nanoparticles. *Macromolecules*, *37*(24), 9114–9122.

Wang, X., Hann, Z., & Maruoka, K. (2007). Convenient Preparation of Chiral Phase-Transfer Catalysts with Conformationally Fixed Biphenyl Core for Catalytic Asymmetric Synthesis of α-Alkyl- and α,α-Dialkyl-α-amino Acids: Application to the Short Asymmetric Synthesis of BIRT-377. *Tetrahedron*, *63*(26), 6042–6050.

Wang, Xudong, Wang, Y., Wei, K., Zhao, N., Zhang, S., & Chen, J. (2009). Drug distribution within poly(ε-caprolactone) microspheres and in vitro release. *J. Mater Process Technol*, *209*(1), 348–354.

Wang, Y.-X., Guo, D.-S., Cao, Y., & Liu, Y. (2013). Phosphatase-responsive amphiphilic calixarene assembly. *RSC Advances*, *3*(21), 8058.

Wang, Y.-X., Guo, D.-S., Duan, Y.-C., Wang, Y.-J., & Liu, Y. (2015a). Amphiphilic *p*-Sulfonatocalix[4]arene as “Drug Chaperone” for Escorting Anticancer Drugs. *Scientific Reports*, *5*, 1–13.

Wang, Y.-X., Guo, D.-S., Duan, Y.-C., Wang, Y.-J., & Liu, Y. (2015b). Amphiphilic *p*-Sulfonatocalix[4]arene as “Drug Chaperone” for Escorting Anticancer Drugs. *Scientific Reports*, *5*, 9019.

Wang, Z., Bao, X., Xu, M., Deng, Z., Han, Y., & Wang, N. (2018). Direct Formation of Amides from Carboxylic Acids and Amines Catalyzed by Niobium(V) Oxalate Hydrate. *ChemistrySelect*, *3*(9), 2599–2603.

Wei, H., Zhuo, R. X., & Zhang, X. Z. (2013). Design and development of polymeric micelles with cleavable links for intracellular drug delivery. *Prog. Polym. Sci.*, *38*(3–4), 503–535.

Weinelt, F., & Schneider, H.-J. (1991). Mechanisms of Macrocycle Genesis. The Condensation of Resorcinol with Aldehydes’. *J Org Chem*, *56*(19), 5527–5535.

Werdehausen, R., Fazeli, S., Braun, S., Hermanns, H., Essmann, F., Hollmann, M. W., Stevens, M. F. (2009). Apoptosis induction by different local anaesthetics in a neuroblastoma cell line. *Br. J. of Anaesth.*, *103*(5), 711–718.

West, J. W., Pattont, D. E., Scheuer, T., Wang, Y., Goldint, A. L., & Catterall, W. A. (1992). A cluster of hydrophobic amino acid residues required for fast Na^+-channel inactivation. *Proc. Natl. Acad. Sci. USA*, *89*, 10910–10914.

Wilczura-Wachnik, H. (2007). *Dynamic Light Scattering application in size detection of molecules and molecular aggregates, 1-8*.

Williams, P. G., Yoshida, W. Y., Quon, M. K., Moore, R. E., & Paul, V. J. (2003). The Structure of Palau ' amide , a Potent Cytotoxin from a Species of the Marine Cyanobacterium Lyngbya. *J. Nat. Prod.*, *66*, 1545–1549.

Wu, S., Yan, Z., Wen, X., Xu, C., & Pan, Q. (2014). Conductometric and fluorescence probe investigations of molecular interactions between dodecyltrimethylammonium bromide and dipeptides Shuangyan. *Colloid Polym Sci*, *292*(11), 2775–2783.

Xue, Y., Guan, Y., Zheng, A., & Xiao, H. (2013). Amphoteric calix[8]arene-based complex for pH-triggered drug delivery. *Colloids Surf. B*, *101*, 55–60.

Yang, W., & de Villiers, M. M. (2004). Aqueous solubilization of furosemide by supramolecular complexation with 4-sulphonic calix[n]arenes. *J. Pharm. Pharmacol.*, *56*(6), 703–708.

Yang, W., Otto, D. P., Liebenberg, W., & Villiers, M. M. De. (2008). Effect of para-Sulfonato-Calix[n]arenes on the Solubility, Chemical Stability, and Bioavailability of a Water Insoluble Drug Nifedipine. *Curr. Drug Discov. Technol.*, *5*(2), 129–

139.

Yang, W., & Villiers, M. M. de. (2004). The solubilization of the poorly water soluble drug nifedipine by water soluble 4-sulphonic calix[n]arenes. *Eur. J. Pharm. Biopharm.*, *58*, 629–636.

Yao, Y., Xue, M., Chen, J., Zhang, M., & Huang, F. (2012). An Amphiphilic Pillar[5]arene: Synthesis, Controllable Self-Assembly in Water, and Application in Calcein Release and TNT Adsorption. *J. Am. Chem. Soc.*, *134*(38), 1–4.

Yokoyama, M., Kwon, G. S., Okano, T., Sakurai, Y., Seto, T., & Kataoka, K. (1992). Preparation of micelle-forming polymer-drug conjugates. *Bioconjug. Chem.*, *3*(4), 295–301.

Yousaf, A., Hamid, S. A., Bunnori, N. M., & Ishola, A. (2015). Applications of calixarenes in cancer chemotherapy : facts and perspectives. *Drug Des. Devel. Ther.*, *9*, 2831–2838.

Zadmard, R., Ataeian, P., & Khalili-foumeshi, M. (2011). C-Silylated Calix[4]Arene as a New Receptor for Aspartate in Polar Solvents. *Chemistry International*, *2011*, 15–19.

Zhang, J., Li, S., Li, X., Li, X., & Zhu, K. (2009). Morphology modulation of polymeric assemblies by guest drug molecules : TEM study and compatibility evaluation. *Polymer*, *50*(7), 1778–1789.

Zhang, L., Wang, S., Zhang, M., & Jie Sun. (2013). Nanocarriers for oral drug delivery. *J Drug Target*, *21*(6), 515–527.

Zhang, X., Chen, Z., & Würthner, F. (2007). Morphology control of fluorescent

nanoaggregates by co-self-assembly of wedge- and dumbbell-shaped amphophilic perylene bisimides. *J. Am. Chem. Soc.*, *129*(16), 4886–4887.

Zhao, H., Guo, D., & Liu, Y. (2013). Binding Behaviors of *p*-Sulfonatocalix[4]arene with Gemini Guests. *J. Phys. Chem. B*, *117*, 1978–1987.

Zhao, Z.-M., Wang, Y., Han, J., Zhu, H.-D., & An, L. (2015). Preparation and characterization of amphiphilic calixarene nanoparticles as delivery carriers for Paclitaxel. *Chem. Pharm. Bull.*, *63*(3), 180–186.

Zhou, R., Ren, J. C., & Yan, C. G. (2010). Novel synthesis of resorcinarene *O*-acetates by BF_3. OEt 2-catalyzed cyclocondensation of 1,3-(dialkoxycarbonylmethoxy)benzenes with aldehydes. *J. Incl. Phenom. Macrocycl Chem.*, *67*, 335–342.

Zhou, Y., Li, H., & Yang, Y.-W. (2015). Controlled drug delivery systems based on calixarenes. *Chin. Chem. Lett,* 26(7), 825-828.

Ziaja, P., Krogul, A., Pawłowski, T. S., & Litwinienko, G. (2016). Thermochimica Acta Structure and stoichiometry of resorcinarene solvates as host–guest complexes–NMR, X-ray and thermoanalytical studies. *Thermochimica Acta*, *623*, 112–119.

Ziganshina, A. Y., Kharlamov, S. V., Kazakova, E. K., Latypov, S. K., & Konovalov, A. I. (2007). Water-soluble tetra(methylviologen)calix[4]resorcinarene: host-guest properties toward aromatic compounds. *Mendeleev Commun.*, *17*(3), 145–147.